TEMPORAL, LITHOSPHERIC AND MAGMATIC PROCESS CONTROLS ON Ni, Cu AND PLATINUM-GROUP ELEMENT (PGE) MINERALISATION:

A CASE STUDY FROM SCOTLAND

HANNAH S. R. HUGHES

Submitted in fulfilment of the requirements for
the degree of PhD

February 2015

Declaration

This work has not previously been accepted in substance for any degree and is not concurrently submitted in candidature for any degree

Signed ..... (candidate)

Date ..17/02/15...

Statement 1

This thesis is being submitted in partial fulfilment of the requirements for the degree of PhD.

Signed ..... (candidate)

Date ..17/02/15..

Statement 2

This thesis is the result of my own independent work/investigation, except where otherwise stated.

Other sources are acknowledged by explicit references

Signed ..... (candidate)

Date ..17/02/15...

Statement 3

I hereby give consent for my thesis, if accepted, to be available for photocopying and for inter-library loan, and for the title and summary to be made available to outside organisations.

Signed ..... (candidate)

Date ..17/02/15..

Statement 4

I hereby give consent of my thesis, if accepted, to be available for photocopying and for inter-library loans after expiry of a bar on access previously approved by the Graduate Development Committee.

Signed ..... (candidate)

Date ..17/02/15..

ACKNOWLEDGEMENTS

There are many people to thank for their contributions and support over the past three and a half years. I hope they know they're appreciated (beyond belief!). They are:

Andrew Kerr, Adrian Boyce, Brian Upton, John Faithfull, Dave Holwell, Tony Oldroyd, Pete Fisher, Alison McDonald, Brett Davidheiser-Kroll, Hazel Prichard, Julian Pearce, Rachel North, Laura Cotton, Hilary Downes, Denis Schlatter (for all the Swiss chocolate!), Josh Hughes, Kevin Murphy, Ella Young, Ben Hayes, Bethan Phillips, Matt Loocke, Henry Coombs, Jake Ciborowski and Rob Knight.

Finally, there are three particular people that deserve highlighting: Kathryn Goodenough, Katie Dobbie and (last, but by no means least) Iain McDonald. What granted me the luck to work and laugh with these people I do not know, but I thank my stars that I know them.

Kathryn – you have stuck with me and nothing is ever too much trouble. Not least, you gave me the confidence to do it all. So here's to many more years to come!

Katie – you have been a true friend (measured of course, proportionally to the volumes of tea consumed in our impossibly-fun 'breaks'). You should probably get a PhD-by-proxy.

And Iain – what would I have done without you? You've been there through thick and thin, encouraged me when I most certainly needed it, and always stood by and cheered me on. I honestly don't think I can put into words how much I appreciate all you've done. And I hope I can say that for a very long time yet.

Iain, Katie and Kathryn – you probably all deserve some kind of a medal!

To all – thank you.

Lastly, Mum & Dad – not too bad for a Pendeen girl, hey! And Dad, yes there really is a paper out there called "Heavy metal, sex and granite".
Love you always. x

PUBLICATION LIST

Chapters 6 to 12 present a series of seven papers. At the time of thesis submission and completion, the papers are in various stages of review, in press, or in print and fully published. The content of the papers has been re-formatted so as to be more suitable for the thesis layout, however the text, figures and tables presented here are the same as those submitted to the journals.

The details of the following papers (chapters), including co-author contributions, are as follows (up to date at the time of thesis submission):

- Hughes, H.S.R., McDonald, I., Goodenough, K.M., Ciborowski, T.J.R., Kerr, A.C., Davies, J.H.F.L., Selby, D. 2014. **Enriched lithospheric mantle keel below the Scottish margin of the North Atlantic Craton: Evidence from the Palaeoproterozoic Scourie Dyke Swarm and mantle xenoliths.** *Precambrian Research,* **250,** 97-126. ***(Chapter 6).***
  Co-author contributions: *I. McDonald, K.M. Goodenough, A.C. Kerr, J.H.F.L. Davies, and T.J.R. Ciborowski were involved in discussions during the writing of this paper. D. Selby processed three bulk samples for Re-Os isotopes. I. McDonald supervised bulk rock analyses. Note that H.S.R. Hughes and J.H.F.L. Davies also co-authored a similar online publication for "Large Igneous Province of the Month" (May, 2014). See: http://www.largeigneousprovinces.org/14may*

- Hughes, H.S.R., McDonald, I., Faithfull, J.W., Upton, B.G.J., Downes, H. (in press). **Trace element abundances in the shallow lithospheric mantle of the North Atlantic Craton margin: Implications for melting and metasomatism beneath Northern Scotland.** *Mineralogical Magazine (North Atlantic Craton Conference Special Issue).* ***(Chapter 7).***
  Co-author contributions: *I. McDonald, J.W. Faithfull, B.G.J. Upton and H. Downes were involved in discussions during the writing of this paper. J.W. Faithfull and B.G.J. Upton provided xenolith specimens for study. I. McDonald supervised bulk rock and LA-ICP-MS analyses.*

- Hughes, H.S.R., McDonald, I., Upton, B.G.J., Faithfull, J.W. (under review). **Sulphides and precious metals in the lithospheric mantle: A multi-event record of sulphur-bearing magmatism and metasomatism through time (Loch Roag, Scotland).** *Geochimica et Cosmochimica Acta.* ***(Chapter 8).***
  Co-author contributions: *I. McDonald, B.G.J. Upton and J.W. Faithfull were involved in discussions during the writing of this paper. B.G.J. Upton provided xenolith specimens for study. I. McDonald supervised bulk rock and LA-ICP-MS analyses.*

- Hughes, H.S.R., McDonald, I., Faithfull, J.W., Upton, B.G.J. (under review). **Cobalt and precious metals in sulphides of peridotite xenoliths and inferences concerning their distribution according to geodynamic environment: A case study from the Scottish lithospheric mantle.** *Lithos.* ***(Chapter 9).***
  Co-author contributions: *I. McDonald, B.G.J. Upton and J.W. Faithfull were involved in*

discussions during the writing of this paper. B.G.J. Upton and J.W. Faithfull provided xenolith specimens for study. I. McDonald supervised bulk rock and LA-ICP-MS analyses.

- Hughes, H.S.R., McDonald, I., Kerr, A.C. (accepted). **Platinum-group element signatures in the North Atlantic Igneous Province: Implications for mantle controls on metal budgets during continental breakup.** *Lithos.* ***(Chapter 10).***
  Co-author contributions: *I. McDonald and A.C. Kerr were involved in discussions during the writing of this paper. A.C. Kerr provided bulk rock major and trace element geochemistry from his thesis (although some samples were re-analysed to check comparability of analytical techniques). Isle of Mull and Morvern lava samples are from A.C. Kerr's PhD thesis collection and were therefore crushed and milled by him during his PhD. All Skye, Rum and Ardnamurchan lava samples were collected as part of H.S.R. Hughes's PhD. I. McDonald supervised bulk rock and LA-ICP-MS analyses.*

- Hughes, H.S.R., Boyce, A.J., McDonald, I., Davidheiser-Kroll, B., Holwell, D.A., McDonald, A., Oldroyd, A. (accepted). **Contrasting mechanisms for crustal sulphur contamination of mafic magma: evidence from dyke and sill complexes from the British Palaeogene Igneous Province.** *Journal of the Geological Society, London.* ***(Chapter 11).***
  Co-author contributions: *A.J. Boyce, I.McDonald, B. Davidheiser-Kroll and D.A. Holwell were involved in discussions during the writing of this paper. A. McDonald and A. Oldroyd advised on bulk rock sulphur extraction methodology. I. McDonald supervised bulk rock analyses at Cardiff, and A. McDonald supervised S-isotopic analyses at SUERC.*

- Hughes, H.S.R., McDonald, I., Boyce, A.J., Holwell, D.A., Kerr, A.C. (under review). **Sulphide sinking in magma conduits: evidence from mafic-ultramafic plugs on Rum, North Atlantic Igneous Province.** *Journal of Petrology.* ***(Chapter 12).***
  Co-author contributions: *I. McDonald, A.J. Boyce, D.A. Holwell and A.C. Kerr were involved in discussions during the writing of this paper. I. McDonald supervised bulk rock and LA-ICP-MS analyses.*

ABSTRACT

A temporal and spatial relationship between plume magmatism, cratonic lithosphere and the occurrences of orthomagmatic Ni-Cu and platinum-group element (PGE) sulphide mineralisation has been documented in the literature. However the underlying causes for this correlation have yet to be resolved – is there an inherent feature of the cratonic lithosphere and its mantle 'keel' that controls mineralisation? Or is this correlation purely a preservational bias in the geological record?

Scotland has experienced multiple tectono-magmatic events and provides an ideal testing ground, or 'framework', in which to assess the role of lithospheric mantle on chalcophile element (Ni and Cu) and precious metal (PGE and Au) abundances through time. Given the well-documented geological history of the region (including several suites of mantle xenoliths), coupled with exploration campaigns in Greenland (with which Scotland has comparable geology), this thesis aims to assess the contributions and influences of lithospheric mantle vs. asthenospheric mantle during melting and mineralisation. It also evaluates the Ni-Cu-PGE mineralisation potential for Scotland, particularly in a Noril'sk-type conduit-hosted setting within the British Palaeogene Igneous Province (BPIP).

The earliest major tectono-magmatic event following cratonisation of the North Atlantic Craton (NAC) occurred c. 2.4 Ga during Palaeoproterozoic extension, forming the mafic-ultramafic Scourie Dyke Swarm. Despite evidence for lithospheric mantle melting at this time, the subcontinental lithospheric mantle (SCLM) below the Scottish portion of the NAC did not become severely depleted in sulphides or PGE. Instead, spinel lherzolite mantle xenoliths from this region (e.g., Loch Roag) record an influx of carbonatite-associated sulphides at this time, enriched in PGE, and providing a deeper indication of continental extension that may be correlated to carbonatitic intrusions in Greenland. Subsequent collision and orogenesis of the NAC in the late Palaeoproterozoic (c. 1.9 to 1.7 Ga) represents a second significant tectono-magmatic event, recorded in the Scottish SCLM as sulphide (re-)melting and formation of discrete Pt-sulphide minerals (cooperite). Hence the lithospheric mantle here became appreciably enriched in precious metals during the Palaeoproterozoic, but crucially this preserved multiple co-existing populations of sulphides, distinct in their petrographic setting and geochemistry.

Cratonic basement and associated mantle lithosphere are absent in the southern terranes of Scotland. This provides a direct comparison between lithospheric mantle geochemistry for Archaean-Palaeoproterozoic terranes north of the Great Glen Fault vs. Palaeozoic terranes south of the Great Glen Fault. Rifting of Rodinia and opening of the Iapetus Ocean in the late Neoproterozoic thus marks a significant change in geodynamic setting. This is especially apparent in the concentration of cobalt in lithospheric mantle sulphides, which appears to be inherently linked with the formation and/or later destruction (subduction) of oceanic crust during the Grampian event of the Caledonian orogeny.

The impingement of the proto-Icelandic mantle plume initiated in the Palaeogene at the base of the NAC lithospheric mantle keel of Scotland and Greenland. The earliest Palaeogene magmas are enriched in Pt (i.e., have a high Pt/Pd ratio), whilst subsequent magmas

associated with the opening of the Atlantic Ocean have successively lower Pt/Pd ratios. High Pt/Pd ratios are therefore coincident with magmas that have intruded through cratonic lithosphere. The SCLM at the margin of this region is known to be Pt-enriched (with cooperite) and therefore the changing Pt/Pd ratio of North Atlantic Igneous Province magmas suggests a fundamental interaction between the mantle plume and pre-enriched SCLM. Thus, whilst the concentration of metals, particularly Ni and Cu, is largely based on the high degree of asthenospheric mantle melting associated with the plume itself, the ratio of precious metals, such as Pt/Pd, can be strongly influenced by SCLM geochemistry.

Overall, the intricate subtleties of metasomatic signatures recorded by mantle xenolith sulphides (or populations of sulphides) could allow for metallogenic 'mapping' of the upper mantle. This may identify areas of geochemical and mineralogical 'preconditioning', and together with geophysical constraints such as major lithospheric lineaments, it may be possible to establish the craton-specific fertility of a region.

Finally, in order for orthomagmatic sulphide mineralisation to occur, magmas must achieve sulphur saturation in the upper crust, forming an immiscible sulphide liquid and thereby collecting PGE and chalcophile elements, possibly to economic grades. Thus a crucial part of assessing the mineralisation potential of a region must entail an investigation into the causes and locations of S-saturation. Given that crustal sulphur contamination is a common trigger for magmatic S-saturation, this thesis establishes the first S-isotopic ($\delta^{34}S$) framework for western Scotland in order to identify areas of sulphur contamination in the BPIP. In Scotland, the most readily available and S-rich rocks occur in the Mesozoic Hebrides Basin. Sulphur contamination of BPIP rocks is widespread and both S-saturation and S-undersaturation can be observed, suggesting that the region may be extremely fertile for orthomagmatic Ni-Cu-PGE mineralisation. By reconstructing the Hebrides Basin stratigraphy we can assess locations of contamination, even if these are above the current level of exposure (and since removed by erosion), and in some situations sulphide liquid sinking may be demonstrated, suggesting further possibilities for mineralisation present 'up-stream' in magmatic conduits. In conclusion, the Scottish BPIP represents a new exploration frontier not yet identified by industry for orthomagmatic Ni-Cu-PGE mineralisation.

The conclusions are based on approximately 500 rock samples from across Scotland, which have been analysed for major elements and over thirty trace elements (including PGE) and S-isotopes. All data are available on an accompanying CD.

CONTENTS

Chapter 1 – Introduction **1**

Chapter 2 – Platinum-group elements as commodities **5**

Chapter 3 – Orthomagmatic Ni-Cu-PGE sulphide mineralisation and geochemistry **10**

3.1. Magmatic sulphide deposit types 11

3.1.1. Ni-Cu dominated mineralisation 11

3.1.2. PGE-dominated mineralisation 11

3.2. Stages of formation of magmatic sulphide deposits 12

3.2.1. Sulphur solubility in silicate magmas and sulphide immiscibility 13

3.2.2. Partial melting in the mantle 15

3.2.3. The chemical partitioning of PGE 18

3.2.4. PGE and sulphides in the mantle 19

3.2.5. The physical state of PGE in magmas 22

3.2.6. Source fertilisation 23

3.2.7. The 'R factor' 23

3.2.8. Sulphide droplets, settling, and coalescence 25

3.2.9. Sulphide upgrading via new magma input 26

3.2.10. Cooling and crystallisation of a sulphide liquid – PGE partitioning behaviour 29

3.3. Orthomagmatic sulphide deposit models 31

3.3.1. The Bushveld Complex (an open system layered intrusion deposit model) 31

3.3.2. The Skaergaard Intrusion (a closed system layered intrusion deposit model) 33

3.3.3. Noril'sk-type sulphide mineralisation (conduit-hosted orthomagmatic sulphides deposit model) 35

Chapter 4 – A review of PGE mineralisation in the British Isles and North Atlantic Igneous Province **38**

4.1. Platinum-group mineral occurrences in the British Isles 39

4.1.1. PGE in the Scourie Dykes 41

4.1.2. PGE in the British Palaeogene Igneous Province 42

4.1.2.1. Scotland 42

4.1.2.2. Northern Ireland and the northern Republic of Ireland 42
4.2. PGE in the wider Palaeogene North Atlantic Igneous Province 46
4.2.1. PGE in NAIP basalts 46
4.2.2. PGE in east Greenland intrusions 46

Chapter 5 – Publications and the layout of Chapters 6 to 12 ..... **53**

Chapter 6 – Enriched lithospheric mantle keel below the Scottish margin of the North Atlantic Craton: evidence from the Palaeoproterozoic Scourie Dyke Swarm and mantle xenoliths **56**
Abstract 57
6.1. Introduction 58
6.2. Regional geology 59
6.2.1. Geology of the Scourie Dyke Swarm and previous work 61
6.2.2. The Loch Roag mantle xenolith locality 64
6.3. Sampling and analytical methods 65
6.4. Scourie Dyke geochemistry 66
6.4.1. Major elements 66
6.4.2. Trace elements 68
6.5. Mantle xenolith petrology and geochemistry 76
6.6. Re-Os isotopes 77
6.7. Discussion 81
6.7.1. Dyke composition in relation to Lewisian terrane 81
6.7.2. Mantle melting regime – evidence of crustal contamination or SCLM melting? 82
6.7.2.1. Dolerite dykes 82
6.7.2.2. Picrite and olivine gabbro dykes 84
6.7.3. Degree of partial melting and crystal fractionation – chalcophile element evidence 87
6.7.4. Summary of mantle sources, melting and modelling 89
6.7.5. Th-Nb-Ta-Ti and Zr-Hf anomalies – a relict Archaean subduction or metasomatic signature? 93
6.7.6. Lewisian SCLM geochemistry: evidence of melting mechanism – plume or no plume? 95
6.8. Conclusions 96

Chapter 7 – Trace element abundances in the shallow lithospheric mantle of the North Atlantic Craton margin: Implications for melting and metasomatism beneath northern Scotland **98**

Abstract 99

7.1. Introduction 100

7.1.1. Overview of the North Atlantic Craton – formation, amalgamation and xenolith localities 101

7.1.2. The Scottish portion of the North Atlantic Craton and neighbouring terranes 103

7.1.2.1. Loch Roag, Isle of Lewis (Hebridean Terrane) 106

7.1.2.2. Rinibar, South Ronaldsey, Orkney Isles (Northern Highland Terrane, NE) 107

7.1.2.3. Streap Com'laidh, near Glenfinnan (Northern Highland Terrane, SW) 107

7.2. Analytical techniques and methodology 110

7.2.1. Petrography and mineral chemistry analysis 110

7.2.2. Whole-rock sample preparation and analysis 111

7.3. Results 115

7.3.1. Petrography and accessory mineralogy 115

7.3.2. Whole-rock element abundances 119

7.3.2.1. Calculated normative mineral abundances 119

7.3.2.2. Major elements 119

7.3.2.3. Trace elements 120

7.3.3. Clinopyroxene compositions 126

7.4. Discussion 130

7.4.1. Terrane-scale variation in the NW Scottish lithospheric mantle 131

7.4.2. Rare earth elements and the fertility of the sub-Lewisian lithosphere 133

7.4.3. 'Primary' vs. 'metasomatic' signatures in the SCLM 134

7.5. Conclusions 138

Chapter 8 – Sulphides and precious metals in the lithospheric mantle: A multi-event record of Sulphur-bearing magmatism and metasomatism through time (Loch Roag, Scotland) ... **140**

Abstract 141

8.1. Introduction 142

8.1.1. Geological setting 143

8.1.2. Host rock for the spinel peridotite xenoliths 145

8.2. Analytical techniques and methodology 145

8.2.1. Whole-rock sample preparation and analysis 145

8.2.2. Petrography and mineral chemistry analysis 146

8.3. Results 147

8.3.1. Bulk PGE and chalcophile element geochemistry 147

8.3.2. Sulphide mineralogy and textures 152

8.3.3. Sulphide compositions 157

8.4. Discussion 164

8.4.1. Sulphide populations in the subcontinental lithospheric mantle 164

8.4.1.1. Group 3 sulphides ('droplets') 164

8.4.1.2. Group 2 sulphides ('spongy') 165

8.4.1.3. Group 1 sulphides ('complex') 166

8.4.2. Implications for bulk rock precious metal geochemistry 168

8.4.3. The complexity of sulphur in the SCLM – a record of S-bearing events as a 'box model' 171

8.4. Conclusions 174

Chapter 9 – Cobalt and precious metals in sulphides of peridotite xenoliths and influences concerning their distribution according to geodynamic environment: A case study from the Scottish lithospheric mantle 175

Abstract 176

9.1. Introduction 177

9.1.1. An overview of Scottish geology 178

9.1.1.1. Scottish terranes 178

9.1.1.2. Mantle xenoliths 182

9.2. Analytical techniques and methodology 182

9.2.1. Whole-rock sample preparation and analysis 184

9.2.2. Petrography and mineral chemistry analysis 184

9.3. Results 185

9.3.1. Xenolith preservation and alteration 185

9.3.2. Whole-rock element abundances 186

9.3.2.1. Major elements and Ni, Cu and Co 186

9.3.2.2. Platinum-group elements and gold 187

9.3.3. Sulphide petrography and mineralogy 188

9.3.4. Sulphide compositions 201

9.3.4.1. Major element compositions of sulphides – Fe, Ni, Cu and Co 201

9.3.4.2. Platinum-group elements..... 202
9.3.4.3. Other trace elements in sulphides..... 206
9.4. Terrane-scale trends in sulphide petrography and precious metals 207
9.4.1. Sulphide mineral abundance and 'populations' 207
9.4.2. Sulphide-carbonate associations 209
9.4.3. Changes in Pt/Pd ratio 210
9.5. Cobalt and the Great Glen Fault – a major lithospheric lineament distinction 211
9.6. Conclusions 217

Chapter 10 – Platinum-group element signatures in the North Atlantic Igneous Province: Implications for mantle controls on metal budgets during continental break-up..... **219**
Abstract 220
10.1. Introduction 221
10.2. Geology and formation of the North Atlantic Igneous Province (NAIP) 222
10.2.1. The Hebridean portion of the BPIP 226
10.3. Analytical methods..... 229
10.4. Geochemistry of NAIP and BPIP volcanics 232
10.4.1. Major elements and petrography..... 232
10.4.2. Chalcophile elements..... 232
10.4.3. Platinum-group elements and Au 233
10.5. Discussion..... 242
10.6. The S-saturation status for BPIP and NAIP lavas – regional mineralisation potential . 244
10.7. Pt/Pd ratio of NAIP magmas throughout continental break-up 246
10.8. Conclusions 256

Chapter 11 – Contrasting mechanisms for crustal sulphur contamination of mafic magma: evidence from dyke and sill complexes from the British Palaeogene Igneous Province..... **259**
Abstract 260
11.1. Introduction 261
11.2. Geology of the Hebridean portion of the British Palaeogene Igneous Province (BPIP) 262
11.2.1. Palaeogene geology of the Isle of Skye..... 263
11.2.1.1. The Trotternish Sill Complex, northern Skye 263
11.2.1.2. Dykes from the Robustan – Kirkibost area of the Strathaird Peninsula, southern Skye..... 266

11.3. Stratigraphy of the Hebrides Basin and potential for crustal S contamination 266
11.4. Methodology 267
11.4.1. Sampling strategy 267
11.4.2. Whole-rock geochemistry 271
11.4.3. Sulphur isotope analyses 271
11.4.4. Whole-rock sulphur concentration analysis 272
11.5. Results of $\delta^{34}S$ and S determinations 273
11.5.1. Trotternish Sill Complex 273
11.5.2. Robustan basalt dyke swarm 273
11.5.3. Sedimentary and contaminant country rock units 275
11.6. Discussion 277
11.6.1. What is the value of the local mantle S-isotope signature in the BPIP? 277
11.6.2. Crustal sulphur contamination in dykes from southern Skye 279
11.6.3. Contrasting S-isotope signatures of sills and dykes on Skye 280
11.6.3.1. The role of emplacement mechanism on the crustal contamination signature 282
11.6.4. Crustal sulphur sources and contamination potential for Hebridean Scotland and the BPIP 287
11.6.5. Implications for Ni-Cu-PGE orthomagmatic sulphide mineralisation 289
11.7. Conclusions 291

Chapter 12 – Sulphide sinking in magma conduits: evidence from mafic-ultramafic plugs on Rum, North Atlantic Igneous Province 294
Abstract 295
12.1. Introduction 296
12.2. Regional geological setting 297
12.2.1. Geology of the Isle of Rum 298
12.2.2. Ultramafic plugs of the Isle of Rum 299
12.2.2.1. Field relations and structural setting 299
12.2.2.2. Mineral compositions and relation to layered intrusions 302
12.2.3. The Hebridean sedimentary succession and country rocks to the Rum plugs 302
12.2.3.1. S-isotope signatures in western Scotland 302
12.2.4. Magmatic sulphide mineralisation and S contamination in the NAIP 303
12.3. Methodology 305
12.3.1. Bulk rock analysis 305

12.3.2. Mineralogy and mineral composition methodology 306
12.4. Results 306
12.4.1. Whole-rock geochemistry 306
12.4.1.1. Platinum-group elements 307
12.4.2. Sulphide mineralogy and trace element compositions 307
12.4.3. S-isotopic compositions and S/Se ratios of the Rum plugs 319
12.5. Discussion 324
12.5.1. Magmatic context of the Rum plugs vs. the Rum Central Complex 324
12.5.1.1. Feeders and magma staging chamber for the plugs and Rum Layered Suite 325
12.5.2. The origin of sulphides within the Rum plugs 326
12.5.3. Potential crustal S sources for West and Loch Sgaorishal plugs (plugs 1 and 2) 328
12.5.4. Dynamic conduit modelling and sulphide sinking 330
12.5.4.1. Hademard-Rybczinski conduit modelling 330
12.5.4.2. N-factor modelling: silicate/sulphide liquid ratios 337
12.5.4.3. Sulphide tenor calculations 338
12.6. Conclusions 340

Chapter 13 – Synthesis **343**
13.1. Cratonisation and 'preconditioning' of the lithospheric mantle 344
13.2. The effects of lithospheric mantle 'preconditioning' on plume-related magmatism in the Palaeogene and regional-scale 'prospectivity' of the Scottish portion of the British Palaeogene Igneous Province 355
13.3. Final statement 358

Reference list **360**

Appendix A (relating to Chapter 6) **401**
Appendix B (relating to Chapter 8) **414**
Appendix C (relating to Chapter 9) **416**
Appendix D (relating to Chapter 10) **419**
Appendix E (relating to Chapter 11) **421**
Appendix F (relating to Chapter 12) **430**

Contents list of supplementary tables on accompanying CD **434**

LIST OF FIGURES

Figure 2.1. – Prices for Pt and Pd 8

Figure 3.1. – Stages of formation for a magmatic sulphide deposit 13

Figure 3.2. – Schematic plot for SCSS of a magma mixing model 14

Figure 3.3. – Variations of S, MgO, Ni, Cu and Pt + Pd concentrations in silicate magma during mantle melting 17

Figure 3.4. – The physical state of mantle sulphides over a range of P-T conditions 21

Figure 3.5. – R-factor diagram 24

Figure 3.6. – Cu and PGE concentrations as a function of R-factor 28

Figure 3.7. – Schematic timeline for the cooling of sulphide liquid 30

Figure 3.8. – Simplified phase diagrams for cooling Fe-Ni-S and Fe-Cu-S systems 31

Figure 4.1. – Principle PGE occurrences in the British Isles 40

Figure 4.2. – Simplified Palaeogene geology of the NAIP 48

Figure 6.1. – Simplified map of NW Scotland 59

Figure 6.2. – Major element plots (bulk rock) for the Scourie Dykes 67

Figure 6.3. – Multi-element normalised diagrams (bulk rock) for the Scourie Dykes 73

Figure 6.4. – Bivariant trace element plots (bulk rock) for the Scourie Dykes 74

Figure 6.5. – PGE multi-element diagrams (bulk rock) for the Scourie Dykes 75

Figure 6.6. – Multi-element diagrams (bulk rock) for Loch Roag mantle xenoliths 73

Figure 6.7. – Trace element AFC modelling for the Scourie Dykes 86

Figure 6.8. – Trace element binary mixing modelling for the Scourie Dykes 87

Figure 6.9. – Model scenario for formation of Lewisian SCLM and the Scourie Dyke Suite 92

Figure 7.1. – Palaeoproterozoic reconstruction of the North Atlantic Craton 102

Figure 7.2. – Terrane map of Scotland and xenolith localities 105

Figure 7.3. – Hand sample photographs of xenoliths 108

Figure 7.4. – Streap Com'laidh back scattered electron SEM images 116

Figure 7.5. – Rinibar back scattered electron SEM images 117

Figure 7.6. – Loch Roag green clinopyroxenite back scattered electron SEM images 118

Figure 7.7. – Cumulative bar charts of calculated mineral abundances in xenoliths 119

Figure 7.8. – Major element bivariant plots (bulk rock) for xenoliths 121

Figure 7.9. – Minor element bivariant plots (bulk rock) for xenoliths..... 123

Figure 7.10. – Rare earth element multi-element diagrams (bulk rock) for xenoliths and host dykes 124

Figure 7.11. – Trace element multi-element diagrams (bulk rock) for xenoliths and host dykes 125

Figure 7.12. – Multi-element diagrams for clinopyroxene in xenoliths 128

Figure 7.10. – Bivariant trace element diagrams for clinopyroxene in xenoliths..... 129

Figure 8.1. – Terrane map of Scotland showing mantle xenolith localities..... 144

Figure 8.2. – Bulk rock geochemistry of Loch Roag xenoliths 149

Figure 8.3. – PGE multi-element diagrams for Loch Roag xenoliths and host dyke 150

Figure 8.4. – PGE bivariant plots for Loch Roag xenoliths 151

Figure 8.5. – Example of xenolith sulphide mineral mapping in a spinel lherzolite slice 153

Figure 8.6. – Back scattered electron SEM images of Loch Roag sulphides (including Groups 1 and 2) 154

Figure 8.7. – Back scattered electron SEM images of Loch Roag sulphides (including Group 3 with cooperite)..... 155

Figure 8.8. – Total PGE + Au + Re vs. major elements for sulphide minerals in Loch Roag xenoliths..... 161

Figure 8.9. – PGE multi-element diagrams for sulphide minerals in Loch Roag xenoliths 162

Figure 8.10. – Bivariant trace element plots for sulphide minerals in Loch Roag xenoliths 163

Figure 8.11. – Mass balance calculations for bulk rock PGE vs. sulphide populations..... 169

Figure 9.1. – Terrane map of Scotland and the North Atlantic Craton showing mantle xenolith localities 181

Figure 9.2. – Bulk rock geochemistry for Scottish mantle xenoliths 192

Figure 9.3. – Bulk rock PGE multi-element diagrams for Scottish mantle xenoliths 193

Figure 9.4. – Bulk rock bivariant diagrams for Scottish mantle xenoliths (Cu, PGE and Au) 194

Figure 9.5. – Classification categories for sulphide petrography and textures in xenoliths..... 196

Figure 9.6. – Rinibar xenolith back scattered electron SEM images of sulphides 197

Figure 9.7. – Streap Com'laidh xenolith back scattered electron SEM images of sulphides.... 198

Figure 9.8. – Colonsay xenolith back scattered electron SEM images of sulphides 199

Figure 9.9. – Coire na Ba xenolith back scattered electron SEM images of sulphides 200

Figure 9.10. – Sulphide chalcophile element bivariant plots..... 203

Figure 9.11. – Sulphide PGE multi-element diagrams per xenolith suite 204

Figure 9.12. – Sulphide trace element bivariant plots..... 205

Figure 9.13. – Sulphide trace element bivariant plots and Co/metal ratios..... 213

Figure 9.14. – Schematic model showing the lithospheric mantle below Scotland and Co enrichment..... 216

Figure 10.1. – Simplified Palaeogene geology of the NAIP..... 223

Figure 10.2. – Geology of the Hebridean portion of the BPIP 224

Figure 10.3. – Simplified timeline of the lava sequences in phases 1 and 2 of the formation of the NAIP 226

Figure 10.4. – Bivariant plots of major elements for BPIP and NAIP lavas..... 231

Figure 10.5. – Bivariant plots of chalcophile elements for BPIP and NAIP lavas 234

Figure 10.6. – PGE multi-element diagrams for BPIP and NAIP lavas 235

Figure 10.7. – Bivariant plots of PGE for BPIP and NAIP lavas..... 236

Figure 10.8. – Bivariant plots of Pt/Pd ratio vs. various trace element ratios for BPIP and NAIP lavas 237

Figure 10.9. – Bivariant plots of PGE and chalcophile elements for BPIP and NAIP lavas..... 240

Figure 10.10. – Cu/Pd ratio plots for BPIP and NAIP lavas 241

Figure 10.11. – Pd/Ir ratio plots for BPIP and NAIP lavas 242

Figure 10.12. – Pt vs. Pd bivariant plots for BPIP and NAIP lavas..... 249

Figure 10.13. – Cratonic block reconstruction for the North Atlantic..... 255

Figure 11.1. – Simplified geological map of part of the BPIP..... 264

Figure 11.2. – Cross-section of the Strathaird Peninsula..... 265

Figure 11.3. – Annotated field photographs from the Trotternish Peninsula..... 269

Figure 11.4. – Sulphur isotope results for the Isle of Skye 274

Figure 11.5. – Sulphur isotope results and bulk rock PGE and Cu concentrations for the Strathaird dykes 275

Figure 11.6. – Sulphur isotope results for Jurassic and Torridonian sedimentary samples 276

Figure 11.7. – Simple binary mixing model between mantle melt and sedimentary contaminants 278

Figure 11.8. – Intrusion models for sulphur contamination (sills vs. dykes) 286

Figure 12.1. – Simplified geological map of the Isle of Rum and Small Isles 299

Figure 12.2. – Geology of three areas of the Isle of Rum 301

Figure 12.3. – Bulk rock PGE multi-element diagrams for Rum peridotite plugs 311

Figure 12.4. – Back scattered electron SEM images of sulphides in Rum peridotite plugs 314

Figure 12.5. – Bivariant diagrams for Rum plug sulphides 318

Figure 12.6. – PGE multi-element diagrams for Rum plug sulphides (plugs 1 and 2 only) 320

Figure 12.7. – PGE multi-element diagrams for Rum plug sulphides (plugs 4 to 12) 321

Figure 12.8. – S-isotopic composition vs. S/Se ratio for Rum plugs and Eastern Layered Series 322

Figure 12.9. – Dynamic conduit modelling for sulphide settling 331

Figure 12.10. – Cartoon cross-section models of crustal sulphur contamination in NW Rum. 334

Figure 12.11. – Calculated PGE tenor of sulphides vs. measured PGE abundance 339

Figure 13.1. – Overview geological model for the Archaean and Palaeoproterozoic 351

Figure 13.2. – Overview geological model for the Neoproterozoic 352

Figure 13.3. – Overview geological model for the Caledonian Orogeny 353

Figure 13.4. – Overview geological model for Permo-Carboniferous extension 354

Figure 13.5. – Overview geological model for the Palaeogene 359

LIST OF TABLES

Table 2.1. – Platinum-group metal prices (February 2015) 7

Table 3.1. – Partition coefficients for Ni, Cu and PGE between sulphide liquid and silicate magma 18

Table 3.2. – Partition coefficients for Ni, Cu and PGE between MSS and sulphide liquid 21

Table 4.1. – Overview of published material for PGM and PGE in the BPIP 44

Table 4.2. – Overview of published material for PGM and PGE in the NAIP basalts 49

Table 4.3. – Overview of published material for PGM and PGE in the NAIP intrusions 51

Table 6.1. – Scourie Dyke major and trace element bulk rock compositions 70

Table 6.2. – Loch Roag mantle xenolith major and trace element bulk rock compositions 79

Table 6.3. – Re-Os isotopic compositions of Scourie Dykes and Loch Roag mantle xenoliths ... 80

Table 6.4. – Parameters required for melting, mixing, contamination and fractional crystallisation modelling 85

Table 7.1. – Overview of published material for Scottish xenolith localities 109

Table 7.2. – Bulk rock major and trace element geochemistry of Scottish xenoliths 112

Table 7.3. – Summary of clinopyroxene compositions in Scottish xenoliths 127

Table 8.1. – Loch Roag spinel lherzolite and clinopyroxenite xenolith bulk rock compositions 148

Table 8.2. – Sulphide compositions from Loch Roag xenoliths 159

Table 9.1. – Overview of xenolith suites 183

Table 9.2. – Bulk rock geochemistry for xenoliths and host dykes 189

Table 10.1. – Bulk rock PGE and Au compositions for BPIP lavas 230

Table 11.1. – Summary of sulphur isotopic composition for sedimentary rocks from western Scotland 270

Table 12.1. – Bulk rock major and trace element compositions for the Rum volcanic plugs .. 308

Table 12.2. – Sulphide mineralogy, textures and sizes in the Rum plugs 312

Table 12.3. – Representative selection of sulphide compositions from the Rum plugs 316

Table 12.4. – Calculated sulphide metal tenors 323

ABBREVIATIONS

AFC	assimilation during fractional crystallisation
BPIP	British Palaeogene Igneous Province
BSE	back scattered electron
ELS	Eastern Layered Series
GGF	Great Glen Fault
HFSE	high field strength elements
HREE	heavy rare earth elements
ICP-MS	inductively coupled plasma mass spectrometry
ICP-OES	inductively coupled plasma optical emission spectroscopy
IPGE	iridium-group platinum-group elements
ISS	intermediate solid solution
LA-ICP-MS	laser ablation inductively coupled plasma mass spectrometry
LGC	Lewisian Gneiss Complex
LILE	large ion lithophile elements
LREE	light rare earth elements
MREE	middle rare earth elements
MSS	monosulphide solid solution
NAC	North Atlantic Craton
NAIP	North Atlantic Igneous Province
PGE	platinum-group elements
PPGE	palladium-group platinum-group elements
REE	rare earth elements
SCLM	subcontinental lithospheric mantle
SCSS	sulphur content at sulphur saturation
SEM	scanning electron microscope
TTG	tonalite trondhjemite granodiorite

CHAPTER 1

Introduction

A strong correlation exists between plume magmatism, ancient cratonic lithosphere, and magmatic sulphide Ni-Cu and platinum-group element (PGE) deposits (Maier & Groves, 2011), with mineralisation typically located within or proximal to Archaean cratons. The largest known examples of primary magmatic PGE-dominated mineralisation occur in Late Archaean to Palaeoproterozoic intrusions, and fewer examples of intrusions containing significant PGE resources appear to be younger, although some notable exceptions such as the Skaergaard Intrusion in east Greenland exist (Groves *et al*., 1987; De Wit & Thiart, 2005; Groves *et al*., 2005; Maier, 2005; Begg *et al*., 2010; Goldfarb *et al*., 2010). This temporal control may reflect the higher geothermal gradient on the Archaean Earth (e.g., Richter, 1988; Korenaga, 2008; Davies, 2009; Herzberg *et al*., 2010) facilitating higher degrees of partial mantle melting and giving rise to magmas with higher MgO, Cr, Ni, and PGE concentrations (e.g., Maier, 2005; Maier & Groves, 2011 and references therein). But this oversimplification between age and metallogenesis is based on an empirical dataset, itself dependent on the preservation potential of individual deposits and an exploration bias (see Groves & Bierlein, 2007 and references therein; Maier & Groves, 2011).

A more reasonable exploration criterion may therefore disregard the age of the intrusion itself, but instead focus on the age of the lithosphere into which the intrusion became emplaced. At a crustal level, the occurrence of mafic or ultramafic magmatism through Archaean or Palaeoproterozoic gneiss terranes (within a craton, but particularly along craton margins) may be prospective for PGE mineralisation (e.g., Lightfoot, 2007; Maier & Groves, 2011). Further, the location of Ni-Cu-PGE mineralisation may be related to the architecture of subcontinental lithospheric mantle (e.g., Groves & Bierlein, 2007; Begg *et al*., 2010).

With this in mind, it is imperative to assess the relative contributions made by plume magmatism vs. the subcontinental lithospheric mantle (SCLM) in order to determine the underlying controls required for producing PGE-rich magmas – a crucial initial stage in forming Ni-Cu-PGE mineralisation (see Chapter 3). It could be that the apparent relationship between Archaean cratons and PGE mineralised intrusions reflects an inherent metallogenic 'fingerprint' of this ancient crust and its underlying SCLM (De Wit & Thiart, 2005) making those areas of old metasomatised lithospheric mantle more enriched in elements such as PGE. Hence, partial melts derived from the SCLM, or deeper mantle melts which geochemically interacted with the SCLM during ascent, may have a higher propensity for PGE mineralisation. Once this is established, debate over the physical constraints that SCLM may impose on magma ascent may help to resolve the empirical spatial and temporal relationships between

Ni-Cu-PGE mineralised systems and ancient (Archaean-Palaeoproterozoic) lithospheric cratonic boundaries (e.g., Kerrich *et al*., 2005; Begg *et al.*, 2010).

A highly desirable combination of plume-related mafic–ultramafic igneous systems and Archaean cratons, underlain by their associated SCLM keel, occurs within the North Atlantic Igneous Province (NAIP). Significant mineralisation has been discovered in the western portion of the NAIP (see Chapter 4). Therefore, the British Palaeogene Igneous Province (BPIP) is potentially the most prospective PGE province in western Europe (Andersen *et al*., 2002).

This thesis focuses on western Scotland, particularly the Scottish sectors of the BPIP and how these relate to the North Atlantic Craton (NAC). Isolated platinum-group mineral occurrences have been documented in BPIP intrusions on the Isles of Rum, Mull and Skye (Table 4.1) but with limited assessment of their relationship to the province as a whole. To evaluate the geochemical inputs of asthenospheric (plume) and lithospheric mantle 'reservoirs', a temporal and spatial evaluation of PGE abundance across the region must be adopted. In short, two key questions have been identified, around which the thesis is centred:

1) Does the SCLM contribute metals to ascending asthenosphere-derived magmas during large igneous province formation?

2) What is the potential for conduit-hosted orthomagmatic Ni-Cu-PGE mineralisation in the Scottish BPIP?

Due to the temporal aspect of question (1) the Palaeoproterozoic mafic–ultramafic Scourie Dyke Swarm, several suites of mantle xenoliths from across Scotland, and Palaeogene lavas and magma conduits are assessed geochemically (and sequentially) in the following chapters. Sampling and analysis combines bulk rock major and trace element analyses (including NiS fire assay for PGE), mineral-specific major and trace element analyses by scanning electron microscope (SEM) and laser ablation inductively coupled mass spectrometry (LA-ICP-MS) in sulphide and silicate minerals. This allows an assessment of temporal, macroscopic and microscopic processes within the SCLM and the magmas that have interacted with it. These are considered to exercise the main controls on Ni-Cu-PGE abundance in the region, providing broad-scale insights for future exploration based on the idea of 'craton-specific exploration'. In particular, sulphide petrography, coupled with *in situ* sulphide compositional analysis (by LA-ICP-MS) has revealed a temporal and spatial 'map' of the lithospheric mantle under Scotland. With regards to question (2), bulk and *in situ* S-isotopic analyses ($\delta^{34}S$), measured by conventional and laser combustion methodologies for crustal country rocks and BPIP igneous

lithologies, have built a framework of sulphur contamination signatures and the behaviour of sulphide liquids in different conduit systems. This is suitable for identifying locations of S-saturation in the magmatic plumbing system, and begins to vector towards areas of possible sulphide accumulation and mineralisation.

Throughout this investigation, approximately 500 new surface rock samples were collected from across western Scotland (Loch Lomond to Durness) during fieldwork by the author that was carried out individually or alongside co-workers. Additionally, a sub-selection of BPIP lava samples from the Isle of Mull (collected during Andrew Kerr's PhD thesis) were re-analysed. Archived and catalogued Scottish mantle xenolith samples from the British Geological Survey (Murchison House, Edinburgh; originally collected by Brian Upton) and the Hunterian Museum (University of Glasgow) were also analysed by bulk and *in situ* methods. A further limited selection of specialised samples from the personal collections of Brian Upton (University of Edinburgh) and John Faithfull (Hunterian Museum) were also used during this investigation.

All bulk rock geochemical and S-isotopic data analysed during this study (alongside all duplicates, blanks and rock standards) have been collated into a specially designed Microsoft Access database, available on the accompanying CD (instructions for database operation are also provided on this disk). Each sample (new and loaned) has been entered into the database with accompanying geographical coordinates (Ordinance Survey British National Grid), location name, lithological details, age relationships, and sample collection and analyses dates. Data can be directly exported from the database, including geographical coordinates, allowing for efficient use in a Geographical Information System (e.g., ArcGIS) and statistical or geochemical plotting software.

CHAPTER 2

Platinum-group elements as commodities

The industrial and non-industrial uses of PGE are reviewed in the British Geological Survey Commodity Summary (2009), the EU Commission Raw Materials Supply Group Report (2010) and Gunn (2014). Principal end-use markets for platinum-group metals are:

- Autocatalysts – where Pt, Pd and Rh are coated onto a honeycomb substrate (usually alumina) of the exhaust system and act to reduce CO, un-combusted hydrocarbons and nitrogen oxide levels in exhaust fumes.
- Jewellery – Pt is alloyed with Au, Pd, Ru, Rh and Ir for constituent parts and decorative uses.
- Electronics and electrics – Pt and Pd-based components are used in multi-layer ceramic capacitors, circuitry and data storage applications.
- Catalysts – Pt-based catalysts are also used widely in the petrochemical industry, alongside Pd and Ir for hydrocracking and petroleum refining.
- Glass – platinum-group metals are used in glass-making equipment.
- Investment – Pt is also used as a store of wealth for investment purposes (as ingots or exchange traded fund products), and since the global credit crisis in 2008, Pd has also been used for the same purpose.
- Magnet technology – Ru is employed in perpendicular magnetic recording technology (hard disk manufacture) as well as flat screen technology.
- New technologies and renewable energy technology – for example, Pt is used in third generation fuel cells to catalyse the oxidation state of hydrogen and generate power for electric motors. Demand for Pt in fuel cells is predicted to increase markedly in the future as this technology becomes more widespread. Ru and Re are increasingly used with Ni-superalloys in turbine blades and other air travel applications.
- Medicine – PGE are widely used in medical applications, including dental alloys, electrodes in pacemakers and defibrillators, as well as anti-cancer drugs, such as cis-platin.

PGE are sold in various forms, ranging from pure metals to various compounds and solutions, and are refined and produced by a select group of companies (e.g., Johnson Matthey and BASF). Almost 90% of global platinum-group metal reserves are located in South Africa, which supplies 77% of global platinum production (according to the EU Minerals Report in 2010). In

the EU, the main sources of platinum-group metals are South Africa (60%) and the Russian Federation (> 30%), with the remainder coming from Zimbabwe, the USA, and as by-products (normally from Cu, Ni and/or Au production) from EU countries (notably Finland and Poland) and Canada. Platinum-group metals are only extracted as by-products of other metal ores (usually Ni, Cu and Au) in Russia and Canada. Conversely, deposits are mined specifically for platinum-group metals (as primary ores) in South Africa (Bushveld Complex), Zimbabwe (Great Dyke), Canada (Lac des Iles) and the USA (Stillwater). When PGE are extracted (either as primary ore or as by-products) they are processed and recovered together as a suite of elements (coupled production), such that the supply of Rh, Ru, Ir and Os depends on the demand and mining of Pt and Pd (alongside Ni).

Despite high recycling rates of platinum-group metals (> 90% recovery of material and a closed loop lifecycle – i.e., metals retain their physical/chemical/conductive properties) recycling cannot sustain growing demands, spurred by a growing global population, demand in developing nations and emerging new technologies. These factors have ensured that the Pt and Pd prices have risen steadily since 2000. Table 2.1 gives the most recent platinum-group metal prices (February 2015), Figure 2.1 displays the price of Pt and Pd from 2000 to 2015, and a review of global platinum supply and demands is given in the World Platinum Investment Council Quarterly Report (www.platinuminvestment.com). Periodic spikes in prices such as the dramatic rises in the Pd price in 2000-2001 (reflecting fears over supply from Russia) and Pt in 2008 (due to the energy crisis in South Africa affecting mining operations), and the fall in prices accompanying the global financial crisis in late 2008, produce short term fluctuations on the rising trend. While Pt prices have stabilised at around $1200 oz-1, Pd prices are at recent historic high (see Table 2.1) reflecting worries over future supplies from Russia.

Table 2.1. Platinum group metal prices (2nd February 2015). Data from www.platinum.matthey.com.

Metal	US$ per troy oz
Platinum	1235
Palladium	776
Rhodium	1180
Iridium	570
Ruthenium	56

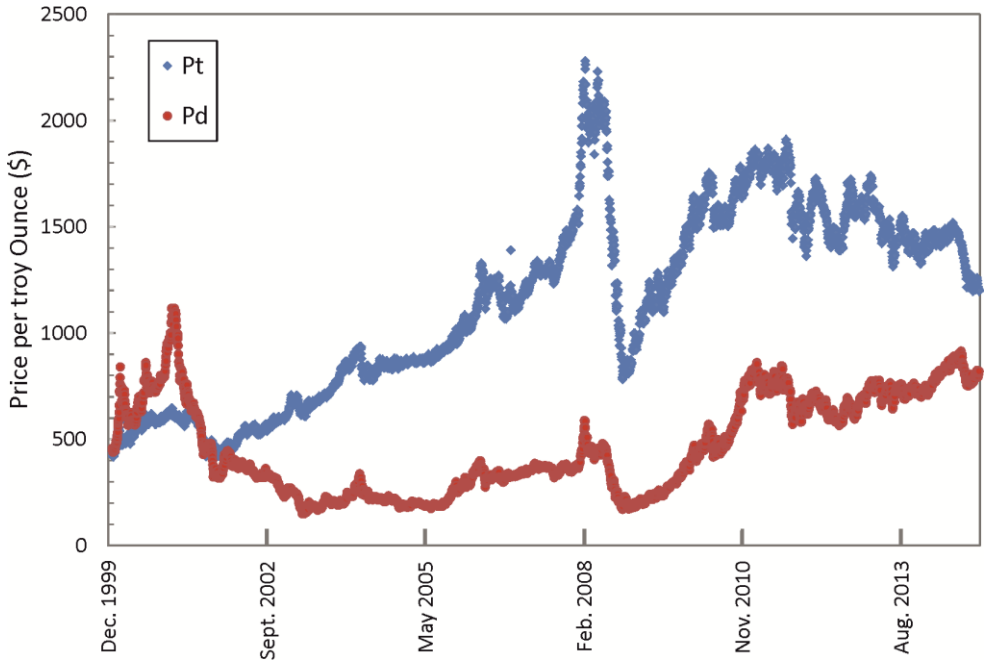

Figure 2.1. Prices of Pt and Pd since December 1999 until January 2015. Data from Johnson Matthey.

Coupled with the rise in Pt and Pd prices, there are growing concerns over security of supply (outside of South Africa and Russia) and this has led to renewed interest in several deposits previously thought uneconomic, as well as encouraging exploration for PGE on a global scale. For example, Greenland and Finland have been at the forefront of 'greenfield' exploration campaigns, led by both major mining and junior exploration companies. There is currently increasing socioeconomic strain on the mining industries of South Africa (e.g., co-ordinated miner strikes over wage disputes from September 2012 until June 2014), political pressures on export tax (e.g., 6.5% on all platinum-group metals in Russia) and enforced majority shares on mines in Zimbabwe and sanctions on ore refining (such that ore produced in Zimbabwe must be beneficiated there and not shipped as concentrate for smelting and refining in South Africa). All of these factors combine so that identifying PGE mineralisation and resources outside of these countries has become a strategic imperative.

The average price for Pt over the last 20 years has been more than double that of Pd. Although the differential has shrunk recently (see Fig. 2.1), the higher price for Pt has resulted in exploration companies favouring Pt-rich orebodies. However the geological controls on Pt/Pd ratio are poorly understood. As already outlined in Chapter 1, few large deposits worldwide have Pt enriched above Pd (Pt/Pd ratio > 1) and notable examples where this is the case tend to be restricted to layered intrusions within Archaean cratons such as the Bushveld Complex

and the Great Dyke of Zimbabwe. However, these intrusions can be compartmentalised metallogenically. The PGE deposits in the Bushveld Complex that lie south of the Thabazimbi-Murchison Lineament (e.g., the Merensky and UG2 Reefs) are Pt-dominant, while all of the deposits north of the lineament have Pt/Pd around unity or lower (McDonald & Holwell, 2011; Naldrett, 2011). Whether this reflects magma evolution, contrasting amounts of sulphide in the orebodies (e.g., Maier *et al*., 2008) or a deeper lithospheric mantle control on the Pt/Pd ratio of the feeder magmas either side of the lineament (McDonald *et al*., 2009) is not fully understood.

A more detailed understanding of these controls and the spatial link between intrusion-hosted PGE deposits and Archaean cratons will feed into regional exploration models and improve discovery rates for PGE. These questions are addressed in later chapters of this thesis.

CHAPTER 3

Orthomagmatic Ni-Cu-PGE sulphide mineralisation and geochemistry

3.1. Magmatic sulphide deposit types

Orthomagmatic sulphide deposits can be divided into two types – those where Ni and Cu dominate the sulphide mineral assemblage as the most valuable metal commodities; and those where the PGE predominate and base metals are subsidiary. Different deposit classes can be assessed in terms of their (Pt + Pd)/(Ni+Cu) metal ratios, such that Ni-Cu dominated ores have low ratios (typically < 0.5), while PGE dominated ores have high ratios (often 10-30, but occasionally >100). Beyond this, each orthomagmatic sulphide mineralisation type can be further subdivided into deposit types based on parameters such as petrology, lithogeochemistry, morphology, mineralogical associations, and physical constraints for mineralised zones (i.e., stratiform reefs or conduit-hosted sulphides) – see Naldrett (2004, 2011).

3.1.1. Ni-Cu dominated mineralisation

This group of deposits are typically hosted by komatiites, flood basalts, or conduit-hosted ferropicritic, noritic and anorthositic rocks. Parental magmas have high MgO contents and deposits are generally rich in sulphide (20-90% sulphides; Naldrett, 2011). Such deposits have a broad temporal distribution, varying from the Late Archaean to Mesozoic. Worldwide examples of Ni-Cu deposits include the komatiite-hosted greenstone belt deposits at Kambalda (Western Australia), flood basalts at Noril'sk (Siberia, Russia), ferropicrite-hosted deposits at Pechenga (Kola Peninsula, NW Russia), the troctolite-anorthosite-granite sill-hosted deposits of Voisey's Bay (Labrador, Canada), and the meteorite impact-related melanorite and pyroxenite-hosted deposit at Sudbury (Ontario, Canada).

3.1.2. PGE-dominated mineralisation

PGE-dominated deposits are chiefly found in association with large mafic or ultramafic layered intrusions and typically show evidence of multiple phases of magmatism, with two or more magma types present within the intrusive system; e.g., an early MgO- and SiO_2-rich magma, and a later Al_2O_3-rich tholeiitic magma (Naldrett, 2011). PGE-dominated deposits generally have significantly lower sulphide contents (0.5-5%) and form stratabound ore bodies, both as stratiform mineralisation horizons ('reefs' – i.e., a rock layer with distinctive texture and mineralogy; Naldrett, 2004) and non-stratiform mineralisation. In contrast to Ni-Cu sulphide mineralisation, PGE-dominated ores are temporally more restricted, and predominantly a feature of the Late Archaean or Palaeoproterozoic (with the notable exception of the Palaeogene Skaergaard Intrusion in east Greenland). But the relative lack of reef-hosted PGE deposits places little statistical value on this temporal distribution pattern.

Examples of PGE-dominated deposits include the intracratonic layered mafic intrusion of the Bushveld Complex (South Africa), the Great Dyke (Zimbabwe), the Stella Complex (Kraaipan greenstone belt, South Africa), the Stillwater Complex (Montana, USA), and the Palaeogene tholeiitic rift-related layered intrusion of the Skaergaard Intrusion (east Greenland). Although PGE-dominated, the calc-alkaline mafic intrusive rocks of the Lac des Iles deposit (Ontario, Canada) and the ultramafic cumulate deposit at Sakatti (Lapland, northern Finland) are not strictly stratabound (Naldrett, 2004 and references therein).

The Bushveld Complex, Skeargaard Complex and Noril'sk conduit-hosted mineralisation are presented as deposit case studies in Section 3.3.

3.2. Stages of formation of magmatic sulphide deposits

The stages and fundamental processes controlling orthomagmatic sulphide mineralisation are outlined in Naldrett (2004) and (2011) and can be subdivided into seven key formational stages (as outlined in Figure 3.1):

1. Partial melting of the mantle and the distribution of chalcophile elements between the mantle source and resultant magmas.
2. Magma ascent into the lithosphere.
3. Sulphur solubility in silicate magma and the timing of S-saturation. Factors include the degree of partial melting that took place in the mantle source region, the availability of sulphur (sulphides) in the source, and the formation of an immiscible sulphide liquid, which is itself dependent on the silicate magma oxidation state, Fe content, pressure, temperature and subsequent fractional crystallisation. Formation of immiscible sulphide liquid results in chalcophile element partitioning from the silicate magma into the sulphide liquid.
4. Ascent of magma (possibly entraining sulphide liquid) to higher crustal levels.
5. Concentration and collection of sulphide liquid droplets to form a potentially economic mineralised zone.
6. Enrichment of sulphide deposits through the interaction of sulphide liquids with new magma batches.
7. Processes during sulphide cooling, including crystallisation of the sulphide liquid to various mineral phases and the effect this may have on the redistribution of Ni, Cu, and PGE.

A broad overview of these factors is covered in this chapter.

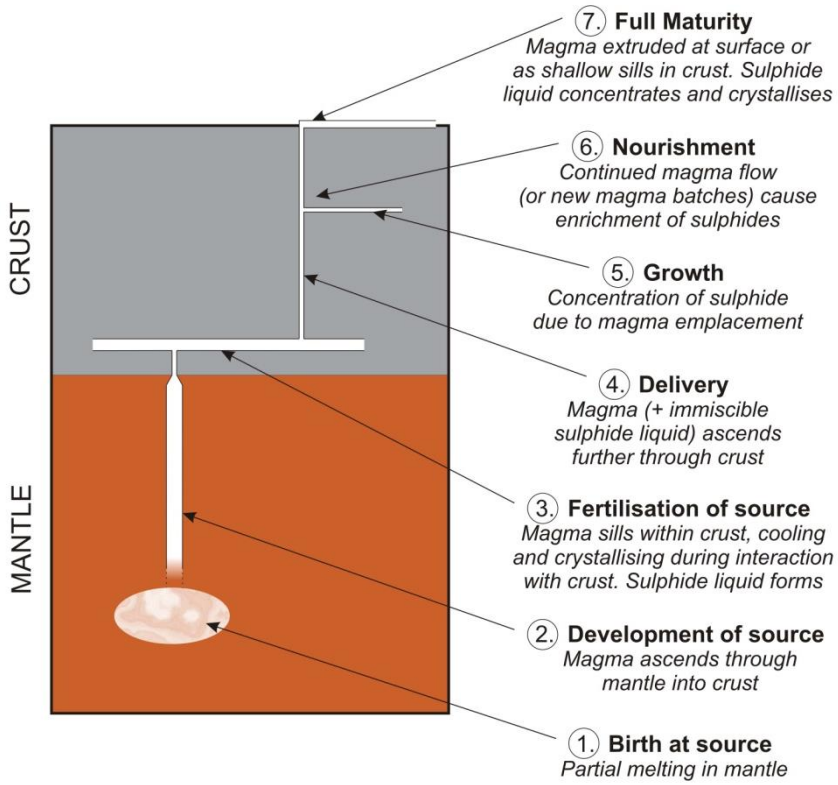

Figure 3.1. Stages of formation for a magmatic sulphide deposit (including both Ni- and PGE-dominated ores). Schematic diagram not to scale. Adapted from Naldrett (2011).

3.2.1. Sulphur solubility in silicate magmas and sulphide immiscibility

The solubility of sulphur in a mafic or ultramafic magma is generally discussed in terms of 'sulphur content at sulphide saturation' (SCSS) – Shima & Naldrett (1975). Principal factors effecting sulphide saturation include pressure, temperature, FeO + TiO_2 concentrations in the magma, oxidation state of the magma, and 'maficity' of the magma (Naldrett, 2004). For example, the sulphur capacity (and therefore SCSS) of a melt increases with decreasing pressure, increasing temperature (Haughton *et al.*, 1974; Shima & Naldrett, 1975), and decreasing fO_2 (Haughton *et al.*, 1974). Under conditions of higher oxygen fugacity (fO_2) sulphur dissolves as SO_2, whereas in lower fO_2 conditions sulphur dissolves in its reduced state of S^{2-}. Sulphur solubility increases with decreasing pressure, thus as a melt ascends adiabatically from a mantle source region, through the crust, the magma will have an increasing capacity to carry more S (Mavrogenes & O'Neill, 1999). Therefore S-saturation may

not be reached purely through changes in the ambient P-T conditions and may instead require some additional mechanism for the melt to reach SCSS, such as significant fractional crystallisation, magma mixing or addition of S through the assimilation of crustal rocks.

For example, S-saturation may be achieved by mixing two magmas – one mafic or ultramafic, and a more felsic magma (perhaps evolved from a main central mafic melt at the marginal zones of an intrusion during crustal ponding). Alternatively, magma injections interacting with partially melted roof rocks might also trigger S-saturation (e.g., Kinnaird *et al.,* 2002). A magma-mixing model could cause a shift in composition into the chromite-only phase volume of a crystallising sequence (thereby forming a chromite cumulate) and trigger sulphide immiscibility (e.g., Irvine, 1975; Naldrett *et al.*, 2011). Even in the absence of chromitite formation, the mixing of basaltic and felsic magmas has been found to be an effective mechanism for the induction of S-saturation, as displayed in Figure 3.2 (Li & Ripley, 2005).

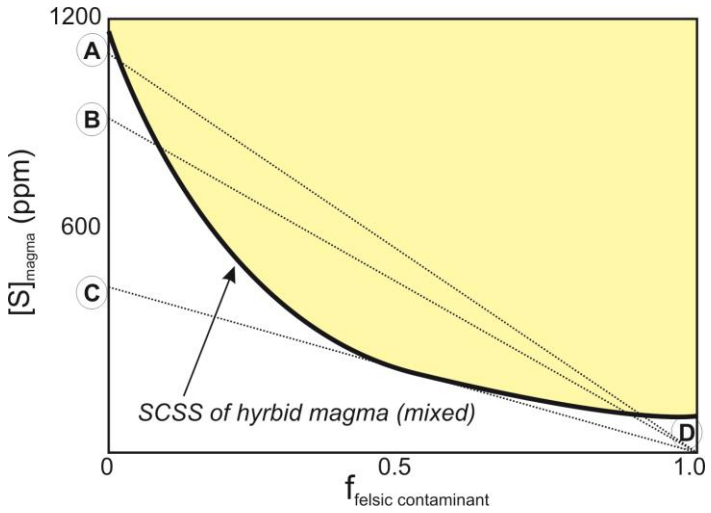

Figure 3.2. Schematic plot for SCSS of a magma mixing model (mafic tholeiitic basalt contaminated by felsic granitic melt). Points A, B, and C are the starting sulphur concentrations in various tholeiite basalts (before mixing) and point D is the starting sulphur concentration of the contaminating granitic melt (also before mixing). 'felsic contaminant' is the proportion of granitic melt present within the system. The yellow shaded area delineates the field in which immiscible sulphide will form. Adapted from Naldrett (2011), after Li and Ripley (2005).

Sources of crustal and/or magmatic sulphur can be traced by stable isotopic ratios, such as $\delta^{34}S$ (mass-dependent fractionation) or $\Delta^{33}S$ (mass-independent fractionation), to understand ore genesis and the processes triggering S-saturation in igneous systems. Due to the chemical fractionation of different sulphur isotopes in various geologic environments, sulphur derived

from a mantle magmatic environment has $\delta^{34}S$ of 0 ± 4 ‰, depending on the oxidation state of the magma (Ohmoto & Rye, 1979). In contrast, sulphur derived from various crustal reservoirs (e.g., evaporites or mudrocks) develops a broader range of both positive and negative $\delta^{34}S$ anomalies (e.g., Seal, 2006). Sulphur isotopes ($\delta^{34}S$) have been used towards terrane and basement discrimination in northern Britain (e.g., Lowry *et al.,* 2005). Lowry *et al.* (2005) also demonstrated that contamination by upper crustal sediments and/or cratonic basement was widespread for Scottish Caledonian sulphide (Pb, Zn, Mo, Au) mineralisation. $\delta^{34}S$ variation is a mass-dependent process and arises from bacterial reduction of seawater sulphate in the contemporaneous diagenetic marine environment (Ohmoto & Goldhaber, 1997). While $\delta^{34}S$ is a crucial means of deciphering crustal contamination in magmas, this can only identify contamination by rocks younger than the great oxidation event in the Mesoproterozoic (cf. Parnell *et al.,* 2010).

Recent advances in mass spectroscopy have allowed for greater precision in isotopic analysis, advancing the use and interpretation of mass-independent fractionation (MIF) isotopic signatures, such as those shown by $\Delta^{33}S$ (where $\Delta^{33}S = \delta^{33}S - 0.515 * \delta^{34}S$) (Hiebert & Bekker, 2010). Photochemical reactions of SO_2 gas in the Earth's Archaean atmosphere resulted in MIF of S-isotopes, as shown by large-magnitude shifts in $\Delta^{33}S$ (Farquhar *et al.*, 2001) prior to 2.5 Ga. If S-isotope MIF is present in magmatic sulphides it indicates the assimilation or contamination of crustal material during the formation of sulphide immiscible liquids and mineralisation. In combination with $\Delta^{36}S$ and Fe isotopic proxies, $\Delta^{33}S$ can also be used to 'fingerprint' sulphur sources from Archaean crust. For example, $\Delta^{33}S$ has been successfully used to identify wall-rock sulphur interaction (controlled by back-diffusion of fluids from magma into the footwall country rocks) in the Platreef (Northern Limb of the Bushveld Complex) not evident in the more traditional use of $\delta^{34}S$ (Penniston-Dorland *et al.*, 2008; Sharman *et al.,* 2013).

3.2.2. Partial melting in the mantle

The SCSS of a magma is a function of the degree of partial mantle melting at source (amongst other factors). During mantle melting, some of the first mineral phases to melt are sulphides, alongside garnet and clinopyroxene (and later incorporating spinel and olivine – see Pearson 2005 and references therein). Thus, with increasing degrees of partial melting (expressed as the melt fraction, F) the amount of sulphur in the melt (in wt.%) increases until no sulphides remain in the mantle source region. Complications to this model may be added depending on

whether an equilibrium batch melting, fractional melting, continuous melting, or dynamic melting model is assumed. However, it has been calculated (assuming a starting S concentration of 200 ppm, or 550 ppm sulphide, in an equilibrium batch melting system; Palme & O'Neill, 2004) that by F = 13.5 %, all sulphides present in the source will have been completely dissolved in the silicate magma (Li & Ripley, 2009; Naldrett, 2011). Beyond this point, continued melting leads to dilution of S concentration in silicate magma (as shown in Figure 3.3). This is in contrast to the concentration of MgO, which continues to increase with increasing F due to the continued melting of clinopyroxene, orthopyroxene, and eventually olivine and spinel. This peak in S concentration (vs. percentage partial melting) has repercussions for the concentrations of chalcophile elements such as Ni, Cu and PGE in silicate magmas and residual mantle (see discussion in Section 3.3.2).

Ni partitions into a number of silicate phases (particularly olivine) as well as sulphides. In contrast, Cu and PGE partition strongly into sulphide phases rather than silicates, unless Pt and Pd are stabilised as alloys with semimetals such as As, Sb, Te, and Bi forming discrete platinum-group minerals (PGM) (Helmy *et al.*, 2007). LA-ICP-MS studies of mantle sulphides have demonstrated the strong affinity of PGE into sulphide phases (Alard *et al.*, 2000), and experimental and empirical studies have shown that the Nernst partition coefficients of PGE into sulphides are several orders of magnitude greater than that for Ni or Cu (e.g., Peach *et al.*, 1990; Gaetani & Grove, 1997; Fleet *et al.*, 1999; Holzheid & Lodders, 2001; Sattari *et al.*, 2002). Hence it is believed that in order for a mantle-derived partial melt to contain significant quantities of PGE, all the sulphides must be melted from the mantle source region such that PGE-hosting phases are not retained in residual sulphides (Peach *et al.*, 1990).

LA-ICP-MS investigations also highlight the differing partitioning of iridium-group PGE (IPGE) and palladium-group PGE (PPGE) into monosulphide solid solution (MSS) and Cu-Ni-rich sulphide phases (Alard *et al.*, 2000), and along with the presence of PGE in silicate minerals such as spinel and olivine, this adds a complicating factor to the modelling of PGE in partial mantle melts, as discussed further in section 3.3.3.

Assuming that sulphides host the greatest concentrations of PGE, then at melt fractions beyond that of complete sulphide melting (e.g., 13.5 % F), PGE become diluted as silicate magma (contributing little or no PGE budget) is added to the magmatic reservoir (Naldrett, 2011). Similarly Cu becomes diluted beyond this point of sulphide exhaustion. However, the concentration of Ni continues to increase with increasing melt fraction due to the progressive

melting of olivine. The partitioning behaviour of these three metals can therefore be shown on graphically simplified plots such as those of Figure 3.3.

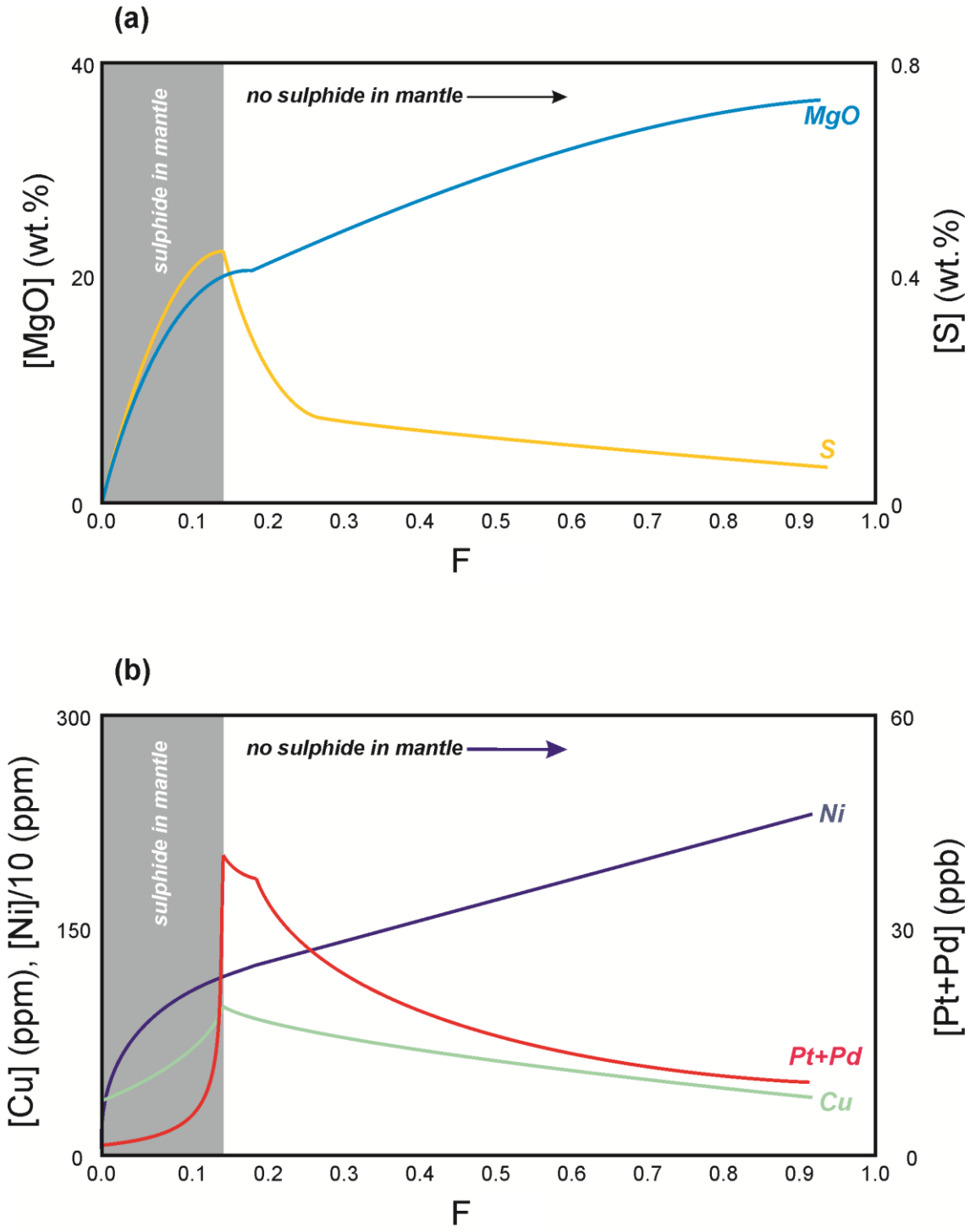

Figure 3.3. a) Diagram showing the variation of S and MgO concentrations in a mantle melt according to F, the fraction of partial melting undergone. b) Diagram showing the variation of Ni, Cu, and Pt+Pd concentrations in the same scenario as (a). Models calculated using the programme pMELTS (Ghiorso *et al.*, 2002) and adapted from Naldrett (2011).

3.2.3. The chemical partitioning of PGE

Nernst partition coefficients are used to quantify the movement or fractionation of trace elements between two phases, whether this is between a melt and residue, a melt and forming crystals, or between two liquids such as a silicate magma and immiscible sulphide liquid.

For the latter situation, the Nernst partition coefficient 'K_D' for metal '*i*' is (Naldrett, 2011):

$$K_{D_i}^{(sulphide/silicate)} = \frac{wt\ \%\ i^{(sulphide)}}{wt\ \%\ i^{(silicate)}}$$

(equation 3.1)

This value, K_{Di}, may be applied for any trace element between any two phases. The cumulative D_i for metal *i* in multiple different phases (1, 2, and 3 for example), each at different proportions in a rock (x), can be applied such that (Wood & Fraser, 1976):

$$D_i = x_1 K_D^1 \cdot\ x_2 K_D^2\ \cdot x_3 K_D^3$$

(equation 3.2)

The partitioning of Ni, Cu, and PGE can be established and used (as in Figure 3.3) to calculate the concentrations of these elements in various liquid and crystal phases. These are given in Table 3.1.

Table 3.1. Partition coefficients for Ni, Cu, and PGE noble metals between sulphide liquids and silicate melts. Source of values referenced given in table.

Trace element	K_D	Empirical/Experimental	*References*
Ni	500	Experimental	*(Mungall & Brenan, 2014)*
	500-900	MORB	*(Peach et al., 1990)*
	410-580	Experimental	*(Gaetani & Grove, 1997)*
	315-424	Experimental	*(Sattari et al., 2002)*
Cu	1470	Experimental	*(Mungall & Brenan, 2014)*
	1383	MORB	*(Peach et al., 1990)*
	230-313	Experimental	*(Gaetani & Grove, 1997)*
	380-1670	Experimental	*(Holzheid & Lodders, 2001)*
Os	740,000	Experimental	*(Mungall & Brenan, 2014)*
	2200-2500	Experimental	*(Fleet et al., 1999)*
	>31,000	Experimental	*(Sattari et al., 2002)*
Ir	458,000	Experimental	*(Mungall & Brenan, 2014)*
	12,000-16,000	MORB	*(Peach et al., 1990)*
	460,000	UG-2	*(Campbell & Barnes, 1984)*
	160	Lac des Iles	*(Campbell & Barnes, 1984)*
	130,000	Experimental	*(Stone et al., 1990)*
	1800-3500	Experimental	*(Fleet et al., 1999)*
	>50,000	Experimental	*(Sattari et al., 2002)*

Table 3.1 *(Continued)*

Trace element	K_D	Empirical/Experimental	*References*
Ru	415,000	Experimental	*(Mungall & Brenan, 2014)*
	2400-2800	Experimental	*(Fleet et al., 1999)*
	>12,000	Experimental	*(Sattari et al., 2002)*
Rh	205,000	Experimental	*(Mungall & Brenan, 2014)*
	>140,000	Experimental	*(Sattari et al., 2002)*
Pt	317,000	Experimental	*(Mungall & Brenan, 2014)*
	>2400	MORB	*(Peach et al., 1990)*
	490,000	UG-2	*(Campbell & Barnes, 1984)*
	120,000	UG-2	*(Campbell et al., 1983)*
	6450	Merensky	*(Campbell et al., 1983)*
	9100	Experimental	*(Stone et al., 1990)*
	1400-3900	Experimental	*(Fleet et al., 1999)*
	>18,000	Experimental	*(Sattari et al., 2002)*
Pd	190,000	Experimental	*(Mungall & Brenan, 2014)*
	35,000	MORB	*(Peach et al., 1990)*
	310,000	UG-2	*(Campbell et al., 1983)*
	6375	Merensky	*(Campbell et al., 1983)*
	120,000	Lac des Iles	*(Campbell & Barnes, 1984)*
	88,000	Experimental	*(Stone et al., 1990)*
	2900-3400	Experimental	*(Fleet et al., 1999)*
	>92,000	Experimental	*(Sattari et al., 2002)*
Au	1000-10,000	Experimental	*(Mungall & Brenan, 2014)*
	15,000-19,000	MORB	*(Peach et al., 1990)*
	600-900	Experimental	*(Fleet et al., 1999)*
Re	400-800	Experimental	*(Mungall & Brenan, 2014)*

3.2.4. PGE and sulphides in the mantle

Fertile mantle has approximately chondritic proportions of each PGE, but their actual abundance in the mantle is lower by a factor of approximately 100-1000, as demonstrated by mantle-derived peridotite xenoliths (Lorand *et al.*, 1999; Lorand & Alard, 2001; Luguet *et al.*, 2003; Lorand *et al.*, 2008). Primitive magmas derived from mantle partial melting are generally enriched in Pt, Pd, and Rh (PPGE) and depleted in Ir, Os and Ru (IPGE) relative to starting chondritic proportions (Bockrath *et al.*, 2004a), as displayed by positive slopes on chondrite-normalised PGE multi-element diagrams, or higher Pd/Ir or Pt/Ir ratios (e.g., Naldrett & von Gruenewaldt, 1989).

Fractionation of PGE in mantle-derived magmas is caused by the differences in compatibility of IPGE and PPGE in mantle sulphide phases. The IPGE behave as though compatible in silicate and oxide minerals, with olivine, spinel and specifically chromite crystals acting as significant IPGE hosts (Maier *et al.*, 2003b; Pritcher *et al.*, 2009). In part, this is due to these crystals including IPGE-rich PGM, such as laurite which is stable at chromite liquidus temperatures (Brenan & Andrews, 2001), Os-Ir and Ir-Rh metallic alloys, and IPGE semimetal alloys (such as sulpharsenides) (Ahmed & Arai, 2002). However, Rh and Ru in particular have also

experimentally been shown to be compatible into the spinel crystal structure itself (Capobianco & Drake, 1990; Capobianco *et al.*, 1994; Puchtel & Humayun, 2001; Righter *et al.*, 2004; Page *et al.,* 2012; Locmelis *et al.,* 2013). Pt and Ru have both been shown to be mildly compatible in clinopyroxene, but Pd is thought to be incompatible in silicate and oxide minerals (e.g., Hill *et al.*, 2000; Righter *et al.*, 2004). PGE may also be partitioned in a speciated form (e.g., Tredoux *et al.*, 1991; Ballhaus *et al.*, 1994; Tredoux *et al.*, 1995) or behave as nanoclusters (e.g., Helmy *et al.,* 2013b and references therein).

Sulphide phases have been shown to be the dominant hosts of mantle PGE (e.g., Mitchell & Keays, 1981; Burton *et al.*, 1999; Alard *et al.*, 2000; Lorand & Alard, 2001). Fractionation of PGE has been proposed to be due to the coexistence of two mantle sulphide phases (e.g., Burton *et al.*, 1999; Alard *et al.*, 2000; Lorand & Alard, 2001; Luguet *et al.*, 2003; Bockrath *et al.*, 2004a; Lorand *et al.,* 2013 and references therein) – see Figure 3.4. These are crystalline monosulphides enriched in Fe, Ni and IPGE, and immiscible sulphides enriched in Cu, Ni and PPGE (Lorand *et al.,* 2013). The former may be retained in the mantle during partial melting and have a tendency to adhere to silicates, while the immiscible sulphide becomes dispersed and segregated in silicate magma during partial melting (e.g., Bockrath *et al.*, 2004a; Lorand *et al.,* 2013 and references therein). However, the sulphide budget of the mantle may be far more complex, particularly in the lithospheric mantle (see Chapters 8 and 9). For example, the presence of several generations of sulphides in mantle sources has also been demonstrated using Re-Os isotopes in peridotitic xenoliths (Pearson *et al.*, 2002). With partial melting of the mantle, PGE are fractionated between mantle monosulphide and immiscible sulphide liquid and partition coefficients as outlined in Table 3.2 (Ballhaus *et al.*, 2001). Thus the PGE ratios of a mantle-derived melt, such as a basalt, are initially controlled by the extent of PGE partitioning between the residual monosulphide and the immiscible sulphide liquid (Ballhaus *et al.*, 2001), as well as the PGE concentration in these mantle sulphides, and the amount of sulphide which becomes dissolved in silicate magmas and extracted from the mantle.

Table 3.2. Partition coefficients for PGE noble metals between MSS and immiscible sulphide liquid. Range of values experimentally determined and taken from Ballhaus et al. (2001).

PGE	K_D
Ir	3.0-11.3
Ru	3.6-19
Rh	1.5-3.2
Pt	0.02-0.14
Pd	0.06-0.16

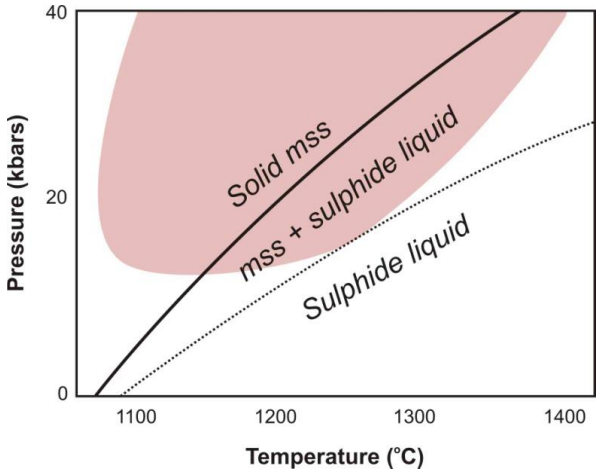

Figure 3.4. The physical state of mantle sulphides over a range of P-T conditions during mantle partial melting. Red shaded area delineates P-T conditions within which most mantle partial melting takes place. Diagram adapted from Bockrath et al. (2004).

The degree of PGE fractionation can be described as a function of magma MgO concentration (as a proxy for silicate magma fractionation) (e.g., Keays, 1982; Keays *et al.*, 1982; Brügmann *et al.*, 1993; Tredoux *et al.*, 1995; Rehkamper *et al.,* 1997, 1999; Maier *et al.*, 2003b). For example basalts tend to have a much higher Pt/Ir or Pd/Ir ratio than komatiites (Tredoux *et al.*, 1995; Rehkamper *et al.,* 1999) because retaining MSS and refractory alloys in the mantle during melting and melt extraction retains IPGE, causing a depletion of Ru, Ir, and Os relative to PPGE in the resultant magma (Bockrath *et al.*, 2004b). The broad observation that lower degrees of melting (with correspondingly lower MgO concentrations) result in a greater divergence from the chondritic proportions of PGE can be expressed as a ratio between PPGE and IPGE, here referred to as the 'PGE fractionation value' (Naldrett, 2011):

$$\boldsymbol{PGE\ fractionation\ value} = \frac{(\boldsymbol{Pd} + \boldsymbol{Pt} + \boldsymbol{Rh})}{(\boldsymbol{Ru} + \boldsymbol{Ir} + \boldsymbol{Os})}$$

(equation 3.3)

Mantle PGE concentrations may be further complicated in the case of previous mantle melting and/or metasomatic events (e.g., Hamlyn *et al.*, 1985; Peach *et al.*, 1990; Alard *et al.*, 2000; Lorand & Alard, 2001; Alard *et al.*, 2002). For example, if an initial period of mantle partial melting (which did not exhaust sulphides in the source region) was followed by a later melting event, PGE could have been pre-enriched in the residual sulphide populations, such that second-stage melting would produce a PGE enriched magma at lower degrees of partial melting than for the first melting stage (e.g., Hamlyn & Keays, 1986).

3.2.5. The physical state of PGE in magmas

The melting behaviour of PGE-bearing minerals and their thermal stabilities must be assessed in order to further understand PGE in magmatic systems. According to Tredoux *et al.* (1995) a model based on the temperature controlled behaviour of certain PGE (specifically their melting temperatures) can allow for these elements to be subdivided into two groups, distinct from the more mainstream groups of IPGE and PPGE. These groups are high-temperature (HTPGE – comprising Ir and Ru) and low-temperature (LTPGE – including Pt, Pd, and Rh). Typically as alloys, HTPGE phases in the mantle are more refractory than LTPGE phases, and thus these may not melt during magma formation and extraction. Instead the unmelted alloys may be included as a whole in silicate melts in a state similar to which they occurred in the mantle source, or as 'micro-xenoliths' (McDonald, 1993). Hence PGE may occur as metallic clusters in a melt (Tredoux *et al.*, 1991; Ballhaus *et al.*, 1994; Capobianco *et al.*, 1994; Tredoux *et al.*, 1995) and not as single atoms or ionic complexes. Clusters may then be stabilised by surface adsorptions onto semimetals (such as As, Sb, and Te), chalcogenides (such as S). If this is the case, the use of partition coefficients would not be suitable in describing the distribution and behaviour of PGE (Tredoux *et al.*, 1995).

In a S-rich environment, PGE clusters may be 'activated' by their semimetal or chalcogenide covering, and therefore be available for scavenging by an immiscible sulphide liquid, coalescing and precipitating to form PGE sulphides, alloys, tellurides, arsenides, or bismuthides (Lindsay, 1989; Tredoux *et al.*, 1995). Any remaining PGE clusters in the cooling sulphide liquid will precipitate with base metal sulphides. Alternatively, in a S-poor environment, clusters will remain in suspension in a silicate melt, until they later coalesce to form alloys (Tredoux *et al.*, 1995). With early coalescence (more likely for Os and Ir-rich clusters) these PGM may provide nucleation centres for early-forming silicate and oxide phases such as olivine and chromite.

3.2.6. Source fertilisation

As magma ascends from the mantle source region, through the crust, the associated decrease in pressure causes the SCSS to increase, so that the magma can dissolve greater amounts of sulphur before sulphur saturation is reached (Mavrogenes & O'Neill, 1999). As a result, without the occurrence of some additional process, left to its own devices a melt is unlikely to reach sulphur saturation, and therefore no Ni-Cu-PGE deposit can be formed. Sulphur saturation can be achieved from prolonged fractional crystallisation (e.g., Platinova Reef of the Skaergaard Intrusion; Andersen *et al.,* 1998 and references therein; Holwell & Keays, 2014 and references therein) but calculations suggest that SCSS is not reached until > 40 % crystallisation (Naldrett, 2011), by which stage the concentration of Ni is markedly reduced due to its incorporation into silicate phases such as olivine.

If a sulphide deposit is to form within a mafic or ultramafic magmatic system, the silicate melt must be 'fertilised' (Naldrett, 2011). This can occur via one of the following mechanisms:

- Mixing of two magmas (mafic and/or ultramafic), both of which must be close to SCSS already. This will form a sparse sulphide deposit.
- A change in pressure associated with the introduction of new magma from depth.
- Contamination of mafic/ultramafic magmas with crustal partial melts.
- Addition of sulphur by assimilation or contamination of S-rich crustal rocks (e.g., Ripley & Li, 2013 and references therein).
- Addition of carbon (as graphite) by assimilation or contamination of crustal C-rich mudrocks (i.e., a redox-controlled S-saturation event; e.g., Turnagain *et al.,* 2012; Tomkins *et al.,* 2012).
- Silica contamination by felsic country rocks. This lowers the solubility of sulphur in a mafic magma (Naldrett *et al.*, 1986b; Li & Naldrett, 1993).
- Increasing magma oxygen fugacity fO_2. This decreases the iron (II) oxide content and in turn the lowers SCSS of a silicate magma (e.g., Buchanan & Nolan, 1979).

3.2.7. The 'R factor'

Once sulphur saturation has been achieved and an immiscible sulphide liquid formed, the ratio of silicate magma to sulphide liquid affects the efficiency of partitioning of Ni, Cu, and PGE into the sulphide phase. This has implications for the volume and grade of any resulting deposit.

To quantify this effect, the mass ratio of silicate melt and sulphide liquid is described as the 'R-factor' (Campbell & Naldrett, 1979):

$$\boldsymbol{R = \frac{m_{silicate}}{m_{sulphide}}}$$

(equation 3.4)

$$\boldsymbol{Y_i = \frac{[D_i X_{oi} R + 1]}{R + D_i}}$$

(equation 3.5)

Where Y_i is the concentration of metal *i* in the sulphide, X_{oi} is the original concentration of metal *i* in the silicate magma, and D_i is the partition coefficient for metal *i* between silicate and sulphide (equation 1).

These equations indicate a large decrease in chalcophile element concentration in silicate magma due to their partitioning into an immiscible sulphide liquid (Figure 3.5).

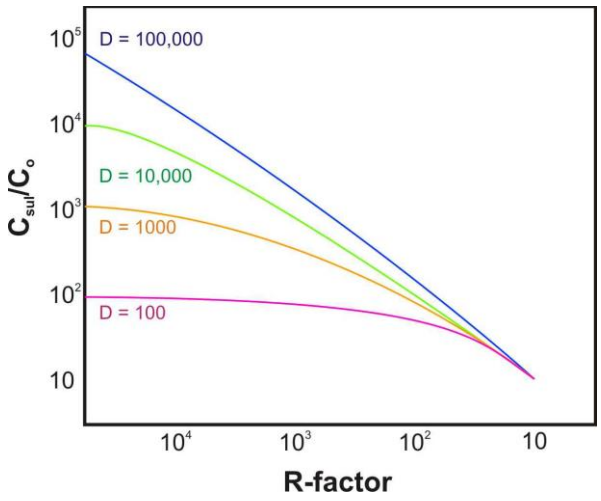

Figure 3.5. The relationship between partition coefficients (D), the mass ratio of sulphide to silicate melt (R-factor) and the degree of enrichment of sulphide liquid compatible trace elements (such as Ni, Cu, and PGE). Diagram adapted from (Robb, 2005). C_{sul} is concentration of element in the sulphide liquid, C_o is initial concentration of element in the total silicate magma reservoir.

The effective R-factor is also a function of the rate at which elements diffuse into the sulphide liquid, along a chemical potential gradient in the surrounding silicate magma (Mungall, 2002). A sulphide droplet displays a zone of influence around itself within the silicate melt. The higher the diffusivity of an element, the greater the effective R-factor. The diffusivities of chalcophile

elements are ranked in the following order: $Cu^{+} > Au^{+} > Ni^{2+} > Pt^{2+}$, Rb^{2+}, Pd^{2+}, Fe^{2+}, $Ir^{2+} > Os^{3+}$, and Ru^{3+} (Mungall, 2002). Diffusivity can also be a function of the silicate melt composition, with more felsic melts enhancing differences in metal diffusivity relative to mafic melts (Mungall, 2002). Overall, the diffusivity effect is not considered of major importance in large deposits, as rapid nucleation of sulphides promotes the establishment of equilibrium throughout the magmatic system, decreasing the diffusivity effect (Naldrett, 2011). In comparison, the rate or effectiveness of circulation of sulphide liquid droplets around a silicate magma body may enhance chalcophile element scavenging (e.g., Naldrett, 2004 and references therein).

3.2.8. Sulphide droplets, settling, and coalescence

In order for a sulphide deposit to be of economic potential, sulphide mineralisation must occur in mineable zones, horizons or 'pockets' for extraction. Therefore it is important to consider mechanisms controlling sulphide droplet entrainment, coalescence and collection in a silicate magma.

Sulphide liquid has a number of distinctive physical properties in comparison to silicate magma. For example, sulphide liquids are significantly denser than silicate liquid (> 5.0 g/cm^3 for NiS and Cu_2S in comparison to 2.7-3.0 g cm^{-3} for silicate magma; Kucharski *et al.*, 1994). As a result, sulphide droplets tend to sink or settle through silicate magma and may be impeded by phenocrysts. The surface tension and viscosity of the host silicate magma will also affect a sulphide droplet's ability to settle due to this density contrast (Naldrett, 2011). Upward transport of sulphide droplets is possible as long as the upward velocity of the silicate magma (for example magma ascent from the mantle to crust) is greater than the sulphide droplet settling rate (de Bremond d'Ars *et al.*, 2001). Sulphide droplets tend not to coalesce during transport (due to a silicate melt rim present around each droplet). Thus, coalescence cannot be considered a significant factor in the concentration of sulphide phases (de Bremond d'Ars *et al.*, 2001).

In a large crystallising magma chamber environment, sulphide settling may be impeded by a silicate and oxide crystal cumulus mush, formed prior to sulphide saturation and collected towards the base of the system (Naldrett, 2011). This may form a barrier to further sulphide settling, so that a sulphide layer forms on top of magmatic cumulates. Alternatively however, sulphide droplets may be able to settle further through this pile, depending on the mineralogy

of the cumulate and the fraction of trapped melt. Wetting behaviour (i.e., the mobility of sulphide liquid within a coexisting crystalline matrix) is quantified by dihedral angle (e.g., in olivine cumulates) which is itself a function of the solid-solid and solid-liquid surface energies (Rose & Brenan, 2001). Experiments reveal that chromitites are relatively permeable to sulphide liquids, and are therefore able to act as channel ways for droplets, as long as there is limited intercumulus silicate melt (Brenan & Rose, 2002). Overall discrete sulphide liquid globules may be impeded from migration through semi-liquid silicates, limiting the sulphide liquids motion into fractures and along silicate grain boundaries (Mungall & Su, 2005). However, the experimental evidence from Mungall & Su (2005) is at odds with observations, for example from the Platreef at Overysel (Northern Limb, Bushveld Complex) where fractionated net textured and massive sulphides have been observed in footwall gneisses, and are thought to have formed by sulphide liquid migration down from the overlying mafic layered intrusion, through partially melted footwall rocks (Holwell & McDonald, 2006).

3.2.9. Sulphide upgrading via new magma input

Upgrading of sulphide liquid may occur via reaction with fresh silicate magma, undepleted in chalcophile elements in a situation analogous to zone refining and described by the N-factor (an open-system equivalent to the R-factor; Naldrett, 2004 and references therein). Chalcophile elements are partitioned from the new magma batch into the pre-existing sulphide liquid. However due to the S-undersaturated state of the new magma batch, S would coevally partially dissolve out of the sulphide liquid and into silicate magma (i.e., self-destructive sulphide system of 'multistage-dissolution upgrading'; Kerr & Leitch, 2005). Due to the greater compatibility of PGE, Se, Ni and Cu into sulphide liquid, Fe may also become slightly re-dissolved into the new magma batch, leaving a sulphide liquid with lower S and Fe concentrations and lower S/Se ratio than if upgrading had never taken place (Kerr & Leitch, 2005). This is particularly important for conduit-hosted orthomagmatic sulphide deposits of Noril'sk and Voisey's Bay (Naldrett *et al.*, 1996; Naldrett *et al.*, 2000).

Calculations for sulphide upgrading can be made using an incremental R-factor ($R_{incremental}$) which is the ratio of new magma to remaining sulphide liquid. For the purposes of calculation, this process continues in a number of steps so that the total $R_{incremental}$ is the sum of all batches of magma that have passed through the system. In this way, the effect of magma interaction can be assessed for Ni, Cu, and PGE. As shown in Figure 3.6, the effect of open system interaction sees an increase in all chalcophile element abundances in sulphide liquid, but is

particularly effective for those elements with exceptionally high partition coefficients, such as the PGE (and especially Pt and Pd).

Sulphide upgrading may also be dependent on certain physical constraints. For example, diffusion rates of S and chalcophile elements would not allow for maximum equilibration rate if the contact between replenishing magma batches and sulphide liquid was 'smooth' (Naldrett, 2011). These conditions could be found in intrusion feeder zones where a narrow conduit allows for this intimate interaction of silicate magma(s) and sulphide liquid (Naldrett, 2011). Instead, more turbulent mixing of sulphide liquids with replenished silicate magma batches would increase the surface area available for chemical equilibration and chalcophile element partitioning (and 'scavenging'), thereby promoting reaction (Naldrett, 2011 and references therein).

It follows that this process should also produce large volumes of PGE-depleted silicate rocks (represented by cumulates or basalts) which crystallised from S-interacted magma. Evidence of such cumulates have been found in some systems including the Main Zone above the Merensky and Bastard reefs of the Bushveld Complex (Maier & Barnes, 1999), Sudbury (Lightfoot, 2007), and at Voisey's Bay (Naldrett, 1997). Basaltic suites such as those of the Nadezhdisnsky and Tuklonsky Formations at Noril'sk also attest to significant depletion of silicate magma which had passed through the PGE-concentrating conduit system (Naldrett *et al.*, 1992; Brügmann *et al.*, 1993; Li *et al.*, 2009; Naldrett *et al.*, 2011).

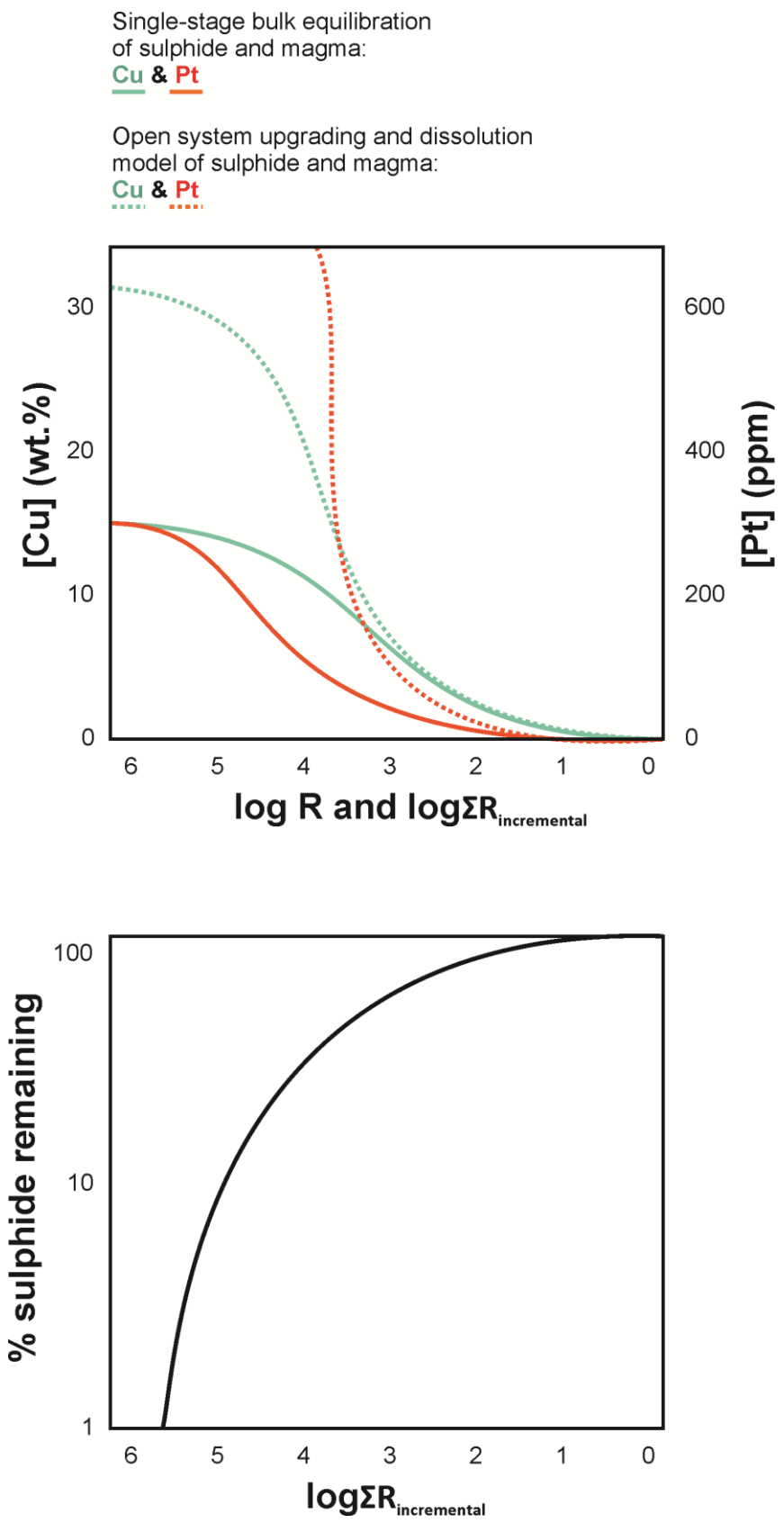

Figure 3.6. Cu and PGE concentration variations of sulphides as a function of R-factor and in comparison to summed $R_{incremental}$ ($\Sigma R_{incremental}$) for the mechanism of sulphide upgrading due to new magma input (Kerr & Leitch, 2005). Diagram adapted from Naldrett (2010).

3.2.10. Cooling and crystallisation of a sulphide liquid – PGE partitioning behaviour

On cooling, a sulphide liquid will at first crystallise a monosulphide solid solution (MSS) – the high temperature equivalent to Ni-rich pyrrhotite (Figure 3.7). Partitioning of chalcophiles will take place between the MSS and remaining sulphide liquid, such that Cu, Pt, Pd and Au become enriched in the sulphide liquid, while Ru, Ir and Os partition into MSS in a S-rich alloy-poor system (Fleet *et al.*, 1993; Barnes *et al.*, 1997; Mungall *et al.*, 2005; Holwell & McDonald, 2010). With further cooling MSS recrystallises as pyrrhotite and pentlandite (with the IPGE remaining in solid solution in these mineral phases; Naldrett, 1989).

Following MSS formation, the concentration of Ni and Cu increases in the residual sulphide liquid. The sulphide liquid may then escape from the MSS, possibly resulting in zonation of sulphide minerals in the resulting orthomagmatic deposit (Naldrett, 2011). For example, the sulphide liquid may penetrate along fractures and grain boundaries in the already-crystallised silicate intrusion or surrounding country rocks, forming a zone of veins surrounding a massive sulphide deposit (itself formed from the MSS). With continued cooling of the Fe-Ni-S system, MSS remains until < 300°C, as shown in Figure 3.8 (Naldrett, 2004). Depending on whether an ore is S-rich or S-poor, determines what minerals will form from the MSS. Sulphur-rich compositions led to the formation of pyrite on cooling, while relatively S-poor compositions cool to form pentlandite. The presence of the MSS between these two end-member minerals prevents their stable coexistence until the temperature of the cooling system drops below 250°C (Figure 3.8). This has implications for the timing of pentlandite formation – the lower the S content of the cooling Fe-Ni-S system, the later the crystallisation of pentlandite at lower temperatures (Naldrett, 2011). Within the Fe-S system various forms of pyrite and pyrrhotite form during cooling (cf. Dare *et al.,* 2010). Lastly, within the Fe-Cu-S system, chalcopyrite is the main phase crystallised from cooling sulphide liquid, following the transitional formation of an ISS (Naldrett, 1989), as shown in Figures 3.7 and 3.8. On further cooling, additional Cu-bearing phases include bornite, chalcocite, covellite, and cubanite.

Overall in a S-rich system, MSS which formed from a cooling immiscible sulphide liquid will be enriched in IPGE and Rh. Recrystallisation products of MSS on further cooling (pyrrhotite and pentlandite) would also be expected to have high concentrations of these elements, present in solid solution. Following initial MSS crystallisation (~ 1000°C) Pt, Pd, and Au remain in the residual Cu-rich sulphide liquid until intermediate solid solution (ISS) crystallises at approximately 900°C (e.g., Fleet *et al.*, 1993; Fleet *et al.*, 1999; Holwell & McDonald, 2010 and references therein). If the original immiscible sulphide melt is enriched in semimetals, PPGE

may become concentrated into a late-stage semimetal rich immiscible liquid, enriched in Te, Bi, As and Sb, exsolving as a discrete bismuthotelluride melt from the re-equilibrating sulphide phases (Helmy *et al.*, 2007). Although semimetals may be present within the magmatic system from source, it is possible that additional semimetals entered the system through the localised contamination of magma via assimilation of Sb- or As-bearing sediments, as identified in the Turfspruit area of the Platreef (Northern Limb, Bushveld; Hutchinson & McDonald, 2008).

With continued cooling of ISS, Pt and Pd are scavenged and combine with semimetals to form discrete PGM, with Au and Ag forming an electrum alloy (Helmy *et al.*, 2007; Holwell & McDonald, 2010). Being some of the last phases to crystallise, these tend to form around the margins of sulphide grains. However, if semimetals are lacking from the sulphide melt, Pt and Pd may instead be present in solid solution in sulphide phases, including low-temperature crystallisation products of MSS (Helmy *et al.*, 2007; Holwell & McDonald, 2010). The incompatibility of PGE in ISS dictates that the final crystallisation product of ISS (chalcopyrite) contains no significant concentration of PGE in solid solution (Holwell & McDonald, 2010). Overall, the abundance of semimetals in magmas and sulphide liquids is an essential factor in determining the mineralogical (and PGM) characteristics of Pt and Pd magmatic sulphide deposits (e.g., Tomkins, 2010; Dare *et al.,* 2011; Helmy *et al.,* 2013a; Prichard *et al.,* 2013a, 2013b).

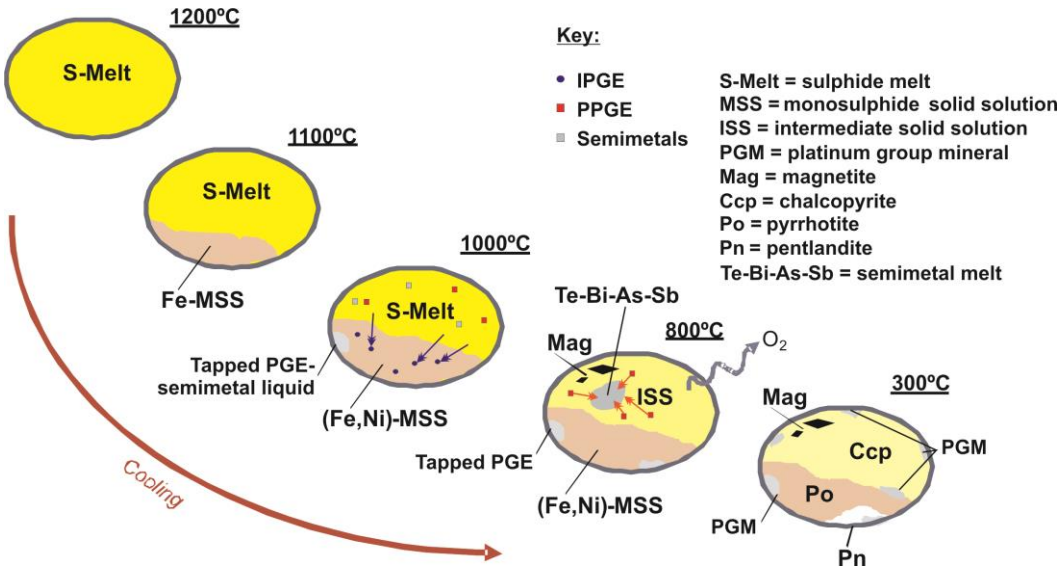

Figure 3.7. Schematic timeline for the cooling and crystallisation of a sulphide liquid to MSS, ISS, a semimetal immiscible phase and low-temperature mineral phases. Diagram adapted from Holwell & McDonald (2010).

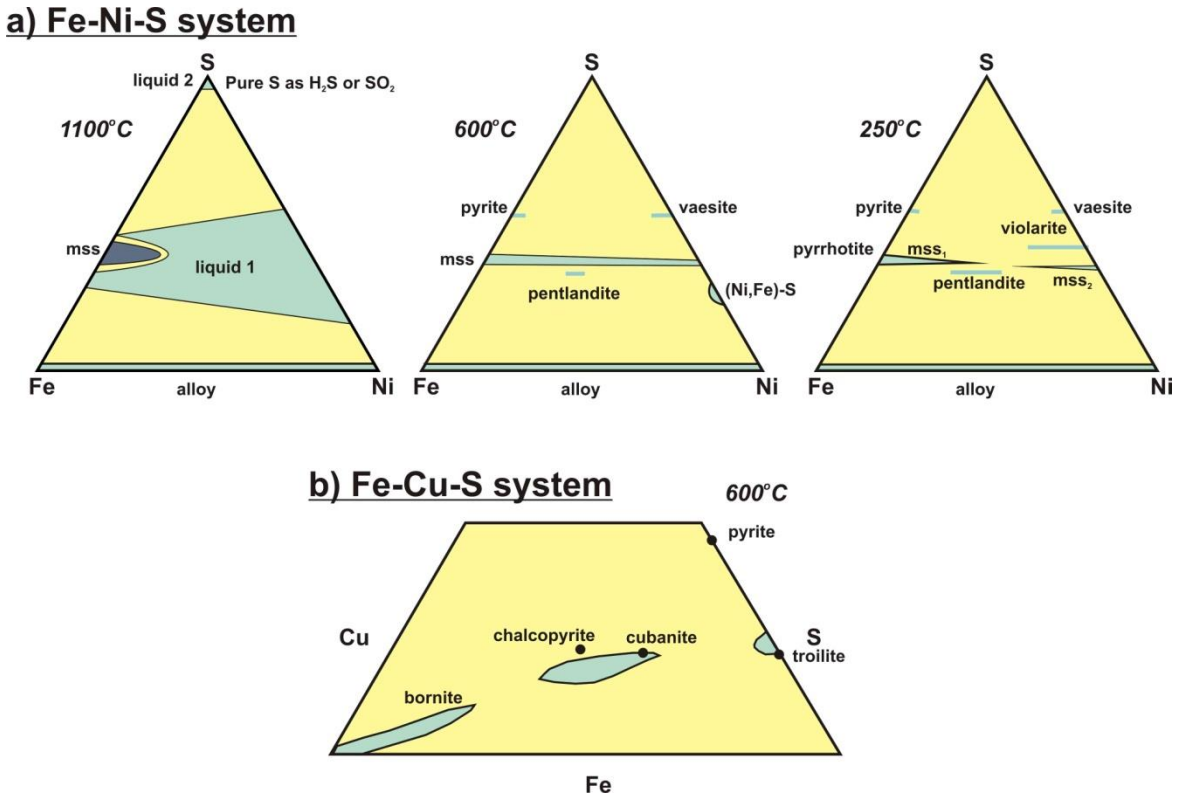

Figure 3.8. Simplified phase diagrams for cooling of the Fe-Ni-S and Fe-Cu-S systems (mms is monosulphide solid solution). Adapted from Naldrett (1989).

3.3. Orthomagmatic sulphide deposit models

3.3.1. The Bushveld Complex (an open system layered intrusion deposit model)

The Bushveld Complex of South Africa is the world's largest known plutonic igneous intrusion, on the order of 1 million km^3 of igneous rocks underlying an area ~ 66,000 km^2, and divided into five main 'limbs': Eastern, Western, Southern, Northern and Far Western. Since the discovery of the Merensky Reef in 1924, the Bushveld Complex has been the largest producer of PGE, currently representing > 80 % of global platinum production (Gunn & Benham, 2009) as well as being a major producer of Ni, Cu, Cr, V, Sn and fluorspar (Cawthorn, 2010). The lower portions of the Bushveld host PGE-dominant mineralisation and platinum is currently mined from three main horizons: the Merensky Reef (in the Eastern and Western Limbs and the type locality of 'Merensky type' mineralisation), UG2 Reef (also in the Eastern and Western Limbs, and representative of 'Chromitite type' mineralisation) and the Platreef (in the Northern Limb, representative of 'Contact type' mineralisation).

The Bushveld Complex was intruded into country rocks of the Transvaal Supergroup (including quartzites, dolomites and argillites) and Archaean granitoids and greenstones. Numerous reviews of the geology and mineralisation of the Bushveld Complex are available, notably in Naldrett (2004), Cawthorn *et al.* (2006), Cawthorn (2010), McDonald & Holwell (2011) and Naldrett *et al.* (2011). Overall, the Bushveld has a bimodal composition, with sub-equal proportions of mafic-ultramafic and felsic rocks. In the lower portions hosting PGE mineralisation (i.e., the Rustenburg Layered Suite) the Bushveld is a layered mafic and ultramafic saucer-shaped intrusion, with layers broadly dipping inwards towards the centre of the intrusion (cf. Webb *et al.,* 2004; Webb *et al,.* 2011). The vertical 'stratigraphy' of the Rustenburg Layered Suite is as follows (bottom to top): Marginal Zone, Lower Zone, Critical Zone, Main Zone and Upper Zone.

Broadly, the Bushveld Complex represents an open magmatic system, with multiple injections of magma batches (of varying geochemical composition) into the main laccolithic deep magma chamber. For the Merensky and chromitite-type mineralised horizons, reefs were probably formed as a direct result of magma replenishment and mixing, resulting in extensive and laterally continuous thin high grade (4-8 g/t Pt+Pd) mineralised layers, with low abundances of base metal sulphide minerals (e.g., Naldrett, 2004 and references therein). These replenishing magmatic injections and subsequent magma mixing triggered changes in fractional crystallisation assemblages now identified as marker horizons in the cumulate pile (e.g., Irvine 1975, 1977). At a microscopic scale, layering may be assessed by mineralogical observations relating to crystal settling and sorting (for example in an analogue model of snowfall vs. rainfall – see Cawthorn *et al.* 2006 and references therein). Crystal settling and sorting may be regulated by the temperature, viscosity and density of the host magmatic system. In comparison, *in situ* crystallisation processes are controlled by nucleation and other thermodynamic parameters. Sudden changes or reversal in mineralogy are coupled with sharp shifts in bulk rock geochemistry (e.g., Mg#), mineral chemistry (e.g., Fo-content in olivine) and isotopic compositions (e.g., $^{87}Sr/^{86}Sr$) – see Cawthorn *et al.* (2006) and references therein.

In comparison, the Contact type mineralisation of the Platreef is an extensive (km-scale) zone of discontinuous PGE mineralisation (1-4 g/t Pt+Pd and therefore lower grade to the Merensky Reef and UG2 – see Gunn & Benham, 2009) associated with disseminated to massive base metal sulphides along basal contact zones of the layered body and can commonly be disrupted, brecciated or heterogeneous (e.g., Kinnaird *et al.,* 2005; Hutchinson & McDonald, 2008; Holwell *et al.,* 2011; McDonald & Holwell, 2011). Localised crustal contamination of

magmas by wall-rock partial melts and sediments (S and C-rich) can be demonstrated in the Platreef (e.g., Buchanan & Rouse, 1984; Barton *et al.,* 1986; Holwell *et al.,* 2007; Penniston-Dorland *et al.,* 2008), exemplifying a major distinction in mineralisation processes here, in comparison to the Merensky and UG2 reefs.

Large-scale complexities pertaining to the formation of layers in an open magmatic system are illustrated by regional magmatic unconformities, and the creation of potholes and gap structures, for example where the Upper Zone transgresses and erodes underlying Main, Lower, and Critical Zones. However an enduring enigma remaining to be solved is how the macroscopic correlation of layering across the Eastern and Western Limbs of the Bushveld (e.g., Lower and Upper Critical Zones, and Main Zone Pyroxenite Marker) relate to the Northern Limb, with its breaks in crystallization (e.g., Holwell & Jordaan, 2006), anomalous Troctolite Marker and different Pt/Pd and Au/PGE budgets (cf. Maier & Barnes, 2010). The Northern Limb is situated on the northern side of the Thabazimbi-Murchison lineament (a deep lineament probably extending to lithospheric mantle depths – e.g., Begg *et al.,* 2010) while the other four limbs of the Bushveld are sited on the southern side of the structure. The significance of the spatial correlation between PGE-rich magmas (e.g., in Bushveld-like layered intrusions) and lithosphere-scale lineaments penetrating through Archaean cratonic crust is a current topic of debate (e.g., Groves & Bierlein, 2007; Maier & Groves, 2011; Arndt, 2013; and see Chapter 1).

3.3.2. The Skaergaard Intrusion (a closed system layered intrusion deposit model)

In contrast to the Bushveld Complex (an open magmatic system), the gabbroic Skaergaard Intrusion of east Greenland is a type locality for a closed system layered magmatic chamber (e.g., Wager & Brown, 1968; Hunter & Sparks, 1987; McBirney, 1989; Holness *et al,* 2007, 2011; Tegner *et al.,* 2009; McKenzie, 2011). The Skaergaard Intrusion was emplaced during the initial breakup of the North Atlantic (c. 55.7 ± 0.03 Ma; Hirschmann *et al.,* 1997). Several initial pulses of Ti-rich tholeiitic basaltic magma (similar to syn-breakup flood basalt compositions elsewhere in east Greenland) culminated in the intrusion of the Skaergaard Intrusion, which subsequently homogenised and became isolated as the intrusion cooled and crystallised (hence becoming a closed system) – see Holness *et al.* (2007).

During cooling, fractional crystallisation in the closed system led to the formation of early Ni- and Cr-poor plagioclase and olivine cumulates, suggesting that substantial fractional crystallisation had already taken place prior to magma emplacement at the crustal level of the

Skaergaard Intrusion itself (see Andersen *et al.,* 2002 and references therein). Trapping of buoyant crystals, such as plagioclase, at the base of liquid zones (e.g., in the Lower Zone cumulate layers) has recently been proposed (Bons *et al.,* 2015) and builds on the work of Irvine *et al.* (1998) whereby cumulate layers are modelled as being sorted and deposited by magmatic crystal-liquid suspension currents. The magma chamber itself caused contact metamorphism and H_2O-fluxed melting close to the contact of the Precambrian gneiss country rocks forming the floor of the intrusion (Bufe *et al.,* 2014).

Broadly, the Skaergaard can be sub-divided into the Lower, Middle and Upper Zones, encompassing a wide variety of gabbros and gabbroic pegmatites (e.g., Hunter & Sparks, 1987; Larsen & Brooks, 1994) with varying degrees of compaction (Tegner *et al.,* 2009; McKenzie, 2011). The Marginal Border Series crystallised *in situ* on the vertical walls of the Skaergaard magma chamber and includes feldspathic autolithic fragments, Precambrian gneiss xenoliths, and xenoliths of metasomatised Cretaceous-Palaeocene sediments (Irvine *et al.,* 1998). Recent studies show that the Marginal Border Series underwent infiltration by reactive fluids through the developing crystal mush (e.g., Namur *et al.,* 2013 and references therein). Autoliths are also found in the Layered Series (Irvine *et al.,* 1998).

PGE exploration targeted a distinctive rhythmically layered zone (the Triple Group) in the upper portions of the intrusion. Platinova Resources Ltd found that this was host to Cu-Fe-Au-Pd mineralisation (e.g., Brooks, 1989; Bird *et al.,* 1991; Andersen *et al.,* 1998; Nielsen *et al.,* 2005; Holwell & Keays, 2014). Mineralisation occurs as a series of stratiform horizons (reefs) known as the Platinova Reef (Bird *et al.,* 1991) with sulphur contents < 100 ppm (Andersen *et al.,* 1998). Due to the low S abundance, sulphides present in the Platinova Reef are high tenor, and estimates of tonnage and grade are 280 Mt at 1.87 g/t Pd and 91 Mt at 1.8 g/t Au (Andersen *et al.,* 2002).

The Triple Group itself consists of plagioclase-augite-titanomagnetite-ilmenite cumulates, with patchy occurrences of pigeonite and olivine (e.g., Andersen *et al.,* 1998 and references therein). However, the factors controlling the origin of the Platinova Reef are still contentious (e.g., Holwell & Keays, 2014). While an initial stage involving the formation of an immiscible sulphide liquid from a metal-rich magma must have taken place (Andersen *et al.,* 1998; Bird *et al.,* 1991), the high tenor and strict Au- and Pd-enrichment suggests a subsequent process (or processes) modified the sulphide liquid (e.g., filter pressing of sulphide liquid, Andersen *et al.,* 1998; Rayleigh fractionation, Prendergast, 2000; modification of sulphides with a metal-rich volatile phase, Andersen, 2006 and references therein; dissolution upgrading, Holwell & Keays,

2014; and/or oxidation of sulphides, Wohlgemuth-Ueberwasser *et al.,* 2013). Regardless of the details of the specific sulphide geochemistry of the Platinova Reef, the closed magmatic system of the Skaergaard Intrusion demonstrates a situation where S-saturation was reached because of extensive fractional crystallisation of a magma (hence the Platinova Reef occurs in the higher portions of the intrusion). Therefore the Platinova Reef was not controlled by external S inputs and was formed in the absence of open system behaviour such as magma mixing or replenishment (Naldrett, 2004 and references therein).

3.3.3. Noril'sk-type sulphide mineralisation (conduit-hosted orthomagmatic sulphides deposit model)

The Noril'sk orthomagmatic Ni-(Cu)-PGE deposits are the type example of conduit-hosted magmatic sulphide mineralisation associated with a large igneous province (LIP), reviewed by Arndt (2011). The deposit (often subdivided into several constituent parts or sub-ranking deposit names, e.g., Kharaelakh) contains approximately 500 million tonnes (Mt) of ore reserves with additional 1000t of indicated resources (Arndt, 2011 and references therein). Noril'sk ores have a (Pt + Pd)/(Ni+Cu) metal ratio of 1 to 5, notably higher than most gabbro-related deposits (0.05 to 0.5) – Naldrett (2004). Mean ore grades are 1.77 wt.% (Ni), 3.57 wt.% (Cu), 1.84 g/t (Pt), 7.31 g/t (Pd) and 9.50 g/t (total PGE) – Naldrett *et al.* (1996).

Magmatic rocks at Noril'sk form part of the Siberian Traps LIP, formed from mantle plume magmatism in the Permo-Triassic (e.g., Reichow *et al.,* 2002; Saunders *et al.,* 2005 and references therein). Hosted in hyperbyssal mafic magmatic conduits, the sulphide ores range from massive to disseminated, and sulphides were accumulated in the lower parts of these conduits. The conduits themselves intrude through a thick sedimentary sequence of evaporites (sulphate-bearing) which underlie the Siberian Trap flood basalt sequence (which have both PGE-rich and PGE-depleted volcanic members - Arndt, 2011 and references therein).

The ore-hosting intrusive conduits, beneath the volcanics, are small (generally < 150m thick) with a 'ribbon-like' form (500-2000 m wide, up to 19 km long) – Arndt (2011). Conduits are predominantly concordant to the sedimentary country rocks but some segments cut up and cross-cut the sedimentary and volcanic units (i.e., stepping sills) – e.g., Czamanske *et al.* (1995). Most conduits have uniform basaltic compositions (with dolerite or gabbro textures) but most of the major ore deposits occur in differentiated intrusions ranging olivine gabbros to diorites (e.g., Talnakh, Kharaelkh and Noril'sk deposits) – see Fedorenk & Czamanske (1997).

The geochemical compositions of silicate rocks hosting the main mineralised bodies are directly comparable to the composition of overlying volcanic rocks (e.g., Fedorenk & Czamanske, 1997; Arndt *et al.,* 2003; Arndt, 2005).

The evaporitic sediments are thought to have acted as a major source of crustal S contamination for some of the Noril'sk conduit magmas, triggering S-saturation (identified by a heavy non-magmatic $\delta^{34}S$ signature in ore sulphides) but other S-isotopic compositions indicate that evaporite contamination was not strictly controlling the formation of all sulphide liquids in the region (Arndt, 2011). For example, weakly mineralised disseminated sulphides in the Lower Talnakh deposit have $\delta^{34}S$ ranging from +4 to +6 ‰, low εNd (-12), high $^{87}Sr/^{86}Sr$, enrichment in incompatible elements and negative Nb-Ta anomalies, suggesting that S-saturation may have been controlled by contamination with old (lower to mid-) granitic continental crust (see Arndt, 2011 and references therein). In comparison, Noril'sk type deposits (hosting substantially more sulphide ore) have higher $\delta^{34}S$ (+6 to +12 ‰) which may indicate a greater control of S-saturation by evaporite contamination (possibly aided by circulation of fluids around the conduits and surrounding metamorphic aureoles as evidenced by crystal-rich magmatic breccias in lower portions of some conduit – e.g., Gorbachev, 2010).

For the main ore-hosting conduits, textural evidence suggests that these did not form by simple differentiation of a single magma batch, but were instead emplaced and formed by a series of magma pulses (e.g., Arndt *et al.,* 2003). Thus the geochemical correlation of volcanic units in the Siberian LIP is a crucial step used in understanding the timing of mineralisation in the coeval and underlying mineralised conduits, and has been widely developed as part of a deposit model used globally for exploration of similar LIP-hosted mineralisation (e.g., Karoo, Deccan and North Atlantic Igneous Provinces – see Andersen *et al.,* 2002 and references therein, and Arndt, 2011).

Several models have been suggested for the entrainment and collection of sulphide liquids in the conduit systems, (see Arndt, 2011 for an overview). The most recent model of sulphide liquid entrainment and accumulation proposes that parental picritic magmas passed through a series of deep chambers, assimilating granitic country rocks and locally segregating immiscible sulphide liquids. Later magmas passing through this magmatic plumbing system resorbed accumulated sulphides (e.g., Li *et al.,* 2009) and ascended to the subvolcanic magma system, at which stage they crystallised Fo-rich olivine (e.g., Czamanske *et al.,* 1994). Heat loss to the wall rocks in the subvolcanic system, coupled with assimilation of evaporitic sediments and organic-rich carbonates led to secondary segregation of immiscible sulphide liquid(s)

concomitant with further olivine crystallisation, resulting in a hyperbyssal magma column with variable olivine mush and sulphide droplets. Episodic eruptions fed by the conduit systems caused pulses or upwards magma surges through the magma column, followed by periods of quiescence during which time the magma drained back through the column (analogous to filling and emptying of lava lakes) – see Arndt (2011) and references therein. During episodic activity, sills on the flanks of the magma column open, allowing for multiple injections of variably phenocryst- and sulphide-poor and rich magmas to interact and segregate, resulting in the range of sulphide compositions (e.g., for $\delta^{34}S$). Within-conduit textures were further complicated by erosion or disruption of conduit walls (e.g., forming brecciated sections).

CHAPTER 4

A review of PGE mineralisation in the British Isles and North Atlantic Igneous Province

4.1. Platinum-group mineral (PGM) occurrences in the British Isles

PGM of magmatic and hydrothermal origin occur in numerous localities across the UK, as displayed in Figure 4.1 (Gunn & Styles, 2002; Gunn *et al.*, 2009). Many of these were discovered or investigated during the Mineral Reconnaissance Programme of the British Geological Survey (BGS), dating back to the early 1970s and 1980s. Most of this mineralisation occurs in Scotland and includes the intrusion-related deposits of Caledonian mafic-ultramafic bodies in NE Scotland such as the Knock Intrusion and intrusives at Huntly and Arthrath (Fletcher & Rice, 1989; Gunn *et al.*, 1990; Gunn & Shaw, 1992; Styles *et al.*, 1992; McKervey *et al.*, 2007); the Loch Borralan and Loch Ailsh Caledonian alkaline intrusions of NW Scotland (Styles *et al.*, 2004); and minor dioritic intrusions such as that at Talnotry in Dumfries and Galloway (Power *et al.*, 2004) and Sron Garbh near Tyndrum (Sangster, 2012). Layered ultramafic rocks in the igneous centres of the British Palaeogene Igneous Province (BPIP) including Rum, Mull, and Skye have also been shown to host PGM and PGE mineralisation (Hulbert *et al.*, 1992; Butcher *et al.*, 1999; Pirrie *et al.*, 2000; Power *et al.*, 2000; Prout *et al.*, 2002; Power *et al.*, 2003). Ophiolite-hosted PGM have been reported from Unst in Shetland (Prichard *et al.*, 1981; Gunn *et al.*, 1985; Prichard & Lord, 1993; Lord & Prichard, 1997; O'Driscoll *et al.,* 2012; Brough *et al.,* 2015) and Ballantrae (Power & Pirrie, 2004), as well as very minor occurrences in the Lizard in Cornwall (McPherson & Lamb, 1921; Hutchinson, 2001). PGM have also been documented in elongate serpentinised ultramafic bodies, exposed along the Highland Boundary Fault of Scotland, at Corrycharmaig (Power & Pirrie, 2000).

Two investigations into the PGE mineralisation potential were carried out across the Lewisian of NW Scotland, including areas in the Outer Hebrides, through the BGS Mineral Reconnaissance Programme (Shaw *et al.*, 1993; Coats *et al.*, 1997 and references therein). In particular, the ultrabasic and basic rocks of the Lewisian Central Block on the mainland were considered favourable for PGE, Cu, Ni, and/or Au mineralisation due to the discovery of similar style deposits in the Fennoscandian (or Baltic) Shield of northern Finland (Alapieti *et al.*, 1990). In 1986, lithogeochemical sampling was carried out between Loch Laxford and Gruinard Bay, and this was followed by a second sampling programme in 1994 from Scourie to Lochinver. The highest PGE concentration reported was 30 ppb Pt and 40 ppb Pd, but the majority of samples were significantly less enriched. Au abundances were low, with a median concentration of 4 ppb and Ni averaged 402 ppm (although this is consistent with most Ni being contained within olivine rather than sulphides). The highest concentration of Cu to be reported was 3351 ppm (Coats *et al.*, 1997).

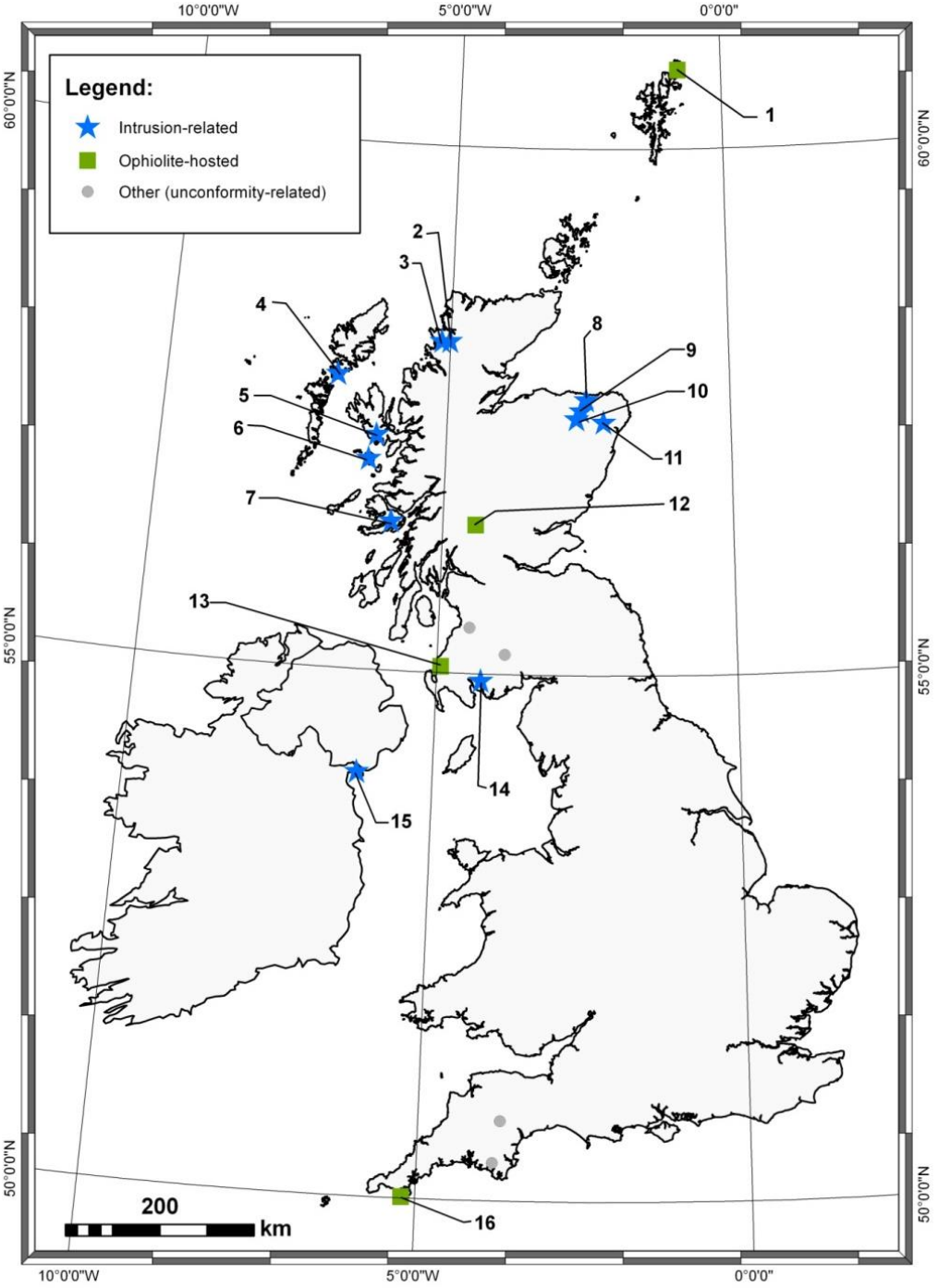

Figure 4.1. Principal PGE occurrences in the British Isles. (1) Unst, (2) Loch Ailsh, (3) Loch Borralan, (4) South Harris, (5) Cuillin Complex, Isle of Skye, (6) Isle of Rum, (7) Ben Buie, Isle of Mull, (8) Knock, (9) Huntly, (10) Upper Deveron, (11) Arthrath, (12) Corrycharmaig, (13) Ballantrae, (14) Talnotry, (15) Carlingford, (16) The Lizard. Map adapted from Gun & Styles (2002). *Map uses OS UK outline EDINA Digimap download (© Crown Copyright Ordnance Survey).*

The apparent lack of Ni-Cu-PGE-(Au) enrichment may be either due to a lack of primary magmatic sulphides, or (particularly in the case of Au) due to the subsequent metamorphism and remobilisation of metals from these Archaean rocks (Cameron, 1994). Sampling across the South Harris Gneiss Complex and surrounding marginal metamorphic belts was completed in 1991 (Shaw *et al.*, 1993). Stream sediment samples indicated no areas of significant PGE enrichment, and gabbro, diorite, and anorthosite rock samples from the complex itself yielded similarly low concentrations (< 15 ppb Pt or Pd). Sulphide mineralisation was found to be more common in the surrounding gneisses of the Leverburgh and Langavat Belts, and a maximum of 210 ppb Pd and 52 ppb Pt were found for a series of tectonised altered ultramafic pods in the Langavat Belt (Shaw *et al.*, 1993).

4.1.1. PGE in the Scourie Dykes

With the exception of work by Frick *et al.* (1994) and Frick (1998), no PGE data are available for the Scourie Dykes. Frick (1998) provides whole-rock PGE data for 5 samples taken from 3 dykes (including a bronzite picrite, an olivine gabbro, and a norite dyke) and showed that Pd abundances range from 3.2 to 13.6 ppb, and from 0.07 to 2.6 ppb for Ir (Frick *et al.*, 1994; Frick, 1998). Overall, mantle-normalised PGE multi-element diagrams show fractionated compositions with PPGE enriched relative to IPGE. Significant Au depletion has been reported from the mafic and felsic Lewisian granulites (Cameron, 1994), averaging 0.54 ppb Au and well below the average crustal concentration of 2.5 ppb (Crocket, 1974), but the Scourie Dykes have higher Au contents (mean 1.20 ppb, maximum 5 ppb Au; Cameron, 1994). High total PGE concentrations indicate that parental magma(s) were derived from an enriched mantle region (Frick *et al.*, 1994). Using Re-Os (Frick *et al.*, 1994) and Sm-Nd, Rb-Sr, and U-Pb isotopic data (e.g., Waters *et al.*, 1990), it has been proposed that magmas were partially derived from the SCLM, and this interpretation is supported by other geochemical studies of the Scourie Dykes (Weaver & Tarney, 1981; Tarney & Weaver, 1987; Condie, 1997).

4.1.2. PGE in the British Palaeogene Igneous Province (BPIP)

4.1.2.1. Scotland

PGM have been discovered in various layered intrusions within the BPIP, including Mull and Skye (Pirrie *et al.*, 2000; Prout *et al.*, 2002) and the Isle of Rum (Hulbert *et al.*, 1992; Butcher *et al.*, 1999; Power *et al.*, 2000). However whole-rock PGE data are relatively scarce as published literature have tended to document mineral species and PGM assemblages associated with layers in particular intrusions. A study was also carried out on a single volcanic plug on the Isle of Rum that identified PGM associated with coarse sulphides in the plug itself, and in sulphide-bearing gabbroic dykes cross-cutting the plug (see Power *et al.*, 2003). Based on the limited published whole-rock PGE data, mineralisation is assumed to be of a primary orthomagmatic type with little evidence for post-magmatic remobilisation processes affecting initial PGE geochemistry (except for minor localised hydrothermal effects; see Gunn & Styles, 2002 and references therein). Prior to this investigation and thesis, only the paper by Andersen *et al.* (2002) has attemped to give a broader review of whole-rock PGE abundance across the BPIP and North Atlantic Igneous Province (NAIP). There are no published whole-rock PGE data available for the BPIP flood basalt lava sequences (unlike in the NAIP flood basalts of Greenland – Section 4.2.1).

An overview of published literature on the occurrences of PGM in the BPIP is given in Table 4.1 and Figure 4.2.

4.1.2.2. Northern Ireland and the northern Republic of Ireland

The potential for PGE mineralisation in Northern Ireland and the bordering regions of the Republic of Ireland has been recognised by the Tellus regional exploration programme (completed in 2007 and led by the Geological Survey of Northern Ireland; GSNI). The Tellus Project involved the collection and analysis of soil and stream sediment samples, along with regional airborne geophysical surveys (Young & Earls, 2007). New targets have been established for an extended prospecting campaign for PGE in areas that cover Counties Antrim, Tyrone and Fermanagh, along with the Sperrin Mountains, and the Slieve Gullion igneous complex. In particular, extensive soil and stream sediment sample anomalies for Pt and Pd have been identified in northwest and east County Antrim, associated with the Antrim

Basalt Plateau and Palaeogene dykes (Smith, 2007). However a challenge presented by the soil sampling methodology used during Tellus is the preferential absorption of trace elements such as Cu and Pd onto organic matter in peat.

PGE mineralisation has also been identified in 'exotic' glacial boulders near the Palaeogene Carlingford Complex of the Republic of Ireland. Mineral exploration across the Carlingford Complex was first carried out by Westland in 1987 to 1989, and followed by BHP (now BHP Billiton) between 1995 and 1998. The BHP prospecting area incorporated two licences in north County Louth over an area of 80 km². During this period, a systematic soil sampling regime was carried out over areas with soil and bedrock anomalies identified by previous prospectors (Hurst, 1997a; Hurst, 1997b). After BHP's withdrawal from the area in 1998, Belmore Resources Ltd took over the lease in 2005. As a result of exploration across the Carlingford Complex, numerous PGE anomalies have been identified. These include a 10 cm section of basic dyke with 0.21 g/t Pt and several boulders located west of Carlingford Village with values up to 1.5 g/t Pt, 1.5 g/t Pd, 0.1 % Ni, 1.7 % Cu and 0.4 g/t Au (Goodman & Slowley, 2005).

By association with Carlingford, the Slieve Gullion Complex of Northern Ireland has become a potential PGE exploration target, but this is an acid-dominated complex at the current level of exposure and is therefore unlikely to host any significant PGE mineralisation. The Tellus dataset has been the catalyst for a renewed exploration campaign being carried out by Lonmin (Smyth, 2014), concentrating on the areas highlighted for their PGE potential, and in particular targeting potential PGE-bearing deposits associated with the Antrim basalts (Heffernan, 2010).

Table 4.1. *(continued overleaf)*

	Mineralisation location	Host lithologies	Host mineralogy & chemistry	PGM species	PGM size	PGM mineral associations	Genesis	Whole-rock PGE concentration	Published sampling	Refs
Rum	• Eastern Layered Series (ELS), Rum Central Complex	6 chromitite layers within 16 alternating units feldspathic peridotites to allivalite (plagioclase-olivine cumulate bytownite troctolites). 750 m total ELS thickness.	PGM are in chromitite layers, and associated with minor concentrations of interstitial sulphides. Sulphide minerals include Fe-rich pentlandite, chalcopyrite, bornite, with subordinate pyrrhotite. Some alteration of chalcopyrite to bornite, digenite, chalcocite, and covellite. Sulphides are sometimes S-poor. Magnetite is Ti-poor, suggesting strong but incomplete local oxidation and alteration (e.g., Platinova Reef, Skaergaard).	Most abundant and diverse PGM recorded in the BPIP. PGM assemblage varies with stratigraphic height: • ***Units 5-6*** (chromitite) = Pt+Pd-Bi-Te (+Au + electrum) • ***Units 7-8*** (chromitite) = laurite, Pt+Pd-Fe alloys & sulphides ***(main PGM layer)*** • ***Units 11-12*** (chromitite) = Pt+Pd arsenides & Bi-Te Most PGM are Pt-Pd bismuthotellurides, with arsenides, sulphides and alloys.	0.2-2 µm (max. 35 µm)	71 % PGM directly in contact with sulphides (mostly pentlandite or chalcopyrite, sometimes chalcocite, bornite and Fe-sulphides). Few PGM enclosed in sulphides. PGM also at silicate, chromite, and Fe-(hydroxyl) oxide boundaries. Very few PGM enclosed in chromite/chrome-spinel. One case noted of discontinuous rim of Pt-As, > 100 µm length around margin of sulphide grain. Pt-Te phases usually euhedral and elongate. Smaller PGM grains anhedral.	PGM of magmatic origin (but some grains show evidence of hydrothermal alteration). Mineralisation by: 1) Initial PGE-rich parental magma (high % melting due to plume) 2) Localised PGE mineralisation due to magma mixing (open-system magma chamber)	Eastern Layered Series [PGE + Au] > 2500 ppb (in chromitites), (~ 232 ppb in sulphide-rich zone of Unit 1). PGE normalised patterns are distinct between stratigraphic levels in the ELS (but consistent within the same stratigraphic level). All have weakly positive trends. No internal fractionation or stratigraphic variation for IPGE, but significant variation for PPGE. Very strong correlation between observed PGM abundance and whole-rock [PGE+Au].	Within and adjacent to chromitite layers or laminae. Sampled Units 5-6, 7-8, 9, and 11-12.	(Hulbert *et al.*, 1992; Butcher *et al.*, 1999; Power *et al.*, 2000; O'Driscoll *et al.*, 2009)
	• Western Layered Series, Rum Central Complex	Dunite and peridotite sequences with discontinuous chromitite laminae (troctolite below chromitite, feldspathic peridotite above).	PGM within discontinuous chromitite lamina (1-2 mm thick, and traceable for up to 5 m). Sulphides: pentlandite, chalcopyrite, pyrrhotite, chalcocite, bornite.	PGM mostly: laurite ($Ru(Os,Ir)S_2$), sperrylite ($PtAs_2$), irarsite (IrAsS). Rare platarsite (PtAsS) and michenerite ((Pd,Cu)(Bi,Te)).	0.3-1 µm	Sulphides interstitial to cumulus chromite and enclosed/intergrown with silicates. PGM in sulphides, clinopyroxne, or at silicate-sulphide grain boundary.	Magmatic	*[No data available]*	Within the Transitional Member	(Butcher *et al.*, 1999)
	Sgaorishal: • Ultramafic Plugs • Cross-cutting sulphide-rich gabbroic dykes	Late-stage ultramafic (and mafic) plugs cut Layered Suite and country rocks. Plugs may represent longer-lived feeder conduits. Sgaorishal ultramafic plugs then cut by cross-cutting sulphide (pyrrhotite vs. chalcopyrite)-rich gabbro dykes (< 200 mm wide).	Plugs show matrix banding with cumulus olivine (and varying % cumulus plagioclase, clinopyroxene and disseminated spinel). Sulphides are more abundant towards contacts with sediments. Primary sulphides include chalcopyrite, pentlandite, pyrrhotite, with alteration products including bornite, digenite, chalcocite, Cu, magnetite, and Fe-hydroxides. Galena is common throughout. $\delta^{34}S$ (plugs) = -9.2 to -18.3 ‰ $\delta^{34}S$ (dykes) = -10.8 to -15.0 ‰ S-isotopes suggest contamination by strongly bacterially reduced crustal S. Note increasingly more negative $\delta^{34}S$ towards plug margin with Triassic sandstone, but this is thought not to be the S-source (calcretes from arid formation should have expected positive $\delta^{34}S$).	*Plugs*: PGM mostly Pd bismuth-tellurides, sperrylite ($PtAs_2$) ± electrum, $PdBi_2$, and Pt-Bi-Te phases. Restricted range of species in comparison to Rum Layered Series. *Dykes*: Pd bismuth-tellurides, sperrylite, and paolovite (Pd_2Sn)	*Plugs:* 0.2 to > 10 µm *Dykes*: < 1 to > 40 µm	PGM are all sulphide-hosted (disseminated sulphides, cumulus & poikilitic). *Plugs*: PGM occur as discrete monomineralic grains (either wholly enclosed by sulphide or at sulphide-silicate boundary). Also relict PGM in altered sulphides. *Dykes*: For pyrrhotite-rich dykes, PGM relatively rare despite abundant sulphide. PGM as anhedral blebs in sulphides. Chalcopyrite-rich dykes have abundant larger PGM. < 10 % PGM in silicates (quartz + chlorite).	Magmatic: Two generations of PGE mineralisation. 1) West Sgaorishal plugs (disseminated Cu-Ni sulphides) 2) Later cross-cutting sulphide-rich gabbro dykes Sulphides in dykes have complex assemblages, related to late-/post-magmatic oxidation. Evidence that plugs are deep-level cross-sections of volcanic conduits (through which olivine-rich magmas flowed for substantial periods).	[PGE + Au]: > 400 ppb (plugs), > 2000 ppb (pyrrhotite-rich dykes) Absolute [PGE] considered to be dependent on sulphide content. Chondrite-norm patterns are weakly positively fractionated (suggesting primitive magma source with slight fractionation) and similar in both plugs and dykes. Degree of fractionation is less than in the ELS. Correlation between PGM and [PGE+Au] observed in disseminated sulphides of plugs, but not in pyrrhotite-rich dykes, suggesting significant % PGE contained in solid solution within sulphides (but not tested in literature).	West Sgaorishal plug only (largest plug at 100 x 500 m size) and cross-cutting dykes	(Power *et al.*, 2003; Holness *et al.*, 2012)

Table 4.1. Overview of published material for PGM and PGE in the British Palaeogene Igenous Province. Literature highlights varying mechanisms for local concentration of PGE (e.g., between Mull, Skye, and Rum) despite their being in a similar tectonic setting. References listed per location. NB. [PGE] notates whole-rock PGE concentrations. Concentrations are given in ppm or ppb and not g/t, to allow for ease of comparison with academic literature.

	Mineralisation location	Host lithologies	Host mineralogy & chemistry	PGM species	PGM size	PGM mineral associations	Genesis	Whole-rock PGE concentration	Published sampling	Refs
Skye	Outer Layered Series, Cuillin Complex: • *Meall na Cuilce (grid ref.: NG 4833 1990)* • *An Garbh Choire (grid ref.: NG 4680 2010)*	Peridotite Series: dunites, peridotites, troctolites, and anorthosites (with chromitite layers in the lower stratigraphic levels, dominated by olivine).	Ca-tholeiitic melt. Pinch and swell of chromitite layers, some steeply dipping. Chrome-spinel compositions range from chromite to hercynite. Sulphides, including chalcopyrite and pentlandite, present as accessories within chromitites. Chalcopyrite is abundant in some marginal areas of small basic intrusions.	~ 60 % of PGM are laurite $(Ru,Os,Ir)S_2$, minor sperrylite, RuAsS (ruasite), ± PGM alteration minerals (Pd-Bi tellurides)	< 1 to 7 µm	PGM in chromite or at chromite-silicate ± chromite-sulphide) boundaries (pentlandite & chalcopyrite). Sulphide-associated PGM are rare.	Orthomagmatic (with little alteration)	[PGE+ Au] up to 508 ppb (in chromitite layers) Chondrite-normalised patterns: flat or with negative trend. Implies IPGE enrichment through chromite crystallisation or PPGE depletion through later hydromagmatic/ hydrothermal processes.	Sampling restricted to chromitite layers.	(Pirrie *et al.*, 2000; Prout *et al.*, 2002)
Mull	Ben Buie Intrusion: • *Craig (grid ref.: NM 5807 2978)* • *Caigeann Doire nan Cuilean (grid ref.: NM 5771 2924)*	Plagioclase-clinopyroxene cumulate bytownite gabbro (eucrite) with leuco-troctolites and feldspathic peridotites (large layered intrusion – chromitite layers)	High-Ca tholeiitic composition (Mull Centre 1) belonging to the Central Mull tholeiitic magma type. Abundant chromite (in peridotites) as chromitite layers or seams (margins of anorthosite pods)	Semi-metals, and complexes of Bi, Te, Sb. *Craig*: Pd-rich species. *Caigeann*: Pt-rich species.	< 1 to 3 µm	PGM within silicates (intercumulus) and chromite, or at grain boundaries. Sulphide-associated PGM are rare.	Significant low-temperature hydromagmatic and hydrothermal alteration.	[PGE + Au] up to 189 ppb (in chromitite layers) Chondrite-normalised patterns: flat or with positive trend (± Rh-enrichment due to PGE concentration through fractional crystallisation of chromite.	Sampling restricted to chromitite layers.	(Pirrie *et al.*, 2000; Prout *et al.*, 2002)

4.2. PGE in the wider Palaeogene North Atlantic Igneous Province

The North Atlantic Igneous Province (NAIP) is thought to have high potential for PGE mineralisation, with numerous documented occurrences of mineralisation in the Greenlandic NAIP (see Tables 4.2 and 4.3 and Andersen *et al.,* 2002 and references therein) most notably in the Platinova Reef of the Skaergaard Intrusion (see Chapter 2). Factors such as the extensive melting and magmatism recorded in the NAIP following impingement of the proto-Icelandic mantle plume, combined with the presence of Archaean cratonic basement (comparable to the Lewisian terranes of Scotland) and younger contaminating sediments in the shallow crust (Permo-Triassic shales in east Greenland vs. Mesozoic Hebrides Basin in Scotland) makes the NAIP, and therefore the BPIP, one of the most prospective regions for PGE mineralisation globally (e.g., Andersen *et al.*, 2002).

An overview of PGE studies and reports from the NAIP outwith the British Isles is presented in the following subsections, and is summarised in Tables 4.2 and 4.3, and on Figure 4.2.

4.2.1. PGE in NAIP basalts

The flood basalts of east and west Greenland have been studied for their potential to host Ni-Cu-PGE mineralisation, analogous to that of Noril'sk (e.g., Lightfoot & Hawkesworth, 1997; Lightfoot *et al.*, 1997; Philipp *et al.,* 2001; Andersen *et al.*, 2002; Momme *et al.,* 2006; Bernstein, 2011). Icelandic basalts have also been analysed by Momme *et al.,* (2003). A summary of published PGE studies for basalts of the NAIP is given in Table 4.2 and an overview of mineralisation potential is given by Andersen *et al.* (2002).

4.2.2. PGE in east Greenland intrusions

Numerous mafic-ultramafic central complexes and dykes (including 'macrodykes') outcrop along the east and west Greenland coast and are associated with the Palaeogene plateau basalts and early-stage NAIP volcanics of Table 4.2. The most famous of these is the Skaergaard Intrusion (see Chapter 2). As outlined in Andersen *et al.* (2002), east Greenlandic major layered intrusions can be divided into two magmatic groups which formed towards the end of continental plateau volcanism: an older group (57-54 Ma) including the Skaergaard Intrusion, Imilik I Intrusion and Sorgenfri Gletcher Sill Complex, and a younger group (50-47 Ma) which includes the Kap Edvard Holm Complex, Kruuse Fjord Complex, Imilik II and III

Intrusions, the Lilloise Intrusion, and the Nordre Aputiteq Complex (Tegner *et al.*, 1998a). Of these, and including macrodykes in the vicinity of Skaergaard, the following have been reported to contain PGM or PGE mineralisation: Skaergaard Intrusion, the Kaerven Gabbro Complex, the Kap Edvard Holm Complex, Krusse Fjord Complex, the Miki Fjord Macrodyke, and the Togeda Macrodyke (cf. Andersen *et al.,* 2002; Thomassen & Nielsen, 2006 and references therein; Holwell *et al.,* 2012). In comparison, few published sources are available detailing potential Ni-Cu-PGE intrusions in west Greenland, although limited information on the Hammer Dal Dyke Complex of NW Disko Island has been included in Table 4.3. A summary of published PGE studies for Palaeogene intrusions of Greenland is given in Table 4.3 and an overview of these sources is available in Andersen *et al.* (2002).

This investigation and thesis sets out to contribute to the wider regional-scale exploration strategy for potential PGE mineralisation in the NAIP by analysing whole-rock PGE geochemistry of magma conduits, dykes, sills, plugs and the extensive lava sequences, putting the BPIP into a wider framework within the NAIP for PGE mineralisation potential. In addition, Scottish mantle xenoliths have been used to establish the sulphide and precious metal contents of the continental lithospheric mantle, and examine the contribution and potential controls that the SCLM may have had on metal budgets (and therefore mineralisation) over time.

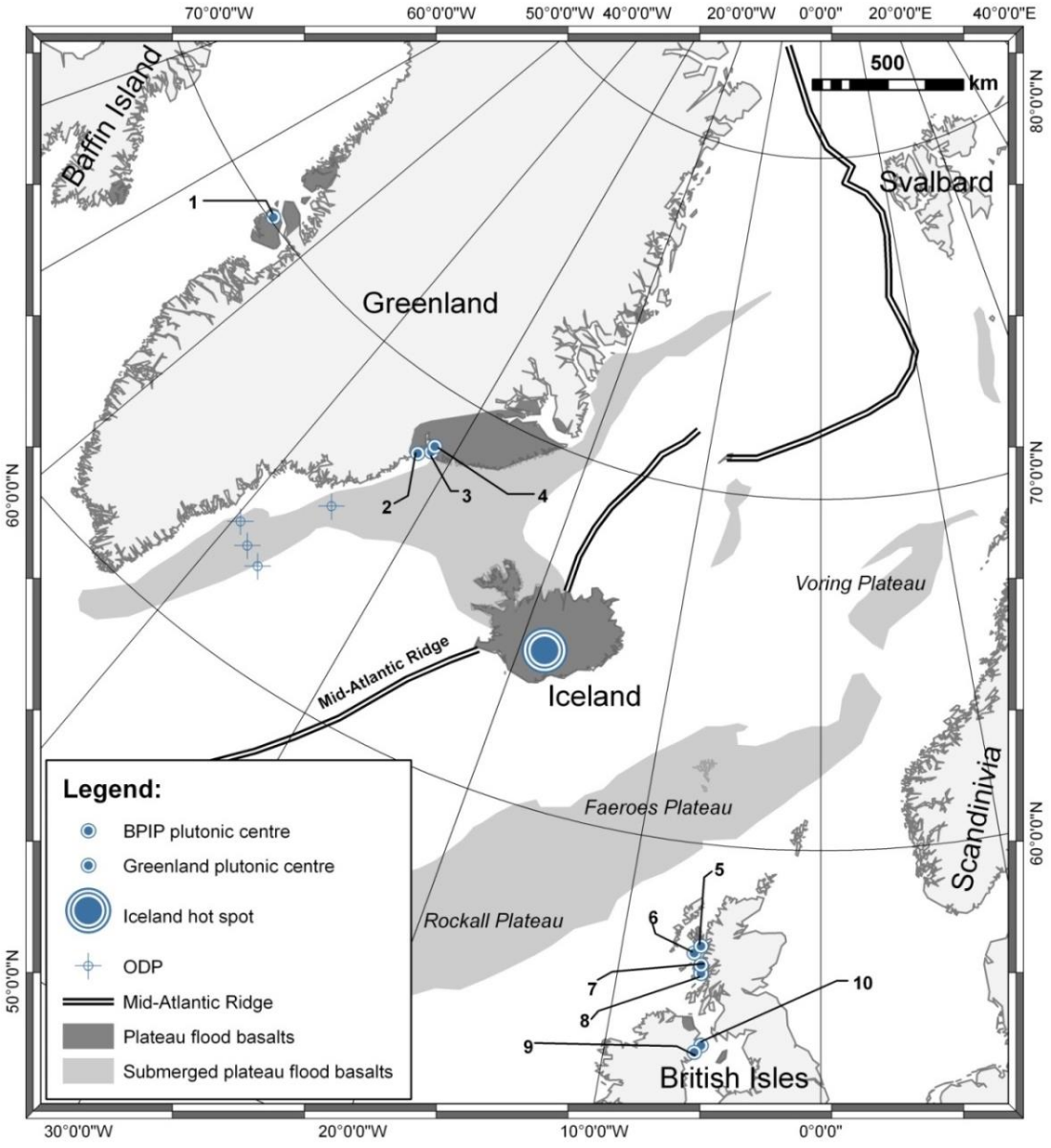

Figure 4.2. Simplified Palaeogene geology of the NAIP, showing locations of the flood plateau basalts associated with early-stage rifting of the Atlantic and a selection of plutonic centres mentioned in Tables 4.1 and 4.3: (1) Hammer Dal Complex, Disko Island, (2) Krusse Fjord Complex, (3) Skaergaard Complex, (4) Miki Fjord and Togeda Macrodykes, (5) Cuillin Central Complex, Isle of Skye, (6) Rum Central Complex, Isle of Rum, (7) Central Complexes of Ardnamurchan, (8) Ben Buie Central Complex, Isle of Mull, (9) Carlingford Complex, (10) Slieve Gulion and Mourne Complexes. ODP are ocean drilling program sites (as in Table 4.2). Map adapted from Andersen *et al*. (2002).

Table 4.2. Overview of published material for NAIP basalts and their PGE and Cu concentrations (excluding the BPIP – refer to Table 4.1). Data from various sources (with specific PGE references in bold font type) and discussed in Andersen et al. (2002). *NB. [PGE] notates whole-rock PGE concentrations. Concentrations are given in ppm or ppb and not g/t, to allow for ease of comparison with academic literature.* † Incompatible trace element behaviour for Cu. Cu is used here as a monitor of S-saturation. Cu is incompatible during oxide/silicate crystallisation (and relatively immobile during minor hydrothermal alteration). Thus magmas become enriched in Cu during fractional crystallisation (as indicated by MgO wt%) so that a semi-hyperbolic Cu-MgO trend is observed (Andersen et al., 2002). If S-saturation is achieved, residual silicate magma (later erupted) is strongly depleted in Cu.

	Locality & Formation	Lava extent	Lithologies	Geochemistry & Cu concentration	Whole-rock PGE concentration	Petrogenesis & comments	Refs
East Greenland	*Onshore: Kangertittivaq to Kangerlussuaq Fjord* 1. Lower Basalts 2. Low-Ti Plateau Basalt Series (LTS) 3. High and Very High-Ti Plateau Basalt Series (HTS & VHTS) 4. Dykes and sills (e.g., THOL-1 and THOL-2 dyke swarms, and Jameson Land and Traill Ø sills) 5. Minor late syenite complexes and alkaline lavas	Area: 65,000 km^2 Stratigraphic thickness: 6.5 km	Initial eruption of picrites and thin units of crustally contaminated tholeiites (1). Followed by eruption of voluminous uncontaminated tholeiitic plateau basalts caused by continental breakup.	Picrites in Lower Basalts have MgO content up to 17 wt.%. Lower Basalts Cu concentration varies 72-182 ppm.	Low PGE concentrations in Lower Basalts: Pt = 3-10 ppb, Pd = 2-9 ppb, Ir = 0.2-1.1 ppb, Au = 2-17 ppb (Picrites have highest concentrations) No correlation of PGE with Mg#. Negative correlation between PGE and Zr (for Lower Basalt tholeiites).	Picrites are S-undersaturated, uncontaminated primitive magmas possibly sourced from differentiated ultramafic cumulates. Lower Basalt tholeiites fractionated due to crustal contamination and sulphide segregation.	**(Nielsen & Brooks, 1995; Momme *et al.*, 2002a; Momme *et al.*, 2002b; Momme *et al.*, 2006)** (Nielsen, 1978; Fram & Lesher, 1997; Pedersen *et al.*, 1997; Tegner *et al.*, 1998b; Hald & Tegner, 2000)
				Main Plateau Basalts are subdivided according to TiO_2 content: LTS = 0.8-2 wt.% HTS = 1.5-4 wt.% VHTS = 4-5.5 wt.% Cu shows incompatible trace element behaviour † (suggesting S-saturation did not occur). LTS [Cu] = 105-248 ppm HTS [Cu] = 43-304 ppm VHTS [Cu] = 239-453 ppm	LTS basalts have broad range of PGE concentrations, with Pt and Ir positively correlated with Mg#, and Pd negatively correlated. LTS [PGE]: Ir = < 0.05-1.01 ppb, Rh = 0.48-1.13 ppb, Ru = < 0.3-1.8, Pt = 2.5-12.6 ppb, Pd = 5.9-23.8 ppb, Au = 5.7-17.4 ppb. HTS & VHTS show relatively constant Cu/Pd ratios, therefore suggesting little or no sulphide fractionation during magma differentiation. HTS [PGE]: Ir = < 0.05-1.58 ppb, Rh = 0.30-0.65 ppb, Ru = < 0.3-2.8 ppb, Pt = 2.63-9.06 ppn, Pd = 3.04-15.1 ppb, Au = 1.5-12.4 ppb. VHTS [PGE]: Ir = 0.10-0.13 ppb, Rh = 0.15-0.48 ppb, Ru = < 03-0.46 ppb, Pt = 2.56-5.76 ppb, Pd = 12.3-25.0 ppb, Au = 6.1-15.2 ppb.	LTS derived from more depleted mantle source than HTS and VHTS. HTS and VHTS are rich in incompatible elements suggesting that these were formed from low degree partial melts segregated from the asthenosphere. Overall the east Greenland flood basalts contain moderate PGE concentrations (between that of komatiites and MORB). Evidence suggests that these did not exsolve sulphide (i.e. S-undersaturated).	
			Skaergaard-like dyke swarms (THOL-2), and other tholeiitic dykes swarms.	THOL-2 Mg# = 46-60 %, 96-263 ppm Cu. Major elements resemble HTS basalts.	THOL-2 dykes are slightly more fractionated than LTS basalts and Lower Basalts (i.e., lower Mg#). THOL-2 [PGE]: Ir = < 0.05-0.4 ppb, Pt = 1-20 ppb, Pd = 15-27 ppb, Au = 4-22 ppb.	Coeval with various basalt generations listed above. Jameson Land and Traill Ø sills are of particular exploration interest due to their intrusion through gypsum-bearing Permo-Triassic sediments.	
	Offshore: SE Greenland coast 1. Pre-breakup (continental) Basalts 2. Syn-breakup (oceanic) Basalts		Predominantly voluminous uncontaminated tholeiitic plateau basalts continue offshore. Pre-breakup Basalts range from picrites to evolved tholeiites (fractionated ± crustal contamination). Syn-breakup Basalts are predominantly evolved oceanic tholeiites, but with some (older) high-Mg basalts and picrites.	Ocean Drilling Program (ODP) offshore basalts predominantly of LTS-type (onshore). Picrites and high-Mg basalts MgO up to 24 wt.%. Syn-breakup evolved tholeiite MgO ranges 8.23-6.26 wt.%. Pre-breakup basalt [Cu] = 42.1-196 ppm Syn-breakup basalt [Cu] = 73.1-237 ppm Syn-breakup basalt [Cu] suggest variable degrees of S-undersaturation and S- saturation.	Pre- and syn-breakup basalts have variable PGE concentrations, with 2 correlation trends with MgO content (for Pt-Pd, and Ir-Rh-Ru respectively). Pre-breakup basalts show a broader scatter of PGE concentrations with MgO, with a lesser correlation between PGE and MgO. Pre-breakup [PGE]: Ir = 0.10-0.60 ppb, Ru = 0.04-0.84 ppb, Rh = 0.02-0.57 ppb, Pt = 0.39-5.55 ppb, Pd = 0.52-5.91 ppb (from the Lower and Middle Series of Drill Site 917). Syn-breakup evolved tholeiites display a positive correlation between PGE and MgO. Syn-breakup [PGE]: Ir = 0.1-2.19 ppb, Ru = 0.08-2.52 ppb, Rh = 0.07-0.90 ppb, Pt = 3.69-14.3 ppb, Pd = 4.63-16.2 ppb (from the Upper Series of Drill Site 917 and Sites 988, 989, and 990).	Comparable in age to east Greenland basalts. Pre- and early syn-breakup basalts are continental (with evidence of contamination by Precambrian material, similar to that in the BPIP). This contamination (and fractionation) led to variable S-saturation. Syn- and post-breakup basalts have oceanic trace element signatures. Overall PGE, REE, and trace element ratios suggest basalts of different units were derived from heterogeneous mantle sources (with cogenetic basalt suites related by fractionation). Syn-breakup basalt S-saturation/undersaturation indicate mixing between two different magma sources – one PGE-poor and Cu-rich, and one PGE-rich and Cu-poor (i.e. an N-MORB and hot spot component).	**(Philipp *et al.*, 2001)** (Larsen *et al.*, 1998; Larsen *et al.*, 1999 ; Andersen *et al.*, 2002)

Table 4.2. *(continued)*

	Locality & Formation	Lava extent	Lithologies	Geochemistry & Cu concentration	Whole-rock PGE concentration	Petrogenesis & comments	Refs
West Greenland	Disko Island (Qeqertarssuaq), the Nuussuaq and Svartenhuk Peninsulas, and Ubekendt Ejland. In particular the Asuk, Kuuganguaq horizons of the Naujanguit Member of the Vaîgat Formation, and the Malîgat basalt Formation.	Area: 55,000km^2 Stratigraphic thickness: 5 km	Lavas range from picrites to olivine and quartz tholeiites. Minor trachyte, trachybasalt, lamprophyre and nepheline normative olivine basalts. No syenites (unlike east Greenland). On Qeqertarssuaq Island continental basalts include ~1000m picrite lavas and discrete 10-15m thick contaminated members (the Vaîgat and Malîgat Formations).	Low Cu and Ni contents are potentially the result of magmatic sulphide scavenging (following S-saturation at an early stage). However [Cu] in these basalts are higher than MORB. Dominant S-saturated lavas are found in the Vaîgat Formation (picrites) and Malîgat Formation (tholeiites). The Naujanguit Member of the Vaîgat Formation has MgO content ranging 7-29 wt%. Within this, the Asuk and Kuuganguaq horizons have elevated SiO_2 (52-58 wt%) and lower MgO (7.5-12.8 wt%). These horizons have low [Cu] and [Ni] (45 and 40 ppm respectively).	Limited data on whole-rock [PGE] of the west Greenland lavas: Picrites display unfractionated PGE patterns (Pd/Ir ratio = 5.8-8.0) and very high Ir and Os concentrations (Os = 0.04-3.71 ppb). The Naujanguit Member picrites (Vaîgat Formation) contain 5.7-9.4 ppb Pt and 4.2-12.9 ppb Pd. The Asuk and Kuuganguaq horizons have very low [Pd] (0.16-0.63 ppb) and [Pd] (0.13-0.68 ppb). The neighbouring Illukunguaq dyke (related to the Asuk and Kuuganguaq horizons) has a massive sulphide lens at the lower dyke contact containing 2 ppm Pd+Pt (and 6.9 wt% Ni, 3.7 wt% Cu).	Picrites are primitive and uncontaminated products of the early mantle plume. Both picrites and tholeiites may have crystallised from a high-Mg parental magma (similar to recent Icelandic picrites). Tholeiites have numerous xenoliths (normally shale) supporting chemical evidence of high-level crustal contamination. Contamination is also possible by Archaean basement. Contamination and resulting increase in magma SiO_2 content probably caused S- saturation. Parental and contaminated magmas likely contained sufficient Ni-Cu-PGE and S to form magmatic sulphide deposits, however the west Greenland basalts occur as isolated units (separated and fed by N-S trending transcrustal rift faults e.g., the Kuuganguaq-Qunnilik fault complex). The possible lack of continued interaction with later magma batches may have prevented the formation of a Noril'sk-type deposit. However, proof of this style of mineralisation is found in the neighbouring Illukunguaq dyke (on Disko) with a massive sulphide lens at the irregular lower dyke contact (sulphide settled here by gravity). Therefore the related Kuuganguaq horizon of the Vaîgat Formation is of particular exploration interest (especially in valley systems that run along and across the Kuuganguaq-Qunnilik fault as these are close to the transition between the Kuuganguaq basalts and underlying contaminating Cretaceous sediments. Lesser known exposed intrusive centres associated with these lavas (in comparison to east Greenland). Larger intrusions with PGE potential include Niaqornarssuit and Ubekendt Ejliand (discussed in Table 4.3).	**(Lightfoot *et al.*, 1997; Pearson *et al.*, 1999; Schaefer *et al.*, 2000; Keays & Lightfoot, 2007; Secher *et al.*, 2007; Bernstein, 2011)** (Clarke & Pedersen, 1976)
Iceland	Samples mostly from central and SE Iceland Holocene volcanics (between Hofsjökull and Vatnajökull, near Bardarbunga Volcano).		Tholeiitic basalts dominate. Minor alkaline activity (off central rift axis).	Basalt types from Iceland are divided into three groups: 1. High-Mg tholeiites (10-14 wt.% MgO) including primitive olivine tholeiites and picrites 2. Evolved olivine tholeiites (7-10 wt.% MgO) 3. Evolved basalts (4-7 wt.% MgO) including quartz tholeiites and alkaline basalts Cu concentrations (vs. MgO content) vary from an incompatible trend (similar to the east Greenland basalts) to a Cu-depleted N-MORB trend[†]. High-Mg tholeiites range from Cu-rich/Pd-poor to Cu-poor/Pd-rich ([Cu] = 74-120 ppm). Evolved olivine tholeiite (2) [Cu] = 100-150 ppm. Evolved basalt (3) [Cu] = 39-155 ppm.	Off-ridge alkaline olivine basalt [PGE]: Ir = 0.157 ppb, Ru = 0.167 ppb, Pt = 4.03 ppb, Pd = 65.9 ppb (sample from Snaefellsnaes Peninsula). High-Mg tholeiites [PGE]: Ir = 0.12-0.32 ppb, Ru = 0.24-0.92 ppb, Rh = 0.15-0.66 ppb, Pt = 3.58-6.93 ppb, Pd = 3.40-17.0 ppb, Au = 3.51-7.44 ppb. Evolved olivine tholeiite [PGE]: Ir = 0.06-0.19 ppb, Ru = 0.17-0.63 ppb, Rh = 0.20-0.38 ppb, Pt = 2.69-10.7 ppb, Pd = 0.40-18.1 ppb, Au = 2.14-5.67 ppb. Mg-poor evolved basalt [PGE]: Ir = 0.04-0.08 ppb, Ru = 0.13-0.17 ppb, Rh = 0.09-0.10 ppb, Pt = 0.31-2.23 ppb, Pd = 0.19-2.4 ppb, Au = 1.09-3.32 ppb. Olivine tholeiite [PGE]: Ir = 0.028-0.223 ppb, Ru = 0.024-0.646 ppb, Pt = 1.21-10.9 ppb, Pd = 0.848-16.7 ppb (data from NW Iceland).	Cu and PGE concentrations from depleted picrites indicate a melting regime of high degrees of partial melting from a highly depleted mantle source. However the presence of a hot mantle plume likely resulted in the formation of PGE-rich magmas (from high degrees of partial melting). In contrast alkaline and quartz tholeiite basalts (3) have low PGE concentrations potentially due to residual sulphides in the mantle source and/or S-saturation and differentiation at an earlier stage. LTS Plateau Basalts from east Greenland have similar Cu/Pd ratios to evolved olivine tholeiites (west Greenland), indicating that these may have been derived from similarly depleted mantle sources which underwent comparable plume-influenced partial melting.	**(Hardarson *et al.*, 1997; Rehkamper *et al.*, 1999; Momme *et al.*, 2003)** (Andersen *et al.*, 2002)

Table 4.3. *(continued overleaf)*

		Lithologies	Intrusion size	Mineralised Units	Host mineralogy & chemistry	Whole-rock PGE concentration	PGM species, size and associations	Petrogenesis & comments	Refs
						See Chapter 3 for Skaergaard Intrusion details			
East Greenland	***Miki Fjord Macrodyke***	Tholeiitic gabbro dyke. Main lithology: olivine gabbro (with some hybrid rocks formed by mixing with contaminating anatectic melts). Some ultramafic xenoliths at a widened point of the dyke (Sødalen Segment) THOL-2 generation of dykes (see Table 4.2) at Kangerlussuaq Fjord.	The Miki Fjord macrodyke is the largest of 3 gabbroic macrodykes (2 km from Skaergaard). It can be traced for 14.5 km (NE-trending). Maximum dyke width is 1 km.	Contact-related sulphide-hosted PGE mineralisation: Cu-PGE-Au sulphide mineralisation along dyke margin. Parts of dyke that cross-cut gneissic basement were initially discovered to be PGE-rich with PGM and sulphides. In southern portions, the dyke intrudes sedimentary rocks, including pyritic quartzites, siltstones, and shales.	Gabbro with medium-coarse grained olivine, clinopyroxene, orthopyroxene, plagioclase (± magnetite and biotite). Gabbro is rhythmically layered (5-10 cm bands) consisting of thick pyroxene-dominated melacratic layers and intervening homogeneous gabbro (0.5-1 m thick). Ultramafic xenoliths (up to 1 m size) are cumulates of ~ 80 % olivine with minor intercumulus plagioclase (MgO = 28 wt.%). Sulphides most abundant at or near the intrusive margin (in contact with gneissic basement), decreasing in abundance towards the dyke centre. Sulphide phases are predominantly: chalcopyrite, pyrrhotite ± bornite and pyrite. Sulphides are disseminated interstitial blebs/rounded globules. In olivine cumulate ultramafic xenoliths, there are minor interstitial sulphides (including pentlandite).	Initial grab samples (Platinvoa Resources Ltd, 1986) showed gabbros from the Sødalen Segment of the dyke with [PGE] up to: 2100 ppb Pd, 70 ppb Pt and 150 ppb Au. Later grab samples from this area (Platinvoa Resources Ltd, 1988) recorded [PGE] up to: 2228 ppb Pd, 100 ppb Pt, and 286 ppb Au. Rock-chip assay results show grades up to 3.2 ppm Pd, 160 ppb Au, 2.2 wt.% Cu and 0.7 wt.% Ni. Cu- and Pd-dominant mineralisation. Cu/Pd and Cu/Au ratios slightly scattered away from linear relationship (with relatively high PGE+Au concentrations). Mean Cu/Au = 90,000 No correlation of Pt with base metals. Poor Cu/Ni ratio correlation with MgO.	PGM grains < 40 µm. PGM associated with sulphides (completely or partially included). PGM chiefly Pd bismuthides and tellurides. PGM phases also include: atokite, kotulskite, and stibiopalladinite. Minor antimonides.	NB. Macrodykes such as this were major feeders to plateau basalts (Table 4.2) during the early stages of rifting in the NAIP. The macrodykes around the Skaergaard Intrusion in the Kangerlussuaq region are probably spatially and temporally related, and may be part of a large complex, connected at depth to a mutual magma chamber. However for the Miki Fjord Macrodyke, footwall contamination (by Archaean basement gneisses, as indicated by rheomorphic melting) is a possible cause of S-saturation. However S-isotopic evidence does not support this, instead indicating the sulphidic units of the Kangerlussuaq Basin sequence as the S source. Hence, the presence of sulphide mineralisation in each macrodyke is dependent on interaction with local country rocks (and therefore the type of country rock contamination). For example these magmas may also have interacted with Cretaceous basinal sediments. PGM-bearing sulphide globules probably formed due to fractionation of trapped droplets of immiscible Cu- and Pd-rich sulphide liquid. Therefore PGE mineralisation and sulphide concentration were reliant on local country rock contamination. The occurrence of PGE- and Pb-antimonides in the Miki Fjord Macrodyke (unlike the Togeda Macrodyke) may be suggestive of addition of Sb during crustal contamination (especially from shales). However coupled with high Pb grades (potentially due to remobilisation in late magmatic fluids) is it possible that the Miki Fjord Macrodyke has undergone more alteration than the Togeda Macrodyke.	**(PlatinaResources; Thomassen & Nielsen, 2006; PlatinaResources, 2009; Holwell *et al.*, 2012; Holwell & Boyce, 2012)** (Deer, 1976; Nielsen, 1978; Blichert-Toft *et al.*, 1992)
	Togeda Macrodyke	Gabbroic dyke surrounded by country rocks of Archaean gneisses (with minor amphibolite) and pre-Tertiary basic dykes.	Dyke thickness: c. 80-100 m	Contact-related sulphide-hosted PGE mineralisation: Cu-PGE-Au sulphide mineralisation along dyke lower margin (SE side of dyke). Sporadic footwall mineralisation observed, but does not extend > 2 m into the gneissic footwall.	Undeformed Ti-rich gabbro. Very similar host mineralogy and petrology to the Miki Fjord Macrodyke (although not layered and no xenoliths discovered). Togeda Macrodykes displays continuous sulphide mineralisation along the whole exposed length of the dyke. Mineralisation is particularly concentrated along a steady 5-6m thick zone at the lower SE margin of the dyke. Both disseminated (interstitial) and globular Cu-PGE sulphide mineralisation is present.	Cu- and Pd-dominant mineralisation. [Cu] up to 4 wt.%, [Pd] up to 3.3 ppm [Pt] up to 136 ppb [Au] up to 493 ppb Cu/Pd and Cu/Au ratios consistent linear relationship. Mean Cu/Au = 149,000 Mean Pd/Au = 11 No clear correlation of Pt with base metals. Poor Cu/Ni ratio correlation with MgO.	85 % of PGM are < 10 µm (one sobolevskite grain 60 µm long). PGM are predominantly (96 % by volume) bismuthides, tellurides, and bismuthotelluride. These include sobolevskite, merenskyite, and froodite. Minor stannides, pallarstenide, paolovite, and electrum. 66 % of PGM (by number) are included in base metal sulphides, with 25 % at sulphide-silicate margins, and only 2 PGM observed enclosed in silicates.	Discovered in 2008, relatively few investigations have been carried out on the Togeda Macrodyke. As for the Miki Fjord Macrodyke, sulphide mineralisation in the Togeda Macrodyke was dependent on country rock contamination; with S-isotopes indicating a marine sediment S source. Due to the Togeda Macrodyke's location, it may be that this dyke is an offshoot or extension of the Miki Fjord Macrodyke. The lack of modal layering in the Togeda Macrodyke, its shallower dip (50°W) and restriction of mineralisation to the lower contact may be evidence that these two dykes are distinct. The presence of two textural types of sulphide mineralisation is likely the result of variable cooling effects within the host gabbro (and not indicative of two different sulphide generations).	**(Holwell *et al.*, 2010; Holwell *et al.*, 2012)**

Table 4.3. Overview of published material for PGE and Cu concentrations in east and west Greenland intrusions. Data taken from various sources (with specific PGE references in bold font type) and summarised in Andersen *et al.* (2002). *NB. [PGE] notates whole-rock PGE concentrations. Concentrations are given in ppm or ppb and not g/t, to allow for ease of comparison with academic literature.*

		Lithologies	Intrusion size	Mineralised Units	Host mineralogy & chemistry	Whole-rock PGE concentration	PGM species, size and associations	Petrogenesis & comments	Refs
	Krusse Fjord Complex	Complex subdivided into an outer gabbro series and an inner troctolite series, both cross-cut by an ultramafic transgressive body (with undulating lower contact and lack of chilled margin). The layered gabbro series consists olivine- and magnetite-gabbro cumulates > 2 km thick (along with a c.20 m thick marginal gabbro) Ultramafic body comprises olivine melagabbro, two wehrlites, and a melatroctolite. PGE-rich zone is within the melagabbro.	Area: 20-13 km Estimated thickness of exposed complex: 5000 m	Contact-related sulphide-hosted PGE mineralisation: PGE-rich zone occurs within 1m of lower undulating contact of transgressive ultramafic intrusion (contact discordant to layered gabbro complex). Mineralised melagabbro zone traced for 100 m along strike.	PGE-rich melagabbro comprises olivine-chromite-diopside-plagioclase cumulate (± phlogopite, apatite, and sulphide) with local lenses of pyroxenite and dunite. Sulphide phases within this occur as interstitial grains or inclusions in silicates. Sulphides include: pyrrhotite, chalcopyrite, pentlandite and cubanite (± violarite, bornite and millerite).	Mineralised zone whole-rock [PGE] up to 690 ppb Pd, 630 ppb Pt and 162 ppb Au. NB. Limited published data for whole-rock [PGE].	PGM < 35 µm. Grains are included in sulphide minerals/grain boundaries between primary magmatic and secondary silicate phases. PGM include: sperrylite, kotulskite, moncheite ± Pt-Fe alloys, Cu-Pd phases, hollingworthite, platarsite, and a Pb-bismuthotelluride.	Undulating contact between ultramafic sill and layered gabbro resembles resorption structures with localised peridotite pods (suggesting chemical reaction between the sill and gabbro complex). Local alteration (hydrothermal) has caused recrystallisation of some gabbros to secondary mineral assemblages. Overall, an igneous lithological control on PGM occurrence suggests a magmatic origin of PGE mineralisation. However PGM association with secondary silicate phases and observations of sperrylite in veinlets indicates some degree of post-magmatic (hydrothermal?) PGE local redistribution. Note that the Kruuse Fjord Complex has not undergone rotation during regional collapse of the coast here (unlike the Kap Edvard Holm Complex and Skaergaard Intrusion) therefore only a small part of the intrusion is exposed. Overall, poor exposure, remote location and inaccessible terrain have limited research into this intrusion.	**(Arnason *et al.*, 1997a; Thomassen & Nielsen, 2006)** (Arnason *et al.*, 1997b)
	Kap Edward Holm Complex	Layered gabbros (Upper, Middle and Lower Layered Series): Lower Series consists of modally layered gabbro and lesser granular anorthosite and troctolites. Mineralised reef associated with plagioclase-augite-olivine orthocumulates (and wehrlite below) in Lower Series.	Area: 360 km^2 Cumulate stratigraphic thickness: 7500 m	Stratiform PGE and Au mineralisation: Willow Ridge Reef (Stratabound) Mineralised horizon (within Lower Layered Series) identified over ~ 30 km along-strike.	Host gabbro to mineralised reef is much the same as other gabbros from the Lower Layered Series. No lithologic discontinuities such as chromitite/sulphide layers or pegmatites. Stratigraphic features associated with the mineralised reef: Parallel wehrlite layer 25 m below reef, 2 cm-wide olivine-rich melacratic layer within Pt- and Au-rich layers of the reef, and a 5-10 m thick anorthosite layer 6-12 m above top of reef.	Mean [PGE]: Pt = 250 ppb, Au = 50 ppb (over a 3m stratigraphic interval). Maximum [PGE] in individual samples report up to 5 ppm Pt, 110 ppb Pd, and 8 ppm Au . Os, Ir, Ru, and Rh all below detection limits in the Willow Ridge Reef. Lower Layered Series olivine-gabbro [MgO] = 4.3-10.9 wt.%, [SiO_2] = 47.950.6 wt.%, [Cu] = 23-448 ppm, [Ni] = 75-274 ppm.	PGM < 100 µm (average 10 µm). PGM chiefly Pt-alloys including sperrylite, cooperate and moncheite. Au as Au-alloys (< 25 µm, averaging 5 µm). PGM and Au-alloys all associated with Cu-Fe sulphides (digenite, bornite and chalcopyrite), secondary hydrothermal minerals, and as inclusions on the post-cumulus rims of silicates.	Numerous magma mixing events (open system, unlike Skaergaard) displayed as quench-zones or reversals in cumulate assemblages. Around the Willow Ridge Reef the cumulate gabbros show gradual compositional reversals. Deposition of the Willow Ridge Reef is spatially and temporally associated with the injection of plagioclase-saturated primitive magma into the resident magma chamber, resulting in the partitioning of PGE and Au into sulphides derived from the large volume of magma. Settling or deposition of the sulphide then formed the mineralised layer. Extensive hydrothermal alteration near a cross-cutting syenite intrusion, where gabbros are replaced by secondary minerals. In addition meteoric hydrothermal solutions also caused widespread alteration, desulphization of Cu-Fe sulphides and recrystallisation of some PGE minerals (and hosts).	**(Bird *et al.*, 1995; Arnason & Bird, 2000; Thomassen & Nielsen, 2006; Secher *et al.*, 2007; PlatinaResources, 2012)** (Bernstein *et al.*, 1996)
West Greenland	***Hammer Dal Dyke Complex (NW Disko Island)***	Subvolcanic intrusive dykes of contaminated basaltic melts (feeders to flood basalts in this area).	No data available	No mineralised units or horizons have been located to date, but iron cumulates and sulphides indicate a Noril'sk-type deposit.	Contains Ni-bearing pyrrhotite and native iron.	Sulphides in enriched basalt (and accumulated metallic iron) show Ni concentrations > 1 % and enriched PGE contents up to 0.5 ppm.	No data available	Intense hydrothermal alteration around this dyke complex and NW Disko Island suggest that a larger feeder intrusion exists at depth. In addition, the presence of Fe-cumulates suggests that considerable magma transport took place through this dyke system and associated conduits. History of Ni-Cu-PGE exploration for the Hammer Dal Complex includes Greenex/Cominco Ltd in the 1980s, Platinova A/S-Falconbridge Greenland A/S joint venture 1991-1996, and Vismand Exploration Plc. since 2003.	**(Vismand, 2006; Secher *et al.*, 2007; Secher *et al.*, 2010)** (Secher & Stendal, 2010)

CHAPTER 5

Publications and the layout of Chapters 6 to 12

Chapters 6 to 12 present a series of seven papers, which are in various stages of review, in press, or in print and fully published. The content of these papers has been re-formatted so as to be more suitable for the layout of this thesis, however the text, figures and tables presented here are the same as those submitted to the journals. For each paper, a cover page detailing the full title, journal of submission/publication, co-authors (and contributions thereof), and the status of the paper (under review, accepted, in press, or published) is provided on the title page of each chapter. A related appendix section in this thesis (for the original supplementary material submitted to journals) is also provided on a paper-by-paper basis. Given the breadth of material and techniques covered within the seven papers, each paper (now Chapters 6 to 12) has its own abstract, introduction, methodology, results, discussion, conclusion and acknowledgement sections. Only the reference lists from each paper have been removed and amalgamated to make a master reference list at the end of this thesis.

The details of the following chapters are as follows (up to date at the time of thesis submission):

Chapter 6:

Hughes, H.S.R., McDonald, I., Goodenough, K.M., Ciborowski, T.J.R., Kerr, A.C., Davies, J.H.F.L., Selby, D. 2014. **Enriched lithospheric mantle keel below the Scottish margin of the North Atlantic Craton: Evidence from the Palaeoproterozoic Scourie Dyke Swarm and mantle xenoliths.** *Precambrian Research,* **250,** 97-126.

Chapter 7:

Hughes, H.S.R., McDonald, I., Faithfull, J.W., Upton, B.G.J., Downes, H. (in press). **Trace element abundances in the shallow lithospheric mantle of the North Atlantic Craton margin: Implications for melting and metasomatism beneath Northern Scotland.** *Mineralogical Magazine (North Atlantic Craton Conference Special Issue).*

Chapter 8:

Hughes, H.S.R., McDonald, I., Upton, B.G.J., Faithfull, J.W. (under review). **Sulphides and precious metals in the lithospheric mantle: A multi-event record of sulphur-bearing magmatism and metasomatism through time (Loch Roag, Scotland).** *Geochimica et Cosmochimica Acta.*

Chapter 9:

Hughes, H.S.R., McDonald, I., Faithfull, J.W., Upton, B.G.J. (under review). **Cobalt and precious metals in sulphides of peridotite xenoliths and inferences concerning their distribution according to geodynamic environment: A case study from the Scottish lithospheric mantle.** *Lithos.*

Chapter 10:

Hughes, H.S.R., McDonald, I., Kerr, A.C. (accepted). **Platinum-group element signatures in the North Atlantic Igneous Province: Implications for mantle controls on metal budgets during continental breakup.** *Lithos.*

Chapter 11:

Hughes, H.S.R., Boyce, A.J., McDonald, I., Davidheiser-Kroll, B., Holwell, D.A., McDonald, A., Oldroyd, A. (accepted). **Contrasting mechanisms for crustal sulphur contamination of mafic magma: evidence from dyke and sill complexes from the British Palaeogene Igneous Province.** *Journal of the Geological Society, London.*

Chapter 12:

Hughes, H.S.R., McDonald, I., Boyce, A.J., Holwell, D.A., Kerr, A.C. (under review). **Sulphide sinking in magma conduits: evidence from mafic-ultramafic plugs on Rum, North Atlantic Igneous Province.** *Journal of Petrology.*

CHAPTER 6

Enriched lithospheric mantle keel below the Scottish margin of the North Atlantic Craton: evidence from the Palaeoproterozoic Scourie Dyke Swarm and mantle xenoliths

Submitted as:

Hughes, H.S.R., McDonald, I., Goodenough, K.M., Ciborowski, T.J.R., Kerr, A.C., Davies, J.H.F.L., Selby, D. 2014. Enriched lithospheric mantle keel below the Scottish margin of the North Atlantic Craton: Evidence from the Palaeoproterozoic Scourie Dyke Swarm and mantle xenoliths. *Precambrian Research*, **250,** 97-126.

Co-author contributions:

I. McDonald, K.M. Goodenough, A.C. Kerr, J.H.F.L. Davies, and T.J.R. Ciborowski were involved in discussions during the writing of this paper. D. Selby processed three bulk samples for Re-Os isotopes. I. McDonald supervised bulk rock analyses.

*Note that H.S.R. Hughes and J.H.F.L. Davies also co-authored a similar online publication for "Large Igneous Province of the Month" (May, 2014).
See: http://www.largeigneousprovinces.org/14may

Abstract

The Lewisian Gneiss Complex of NW Scotland represents the eastern margin of the North Atlantic Craton. It comprises mid-late Archaean tonalite-trondhjemite-granodiorite gneisses that were metamorphosed and deformed during the Late-Archaean and Palaeoproterozoic. A major swarm of mafic-ultramafic dykes, the Scourie Dyke Swarm, was intruded at ca. 2.4-2.3 Ga during a period of extension that can be correlated across the North Atlantic Craton. The majority of dykes are doleritic, with volumetrically minor picrite and olivine gabbro suites.

New major and trace element geochemical data and Re-Os isotopes indicate that the Scourie Dyke Swarm was not solely derived from a 'typical' asthenospheric mantle source region. The geochemical signatures of the dykes show significant negative Nb, Ta and Ti anomalies, coupled with enrichment in Th, Light Rare Earth Elements and other large ion lithophile elements. These features cannot be reproduced by simple contamination of asthenospheric sources with Lewisian granulite-facies crust. Instead they are a feature of the mantle source that produced the Scourie Dykes and may have developed during Archaean subduction episodes.

Spinel lherzolite mantle xenoliths from the Isle of Lewis offer direct insight into the lithospheric mantle below this region. They display similar geochemical 'enrichments' and 'depletions' observed in the Scourie Dykes and the magma source is thus considered to reside primarily in the sub-continental lithospheric mantle (SCLM), with some potential contribution from asthenospheric melts. Platinum-group element geochemistry and trace element modelling indicate that the dolerite dykes were formed by moderate (< 15 %) partial melting of the source, whilst higher degrees of partial melting led to the formation of picritic and olivine gabbro suites. Magma production was triggered by significant crustal and lithospheric extension, causing both asthenospheric and substantial lithospheric melting.

6.1. Introduction

The Lewisian Gneiss Complex crops out in NW Scotland and the Outer Hebridean Islands. It comprises mid-late Archaean tonalite-trondhjemite-granodiorite (TTG) gneisses, with minor mafic-ultramafic and metasedimentary components, that have been reworked by several Late Archaean and Palaeoproterozoic tectonic events. The Complex contains an extensive swarm of early Palaeoproterozoic mafic to ultramafic dykes (the Scourie Dykes) which can be correlated with dykes across the wider North Atlantic Craton (Bridgwater *et al.*, 1995). The Scourie Dykes were first mapped by Peach *et al.* (1907) and were recognised as an important time marker by Sutton and Watson (1951). Distinctions were made between the dykes according to their relict igneous mineralogy and bulk geochemical properties (Weaver & Tarney, 1981b; Tarney & Weaver, 1987). Initial dating suggested that the dykes were intruded in two episodes, at ca. 2.4 and 2.0 Ga (Heaman and Tarney, 1989) but only one dyke recorded the younger age. The majority of the dykes are now considered to have been emplaced in one magmatic event at ca. 2.418-2.375 Ga (Davies & Heaman, 2014).

The Lewisian Gneiss Complex is divided into a number of regions or terranes separated by major shear zones (Kinny et al., 2005; Fig. 6.1) with Scourie Dykes present in all terranes. Substantial work has focused on the Assynt Terrane, which comprises Archaean granulite-facies TTG gneisses locally reworked by post-Scourie Dyke amphibolite-facies metamorphism and deformation. To the north and south respectively, the Rhiconich and Gruinard Terranes were more thoroughly reworked at amphibolite-facies. Thus, igneous textures and mineralogy of the Scourie Dykes are best preserved in the Assynt Terrane (Tarney and Weaver, 1987). Scourie and 'Scourie-like' dykes have also been studied from the Rhiconich (Northern) Lewisian Terrane, the Isles of Coll and Tiree, and the Outer Hebrides (Fettes & Mendum, 1987; Muir *et al.*, 1993; Mason & Brewer, 2004; Goodenough *et al.*, 2010). In total this data set comprises ~50 Scourie Dyke analyses, spanning almost 30 years of varying analytical methods and differing element suites, for dykes found across the entire Lewisian Gneiss Complex.

In this paper, we present an updated data set of whole-rock geochemical analyses, including the platinum-group elements (PGE), for the Scourie Dykes based on new sampling carried out across the three mainland Lewisian Terranes (Rhiconich, Assynt and Gruinard) using modern and consistent analytical techniques. These new data are used to re-assess the potential magma sources and provide insights into the geochemistry of Archaean subcontinental lithospheric mantle (SCLM) and melting regimes. In addition, we present whole-rock

geochemical analyses and PGE concentrations of upper mantle (lithospheric) spinel lherzolite xenoliths from the Isle of Lewis, to directly investigate the geochemistry of the SCLM that underlies the Lewisian Gneiss Complex.

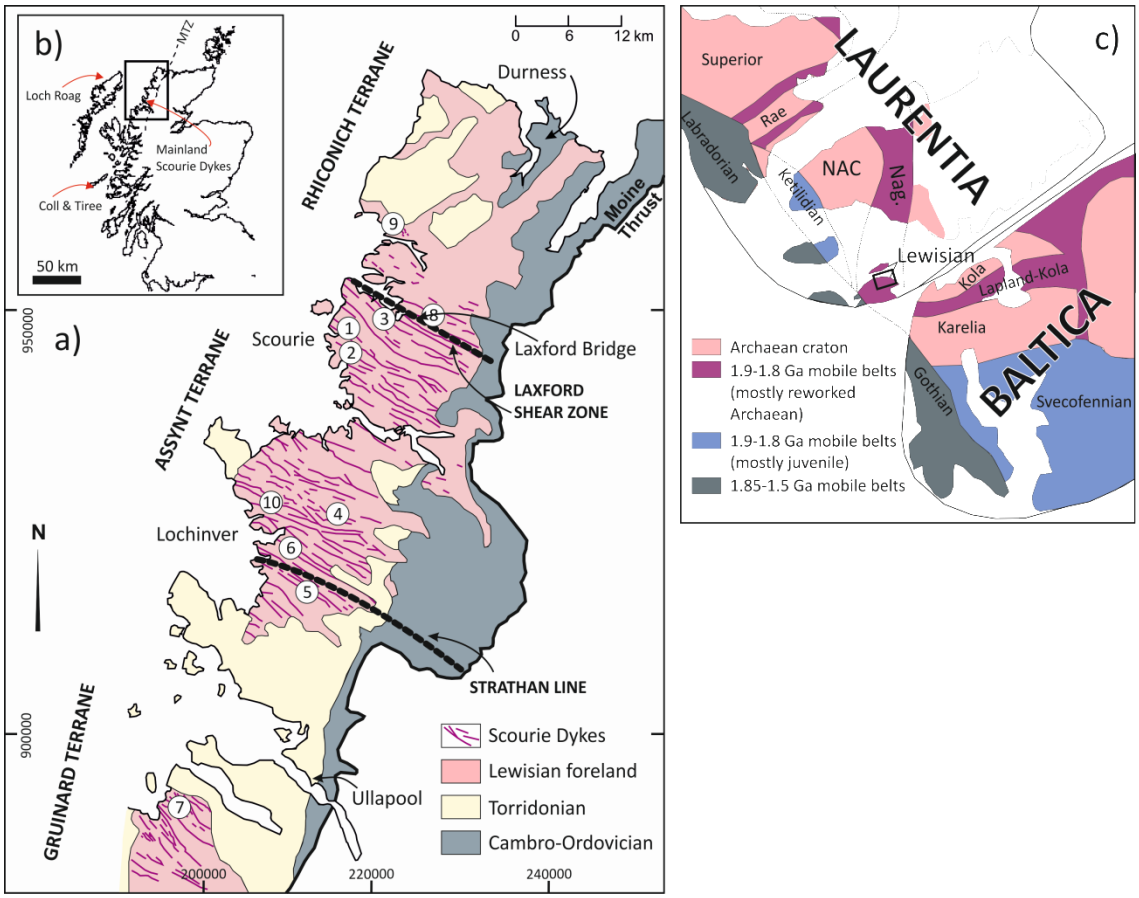

Figure 6.1. (a) Simplified map of NW Scotland, showing main geological units and the Scourie Dykes and location of Loch Roag mantle xenolith site (b). MTZ is Moine Thrust Zone, delineating the Caledonian Foreland. Numbered localities indicate approximate dyke sampling locations. Terrane nomenclature based on (Kinny *et al.*, 2005). (c) Larger scale simplified map showing the early Palaeoproterozoic relationship between the Lewisian of Scotland and the North Altantic Craton, as part of Laurentia and Baltica, based on Buchan *et al.* (2000).

6.2. Regional geology

The Lewisian Gneiss Complex is a small fragment of the much larger North Atlantic Craton (NAC; Fig. 6.1c) that includes Greenland, Labrador and parts of Canada and which consists of Archaean protoliths with zones of Palaeoproterozoic reworking. Tectonic events within the Lewisian fragment were as follows: (1) 3.0-2.8 Ga – magmatic protolith formation, (2) 2.8-2.5 Ga high-grade metamorphism and deformation including initiation of shear zones, (3) 2.4-2.0 Ga – intrusion of mafic and ultramafic dyke swarms (the Scourie Dykes), (4) 2.0-1.8 Ga –

formation and accretion of arc terranes, marked by calc-alkaline granitoid emplacement and related volcanics, and formation of localised high-grade Laxfordian metamorphic belts in the Lewisian portion of the NAC, (5) 1.8-1.5 Ga – continued calc-alkaline igneous activity, amphibolite-facies metamorphism and deformation, and crustal anatexis during the Laxfordian event (Park, 1994; Park, 1995; Kinny *et al.*, 2005; Goodenough *et al.*, 2013; Vernon *et al.*, 2014).

The mainland Lewisian Gneiss Complex has traditionally been sub-divided into three districts (Peach *et al.*, 1907; Sutton & Watson, 1951): the Central granulite-facies district, which was only partially affected by Laxfordian-age reworking, and the North and South amphibolite-facies districts that were extensively reworked in the Laxfordian (Fig. 6.1a). Recent geochronological data have shown that these crustal blocks also have different protolith ages, and they are now considered to represent separate terranes divided by major shear zones (Friend & Kinny, 2001; Love *et al.*, 2003; Kinny *et al.*, 2005; Park *et al.*, 2005; Goodenough *et al.*, 2010; Love *et al.*, 2010). The number of terranes or 'blocks' and the details of this model are still contentious, and timing and composition of the Scourie Dykes are important (Goodenough *et al.*, 2010). The terrane nomenclature of Kinny *et al*. (2005) has been adopted here (Fig. 6.1) with the Rhiconich, Assynt and Gruinard Terranes being broadly comparable to the North, Central, and South districts respectively.

The Assynt and Rhiconich Terranes are separated by the Laxford Shear Zone, inferred to be a boundary between two crustal blocks (Goodenough *et al.*, 2010). The Assynt Terrane consists of banded felsic gneisses of classic TTG composition, with mafic-ultramafic pods and lenses on scales from 1 cm to 10 m across. The typical granulite-facies gneisses are coarse-grained rocks containing clino- and ortho-pyroxene, hornblende, plagioclase and occasionally retrograde biotite (Johnstone & Mykura, 1989). However, unretrogressed granulite-facies lithologies are relatively rare; the majority of the Assynt gneisses display some degree of amphibolite-facies reworking, typically in discrete Laxfordian shear zones (Kinny *et al.*, 2005). The Assynt gneisses are characterised by a marked depletion in U, Th, and the LILE (Sheraton *et al.*, 1973).

The amphibolite-facies Rhiconich Terrane consists of more homogeneous biotite-hornblende gneisses of granodioritic composition (Goodenough *et al.,* 2010). Lenses, sheets, and veins of Laxfordian pegmatite and granite are also present. In comparison with the Assynt Terrane, the Rhiconich amphibolite gneisses are richer in U, Th and the LILE (Holland & Lambert, 1973; Sheraton *et al.*, 1973).

The Gruinard Terrane comprises hornblende-biotite-feldspar-quartz gneisses (amphibolite-facies) with a variety of mafic to ultramafic bodies on a range of scales (Fowler, 1986; Rollinson & Fowler, 1987). Geochemically, the Gruinard Terrane gneisses are more similar to those of the Rhiconich Terrane than the Assynt Terrane, and lack the strong U, Th and LILE depletion found in the latter.

6.2.1. Geology of the Scourie Dyke Swarm and previous work

The approximately NW-SE trend of the Scourie Dyke Swarm is thought to have been controlled by pre-existing shear zones that were exploited during crustal extension (Tarney, 1973). Many of the Scourie Dykes have been deformed and metamorphosed by Laxfordian shearing, but their igneous mineralogy and textures are still preserved at some localities in the Assynt Terrane. Similar dykes (the 'Older Basics') have also been described from the Outer Hebrides (Fettes & Mendum, 1987) but were not sampled during this study. The Scourie Dyke Swarm forms part of a wider Palaeoproterozoic group of basic dyke swarms extending throughout Labrador, western and eastern Greenland, and Baltica. These include the Kangâmiut, Graedefjord and Avayalik mafic dykes in W Greenland (Kalsbeek *et al.*, 1987; Bridgwater *et al.*, 1995; van Gool *et al.*, 2002; Nilsson *et al.*, 2013); high-Mg dyke swarms in Karelia and Kola (Fennoscandia); and Eqaluk, Kangeq, and Aornit high-Mg dykes in SW Greenland (Bridgwater *et al.,* 1995, and references therein).

In the Assynt Terrane, two generations of Scourie dykes are apparent: a mafic suite trending NW-SE, and an ultramafic E-W trending suite (Weaver & Tarney, 1981b; Tarney & Weaver, 1987). Both suites are steep-sided, ranging in width from 30 to 100 m, and some dykes can be traced along strike for up to 15 km, often with tapering offshoots (Weaver & Tarney, 1981b). They display sharp contacts with the host gneisses, and cross-cut pre-existing structures.

Petrological and geochemical features of the Scourie Dyke Swarm in the Assynt Terrane were reported by Tarney (1963; 1973), Weaver & Tarney (1981b), and Tarney & Weaver (1987) who grouped the dykes according to their original igneous mineralogy and composition. Four suites of dyke were identified: a main 'quartz-dolerite' or 'dolerite' suite (comprising 90-95 % of all dykes in the Assynt Terrane), and comparatively minor 'bronzite-picrites' (here referred to as 'picrites'), 'olivine-gabbro', and rare 'norite' suites which were not collected during this study (Tarney, 1973; Weaver & Tarney, 1981b; Tarney & Weaver, 1987). Field evidence suggests that the main dolerite suite was the first dyke group to be intruded, with subsequent picrite and

olivine gabbro dykes cross-cutting them (Tarney 1973). Due to limited exposure, and the general scarcity of ultramafic relative to mafic dykes, there are only a few places where this relationship can be observed. Recent geochronological work on the Scourie Dyke Swarm reveals that the main pulse of dolerite dyke intrusion occurred between 2.418-2.375 Ga (Davies & Heaman, 2014). However subtleties of the timing within this event have also been identified. For example some of the ultramafic dykes are in fact older than the mafic dykes (Davies & Heaman, 2014) so that within this 'main' event the Scourie Dykes were intruded in the following order; (1) an older minor suite (2418-2408 Ma) of ultramafic dykes, (2) the major suite of mostly mafic dykes with some ultramafics (2395-2390 Ma), and (3) a late suite of mafic dykes (2385-2375 Ma). The very late event at ~2000 Ma, identified by Heaman and Tarney (1989) has not been recognised again in recent studies, suggesting that it was a comparatively minor component of magmatism.

The dyke grouping criteria, maps and sampling locations for the Assynt Terrane from Tarney and Weaver (1981 b, 1987) were used during this study, in an attempt to ensure that all dyke suites were characterised. Dykes were also sampled from the Rhiconich and Gruinard Terranes. Geochemically, these are all basaltic dykes, rather than picrite or olivine gabbro.

The mineralogy and petrology of the three analysed dyke suites are as follows (Weaver & Tarney, 1981b; Tarney & Weaver, 1987):

1) Dolerite dykes – These are texturally and mineralogically uniform with chilled margins. Almost complete amphibolitisation is common, with acicular networks of tremolite-actinolite (or 'uralisation'). Reliable estimates of primary mineral modal abundances are difficult, but overall they consist of (partially) amphibolitised clinopyroxene, (partially) amphibolitised minor orthopyroxene, plagioclase, hornblende, quartz, and biotite. Accessory magnetite, ilmenite, pyrite, pyrrhotite and apatite are present.
2) Picrite dykes comprise up to 55 % olivine, 5-80 % orthopyroxene, 7-30 % clinopyroxene, interstitial plagioclase (7-25 %), minor phlogopite (1-4 %), accessory chromite, Fe-Ti oxides and pyrite. Each dyke has a distinctive texture and olivine size range (uniform per dyke) and plagioclase is interstitial to pyroxenes. No chilled margins are observed in these dykes, which instead have coarse pyroxene-rich margins.
3) Olivine gabbro dykes are composed of 3-6 % orthopyroxene, 20-38 % clinopyroxene, 12-20 % olivine, 20-35 % plagioclase, 8-16% hornblende and minor phlogopite (3-8 %).

Accessory magnetite, ilmenite, pyrite and pyrrhotite are present, and spherulitic clinopyroxene is generally concentrated at dyke margins.

Primary hydrous phases such as hornblende, phlogopite or biotite indicate a deep intrusion level of dykes (O'Hara, 1961; Tarney, 1963; Tarney, 1973), where magmatic volatile components were retained, and could be suggestive of a hydrated magma source. Where undeformed, dyke chilled margins are composed of hornblende, plagioclase, and sometimes garnet, implying a high ambient temperature of the crust during emplacement (300-500°C). This could also suggest a deep level of intrusion (O'Hara, 1961; Tarney, 1973) and is consistent with the mineralogy and the coarse-grained gabbroic textures observed at dyke centres. Dyke margins are sharp and well defined with rare examples of marginal xenoliths (e.g., at Upper Badcall, dyke samples X40, 41 and 42) but little other observable evidence of contamination.

Laxfordian amphibolite-facies metamorphism of the dykes is common as shown by variable amounts of 'amphibolisation' to tremolite and actinolite (Tarney, 1963). Garnet occurs in some Assynt Terrane dolerite dykes, sometimes as coarse stringers (e.g., 'the Graveyard dyke', Scourie Bay). Garnet is also prevalent in dykes around Gairloch (Gruinard Terrane) as patches or lenses. These dykes have compositions distinct from other members of the Scourie Dyke Swarm (Park 2002a – Shieldaig dykes) and this may have facilitated the growth of garnet during metamorphism. Although primary igneous mineralogy is retained to some degree at localities in the Assynt Terrane, an amphibolite-facies overprint is often present. This is particularly the case for earlier mafic dykes, with primary mafic silicates almost entirely replaced by hornblende. Amphibolitisation increases from the dyke centres to their margins (Tarney, 1973) and is particularly common in the dolerite suite. However, some Assynt dykes sampled during this study were almost entirely fresh (particularly the picrite suite), displaying a primary igneous mineralogy. In the Rhiconich Terrane, the dykes have been pervasively deformed and amphibolitised during the Laxfordian, with the development of a strong and pervasive mineral foliation defined by aligned hornblendes. A similar mineral foliation can be observed in Laxfordian-age shear zones within the Assynt Terrane, and samples were collected from outside shear zones where possible.

The complex tectonometamorphic history of the area post-Scourie Dyke emplacement means that the effects of post-intrusion alteration must be considered. The chief controls on trace element mobility are the availability of fluid phases, the composition of the fluids (e.g., CO_2 or halogen-bearing fluids) and the type of alteration. Geochemical interpretations in this study are predominantly based on the elements generally regarded to be 'immobile' at low to

moderate degrees of alteration and metamorphism, such as Th, Ti, P, Zr, Y, Nb and other high field strength elements (HFSE) (e.g., Jenner, 1996; Pearce, 1996). Early investigations of the Scourie Dykes (Weaver & Tarney, 1981a) suggested that element mobility only become significant after considerable recrystallisation, during which the large ion lithophile elements (LILE) were particularly mobile. In the absence of significant fluid-based alteration and circulation, rare earth elements (REE) appear to be stable up to granulite-facies metamorphism (Weaver & Tarney, 1981a; Jenner, 1996) and REE abundances in the Scourie Dyke Swarm are therefore unlikely to have been significantly affected by post-intrusion metamorphism. LILE such as Ba, K, Rb and Sr have also been tentatively used in geochemical interpretations of the dykes, despite their apparent mobility during metamorphism. These data are particularly relevant in light of the lack of LILE-rich host rocks in the Assynt Terrane, suggesting that any enrichment in these elements was a primary feature of the Scourie Dyke magma. However, these mobile elements have not been used for modelling of magma fractionation. Finally, PGE are effectively immobile in the absence of fluid-rich alteration (Gammons & Bloom, 1993; Crocket, 2000), so they are regarded in this study as relatively immobile. However Au is significantly more mobile during metamorphism and fluid-based alteration (Crocket, 2000), but is not directly used in interpretations in this study.

6.2.2. The Loch Roag mantle xenolith locality

Direct evidence about the lithospheric mantle beneath NW Scotland is limited to a few xenolith localities. One of these is a Tertiary monchiquite dyke (45.2 Ma; Faithfull *et al.,* 2012) that intrudes the Lewisian Gneiss Complex near Loch Roag on the Isle of Lewis (Fig. 6.1b). This dyke contains numerous xenoliths, xenocrysts and megacrysts from the lower crust and lithospheric upper mantle (Faithfull *et al.*, 2012). Previous detailed work has highlighted the metasomatised state of this region of lithospheric upper mantle (Upton *et al.*, 1983; 2011 Menzies *et al.*, 1987; Long *et al.*, 1991). Sr, Nd and Pb isotopic analyses of the spinel lherzolite and pyroxenite xenoliths suggest the presence of an old, stable keel below the Lewisian Gneiss Complex, which has been enriched over a period of 1000-1500 Myr in incompatible elements, particularly Ba, Rb, Sr, P and the LREE (Menzies *et al.*, 1987; Long *et al.*, 1991). Time-integrated Nd and Sr isotope systematics indicate a geochemical enrichment event at ca. 2.5-2 Ga, involving interaction with carbonatite (Long *et al.*, 1991). The only magmatic event known to have occurred within this time period is the intrusion of the Scourie Dykes, and thus the Loch Roag xenoliths may provide information about the source of these dykes.

6.3. Sampling and analytical methods

Samples were collected to include the picrite, olivine gabbro, and dolerite dyke varieties. In all, 50 samples were collected from 40 individual dykes for analysis of major and trace elements, and a representative selection of 25 samples were assayed for bulk rock PGE and gold (Appendix A.1). Most samples were collected from dyke centres to minimise effects of local crustal contamination, but some were also collected from dyke margins for comparison. The most common dolerite dykes were sampled from each of the three Lewisian Terranes, (39 samples from the Assynt Terrane, 9 from the Gruinard Terrane, and 6 from the Rhiconich Terrane; Fig. 6.1). The samples have been assigned to the dolerite, olivine gabbro, and picrite suites based on their petrology, mineralogy and geochemistry. The suite includes 4 olivine gabbro dyke samples, 6 picrites and 40 dolerite dykes.

Spinel lherzolite mantle xenolith samples from Loch Roag were provided by the British Geological Survey, including 4 rounded xenoliths approximately 3-6 cm in diameter. When cut, the peridotite xenoliths show mostly green alteration halos, with visible replacement-reaction textures in these areas. In some samples (e.g., LR80) a grey-black, relatively 'unaltered' central zone in the xenolith was cut out and analysed separately to its green halo. Overall these peridotite xenoliths are medium- to coarse-grained (crystals ranging 0.5-2 mm). Samples weighed at least 25-50 g (maximum available), to ensure that as large a sample as possible was homogenized for whole-rock geochemical analyses.

For the dyke samples, weathered material was removed from each sample before being crushed, split, and milled to a fine powder in an agate planetary ball mill at Cardiff University. Major and trace elements were analysed by inductively coupled plasma optical emission spectrometry (ICP-OES) and inductively coupled plasma mass spectrometry (ICP-MS), respectively, at Cardiff University using methods and instrumentation described by McDonald & Viljoen (2006). Samples were analysed for PGE and Au by Ni sulphide fire assay followed by tellurium co-precipitation and ICP-MS (Huber *et al.*, 2001; McDonald & Viljoen, 2006). Accuracy was constrained by analysis of the certified international reference materials TDB1 and WMG1 for PGE + Au, and JB1a for all other trace and major elements (see Appendix A.2). Precision was estimated by repeat analysis of a sub-set of samples (Appendix A.2). Representative data for each dyke suite are listed in Table 6.1. A full table of results is available in Appendix A.1.

For determination of rhenium-osmium abundances and isotopic composition, analyses were carried out at the TOTAL Laboratory at Durham University and follow the analytical procedures of Selby *et al.* (2009). Whole-rock powders were weighed and loaded into carius tubes with a known amount of spike solution (^{185}Re + ^{190}Os) together with 9 ml of inverse *aqua regia*. Tubes were sealed and heated to 220°C for 48 hours. $CHCl_3$ solvent extraction and micro-distillation isolated Os, and Re was separated using an anion exchange column and single-bead chromatography. Resulting Re and Os were loaded onto Ni and Pt filaments for isotopic analysis using negative-ion mass spectrometry on a Thermo Electron TRITON mass spectrometer. Results and uncertainties (2σ) are presented in Table 6.3, and model age equations in Appendix A.3.

6.4. Scourie Dyke Geochemistry

6.4.1. Major elements

All the analysed dykes contain < 53 wt.% SiO_2 and on an AFM diagram (Fig. 6.2a – anhydrous data plotted for all major element diagrams) they display an Fe-enriched tholeiitic trend. The total alkalis vs. silica (TAS) classification shows that most dykes fall within the basaltic field (Le Maitre *et al.*, 2002), with some overlap into the picrobasalt, trachybasalt and basaltic andesite fields (Fig. 6.2b) and unusually high SiO_2 contents in the picrites. Major element bivariant diagrams (anhydrous) plotted against MgO content (Figs. 6.2c-f) highlight clear separation between the dyke groups. These diagrams display considerable major element variability in the dolerites, particularly notable for Fe_2O_{3T}, CaO and TiO_2, due to fractional crystallisation of minerals such as olivine, pyroxenes, spinel and magnetite/ilmenite. The clustered Al_2O_3 composition (Fig. 6.2c) of the dolerites indicates little or no plagioclase fractionation took place in the magma, therefore the variation of CaO in the dolerites is a response to clinopyroxene fractionation. Variable K_2O content of dolerites, with no clear corresponding variation for Na_2O (Appendix A.1), is likely due to the mobility of these elements during metamorphism and alteration. The picrite and olivine gabbro suites have low TiO_2 (< 0.7 wt.% and < 2 wt.% in picrites and olivine gabbros respectively), and low Al_2O_3, Na_2O, CaO, Fe_2O_{3T} and P_2O_5 concentrations in comparison to the dolerite suite, but substantially higher MgO contents. Picrite dykes contain > 17 wt.% MgO, while olivine gabbro dykes contain 11-17 wt.% MgO (hydrous). While evidence of a fractional crystallisation trend is observed for the dolerites, the variability of major elements such as Fe_2O_{3T}, CaO and TiO_2 with MgO for picrites and olivine gabbros is less

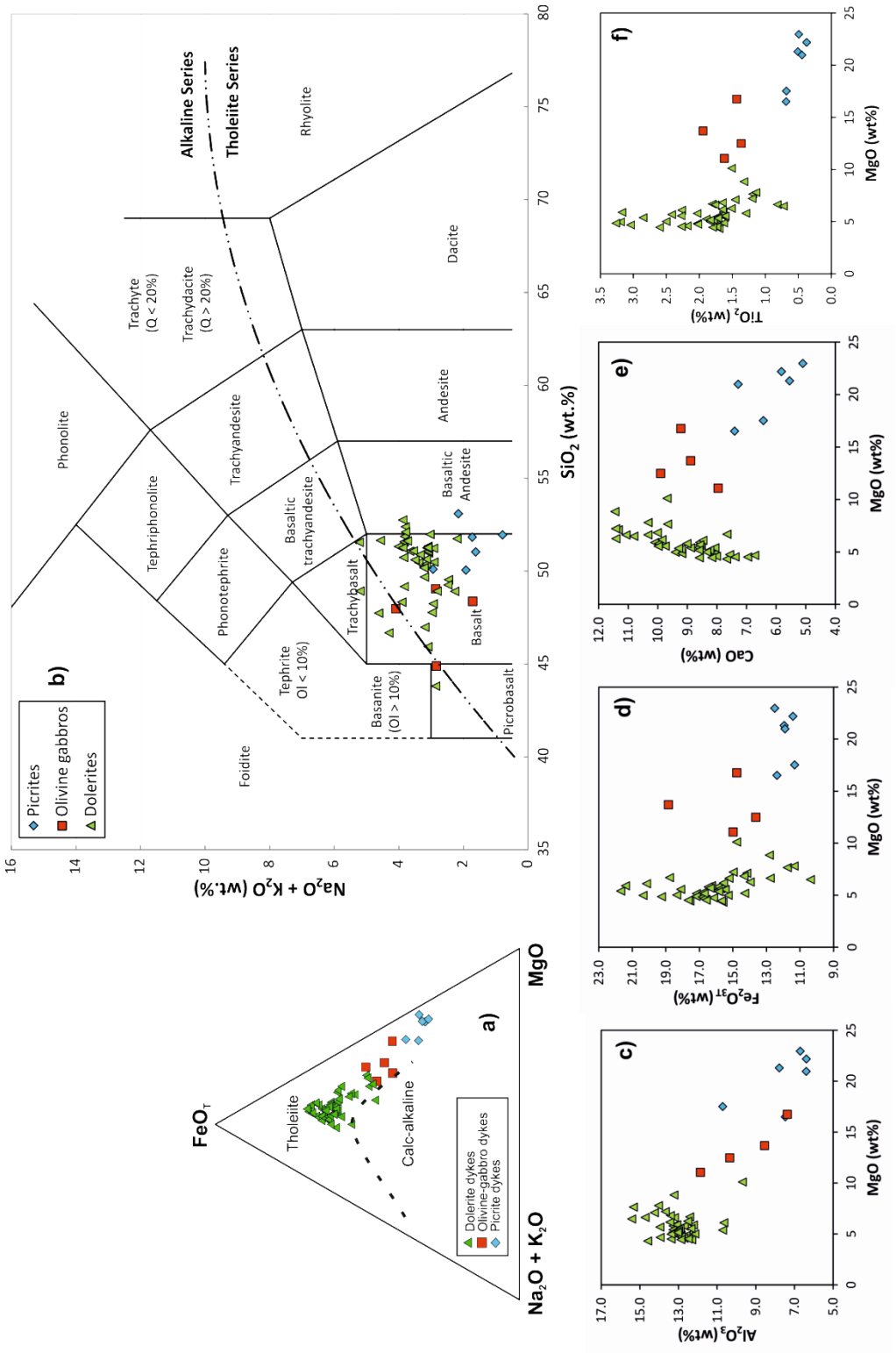

Figure 6.2. Major element plots (anhydrous). (a) AFM classification of Scourie Dyke Suite. Fe_2O_{3T} where $_T$ denotes total iron. FeO_T in AFM diagram was converted from analysed Fe_2O_{3T} (total iron). FeO for use in calculating Mg-number (Mg#) was calculated by assuming actual Fe2O3 (Fe_2O_3*) content = 1.5+TiO_2. Then, FeO = (Fe_2O_{3T} – Fe_2O_3*)/1.1. (b) Total alkali silica (TAS) classification diagram. (c) to (f) Major elements versus MgO (wt.%). Note that all major element abundances have been recalculated as anhydrous for use in diagrams of Figure 6.2. Concentrations cited in the main text are hydrous, for comparison to Table 6.1.

clearly related to fractionation, with the exception of Al_2O_3 for olivine gabbros, where plagioclase may have fractionated.

Despite some degree of mobility of K_2O and Na_2O during amphibolite facies metamorphism, picrites have < 3 wt.% total alkalis (Na_2O+K_2O), whilst the olivine gabbro and dolerite suites are considerably more variable with up to 5.2 wt.% Na_2O+K_2O. Loss on ignition (LOI wt.%) values do not vary systematically between dyke suites (see Table 6.1 and Appendix A.1) with most samples ranging from 0.25 to 3 wt.%. Finally, no systematic variation can be observed for the dolerite dyke group throughout the three Lewisian Terranes. Whole rock major element geochemical compositions of these samples do not vary according to the terrane in to which they were intruded.

6.4.2. Trace elements

All dyke suites are depleted in high field strength elements (HFSE). Mantle-normalised multi-element patterns (Fig. 6.3a-c) show a negative Nb-Ta anomaly, and the picrite suite also displays a trough at Ti (corresponding to TiO_2 < 1 wt.%). Most dolerite dykes have a positive Ti anomaly and show Th enrichment, but a small sub-group of dolerite dykes display negative Ti anomalies, and more pronounced negative Nb-Ta anomalies (Fig. 6.3c). Most of the olivine gabbro dykes do not display a trough for Ti in the multi-element diagram (Fig. 6.3b) corresponding to TiO_2 = 1-2 wt.%, but still show significant negative anomalies for Nb and Ta – a feature that could be reconciled by inferring Ti-magnetite accumulation. Rare dolerite dyke samples (e.g., X39 and X71) display very flat multi-element patterns. These samples have low to mid-range K_2O and Rb concentrations in comparison to other dolerite dykes, and coupled with their flat multi-element patterns (i.e., no Th enrichment, Nb-Ta-Ti trough) these may represent rare 'uncontaminated' asthenospheric magmas. However these dykes are also located in Laxfordian shear zones and show evidence of alteration textures as well as an increase in serpentine, talc or mica, indicating that they have been altered by fluids circulating in the shear zones.

All dyke suites are enriched in Th, LREE and LILE (Figures 6.3 and 6.4) and have slight positive Zr-Hf anomalies (Fig. 6.3). The Th and some LILE enrichment of Scourie Dykes (e.g., Rb and K) is in stark contrast to the whole-rock geochemistry of the Lewisian granulite-facies TTG of the Assynt terrane, which is notably depleted in these elements. However, the amphibolite-facies gneisses of terranes to the north and south are less depleted in these elements (Fig. 6.3d and

4a-b). Both amphibolite- and granulite-facies gneisses are more enriched in Ba (Fig. 6.4c) and Sr than the dykes (Table 6.1 and Appendix A.1).

All dyke suites display chondrite-normalised rare earth element (REE) patterns that are enriched in the light REE (LREE) (Fig. 6.3e-g), but the dolerite dykes are most enriched with concentrations of La up to 100 x chondrite values (Fig. 6.3g). The dolerite dykes have flatter middle REE (MREE) patterns, with no fractionation of the heavy REE (HREE), unlike that shown by the picrite and olivine gabbro suites. Overall, dolerites have the highest total REE concentrations. Picrites have the highest La/Sm ratio, while the olivine gabbro suite has the highest Gd/Yb. Variability in LREE of the olivine gabbros (Fig. 6.3f) could indicate fractionation of clinopyroxene. Picrites and olivine gabbros also have the highest Th/Yb ratios and olivine gabbros have the highest TiO_2/Yb ratios. Picrite dykes have the highest La/Nb and Ce/Sm ratios of all the dyke suites (Fig. 6.4d), but the olivine gabbro and dolerite suite are not distinguishable using these trace element ratios.

The different suites also have distinctive Co concentrations (up to 157 ppm and 72 ppm in picrites and dolerites respectively). MgO and Ni concentrations are positively correlated between the three dyke groups (Fig. 6.4e) reflecting the observed olivine content of these dykes. Similarly this is the case for Ni and Co (Fig 6.4f). However on close inspection, the dolerites tend to cluster (particularly for Co; Fig. 6.4f close-up) with no clear fractionation trend, suggesting little or no olivine fractionation within this suite. Further, there is a poor positive correlation (R^2 = 0.61) between Ni and Co for the olivine gabbro and picrite suites together. It is possible that the broad positive Ni-MgO and Ni-Co trends for the Scourie Dykes indicate control by olivine crystallisation (particularly in the picrites). Overall, the geochemical compositions of the three dyke suites signal that they are not cogenetic and cannot be related to one another by a simple fractionation trend from the same magma source. Instead these indicate at least two, magma sources (dolerites vs. picrites, while olivine gabbros may be related by fractionation to the dolerites). No systematic variation can be identified in the trace element abundances of dolerite dykes intruded into the three mainland Lewisian terranes.

Table 6.1. *(continued overleaf)*

Sample	X23	X25	X26	X27	X68	X10	X36	X37
	P.4.c	*P.4.c*	*P.4.c*	*P.4.m*	*P.10.c*	*OG.1.c*	*OG.5.c*	*OG.6.c*
Grid ref.	NC 1447 2256	NC 1451 2283	NC 1448 2283	NC 1487 2395	NC 0498 2710	NC 1548 4474	NC 1197 1590	NC 0741 2105
	(wt.%)							
SiO_2	49.63	47.43	50.25	52.5	50.46	47.64	47.97	45.27
Al_2O_3	10.61	7.23	6.19	7.39	6.21	7.26	11.86	8.62
Fe_2O_3*	11.21	11.1	11.07	12.23	11.55	14.54	14.98	19
MgO	17.36	19.81	21.52	16.34	20.38	16.51	11.07	13.82
CaO	6.37	5.16	5.64	7.32	7.07	9.08	7.96	8.96
Na_2O	2.22	0.47	1.22	1.37	0.76	1.56	3.32	2.34
K_2O	0.69	1.03	0.46	0.76	0	0.12	0.77	0.52
TiO_2	0.67	0.47	0.36	0.68	0.43	1.41	1.62	1.96
MnO	0.16	0.15	0.17	0.19	0.19	0.22	0.2	0.23
P_2O_5	0.11	0.07	0.05	0.1	0.05	0.12	0.21	0.11
LOI	2.06	6.88	2.54	1.18	2.07	0.62	0.36	0.25
Total	101.09	99.8	99.46	100.04	99.18	99.09	100.32	101.07
Mg#	0.79	0.81	0.82	0.76	0.81	0.74	0.65	0.64
	(ppm)							
Sc	19	18	19	25	23	28	25	30
V	176	146	132	218	162	255	304	435
Cr	1918	3891	4432	2823	2949	1689	910	1294
Co	114	142	157	93	87	129	85	142
Ni	1261	1474	1587	909	1209	1213	709	844
Cu	112	167	54	42	66	139	122	131
Rb	22	31	12	22	1	1	18	12
Sr	258	109	155	78	12	135	332	200
Y	14	10	9	15	10	15	23	20
Zr	73	70	55	81	53	80	182	109
Nb	3.1	2.9	1.6	3.7	1.4	6.3	7.7	5
Ba	366	174	315	239	1	73	266	175
La	13.87	10.78	8.43	14.02	7.34	9.34	15.93	9.79
Ce	28.58	21.75	17.27	30.45	15.36	23.66	35.62	23.22
Pr	3.76	2.84	2.23	3.97	2.12	3.64	5.12	3.53
Nd	14.11	10.3	8.42	14.65	8.27	15.4	21.81	15.76
Sm	2.8	2	1.68	2.88	2	3.74	5.63	4.19
Eu	0.8	0.62	0.52	0.75	0.45	1.08	1.5	1.19
Gd	2.41	1.83	1.54	2.62	1.69	3.21	4.59	3.63
Tb	0.38	0.27	0.24	0.42	0.27	0.51	0.73	0.61
Dy	2.15	1.6	1.37	2.44	1.65	2.79	4.12	3.5
Ho	0.42	0.31	0.27	0.48	0.33	0.52	0.76	0.64
Er	1.2	0.91	0.81	1.38	0.95	1.41	2.04	1.75
Tm	0.18	0.13	0.11	0.2	0.13	0.19	0.26	0.23
Yb	1.15	0.88	0.75	1.23	0.88	1.15	1.59	1.44
Lu	0.17	0.13	0.11	0.19	0.14	0.17	0.27	0.23
Hf	1.66	1.85	1.18	1.89	1.21	2.4	4.45	3.31
Ta	0.21	0.21	0.09	0.19	0.11	0.46	0.49	0.28
Th	1.66	1.42	1.22	2.58	1.2	1.25	2.9	1.15
U	0.35	0.28	0.21	0.6	0.29	0.31	0.37	0.24
	(ppb)							
Os	0.59	0.95	1.26	0.36	0.43	0.42	1.44	1.53
Ir	0.71	1.12	1.23	0.68	1.01	1.4	1.75	2.53
Ru	1.95	3.33	3.46	2.01	2.56	2.13	2.39	3.47
Rh	0.59	0.88	1.38	0.62	0.97	0.92	0.81	1.09
Pt	1.89	2.78	4.17	5.61	5.59	8.38	6.91	9.2
Pd	2.65	1.83	3.13	2.86	4.92	8.31	5.85	7.9
Au	1.23	12.31	1.17	1.43	0.82	3.26	1.5	2.17
Cu/Pd	42.4	90.9	17.4	14.7	13.5	16.7	20.9	16.6
Pd/Ir	3.7	1.6	2.5	4.2	4.9	5.9	3.3	3.1

Table 6.1. *(continued overleaf)*

Sample	X52	X8	X12	X28	X31	X33	X34	X35
	OG.7.c	*D.1.c*	*D.3.c*	*D.4.c*	*D.4.c*	*D.5.c*	*D.5.c*	*D.5.c*
Grid ref.	NG 9602 9276	NC 1473 4488	NC 1637 4872	NC 1698 2581	NC 1717 2602	NC 1197 1605	NC 1197 1605	NC 1201 1606
SiO_2	48.1	43.43	48.55	51.12	51.07	50.59	50.3	50.41
Al_2O_3	10.14	12.12	10.57	15.13	12.86	12.83	12.88	12.94
Fe_2O_3*	13.37	21.21	20	10.17	17.19	15.63	16.51	16.84
MgO	12.25	5.85	6.07	6.37	4.89	5.27	5.1	5.28
CaO	9.71	10.01	8.41	10.6	8.23	9.17	8.5	9.23
Na_2O	2.52	2.43	2.02	3.07	3	2.4	2.57	2.54
K_2O	0.28	0.4	0.77	0.65	0.66	0.66	0.73	0.7
TiO_2	1.34	3.14	2.25	0.71	1.63	1.7	1.82	1.9
MnO	0.21	0.28	0.35	0.18	0.27	0.24	0.24	0.24
P_2O_5	0.12	0.22	0.24	0.07	0.18	0.17	0.17	0.2
LOI	1.44	0.31	1	0.99	0.77	0.31	0.43	0.31
Total	99.49	99.41	100.23	99.06	100.73	98.97	99.25	100.58
Mg#	0.7	0.41	0.42	0.61	0.41	0.46	0.43	0.44
Sc	25	50	50	32	38	42	40	42
V	297	566	559	250	410	450	388	429
Cr	965	33	106	320	56	160	126	151
Co	69	59	59	48	60	59	51	54
Ni	801	70	115	161	99	93	77	89
Cu	90	88	57	56	164	196	149	185
Rb	4	10	25	6	15	19	19	21
Sr	199	149	169	339	218	173	175	166
Y	17	35	45	20	37	41	39	43
Zr	93	115	151	65	153	174	131	188
Nb	2.7	7.6	11.7	3.5	7.8	7.9	7.8	8.6
Ba	92	123	190	261	159	227	249	255
La	4.43	9.23	11.76	12.92	12	15.15	14.42	17.03
Ce	12.79	22.63	27.77	29.31	27.41	34.16	32.67	38.35
Pr	2.13	3.58	4.44	4.08	4.04	4.95	4.83	5.65
Nd	10.54	16.16	19.8	15.72	17.66	21.07	20.53	23.54
Sm	3.43	4.62	5.39	3.29	4.83	5.27	5.6	6.07
Eu	1.04	1.52	1.68	1.13	1.52	1.49	1.49	1.56
Gd	2.93	4.72	5.73	3.1	4.74	5.42	5.24	5.81
Tb	0.51	0.87	1.04	0.51	0.87	0.96	0.92	1.03
Dy	2.97	5.54	6.79	3.15	5.67	6.1	6.19	6.67
Ho	0.56	1.14	1.42	0.64	1.15	1.28	1.25	1.34
Er	1.49	3.38	4.29	1.85	3.44	3.8	3.72	4.03
Tm	0.2	0.49	0.61	0.27	0.48	0.57	0.54	0.58
Yb	1.27	3.08	4.08	1.84	3.38	3.87	3.58	3.92
Lu	0.18	0.5	0.66	0.28	0.51	0.59	0.59	0.64
Hf	2.71	3.1	4.02	1.53	3.79	4.15	3.6	4.82
Ta	0.21	0.41	1.05	0.22	0.49	0.44	0.37	0.44
Th	1.08	1.09	1.34	0.39	1.79	2.12	1.96	2.31
U	0.18	0.26	1.25	0.12	0.35	0.52	0.56	0.6
Os	0.96	0.06	0.06	0.07	0.05	0.09	0.05	0.04
Ir	1.36	0.22	0.07	0.14	0.07	0.08	0.08	0.05
Ru	2.13	0.43	0.14	0.57	0.11	0.18	0.13	0.27
Rh	0.67	0.36	0.11	0.24	0.1	0.23	0.28	0.22
Pt	9.81	2.11	0.7	2.99	0.92	3.58	5.42	3.3
Pd	6.24	1.33	0.57	3.56	0.78	2.73	4.96	3.31
Au	1.7	1.2	1.75	2.12	0.7	1.06	1.42	1.01
Cu/Pd	14.4	66.4	100	15.6	209.7	71.9	30.1	55.7
Pd/Ir	4.6	5.9	7.7	24.9	11.5	34.6	63.1	73.5

Table 6.1. Scourie Dyke major and trace element whole-rock analyses for a representative selection of picrite, olivine gabbro, and dolerite dykes suites. Sample code: P (picrite), OG (olivine gabbro), D (dolerite), c (dyke centre) and m (dyke margin). Numbers 1 to 10 correspond to approximate locations marked on Figure 6.1. Totals are those from oxides with 4 decimal places, displayed to 2 decimal places.

Sample	**X39** *D.6.c*	**X40** *D.2.m*	**X44** *D.7.c*	**X50** *D.7.c*	**X53** *D.8.c*	**X58** *D.9.c*	**X69** *D.10.c*	**X71** *D.10.c*
Grid ref.	NC 0820 2057	NC 1455 4161	NG 9867 9240	NG 9552 9044	NC 2481 4691	NC 2409 4979	NC 0498 2712	NC 0593 2510
SiO_2	47.92	51.13	50.05	51.94	50.67	52.05	49.38	48.01
Al_2O_3	12.31	13.13	9.57	12.56	13.06	12.76	13.23	13.43
Fe_2O_3*	18.61	15.83	14.6	14.02	14.05	16.04	15.26	14.7
MgO	6.64	5.39	10	6.3	5.09	4.72	6.64	7.08
CaO	7.6	8.86	9.57	11.45	8.1	7.52	11.1	11.21
Na_2O	3.16	2.43	2.39	1.8	3.42	2.74	1.69	1.8
K_2O	0.71	0.69	0.72	0.4	1.71	1.03	0.78	0.42
TiO_2	1.79	1.75	1.49	1.52	1.75	2.01	1.77	1.18
MnO	0.28	0.23	0.22	0.22	0.25	0.23	0.23	0.22
P_2O_5	0.11	0.29	0.18	0.13	0.16	0.22	0.14	0.08
LOI	1.96	0.7	1.46	0.89	1	2.04	0.66	0.93
Total	101.09	100.44	100.26	101.23	99.27	101.37	100.89	99.07
Mg#	0.46	0.46	0.63	0.53	0.48	0.43	0.52	0.54
Sc	48	37	24	42	38	36	41	41
V	556	341	234	444	325	460	353	326
Cr	186	61	837	58	24	19	62	129
Co	68	48	73	57	45	45	49	53
Ni	93	261	323	85	55	23	83	129
Cu	1055	125	143	314	103	45	127	119
Rb	15	7	19	5	61	26	9	3
Sr	132	262	271	141	316	148	199	169
Y	31	34	32	31	31	37	22	24
Zr	93	183	256	96	161	161	91	68
Nb	4.4	8.3	16.5	5.8	12.8	6.6	8.9	3.7
Ba	168	240	322	79	302	147	253	115
La	5.34	22.67	24.38	9.1	13.71	12.06	9.84	3.65
Ce	13.83	49.13	54.09	20.77	31.58	26.48	23.18	9.6
Pr	2.31	6.85	7.67	3.12	4.52	3.7	3.46	1.61
Nd	11.13	27.5	30.69	13.26	18.82	15.41	14.82	7.81
Sm	3.62	6.34	7.16	3.95	4.82	4.4	3.91	2.71
Eu	1.1	1.6	1.62	1.06	1.27	1.23	1.17	0.85
Gd	3.74	5.36	6.26	3.76	4.12	4.36	3.32	2.64
Tb	0.72	0.86	0.96	0.67	0.72	0.84	0.56	0.52
Dy	4.86	5.19	5.53	4.39	4.45	5.45	3.47	3.64
Ho	1.02	1.04	1.06	0.91	0.93	1.14	0.68	0.77
Er	2.92	3.06	2.99	2.74	2.76	3.49	1.97	2.33
Tm	0.43	0.43	0.41	0.39	0.4	0.51	0.28	0.34
Yb	2.84	2.89	2.62	2.63	2.69	3.48	1.81	2.31
Lu	0.49	0.47	0.41	0.43	0.42	0.53	0.28	0.36
Hf	2.49	4.49	6.12	2.95	3.71	4.09	2.62	1.72
Ta	0.27	0.44	0.85	0.33	0.71	0.38	0.53	0.19
Th	0.82	2.93	3.81	1.24	2	2.49	1.14	0.38
U	0.25	0.67	1.27	0.34	0.7	1.84	0.3	0.09
Os	0.05	0.05	0.07	0.06	0.09	0.1	0.06	0.04
Ir	0.07	0.06	0.27	0.08	0.09	0.09	0.11	0.06
Ru	0.16	0.13	0.64	0.29	0.25	0.27	0.28	0.17
Rh	0.41	0.15	0.18	0.57	0.26	0.13	0.57	0.58
Pt	2.3	1.9	2.31	5.73	7.61	2.45	11.55	8.58
Pd	3.27	1.48	2.21	5.94	9.31	1.64	10.98	12.18
Au	1.45	1.45	0.61	3.48	1.06	0.68	3.7	6.02
Cu/Pd	322.9	84.4	64.6	52.9	11.1	27.7	11.5	9.8
Pd/Ir	44	26.9	8.3	74.7	105.7	18.3	96.3	221.3

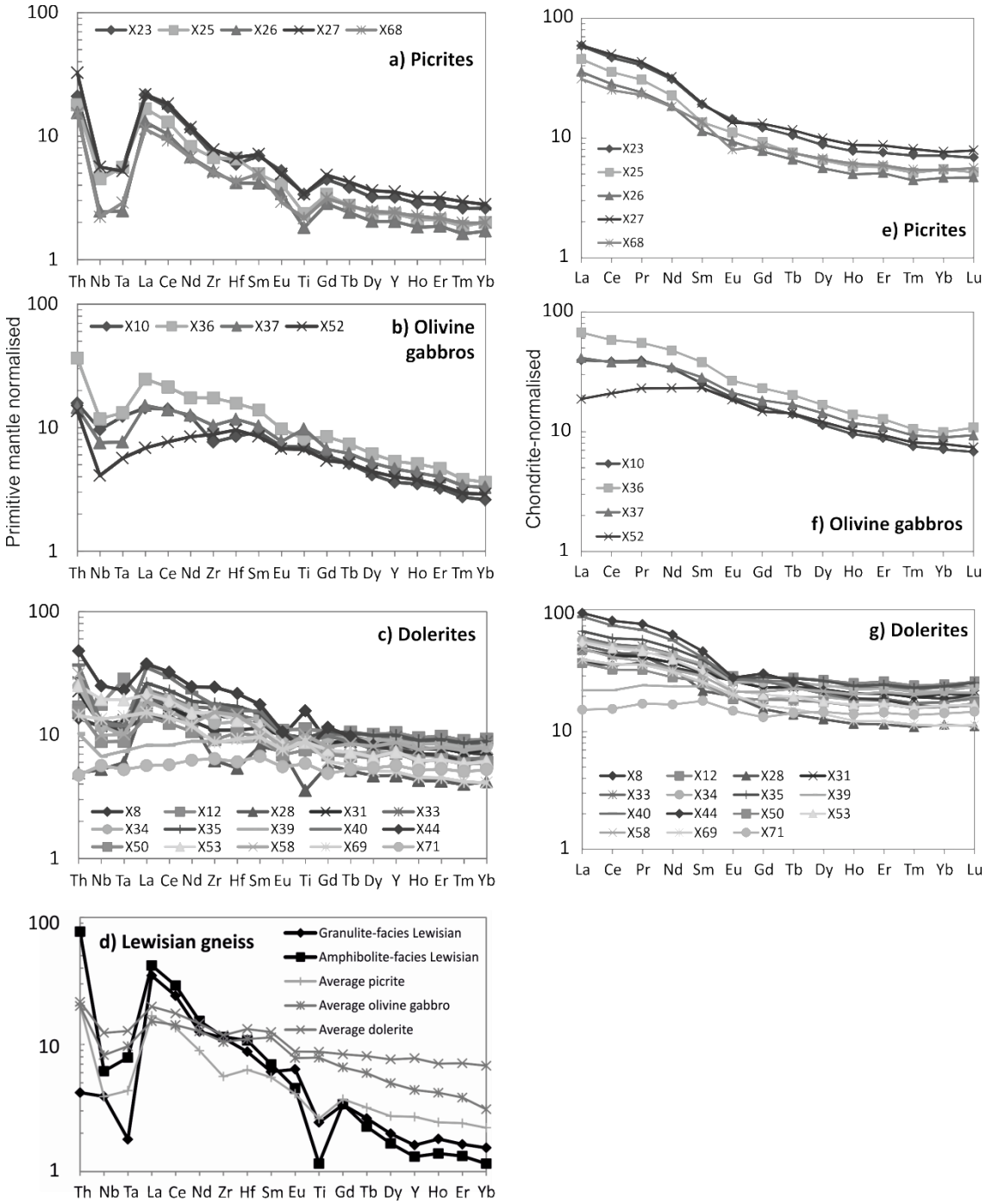

Figure 6.3. (a) to (c) Multi-element normalised diagrams for each dyke suite. Plots are primitive mantle normalised (McDonough & Sun, 1995). (d) Comparison plot with Rollinson (2012) average granulite- and amphibolite-facies gneiss. (e) to (g) Chondrite-normalised (McDonough & Sun, 1995) rare earth element multi-element diagrams per dyke suite.

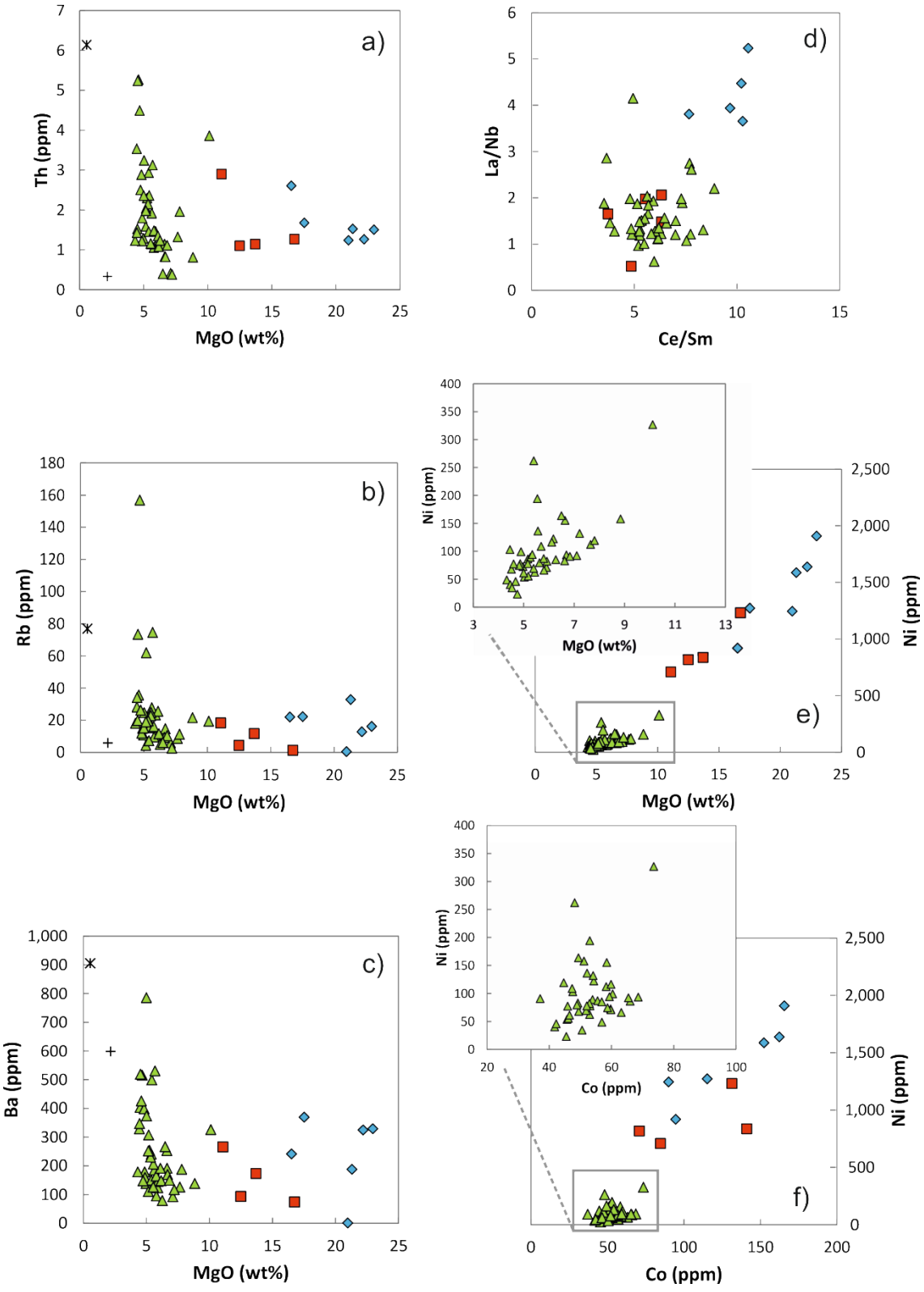

Figure 6.4. Trace element plots. (a) Th-MgO and (b) Rb-MgO showing LILE enrichment of Scourie Dyke Suite relative to granulite-facies Lewisian TTG (plus sign) except for (c) Ba-MgO. Amphibolite-facies Lewisian gneiss also shown for reference (star). All Lewisian gneiss data is averaged from Rollinson (2012). (d) La/Nb – Ce/Sm bivariant plot to assess garnet-bearing component of source for the dyke suites. (e) and (f) show Ni and Co vs. MgO (anhydrous, wt.%). Inset plots for both (e) and (f) are close-up views for dolerite dyke data only.

Total PGE+Au concentrations range from 38.3 ppb (olivine gabbro) to 2.7 ppb (dolerite). All dyke suites display fractionated chondrite-normalised PGE profiles (Fig. 6.5a-d) enriched in palladium-group PGE (PPGE) and the dolerite suite has notable iridium-group PGE (IPGE) depletion. The picrite and olivine gabbro dykes have relatively flat PGE+Au patterns, although these are still slightly fractionated. The picrite and olivine gabbro suites have significantly higher concentrations of Ni, Cr and Co than the dolerites, whilst Cu concentration varies widely across and within the dyke suites. This variation in Cu is predominantly due to its fractionation as an incompatible element in silicate magma.

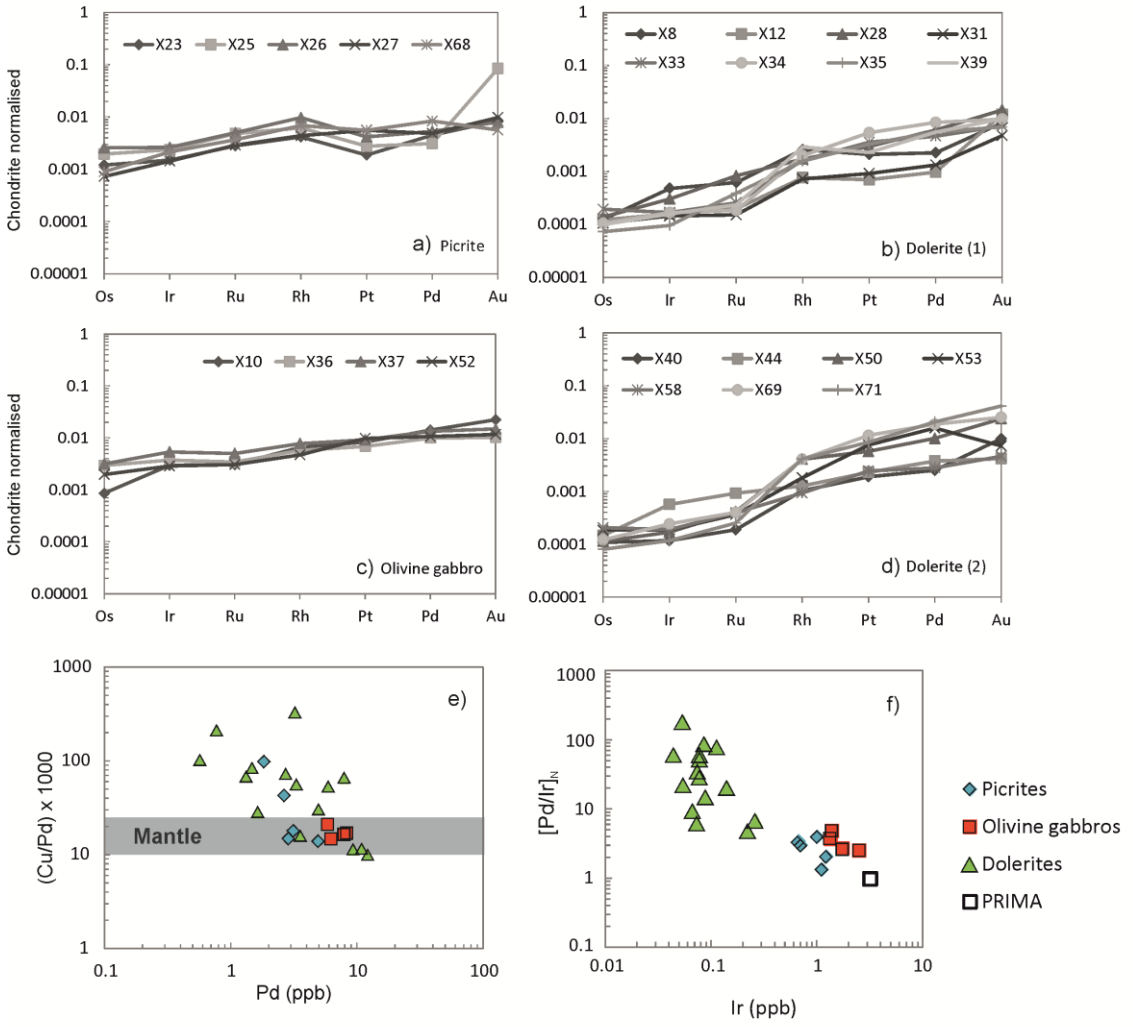

Figure 6.5. (a) to (d) Platinum-group element multi-element plots (chondrite normalised using McDonough & Sun, 1995) for picrite dykes, olivine gabbros, and dolerite dykes. (e) and (f) Platinum-group element bivariant plots. Grey area in (e) indicate typical mantle ratios for Cu/Pd. (f) $[Pd/Ir]_N$ is chondrite-normalised Pd/Ir ratio. PRIMA is typical $[Pd/Ir]_N$ for primitive mantle (McDonough & Sun, 1995).

Chalcophile element ratios, such as Cu/Pd, are typically higher than primitive mantle ratios. There is little consistent variation in Cu/Pd between dyke suites, although olivine gabbros tend to have the most primitive values (Fig. 6.5e). $[Pd/Ir]_N$ ratios from all the dyke suites are higher than typical mantle values (PRIMA (primitive mantle) ~ 0.97) and those from dolerite dykes are significantly higher than those in both picrites and olivine gabbro dykes (Fig. 6.5f). There is no correlation between dyke alteration (using Alteration Index = $(K_2O+MgO)/(Na_2O+K_2O+CaO+MgO)*100$ (Ishikawa *et al.*, 1976), LOI wt.%, and extent of amphibolitisation as a qualitative proxy) and PGE concentrations, suggesting that PGE were immobile during alteration and metamorphism and that variation in PGE geochemistry between dykes is a primary feature (Appendix A.2).

6.5. Mantle Xenolith Petrology and Geochemistry

The Loch Roag spinel lherzolite mantle xenoliths consist of olivine, clinopyroxene, orthopyroxene and spinel, with accessory sulphides (mostly chalcopyrite, with some pentlandite). A Pt-sulphide grain (~ 3 µm diameter) has been observed at the margin of a chalcopyrite droplet in LR80. Major silicate mineral phases are equigranular, with minor interstitial Fe-Ni-Cu sulphides (generally up to 150 µm diameter). Samples are generally fresh, with fresh olivine throughout (particularly in the grey centres – e.g., sample LR80). On the outer rims of the xenoliths, a green rim of partial alteration is observed (generally 2-5 mm in width), in which replacement reaction textures are more prevalent, and sulphides tend to be absent, but there are rounded baryte-filled vugs. In sample LR80, this outer green material was easily removed, and thus the powdered sample was the most pristine (thus used for trace element geochemical modelling later in the paper). For more detailed descriptions of these samples, and their mineral chemistry, see Upton *et al.* (2011) and references therein.

Table 6.2 shows the first whole-rock geochemical analyses of the Loch Roag peridotite xenoliths. Their MgO contents (anhydrous) vary from 36.7 to 39.4 wt.% (comparable to primitive mantle composition; McDonough & Sun, 1995). Fe_2O_{3T} is slightly elevated in comparison to primitive mantle, ranging from 10.3 to 11.9 wt.% (anhydrous), but Al_2O_3 (1.1 – 2.5 wt.%) and CaO (2.3 – 2.7 wt.%) are lower than primitive mantle and Ti is significantly depleted, (only 13 to 30 % of Ti in primitive mantle). This depletion in CaO and Al_2O_3 may indicate partial melting and depletion of the mantle (by initial melting of clinopyroxene), which was subsequently re-enriched. But this would have caused an increase in MgO above primitive

mantle levels which is not observed in these xenoliths, and coupled with their abundant clinopyroxene, makes this an unlikely scenario.

Nb and Ta, Zr and Hf, and Ti show negative anomalies (Fig. 6.6a) when normalised to primitive mantle, however Nb and Ta are not depleted below primitive mantle concentrations (i.e., not < 1 when normalised). HREE are not depleted either, but show flat trends similar to primitive mantle concentrations. Zr, Hf and Ti are however < 1 on Figure 6.6a. In contrast, Th and the LREE and MREE are markedly enriched to levels many tens of times more abundant than in primitive mantle (Fig. 6.6a). Chondrite normalised REE patterns (Fig. 6.6b) show a consistent negative Eu anomaly, or positive Gd anomaly. PGE and Au analyses indicate that the lithospheric mantle below this region of NW Scotland is fertile for these elements. Primitive mantle estimates for Au and Pd are 1 and 3.9 ppb, respectively (McDonough & Sun, 1995), but the Loch Roag xenoliths contain 2.0 – 3.3 ppb Au, and 4.7 – 11.5 ppb Pd. Pt is also elevated (11 – 16.9 ppb, compared with 7 ppb for primitive mantle) suggesting that the PGE and Au underwent enrichment, in addition to Th, LILE and LREE. Finally the IPGE occur in concentrations comparable to primitive mantle, with Ir concentrations ranging from 2.9 to 3.6 ppb. This gives a slightly positive trend to the PGE+Au multi-element diagram (Figure 6.6c), with enrichment in PPGE, but no depletion in IPGE.

6.6. Re-Os isotopes

Three whole-rock samples were analysed for Re and Os abundances and isotopic composition. This included two Scourie Dykes (X8 – the dolerite 'Graveyard dyke'; and X23 – a picrite dyke from the north shore of Loch an Leathaid) and the freshest spinel lherzolite xenolith sample from Loch Roag (LR80). Results are displayed in Table 6.3, and calculated parameters include Os_i (initial $^{187}Os/^{188}Os$), γOs (calculated from the initial $^{187}Os/^{188}Os$ and $^{187}Re/^{188}Os$ ratios), T_{MA} (model age using Re/Os and assumed chondritic initial values), T_{RD} (Re-depletion Os model age assuming all Re is metasomatic) and T_{RD}^{erupt} (Re-depletion model eruption age assuming all Re is metasomatic and calculated prior to the time of eruption). In Table 6.3, *Age are based on various published geochronology sources for the age of eruption (see caption). For further details, refer to the Appendix. X8 and X23 were analysed for comparison to earlier data collected by Frick (1998), in the light of new Re-Os methodologies and modern dating of the Scourie Dykes (Davies & Heaman, 2014). LR80 was run as an unknown sample, with no previous Re-Os data for the Loch Roag mantle xenoliths available in the literature.

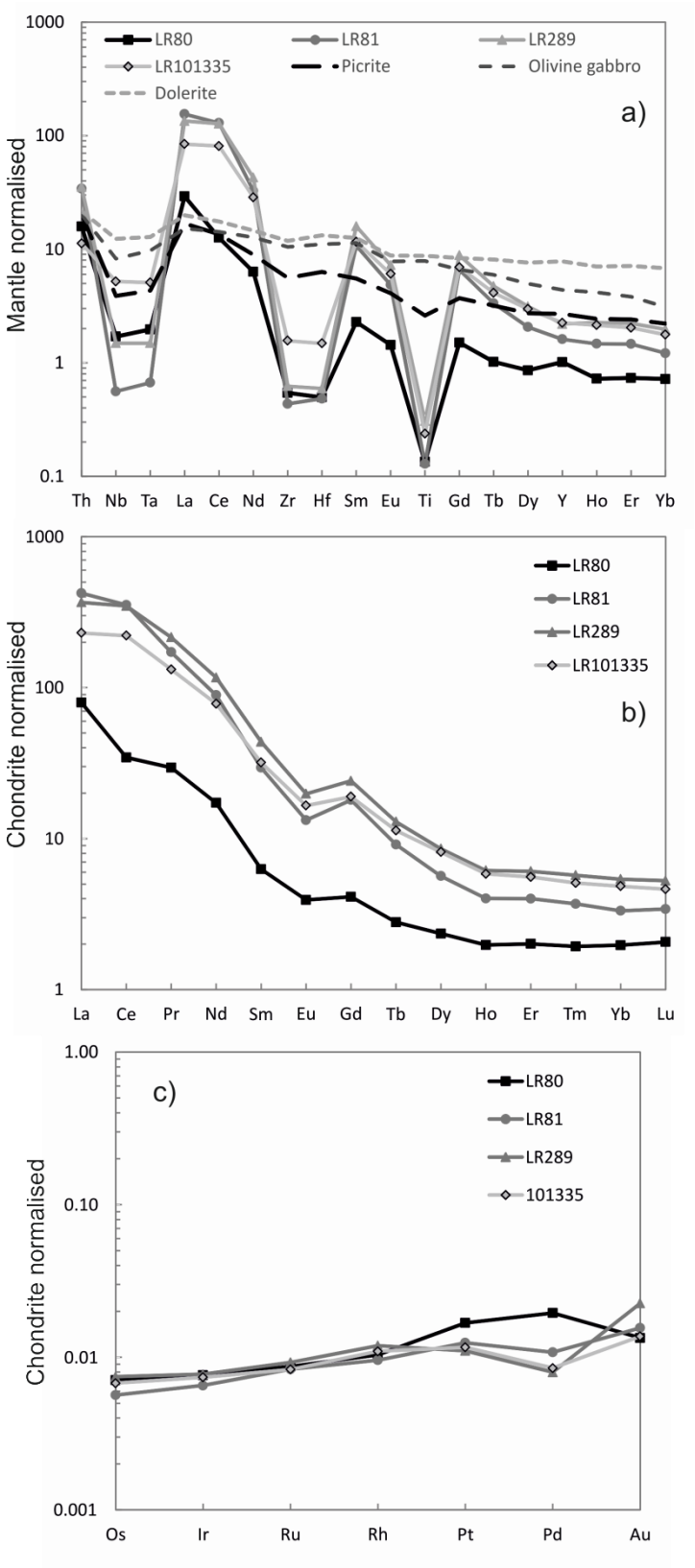

Figure 6.6. Loch Roag multi-element diagrams: (a) primitive mantle normalised trace element multi-element diagram, (b) REE chondrite-normalised plot, and (c) chondrite-normalised PGE+Au plot.

Table 6.2. Loch Roag major and trace element whole-rock analyses.

Sample	LR80	LR81	LR289	LR101335
	(wt.%)			
SiO_2	45.33	45.34	43.97	42.85
Al_2O_3	1.59	2.4	1.89	1.06
Fe_2O_3*	10.2	10.12	10.05	11.48
MgO	38.71	35.78	37.04	38.16
CaO	2.22	2.54	2.53	2.61
Na_2O	0.44	0.46	0.3	0.16
K_2O	0.09	0.54	0.11	0.03
TiO_2	0.03	0.03	0.06	0.05
MnO	0.13	0.16	0.17	0.25
P_2O_5	0.04	0.15	0.12	0.22
LOI (%)	0.92	3.25	3.29	2.37
Total	99.7	100.78	99.53	99.23
	(ppm)			
Sc	12	13	12	9
V	47	60	48	37
Cr	2427	2935	3047	2607
Co	104	112	132	131
Ni	2117	1743	2015	2331
Cu	175	90	101	66
Rb	2	6	3	1
Sr	28	256	250	94
Y	4	7	9	10
Zr	6	5	7	16
Nb	1.1	0.4	1	3.4
Ba	13	48	38	26
La	18.91	100.23	87.14	54.65
Ce	21.13	216.44	213.27	135.63
Pr	2.74	15.96	20.02	12.26
Nd	7.89	40.74	53.41	35.78
Sm	0.93	4.36	6.47	4.72
Eu	0.22	0.75	1.12	0.93
Gd	0.82	3.59	4.8	3.78
Tb	0.1	0.33	0.47	0.41
Dy	0.58	1.39	2.11	2
Ho	0.11	0.22	0.34	0.32
Er	0.32	0.64	0.97	0.89
Tm	0.05	0.09	0.14	0.13
Yb	0.32	0.54	0.87	0.78
Lu	0.05	0.08	0.13	0.11
Hf	0.14	0.14	0.17	0.42
Ta	0.07	0.02	0.06	0.19
Th	1.26	2.71	2.81	0.89
U	0.33	0.73	1.02	0.24
	(ppb)			
Os	3.45	2.75	3.63	3.29
Ir	3.6	3.08	3.64	3.48
Ru	6.03	5.79	6.41	5.77
Rh	1.47	1.35	1.68	1.54
Pt	16.88	12.52	11.07	11.69
Pd	11.48	6.35	4.7	5
Au	1.96	2.28	3.3	2

Table 6.3. Re-Os isotope data (whole-rock) for dolerite dyke (X8 – 'the Graveyard Dyke'), picrite dyke (X23) and Loch Roag spinel lherzolite xenolith (LR80). Calculated parameters include Os_i (initial $^{187}Os/^{188}Os$), γOs (calculated from the initial $^{187}Os/^{188}Os$ and $^{187}Re/^{188}Os$ ratios), T_{MA} (model age using Re/Os and assumed chondritic initial values), T_{RD} (Re-depletion Os model age assuming all Re is metasomatic) and T_{RD}^{erupt} (Re-depletion model eruption age assuming all Re is metasomatic and calculated prior to the time of eruption). In Table 6.3, $^{187}Os/^{188}Os$ initial (Os_i) is calculated from eruption ages as indicated (*Age). *Age are based on various published geochronology sources for the age of eruption. Note that dykes ages from U-Pb isotopic ages from Davies & Heaman (2014) for X8 (Graveyard Dyke) and X23 (Cnoc an Leathaid). Eruption age of LR80 based on $^{40}Ar/^{39}Ar$ date (Faithfull *et al.,* 2012). All uncertainties reported to 2 s.d. level, all data are blank corrected. Blanks for Re and Os are 1.3pg and 0.1pg respectively, and mean $^{187}Os/^{188}Os$ of 0.173. For model age equations, refer to Appendix A.3.

Sample / Batch	**Rock type**	**Re** (ppb) total	±	**Os** (ppt) total	±	$^{187}Re/^{188}Os$	±	$^{187}Os/^{188}Os$	±	**rho**	Os_i	**γOs**	***Age** (Myr)	T_{MA} (Myr)	T_{RD} (Myr)	T_{RD}^{erupt} (Myr)
X8 / RO538-7	Dolerite dyke	3.42	0.02	108.3	5.5	1784.8	135.1	82.3096	7.0381	0.882	9.731	8655.01	2391.7	2702	-	-
X23 / RO538-9	Picrite dyke	0.4	0.01	1089.9	19.5	1.8	0.1	0.1767	0.01	0.566	0.103	-7.24	2418	2080	-7307	3505
LR80 / RO538-8	Spinel lherzolite xenolith	0.51	0.01	1755.2	31.2	1.4	0.1	0.1278	0.0072	0.609	0.127	-0.94	45.2	-28	66	217

For the two dykes, X8 has significantly higher Re and Os abundances than X23 (3.4 vs 0.4 ppb and 1090 vs. 108 ppt, respectively). Therefore X8 has high $^{187}Re/^{188}Os$ and very radiogenic Os_i and γOs, suggesting significant disturbance of the isotopic system, post-intrusion. This is comparable to previous measurements of the 'Graveyard dyke' by Frick (1998). In contrast picrite dyke X23 has γOs = -6.73 and Os_i = 0.104 (lower than the predicted mantle range of 0.11 – 0.50 at 2400 Ma), and its $^{187}Re/^{188}Os$ and $^{187}Os/^{188}Os$ are within the range of results by Frick (1998).

The Os_i (0.127) and γOs (-0.94) of xenolith LR80 has been calculated at 45.2 Ma, based on the age of the host dyke at Loch Roag (Faithfull *et al.,* 2012). However, Long *et al.* (1991) used time integrated Nd-isotopes to suggest there was a major metasomatic event between 2.3 – 2.5 Ga and 1.0 – 1.5 Ga. If we recalculate $Os_{initial}$ for LR80 at 2.4 Ga, this is 0.07 – a result too unradiogenic for mantle at that time, and suggesting that the Re-Os system has been disturbed slightly.

6.7. Discussion

The geochemistry of the mafic and ultramafic rocks of the Scourie Dyke swarm fits with structural and metamorphic observations, and the commonly accepted view that these magmas were derived from the mantle during extension (Tarney & Weaver, 1987; Bridgwater *et al.*, 1995; Park, 1995), and intruded into the Lewisian lower to middle crust. On the basis of the new geochemical data several further inferences can be made about the mantle sources of these dykes and the mantle beneath the Lewisian gneiss Complex at the time of their formation.

6.7.1. Dyke composition in relation to Lewisian terrane

Although the compositions of the doleritic Scourie Dyke swarm are variable, no systematic geochemical difference was observed across the three Lewisian terranes (Rhiconich, Assynt and Gruinard). Picrite and olivine gabbro dykes are rare in the granulite facies Assynt Terrane, and absent in the amphibolite facies Gruinard and Rhiconich Terranes to the south and north. This may be due to the depth of current erosion levels across the Lewisian terranes. The granulite-facies Assynt Terrane is considered to represent the lower crust (Park & Tarney, 1987), while the amphibolite-facies terranes represent mid-crustal levels. The absence of picrite and olivine gabbro dykes from the amphibolite-facies terranes might imply that these more MgO-rich magmas did not ascend as high into the crust, becoming trapped in lower

crustal regions. Their elevated MgO contents imply their parental magmas were considerably denser than the dolerite dyke magmas, restricting their ascent. In addition, the homogeneity of the dolerite dyke suite across the three Lewisian terranes suggests that these Lewisian blocks had been accreted onto each other before dyke intrusion, confirming the conclusions of Goodenough *et al.* (2010), and supporting those of Davies and Heaman (2014). However this excludes the dykes at Shieldaig near Gairloch, which occur south of the Loch Maree Group (itself accreted in an arc setting after c. 1900 Ma; Park, 2002).

6.7.2 Mantle melting regime – evidence of crustal contamination or SCLM melting?

The ultimate mantle source of the Scourie Dyke magmas could potentially be either the convecting asthenosphere or the subcontinental lithospheric mantle. Enriched LREE patterns and trace element ratios indicate that dyke suites were derived from a mantle source with significantly higher LILE concentrations than the Lewisian TTG of the Assynt terrane (Rollinson, 2012). The high La/Sm ratio of picrite dykes in particular is suggestive of a relatively enriched mantle source, while the high Gd/Yb of olivine gabbros and picrites (relative to the dolerite suite) could indicate a comparatively deep garnet-bearing source region, or at least a source with a garnet-like signature, irrespective of actual depth. HREE patterns in the dolerite dyke suite are flatter ($[Gd/Yb]_N$ generally < 1.5; Fig. 6.3g) likely due to an absence of garnet in the source (i.e., in the spinel lherzolite stability field).

In order to test the possible mantle sources, trace element modelling is used. Details of the methods, equations, conditions and geochemical parameters used in the modelling presented below are provided in Appendix A.2. A summary of modelling parameters is given in Table 6.4.

6.7.2.1 Dolerite dykes:

Trace element modelling based on recent asthenospheric type sources (e.g., primitive mantle (PM), and enriched mantle EM1 and EM2) was initially employed. Partial melting was used for the dolerite dyke suite. As a starting point, modelling of 30 % partial melting of a spinel lherzolite primitive mantle source (McDonough & Sun, 1995) with 45-50 % fractional crystallisation of olivine was attempted; however this cannot replicate the trace element composition of the dolerite dykes. Fractional crystallisation of various modal proportions of olivine, orthopyroxene, clinopyroxene, plagioclase, and accessory minerals including magnetite and rutile, also failed to reproduce the multi-element patterns of the dolerites without invoking an unreasonably high degree of crystal fractionation (> 80 %) for an poorly acceptable model fit. Modelling using an enriched mantle source (EM1) – potentially more

fitting to the Scourie dolerite dyke geochemistry – produces a similarly poor fit to multi-element spectra. In particular, modelling using either PM or EM1 sources is unable to replicate the characteristic anomalies for Th, Nb, Ta and Ti in the dolerites. Overall, this implies that the dolerites have experienced some degree of lithospheric contamination, either involving the crust or SCLM, or that the source regions of the parental magmas are significantly different from more recent asthenospheric compositions used in modelling.

The dolerite suite can be subdivided into two broad groups – high-TiO_2 (> 2 wt.%, with positive Ti-anomaly) and low-TiO_2 group (< 2 wt.%, with negative Ti-anomaly) (Fig. 6.3g). Geochemical modelling cannot replicate this positive Ti anomaly using any realistic contamination components, and the presence for the Ti anomaly does not consistently coincide with any effect for Nb or Ta. High-Ti dolerite dykes commonly have higher Fe contents (> 17 wt.% Fe_2O_{3T}) and this might suggest a higher magnetite and/or ilmenite content.

AFC modelling using Lewisian amphibolite-facies gneiss (Rollinson, 2012) as the contaminant with low to moderate rates of assimilation (r = 10-20 %) and fractionation of 40-65 % olivine, can successfully reproduce the trace element signature of the dolerite dykes from a 30 % melt of a spinel lherzolite primitive mantle (PM) source (Fig. 6.7a-b). Indeed, lower degrees of partial melting of this source (10-25 %) can still successfully replicate the range of dolerite dyke trace element compositions (Fig. 6.7a). However this modelling has a major flaw – most samples in this study were intruded into LILE- and Th-poor granulite-facies gneisses of the Assynt terrane (a geochemical feature common to deep continental crustal material; Rudnick & Fountain, 1995)). The granulite-facies metamorphism predates the Scourie Dyke intrusion, and there is no evidence for post-intrusion tectono-metamorphic events that could have removed the LILE and/or Th. LILE-enriched amphibolite-facies gneiss only occurs in the Rhiconich and Gruinard terranes, and therefore was not available to contaminate the dolerite dykes in the Assynt Terrane. Additionally, a mechanism of contamination followed by prolonged lateral movement of the magmas would also provide an unsatisfactory explanation, as the same problem of the availability of a suitable contaminant would apply. Furthermore, there is no systematic change in composition of the Scourie Dykes across the basement terrane boundaries, indicating that local crustal contamination could not have been a major factor. Therefore this model is inappropriate for most Scourie dolerite dykes.

Assimilation of Lewisian granulite TTG (Rollinson, 2012) in AFC models cannot fully reproduce the dolerite trace element geochemistry, with a particularly poor correlation for Th (Fig. 6.7c). Varying the degree of fractional crystallisation of pyroxenes and plagioclase, in addition to

olivine, can explain slight nuances in individual dyke geochemistry, especially for Eu, but cannot reproduce the main geochemical features. It is noted however, that the modelled Zr and Hf concentrations can be elevated by contamination of a mantle magma with a partial melt of any Lewisian TTG composition (granulite or amphibolite), although this is insensitive to changes in melting or contamination parameters and does not account for the other trace element features of the dolerites. Principally, where did the enrichment in Th and LILE present in the dykes, but absent in Lewisian granulite-facies gneisses, come from (see Section 7.5)?

6.7.2.2 Picrite and olivine gabbro dykes:

The presence of garnet is suggested by high $[Gd/Yb]_N$ ratios of the olivine gabbros and picrite dykes, but trace element modelling of partial melting of a garnet lherzolite enriched mantle (EM1) source and olivine fractionation could not reproduce the normalised multi-element pattern for these two dyke sets. Furthermore, fractionation of additional mineral phases could not reproduce the Th, Nb-Ta-Ti, and LREE systematics of the picrite suite. As with dolerite dyke modelling, this implies involvement of a contaminant or a significantly modified mantle source. Although attempts to model an AFC scenario similar to that for the dolerite dykes can reproduce the trace element fingerprint of the picrite dykes, this requires contamination by Lewisian amphibolite-facies gneiss which would similarly have been unavailable in the granulite facies Assynt Terrane. An AFC model involving this material is thus unfeasible. Attempts to model the picrite and olivine gabbro dyke compositions by re-melting the residue from previous dolerite dyke magma extraction similarly failed.

Having discounted the likelihood of crustal contamination of asthenospherically-derived magmas for the Scourie Dykes, we must further consider evidence for significant addition of SCLM to their parental magmas, or the possibility of a parental magma source within the SCLM.

Although major element, mineralogical and isotopic analyses of the SCLM below the North Atlantic Craton in Greenland exist (Bernstein *et al.*, 1998; Hanghoj *et al.*, 2001; Bizzarro & Stevenson, 2003; Griffin *et al.*, 2003; Griffin *et al.*, 2008; Wittig *et al.*, 2008; Sand *et al.*, 2009; Wittig *et al.*, 2010; Tappe *et al.*, 2011), estimates of its trace element composition are not currently available. Therefore whole-rock geochemical analyses of spinel lherzolites from Loch Roag offer the best approximation of the sub-Lewisian SCLM. These xenoliths have been entrained in a much younger (Eocene) dyke, but nonetheless there is good evidence that once formed, lithospheric keels of Archaean cratons remain both physically stable and directly

associated with their overlying ancient crust (O'Reilly *et al.*, 2001; Griffin *et al.*, 2003; Griffin *et al.*, 2008; Begg *et al.*, 2010). The Lewisian Gneiss Complex has remained relatively unaffected by magmatic events since the Palaeoproterozoic (Long *et al.*, 1991; Upton *et al.*, 2011). Therefore for the purposes of this investigation, fresh xenolith LR80 is taken as the best available model composition for the SCLM below NW Scotland at the time of Scourie Dyke emplacement.

Modelling results indicate that, by mixing of a small degree asthenospheric partial melt (referred to here as a 'catalyst melt') with a volumetrically larger lithospheric partial melt (derived from xenolith LR80), magmas with the compositions of the various Scourie Dyke groups can be replicated. A catalyst melt representing 2-5 % melting of spinel lherzolite depleted mantle (DMM), mixed with a 15 % partial melt of LR80 can reproduce the trace element and general geochemical features of the dolerites (Fig. 6.8a-b). Furthermore, a 10 % garnet lherzolite DMM catalyst melt mixed with a 30 % LR80 melt reproduces the composition of the picrite dykes (Fig. 6.8c-d). By varying the amount of garnet and spinel in the catalyst melt, and the fraction of the melt derived from LR80 added to the mix (x), the trace element variability of the entire Scourie Dyke Suite can be replicated.

Table 6.4. Parameters required for melting, mixing, contamination, and fractional crystallisation during dyke magma evolution. F is % partial melting, r is % ratio of assimilation rate to fractional crystallisation, and x is % of contaminant added to primary melts in binary mixing model. Percentage olivine fractional crystallisation provided (ol. FC). Mantle sources used include primitive mantle† (McDonough & Sun, 1995), enriched mantle (EM1)‡ (Willbold & Stracke, 2006) and depleted mantle (DMM)® (Workman & Hart, 2005). Lewisian contaminants* (Rollinson, 2012) and SCLM partial melts**, based on fresh xenolith material of sample LR80 (see Table 6.2).

Dyke suite	Mantle source modelled (non-batch melting)	% partial melting (F) asthenos.	% partial melting (F) lithos (SCLM)	% mixing (binary mixing model)
Dolerite	Spinel lherzolite DMM® asthenospheric melt + spinel lherzolite SCLM melt (based on LR80)	c. 2%	15% LR80 melt	x = 0.1 – 0.3
Picrite	Garnet lherzolite DMM® asthenospheric melt + spinel lherzolite SCLM melt (based on LR80)	c. 10%	30% LR80 melt	x = 0.2 – 0.4

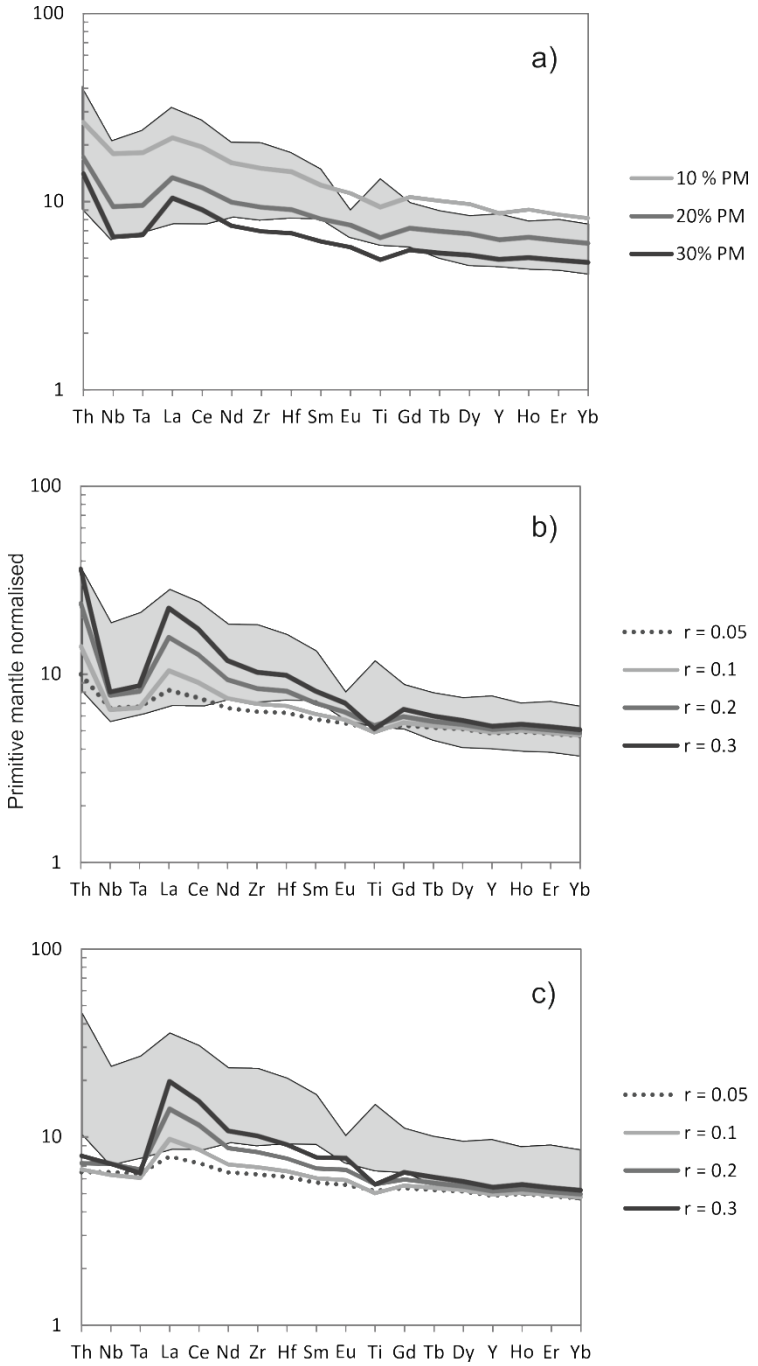

Figure 6.7. Trace element AFC modelling for primary mantle melts with Lewisian contamination. (a) 10-30 % partial melting of a spinel lherzolite primitive mantle (PM) source with assimilation (r = 0.10) of Lewisian amphibolite and fractional crystallisation fixed at 47.5 % olivine. (b) 30% partial melting of a spinel lherzolite PM source with fixed fractional crystallisation of 47.5 % olivine, and varying Lewisian amphibolite assimilation rates (r = 0.05-0.30). (c) Same as (b) but with assimilation of Lewisian granulite TTG. Lewisian contaminants based on Rollinson (2012).

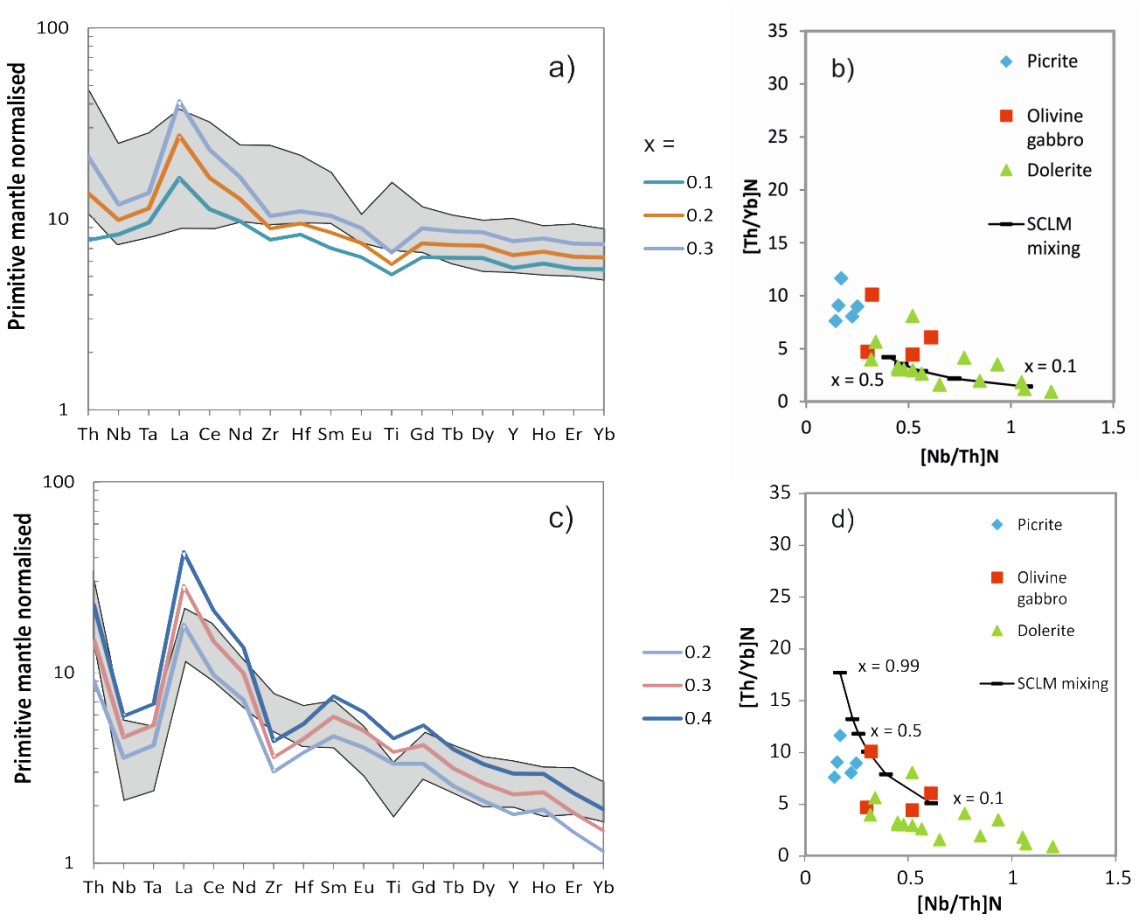

Figure 6.8. Trace element modelling for binary mixing between primary asthenospheric mantle melts (DMM) and SCLM partial melts (using LR80 starting composition). (a) Modelling for dolerite dykes: 2-5 % partial melting of a spinel lherzolite depleted mantle (DMM) source mixing with a 15 % SCLM partial melts (x = 0.10-0.30). No subsequent crystal fractionation used in model. (b) Th/Yb vs Nb/Th bivariant plot for (a). (c) Modelling for picrite dykes: 10 % partial melt of a DMM garnet lherzolite mixed with a 30% SCLM partial melt of LR80 (x = 0.20-0.40). (d) Th/Yb vs Nb/Th bivariant plot for (c).

6.7.3. Degree of partial melting and crystal fractionation – chalcophile element evidence

The picrite and olivine gabbro dyke suites have relatively unfractionated PGE spectra. However, although the dolerite dykes show significant IPGE depletion (Fig. 6.5f), there is no systematic variation in PPGE concentration between the three dyke suites. Partial melting of the asthenospheric mantle initially increases Pd/Ir ratio of the melt (Keays, 1982; Barnes *et al.*, 1988; Barnes, 1990; McDonald *et al.*, 1995; Maier & Barnes, 2004). This is because mantle IPGE (including Ir) are mainly hosted by an Fe-rich monosulphide solid solution (MSS) often included in silicate minerals, and/or as refractory metal alloys (Os-Ir-Ru-Rh-Pt) (Brenan & Andrews, 2001; Ahmed & Arai, 2002; Sattari *et al.*, 2002; Bockrath *et al.*, 2004b). In contrast, Pd is predominantly hosted by interstitial Cu-rich sulphides (Sattari *et al.*, 2002; Bockrath *et al.*,

2004a). Under anhydrous melting conditions, refractory MSS and metal alloys (and Ir) are retained in the residue, while Pd is gradually removed with the Cu-sulphide melt. With increasing degrees of partial melting, the Pd/Ir ratio of partial melts increases until mantle sulphides become exhausted in the source region while Ir-bearing alloys are retained. At 15-20% partial melting of fertile mantle, magmas are most fractionated with the highest Pd/Ir ratios (Naldrett, 2011). If partial melting exceeds this point, Ir-bearing alloys enter the melt, progressively lowering the Pd/Ir ratio of the magma as melting proceeds.

Assuming an initial mantle concentration of approximately 250 ppm sulphur (McDonough & Sun, 1995; Bockrath *et al.*, 2004a) and a columnar melting regime, 15-20 % partial mantle melting would almost exhaust Cu-rich sulphides, providing positively fractionated PGE spectra and Pd/Ir and Cu/Pd ratios significantly higher than mantle values. This signature can be identified in the dolerite dyke suite, but the olivine gabbros and picrites do not have such elevated Pd/Ir ratios, and overall their PGE patterns are relatively unfractionated. This implies that parental melts of the picrite and olivine gabbro dykes were generated through significantly higher degrees of mantle melting, exceeding the point of solely PPGE-bearing sulphide extraction and melting IPGE-rich phases, entraining these into the magma.

Similarly low Pd/Ir ratios might also be observed in cases of second-stage melting of a depleted or refertilised mantle source. In such environments, sulphur and Pd-bearing sulphides would have already been partially extracted, and a second melting event would effectively short-cut this process, producing comparatively IPGE-rich magmas (Keays, 1995; McDonald *et al.*, 1995; McDonald & Viljoen, 2006). For the Scourie Dyke picrite and olivine gabbro suites however, other trace element evidence cannot be reconciled with this two-stage melting scenario, with models particularly unable to recreate the HREE fractionation so characteristic of these dyke suites.

Pd/Ir ratios of some intra-craton magmas can be lower than off-craton magmas, as exemplified by comparison of on- and off-craton kimberlites (McDonald *et al.*, 1995). On-craton kimberlites are IPGE-rich, however this is not due to any particular Ir-rich melting process, but instead a physical entrainment of xenolithic SCLM material (including IPGE-alloy inclusions in chromite, and olivine and other silicates) during ascent. Previous work has implied that Pt/Pd ratios might be utilised to infer a metasomatic and 'on-craton' signature in magmas (Maier & Barnes, 2004) with an increased Pt/Pd ratio limited to metasomatic fluid-alteration effects. However, this does not reflect the physical nature of entrainment originally proposed for kimberlites (McDonald *et al.*, 1995), and can readily be tested by plotting Pt/Pd

against another metasomatic indicator, Nb/La for example. No correlation exists between Pt/Pd and Nb/La ratios for the Scourie Dyke Suite, suggesting that the Pt/Pd ratio is insensitive to SCLM magma input or changes in SCLM geochemistry. However, the range of Pt/Pd in the Scourie Dykes is comparable to that in komatiites and continental flood basalts (Maier & Barnes, 2004).

Although it cannot be entirely discounted that the relatively high IPGE content of the picrite and olivine gabbro dyke suites could arise from physical entrainment of SCLM material, mineralogical and textural evidence does not support this, as no xenolithic material occurs in these dykes. Instead, geochemical evidence such as high MgO contents and raw PGE concentrations supports the interpretation that these are high MgO magmas, produced by higher degrees (> 25-30 %) of partial mantle melting than the dolerites.

Finer points may also be noted from the PGE geochemistry of the Scourie Dyke Suite. Slight positive anomalies for Rh concentrations of the picrite dyke suite (Fig. 6.5a) are potentially indicative of Cr-spinel accumulation in these dykes, as supported by significantly higher proportions of chromite of this suite. Olivine fractionation has apparently had very little or no effect on the PGE geochemistry of both the picrite and olivine gabbro suites, suggesting that no significant olivine fractionation took place in the parental magmas of these dykes prior to emplacement, highlighting the primitive nature of these dyke suites.

6.7.4. Summary of mantle sources, melting and modelling

From the models presented in Section 6.2, we propose that the Scourie parental magmas are derived from both the asthenosphere and lithosphere, but predominantly it was the lithospheric mantle melting that contributed most of the melt and the observed trace element signature that we observe. In other words, 30 % partial melting of LR80 modelled in Fig 6.8b for the picrite suite, resulted in the extraction of almost all of the sulphide component, and with it the PPGE, along with a significant proportion of the IPGE budget.

In summary, simple partial melting of asthenospheric mantle sources (i.e., PM and EM1) cannot reproduce the ‘continental-like signature’ of the Scourie Dykes. Some subtleties of the trace element signatures, particularly for dolerites, can be accounted for by inferring some degree of crustal contamination, but by components not available to the magma at the observed level of intrusion. Moreover this contamination signature is highly variable and a very minor feature of very particular trace element abundances (Zr-Hf) in the dykes. Models

highlight the insensitivity of Zr and Hf abundances during AFC or any mechanism of crustal contamination, and any 'crustal' signature is easily out-weighed by the strong component of lithospheric mantle.

Comparison of whole-rock geochemistry of the Scourie Dykes to that of spinel lherzolite xenoliths of Loch Roag can account for many significant similarities (e.g., Nb-Ta-(Ti) negative anomalies, and positive anomalies for Th, LILE and LREE). SCLM compositions underlying Archaean cratons are extremely variable. However the position of the Loch Roag xenoliths within the undisturbed Lewisian Gneiss Complex at the margin of the fragmented NAC provides a rare and valuable insight into the ancient shallow mantle composition and its potential to produce later melts.

The hypothesis that all parental magmas of the Scourie Dyke Suite involved melting of enriched and modified SCLM, with a trigger input from asthenospherically-derived melts, is supported by the Re-Os isotope data (Frick, 1998; this study). The $\gamma Os_{(initial)}$ values for the picrites[1] (-1.89 to 4.30; Frick, 1998; -6.84 for X23, this study) indicate significant and prolonged isolation of the magma source from a convecting asthenospheric source, suggesting that the Scourie Dyke magmas were lithospheric. The $^{187}Os/^{188}Os_{(initial)}$ obtained for picrite dyke (sample X23) is 0.10. In comparison the $\gamma Os_{(initial)}$ value of an earlier dolerite dyke is 2470, significantly more radiogenic that the later picrite values, and could suggest no prolonged isolation had occurred in the parental magma source of the dolerites (Frick, 1998). An $^{187}Os/^{188}Os_{(initial)}$ of 9.73 was obtained for the centre of the 'Graveyard' dolerite dyke (this study) but we suggest that the high Re content of the dyke indicates re-setting of the isotopic system for this sample. New Re-Os analyses of the xenolith LR80 yields $^{187}Os/^{188}Os_{(initial)}$ = 0.127 (using 45.2 Ma age; Faithfull *et al.,* 2012)) or 0.07 (using 2400 Ma age of dykes). At 2400 Ma or 45.2 Ma, the $^{187}Os/^{188}Os_{(initial)}$ is too unradiogenic for the calculated mantle ranges at those times (0.11-0.5 at 2400 Ma, 0.128 at 45.2 Ma). This suggests isolation from the convecting mantle by 2400 Ma, but there may also be some disturbance of the isotopic system.

Sm-Nd and U-Pb isotopic analyses of the dykes in Waters *et al.,* (1990) have a considerable range of initial compositions which indicated a component of old and enriched lithosphere. Waters and co-authors propose that a complex mixing between depleted mantle melts and enriched mantle lithosphere, isolated from the convecting asthenosphere, could have caused and dominated the combined isotope systematics of the Scourie Dykes.

[1] $\gamma Os_{(initial)}$ calculated at an emplacement age of 2400 Ma and 2000 Ma for the picrite and dolerite dykes respectively (Frick, 1998). See Appendix A.3.

The trigger for lithospheric melting might have been the thermal anomaly associated with an impinging mantle plume. However, continental extension alone could be sufficient to initiate a significant degree of partial melting both in the asthenosphere and in the fluid-rich metasomatised SCLM. Extension of the continental lithosphere generates little melt unless β (amount of crustal stretching) > 2 and T_p (mantle potential temperature) > 1380^oC (McKenzie & Bickle, 1988) at which point melting will occur in the asthenosphere and also the hydrous lithosphere (Gallagher & Hawkesworth, 1992). Based on field evidence, it is reasonable to suggest that a very significant degree of stretching took place during the emplacement of the Scourie Dyke swarm (β > 2). In addition, numerous models (Richter, 1988; Korenaga, 2008; Davies, 2009; Herzberg *et al.*, 2010) indicate that the mantle temperature in the Late Archaean/Palaeoproterozoic exceeded 1380^oC. Once β > 2, alkali basalts are produced by decompression melting, and as the degree of melting increases, tholeiites are produced.

Gd/Yb ratios and HREE spectra indicate a significantly different magma source for picrites and olivine gabbro dykes relative to the more abundant dolerite dyke suite – dolerites were derived from a source producing a flat HREE signature but olivine gabbro and picrite suites stem from a source producing a HREE-depleted signature. This is not explicable by only a change in the degree of partial melting, or by subsequent crystal fractionation. If the Scourie Dykes display a predominantly SCLM geochemical signature, then a change in the degree and depth or loci of melting, and proportions of magma inputs from the lithospheric and asthenospheric mantle, could cause the change in geochemical signature apparent between dyke groups. However we hesitate to suggest that any garnet-bearing signature in this environment would truly be at the garnet stability depth. Instead it is likely that a lithospheric source might have undergone numerous melting/freezing magmatic events, and hence a garnet-like signature could have migrated from deeper levels and solidified in shallower lithospheric zones, resulting in an inherent heterogeneity of the Scottish lithosphere. These frozen melts could have subsequently been remobilised by the Scourie magmatic event (Fig. 6.9). This is supported by whole-rock geochemical evidence from the Loch Roag spinel lherzolite xenoliths. The NW Scottish SCLM's apparent heterogeneity may be due to the variable penetration of fluids, volatiles and low-degree partial melts (e.g., carbonatite or alkaline) (Fig. 6.9). Whether through a subduction process, or via some other metasomatic mechanism (Section 7.5), this resulted in alteration, thickening, and continued preservation of the Lewisian mantle keel (Rollinson, 2012).

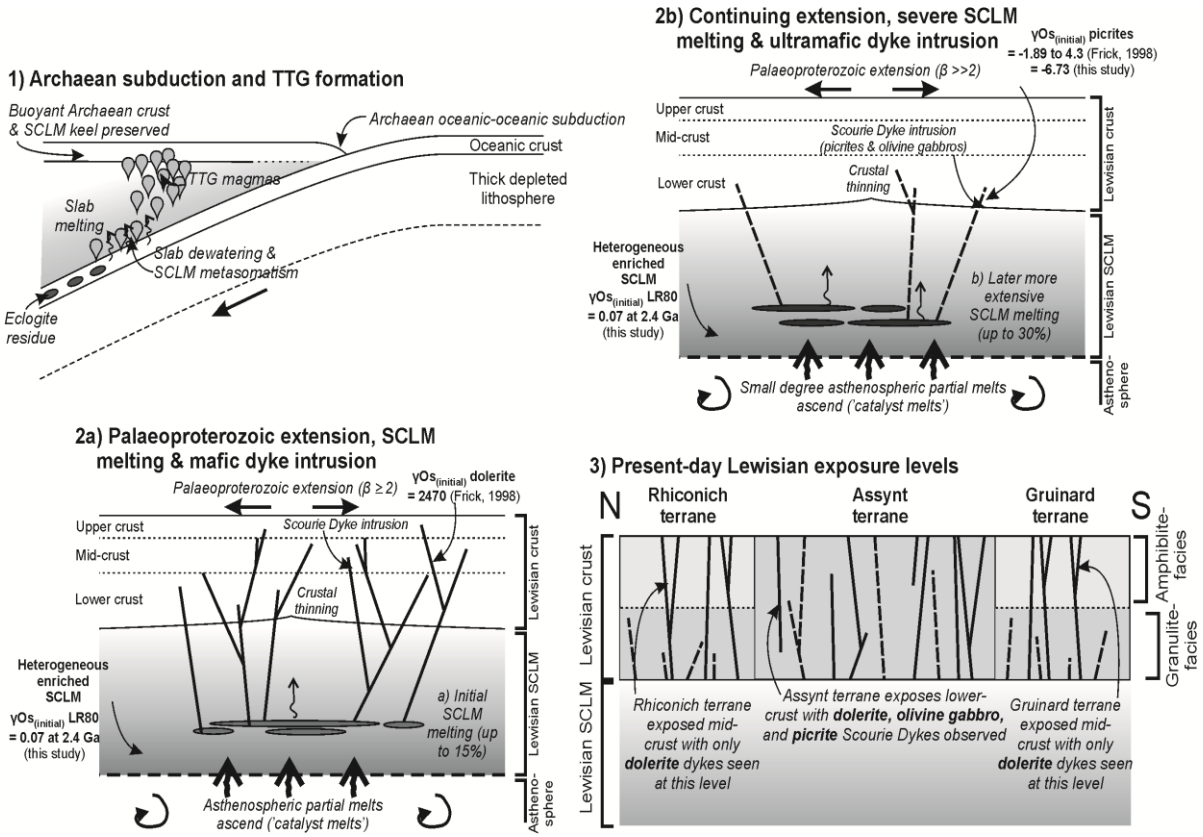

Figure 6.9. Model scenario for formation of Lewisian depth-zoned SCLM and Scourie Dyke Suites. (1) Archaean subduction during Lewisian TTG formation (based on Rollinson, 2010) – subduction of dense Fe-rich oceanic crust and thick depleted lithosphere, causing slab dewatering and melting and over-riding mantle wedge (SCLM) metasomatism. Slab melts (TTG magma precursors) eventually form buoyant Archaean crust and preserved buoyant SCLM. (2a) Palaeoproterozoic extension causes decompression melting in asthenosphere and subduction-enriched SCLM producing dolerite dyke parental magmas. This is followed by (2b) higher degree partial melting of subduction-enriched SCLM producing parental magmas of the olivine gabbro dykes and picrite dykes. Magmas ascend and are emplaced into Lewisian crust, although denser Mg-rich olivine gabbro and picrite dyke magmas only penetrate lower crustal levels. $\gamma Os_{initial}$ values from Frick (1998) and this study. (3) Later tectonic displacement and erosion to present-day exposure levels see the Rhiconich and Gruinard Terranes with mid-crustal amphibolite-facies Lewisian gneiss and only the dolerite dyke suite encountered. In contrast, the Assynt Terrane is a lower crust granulite-facies block with all three dyke suites exposed. See text for discussion.

6.7.5. Th-Nb-Ta-Ti and Zr-Hf anomalies – a relict Archaean subduction or metasomatic signature?

Significant negative Nb-Ta-(Ti) anomalies can be identified on the primitive mantle-normalised multi-element diagrams (Fig. 6.3 and 6.6), particularly in the picrite dykes and Loch Roag xenoliths. Modelling (Section 7.4) has shown that it is unlikely to be due to crustal contamination and may represent variation in the parental magma source. While the Scourie Dykes themselves were formed during the early Palaeoproterozoic, their lithospheric mantle source regions would have an older enrichment signature. Thus, this geochemical signature could likely be traced back into the Archaean. When seen in younger Palaeozoic to Cenozoic-age rocks, this geochemistry can be characteristic of subduction-related volcanic arc rocks. Modern basalt geochemistry can be used to infer differing tectonic environments (Hofmann, 1997; Pearce, 2008) and consistent chemical behaviour of element groups supports the idea that this can be extended to Archaean rocks (Polat & Kerrich, 2006). However controversy still surrounds the interpretation and implications of this in Archaean-Palaeoproterozoic rocks (Jenner *et al.*, 2013) although sanukitoid occurrences across the Archaean-Proterozoic transition may mark a transition from TTG-dominated granitoid magmatism to modern-style arc magmatism (Martin *et al.,* 2010).

Evidence for the inheritance of an Archaean metasomatised signature (rather than crustal contamination) is particularly supported by the enrichment of Th and LILE in the dyke suite relative to the Th- and LILE-depleted Lewisian granulite-facies TTG. All members of the Scourie Dyke Suite sampled during this study (regardless of terrane – see Section 7.1) have much higher concentrations of these elements. This implies that combined LILE and Th enrichment is a key feature of the mantle that produced the Scourie Dykes, i.e., akin to the Loch Roag xenoliths. These features are suggestive of upper mantle alteration and enrichment via a metasomatic mechanism (Hawkesworth *et al.*, 1994; Pearce *et al.*, 2005). But the negative Zr-Hf anomaly observed in Loch Roag in particular indicates a carbonate/carbonatite-metasomatic event, rather than solely a silicate alkali or volatile-only event (Yaxley *et al.*, 1991; Yaxley *et al.*, 1998; Ionov & Harmer, 2002; Pearson *et al.*, 2003). This may have been related to subduction in the Archaean, which is possibly suggested by $\delta^{18}O$ data for the dykes (Davies *et al.* 2012) and previously published whole-rock and mineral $\delta^{18}O$ (Cartwright & Valley, 1995). Cartwright and Valley (1995) demonstrated that the low- $\delta^{18}O$ magmas of the Scourie Dykes were unlikely to have been caused by the assimilation of large volumes of

continental crust, and this signature was more probably derived from a low- $\delta^{18}O$ subduction-modified lithospheric mantle source.

Modification of the sub-Lewisian shallow mantle took place prior to xenolith entrainment, but the timing of this event is uncertain. Time-integrated Nd isotopic ratios of the Loch Roag peridotite xenoliths and associated xenocrysts have suggested two or more periods of lithospheric mantle metasomatism – one at 1.0-1.5 Ga (Menzies *et al.*, 1987), and one at 2.3-2.5 Ga (Long *et al.*, 1991). On this basis, at least some upper mantle metasomatism and enrichment was already underway by the time of Scourie Dyke magmatism. Long et al. (1991) suggest that carbonatite-based metasomatism was prevalent during the 2.3-2.5 Ga event. If this is the case, this age overlaps with that of the age of the Scourie Dykes, and may be a deeper indication of continental rifting. Alternatively, a similar metasomatic signature might have occurred in addition to, or prior to extension, via an older subduction process recorded in the lithospheric mantle – a 'relict' Archaean subduction signature preserved in Archaean SCLM, and incorporated into dyke magmas during Palaeoproterozoic extension.

The protoliths to the Lewisian TTG gneisses are 3.0-2.7 Ga (Kinny *et al.*, 2005). Recent work on the Re-Os isotopic composition of peridotite xenoliths from the NAC in W Greenland has discovered significant metasomatic enrichment and melt extraction at 2.0 Ga, but other xenoliths from a similar area have model Re depletion ages of 2.7-3.1 Ga (Wittig *et al.*, 2010). Overall these xenoliths record lithospheric stabilization between the Meso- to Neoarchaean, followed by metasomatic alteration and overprinting magmatic events. In particular, the FeO enrichment of some of the W Greenland peridotites (comparable to the Fe enrichment observed in the Loch Roag xenoliths), and HREE abundances, are thought to require SCLM depletion in a relatively shallow subduction zone and/or mid-ocean ridge setting (Wittig *et al.*, 2010).

Overall, if a mid-late Archaean slab subduction regime is accepted (Rollinson, 2010), it has implications for Archaean mantle and cratonic SCLM geochemistry. We may expect an enrichment of LILE and LREE, and mobilisation of sulphur through mantle wedge metasomatism and hydrous partial melting. Thus the SCLM keels of Archaean cratons may host complex and heterogeneous hydrous subduction-modified geochemical signatures. Indeed, we find that direct samples of the SCLM below NW Scotland share these geochemical facets. This complexity would only be expected to be preserved in the lithospheric mantle (and likely in a heterogeneous manner), with convecting asthenosphere not retaining the subduction/metasomatic signature. As previously discussed in Sections 7.2-7.4, the

metasomatised complexities of the Lewisian lithospheric mantle keel are vital for understanding the trace element characteristics of the Scourie Dyke Swarm.

6.7.6. Lewisian SCLM geochemistry: evidence of melting mechanism – plume or no plume?

With the acceptance of an ancient subduction signature being present in the Palaeoproterozoic Scourie Dyke Swarm, the intricacies of this scenario and the melting mechanism may be scrutinized further. LREE concentrations of the Scourie Dyke suites are very enriched (Fig. 6.3), comparable to some alkaline magmas globally (e.g., McDonald *et al.,* 1995), especially taking into consideration the high degrees of partial melting indicated for the ultramafic magmas by the IPGE data. This further highlights the substantial LREE metasomatic enrichment of the mantle source. Multi-element plots (e.g., Fig. 6.6a) of each of the dyke suites show a comparable, but progressively exaggerated 'metasomatic' signature, which becomes increasingly more discernible from the dolerites through to the olivine gabbro and picrite suites (i.e., from mafic to ultramafic compositions). This presents a paradox for any melting model incorporating a plume (with contamination).

Asthenospheric melts producing progressively increasing degrees of melting should dilute any initial geochemical anomaly such as that for Nb-Ta-Ti. In addition the relative ages of the dolerite (mafic) and picrite (ultramafic) dyke groups may provide clues as to the presence of a plume. Recent geochronological work has highlighted the long time-period over which Scourie dykes were intruded (400 Myr) (Davies & Heaman, 2014) but the majority were apparently intruded over a shorter 'main' period spanning ~ 40 Myr between 2418-2375 Ma (Davies & Heaman, 2014) which itself has apparent temporal subdivisions. Overall, this prolonged phase of dyke intrusion is exceptional for any Large Igneous Province (LIP) globally (flood basalt-related events are observed to last ~ 1-5 Myr, Ernst *et al.,* 2013), but in Scourie these appear to have been intruded in 'pulses' over at least 40 Myr. The uniformity of dyke azimuth and longevity of intrusion dates could instead be the result of persistent rifting, as observed in the Tarim block of NW China (Zhu *et al.,* 2008; Davies & Heaman, 2014).

6.8. Conclusions

1. Geochemical modelling of the Scourie Dyke Swarm has shown that the swarm could not have been derived from an asthenospheric mantle region with variable crustal contamination using the available crustal components. Therefore we investigate where such an enriched geochemical signature could have been sourced.
2. Negative Nb-Ta-Ti anomalies, and enrichments in Th, LREE and other LILE, particularly in the picrite suite represent an Archaean metasomatic geochemical signature in the lithospheric mantle. This could indicate that a shallow-angle subduction regime was present during formation of the Lewisian portion of the North Atlantic Craton, and/or that carbonatite-induced metasomatism was coeval with the rifting event that led to the intrusion of the Scourie Dykes themselves.
3. Whole-rock geochemical analyses, and a new measurement of the Re-Os isotopic composition of spinel lherzolite mantle xenoliths from Loch Roag confirm the presence of this signature in the shallow mantle underlying this region of Scotland, and corroborate the presence of significant metasomatic enrichment of the mantle lithospheric keel of the Lewisian portion of the NAC.
4. Despite Loch Roag xenolith chemical continuity, the Archaean sub-Lewisian SCLM is likely to be heterogeneous, due to varying degrees of metasomatism and partial melting throughout Lewisian TTG and SCLM keel formation.
5. Dolerite and picrite dykes were derived from different parts of the heterogeneous lithosphere, with variable HREE signatures. However, using HREE to make interpretations of the depth of melting within the heterogeneous SCLM is inappropriate due to the possibility of 'frozen-in' signatures imparted during prolonged formation and alteration.
6. PGE can be used to further characterise mantle melting regimes and the extent of partial melting. Ir-group PGE depletion in dolerite dykes suggests up to 15 % partial melting of the SCLM source, while low Pd/Ir ratios in both the picrite and olivine gabbro dyke suites highlight a significantly higher degree of melting (> 25-30 %) within a fluid-rich lithospheric mantle source.
7. Our trace element geochemical modelling suggests that the Scourie Dykes have variably sampled this enriched and fusible lithospheric mantle region through direct partial melting of the metasomatised SCLM itself, possibly coupled with, or triggered by, some degree of asthenospheric melting. This was a direct result of tectonic extension causing lithospheric thinning and decompression.

Acknowledgements

HSRH would like to acknowledge the financial support of the Natural Environment Research Council (NERC) for funding this work which has been undertaken as part of her PhD (studentship NE/J50029X). Hilary Downes and Hugh Rollinson are thanked for their thorough and detailed review of the manuscript, and Randy Parrish is thanked his for constructive comments. HSRH and co-authors wish to thank Scottish Natural Heritage (SNH) and numerous landowners for their kind permission to sample the Scourie Dykes. Lawrence Badham is thanked for his assistance in making polished thin sections for study. K.M. Goodenough publishes with the permission of the Executive Director of the British Geological Survey. Discussions with Julian Pearce and Nicholas Arndt were much appreciated during the writing of this manuscript.

CHAPTER 7

Trace element abundances in the shallow lithospheric mantle of the North Atlantic Craton margin: Implications for melting and metasomatism beneath Northern Scotland

Submitted as:

Hughes, H.S.R., McDonald, I., Faithfull, J.W., Upton, B.G.J., Downes, H. (in press). Trace element abundances in the shallow lithospheric mantle of the North Atlantic Craton margin: Implications for melting and metasomatism beneath Northern Scotland. *Mineralogical Magazine (North Atlantic Craton Conference Special Issue).*

Co-author contributions:

I. McDonald, J.W. Faithfull, B.G.J. Upton and H. Downes were involved in discussions during the writing of this paper. J.W. Faithfull and B.G.J. Upton provided xenolith specimens for study. I. McDonald supervised bulk rock and LA-ICP-MS analyses.

Abstract

Bulk major and trace element geochemistry in clinopyroxene have been determined in three suites of peridotitic mantle xenoliths from the North Atlantic Craton (NAC) in northern Scotland, to establish the magmatic and metasomatic history of subcontinental lithospheric mantle (SCLM) below this region. Spinel lherzolites from the southernmost locality (Streap Com'laidh) have non-NAC mantle composition, while the two northern xenolith suites (Loch Roag and Rinibar) are derived from the thinned NAC marginal keel. Clinopyroxene compositions have characteristic trace element signatures which show both 'primary' and 'metasomatic' origins. We use Zr and Hf abundances to identify ancient cryptic refertilisation in 'primary' clinopyroxenes. We suggest that Loch Roag and Rinibar peridotite xenoliths represent an ancient Archaean-Palaeoproterozoic SCLM with original depleted cratonic signatures which were overprinted by metasomatism around the time of intrusion of the Scourie Dyke Swam (c. 2.4 Ga). This SCLM keel was preserved during Caledonian orogenesis, although some addition of material and/or metasomatism probably also occurred, as recorded by Rinibar xenoliths. Rinibar and Streap xenoliths were entrained in Permo-Carboniferous magmas and thus were isolated from the SCLM c. 200 Ma before Loch Roag xenoliths (in an Eocene dyke). Crucially, despite their geographical location, lithospheric mantle peridotite samples from Loch Roag show no evidence of recent melting or refertilisation during the Palaeogene opening of the Atlantic.

7.1. Introduction

Mantle xenoliths provide a direct (if incomplete) view into the lithospheric mantle underlying the Earth's crust. Xenolith assemblages are the composite result of magmatic and/or metasomatic events and record transient volatiles and fluids. Interest in the subcontinental lithospheric mantle (SCLM) and its role as a source or sink of metals such as Cu, Mo and Au, has been discussed in the literature for decades (c.f. Groves *et al.,* 1987; Groves & Bierlein, 2007 and references therein). However, recent interest in how the SCLM relates to critical metals and metals of strategic and economic importance (such as the platinum-group elements (PGE) and rare earth elements (REE)) has re-ignited this debate (e.g., Arndt, 2013).

The composition of the ancient Archaean SCLM beneath the North Atlantic Craton (NAC) has already been explored in various studies in Greenland (e.g., Bernstein *et al.,* 1998; Hanghøj *et al.,* 2001; Bizzarro & Stevenson, 2003; Bernstein *et al.,* 2006; Wittig *et al.,* 2008; 2010; Tappe *et al.,* 2011; Bernstein *et al.,* 2013). Xenolith suites from both W and E Greenland comprise a mix of depleted harzburgitic lithologies, eclogites, dunites and wehrlites, as well as more 'fertile' lherzolite peridotites. Typically NAC mantle xenoliths encompass both spinel and garnet-bearing rocks, corroborating seismic tomographic evidence that these ancient lithospheric keels extend to depths in excess of 100 km (Kumar *et al.,* 2005). Research into the mineralogy and isotopic composition of mantle xenoliths from the eastern fragment of the NAC margin in NW Scotland (UK) has resulted in the identification of several suites of spinel lherzolite xenoliths (see Upton *et al.,* 2011 and references therein). These localities are all situated north of the Great Glen Fault, and are hosted in Permo-Carboniferous and Eocene basic dykes (Upton *et al.,* 2011).

In this study, we present whole-rock major and trace element geochemistry for a selection of NW Scottish spinel lherzolite mantle xenoliths. Samples were chosen to represent the freshest lithospheric mantle material in this region, and therefore provide an excellent opportunity to study the composition of the mantle of the cratonic margin of the NAC. We compare these xenoliths to suites from the centre of the NAC in Greenland, and investigate their whole-rock compositions, silicate mineral trace element chemistry (specifically clinopyroxene) and accessory mineralogy to identify various metasomatic signatures and constrain the evolution of this part of the NAC.

7.1.1. Overview of the North Atlantic Craton – formation, amalgamation and xenolith localities

The North Atlantic Craton (NAC) extends from eastern Canada (Nain Province), through Greenland, and includes a fragment in the United Kingdom known locally as the Lewisian Gneiss Complex (Fig. 7.1). The NAC consists of amalgamated Archaean domains with zones of Palaeoproterozoic reworking (e.g., Bridgwater *et al.*, 1973). The geological history of the Lewisian fragment can be subdivided according to the following major tectonic events (see Park, 2005 and references therein): (a) magmatic protolith formation (including ultramafic-mafic bodies now preserved as pods within tonalite-trondhjemite-granodiorite (TTG) gneisses) at 3.0-2.8 Ga; (b) high-grade regional metamorphism followed by initiation of shear zones and associated metamorphism at 2.8-2.5 Ga. Undeformed granitoids from parts of the Lewisian date from 2.8-2.7 Ga and could be coincident with the alkaline province of Skjoldungen in E Greenland (Goodenough *et al.,* 2014 and references therein). This was associated with extensive partial melting (known as the 'Badcallian' event) however the precise dating of this melting event is difficult to constrain (Goodenough *et al.,* 2014). Orogenic events elsewhere in the Greenlandic portion of the NAC at ca. 2.86-2.60 Ga are associated with gold mineralisation (e.g., Kolb *et al.,* 2013). (c) Intrusion of mafic-ultramafic dykes (Scourie Dykes) ca. 2.4-2.3 Ga during a period of continental rifting and extension (Davies & Heaman, 2014); (d) ca. 2.0-1.8 Ga calc-alkaline magmatism and volcanic arc accretion, with formation of Laxfordian high-grade metamorphic belts; (e) continued calc-alkaline magmatism ca. 1.8-1.7 Ga, including further deformation and prograde amphibolite-facies metamorphism and Laxfordian crustal anatexsis (Bridgwater *et al.*, 1973; Park, 1994; Park, 1995; Kinny *et al.*, 2005a; Park, 2005; Hughes *et al.*, 2014 (Chapter 6); Vernon *et al.*, 2014).

The western part of the NAC in Greenland hosts abundant late Proterozoic ultramafic lamprophyre kimberlite dykes and sills, which contain mantle xenoliths (c.f., Bizzarro & Stevenson, 2003; Tappe *et al.,* 2006; Bernstein *et al.,* 2007; Tappe *et al.,* 2007; Wittig *et al.,* 2010 and references therein). Xenolith/xenocryst suites comprise (variably) serpentinised ultra-refractory dunites, harzburgites, eclogites, wehrlites and minor lherzolites (e.g., Hutchison & Frei, 2009). The mantle lithologies have unradiogenic Os-isotope compositions (mean γOs = -9.2) and Re-depletion model eruption ages (T_{RD}^{erupt}) of 3.2 to 2.7 Ga and ca. 2.0 Ga (Wittig *et al.,* 2010). In the SW portion of the NAC, xenoliths entrained in Mesozoic kimberlites have undergone comparatively little serpentinisation. Whilst the silicate mineralogy and whole-rock major element composition of these xenoliths record severe

depletion, they have more radiogenic Os-isotope compositions (mean γOs = -7.2) and a single T_{RD}^{erupt} at 2.0 Ga (Wittig *et al.,* 2010). Overall, thermobarometric studies of western Greenlandic NAC xenoliths suggest that most were derived from 180 to 220 km depth (Bizzarro & Stevenson, 2003; Sand *et al.,* 2009). Studies by Bizzarro & Stevenson (2003) indicate that the western Greenlandic NAC may be stratified, consisting of two major 'units': an upper zone of more refractory peridotites (70-180 km depth), and a lower 'fertile' clinopyroxene-bearing lherzolite zone (180-225 km).

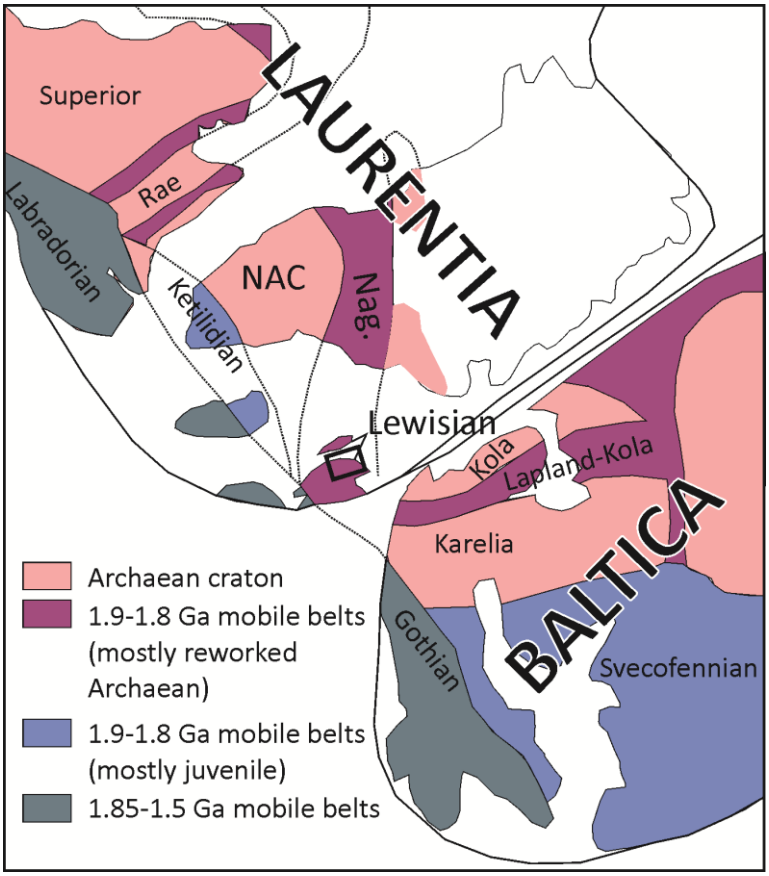

Figure 7.1. Palaeoproterozoic reconstruction of the North Atlantic Craton (NAC), reworked NAC mobile belts and other 'juvenile' mobile belts. Based on Buchan *et al.* (2000). The Scottish portion of NAC is labelled 'Lewisian'.

Palaeogene dykes at the eastern Greenlandic margin of the NAC, at Wiedemann Fjord, have also yielded xenoliths of depleted peridotites, predominantly spinel harzburgites (Bernstein *et al.,* 1998; Hanghøj *et al.,* 2001 and references therein). East Greenlandic xenoliths preserve highly refractory and severe melt depletion signatures (including highly forsteritic olivine and low modal orthopyroxene) and are thought to record formation of the NAC cratonic mantle

keel with further Palaeogene partial melting and depletion during the opening of the Atlantic (Bernstein *et al.,* 1998). The same xenolith suite however also contains a spectrum of peridotite compositions which include lherzolites with variable olivine content (down to 50 %) and up to 25 % clinopyroxene (Hanghøj *et al.,* 2001). As with the western Greenlandic NAC, Os-isotopic compositions from these eastern Greenlandic NAC xenoliths record Archaean polybaric melt depletion for the harzburgites, initiating at ≥ 7 GPa (~ 210 km) and continuing at 2-3 GPa (65-100 km) (Bernstein *et al.,* 1998). Later refertilization of restites added pyroxene (particularly clinopyroxene) and re-equilibrated the modal mineral and isotopic compositions at high temperatures (up to 980°C). This may have taken place during Palaeogene magmatism associated with the opening of the Atlantic and impingement of the Icelandic mantle plume (e.g., Hanghøj *et al.,* 2001). Hence, both depletion and refertilisation are thought to be recorded in the keel of the NAC SCLM in eastern Greenlandic, following Palaeogene mantle plume magmatism.

7.1.2. The Scottish portion of the North Atlantic Craton and neighbouring terranes

In Scotland, mantle xenolith localities occur within five tectonic terranes, delineated by major crustal (and probably lithospheric) lineaments (Fig. 7.2). In the far NW of Scotland, the Archaean – Mesoproterozoic Lewisian Gneiss Complex makes up much of the British portion of the North Atlantic Craton, and is the exposed basement of the Caledonian foreland bounded to the east by the Moine Thrust Zone. Adjacent to this, and bounded to the SE by the Great Glen Fault, is the Northern Highland Terrane which at surface comprises predominantly c. 1 Ga Moinian metasediments, intercalcated with 'Lewisianoid' inliers (Tanner, 1970) which suggest that Archaean basement (at least at the crustal level) extends east beyond the Moine Thrust Zone and underlies the Northern Highland Terrane (e.g., Moorhouse & Moorhouse, 1977). Ordovician-Silurian high Ba-Sr mixed diorite-granitoid, syenite and pyroxenite-syenite alkaline intrusions occur across the Northern Highland Terrane and includes the only carbonatite intrusion in the UK (Loch Urigill; Young *et al.,* 1994). Further, peralkaline granite intrusion occurred in the late Proterozoic (Carn Cuinneag granite at 594 Ma; Oliver *et al.,* 2008) and could attest to a lithospheric mantle magmatic event at this time.

Subduction of Iapetus oceanic lithosphere below Avalonia initiated during the Grampian Event (478-460 Ma) and resulted in the tectonic stacking and metamorphism of Dalradian strata and deformation of the Southern Uplands (Stone et al., 1987; Kinny et al., 2003). Iapetus

subduction ended c. 450 Ma (Neilson *et al.*, 2009) and by c. 430 Ma continent-continent collision had commenced with the edge of Avalonia emplaced beneath that of Laurentia (Stone *et al.*, 1987; Kneller, 1991). The Moine Thrust Zone (MTZ; Fig. 7.2) was formed by large-scale horizontal shortening of the crust in the early Silurian. Movement along the MTZ largely ceased at c. 429 Ma (Goodenough *et al.,* 2011). The Great Glen Fault (GGF; Fig. 7.2) forms the most important terrane boundary and lineament in Scotland. Fundamentally, the GGF separates northern terranes where Lewisian (NAC) Archaean basement is present, from southern terranes where NAC rocks are absent. Faulting was initiated in the Caledonian (428 ± 1.9; Stewart *et al.,* 2001 and references therein) and involved at least 200 km sinistral strike-slip movement. The GGF was reactivated with comparatively minor dextral motion (10-18 km) during the Cenozoic due to differential spreading from the opening of the Atlantic (Le Breton *et al.,* 2013). Various seismic tomographic studies and deep seismic surveys, including the N-S LISPB survey line of Barton *et al.,* (1992) are ambiguous in their exact details of NAC or Lewisian cut-off south of the GGF. For this reason, our xenolith localities have focussed on sites north of the GGF.

Xenolith suites from the Northern Highland Terrane were entrained by Permo-Carboniferous intraplate silica-poor mafic dykes (basanite, mela-nephelinite and monchiquites), formed by tectonic decompression during continental extension (Kirstein *et al.*, 2006). These dykes have ocean island basalt (OIB)-like mantle source compositions (Upton *et al.,* 2004; Kirstein *et al.,* 2006). Whilst debate continues about the involvement of a mantle plume during Permo-Carboniferous rifting, He-isotope data from the Scottish mantle lithosphere (including Streap Com'laidh xenoliths) do not support the hypothesis of involving a mantle plume (Kirstein *et al.,* 2004; Wilson *et al.,* 2004) and instead suggests that magma was generated as a complex response to tectonic collapse of the Variscan Orogen (Wilson *et a.l.,* 2004 and references therein). An overview of this period of magmatic activity in Scotland can be found in Upton *et al.* (2004).

Most recently, the North Atlantic Igneous Province (NAIP) erupted as a widespread continental flood basalt event formed by the impingement of the Icelandic mantle plume beneath overlying lithosphere. Active continental rifting was initiated at approximately 62 Ma in the UK, Greenland and Baffin Island, and ultimately led to the opening of the Atlantic Ocean (Saunders *et al.*, 1997). The British Palaeogene Igneous Province is part of the earliest magmatic expression in the NAIP and is developed through the Hebrides, the W coast of Scotland and Northern Ireland (Saunders *et al.,* 1997).

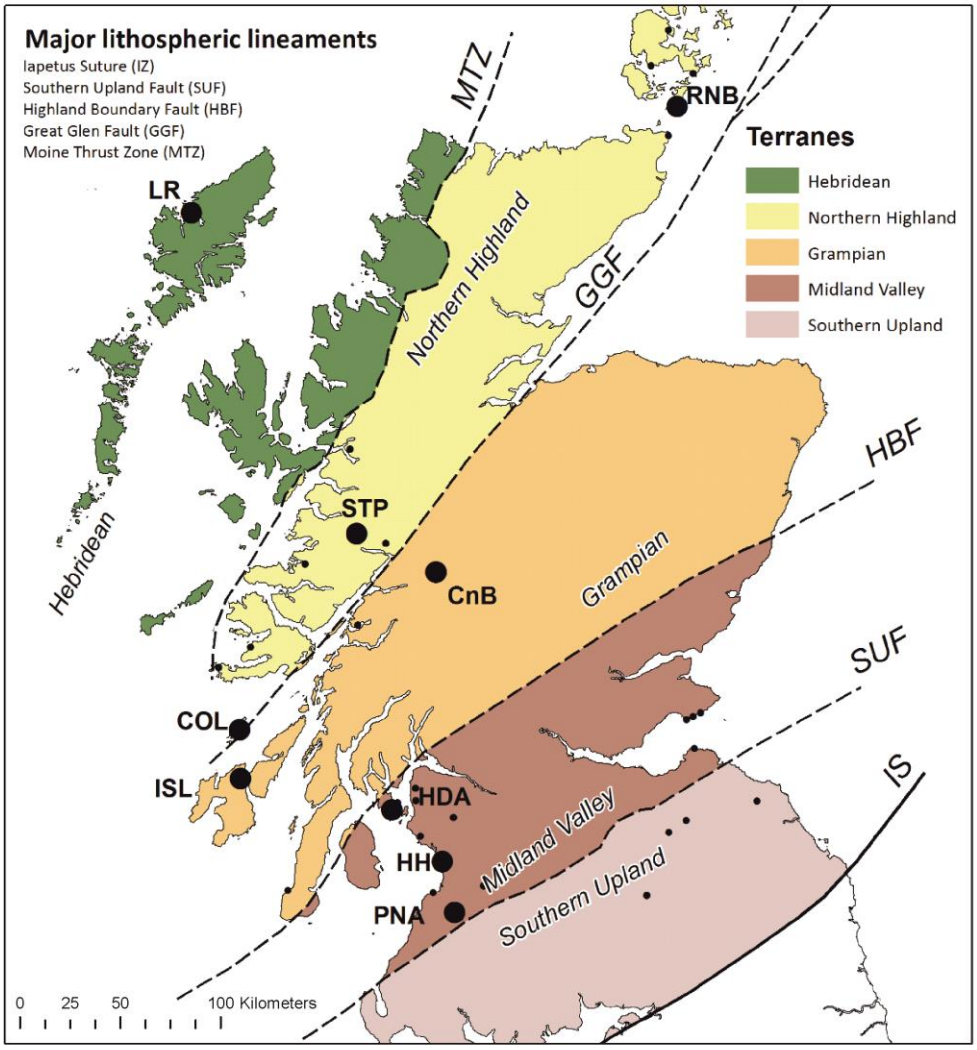

Figure 7.2. Terrane map of Scotland, highlighting major mantle xenolith localities. The three suites N and NW of the Great Glen Fault (GGF) are included in this study; Loch Roag (LR), Streap Com'laidh (STP) and Rinibar (RNB). These span two terranes – the Hebridean Terrane and Northern Highland Terrane – both of which are through to be underlain by (re-worked) NAC basement. Other xenolith localities labelled are: Colonsay (COL), Islay (ISL), Coire na Ba (CnB), Heads of Ayr (HDA), Hillhouse (HH) and Patna (PNA).

The map in Figure 7.2 highlights sites of xenolith suites in Scotland, including the three localities used in this study: Loch Roag (LR), Streap Com'laidh (STP) and Rinibar (RNB). These three localities were selected for their large and comparatively fresh peridotite mantle xenoliths, which yield sufficient material to process for whole-rock chemical analyses alongside mineral chemistry studies. All three xenolith localities are on the north side of the GGF, and thus are the most likely to have sampled the margin of the NAC. All of the studied mantle xenoliths are spinel lherzolites (stable at depths of 55-60 km; Griffin & O'Reilly, 1987). No garnet-peridotite xenoliths are recorded in Scotland suggesting that the deeper

lithospheric root beneath the Scottish portion of the NAC has been lost during multiple tectonic events (e.g., Menzies & Halliday, 1988). A similar apparent loss of deep cratonic keel is described for the Labrador portion of the NAC, for which a cratonic rifting model was proposed (see Tappe *et al.,* 2007). However, while a deep (garnet- or diamond-bearing) cratonic lithospheric mantle keel may be lacking in Scotland, the spinel lherzolites xenoliths from terranes N of the GGF represent the shallow regions of this cratonic SCLM (see Upton *et al.,* 2011 and references therein). These localities provide an opportunity to investigate the pre-Mesozoic shallow lithospheric mantle, as entrained in basaltic magmatism rather than kimberlites (Bonadiman *et al.*, 2008). By contrast the Loch Roag xenolith suite is entrained in an Eocene monchiquite dyke (Faithfull *et al.*, 2012) and represents mantle potentially modified by the Icelandic plume. A description of each xenolith locality can be found in the following subsections, summarised in Table 7.1.

7.1.2.1. Loch Roag, Isle of Lewis (Hebridean Terrane)

The 70 cm wide monchiquite dyke near Loch Roag (Isle of Lewis) cross-cuts Archaean Lewisian gneisses and contains a suite of upper mantle and crustal xenoliths and xenocrysts. Recent Ar-Ar dating has confirmed this dyke to be mid-Eocene in age (45.2 ± 0.2 Ma; Faithfull *et al.,* 2012) and is therefore the youngest known magmatic intrusion in the UK. The xenolith/xenocryst assemblage of the Loch Roag dyke is unusual in comparison to elsewhere in the UK and Europe (Upton *et al.,* 1983). It comprises a diverse range of lithologies and megacrysts; including spinel lherzolites, glimmerites, anothosites/anorthoclasites, gabbros and syenite xenoliths, and phlogopite 'books', apatite and corundum xenocrysts (Upton *et al.,* 1983; Hunter & Upton, 1987; Menzies *et al.,* 1987; Menzies & Halliday, 1988; Long *et al.,* 1991; Upton *et al.,* 1999 and Upton *et al.,* 2011). Previous studies on the spinel lherzolites were concerned with the isotopic composition and mineral chemistry of the major rock-forming minerals (see Upton *et al.,* 2011 and references therein). New Re-Os whole-rock isotopic data for a Loch Roag spinel lherzolite are also available in Hughes *et al.* (2014) (Chapter 6) – see Table 7.1. Overall, the spinel lherzolites are granoblastic, porphyroblastic to sub-equigranular with crystal sizes typically ranging 200 µm to 1 mm in size. Porphyroblasts of orthopyroxene, up to 10 mm wide, are also common. Spinel grains appear 'corroded' and are intergrown at the rim by anorthoclase and/or anorthoclase-clinopyroxene (Na-enriched) 'symplectites' (Hunter & Upton, 1987; Upton *et al.,* 2011). Spinel lherzolite xenoliths typically have an oxidised or altered green-orange-brown 'halo' (cm-scale) around their rim (in contact with the host dyke) with unaltered or 'fresh' grey-coloured peridotite at the xenolith core (e.g., Fig

7.3a-b). A suite of bright apple-green clinopyroxene-rich xenoliths (from hereon referred to as *'green clinopyroxenites'*; Fig. 7.3c) is present at Loch Roag. These consist of granular olivine and orthopyroxene, with rare chromite, but are dominated by granular polycrystalline green clinopyroxene.

7.1.2.2. Rinibar, South Ronaldsey, Orkney Isles (Northern Highland Terrane, NE)

The Rinibar xenolith locality is an approximately 1m wide alkali basalt dyke, cross-cutting Devonian sandstones (UK grid reference [412 929]). The xenolith suite comprises spinel lherzolites, which have been subjected to partial secondary hydration of ferromagnesian silicates along parallel fracture sets (such that xenoliths appear tan-brown; Fig. 7.3d) and have minor veining by calcite, magnetite and clays. The suite also includes clinopyroxene megacrysts. The host dyke is dated by whole-rock K-Ar methods at 252 ± 10 Ma (Baxter & Mitchell, 1984). Xenoliths from Rinibar have previously been investigated for their silicate and spinel trace element compositions, in addition to whole-rock Sr, Nd and Hf isotopes (Bonadiman *et al.*, 2008) – see Table 7.1. The spinel lherzolites still largely record protogranular textures (Bonadiman *et al.,* 2008) with fine-grained (≤ 0.5 mm) silicates and spinels and protogranular to porphyroclastic textures (Mercier & Nicholas, 1975). However the mineral crystal sizes are typically less than what would be expected in cratonic peridotite xenoliths (2-10 mm; Pearson *et al.,* 2003 and references therein).

7.1.2.3. Streap Com'laidh, near Glenfinnan (Northern Highland Terrane, SW)

The 70 cm wide host monchiquite dyke is part of a NE-SW trending swarm which intrudes Moinian metasediments (UK grid reference [945 844]), and is thought to date from c. 290 Ma (Walker & Ross, 1954; Praegel, 1981; Upton *et al.,* 1983, 2004). The mantle xenolith suite is dominated by spinel lherzolites, but also includes websterites (Bonadiman *et al.,* 2008 and references therein). Whole-rock analyses of the Streap Com'laidh spinel lherzolites have previously been presented in Praegel (1981). Whole-rock and clinopyroxene Sr, Nd and Hf isotopes, and silicate mineral trace element compositions have been reported in Bonadiman *et al.* (2008) – see Table 7.1. The Streap Com'laidh spinel lherzolites show primitive granoblastic mantle textures, similar to Rinibar lherzolites, however silicates (especially olivine) are notably fresher and the xenoliths as a whole have undergone significantly less alteration (e.g., Fig. 7.3e-f). Lherzolites from Streap are protogranular but distinctly fine grained (200-400 μm); olivine crystals are fresh, < 0.5 mm with rounded grain boundaries and occasionally with undulose extinction. Orthopyroxene may also be kinked (Bonadiman *et al.,* 2008).

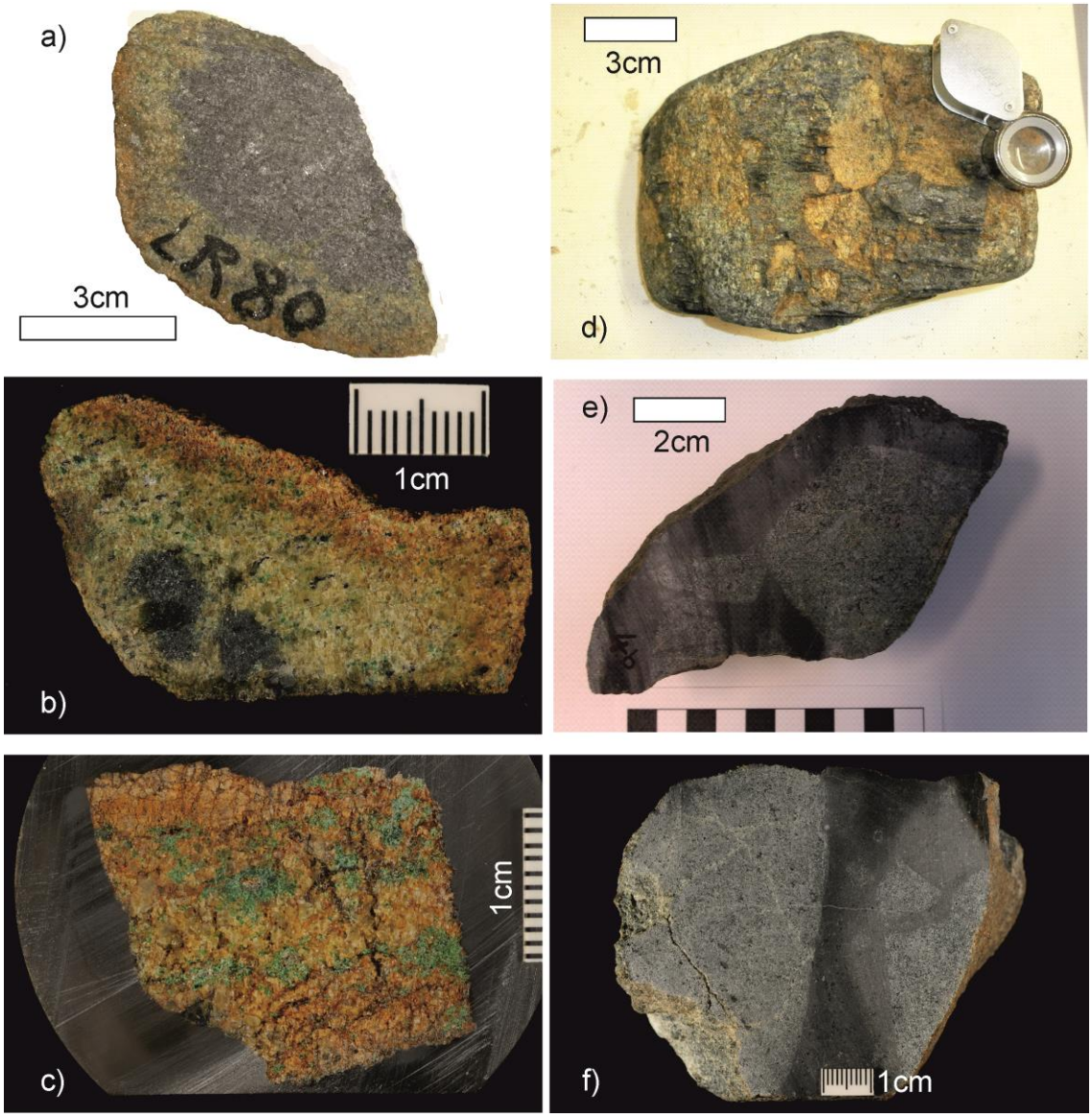

Figure 7.3. Hand sample photos of xenolith slices or xenoliths or xenoliths in dyke sample. (a) Slice of LR80 (Loch Roag spinel lherzolite) showing green-orange-brown 'halo' of oxidation and alteration surrounding grey 'fresh' peridotite interior. (b) Slice of LR90 (Loch Roag spinel lherzolite), showing similar features to (a), but with a greater thickness of the oxidised 'halo'. (c) Chip of LR100 (Loch Roag green clinopyroxenite) mounted in epoxy resin block (unpolished) showing thick 'stringers' or 'veins' of apple green clinopyroxene through brown-orange nodules or olivine and chromite. (d) Weathered surface of hand sample G8 (Rinibar spinel lherzolite) with multiple peridotite xenoliths (weathered tan-brown). (e) Cut surface of hand sample of R2 (Rinibar spinel lherzolite) xenolith in alkali basalt dyke. (f) Cut surface of hand sample ST5 (Streap Com'laidh spinel lherzolite) xenoliths in darker alkali basalt dyke material.

Table 7.1. Overview of xenolith localities in this study, including information available in the published literature.

Xenolith Suite	Terrane	Host dyke/sill	Thickness, strike/dip of host	Host dyke age	Xenoliths/Xenocryst suite
Loch Roag	Hebridean	Monchiquite dyke	approx. 70cm wide, 075°/ subvertical	45.2 Ma (Ar/Ar dating, Faithfull et al., 2012)	Lower crustal and mantle xenoliths (peridotites, pyroxenites, glimmerites, granulites, anorthosite, gabbros, syenites). Megacrysts (corundum/sapphires, feldspars, apatite, phlogophite)
Rinibar	Northern Highland (NE)	Alkali basalt dyke	approx. 1m wide dyke, striking NE-SW	252 ± 10Ma (K/Ar age, Baxter & Mitchell, 1984)	Spinel lherzolites and pyroxenite megacrysts
Streap Com'laidh	Northern Highland (SW)	Monchiquite dyke	approx. 70cm, NE-SW trending/subvertical	c. 290Ma (Walker & Ross, 1954; Upton *et al.*, 2004)	Spinel lherzolites, websterites, granulite-facies metagabbros and quartzo-feldspathic gneisses

Xenolith Suite	Mantle xenolith and xenocryst isotopic data	P-T estimates	Spinel lherzolite textures
Loch Roag	$^{143}Nd/^{144}Nd$ 0.5118-0.5124, $^{87}Sr/^{86}Sr$ 0.7048-0.7051 (Upton et al., 2011), $^{206}Pb/^{204}Pb$ 17.139-17.348, $^{208}Pb/^{204}Pb$ 36.911-37.570 (Menzies et al., 1987), $^{187}Re/^{188}Os$ 1.411, $^{187}Re/^{188}Os_{initial}$ 0.0703 (Hughes *et al.*, 2014)	-	200 µm to 1 mm crystal size (all silicates). Some orthopyroxene porphyroblasts up to 10mm.
Rinibar	$^{143}Nd/^{144}Nd$ 0.5124-0.5128, $^{87}Sr/^{86}Sr$ 0.7033-0.7038, $^{176}Hf/^{177}Hf$ 0.2828-0.2830 (CPX; Bonadiman et al., 2008). Fluid inclusions in olivine $^{3}He/^{4}He$ 2.84 ± 0.29, [^{4}He] 2.78 (Kirstein et al., 2004).	870-1000°C (opx-cpx Fe-Mg exchange thermometer); 1.2-1.8 GPa (Bonadiman *et al.*, 2008)	≤ 500 µm crystal size (all silicates)
Streap Com'laidh	$^{143}Nd/^{144}Nd$ 0.5121-0.5127, $^{87}Sr/^{86}Sr$ 0.7065-0.7083, $^{176}Hf/^{177}Hf$ 0.2825-0.2831 (Bonadiman et al., 2008). Fluid inclusions in olivine $^{3}He/^{4}He$ 6.01-6.33, [^{4}He] 9.26-63.3 (Kirstein *et al.*, 2004).	840-1000°C (opx-cpx Fe-Mg exchange thermometer); 1.2-1.8 GPa (Bonadiman *et al.*, 2008)	200-400 µm crystal size (all silicates)

7.2. Analytical techniques and methodology

7.2.1. Petrography and mineral chemistry analysis

Petrographic studies on polished thin-sections were employed to identify xenolith textures. Further thin-section examination, mapping and quantitative microanalysis was carried out on a Cambridge Instruments S360 scanning election microscope (SEM) at Cardiff University. Quantitative microanalyses were obtained using an Oxford Instruments INCA Energy EDX analyser attached to the SEM, with operating conditions set at 20kV and specimen calibration current of ~2 nA at a fixed working distance of 25 mm. Analytical drift checks were carried out every 2 hours using the Co reference standard and a comprehensive suite of standards from MicroAnalysis Consultants Ltd were used to calibrate the EDX analyser.

Laser Ablation-Inductively Coupled Plasma-Mass Spectrometry (LA-ICP-MS) was performed on clinopyroxenes at Cardiff University. The system comprised a New Wave Research UP213 laser system coupled to a Thermo X Series 2 ICP-MS. The laser was operated using a frequency of 20 Hz that developed pulse energy of 1-2 mJ for a 40 µm diameter beam. Samples were analysed using an acquisition time of 90 seconds, comprising a 20 second gas blank, 60 second ablation and 10 second wash-out. Calibration of the ICP-MS was accomplished using the USGS glass standards BIR-1a and BHVO-2G with certified USGS basalt glass BCR-2G analysed as an unknown every 10-12 samples to check the accuracy of the analysis. A summary of the measured concentrations in the BCR-2g unknowns versus expected concentrations is given in Table A in the supplementary information (on disk).

The suite of isotopes analysed were ^{23}Na, ^{25}Mg, ^{29}Si, ^{39}K, ^{44}Ca, ^{47}Ti, ^{51}V, ^{52}Cr, ^{55}Mn, ^{60}Ni, ^{71}Ga, ^{85}Rb, ^{88}Sr, ^{89}Y, ^{90}Zr, ^{93}Nb, ^{133}Cs, ^{137}Ba, ^{139}La, ^{140}Ce, ^{141}Pr, ^{146}Nd, ^{147}Sm, ^{153}Eu, ^{157}Gd, ^{159}Tb, ^{163}Dy, ^{165}Ho, ^{166}Er, ^{169}Tm, ^{172}Yb, ^{175}Lu, ^{178}Hf, ^{181}Ta, ^{208}Pb, ^{232}Th and ^{238}U. Calcium concentrations of clinopyroxene cores and rim, as determined using SEM, were used as an internal standard to correct for matrix and drift effects in the calculation of the trace-element abundances. Blank correction, drift corrections and conversion of ICP-MS output data (counts/sec) to concentrations (wt.% or µg/g) was accomplished using the Thermo Plasmalab software. Full data for major and trace element concentrations in clinopyroxene from the xenolith samples are given in Table B of the supplementary information (on disk).

7.2.2. Whole-rock sample preparation and analysis

Mantle xenolith samples were provided by the British Geological Survey and Hunterian Museum (University of Glasgow). For whole-rock analyses this included 7 separate xenoliths of approximately 3-6 cm diameter from Loch Roag (e.g., Fig. 7.3a-c), 2 larger angular xenoliths (10-20 cm) from Rinibar, and 5 large xenoliths (ranging 10-15 cm diameter) from Streap Com'laidh (e.g., Fig. 7.3e-f). When cut, some of the Loch Roag peridotite xenoliths display dark green 'alteration' rims, with orange-brown vein-like infills. In one of these samples (LR80; Fig. 7.3a) a grey-black, visually 'unaltered' central zone in the xenolith was large enough to be extracted and analysed separately. Only xenoliths large enough for powdering were selected for whole-rock analysis but where material was limited, powdered samples weighed at least 25 g (typically 80-150 g for larger xenolith samples). The dykes hosting the xenolith suites were also analysed in order to compare the compositions of the dykes and xenoliths, and therefore to assess if dyke material remained during xenolith sample preparation.

All samples were crushed to chips either by hand (smaller samples) in a hardened steel pestle and mortar, or crushed through a hardened steel jaw crusher (larger samples). Gravels were then milled to a fine powder in agate planetary ball mills at Cardiff University. Major and trace elements were analysed by inductively coupled plasma optical emission spectrometry (ICP-OES) and inductively coupled plasma mass spectrometry (ICP-MS), respectively, at Cardiff University using methods and instrumentation described by McDonald & Viljoen (2006). Accuracy was constrained by analysis of the certified international reference materials JB1a, JB3, NIM-P, NIM-N, JA2 and JP1. Precision was estimated by repeat analysis of a sub-set of samples. Whole-rock geochemical results for all xenoliths and dykes analysed during this study are presented in Table 7.2.

Table 7.2. *(continued overleaf)*

Sample number	LR81*	LR101335*	LR289*	LR80*	LR84
Location	Loch Roag	Loch Roag	Loch Roag	Loch Roag	Loch Roag
Rock type	Spinel lherzolite xenolith	Spinel lherzolite xenolith	Spinel lherzolite xenolith	Spinel lherzolite xenolith	Green clinopyroxenite
Terrane	Hebridean	Hebridean	Hebridean	Hebridean	Hebridean
(wt.%)					
SiO_2	45.34	42.85	43.97	45.33	41.69
Al_2O_3	2.40	1.06	1.89	1.59	1.06
Fe_2O_3*	10.12	11.48	10.05	10.20	9.77
MgO	35.78	38.16	37.04	38.71	42.55
CaO	2.54	2.61	2.53	2.22	1.98
Na_2O	0.46	0.16	0.30	0.44	0.23
K_2O	0.54	0.03	0.11	0.09	0.02
TiO_2	0.03	0.05	0.06	0.03	0.02
MnO	0.16	0.25	0.17	0.13	0.13
P_2O_5	0.15	0.22	0.12	0.04	0.02
LOI	3.25	2.37	3.29	0.92	1.66
Total	100.78	99.23	99.53	99.70	99.13
Mg#	0.89	0.88	0.89	0.90	0.91
(ppm)					
Sc	13	9	12	12	10
V	60	37	48	47	22
Cr	2910	2599	3001	2456	2504
Co	107	130	133	103	131
Ni	1756	2404	2022	2144	2301
Cu	98	70	97	182	29
Rb	5.5	1.2	2.7	2.3	1.1
Sr	256	94	250	28	50
Y	6.9	9.7	9.4	4.4	9.3
Zr	5	16	7	6	89
Nb	0.37	3.42	0.98	1.12	4.87
Ba	48	26	38	13	20
La	100.23	54.65	87.14	18.91	22.02
Ce	216.44	135.63	213.27	21.13	46.50
Pr	15.96	12.26	20.02	2.74	5.80
Nd	40.74	35.78	53.41	7.89	16.27
Sm	4.36	4.72	6.47	0.93	3.17
Eu	0.75	0.93	1.12	0.22	0.77
Gd	3.59	3.78	4.80	0.82	2.70
Tb	0.33	0.41	0.47	0.10	0.33
Dy	1.39	2.00	2.11	0.58	1.74
Ho	0.22	0.32	0.34	0.11	0.30
Er	0.64	0.89	0.97	0.32	0.78
Tm	0.09	0.13	0.14	0.05	0.12
Yb	0.54	0.78	0.87	0.32	0.76
Lu	0.08	0.11	0.13	0.05	0.11
Hf	0.14	0.42	0.17	0.14	1.93
Ta	0.02	0.19	0.06	0.07	0.28
Th	2.71	0.89	2.81	1.26	0.48
U	0.73	0.24	1.02	0.33	0.40

Table 7.2. *(continued overleaf)*

Sample number	LR90	LR100	E19	R2	ST2
Location	Loch Roag	Loch Roag	Rinibar	Rinibar	Streap
Rock type	Spinel lherzolite xenolith	Green clinopyroxenite	Spinel lherzolite xenolith	Spinel lherzolite xenolith	Spinel lherzolite xenolith
Terrane	Hebridean	Hebridean	Northern Highland (NE)	Northern Highland (NE)	Northern Highland (SW)
(wt.%)					
SiO_2	43.23	42.12	42.34	42.03	45.77
Al_2O_3	1.84	1.31	1.46	2.37	3.16
Fe_2O_3*	9.68	11.88	7.86	8.59	9.11
MgO	41.37	38.84	32.90	34.01	36.82
CaO	1.29	4.39	2.30	3.81	2.77
Na_2O	0.49	0.46	0.21	0.28	0.26
K_2O	0.13	0.03	0.07	0.07	0.03
TiO_2	0.03	0.02	0.07	0.16	0.14
MnO	0.15	0.23	0.11	0.15	0.12
P_2O_5	0.00	0.05	0.07	0.02	0.01
LOI	1.54	2.02	11.92	7.73	1.61
Total	99.76	101.34	99.30	99.22	99.81
Mg#	0.91	0.88	0.91	0.91	0.91
(ppm)					
Sc	12	12	10	11	15
V	56	38	44	55	57
Cr	2646	4221	2212	2454	2274
Co	108	101	99	91	88
Ni	1892	1702	2040	1663	2038
Cu	35	21	67	27	41
Rb	2.8	2.0	2.8	2.6	1.0
Sr	20	102	148	209	26
Y	3.5	14.2	2.2	3.5	3.2
Zr	8	77	5	31	5
Nb	3.80	9.64	3.16	5.70	1.83
Ba	35	15	64	78	8
La	34.54	37.56	10.45	10.09	0.50
Ce	75.52	75.57	17.57	15.73	1.07
Pr	6.45	9.72	2.00	1.68	0.16
Nd	15.49	26.61	6.90	5.87	0.84
Sm	2.02	5.10	1.06	1.02	0.27
Eu	0.31	1.20	0.27	0.32	0.11
Gd	1.71	4.11	0.82	0.95	0.32
Tb	0.17	0.52	0.09	0.13	0.07
Dy	0.78	2.73	0.41	0.65	0.48
Ho	0.13	0.45	0.08	0.12	0.10
Er	0.33	1.15	0.24	0.34	0.31
Tm	0.05	0.18	0.04	0.05	0.05
Yb	0.27	1.12	0.19	0.31	0.33
Lu	0.04	0.17	0.03	0.06	0.06
Hf	0.29	1.99	0.09	0.77	0.09
Ta	0.29	0.65	0.17	0.34	0.10
Th	0.72	0.73	0.82	1.37	0.27
U	0.37	0.65	0.22	0.41	0.06

Table 7.2. Whole-rock major and trace element geochemistry of spinel lherzolite xenoliths analysed during this study. Also presented are the whole-rock analyses of host dykes to the xenoliths. Note that results from Loch Roag marked with (*) have previously been reported in Hughes et al. (2014) – Chapter 6. Totals are those from oxides with 4 decimal places, displayed to 2 decimal places.

Sample number	ST5	ST4b	ST4a	ST4c	LRh	R2dyke
Location	Streap	Streap	Streap	Streap	Loch Roag	Rinibar
Rock type	Spinel lherzolite xenolith	Spinel lherzolite xenolith	Spinel lherzolite xenolith	Spinel lherzolite xenolith	Monchiquite dyke	Lamprophyre dyke
Terrane	Northern Highland (SW)	Northern Highland (SW)	Northern Highland (SW)	Northern Highland (SW)	Hebridean	Northern Highland (NE)
(wt.%)						
SiO_2	47.56	46.85	43.96	47.53	44.88	38.51
Al_2O_3	3.37	3.42	3.11	3.19	14.85	9.56
Fe_2O_3*	8.96	9.75	9.84	9.51	8.48	10.33
MgO	34.44	35.59	37.12	34.43	7.75	20.36
CaO	3.46	2.75	2.71	2.89	10.84	8.48
Na_2O	0.29	0.26	0.21	0.29	1.91	0.79
K_2O	0.01	0.06	0.04	0.05	3.49	0.81
TiO_2	0.15	0.12	0.12	0.13	2.73	1.91
MnO	0.12	0.13	0.13	0.13	0.21	0.22
P_2O_5	0.02	0.01	0.02	0.02	1.19	0.74
LOI	1.20	2.31	2.61	0.96	4.65	8.30
Total	99.58	101.24	99.87	99.13	100.95	100.01
Mg#	0.90	0.90	0.90	0.90	0.78	0.85
(ppm)						
Sc	13	13	13	14	22	22
V	69	60	58	59	213	185
Cr	3167	2399	2656	2531	230	944
Co	99	95	100	96	36	59
Ni	1882	2227	2380	2127	136	568
Cu	137	74	58	153	52	75
Rb	0.8	2.1	1.4	1.2	39.9	34.7
Sr	46	38	101	54	1797	393
Y	3.7	3.0	3.0	3.0	28.0	22.2
Zr	7	3	5	4	347	120
Nb	1.43	1.90	2.18	1.82	100.76	72.80
Ba	3	15	9	8	2558	649
La	1.06	1.26	1.31	1.08	132.11	52.00
Ce	2.32	2.24	2.41	2.18	239.79	92.65
Pr	0.31	0.28	0.30	0.29	27.04	10.90
Nd	1.38	1.16	1.29	1.25	91.41	40.14
Sm	0.39	0.29	0.33	0.32	12.87	7.32
Eu	0.13	0.11	0.11	0.11	3.65	2.18
Gd	0.39	0.31	0.35	0.31	10.72	6.79
Tb	0.07	0.06	0.06	0.06	1.24	0.90
Dy	0.55	0.44	0.46	0.47	5.48	4.27
Ho	0.11	0.09	0.09	0.09	0.95	0.74
Er	0.34	0.28	0.28	0.27	2.55	1.97
Tm	0.05	0.05	0.04	0.04	0.34	0.26
Yb	0.34	0.30	0.28	0.31	2.06	1.54
Lu	0.06	0.05	0.05	0.05	0.31	0.25
Hf	0.17	0.08	0.11	0.10	8.42	3.08
Ta	0.08	0.11	0.11	0.11	4.97	3.85
Th	0.29	0.41	0.40	0.34	8.59	6.35
U	0.07	0.09	0.09	0.12	2.56	2.03

7.3. Results

7.3.1. Aspects of petrography and accessory mineralogy

Representative back scattered electron (BSE) images obtained by scanning electron microscope (SEM) are presented in Figures 7.3-7.5. In lherzolites from Streap Com'laidh we highlight the effects of peripheral xenolith melting during entrainment in the host dyke. This is manifest by Al-Mg spinel melting reactions to produce 'disaggregated' chromite, which penetrates along silicate grain boundaries and into the host dyke (e.g., Fig. 7.4a-b). In some cases, tiny micron or sub-micron scale Ni-Fe sulphide droplets are associated (and entrained?) with the melted chromite (e.g., Fig. 7.4c). Elsewhere, partially melted clinopyroxene is also observed, however this is not restricted to the xenolith margins and is not obviously associated with any foreign melt ingress. Micron scale Ni-Fe sulphide droplets are also present at the clinopyroxene melting interface (Fig. 7.4d). In Rinibar xenoliths, silicates (especially olivine) are notably altered and hydrated – for example in serpentinised Fe-oxide and Ni-Fe sulphide droplet-bearing olivine of Figure 7.5a. Melting reactions occur at the xenolith margins in contact with the host dyke, however these appear to re-anneal the xenolith, sealing it off at the rim such that serpentinised fractures are 'healed' (Fig. 7.5b). In some Rinibar samples, clinopyroxene contains elongate inclusions or 'lamellae' of chromite, which have then been cross-cut and fractured by serpentine-filled veinlets (Fig. 7.5c). Mg-Al spinel is absent in Rinibar, and instead the majority of spinel-group minerals in these xenoliths are chromite. In some cases, the xenoliths contain clinopyroxene, plagioclase and orthoclase different from the composition of the host dyke (Fig. 7.5d).

Apple-green polycrystalline clinopyroxene-bearing xenoliths (*'green clinopyroxenites'*) were also analysed from Loch Roag (Figure 7.6). Clinopyroxene occurs as anastomosing green 'veins' and 'stringers' across these rocks (e.g., Fig. 7.3c). These xenoliths are highly friable and show polycrystalline clinopyroxenes surrounding and including fine granular olivine and chromite crystals (Fig. 7.6a,c,d). Sulphides are extremely rare, in contrast with other Loch Roag spinel lherzolites and, where present, these consist of pentlandite and pyrrhotite only (Fig. 7.6b). Intriguingly, the clinopyroxene-rich specimens also retain white chlorite-filled veinlets (up to 1 mm wide) with minor phlogopite. Within these veinlets, chlorite has been overprinted by a Ce-carbonate, possibly bastnaesite-(Ce) [i.e., $(Ce,La)(CO_3)F$] which has infilled cleavage planes and fractures, sometimes associated with serpentine, along the chlorite 'books' (Fig. 7.6e-f).

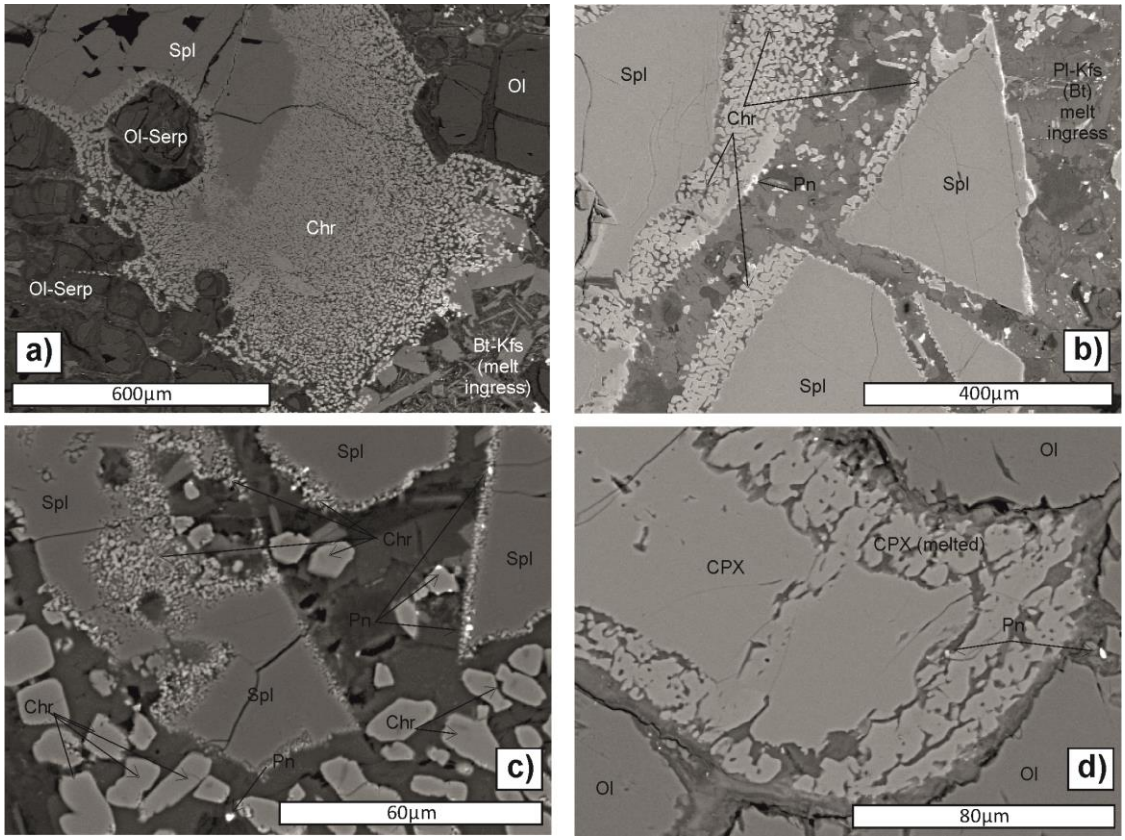

Figure 7.4. Streap Coml'aidh BSE SEM images: (a) Al-Mg spinel reacting and melting to fine granular chromite at spinel grain boundary and enclosing granular serpentinised olivine. Lower right hand corner of image shows ingressed orthoclase and biotite-rich melt, possible from the host dyke entraining the xenolith (sample 4a1). (b) Al-Mg spinel reacting and melting to chromite. Note the tiny µm-scale rounded pentlandite globules associated with spinel-chromite melting (sample 4a1). (c) Similar to (b) Al-Mg spinel melting at rim and forming granular chromite. Note the two crystal size populations of chromite: > 5 µm granular, sub-euhedral chromite crystals vs. µm-scale rounded chromites. Both chromite populations are associated with µm-scale pentlandite globules at crystal margins (sample 4a1). (d) Protogranular clinopyroxene and olivine. Clinopyroxene is melting to form finger-like crystals at its margins. This melt zone is again associated with µm-scale pentlandite globules (sample 4a1). Mineral abbreviations clinopyroxene (CPX), orthopyroxene (OPX), olivine (Ol), spinel (Spl), chromite (Chr), serpentine (Serp), pentlandite (Pn).

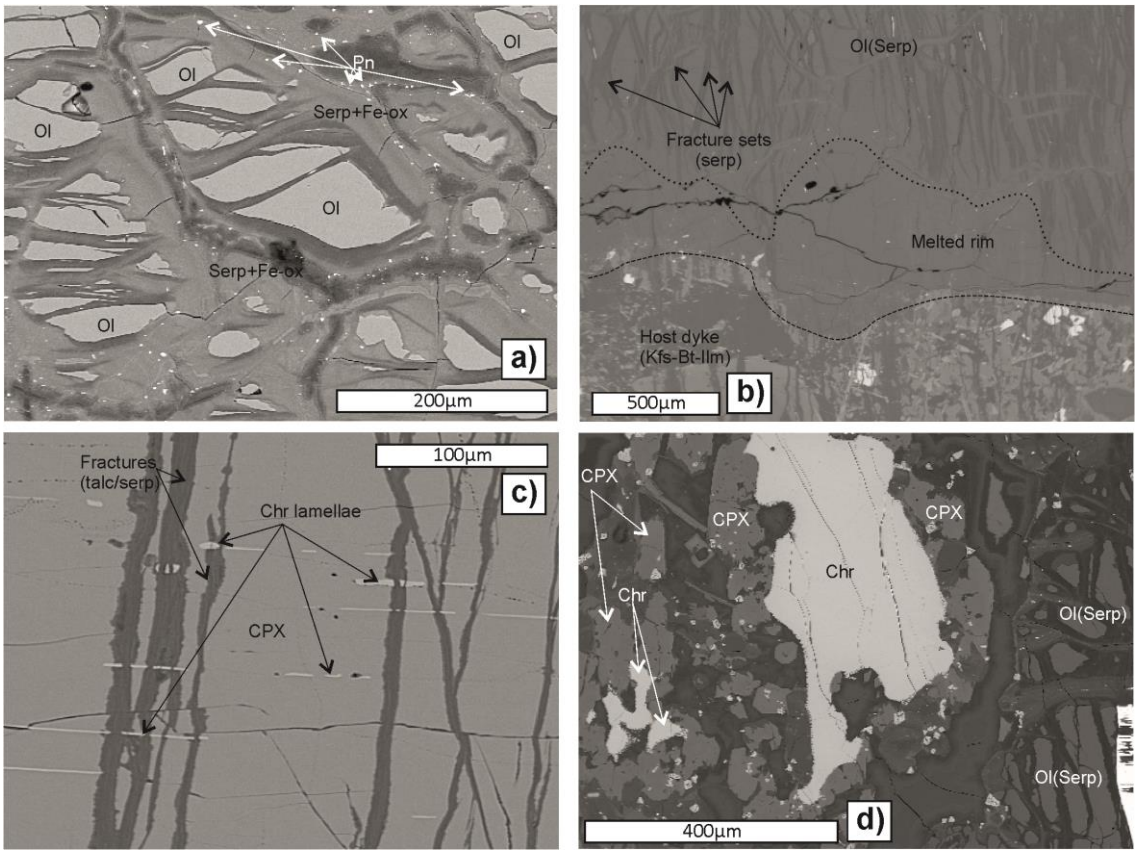

Figure 7.5. Rinibar BSE SEM images: (a) µm-scale pentlandite globules associated with serpentinised olivine (sample E19). (b) Image shows edge of xenolith in contact with the host dyke. Dyke consists of finely crystalline orthoclase, biotite and ilmenite and has a sharp contact with the xenolith. The inner portion of the xenolith (top of image) has widespread anastomosing fractures (serpentine- and talc-filled) but a melted and 'annealed' zone (free of fractures) sits in contact with the dyke (sample R2). (c) Clinopyroxene with parallel set of serpentine and talc-filled fractures. Note the chromite lamellae throughout clinopyroxene, orthogonal to the fractures. Chromite lamellae are cross-cut by the fractures (sample R2). (d) Melt pocket consisting of chromite (with very fine granular rim) and clinopyroxene with interstitial plagioclase and orthoclase feldspars. Serpentinised olivine on right hand side of image is protogranular. Mineral abbreviations olivine (Ol), serpentine (Serp), clinopyroxene (CPX), dolomite (Dol), magnesite (Mag), plagioclase (Pl), chromite (Chr), apatite (Ap), iron oxides (Fe-ox), orthoclase (Kfs), biotite (Bt), ilmenite (Ilm).

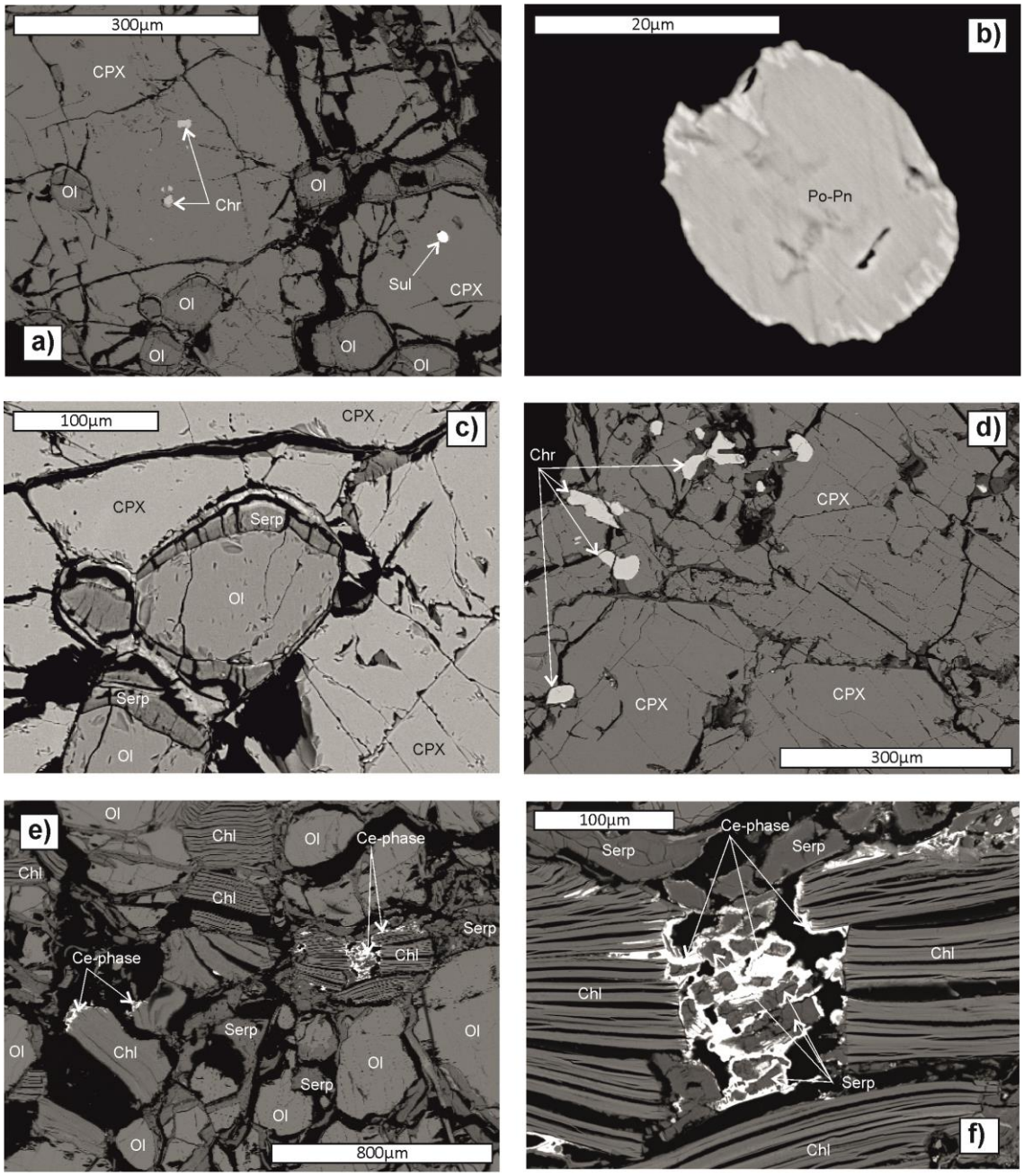

Figure 7.6. Loch Roag green clinopyroxenite sample (LR84) BSE SEM images: (a) Anhedral clinopyroxene (apple-green in thin section) with small granular inclusions of olivine (partially serpentinised), chromite, and a rare rounded sulphide. (b) Close-up of the sulphide in (a), showing simple rounded shape and simple internal texture of pentlandite flames in pyrrhotite. (c) Close-up of partially serpentinised (at rim) olivine inclusions in clinopyroxene of (a). (d) Irregular-shaped chromite inclusions in metasomatic clinopyroxene (apple-green in thin section). (e) Close-up of a section of a chlorite-filled veinlet that cross-cuts the xenolith. Books of chlorite within the vein are surrounded by granular serpentinised olivine. Chlorite books have a Ce-mineral (carbonate or oxide) mineralising along the chlorite cleavage and ends of crystals. (f) Close-up of Ce-mineral in (e) showing chlorite book with Ce-mineral encasing 'book ends' and granular serpentine (presumably olivine prior to serpentinisation). Mineral abbreviations olivine (Ol), clinopyroxene (CPX), chromite (Chr), sulphide (Sul), serpentine (Serp), chlorite (Chl), Ce-carbonate/bastnaesite (Ce-phase), pentlandite (Pn), pyrrhotite (Po).

7.3.2. Whole-rock element abundances

7.3.2.1. Calculated normative mineral abundances

CIPW norm calculation results for mineral abundances based on anhydrous whole-rock major oxide (with FeO calculated from $\{Fe_2O_3^{measured} - (TiO_2 + 1.5)\}/1.1$), and Sr, Ba, Ni, Cr and Zr concentrations based on the method of Johannsen (1931) are shown in Table C (Supplementary Material – on disk) and Figure 7.7. Spinel lherzolite xenoliths from Loch Roag have the highest modal olivine contents (56-70 wt.%), generally lowest orthopyroxene abundances (0.8-24 wt.%) and variable clinopyroxene content (up to 14 wt.%). By contrast, xenoliths from the Northern Highland Terrane have substantially lower olivine contents (39-59 wt.%) and a narrower range of clinopyroxene abundances (4.5-7.4 wt.%). Xenoliths from the Northern Highland Terrane also have a higher calculated abundance of plagioclase feldspars (5.3-10.5 wt.%) consistent with observed occurrences of 'corroded' spinels with a halo of anothosite symplectites in the Loch Roag xenoliths (e.g., Hunter & Upton, 1987).

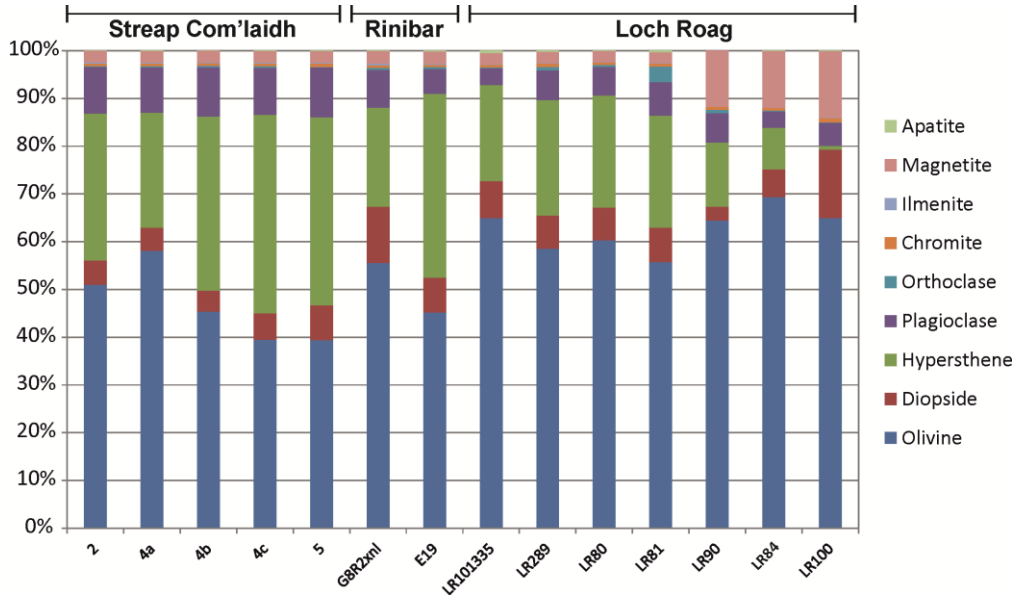

Figure 7.7. Cumulative bar chart of calculated mineral abundances in xenoliths analysed by whole-rock ICP-OES and ICP-MS. Mineral abundances calculated by CIPWnorm method

7.3.2.2. Major elements

Bivariant plots of major element oxides against Al_2O_3 content (as a proxy for the degree of depletion by partial melting) are presented in Figures 7.8a-f, in comparison to published

xenolith data from the Greenlandic NAC (western and eastern coasts) and 'primitive upper mantle' (PUM; see figure caption for details). The Al_2O_3 contents of the Scottish peridotites range from compositions overlapping typical NAC (for Loch Roag) to those approaching PUM (for Streap Com'laidh). Al_2O_3 in Loch Roag varies by a factor of 3, whereas Streap Com'laidh has a tightly clustered Al_2O_3 ranging 3.1-3.4 wt.% (anhydrous). Rinibar xenolith Al_2O_3 compositions in Figure 7.8 are heavily dependent on their re-normalisation to anhydrous values. In comparison to other NAC, the Scottish peridotites have notably lower MgO contents (35-43 wt.% anhydrous), and higher FeO^T (8-11 wt.% anhydrous) and CaO (1.3-4.4 wt.% anhydrous) – see Figures 7.8a-c. Na_2O contents of Loch Roag appear to form a bimodal distribution, with samples LR81, LR90, LR100 and LR80 having substantially higher concentrations that other Scottish or NAC peridotites (Fig. 7.8d). TiO_2 contents of the Scottish xenoliths are comparable to elsewhere in the NAC, with Streap Com'laidh forming a cluster along the chondrite Al_2O_3-TiO_2 ratio (Fig. 7.8e). MnO content is higher in two Loch Roag xenoliths (one spinel peridotite and one clinopyroxenite) than in other N Scottish xenoliths and other NAC xenoliths (Fig. 7.8f). Using elemental ratio plots of Mg/Si, Al/Si and Cr/Al, the Scottish lherzolite xenoliths appear to continue along a trend from the depleted cratonic peridotites of NAC towards PUM (Figs. 7.8g-h).

7.3.2.3. Trace elements

Bivariant plots for trace elements in Figure 7.9 are plotted versus Al_2O_3. Scottish xenoliths have higher Sc concentrations than elsewhere in the NAC, reflecting higher modal clinopyroxene abundances (Figs. 7.8a and 7.6 respectively). Xenoliths from both the Hebridean and Northern Highland Terranes have variable Ni contents (ranging 1500-2500 ppm; Fig. 7.9b) but do not fall along a positive fractionation trend relating to partial melting, as seen for Greenlandic NAC peridotites at high MgO content (i.e., Ni/Mg ratio is highly variable). Hence for the Scottish xenoliths and low-MgO NAC xenoliths, Ni concentration is predominantly controlled by sulphide abundance, rather than olivine. Co content is similarly variable (Fig. 7.9b) however Cu abundances in the Scottish xenoliths are extremely variable and are several orders of magnitude greater than measured elsewhere in the Greenlandic NAC (Fig. 7.9d). Cu appears to vary independently of Al_2O_3 (or MgO) and probably tracks sulphides which are abundant in some xenoliths. In contrast, V concentrations in Loch Roag xenoliths overlap Greenlandic NAC compositions (Fig. 7.9e), however Cr concentrations fall along a trend with Al_2O_3 which is distinct from other eastern NAC xenoliths (Fig. 7.9f).

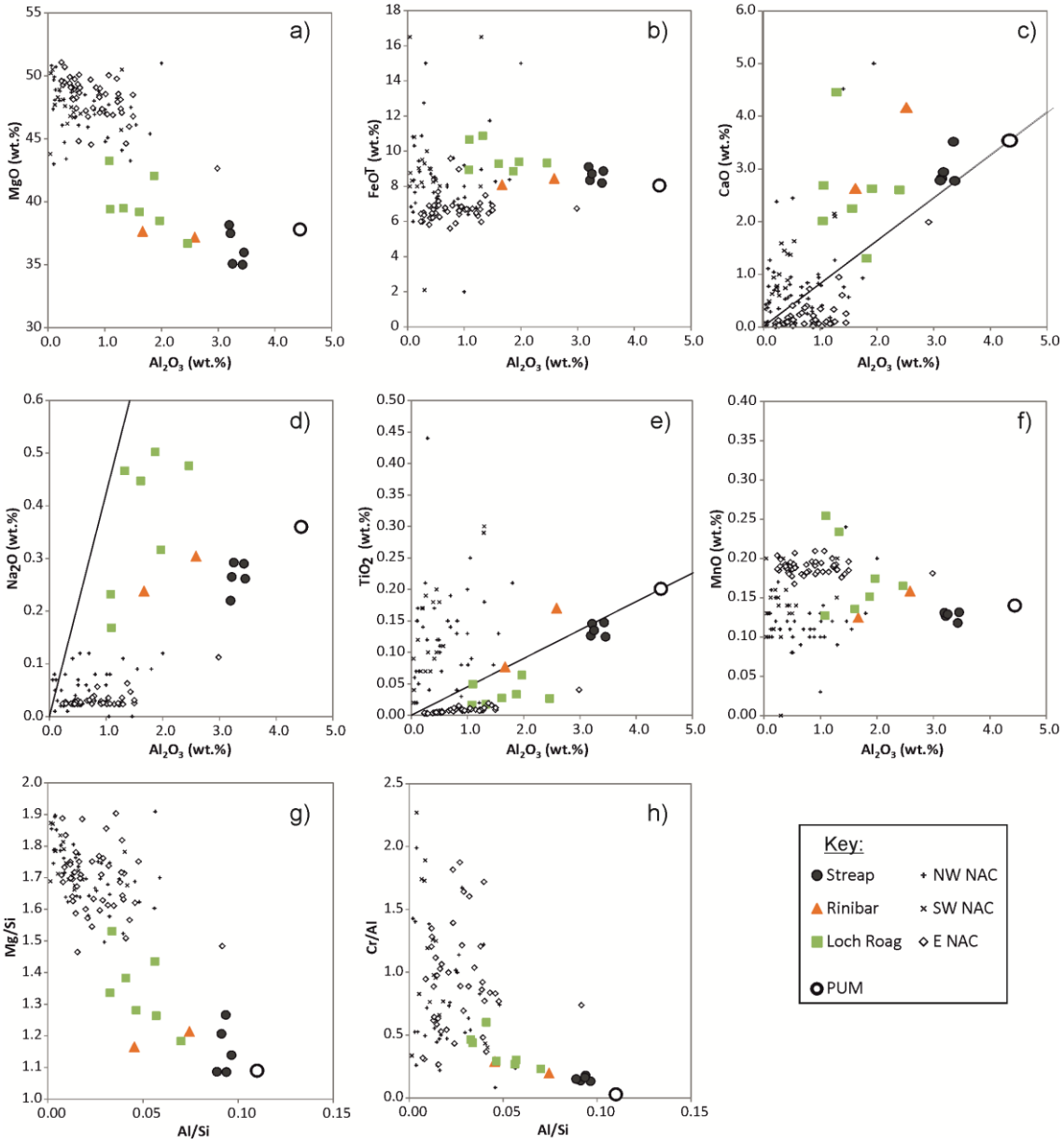

Figure 7.8. Major element bivariant plots (whole-rock) for Loch Roag, Streap Com'laidh and Rinibar spinel lherzolites (this study) in comparison to western ('NW NAC' and 'NW NAC'; from Wittig *et al.,* 2010) and eastern ('E NAC'; from Bernstein *et al.,* 1998) North Atlantic Craton mantle peridotites. Western NAC data are a mix of garnet and spinel peridotites. Eastern NAC data are all spinel peridotites. Black line indicates chondrite ratio of elements (as defined by McDonough & Sun, 1995).

Figure 7.10 compares the chondrite-normalised rare earth element (REE) abundances of the lherzolite xenoliths with their host dykes, and can be used to assess if the dyke has become mixed with the xenoliths either during entrainment itself, or sample crushing and homogenisation. For Loch Roag, the host dyke has higher overall REE abundances, and notably lacks the negative Eu anomaly observed in the lherzolites. The overall REE abundances of the Rinibar dyke are an order of magnitude greater than those of the peridotite xenoliths analysed, and show subtle differences in light REE (LREE), middle REE (MREE) and heavy REE (HREE) patterns. Both Loch Roag and Rinibar xenoliths have highly fractionated REE abundances, such that LREE are elevated above HREE, but by contrast the Streap Com'laidh xenoliths have comparatively flat REE patterns, such that chondrite-normalised LREE are only marginally more enriched than HREE. Further, HREE in Streap Com'laidh are inversely fractionated, increasing from Ho to Lu. Loch Roag spinel lherzolites have $(La/Yb)_N$ ragning from 40 to 127, Rinibar ranges 22 to 37 and Streap Com'laidh $(La/Yb)_N$ ranges from 1 to 3.

The trace element compositions of the xenoliths and host dykes can be further compared using the primitive mantle normalised multi-element diagrams in Figure 7.11. Incompatible element abundances are highly elevated in the host dykes of Rinibar and Loch Roag in comparison to the xenoliths. For certain key elements (e.g., Nb, Ta, Sr, P, Zr, Hf and Ti) the trace element systematics between the dyke and corresponding xenoliths are entirely different, suggesting that host dyke contamination was not an issue during sample preparation and/or xenolith entrainment in the alkali basalt dykes. Thus, the trace element abundances and patterns in the xenoliths are primary features, largely unaffected by the host magmas.

Differences in the normalised trace element patterns of Figure 7.11 are seen between each Scottish xenolith suite. For example, all Loch Roag xenoliths (spinel lherzolites and clinopyroxenites) display consistent negative Nb, Ta, Sr and Ti anomalies, with most also having a notable negative Zr and Hf anomaly. The Zr and Hf abundances in Rinibar samples are strikingly different for the two xenoliths analysed (one has a negative Zr-Hf anomaly on Fig. 7.11b while the other lacks any anomaly), while the other trace elements on the diagram show more consistent features between Rinibar xenoliths. In the Streap Com'laidh suite, Ba is depleted in comparison to Rb, and there is a consistent positive Sr anomaly, unlike any of the other suites.

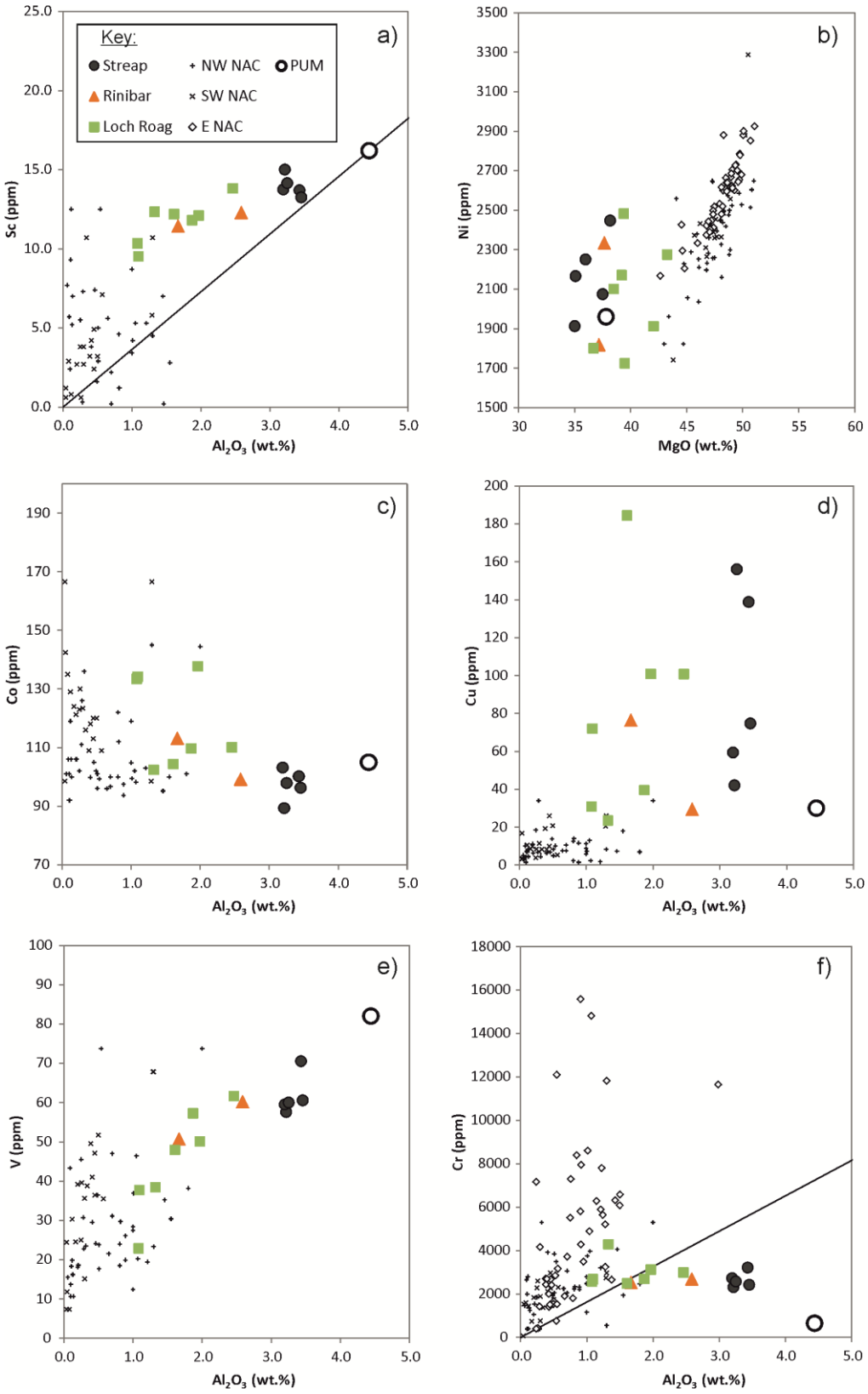

Figure 7.9. Minor element bivariant plots (whole-rock) for Loch Roag, Streap Com'laidh and Rinibar spinel lherzolites (this study) in comparison to western ('NW NAC' and 'NW NAC'; from Wittig *et al.,* 2010) and eastern ('E NAC'; from Bernstein *et al.,* 1998) North Atlantic Craton mantle peridotites. Western NAC data are a mix of garnet and spinel peridotites. Eastern NAC data are all spinel peridotites. Black line indicates chondrite ratio of elements (as defined by McDonough & Sun, 1995).

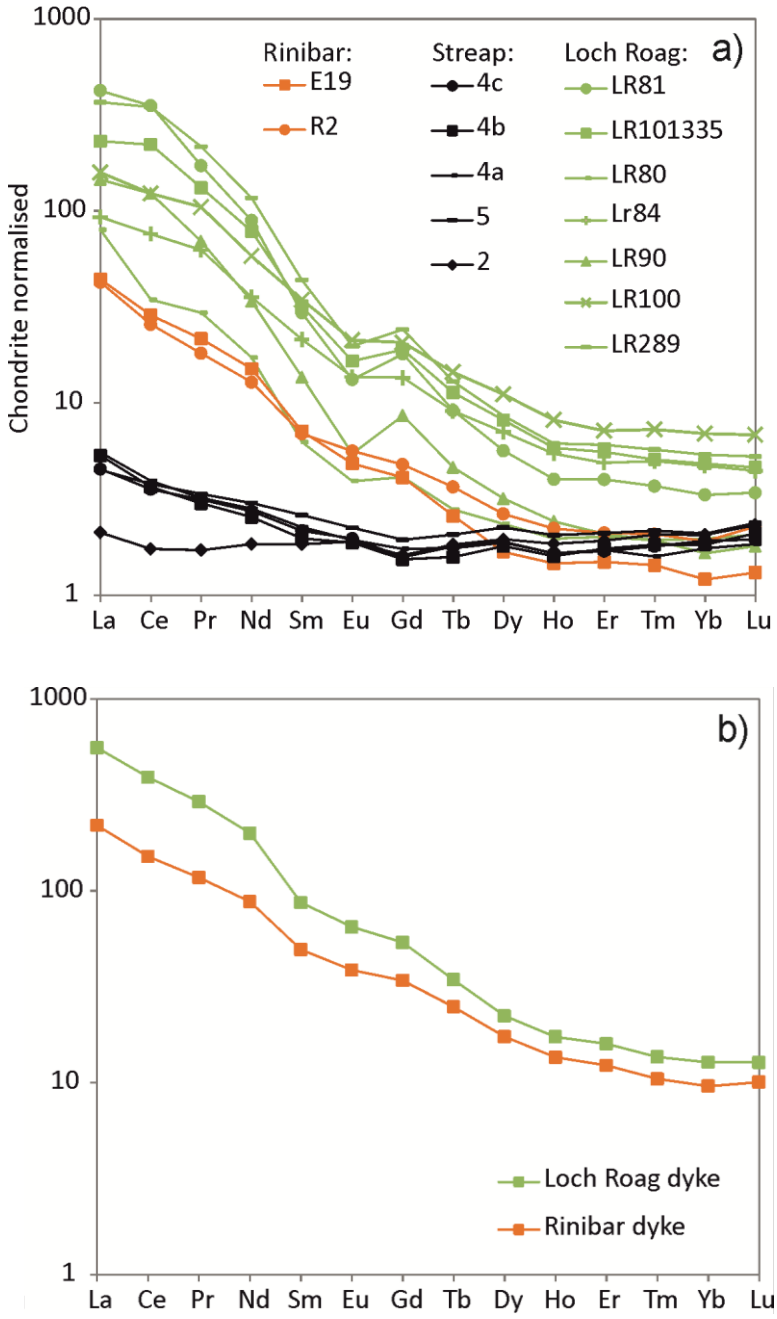

Figure 7.10. Rare Earth Element (REE) chondrite-normalised multi-element diagrams (whole-rock) for Loch Roag, Streap Com'laidh and Rinibar spinel lherzolites (a) and the host dykes to the xenolith suites (b). Chondrite normalising values from McDonough & Sun (1995).

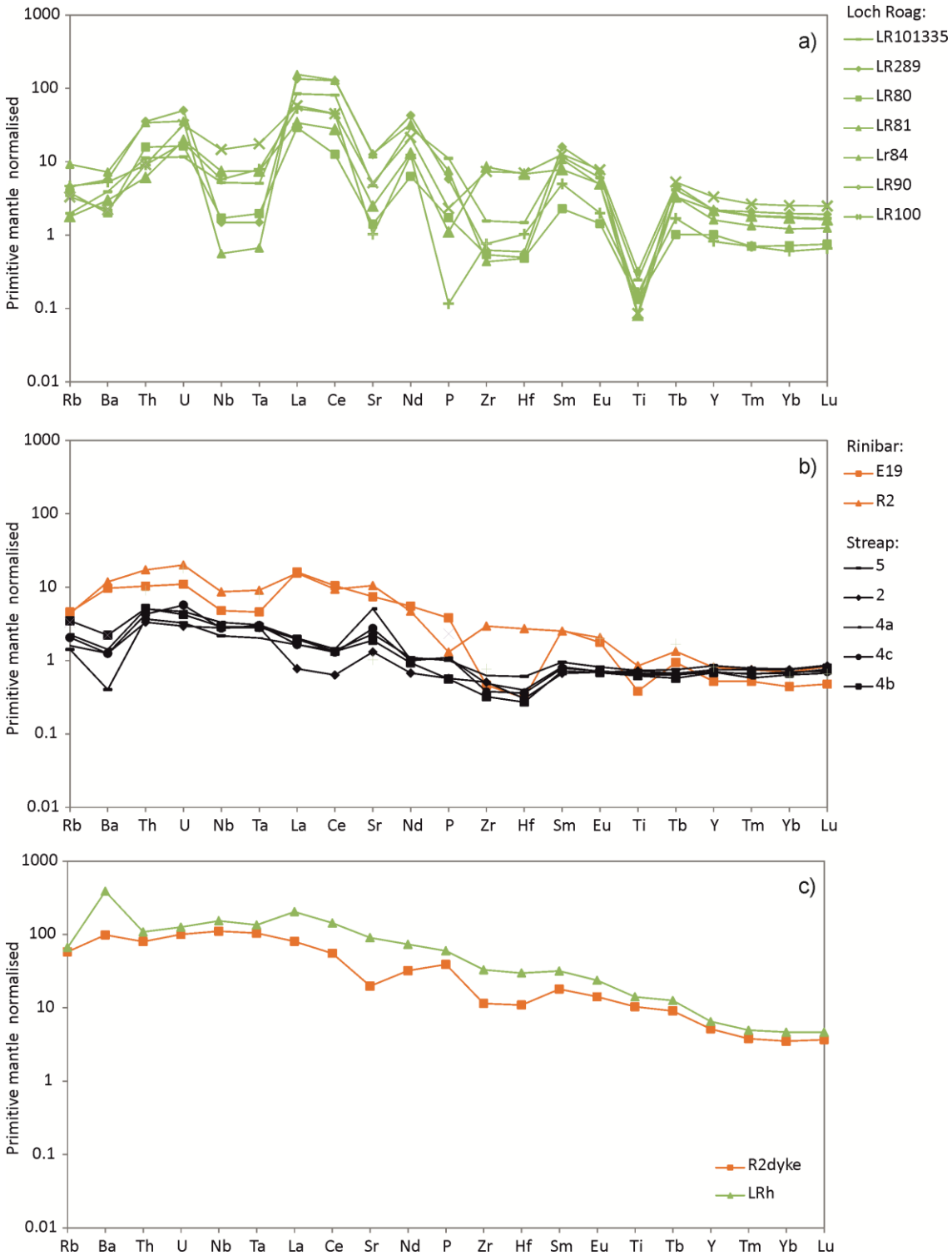

Figure 7.11. Primitive mantle-normalised multi-element diagrams (whole-rock) for Loch Roag (a), Streap Com'laidh and Rinibar spinel lherzolites (b) and the host dykes to the xenolith suites (c). Primitive mantle (pyrolite) normalising values from McDonough & Sun (1995).

7.3.3. Clinopyroxene compositions

Fully quantitative SEM EDS analyses were undertaken on a series of clinopyroxene crystals from various peridotite xenoliths of Loch Roag and Rinibar. Analogous clinopyroxene trace element compositions from Streap Com'laidh were already given by Bonadiman *et al.* (2008). This was followed by LA-ICP-MS line analyses, and a selection of clinopyroxene major and trace element abundances are presented in Table 7.3 with full results available in the Supplementary Material (on disk). Primitive mantle and chondrite normalised trace element spidergrams and REE plots (Fig. 7.12 a-g) show that clinopyroxenes from each xenolith samples analysed define distinct compositions. For example, Loch Roag sample LR80 is a comparatively 'fresh' spinel lherzolite with measured clinopyroxene compositions which have consistent negative anomalies for Ba, Nb, Ta, Sr, Hf and Ti (Fig. 7.12a). The REE profiles of clinopyroxene from this sample (Fig. 7.12b) show LREE enrichment, with La enriched over Ce and a flat HREE pattern. A striking observation for LR80 is the depletion of Hf_N relative to Zr_N. Also noteworthy is the slight enrichment of U over Th.

The trace element and REE profiles of pyroxenes in green clinopyroxenite xenoliths LR84 and LR100 (Figs. 7.12c-d, e and f) are markedly different from that of LR80 – negative anomalies for Nb, Ta, Sr and Ti are smaller than those in LR80. Additionally, U and Th both show positive anomalies, again with U enriched over Th, but these are less pronouced than in LR80. Most strikingly however, in both LR84 or LR100, there is no negative anomaly for either Zr or Hf; Hf_N appears to be slightly enriched over Zr_N, in complete contrast to LR80. REE profiles for clinopyroxene from both LR84 and LR100 are significantly elevated to normalised abundances greater than those in LR80, and the REE patterns define a convex shape for LREE, such that Ce and Pr are enriched over La. Between LR84 and LR100 there are yet more subtle differences, for example between relative abundances of Nb to Ta and Zr to Hf. Lastly, the clinopyroxene REE compositions of Rinibar xenoliths are more akin to that of LR80 than other Loch Roag samples (Fig. 7.12g), although this is not strictly the case for all trace elements (Fig. 7.12f). For example, Rinibar clinopyroxenes have a positive Sr anomaly (rather than Loch Roag's negative one) and Zr-Hf decoupling is even more pronounced, such that Zr_N is notably enriched over Hf_N, but Hf is not depleted below PUM levels (Fig. 7.12f). Notably, none of the clinopyroxenes analysed from any of the Loch Roag xenoliths display a negative Eu anomaly, unlike those shown in some of the whole-rock REE diagrams (Fig. 7.10). In fact, some of the clinopyoxenes in LR80 have a slight positive Eu anomaly. Therefore the negative bulk Eu anomaly must relate to a different mineral phase (or phases) within the xenoliths.

Table 7.3. Summary of SEM EDS quantitative analyses and LA-ICPMS results for major and trace element composition (respectively) of clinopyroxenes from Loch Roag and Rinibar.

SEM EDX quantitative results (major elements):

Sample	Locality	Clinopyro Na	Mg	Al	Si	Ca	Cr	Fe
LR84CPX mean	Loch Roag	green mel	1.41	9.25	1.10	24.98	15.53	1.41	2.36
LR80CPX mean	Loch Roag	primary	2.18	8.78	2.57	25.29	14.58	0.72	2.58
LR100CPX mean	Loch Roag	green mel	1.00	9.71	1.05	24.89	16.30	1.40	2.22
R2CPX mean	Rinibar	primary	0.73	9.40	2.72	23.57	15.39	0.48	2.32

LA-ICP-MS results:

Sample	$^{23}Na_2O$ (wt.%)	^{25}MgO (wt.%)	$^{29}SiO_2$ (wt.%)	$^{39}K_2O$ (wt.%)	^{47}Ti (ppm)	^{51}V (ppm)	^{52}Cr (ppm)	^{55}Mn (ppm)	^{60}Ni (ppm)	^{71}Ga (ppm)	^{85}Rb (ppm)	^{88}Sr (ppm)	^{89}Y (ppm)	^{90}Zr (ppm)	^{93}Nb (ppm)	^{133}Cs (ppm)	^{137}Ba (ppm)
LR84CPX mean	2.01	16.20	52.10	<0.04	312	256.2	18755	957	359	7.95	1.17	630	52.32	668	1.03	0.04	3.57
LR80CPX mean	2.43	13.44	46.40	<0.04	1665	233.8	8309	651	345	4.83	1.36	67	12.15	14	3.45	0.05	3.14
LR100CPX mean	1.60	14.95	48.75	<0.04	539	112.5	20889	929	314	7.68	1.75	380	41.92	329	2.71	0.15	10.22
R2CPX mean	0.86	14.53	46.51	<0.04	1282	165.7	8695	733	570	5.17	0.78	371	9.10	6	0.18	0.03	0.89

Sample	^{139}La (ppm)	^{140}Ce (ppm)	^{141}Pr (ppm)	^{146}Nd (ppm)	^{147}Sm (ppm)	^{153}Eu (ppm)	^{157}Gd (ppm)	^{159}Tb (ppm)	^{163}Dy (ppm)	^{165}Ho (ppm)	^{166}Er (ppm)	^{169}Tm (ppm)	^{172}Yb (ppm)	^{175}Lu (ppm)	^{178}Hf (ppm)	^{181}Ta (ppm)	^{208}Pb (ppm)	^{232}Th (ppm)	^{238}U (ppm)
LR84CPX mean	41.01	135.83	21.66	88.33	23.39	5.74	10.66	1.71	11.37	1.53	4.51	0.65	5.28	0.76	23.18	0.07	1.97	0.26	0.09
LR80CPX mean	43.16	83.79	7.27	19.37	3.59	0.93	2.23	0.40	2.19	0.43	1.25	0.17	1.29	0.22	0.47	0.30	1.53	3.58	1.24
LR100CPX mean	35.80	111.83	16.39	66.92	17.83	4.18	10.41	1.51	8.62	1.30	3.95	0.50	3.36	0.50	8.10	0.13	0.95	0.65	0.19
R2CPX mean	37.54	48.02	3.76	8.92	1.66	0.55	1.24	0.21	1.61	0.32	1.24	0.15	0.99	0.17	0.46	0.01	1.35	3.59	0.57

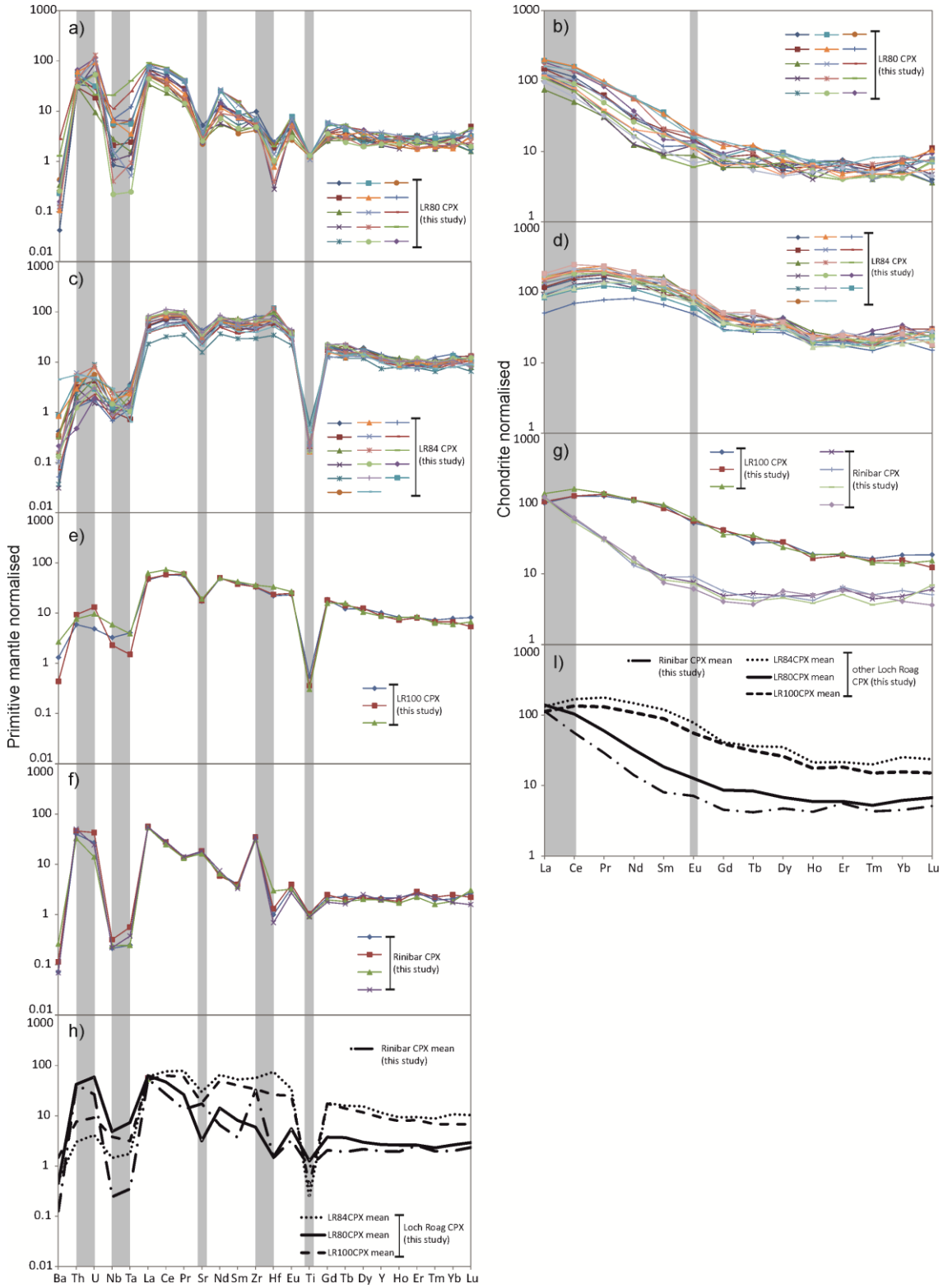

Figure 7.12. Primitive mantle-normalised multi-element diagrams and chondrite-normalised REE diagrams for clinopyroxene (determined by LA-ICPMS) from Loch Roag and Rinibar spinel lherzolites. (a) and (b) for sample LR80 ('fresh' spinel lherzolite). (c) and (d) for LR84 (green clinopyroxenite xenolith). (e) and (g) for LR100 (green clinopyroxenite xenolith). (f) and (g) for Rinibar xenolith 'R2' (partially serpentinised spinel lherzolite). Average (mean) clinopyroxene compositions per sample are displayed in (h) and (i). Primitive mantle (pyrolite) and chondrite normalising values from McDonough & Sun (1995).

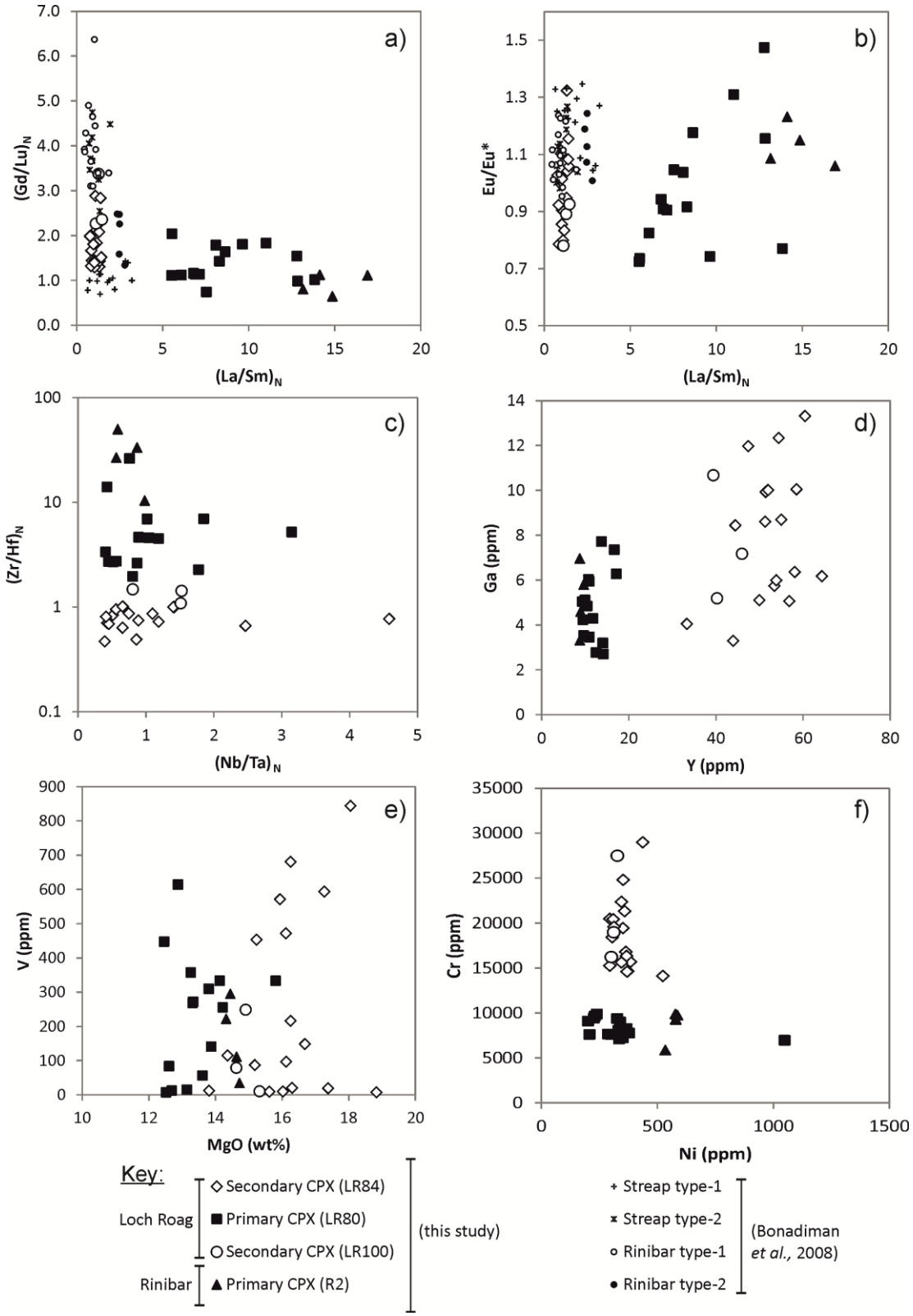

Figure 7.13. Bivariant plots for clinopyroxene from Loch Roag and Rinibar spinel lherzolites (this study). Also comparison with results for Streap Com'laidh and Rinibar lherzolites from Bonadiman *et al.* (2008). Eu/Eu* anomaly is calculated as $Eu_N/((Sm_N + Gd_N) \times 0.5)$ where '$_N$' denoted chondrite normalisation.

The trace element characteristics of clinopyroxenes can be simplified in a series of bivariant diagrams, plotted in comparison with previous analyses of metasomatic clinopyroxenes from Rinibar and Streap Com'laidh (Bonadiman *et al.,* 2008) – see Figure 7.13. These provide clear separation of pyroxene compositions according to $(La/Sm)_N$, Cr, Y and $(Zr/Hf)_N$ (Fig. 7.13). Bonadiman *et al.* (2008) identified 'kimberlite' and 'carbonatite'-related metasomatic clinopyroxene compositions in Northern Highland Terrane xenoliths. Secondary clinopyroxene identified in LR84 and LR100 plot in the same cluster as these two metasomatic compositions ('Streap type-1' and 'Rinibar type-2' from Bonadiman *et al.,* 2008 as a function of $(Gd/Lu)_N$). By contrast, according to $(La/Sm)_N$ (Fig. 7.13a), LR80 and our Rinibar sample (R2) plot entirely separately from the 'metasomatic' pyroxene compositions and must reflect a different origin.

We have further experimented with ways by which to characterise clinopyroxene composition in the mantle – for example according to $(Zr/Hf)_N$ and $(Nb/Ta)_N$ (Fig. 7.13c). Metasomatic clinopyroxenes have a low $(Zr/Hf)_N$ typically ≤ 1.5, while 'primary' clinopyroxene has substantially greater $(Zr/Hf)_N$ ranging > 1.5 to 50. Good characterisation of clinopyroxene compositions ('primary' vs. 'metasomatic') can also be based on Ga, Y, MgO, Cr and Ni contents (Fig. 7.12 d-f). In detail, 'primary clinopyroxenes have a wide range of Ni contents (200 to >1000 ppm) but limited variation in Cr. In contrast metasomatic clinopyroxenes have elevated and wide-ranging Cr concentrations (approximately 1.4 to 3 wt.% Cr).

7.4. Discussion

In this study, we have compared the compositions of Scottish spinel lherzolites with those from elsewhere in the North Atlantic Craton (in western and eastern Greenland). On a terrane-scale in NW Scotland, xenoliths appear to fall into two groups – one which overlaps Greenlandic cratonic NAC xenolith major element abundances (e.g., Loch Roag and Rinibar) and one which does not and is more akin to 'primitive upper mantle' (e.g., Streap Com'laidh). The question arises whether this discrepancy reflects terrane-scale mantle heterogeneity between the Hebridean and Northern Highland Terranes, or whether they form a continuous range in a heterogeneous lithospheric mantle? Are these simply the consequence of limited samples from heterogeneous mantle lithosphere? Cu abundances of the Scottish xenoliths are unusually elevated above concentrations elsewhere in the NAC, or globally for cratonic SCLM – are these 'primary' abundances or have these been recently re-enriched? Similarly, are the critical metal (e.g., REE) concentrations of the Scottish SCLM a 'primary' or 'metasomatic'

feature? And what are the overall mineralogical controls on REE and trace element abundance in the SCLM?

7.4.1. Terrane-scale variation in the NW Scottish lithospheric mantle

As outlined previously, the lithospheric terranes of Scotland were largely amalgamated and assembled into their present positions during the Caledonian Orogeny. At the surface, Lewisian and/or 'Lewisianoid' exposures suggest that the British portion of the NAC (at least at a crustal level) includes the land masses to the north and northwest of the Great Glen Fault (GGF).

All three suites of xenoliths from the Scottish margin of the NAC (i.e., north of the GGF) are notably less refractory (lower MgO, higher Al_2O_3 and generally higher FeO^T) than their Greenlandic counterparts (Fig. 7.8a-b). While the major element compositions of these Scottish xenoliths is similar to that of ultramafic cumulate rocks from the Archaean Tartoq supracrustal belt of SW Greenland (e.g., Szilas *et al.,* 2014) we see no textural or mineralogical evidence to suggest that the spinel peridotite xenoliths of Loch Roag, Rinibar and Streap Com'laidh are anything other than upper mantle lithologies (see Upton *et al.,* 2011 and references therein and c.f., Downes *et al.,* 2007). This suggests that the Scottish margin has either been re-fertilized separately from the wider NAC, or was not as extensively depleted. In detail however, there are differences in xenolith composition between the three Scottish xenolith localities – for example, between the SW and NE portions of the Northern Highland Terrane. Whilst the Rinibar xenoliths are more serpentinised than those from Streap Com'laidh, their anhydrous major element compositions overlap those from elsewhere in the NAC and other cratons (Figs. 7.12 a-b and d-h). In contrast the fresher Streap Com'laidh xenoliths show a very narrow range in major element abundances, more similar to the 'primitive upper mantle' of McDonough & Sun (1995).

Both Northern Highland Terrane xenolith suites were entrained into Permo-Carboniferous dykes, and thus they were removed and isolated from the SCLM well before the Palaeogene impingement of the Icelandic plume. Despite the major elements of Streap Com'laidh xenoliths recording a comparatively undepleted mantle composition, in agreement with other isotopic evidence (e.g., $^3He/^4He$ of fluid inclusions in olivine, Kirkstein *et al.,* 2004; and whole-rock and clinopyroxene Sr- and Nd-isotopes, Menzies & Halliday, 1988; Downes *et al.,* 2001,2007; Bonadiman *et al.,* 2008), Streap Com'laidh xenoliths do not display any of the

characteristic positive or negative anomalies seen in samples from Loch Roag or Rinibar (e.g., for Nb, Ta, Zr, Hf, Ti and LREE). Similarly, trace elements such as Co (Fig. 7.9c) occur at lower concentrations, with correspondingly higher V, than in the other Scottish or cratonic xenoliths globally. Thus in many ways, both geochemically and isotopically, the Streap Com'laidh spinel lherzolites resemble shallow upper mantle compositions underlying MORB, high-temperature off-craton settings, or truly primitive upper mantle. Although the xenoliths were derived from the lithospheric mantle underlying Streap Com'laidh, the very process of xenolith entrainment in the magmas of the host dyke is likely to have introduced a natural sampling bias, such that not all SCLM lithologies will have been entrained into the dyke or preserved at the current level of exposure. As such Streap Com'laidh spinel lherzolites may not in fact be representative of the truly cratonised margin of the NAC at all, and could instead constitute fragment(s) of 'exotic' mantle (possibly part of the Iapetus slab subducted during the Caledonian orogeny). This is corroborated by Bonadiman *et al.* (2008) who highlighted that the fine crystal sizes prevalent in Streap Com'laidh peridotite xenoliths concur with neither simple 'pure' Archaean to Phanerozoic cratonic, nor Phanerozoic off-cratonic environments. Rheological and thermal evidence may suggest that the Streap Com'laidh xenoliths crystallised in a high-stress environment, which allowed for efficient dynamic recrystallization and perturbing the Ostwald ripening long-term high-temperature low-stress regime dominant in Archaean subcratonic mantle (Silver *et al.,* 1999; Pearson *et al.,* 2003).

By contrast, the spinel lherzolites of Rinibar and Loch Roag are geochemically similar, despite being entrained in host dykes separated in age by more than 200 Myr. For example, the whole-rock major element compositions of both suites overlap, and the REE abundances in both Rinibar samples and LR80 (fresh spinel lherzolite xenolith 'core') are very similar. Both Loch Roag and Rinibar lherzolites display negative whole-rock Nb, Ta and Ti anomalies (Fig. 7.11a). Other trace elements however, reveal subtle discrepancies; for example Ba and Sr (and P in one sample) are enriched in Rinibar samples in comparison to those from Loch Roag. Given the relative proximity of a suite of late-Caledonian (c. 430-420 Ma) high Ba-Sr mixed diorite-granitoid, syenite and pyroxenite-syenite intrusions in northern Scotland (for example at Loch Borralan, Loch Loyal, Helmsdale, Rogart and Ach' Uaine) and especially accounting for Caledonian westward motion along the Moine Thrust Zone, it is plausible that the SCLM of this NE region was affected by the transient LILE-rich melts or fluids of that time. This would suggest that a Caledonian subduction-related signature has (in part) been recorded or preserved in this region of the SCLM, for example representing part of the Caledonian Parental Magma Array (Fowler *et al.,* 2008).

The spinel lherzolites from Loch Roag (e.g., samples LR80, LR81, LR90, LR289 and LR101335) have more steeply fractionated chondrite-normalised REE patterns, with notable negative Eu anomalies in comparison to the green clinopyroxenite samples of LR84 and LR100. LR80 has the smallest negative Eu anomaly in comparison to the other spinel lherzolites, and given that the bulk powdering of LR80 involved the removal of the oxidised and baryte-bearing outer 'altered' rim of this xenolith, it might suggest that the negative Eu anomaly is largely controlled by this 'altered' rim material. Otherwise the relative depletion in Eu on Figure 7.10a for Loch Roag lherzolites suggests that at some point during the history of the xenoliths, plagioclase feldspar was fractionating (melted out) of a pre-spinel lherzolite protolith, or that metasomatism from a fluid in equilibrium with plagioclase had occurred. Both of these scenarios would be highly unusual in mantle lithologies.

For the green clinopyroxenites (LR84 and LR100), Zr and Hf concentrations are an order of magnitude higher than other Loch Roag whole-rock samples; a result of elevated Zr and Hf contents of their component clinopyroxene (e.g., Fig. 7.12). However beyond this, no systematic differences in whole-rock geochemistry can be established between the lherzolites and green clinopyroxenites except for slightly higher K_2O and TiO_2 concentrations in the spinel lherzolites. Therefore, if the green clinopyroxenite samples truly represent modally metasomatised SCLM peridotites, they have largely retained the major and trace element bulk compositions of the spinel lherzolites (including the 'fresh' xenolith core composition of LR80).

7.4.2. Rare earth elements and the fertility of the sub-Lewisian lithosphere

The Loch Roag and Rinibar xenoliths are unusually rich in LREE. The Rinibar spinel lherzolites and sample LR80 from Loch Roag (which sampled only the 'fresh' black peridotite interior of the xenolith) have LREE abundances elevated well above chondrite (Fig. 7.10a) but these are not as enriched as other Loch Roag xenoliths. Samples LR90, LR81, LR101335 and LR289 are also spinel lherzolites, but whole-rock powder included green-brown xenolith rims which contain traces of baryte, Fe^{3+} oxides and serpentine. This is reflected in their higher LOI values (> 1 wt.% - Table 7.2). These xenoliths with altered rims also have extremely enriched LREE patterns, well in excess of 100 x chondrite (Fig. 7.10a), with negative Eu anomalies. This clearly indicates that the haloes are not simply surface weathering artefacts. The REE pattern of the Loch Roag monchiquite dyke lacks a Eu anomaly, so a simple link to the host rock seems unlikely. Currently we do not know whether the enhanced LREE is caused by the same process

as the alteration/oxidation, or whether the association is incidental, and instead reflects an increased susceptibility to such alteration in the LREE-enriched peridotites.

The effect of accessory mineralogy on REE whole-rock geochemistry can be significant and is easily overlooked. In one Loch Roag xenolith (LR84) a chlorite- and serpentine-filled veinlet has been overprinted by bastnaesite (Ce-carbonate) – Figure 7.6e-f. Clearly Ce (and La) are major constituents of this mineral, and thus only trace amounts of bastnaesite would have a significant impact on the whole-rock geochemistry of the powdered rock. Similar bastnaesite-filled veins have not been found in any other xenoliths in this study. Nonetheless this highlights the importance of detailed petrography in mantle xenolith studies.

At least under H_2O-rich conditions, (e.g., in mantle wedges above subduction zones) chlorite can be stable to temperatures just above the H_2O-saturated solidus between 2 and 3.6 GPa (Till *et al.,* 2012; Grove *et al.,* 2006). Chlorite is not uncommon in kimberlites and associated mantle xenoliths. Tompkins *et al.* (1984) reviews occurrences, and describes chlorite from kimberlites in Sierra Leone. They propose that chlorite is formed by relatively low-temperature alteration of phlogopite by a late H_2O and CO_2-rich fluid exsolved from kimberlites. Upton *et al.* (2009) describe chloritic rims around ocelli from a range of Scottish monchiquite/nephelinitic dykes, and ascribe these to separation of a carbonate-rich melt/fluid. A similar effect seems a very plausible process within Loch Roag dyke, and the occurrence of LREE-rich bastnaesite would be consistent with a carbonatitic melt/fluid. Such LREE-rich fluids may also explain the 'altered' outer zones of xenoliths with high LREE abundances, although the serpentine-oxide-baryte assemblage might suggest a more oxidised, and perhaps less CO_2-rich (perhaps lower temperature) fluid than that responsible for the chlorite-bastnasite vein.

The Loch Roag dyke displays clear evidence for at least limited post-magmatic fluid flow in the form of zeolites on some joint planes and lining vesicles (Faithfull *et al.,* 2012). REE can be mobile in zeolite-facies fluids: ancylite-(Ce) and kainosite-(Y) are found in zeolite-rich veins at Strontian for example (Green & McCallum, 2005). All of these possible origins would imply that the LREE-enriched crusts and veins are syn- or post-emplacement features, but such processes make it hard to explain the negative Eu anomalies in the LREE-rich zones of the mantle peridotite xenoliths.

7.4.3. 'Primary' vs. 'metasomatic' signatures in the SCLM

Whole-rock geochemistry involves the homogenisation of a xenolith, incorporating a variety of silicate, oxide, sulphide and other accessory mineralogies for a combined analytical result. These data composite the sample mineralogy and must be put into context at an individual mineralogical scale. Olivine and orthopyroxene will only incorporate very low abundances of incompatible lithophile trace elements, while controlling a large proportion of the MgO, FeO, Al_2O_3, Ni and Cr whole-rock budget. Orthopyroxene may also regulate a significant component of whole-rock trace element geochemistry, despite its low overall abundances. Clinopyroxene will incorporate a variety of incompatible lithophile trace elements in significant quantities in addition to CaO, Na_2O and Cr_2O_3. In terms of whole-rock geochemistry, an increase in clinopyroxene abundance correlates with an elevation in Sc and other trace elements (e.g., Fig. 7.9a) and the composition of SCLM clinopyroxene may be sensitive to magmatic and/or metasomatic events.

Clinopyroxenes from Rinibar and Streap Com'laidh reported in Bonadiman *et al.* (2008) are spongy in texture, with inclusions of other clinopyroxenes, olivine and spinel. From the trace element composition of these 'spongy' clinopyroxenes, we support the interpretation of Bonadiman *et al.* (2008) that they are secondary and likely metasomatic in origin. Similar 'spongy' clinopyroxene textures with olivine and chromite inclusions occur in Loch Roag green clinopyroxenite xenoliths (LR84 and LR100). LA-ICP-MS trace element analyses closely correspond with those from Bonadiman *et al.* (2008). In particular, chondrite-normalised REE patterns of their metasomatic pyroxenes display characteristic convex LREE patterns with Ce_N enriched over La_N matching the LR84 and LR100 clinopyroxenes (e.g., Fig. 7.12 d and g). Using $(Gd/Lu)_N$ as a proxy for kimberlite vs. carbonatite metasomatic clinopyroxene (the former having high $(Gd/Lu)_N > 2.5$, and the latter with low $(Gd/Lu)_N < 2.5$ based on Bonadiman *et al.,* 2008), we suggest that the 'spongy' clinopyroxenes of Loch Roag formed during a carbonatite-related metasomatic event and supports isotopic evidence from Long *et al.* (1991) which cited time-integrated Nd-isotopes as recording carbonatite-related metasomatism at c. 2.4 Ga. Other metasomatic influxes are indicated across the Hebridean and Northern Highland Terranes. For example, Sr-Nd isotopic compositions from metasomatic clinopyroxenes indicate an overprinting event for Rinibar at 550 ± 50 Ma (Bonadiman *et al.,* 2008) – prior to both Iapetus oceanic subduction and any possible melt/fluid mobilisation associated with the initiation of the Great Glen Fault.

By contrast, we suggest that the comparatively homogeneous clinopyroxenes in spinel lherzolites from Loch Roag (e.g., LR80) and Rinibar (see Fig. 7.12) are of primary origin. Texturally, these clinopyroxenes are part of a protogranular to sub-equigranular suite of peridotites, and do not contain granular mineral inclusions of any type. Their trace element compositions are distinct from the metasomatic clinopyroxene compositions previously discussed. For instance, $(La/Sm)_N$ in 'primary' clinopyroxene is somewhat counterintuitively elevated by more than 5 to 10 times above that of the metasomatic compositions (Fig. 7.13a). Primary clinopyroxenes also have comparatively low Y and Cr concentrations (Figs. 7.13d and f) and substantial enrichment in U and Th (Fig. 7.12a,f). Hence, these 'primary' pyroxenes represent the original cratonic clinopyroxene prevalent at the Scottish margin of the NAC, although some aspects of their geochemistry may have since been cryptically modified, as discussed later.

The Hf-Zr systematics of clinopyroxenes in the Scottish peridotite xenoliths are highly variable (Figs. 7.12 and 7.13c). In our study, 'metasomatic' clinopyroxenes from LR84 and LR100 have Zr and Hf concentrations elevated to more than 10 times that of the primitive mantle and $(Zr/Hf)_N$ ratios ≤ 1.5. Crucially these clinopyroxenes also have very elevated Cr contents, a feature well documented in other 'metasomatic' mantle clinopyroxenes across the world (e.g., Lloyd *et al.,* 1991; Gysi *et al.,* 2011). By contrast, 'primary' Rinibar (R2) and Loch Roag (LR80) clinopyroxenes have severely decoupled Zr and Hf, with $(Zr/Hf)_N$ ranging 2-50 (Fig. 7.13), as a result of enrichment in Zr, with Hf_N typically around 1 (Fig. 7.12). The 'metasomatic' pyroxenes from Rinibar (Bonadiman *et al.,* 2008) have similarly decoupled Zr and Hf in carbonatite-associated phases, as in our 'primary' pyroxenes, but kimberlite-associated metasomatic pyroxenes have elevated Hf_N more akin to Loch Roag metasomatic types. Streap Com'laidh clinopyroxenes from Bonadiman *et al.* (2008) have similar $(Zr/Hf)_N$ ratios as in 'primary' Loch Roag (LR80), but characteristic convex LREE pattern of modal metasomatic phases, and substantially lower Th and U concentrations.

Downes *et al.* (2014) recently investigated the Zr and Hf composition of clinopyroxenes from French and Polish spinel peridotite mantle xenoliths. Initial extensive partial melting of primitive mantle removed both Zr and Hf, but these extreme depletions are rarely identified in mantle xenoliths globally. Modelling of Hf-depletion in clinopyroxenes from the French Massif Central has been suggested to result from up to 30 % partial melting in the spinel peridotite stability field (Wittig *et al.,* 2006). In their study, Downes *et al.* (2014) identified metasomatism in clinopyroxenes by the substantial elevation of either Zr abundances only, or both Zr and Hf,

depending on the metasomatising agent (i.e., a subduction-related fluid, alkaline silicate melt, or carbonatite).

Taking into account the study of Downes *et al.* (2014) and the other distinct trace element characteristics of each xenolith clinopyroxene population (e.g., Th, U, Nb, Ta and LREE patterns), we suggest that the spongy metasomatic clinopyroxenes of Loch Roag (e.g., LR84, LR100) demonstrate the modal metasomatic record of lithospheric mantle. Both Zr_N and Hf_N are elevated in secondary pyroxenes to > 10 x PUM whereas 'primary' clinopyroxenes may record secondary cryptic metasomatism, revealed by a substantial elevation in Zr_N over Hf_N (e.g., Rinibar, sample R2) with Hf_N remaining at ≤ 1.5 primitive mantle concentrations. Based on the similarity of LREE, U and Th abundances to 'primary' Rinibar compositions, this explanation may therefore be extended to 'primary' Loch Roag clinopyroxenes (i.e., LR80). Thus 'primary' clinopyroxene compositions may largely record initial subcratonic lithospheric geochemistry, however certain high field strength elements, widely regarded as 'immobile' (e.g., Pearce, 1996), may record significant cryptic geochemical evidence of subsequent modification. Importantly, the absence of a true depletion in Hf_N in 'primary' clinopyroxenes of both suites, suggests that no severe partial melting event(s) are recorded in the spinel lherzolites from the Scottish portion of the NAC SCLM.

The Scottish xenoliths enable us to understand the SCLM record. Xenoliths in Loch Roag are entrained in an Eocene-aged dyke, emplaced at the end of magmatism recorded in the UK during the Palaeogene impingement of the Icelandic mantle plume under western Scotland. By contrast the Rinibar xenoliths were entrained in a Permo-Carboniferous dyke and predate the effects of the Icelandic plume. Given the timescale between cratonization of the NAC and the Permo-Carboniferous entrainment (and thus isolation) of the Rinibar xenoliths (in the order of billions of years) vs. the timescale between isolation of the Rinibar and Loch Roag xenoliths (approximately 250 Myr), it seems sensible to suggest that they document a prolonged Archaean and Proterozoic history at the margin of the NAC SCLM, rather than subsequent Phanerozoic events. Therefore similarities in clinopyroxene (and other mineralogical) compositions are unlikely to be coincidental. Loch Roag spinel lherzolites likely record ancient lithospheric shallow mantle compositions (although not notably depleted relative to PUM – e.g., Al_2O_3) and were not been substantially reset, destroyed or recrystallized during the Palaeogene plume event. A new study investigating the common similarities between Loch Roag spinel lherzolite trace element compositions and that of the Scourie Dyke Swarm (erupted during an extensional tectonic event in the Palaeoproterozoic)

highlighted that, despite their Eocene entrainment age, the lithospheric mantle as represented by the Loch Roag xenoliths retained bulk geochemical features that are important to the geochemistry of the 2.4 Ga Scourie Dyke magmas (Hughes *et al.,* 2014; Chapter 6). In short, upper mantle of similar/the same composition to that of xenolith LR80 was partially melted during the Palaeoproterozoic, and fed magmas (predominantly sourced in the lithospheric mantle) which ultimately formed the Scourie Dyke Swarm (Hughes *et al.,* 2014; Chapter 6). Combined, these are essential observations for further investigations into the cratonic or marginal cratonic lithospheric mantle's geochemistry and metal abundances, and for understanding whether these xenoliths record a 'primary' metal enrichment as part of the ancient SCLM keel.

7.5. Conclusions

1. According to major element abundances, spinel lherzolite xenoliths from the Scottish margin of the NAC do not show evidence of severe depletion, unlike xenoliths from the Greenlandic NAC.
2. Ce-carbonate (bastnaesite) has been discovered in a Loch Roag clinopyroxene-rich mantle peridotite, however the provenance of this mineral is likely to be a secondary lower-temperature (hydrothermal?) event and not associated with the lithospheric mantle itself. Overall we highlight the importance of petrography, particularly for accessory minerals, before whole-rock geochemical or isotopic analyses, in order to put into context the main controls on metal abundance.
3. Cu abundances in the spinel lherzolites of Loch Roag are extremely enriched and are elevated above cratonic or Archaean-Proterozoic mantle peridotite compositions worldwide, currently available in the published literature. Specifically this is an enrichment in sulphide and Cu associated with a melt/fluid event although the timing is poorly constrained.
4. Clinopyroxene compositions from Rinibar and Loch Roag have characteristic features including depletions in Nb, Ta and Ti, and clinopyroxenes formed from metasomatic events can be identified by enriched LREE such that Ce is enriched over La (on chondrite-normalised diagrams) and elevated Cr content. Cryptic 'refertilisation' or metasomatism of 'primary' clinopyroxenes can be identified by decoupling of Zr from Hf, such that Zr becomes enriched. The lack of true Hf depletion in these 'primary' clinopyroxenes suggests that the xenoliths have not undergone severe partial melting.

5. We use clinopyroxene compositions, in context with accessory mineral occurrences, to suggest that the Scottish NAC margin has not undergone recent Phanerozoic melting or refertilisation, despite the proximity of the Icelandic mantle plume during the Palaeogene opening of the Atlantic. Further, similarities in trace element systematics between the Loch Roag spinel lherzolites and Palaeoproterozoic Scourie Dyke Swarm (Hughes *et al.,* 2014; Chapter 6) would suggest that these xenoliths represent the composition of shallow mantle that is at least Palaeoproterozoic in age. As such we suggest that the whole-rock REE and other trace element abundances in these xenoliths either represent the original cratonic composition or ancient metasomatised Archaean-Palaeoproterozoic compositions, and that the green clinopyroxenites from Loch Roag may represent a different, more recent volatile-rich or metasomatic event.

Acknowledgements

Much of the material (xenolith and dyke) used throughout this study is from B.G.J. Upton's personal collection, now held at the British Geological Survey (BGS), Murchison House, Edinburgh. The BGS, particularly Michael Togher, is thanked for the curation, access and use of these samples. New samples from Streap Com'laidh were collected by J.W. Faithfull, and are henceforth curated at the Hunterian Museum, University of Glasgow. Anthony Oldroyd is thanked for his preparation of polished thin sections, and Peter Fisher for his assistance and guidance at Cardiff University's SEM facility. This manuscript greatly benefitted from discussions with Graham Pearson, Andrew Fagan, and Nicholas Arndt. Reviews from Sebastian Tappe, Kristoffer Szilas and Fanus Viljoen helped to improve the paper. H.S.R. Hughes is funded by the Natural Environment Research Council (NERC) studentship NE/J50029X.

CHAPTER 8

Sulphides and precious metals in the lithospheric mantle: A multi-event record of sulphur-bearing magmatism and metasomatism through time (Loch Roag, Scotland)

Submitted as:

Hughes, H.S.R., McDonald, I., Upton, B.G.J., Faithfull, J.W. (under review). Sulphides and precious metals in the lithospheric mantle: A multi-event record of sulphur-bearing magmatism and metasomatism through time (Loch Roag, Scotland). *Geochimica et Cosmochimica Acta*

Co-author contributions:

I. McDonald, B.G.J. Upton and J.W. Faithfull were involved in discussions during the writing of this paper. B.G.J. Upton provided xenolith specimens for study. I. McDonald supervised bulk rock and LA-ICP-MS analyses.

Abstract

The role of the lithospheric mantle as a source of precious metal is contentious, and given the chalcophile nature of metals such as the platinum-group elements, Re, Cu and Au, the mobility and stability of these metals is intimately linked with that of sulphur. Hence the age and stability of the subcontinental lithospheric mantle (SCLM) may be of critical importance. We investigate the sulphide mineralogy and trace element composition of a suite of spinel lherzolite mantle xenoliths from northwest Scotland (Loch Roag, Isle of Lewis). This area straddles the margin of the North Atlantic Craton which has been overprinted by a Palaeoproterozoic orogenic belt, and occurs in a region which has undergone a series of magmatic events as recent as the Eocene.

We identify three populations of base metal sulphides within the xenolith suite as a whole and which can also be recognised in a single xenolith. Each population consists of a mixture of Fe-Ni-Cu sulphides, and we distinguished between these according to sulphide morphology and texture, petrographic setting (in relation to silicate and oxide minerals) and sulphide mineral trace element composition (particularly for Re, PGE and Au). The oldest sulphides are coarse, with complex internal textures, have low concentrations of total PGE and high $(Re/Os)_N$ (ranging 1 to 400). A rare group of sulphides with co-existing rounded Ca-carbonate inclusions and polygonal serpentine-filled inclusions are identified along silicate grain boundaries and have high total PGE concentrations and $(Re/Os)_N$ of 0.1–2. The texturally youngest group of sulphides strictly occur within eutectic melt intergrowths of spinel and plagioclase. These sulphides are rounded and droplet-like with micron-scale PtS (cooperite). They have the highest total PGE concentrations and lowest $(Re/Os)_N$ ratio (> 0.04). The co-existence of multiple sulphide populations with distinctly different PGE content and Re/Os ratios in a single xenolith reveals a complexity to the upper mantle S-budget thus far not reported, and highlights that the precious metal budget of the SCLM depends on the composition and petrographic setting of each of these populations. For example, the Pt content of an ascending asthenosphere-derived magma may be significantly increased if this incorporates sulphides similar to Group 3. Assimilation or melting of such sulphides may impart an unradiogeneic Os-isotopic signature. Furthermore we demonstrate that bulk rock PGE compositions represent the integrated effect of multiple sulphide-bearing mantle processes, which may add or remove PGE selectively.

8.1. Introduction

Mantle xenoliths provide a direct but incomplete view into the lithospheric mantle and the composite and complex magmatic and/or metasomatic events that it has experienced over time. Interest in the subcontinental lithospheric mantle (SCLM) and its role in the trapping of, or as a source of metals, such as Cu, Mo the platinum-group elements (PGE) and Au, has been discussed in the literature for over 30 years (cf. Groves *et al.,* 1987; Groves & Bierlein, 2007; Arndt, 2013, and references therein). Many of these metals are strongly chalcophile and thus theoretically should track the sulphur budget of the mantle. Hence, the ability of the shallow mantle to store or release precious metals is thought to be largely dependent on the mobility of sulphur (e.g., Naldrett, 2004 and references therein; Lorand *et al.,* 2013).

The precious metal and chalcophile element composition of the lithospheric mantle (sampled by xenoliths) has been widely documented over the course of several decades, and studied in the context of lithospheric age and tectonic/geodynamic setting and the presence and composition of the late veneer (e.g., Pattou *et al.,* 1996; Rekhamper *et al.,* 1999; Holzheid *et al.,* 2000). Studies have commonly centred on bulk rock geochemistry, isotopic compositions (e.g., Re-Os) and sulphide mineralogy (see Lorand *et al.,* 2013 and references therein). Less widely investigated however, are the morphologies and temporal relationships of sulphide minerals and how these relate to sulphide trace element compositions. Certain questions arise from this topic – for example, are sulphides in a particular region of the lithospheric mantle homogeneous and closely related, or could multiple (recognisably different) generations or populations of sulphides be present? Can these sulphide populations be defined broadly by their mineralogy and/or texture alone, or can they also be defined by significant differences in their trace element composition? Can sulphide populations be correlated with other modal or chemical evidence for mantle metasomatism? And depending on where these sulphides are located within a given mantle sample (i.e., as inclusions or interstitially to various silicate minerals) could these record more than one transient magmatic/metasomatic event and are these capable of being remobilised during subsequent partial melting?

In this study, we present bulk rock chalcophile and PGE concentrations from spinel lherzolite mantle xenoliths from the Eocene-aged Loch Roag monchiquite dyke in NW Scotland. The dyke entrains xenoliths from the lithospheric mantle underlying a marginal region of the Archaean-aged North Atlantic Craton. Based on petrography we identify a variety of 'populations' of mantle sulphides within a single spinel lherzolite xenolith and across the suite of spinel lherzolites hosted in the dyke. Sulphide 'populations' are identified based on their trace

element composition (including PGE, Re and Au) in conjunction with distinct textural characteristics and petrographic settings within the peridotite.

8.1.1. Geological setting

In Scotland, documented mantle xenolith localities span five tectonic terranes (see Upton *et al.,* 2011 and references therein), delineated by major lithospheric lineaments and faults (Fig. 8.1). In the far NW of Scotland, the Archaean – Mesoproterozoic Lewisian Gneiss Complex makes up much of the British portion of the North Atlantic Craton (NAC), and is the exposed basement of the Caledonian foreland bounded to the east by the Moine Thrust Zone (MTZ). Broadly, the NAC (and hence Lewisian) consists of amalgamated Archaean domains with zones of Palaeoproterozoic reworking along the craton margin particularly highlighted by the 1.9 Ga South Harris Igneous Complex (e.g., Bridgwater *et al.*, 1973; Park & Tarny, 1987; Park, 1994; Park, 1995; Baba, 2002; Kinny *et al.*, 2005a; Park, 2005; Goodenough *et al.*, 2013).

The Moine Thrust Zone (MTZ) delineates the boundary between the Hebridean Terrane (where Archaean Lewisian rocks are widely exposed at surface) and the Northern Highland Terrane which, at the surface, comprises predominantly of c. 1 Ga Moinian metasediments, intercalcated and folded during Caledonian deformation with 'Lewisianoid' inliers (Tanner, 1970). Hence it is suggested that this Archaean basement (at least at the crustal level) extends east beyond the Moine Thrust Zone and partially underlies the Northern Highland Terrane (e.g., Moorhouse & Moorhouse, 1977; Hughes *et al.,* in press – Chapter 7).

Most recently, the North Atlantic Igneous Province (NAIP) erupted as a widespread continental flood basalt event formed by the impingement of the Icelandic mantle plume beneath overlying lithosphere. Active continental rifting was initiated at approximately 62 Ma in the UK, Greenland and Baffin Island (Saunders *et al.*, 1997). This ultimately led to the opening of the Atlantic Ocean and hence the fragmentation of the Archaean North Atlantic Craton. The British Palaeogene Igneous Province is part of the earliest magmatic expression in the NAIP and is developed through the Hebrides, the west coast of Scotland and Northern Ireland (Saunders *et al.,* 1997).

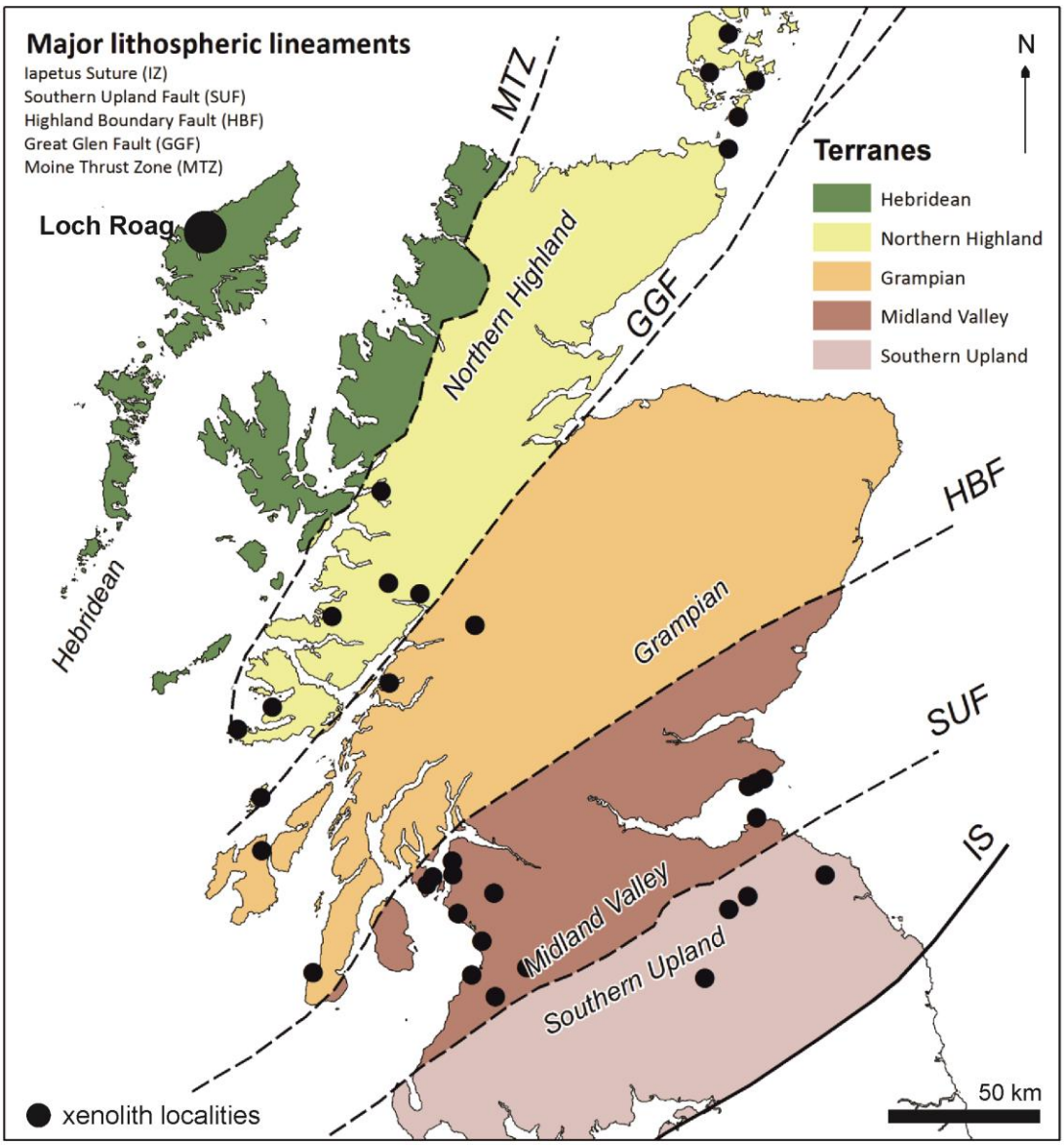

Figure 8.1. Terrane map of Scotland and mantle and lower crustal xenolith localities. These span four terranes – the Hebridean Terrane, Northern Highland Terrane, Grampian Terrane and Midland Valley Terrane. The Hebridean and Northern Highland Terranes are thought to be underlain by (re-worked) North Atlantic Craton basement. The Loch Roag xenolith locality (hosted in a monchiquite dyke) occurs within the Hebridean Terrane.

8.1.2. Host rock for the spinel peridotite xenoliths

The 70 cm wide monchiquite dyke near Loch Roag (Isle of Lewis) cross-cuts Archaean Lewisian gneisses and contains a suite of upper mantle and crustal xenoliths and xenocrysts (see Faithfull et al., 2012 and references therein). Recent ^{40}Ar-^{39}Ar dating has confirmed this dyke to be mid-Eocene (45.2 ± 0.2 Ma; Faithfull *et al*., 2012) and is therefore the youngest known magmatic intrusion in the UK. The xenolith/xenocryst assemblage is unusual in comparison to elsewhere in the UK and Europe (Upton *et al*., 1983) as it comprises a diverse range of lithologies and megacrysts; including spinel lherzolites, glimmerites, anorthosites/anorthoclasites, gabbros and syenite xenoliths, phlogopite 'books', apatite and corundum xenocrysts (Upton *et al*., 1983; Hunter & Upton, 1987; Menzies *et al*., 1987; Menzies & Halliday, 1988; Long *et al*., 1991; Upton *et al*., 1999 and Upton *et al*., 2011).

For the spinel lherzolites, studies have previously investigated the isotopic composition and mineral chemistry of the major rock-forming minerals (see Upton *et al*., 2011 and references therein). New Re-Os whole-rock isotopic data for a Loch Roag spinel lherzolite are also available in Hughes *et al*. (2014) – Chapter 6. Overall, the spinel lherzolites are granoblastic, porphyroblastic to sub-equigranular with crystal sizes typically ranging 200 µm to 1 mm in size. Porphyroblasts of orthopyroxene, up to 10 mm wide, also occur. Spinel grains appear 'corroded' and are intergrown at the rim by thin (< 50 µm) anorthoclase and/or anorthoclase-clinopyroxene (Na-enriched) 'symplectites' (Hunter & Upton, 1987; Upton *et al.,* 2011). Spinel lherzolite xenoliths typically have an oxidised or altered green-orange-brown 'halo' (cm-scale) around their rim (in contact with the host dyke) with unaltered or 'fresh' grey-coloured peridotite at the xenolith core. A suite of bright apple-green clinopyroxene-rich xenoliths (referred to as 'green clinopyroxenites') is also present. These consist of granular olivine and orthopyroxene, with rare chromite, but are dominated by granular polycrystalline green Cr-diopside clinopyroxene.

8.2. Analytical techniques and methodology

8.2.1. Whole-rock sample preparation and analysis

Seven separate mantle xenoliths of 3-6 cm diameter used in this study were provided by the British Geological Survey. When cut, all of the Loch Roag peridotite xenoliths display dark green 'alteration' rims of variable thickness, with orange-brown vein-like infills (see Hughes *et al.,* in press – Chapter 7). One of the largest spinel lherzolite xenoliths (LR80) had a preserved

grey-black, visually 'unaltered' central zone which was large enough to be extracted and analysed separately. Only xenoliths large enough for powdering were selected for whole-rock analysis but where material was limited, powdered samples still weighed at least 25 g (up to 80-150 g for larger xenolith samples). The Loch Roag monchiquite dyke, hosting the xenolith suite, was also analysed in order to compare the composition of the dyke and xenoliths, to assess if dyke material remained during xenolith sample preparation.

Major and trace elements were analysed by inductively coupled plasma optical emission spectrometry (ICP-OES) and inductively coupled plasma mass spectrometry (ICP-MS), (see McDonald & Viljoen, 2006). Samples were analysed for PGE and Au by Ni sulphide fire assay followed by tellurium co-precipitation and ICP-MS (Huber *et al.,* 2001; McDonald & Viljoen, 2006). Fire assay samples included multiple blanks and duplicate samples per assay batch, to assess any degree of procedural contamination and nugget effect for smaller samples. Accuracy was constrained by analysis of the certified international reference materials TDB1, WMG1, WPR1 and WITS1 (for PGE + Au fire assay) and JB1a, NIM-P and NIM-N (for all other major and trace elements). Precision was estimated by repeat analysis of a sub-set of samples (see Supplementary Material on disk). Whole-rock geochemical results for all xenoliths and dykes analysed during this study are presented in Table 8.1.

8.2.2. Petrography and mineral chemistry analysis

Petrographic studies on polished thin sections were employed to identify xenolith textures. Further examination, mapping and quantitative microanalysis was carried out on a Cambridge Instruments S360 scanning election microscope (SEM) at Cardiff University. Quantitative microanalyses were obtained using an Oxford Instruments INCA Energy EDX analyser attached to the SEM, with operating conditions set at 20 kV and specimen calibration current of ~2 nA at a fixed working distance of 25 mm. Analytical drift checks were carried out every 2 hours using the Co reference standard and a comprehensive suite of standards from MicroAnalysis Consultants Ltd were used to calibrate the EDX analyser.

Polished thin sections, and some corresponding polished blocks for samples requiring sulphide trace element analysis were selected for laser ablation ICP-MS (LA-ICP-MS). LA-ICP-MS was performed on sulphide minerals at Cardiff University on a New Wave Research UP213 UV laser system attached to a Thermo X Series ICP-MS. Analytical procedures and standards followed those of Prichard *et al.* (2013) and Smith *et al.* (2014). Both line and spot analysis were used and independently calibrated, depending on the size of the sulphides. For lines, a minimum

line length of ~ 80 µm and a beam diameter of 15 µm was used, with laser operating conditions of 10 Hz frequency, 0.063 mJ at 4.98 Jcm^{-2} and sample translation at 6 µm sec^{-1}. For spot analysis, beam size was 40 µm and the same laser operating conditions were employed. Individual sulphide minerals (or mineral clusters) < 80 µm across were analysed by spot analysis. Acquisition times ranged 40 to 180s with a gas blank measured for 30s prior to laser ablation. Major element concentrations were measured prior to LA-ICPMS on the SEM, and ^{57}Fe was used as an internal standard for trace element calibration. Gas blank subtraction and internal standard corrections were carried out on Thermo Plasmalab software. Further procedural details are available in Smith *et al.* (2014).

The PGE procedure for LA-ICPMS was checked by analysis of the standard, Laflamme-Po724 as an unknown against the Cardiff quenched sulphide standards (results in Supplementary Material on disk). A representative selection of time resolved analysis spectra (TRA) for Group 1 and 3 sulphides are presented in Appendix B.

8.3. Results

8.3.1. Bulk PGE and chalcophile element geochemistry

Bulk rock Cr/Al and Al/Si ratios are used as a proxy for depletion by partial melting in Figure 8.2a. Mantle xenoliths (harzburgites and lherzolites, with some wehrlites) from the North Atlantic Craton (NAC) keel in west Greenland have low Al/Si and extremely variable Cr/Al (Wittig *et al.,* 2010) relative to 'Primitive Upper Mantle' (PUM; McDonough & Sun, 1995). By comparison, the Loch Roag lherzolites and clinopyroxenites form an intermediate group between Greenlandic and PUM compositions, and are less refractory than the Greenlandic NAC garnet and spinel-bearing peridotite xenoliths (Fig. 8.2a). Anhydrous Cu and Ni concentrations are plotted versus MgO (anhydrous) as a proxy for fractionation (Figs. 8.2b-c). This highlights a significant enrichment in Cu for Loch Roag in comparison to other Greenlandic NAC xenolith and PUM, and again demonstrates that the Scottish xenoliths are less refractory than their Greenlandic counterparts (Fig. 8.2b). By contrast, the Loch Roag xenoliths have lower Ni abundance than Greenlandic NAC (Fig. 8.2c). The elevated concentration of Cu in Loch Roag xenoliths, particularly lherzolites, does not correspond with a systematic change in Ni (Fig. 8.2d).

Table 8.1. Loch Roag spinel lherzolite and clinopyroxenite xenolith bulk rock PGE, Cu, Ni, Cr, MgO, Fe_2O_3* (total iron calculated as Fe_2O_3) and Mg#.

Sample		LR81*	LR101335*	LR289*	LR80*	LR90	LR100	LR84	LRh
Lithology		Spinel lherzolite	Spinel lherzolite	Spinel lherzolite	Spinel lherzolite	Spinel lherzolite	Green clinopyroxenite	Green clinopyroxenite	Monchiquite dyke
MgO	*wt.%*	35.78	38.16	37.04	38.71	41.37	38.84	42.55	7.75
Fe2O3*	*wt.%*	10.12	11.48	10.05	10.20	9.68	11.88	9.77	8.48
Mg#		0.89	0.88	0.89	0.90	0.91	0.88	0.91	0.78
Ni	*ppm*	1756	2404	2022	2144	1892	1702	2301	136
Cu	*ppm*	98.3	69.7	97.0	182.2	34.8	21.1	29.2	51.6
Cr	*ppm*	2910	2599	3001	2456	2646	4221	2504	230
Os	*ppb*	2.75	3.29	3.63	3.45	4.63	3.11	5.16	0.02
Ir	*ppb*	3.08	3.48	3.64	3.60	4.23	5.38	5.51	0.05
Ru	*ppb*	5.79	5.77	6.41	6.03	8.40	11.13	11.02	0.15
Rh	*ppb*	1.35	1.54	1.68	1.47	2.18	2.88	3.71	0.05
Pt	*ppb*	12.52	11.69	11.07	16.88	16.08	5.70	17.47	0.68
Pd	*ppb*	6.35	5.00	4.70	11.48	12.65	3.44	3.15	0.44
Au	*ppb*	2.28	2.00	3.30	1.96	3.58	3.40	1.16	0.05

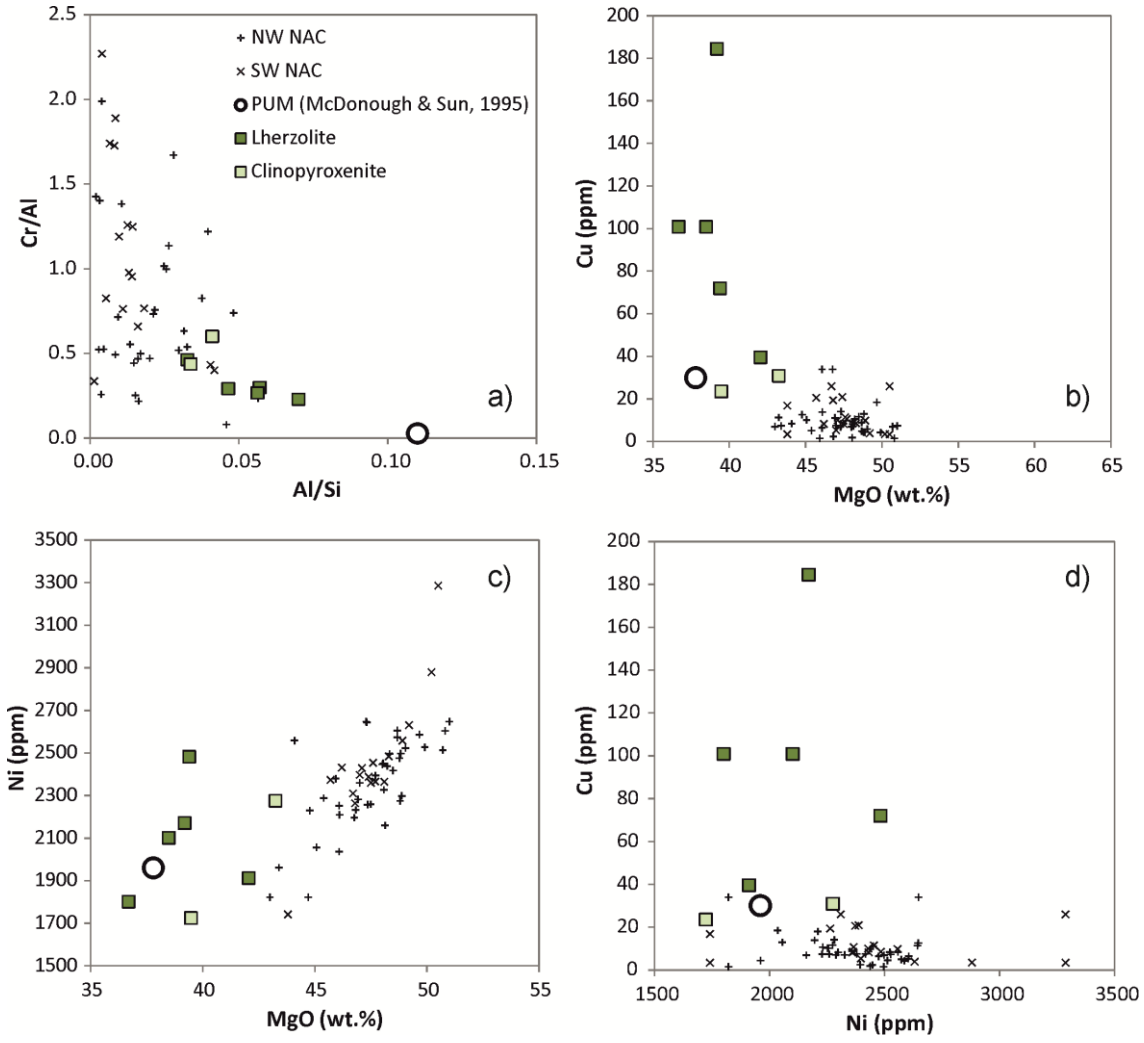

Figure 8.2. Bulk rock geochemistry (a) Cr/Al vs. Al/Si ratio (anhydrous) as proxy for fractionation of xenoliths. High Cr/Al and low Al/Si infers more refractory (depleted) compositions than 'Primitive Upper Mantle' (McDonough & Sun, 1995). (b) Cu vs. MgO (MgO also as fractionation proxy). (c) Ni vs. MgO. (d) Cu vs. Ni bivariant plot. All plots show Loch Roag spinel lherzolite and clinopyroxenite xenoliths (this study) in comparison to western North Atlantic Craton mantle peridotites ('NW NAC' and 'NW NAC'; from Wittig *et al.,* 2010) and PUM (pyrolite, as defined by McDonough & Sun, 1995).

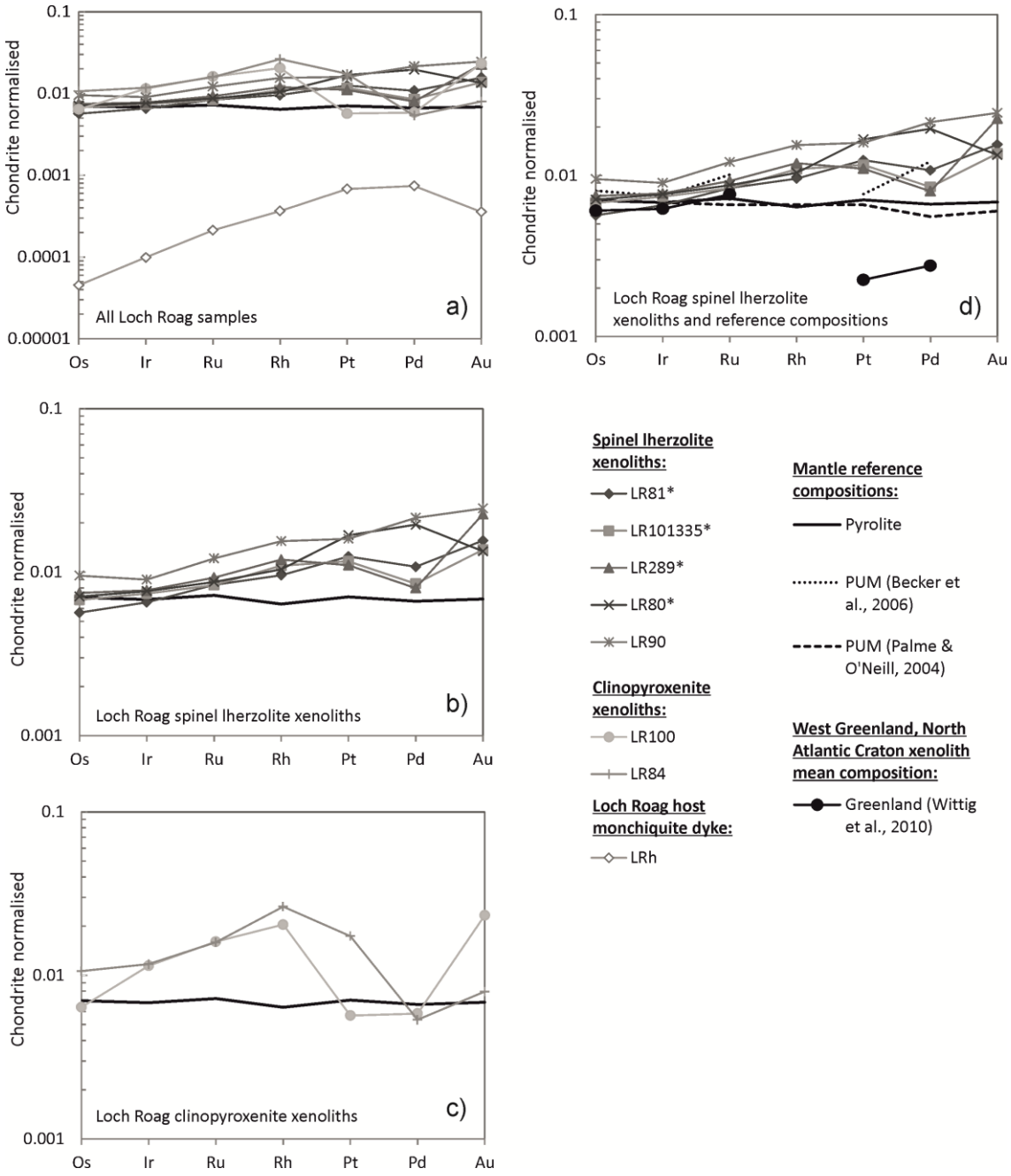

Figure 8.3. Platinum-group element (PGE) chondrite-normalised multi-element diagrams (bulk rock) for Loch Roag spinel lherzolites and clinopyroxenites. (a) All xenoliths and the host monchiquite dyke, relative to PUM (McDonough & Sun, 1995). (b) Spinel lherzolite xenoliths only. (c) Clinopyroxenite xenoliths only. (d) Loch Roag spinel lherzolite plotted in comparison to mean Greenlandic NAC xenoliths (Wittig *et al.,* 2010) and various estimates of 'primitive upper mantle' (PUM) from Palme & O'Neill (2004) and Becker *et al.* (2006) as well as 'pyrolite' (also PUM) from McDonough & Sun (1995). Chondrite normalising values from McDonough & Sun (1995). *denotes bulk rock geochemistry of xenolith samples previously published in Hughes *et al.* (2014) – Chapter 6.

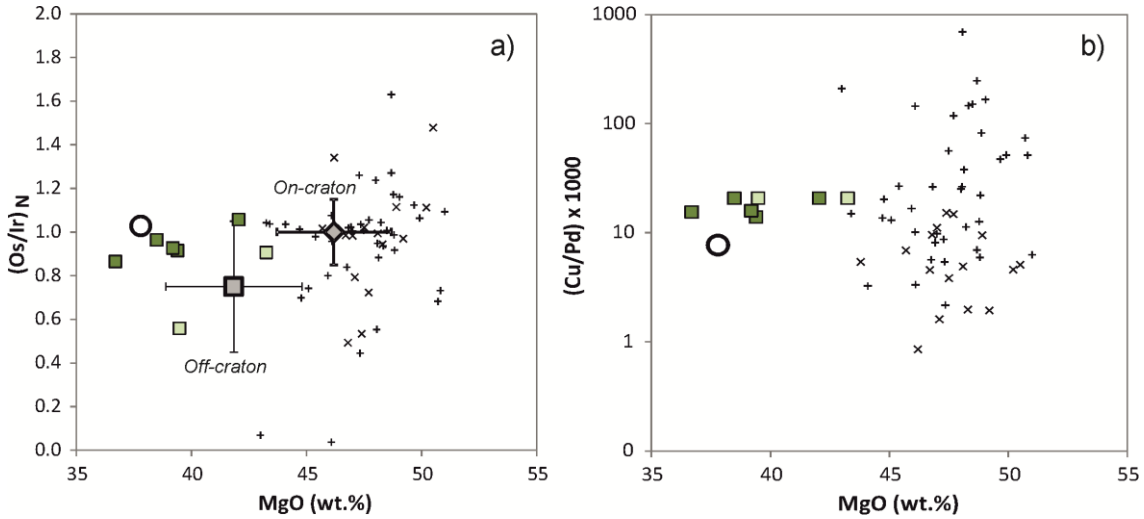

Figure 8.4. Platinum-group element (PGE) bivariant plots, including PGE ratio plots (bulk rock) for Loch Roag xenoliths (this study) in comparison to western North Atlantic Craton mantle peridotites ('NW NAC' and 'NW NAC'; from Wittig *et al.,* 2010) and PUM (pyrolite; McDonough & Sun, 1995). (a) Chondrite-normalised Os/Ir ratio (i.e., $(Os/Ir)_N$) vs. MgO, also showing average on- and off-craton peridotite xenolith compositions ± 3 x standard deviation (see Pearson *et al.,* 2005 and references therein). (b) Cu/Pd ratio (x 1000) vs. MgO.

Chondrite-normalised PGE plots of xenoliths and the host monchiquite dyke are presented in Figure 8.3a. All Loch Roag xenoliths are PGE-enriched by several orders of magnitude above the composition of the dyke, and the fractionation patterns are different, confirming that PGE contamination from the dyke is insignificant. Broadly spinel lherzolites and clinopyroxenites alike form a cluster of chondrite-normalised patterns at approximately 0.01 x chondrite. Palladium-group PGE (PPGE) are enriched above iridium-group PGE (IPGE), but Pt and Pd anomalies are variable. There is a small negative anomaly for Ir in the spinel lherzolite xenoliths (Fig. 8.3b) but Ir, Ru and Rh are consistently enriched in clinopyroxenite xenoliths (Fig. 8.3c) above corresponding concentrations in the lherzolites. All Loch Roag xenoliths display a positive Au anomaly, with the exception of LR80 (Fig. 8.3b). Figure 8.3d displays Loch Roag lherzolite xenolith compositions relative to estimates of PUM (Palme & O'Neill, 2004; Becker *et al.,* 2006), pyrolite (McDonough & Sun, 1995) and the mean composition of mantle xenoliths from beneath the NAC in west Greenland (Wittig *et al.,* 2010). Loch Roag xenoliths are enriched in PPGE above estimates of PUM and pyrolite, and considerably enriched compared to their Greenlandic counterparts, especially for Pt.

Figure 8.4a compares chondrite-normalised Os/Ir ratio of Loch Roag xenoliths with PUM (McDonough & Sun, 1995) and mean compositions of on- and off-craton xenoliths globally (see Pearson *et al.,* 2005 and references therein). The Scottish xenoliths have greater

similarities with PUM and off-craton compositions, than on-craton compositions including the Greenlandic NAC. The Cu/Pd ratio of Loch Roag xenoliths generally clusters near to PUM, and they sit at a ratio value between that of NW and SW Greenlandic NAC margin, and close to PUM (Fig. 8.4b).

8.3.2. Sulphide mineralogy and textures

Detailed petrography and SEM mapping of xenolith polished thin sections and blocks have allowed for the identification and characterisation of various sulphide mineral 'populations'. Initially this was based on textural features of the sulphides themselves, in addition to petrographic setting (e.g., interstitial to coarse protogranular silicates, vs. within symplectite 'pockets'). One spinel lherzolite sample (LR80) was large enough (approximately 6cm diameter) to be cut into slices, sampled by multiple thin sections and polished blocks, and petrographically mapped (Fig. 8.5). Thus LR80 provided a rare opportunity to document the occurrences and 'populations' of sulphides according to their location within the xenolith as a whole, based on SEM backscattered electron (BSE) imaging of 8 polished blocks and thin sections. All sulphides are Fe-Ni-Cu base metal sulphides (pyrrhotite, pentlandite and chalcopyrite), but 3 populations of sulphide blebs can be identified.

Group 1 sulphides (Fig. 8.6a-b) are most abundant in all samples. They are coarse (generally 50-500 μm) and always interstitial to silicate minerals, often occurring at protogranular triple junctions. These Group 1 grains have highly variable and 'complex' internal textures. For example, granular single- or multi-phase base metal sulphide (BMS) 'aggregates' that appear fragmented and re-enclosed within other single- or multi-phase BMS. Both aggregate and enclosing BMS may have distinct and often complex textures, such as striations, flame-textures or intergrown lamellae, stockworks and cross-hatched intergrowth. The distinct shapes of the aggregate BMS, formed prior to their inclusion in the enclosing BMS, and suggest a lengthy formation history.

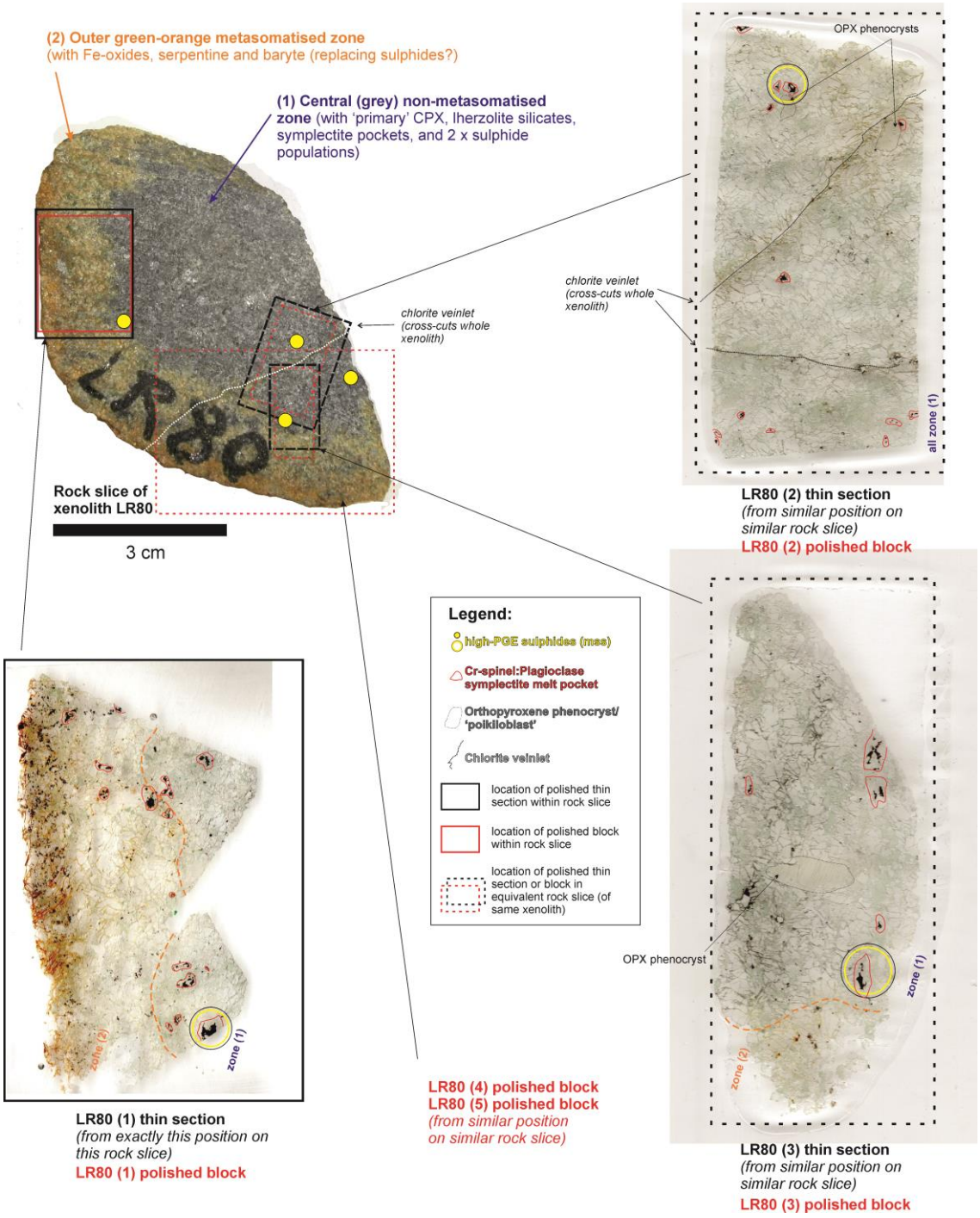

Figure 8.5. Example of xenolith sulphide mineral mapping for spinel lherzolite LR80 rock slice.

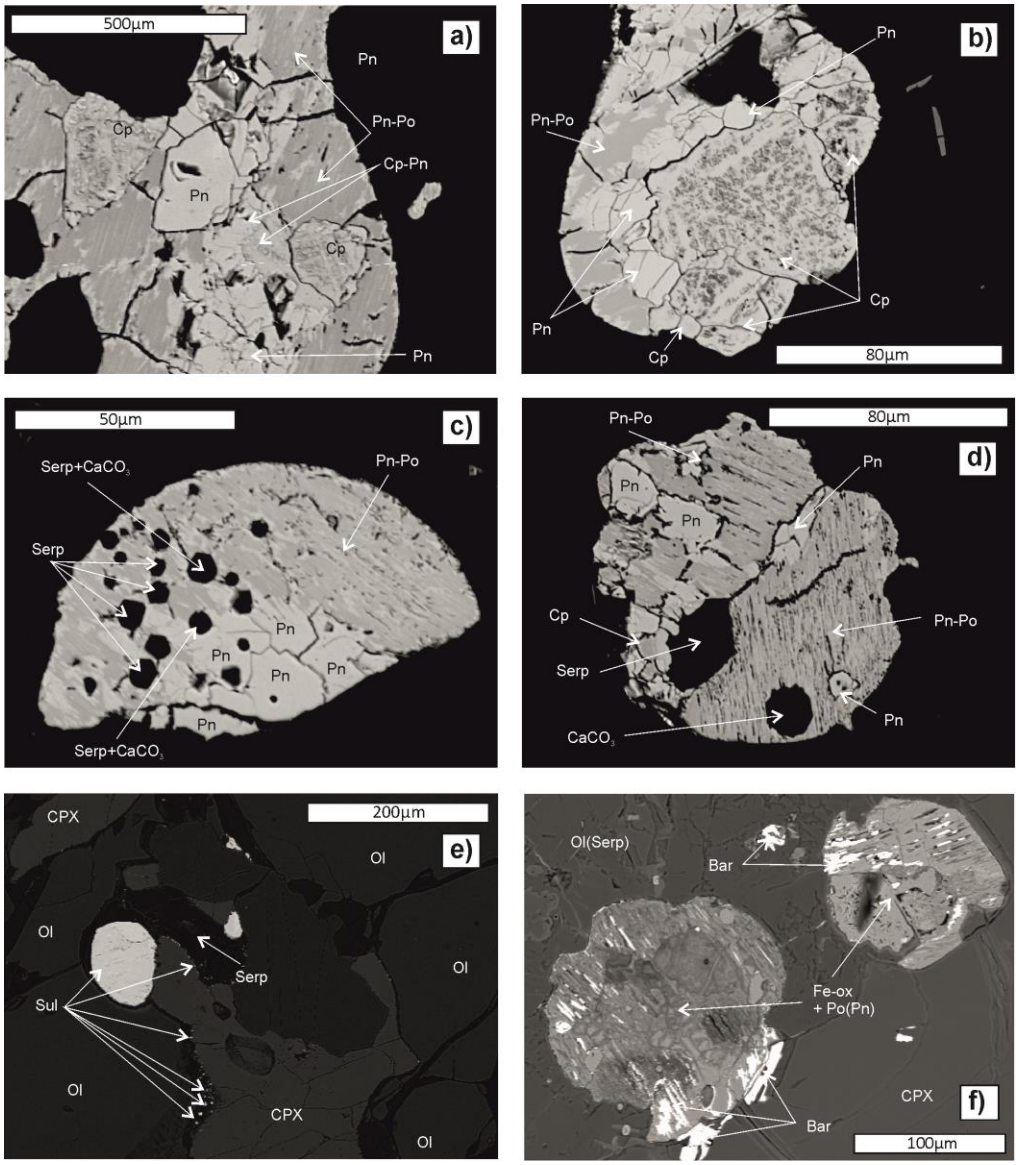

Figure 8.6. Back scattered election (BSE) SEM images of Loch Roag xenoliths. (a) Irregular-shaped complex texture of a Group 1 sulphide grain. Note the granular appearance of pentlandite and cross-hatched chalcopyrite, which are texturally distinct from the surrounding pentlandite, pentlandite-pyrrhotite stockwork, and striated pyrrhotite. (b) Complex multi-phase internal textures of coarse Group 1 sulphides, again showing granular cross-hatched chalcopyrite with granular pentlandite and intergrown flames of pentlandite and pyrrhotite. (c) 'Spongy' textured sulphide grain (Group 2) within chlorite-bearing 'melt pocket' in the xenolith, associated with anorthoclase along a protogranular silicate boundary. Sulphide has rounded- to angular-shaped inclusions of serpentine and rounded $CaCO_3$ inclusions. Note that similar examples of spongy Group 2 sulphides are found in apatite- and chlorite-bearing 'melt pockets'. (d) A 'spongy' Group 2 sulphide. This example is within a chlorite-filled vug surrounded by protogranular coarse olivine. The sulphide dominates the vug in comparison to chlorite. Serpentine (angular) and $CaCO_3$ (rounded) inclusions labelled. Chalcopyrite and pentlandite form discrete phases within the sulphide globule, and two phases of pentlandite-pyrrhotite intergrowths with different scale lamellae at different orientations are present. (e) Rounded sulphide at clinopyroxene and olivine grain boundaries. Note the µm-scale rounded sulphide globules along clinopyroxene grain boundaries. (f) Rounded to irregular-shaped sulphides in the orange-green oxidised alteration rim of xenolith LR80. Sulphides are interstitial to olivine and clinopyroxene, but have become almost completely overprinted by baryte and Fe-oxides. Pyrrhotite is the only sulphide that remains and is oxidising. Mineral abbreviations: olivine (Ol), clinopyroxene (CPX), serpentine (Serp), iron oxide (Fe-ox), baryte (Bar), calcite or Ca-carbonate ($CaCO_3$), pentlandite (Pn), pyrrhotite (Po), chalcopyrite (Cp).

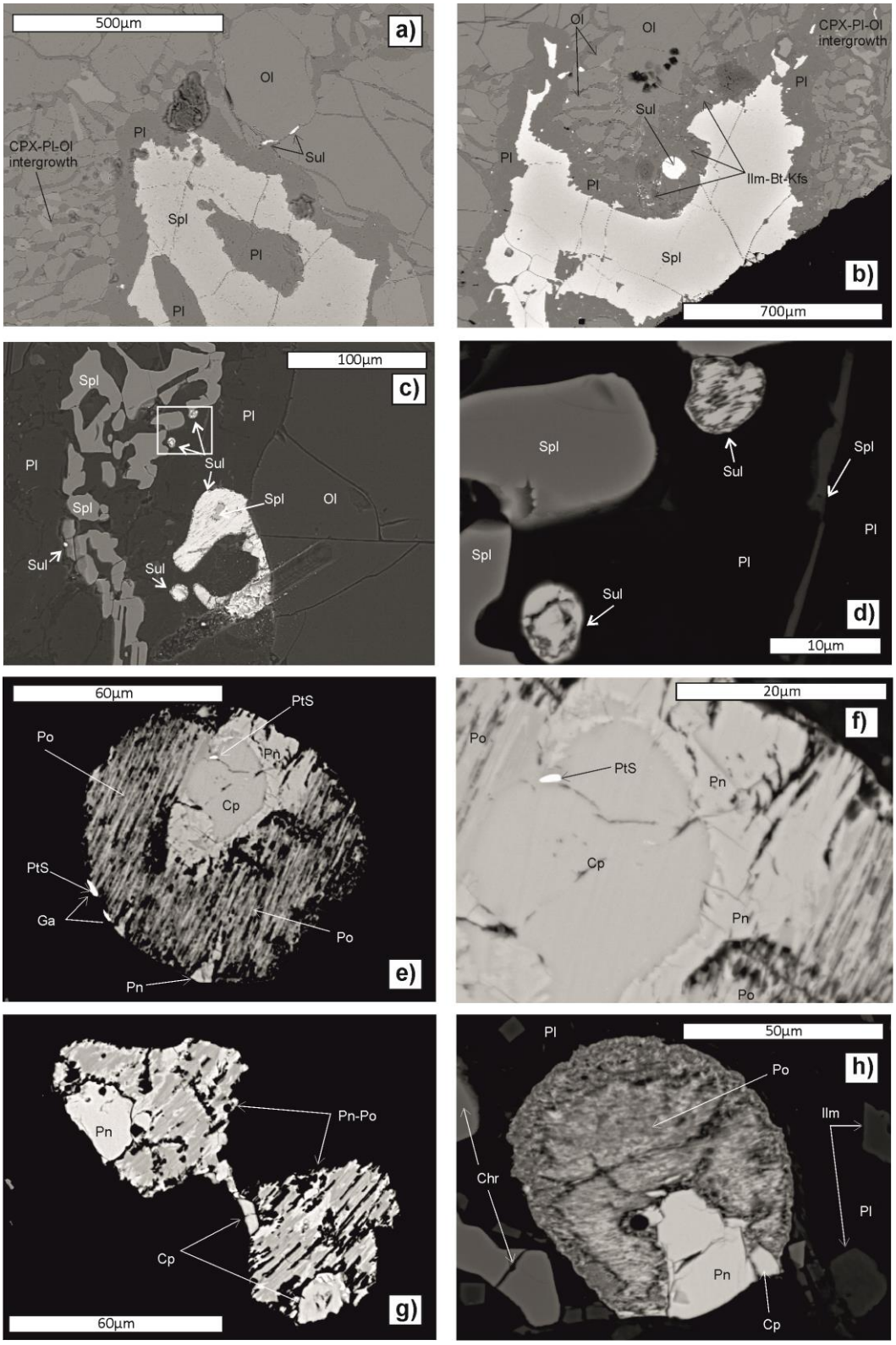

Figure 8.7. *(caption overleaf)*

A second distinct group of BMS with a spongy appearance can also be defined. Group 2 sulphide grains are characterised by a 'spongy' appearance due to multiple non-sulphide inclusions. These grains are < 100 µm in diameter and composed of Fe-Ni-Cu BMS with comparatively simple internal textures with an overall rounded outer shape (Fig. 8.6c-d). Inclusions are presently composed either of serpentine or $CaCO_3$. Serpentine-filled inclusions are generally polygonal in shape, while $CaCO_3$ inclusions are rounded. This group of sulphides is comparatively rare, generally occurring near spinel-feldspar symplectite pockets or melt pockets. Other similarly rounded sulphides with simple internal textures (but within serpentine or $CaCO_3$ inclusions) were identified in LR90, particularly at clinopyroxene crystal boundaries and sometimes with 'trails' of smaller (micron-scale) sulphides (e.g., Fig. 8.6e). In the outer orange-green coloured oxidised alteration halo of xenoliths (labelled in Fig. 8.5) sulphide grains have either been partially of wholly overprinted by baryte and iron oxides (e.g., Fig. 8.6f).

Group 3 sulphide grains (Fig. 8.7) with rounded or 'droplet' shapes occur exclusively within spinel-feldspar symplectites, or at the margins of associated finely crystalline clinopyroxene-plagioclase-olivine haloes to the symplectites (Figs. 8.7a-d). The symplectites themselves often appear skeletal or irregular in shape, where a core of Al-Mg spinel has become intergrown and

Figure 8.7. BSE SEM images of Group 3 sulphides (droplets) in Loch Roag xenoliths (a) Spinel and feldspar symplectite with clinopyroxene-orthopyroxene-plagioclase melted intergrowth on left hand side with 'primary' coarse granular olivine crystals on the right of the symplectite. (b) Spinel and feldspar symplectite bounded by clinopyroxene-plagioclase-olivine melted intergrowths. Note patches of ilmenite, biotite and orthoclase are from a separate melt from that which formed the symplectite and CPX-Pl-Ol intergrowths. Rounded Group 3 sulphide droplet (labelled 'Sul') occurs within symplectite. (c) Multiple Group 3 sulphide droplets of various sizes within a skeletal spinel-feldspar symplectite pocket. Note that the largest sulphide droplet (with irregular curved shape) as a small spinel inclusion within it. Image shows a LA-ICP-MS laser line through the lower portion of the largest sulphide droplet. (d) Close-up image of boxed area in (c) showing simple internal textures within sulphide droplets. (e) Close-up of rounded Group 3 sulphide droplet in (b) with contrast adjusted to display internal texture and sulphide phases. Pentlandite and chalcopyrite have exsolved from pyrrhotite (striated with minor pentlandite flames). Discrete µm-scale platinum-group minerals (labelled PtS) occur within this Group 3 sulphide droplet. Pt-sulphide (cooperite) is within the chalcopyrite portion and at the margin of the droplet. Pt-sulphide at the droplet margin occurs with galena. (f) Close-up of Pt-sulphide within chalcopyrite of (e). (g) Double-ended droplet of Group 3 sulphide located within another spinel-feldspar symplectite. Note similar internal texture of droplets to (e) such that chalcopyrite and pentlandite form discrete phases, from pyrrhotite-pentlandite lamellae, due to cooling stages from previously molten sulphide droplet. (h) Group 3 sulphide droplet within spinel-feldspar symplectite (with accessory ilmenite from separate melt ingress). Sulphide droplet has similar simple internal textures as (e) and (g) but has become partially oxidised due to its location within the green-orange oxidised/altered halo of the xenolith. Mineral abbreviations as in Fig. 8.6 plus: plagioclase (Pl), spinel (Spl), ilmenite (Ilm), orthoclase (Kfs), biotite (Bt), galena (Ga), cooperite (PtS).

surrounded by anorthoclase-oligoclase – see Hunter & Upton (1987). In some symplectites near the margin of the xenolith, feldspar has become partially overprinted by finely crystalline biotite, ilmenite and orthoclase (presumably from an external infiltrating melt), however this is rare. Group 3 sulphides have simple internal textures (e.g., Fig 8.7e), akin to those observed once a sulphide liquid has cooled, forming a monosulphide solution (MSS) at first, and then an intermediate sulphide solution (ISS). Throughout this process Cu and Ni-rich liquids segregate (see Craig & Vaughan, 1990; Holwell & McDonald, 2010 and references therein; Naldrett 2011 and references therein). In some cases cooperite (PtS) has exsolved from Group 3 sulphides and formed discrete platinum-group mineral (PGM) phases (Fig. 8.7e-f). PGM are only observed in Group 3 sulphides. Sometimes Group 3 sulphides appear as double-ended droplets (e.g., Fig. 8.7g) and where these occur within the orange-green oxidised alteration haloes of the xenolith, partial oxidation can occur (e.g., Fig. 8.7h – overprinting by iron oxides).

8.3.3. Sulphide compositions

The trace element composition of 78 sulphide grains from Loch Roag spinel lherzolite xenoliths were analysed *in situ* by LA-ICP-MS (see Table 8.2). Only one analysis of a sulphide grain in a clinopyroxenite xenolith was possible. Due to their variable size, mixed textures of BMS, and the nature of 'incision' by the laser, LA-ICP-MS analyses commonly incorporated multiple sulphide phases resulting in mixed spectra (i.e., pentlandite mixed with pyrrhotite, etc). To account for these mixed spectra, results in Table 8.2 have been classed according to the major BMS end member (pyrrhotite, Po; pentlandite, Pn; chalcopyrite, Cp). Analyses with < 5 wt.% Ni+Cu are classified as Po; 5-15 wt.% Ni or Cu are Po-Pn or Po-Cp respectively; 15-22 wt.% Ni or Cu are Pn-Po or Cp-Po respectively; and analyses with ≥ 22 wt.% Ni or Cu are classified as Pn or Cp. In results where both Ni and Cu abundances are > 5 wt.% each, analyses have been labelled Cp-Pn or Pn-Cp (depending on which metal is dominant). This classification scheme distinguishes details of trace element compositions of Cp, Pn and Po end members of each 'population' of sulphides (i.e., Groups 1, 2 and 3). In the spinel lherzolites, all Group 3 sulphides (i.e., droplets) have high total PGE + Au + Re concentrations (17 to 380 ppm), irrespective of BMS class (defined by wt.% Ni and Cu) – see Figures 8.8a-b. By contrast, Group 1 (complex) sulphides consistently had low total PGE + Au + Re concentrations (0.4 to 40 ppm). Spongy Group 2 sulphides have intermediate total PGE + Au + Re abundances ranging 12 to 92 ppm. The sulphide analysed from a clinopyroxenite xenolith had very low total PGE concentration.

Chondrite-normalised multi-element diagrams for Re, PGE and Au, in the different sulphide groups are displayed in Figure 8.9. Group 1 sulphides have low overall PGE abundances, often sub-chondritic, with characteristic $(Re/Os)_N$ typically > 10 (Fig. 8.9a). Group 2 sulphides have higher PGE abundances (mostly > chondrite) with little variation in Re at approximately 10 x chondrite (Fig. 8.9b) and $(Re/Os)_N$ 0.2 – 2. The IPGE and Rh are enriched above Pt, Pd and Au. Group 3 sulphides have the highest PGE abundances, with low $(Re/Os)_N$ 0.2 – 0.01 (Fig. 8.9c). With the exception of Au and Re, the PGE define a broadly flat chondrite-normalised pattern although Pd is also depleted in a number of cases. Figure 8.9d displays multi-element patterns for LA-ICP-MS lines that intersected PGM (Pt- and Pd-species) within Group 3 sulphides. Where Pt or Pd dominant PGM have been intersected, Pt and Pd are elevated as positive anomalies. In order to be identified by SEM, PGM were generally > 1 µm diameter and exposed on the polished surface. Further PGM were discovered during cross-checking of time resolution analysis (TRA) spectra from raw LA-ICP-MS results (see Appendix B), identifiable as discrete peaks in Pt or Pd.

For spinel lherzolites, S/Se measured in sulphides (all groups) ranges from 2000 to 5000 (Fig. 8.10a), however the S/Se ratio of the clinopyroxenite sulphide was considerably higher (~ 14,800). The majority of sulphides from Loch Roag xenoliths have Se/Te ratios > chondrite, due to their very low Te abundances (Fig. 8.10b). 'Spongy' Group 2 sulphides are transitional between Groups 1 and 3, according to raw Os abundance. This can be further visualised according to normalised Re/Os ratio such that all Group 3 sulphides have $(Re/Os)_N < 1$, and Group 1 sulphides $(Re/Os)_N > 1$ (with the exception of 4 analyses which were visibly altered) – Figure 8.10d. All sulphide groups generally show chondritic Os/Ir (Fig. 8.10e) although Group 1 sulphides are much more scattered. By contrast, sulphides display highly variable Pt/Pd ratios; generally Group 1 sulphides have lower Pt/Pd ratios than Group 3, and Group 3 sulphides display greater variation in Pt abundance (due to their hosting Pt-sulphide PGM).

Table 8.2. *(continued overleaf)*

Analysis code	Sample number	Mineral	Group	*S	Se	S/Se	Fe	Ni	Cu	Co	Zn	As	Ru	Rh	Pd	Ag	Cd	Sb	Te	Re	Os	Ir	Pt	Au	Bi
Mantle xenolith:				*(wt. %)*	*(ppm)*		*(wt. %)*	*(wt. %)*	*(wt.%)*	*(ppm)*	*(ppm)*	*(ppm)*	*(ppm)*	*(ppm)*	*(ppm)*	*(ppm)*	*(ppm)*	*(ppm)*	*(ppm)*	*(ppm)*	*(ppm)*	*(ppm)*	*(ppm)*	*(ppm)*	*(ppm)*	*(ppm)*
LR80(1) ln1	LR80(1) block	Pn	group 3	36.00	156.39	2302.01	37.31	26.22	0.05	3617	1667	<8	8.81	1.27	5.36	6.48	2.99	<0.9	4.67	0.16	5.52	4.28	3.41	0.27	2.14
LR80m5L1 po-pn2	LR80(1)	Pn	group 3	35.00	179.36	1951.40	36.20	27.98	0.82	2779	192	<8	88.69	14.25	62.34	1.67	<0.98	<0.9	19.35	0.03	60.20	62.43	28.51	0.32	0.85
LR80(1) line 4	LR80(1) block	Po-Pn	group 3	36.00	122.45	2939.94	55.52	6.75	0.29	1531	3468	<8	17.19	2.65	<0.2	26.20	3.54	<0.9	6.13	0.61	15.95	11.53	3.49	0.22	1.95
LR80(2) line2	LR80(2) block	Po-Pn	group 3	36.00	167.07	2154.77	49.52	14.64	0.34	1996	1501	<8	25.89	4.51	0.53	7.69	<0.9	<0.9	7.41	0.61	17.70	11.94	6.28	0.35	1.38
LR80(2) line 3	LR80(2) block	Pn	group 3	36.00	114.30	3149.61	34.31	27.69	0.10	3923	351	<8	20.37	3.39	97.65	16.36	1.56	<0.9	7.07	0.24	12.83	10.37	21.28	0.09	1.07
LR80(2) line 4	LR80(2) block	Pn-Po	group 3	36.00	154.80	2325.58	52.85	15.62	0.07	1847	1422	<8	60.06	11.33	<0.2	8.51	<0.9	<0.9	8.01	0.29	48.34	38.07	1.28	0.03	1.50
LR80(2) line 5	LR80(2) block	Pn-Po	group 3	36.00	119.62	3009.65	47.17	15.12	0.06	2149	1466	<8	10.62	1.52	<0.2	5.56	2.85	<0.9	6.18	0.55	6.57	4.91	0.94	0.26	2.09
LR80(2) line 6	LR80(2) block	Pn	group 3	36.00	105.90	3399.43	36.99	24.35	0.07	3401	815	<8	7.02	1.27	6.11	5.69	<0.9	<0.9	6.31	0.37	5.31	4.04	5.40	0.19	1.87
LR80(2) line 8	LR80(2) block	Pn	group 3	36.00	128.14	2809.34	34.73	28.93	0.08	2720	721	<8	5.27	1.16	<0.2	3.60	2.15	<0.9	7.56	0.80	13.78	16.47	0.71	0.80	6.58
LR80(3) m1L1 + Pt PGM	LR80(3) block	Po-Pn (PGM)	group 3	36.00	115.98	3104.05	50.92	13.50	<0.04	1937	486	<8	131.29	21.80	1.61	4.44	<0.9	<0.9	1.28	0.35	75.30	53.35	120.41	0.17	1.10
LR80(3)m1L2	LR80(3) block	Pn-Po (PGM)	group 3	36.00	123.89	2905.80	45.77	17.67	0.95	2892	995	<8	160.34	25.79	34.31	4.70	<0.9	<0.9	2.61	0.58	83.73	69.26	6.01	0.35	1.67
LR80(5) line 1 mix +Pt PGM	LR80(5) block	Pn	group 3	36.50	162.84	2241.44	33.67	23.16	6.47	4627	3811	<8	48.56	6.63	107.53	7.53	7.05	<0.9	2.29	0.45	21.52	23.88	552.74	<0.02	0.51
LR90 m1s1_sulphide	LR90	Pn-Po	group 3	35.40	91.98	3848.59	47.57	16.13	0.06	2098	12	<7	28.26	4.07	0.46	<0.2	2.33	<0.8	7.12	0.35	14.45	12.01	8.37	0.62	1.81
LR90 m1s1_Pt-PGM(1)	LR90	Pn-Po (PGM)	group 3	35.40	94.63	3740.92	47.88	17.59	0.06	2325	12	<7	29.67	4.43	0.33	0.30	5.39	<0.8	11.17	0.64	15.68	11.87	154.76	0.89	1.95
LR90 m1s1_Pt-PGM(2)	LR90	Po-Pn (PGM)	group 3	35.40	103.00	3436.99	49.95	13.78	0.05	1843	5	<7	31.38	3.98	0.38	<0.2	1.22	<0.8	6.98	0.55	10.74	12.05	275.05	<0.02	2.53
LR90 m2s1_sulphide	LR90	Pn-Po	group 3	35.99	89.66	4014.05	45.97	18.33	0.90	2844	6	<7	17.21	2.50	6.27	1.82	<0.95	<0.8	6.87	0.37	11.49	8.97	9.11	0.20	1.57
LR90 m2s1_Pt-PGM	LR90	Pn-Po (PGM)	group 3	35.99	84.21	4273.96	46.40	18.39	2.17	2620	7	<7	17.74	2.74	8.32	2.49	2.41	<0.8	10.36	0.47	14.32	10.23	49.03	0.20	2.12
LR90 m3s1_sulphide	LR90	Pn-Po	group 3	36.00	97.50	3692.12	48.56	15.16	0.18	2197	103	8.47	11.67	1.67	14.37	0.93	<0.95	<0.8	5.86	0.33	6.79	5.97	4.43	0.07	1.52
LR90 m3s1_Pt-PGM	LR90	Pn-Po (PGM)	group 3	36.00	95.31	3777.24	49.80	17.74	0.37	3095	138	<7	11.21	1.43	29.63	2.62	<0.95	<0.8	9.07	0.24	6.92	5.84	15.31	<0.02	1.20
LR90 m3s2	LR90	Po-Pn	group 3	36.00	100.65	3576.70	50.38	13.07	2.38	1906	69	140.80	5.88	0.69	0.43	1.53	<0.95	<0.8	4.23	0.27	3.54	3.92	1.80	0.14	1.51
LR80(3) m1s1	LR80(3)	Pn-Po	group 2	36.00	72.26	4982.25	46.12	15.92	0.87	1980	19036	<7	3.69	0.58	0.88	1.43	<0.95	<0.8	2.79	0.37	2.24	2.45	1.79	0.10	1.65
LR80(3) m1s2	LR80(3)	Pn-Po	group 2	36.00	74.10	4858.56	44.38	19.99	0.68	2573	2919	<7	4.16	0.54	2.16	1.01	<0.95	<0.8	2.66	0.37	1.70	1.89	2.25	0.28	1.37
LR80(3) m2s1	LR80(3)	Pn-Po	group 2	34.93	88.44	3949.49	44.00	21.50	0.36	2931	46	34.53	14.20	2.05	8.54	2.67	<0.95	<0.8	3.73	0.30	7.28	6.10	4.51	0.24	2.25
LR80(2) m1s1	LR80(3)	Pn-Po	group 2	37.87	78.13	4846.84	44.07	20.28	0.02	2179	40	<7	3.71	0.54	0.31	1.14	<0.95	<0.8	6.29	0.53	2.36	2.17	2.33	0.59	2.54
LR80(2) m2s1	LR80(3)	Pn-Po	group 2	36.00	98.07	3671.03	47.42	18.66	0.07	2255	27	<7	41.85	6.38	0.29	0.27	<0.95	<0.8	7.70	0.32	22.23	19.14	1.37	0.37	2.05
LR80m1L1 sul2 - cp	LR80(1)	Cp-Pn	group 1	34.80	106.92	3254.68	39.93	12.47	13.60	1231	5349	<8	0.63	0.22	0.35	4.83	9.91	<0.9	<0.95	1.03	0.08	0.42	0.60	<0.02	0.32
LR80m1L1 sul6 - cp	LR80(1)	Cp-Pn	group 1	34.50	122.58	2814.43	36.04	18.06	9.90	1853	3178	<8	1.37	0.61	4.58	9.61	5.40	<0.9	<0.95	0.45	1.20	0.70	1.78	<0.02	0.50
LR80m4L1 cp	LR80(1)	Po-Cp	group 1	35.00	95.87	3650.61	45.55	3.14	13.32	1929	6483	<8	<0.08	<0.11	<0.2	9.66	1.21	<0.9	2.04	0.23	0.07	0.05	0.12	<0.02	0.25
LR80m1L1 sul3 - cp-pn	LR80(1)	Pn-Cp	group 1	34.00	142.14	2392.06	35.29	17.17	9.53	1787	1736	<8	0.75	0.71	3.64	9.14	2.10	<0.9	<0.95	0.64	0.33	0.41	1.33	<0.02	0.29
LR80m3L1 cp+pn	LR80(1)	Pn-Po	group 1	35.00	114.19	3065.04	39.42	15.91	4.67	2393	490	<8	2.87	0.28	10.67	2.08	3.25	<0.9	1.41	0.73	0.30	0.37	1.27	0.26	1.44
LR80m1L1 sul4 - pn	LR80(1)	Pn	group 1	33.00	154.17	2140.52	33.37	30.85	2.78	5017	1059	<8	1.54	1.16	29.71	7.76	<0.98	<0.9	<0.95	0.34	0.39	0.50	6.61	<0.02	0.69
LR80m1L2 pn +po	LR80(1)	Pn	group 1	37.00	130.34	2838.66	37.68	27.30	<0.04	4338	44	<8	2.67	0.31	11.11	2.31	<0.98	<0.9	3.08	<0.03	0.81	0.77	2.61	<0.02	1.51
LR80m1L1 sul1 - po	LR80(1)	Po-Pn	group 1	38.00	137.19	2769.98	53.28	10.21	0.51	1609	817	<8	4.87	0.86	0.38	5.82	<0.98	<0.9	3.73	0.30	0.82	0.86	0.17	0.12	0.71
LR80m1L1 sul5 - po	LR80(1)	Pn-Po	group 1	39.00	157.34	2478.72	45.31	17.53	1.16	2970	190	<8	1.07	0.79	14.38	7.38	<0.98	<0.9	<0.95	0.50	0.91	0.13	0.62	<0.02	1.13
LR80m1L1 sul7 - po	LR80(1)	Po-Pn	group 1	39.00	120.90	3225.78	46.80	14.25	0.95	1964	785	<8	2.21	0.30	0.43	1.86	<0.98	<0.9	<0.95	0.56	0.95	0.86	0.26	<0.02	1.30
LR80m1L2po1	LR80(1)	Pn-Po	group 1	39.00	105.75	3687.91	48.31	17.67	<0.04	2133	25	<8	1.81	0.39	0.29	0.43	<0.98	<0.9	3.82	<0.03	0.78	0.80	0.17	0.11	1.32
LR80m1L2po2	LR80(1)	Po-Pn	group 1	39.00	77.76	5015.20	48.81	11.13	0.05	1786	65	<8	1.21	<0.11	0.40	0.56	<0.98	<0.9	3.50	0.23	0.78	0.82	0.40	0.17	1.32

Table 8.2. LA-ICP-MS major and trace element data for sulphide grains in Loch Roag spinel lherzolite xenoliths, organised by population (i.e., Group 1, 2 and 3). Also one result for a single sulphide analysed in a clinopyroxenite xenolith. *S indicates calibration of LA-ICP-MS data to S abundance according to sulphide stoichiometry.

Analysis code	Sample number	Mineral	Group	*S	Se	S/Se	Fe	Ni	Cu	Co	Zn	As	Ru	Rh	Pd	Ag	Cd	Sb	Te	Re	Os	Ir	Pt	Au	Bi
LR80m3L1 po-pn	LR80(1)	Po-Pn	group 1	37.00	144.88	2553.78	53.80	6.09	0.11	2251	305	<8	1.82	0.18	0.27	0.71	<0.98	<0.9	4.87	0.43	0.39	0.49	0.13	0.66	1.78
LR80m4L1 po-pn1	LR80(1)	Po-Pn	group 1	35.50	94.84	3743.05	47.67	14.13	0.19	2217	334	10.50	0.25	0.15	<0.2	0.75	<0.98	<0.9	3.62	0.49	0.03	0.03	0.08	0.10	0.77
LR80m4L1 po-pn1	LR80(1)	Po-Pn	group 1	35.50	108.91	3259.61	49.15	13.61	1.24	2089	730	<8	<0.08	<0.11	0.30	1.61	1.12	<0.9	2.76	0.54	0.17	0.10	0.21	<0.02	1.04
LR80m1L1 all	LR80(1)	Pn-Po	group 1	36.50	119.83	3045.98	42.53	16.38	5.08	2169	622	<8	1.78	1.25	5.23	5.70	2.60	<0.9	<0.95	0.56	0.74	0.64	1.19	<0.02	0.82
LR80m1L2 all	LR80(1)	Pn-Po	group 1	37.00	164.03	2255.62	44.79	19.18	0.05	2706	11	<8	1.84	0.28	3.33	1.04	<0.98	<0.9	3.60	0.07	0.82	0.83	0.99	0.11	1.42
LR80m3L1 all	LR80(1)	Po-Pn	group 1	38.00	103.64	3666.49	51.85	7.69	0.46	1999	287	<8	1.60	0.15	0.52	0.75	<0.98	<0.9	4.04	0.41	0.43	0.42	0.22	0.55	1.55
LR80m4L1 all	LR80(1) block	Po	group 1	37.00	84.82	4361.93	56.57	2.37	3.06	2548	1676	<8	0.21	<0.11	<0.2	2.82	<0.98	<0.9	3.79	0.53	0.06	0.03	0.07	0.04	0.92
LR80(1) line 2 mix	LR80(1) block	Po-Pn	group 1	36.00	109.51	3287.45	49.01	14.18	0.22	3219	964	<8	1.28	0.24	0.35	6.44	35.34	<0.9	3.92	0.45	1.29	0.94	0.39	0.70	2.15
LR80(1) line 3 ALL	LR80(1) block	Po-Pn	group 1	36.00	98.05	3671.45	51.78	8.25	5.29	2935	2631	<8	0.60	<0.11	<0.2	13.72	15.98	1.47	3.84	0.45	0.42	0.23	0.52	1.47	1.79
LR80(1) line 3 Cp	LR80(1) block	Po-Cp	group 1	35.50	76.72	4627.45	49.63	3.65	12.83	747	5641	<8	0.34	<0.11	<0.2	24.04	3.33	<0.9	2.23	0.46	0.12	0.13	0.69	2.15	0.40
LR80(1) line 3 Pn-Po	LR80(1) block	Po-Pn	group 1	36.00	111.83	3219.06	51.04	12.52	0.83	4473	511	<8	0.77	0.17	<0.2	6.06	24.76	1.97	4.95	0.42	0.44	0.31	0.37	1.02	2.74
LR80(1) line 5	LR80(1) block	Pn-Po	group 1	36.00	122.10	2948.40	44.13	16.38	0.47	2205	5190	8.96	<0.09	<0.11	<0.2	2.22	<0.9	<0.9	6.35	0.64	0.18	<0.02	0.48	0.48	2.20
LR80(1) line 6	LR80(1) block	Po-Pn	group 1	36.00	139.44	2581.72	52.04	11.01	0.65	2888	1054	8.08	0.19	0.16	<0.2	4.19	67.65	<0.9	4.13	0.35	0.08	0.13	<0.02	0.30	2.08
LR80(1) line 7 all	LR80(1) block	Pn-Po	group 1	37.00	118.82	3114.08	42.05	19.01	2.36	2827	-25	<8	<0.09	<0.11	0.90	3.12	1.35	<0.9	3.39	0.76	<0.03	<0.02	0.27	0.30	1.28
LR80(1) line7 Pn-Po	LR80(1) block	Pn-Po	group 1	35.50	115.64	3069.78	49.47	18.07	0.16	2880	894	<8	<0.09	<0.11	0.87	3.95	1.63	<0.9	3.36	0.55	<0.03	<0.02	0.33	0.31	1.14
LR80(2) line1	LR80(2) block	Pn	group 1	36.00	134.97	2667.35	42.42	22.04	<0.04	2881	1224	<8	0.10	<0.11	0.33	12.89	<0.9	<0.9	7.71	0.61	<0.03	<0.02	<0.02	0.42	1.39
LR80(2) line 7	LR80(2) block	Pn	group 1	35.50	132.77	2673.80	30.64	32.18	0.08	4288	604	<8	0.65	0.12	1.98	9.61	<0.9	<0.9	6.44	0.23	3.04	0.33	1.18	0.34	2.91
LR80(3) m1L2 cp2	LR80(3)	Cp	group 1	36.50	108.73	3356.90	27.05	4.15	33.80	635	2787	<8	<0.08	<0.11	0.24	2.02	5.40	<0.9	3.11	0.32	0.06	0.05	0.42	0.17	<0.09
LR80(3)m3L1 cp	LR80(3)	Cp-Po	group 1	37.50	82.90	4523.33	37.27	7.19	19.55	884	2322	<8	0.12	<0.11	0.35	9.98	<0.98	<0.9	9.61	1.08	0.07	0.18	0.06	0.33	0.60
LR80(3)m1L1 pn	LR80(3)	Pn	group 1	34.50	167.30	2062.12	32.26	33.73	<0.04	5824	112	<8	0.79	0.13	5.57	2.53	<0.98	<0.9	8.47	0.48	0.18	0.21	4.96	<0.02	1.07
LR80(3) m1L2 pn1	LR80(3)	Pn-Po	group 1	34.50	175.20	1969.13	38.59	21.17	6.24	3325	1096	<8	0.89	<0.11	2.32	5.14	<0.98	<0.9	1.00	0.46	0.75	0.69	2.00	0.39	1.18
LR80(3)m2L1 pn1-2	LR80(3)	Pn	group 1	34.00	130.49	2605.48	38.09	27.86	0.05	4050	137	14.33	0.88	<0.11	0.53	2.11	<0.98	<0.9	3.88	0.35	0.55	0.50	0.19	0.15	1.34
LR80(3)m1L3 pn-po	LR80(3)	Pn	group 1	36.50	137.71	2650.58	35.16	30.75	0.09	3720	83	<8	0.62	0.43	1.19	0.92	<0.98	<0.9	<0.9	<0.03	0.56	0.59	0.37	<0.02	0.79
LR80(3)m3L1 pn-po	LR80(3)	Po-Pn	group 1	35.00	127.69	2741.05	49.78	13.13	0.08	1756	123	<8	0.22	<0.11	<0.2	0.53	<0.98	<0.9	4.76	0.78	0.27	0.35	0.06	0.42	2.03
LR80(3)m1L1 Po+Pn	LR80(3)	Po	group 1	37.00	142.82	2590.66	60.14	2.78	0.08	2656	167	<8	1.25	0.22	0.27	0.33	<0.98	<0.9	5.98	0.64	0.31	0.27	0.29	0.19	1.67
LR80(3)m2L1 po-pn	LR80(3)	Pn-Po	group 1	38.50	137.40	2801.98	46.06	16.92	<0.04	2274	52	9.76	0.10	<0.11	0.28	0.43	<0.98	<0.9	2.03	0.53	0.21	0.25	0.06	0.47	1.36
LR80(3)m1L1 all	LR80(3)	Pn-Po	group 1	38.00	153.65	2473.08	44.55	19.39	0.05	2698	127	<8	0.56	0.17	1.11	0.64	<0.98	<0.9	5.36	0.50	0.24	0.21	1.08	0.09	1.28
LR80(3) m1L2 all	LR80(3)	Cp-Pn	group 1	38.00	138.98	2734.28	36.52	10.92	17.56	1650	1793	<8	<0.08	<0.11	0.85	4.17	3.36	<0.9	2.35	0.47	0.04	0.08	1.56	0.25	0.58
LR80(3)m2L1 all	LR80(3)	Pn-Po	group 1	37.00	142.92	2588.93	43.30	19.67	<0.04	2791	78	9.56	0.35	<0.11	0.29	0.88	<0.98	<0.9	2.71	0.47	0.35	0.24	0.10	0.39	1.36
LR80(3)m3L1 all	LR80(3)	Pn-Cp	group 1	35.50	110.87	3201.95	42.17	9.63	8.20	1282	956	<8	0.32	<0.11	<0.2	4.41	<0.98	<0.9	6.36	0.82	0.22	0.32	0.05	0.33	1.29
LR80(3) line 3	LR80(3) block	Po-Pn	group 1	35.00	138.15	2533.50	49.37	14.00	0.07	1935	1160	<8	<0.09	<0.11	<0.2	5.19	<0.9	<0.9	6.62	0.38	<0.03	0.11	0.99	0.27	1.05
LR80(3) line 4	LR80(3) block	Pn-Po	group 1	35.50	124.78	2845.07	48.21	15.36	<0.04	2208	525	<8	<0.09	<0.11	0.25	1.85	<0.9	<0.9	7.72	0.85	<0.03	<0.02	<0.02	0.20	1.67
LR80(4) line 1	LR80(4) block	Pn-Po	group 1	36.00	132.30	2721.09	41.22	20.85	<0.04	2849	1063	<8	0.14	0.13	1.86	5.52	<0.9	<0.9	4.12	0.15	0.11	0.04	0.71	0.28	2.71
LR80(4) line 2	LR80(4) block	Po-Pn	group 1	36.00	133.47	2697.23	50.42	12.23	1.14	2913	511	<8	0.59	<0.11	<0.2	2.12	3.82	<0.9	3.39	0.62	0.67	0.25	0.21	0.69	1.83
LR80(4) line 2 Po-Pn-Cp	LR80(4) block	Cp-Pn	group 1	35.50	119.59	2968.59	43.25	9.15	11.38	1635	2175	<8	0.51	<0.11	<0.2	4.64	15.61	<0.9	4.80	0.51	0.10	0.38	0.21	2.19	0.53
LR80(4) line 3	LR80(4) block	Po-Pn	group 1	36.00	131.78	2731.87	50.87	13.03	0.18	2697	1872	<8	1.04	0.11	0.36	8.19	9.13	<0.9	6.11	0.17	0.17	0.54	0.28	1.14	2.96
LR80(4) line 4	LR80(4) block	Pn-Po	group 1	36.00	100.40	3585.66	43.67	15.76	0.10	2432	1894	<8	<0.09	<0.11	<0.2	1.67	<0.9	<0.9	3.81	0.32	<0.03	<0.02	<0.02	0.10	1.63
LR80(4) line 5	LR80(4) block	Pn-Po	group 1	36.00	101.60	3543.31	38.95	18.90	1.70	2734	1087	<8	0.09	<0.11	0.57	3.01	<0.9	<0.9	6.29	0.26	<0.03	<0.02	0.32	0.17	1.64
LR80(4) line 6	LR80(4) block	Pn-Po	group 1	36.00	133.70	2692.60	43.97	17.38	<0.04	2386	1038	<8	1.51	<0.11	<0.2	0.42	<0.9	<0.9	2.72	0.53	0.30	0.38	0.03	0.14	2.47
LR80(5) line 2	LR80(5) block	Po-Pn	group 1	36.00	104.55	3443.33	46.47	14.22	1.55	1888	1008	<8	<0.09	<0.11	<0.2	2.62	<0.9	<0.9	4.58	0.45	<0.03	<0.02	0.09	0.09	1.13
LR84 m1s1	LR84 (clinopyroxenite)	Pn-Po	n/a	39.03	26.33	14822.48	44.05	15.38	0.87	2024	82	<7	<0.13	<0.16	0.10	1.34	1.40	<0.8	<0.9	0.23	<0.03	<0.02	<0.03	0.17	0.89

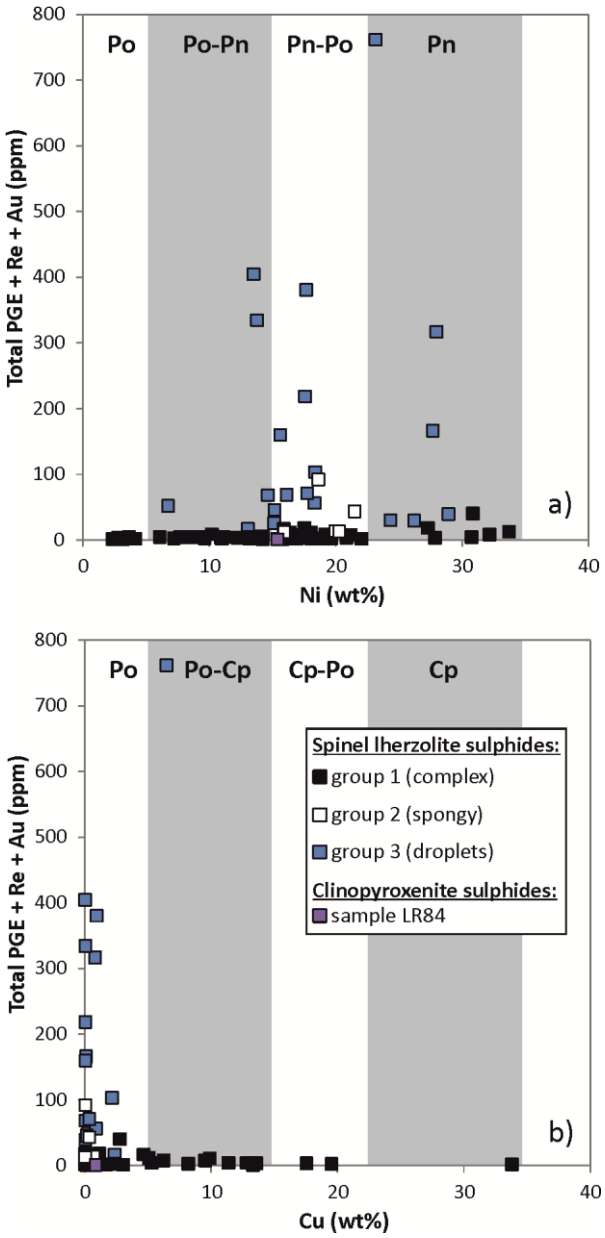

Figure 8.8. Total PGE + Au + Re vs. major elements, delineating end member base metal sulphide components for mixed LA-ICP-MS spectra (a) Ni and (b) Cu. Sulphide data are also distinguished by texture – i.e., Group 1 (complex), Group 2 (spongy) and Group 3 (droplet). See main text for further details.

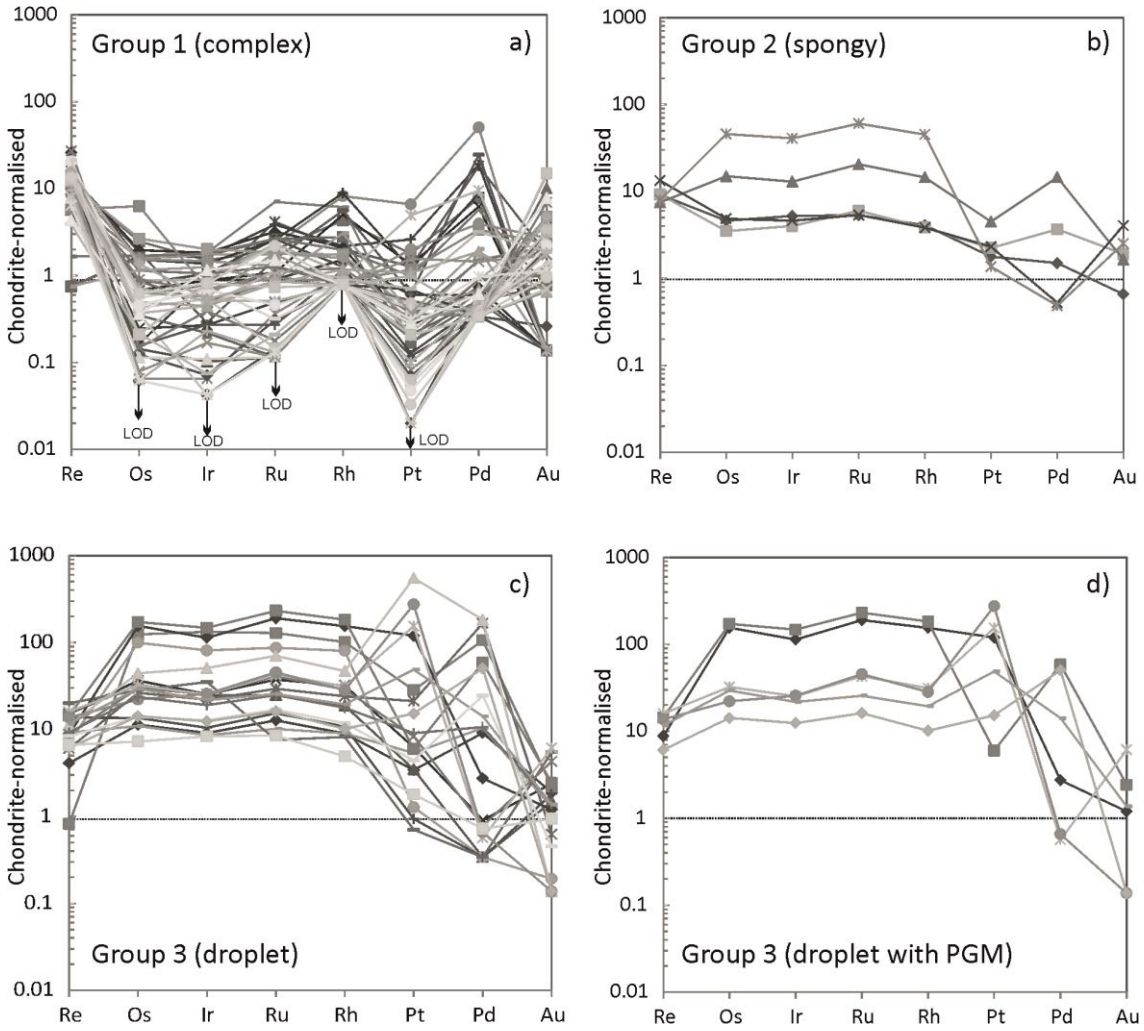

Figure 8.9. Chondrite-normalised Re, PGE and Au multi-element diagrams, per sulphide group. (a) Group 1 (complex), (b) Group 2 (spongy), (c) Group 3 (droplet) and (d) Group 3 (droplet) with observed platinum-group minerals within the LA-ICP-MS analyses. Dashed line at 1 x chondrite (McDonough & Sun, 1995).

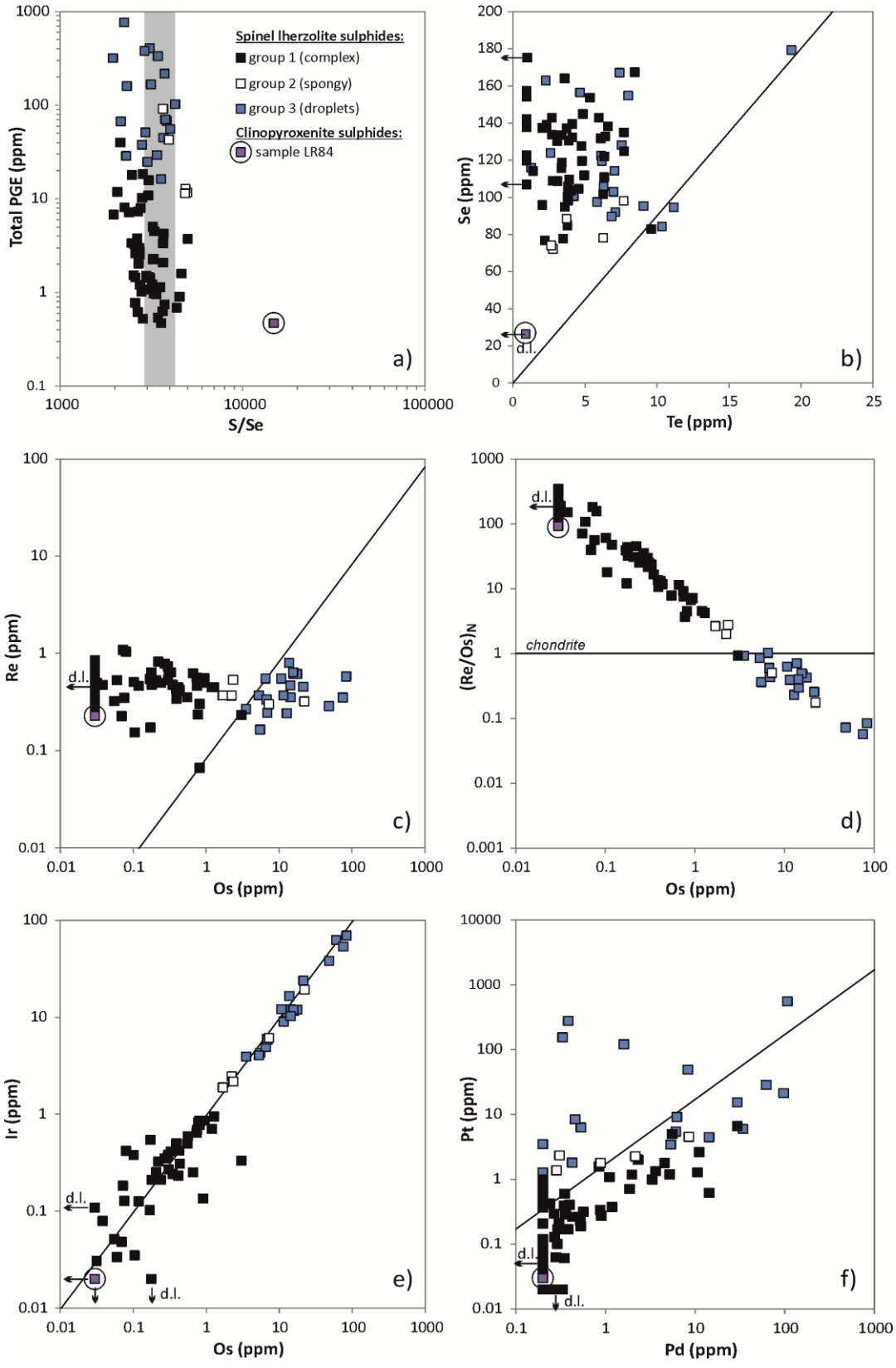

Figure 8.10. Bivariant sulphide trace element plots for (a) total PGE vs. S/Se ratio; (b) Se vs. Te; (c) Re vs. Os; (d) $(Re/Os)_N$ vs. Os where $(Re/Os)_N$ is chondrite-normalised (McDonough & Sun, 1995); (e) Ir vs. Os and (f) Pt vs. Pd.

8.4. Discussion

8.4.1. Sulphide populations in the subcontinental lithospheric mantle

Based on characteristic textural features (Figs. 8.6-8.7) and geochemistry (e.g., Fig. 8.9), three distinct populations of base metal sulphides are recognised. Based on their petrographic setting (e.g., intergranular to olivine and pyroxenes vs. strict occurrences within feldspar-spinel symplectites – Fig. 8.5) we suggest that these record multiple sulphur-bearing magmatic and/or metasomatic events.

8.4.1.1. Group 3 sulphides ('droplets')

The morphology and comparative textural simplicity of Group 3 sulphides, resembling 'droplets', implies these are analogous to sulphide liquid globules which cooled and became frozen into their symplectite hosts. In an ideal high-temperature magmatic environment, molten immiscible sulphide liquids will cool and fractionate PGE through several stages involving Fe-rich monosulphide solid solution (MSS) and Cu-rich intermediate solid solution (ISS) sulphide products along with PGM (see Holwell & McDonald, 2010 and references therein).

The Group 3 droplets display internal textural features resembling those expected from sulphide liquids which have cooled and differentiated through MSS and ISS stages. Group 3 sulphides have very high total PGE abundances (up to ~ 1000 ppm) and Pt occurs at sufficient concentration to have saturated and formed PtS (cooperite) as a discrete mineral phase (Fig. 8.7c-d). The concentration and chondrite normalised profiles (Fig. 8.9c-d) resemble that of sulphide inclusions found in Siberian diamonds by Bulanova *et al.* (1996), but without the obvious Pt and Pd depletion relative to Os, Ir and Ru found in the latter.

The restricted occurrence of Group 3 sulphides within spinel-feldspar symplectites also provides indirect information about the timing of their formation. Symplectites are observed throughout Loch Roag spinel lherzolite xenoliths (Hunter & Upton, 1987) including at the unaltered cores, and are not restricted to xenolith margins. This excludes the possibility that symplectites were formed directly from the monchiquite dyke during xenolith entrainment and instead represent reaction zones of eutectic melts, and by inference, that the Group 3 sulphides formed in relation to these eutectic zones. Currently, it is not possible to demonstrate whether the symplectites are interlinked throughout a single xenolith, however the occurrence of very finely crystalline anorthoclase feldspars of similar composition to those in the symplectites, along spinel-clinopyroxene, olivine-olivine and olivine-clinopyroxene

contacts (Hunter & Upton, 1987) suggests that an interconnected network existed. Therefore symplectites (and associated feldspar networks) could represent frozen-in melt infiltration within the Scottish lithospheric mantle keel, and hence a geochemically open system which allowed co-migration of sulphide liquid from an external source.

8.4.1.2. Group 2 sulphides ('spongy')

Group 2 sulphides are the least common of the three sulphide populations and are characterised by distinctive and abundant rounded $CaCO_3$ and polygonal serpentinised (silicate) inclusions (e.g., Fig. 8.6c-d), but geochemically these are most similar to Group 3 ('droplet') sulphides (e.g., chondrite-normalised Re-PGE-Au patterns, Fig. 8.9c-c). The petrographic setting of this Group is also similar to Group 3 (neighbouring spinel-feldspar symplectites, or along feldspar-bearing interstitial 'networks'). Regarding the silicate-carbonate inclusions within Group 2 sulphides, we are aware of only one other similar sulphide-carbonate association where carbonates occur as inclusions within the sulphides of mantle xenoliths from the Canary Islands (Kogarko *et al.,* 1995). During their study, Kogarko *et al.* (1995) envisaged a three-component immiscibilty system between silicate, carbonate and sulphide liquids. A sulphide-carbonate association has also been found in Kerguelen mantle xenoliths, but in this case the sulphides and carbonates occur together as pockets interstitial to silicate crystals, and not as carbonate inclusions in the sulphides themselves (Lorand *et al.,* 2004; Moine *et al.,* 2004; Delpech *et al.,* 2012). On a smaller scale, melt and fluid inclusions of coexisting silica-rich glasses, solidified sulphide melt and carbonate (mostly present as CO_2 fluid inclusions as well as carbonate-bearing inclusions) trapped in individual olivine and pyroxene crystals of mantle xenoliths (Andersen & Neumann, 2001) provides further evidence of silicate-sulphide-carbonatite immiscibility in the upper mantle. The formation and preservation of such three-way (silicate-carbonate-sulphide) immiscibility is probably a sensitive process and rarely preserved.

Carbonatites have been documented in association with various magmatic and geodynamic regimes, including continental rifting and mantle plumes (e.g., Ernst & Buchan, 2003 and references therein), and frequently these are referred to as causes for cryptic and modal metasomatism of silicate minerals in the upper mantle (Green & Wallace, 1988; Sweeney, 1994). Indeed, isotopic studies (e.g., Long *et al.,* 1991) and trace element geochemistry of silicate mineral phases such as clinopyroxene (e.g., Hughes *et al.,* in press – Chapter 7) have already provided evidence for interaction between the Hebridean SCLM and carbonatitic melts/fluids, as well as in other mantle xenolith suites elsewhere in northern Scotland (e.g.,

Streap Com'laidh and Rinibar; Bonadiman *et al.,* 2008). Given their constraint within eutectic symplectite pockets or the associated feldspathic interstitial network, we suggest that Group 2 and/or 3 sulphides represent the youngest S-bearing event to be recorded in this region of the Scottish lithospheric mantle, post-dating the coarser complex sulphide grains of Group 1 that are interstitial to protogranular or granoblastic silicate minerals.

If Group 2 and 3 sulphides are linked in some way, the geochemical and textural observations are most consistent with Group 3 sulphides having formed following the re-melting and homogenisation of Group 2, with the loss of carbonate and silicate intrusions, partial loss of S and Re, but preservation of the other PGE and Se due to their higher $D_{sulphide/silicate}$ partition coefficients (e.g. Peach *et al.*, 1990; Mungall and Brenan 2014). During this process, PGE concentrations increased in the new re-melted sulphide liquid, enough to form discrete PtS PGM (cooperite). This was coupled with a general decrease in both the S/Se and Re/Os ratios. Re-melting allowed for re-homogenisation of the sulphide liquid, forming the rounded globule or droplet shapes so characteristic to Group 3. The cause for this re-melting event is probably linked to the formation of the feldspar-spinel symplectites. The precise timing of the formation of these features and Group 3 sulphides remains poorly constrained. They might relate to the elevated temperatures associated with the impingement of the proto-Icelandic plume at the base of the lithosphere during the Palaeogene or to an earlier event that (at least partially) survived Palaeogene magmatism (potentially Palaeoproterozoic, Caledonian or Permo-Carboniferous in age, given the magmatic history of this part of Scotland).

8.4.1.3. Group 1 sulphides ('complex')

If PGE concentrations in molten sulphide liquid are very low, all PGE will remain in solid solution within the cooling sulphide liquid. PGM have not been observed (either during SEM studies or LA-ICP-MS analyses) in Group 1 (complex) sulphides and the total concentration of PGE for this population is low in comparison the Group 2 and 3 sulphides (Fig. 8.10a). The complex internal structures and textures of Group 1 sulphides are unlikely to have formed by the simple cooling of sulphide liquid through MSS and ISS stages, and therefore either represent multiple periods of growth (i.e., the cumulative 'accretion' of sulphides) or subsolidus alteration fabrics. In the case of the former and absence of the latter, each generation of sulphide liquid would have to have had very low PGE concentrations and elevated Re/Os. Although this is possible, subsolidus mobilisation of precious metals from sulphides (as highly reactive nanoparticles) has recently been documented in mantle peridotites (Ferraris & Lorand, 2014). However observations of what the resulting textural

changes in the 'source' sulphides might be, remain to be reconciled. In fact, studies of textures and fabrics of sulphide minerals in upper mantle lithologies are rare in the published literature in comparison to geochemical investigations, with notable exceptions (e.g., Guo *et al.,* 1999; Bockrath *et al.,* 2004; Ballhaus *et al.,* 2006; Lorand *et al.,* 2010; Alard *et al.,* 2011; Delpech *et al.,* 2012; Warren & Shirey, 2012 and references therein; Lorand *et al.,* 2013). However even these latter studies emphasise either experimental results or deal with orogenic peridotites from continental massifs rather than SCLM sulphide textures.

Due to the high ambient temperatures and pressures in the lithospheric mantle, subsolidus alteration of sulphides will be a plastic effect, rather than brittle. Flow mechanisms in sulphide minerals and plastic deformation is outlined in Cox (1987), and for high-temperature settings this can broadly be summarised by three creep processes; solution-precipitation, grain-boundary diffusion, or lattice-diffusion creep (assuming a low stress or isotropic regime), in addition to grain-boundary sliding. The dominant process depends on the presence or absence of fluids, with lattice-diffusion creep being of particular importance in fluid-poor settings. This plastic deformation could well have been accompanied by changes in the trace element chemistry of base metal sulphides, especially if fluids were present, and this may promote diffusive exchange with neighbouring mineral phases such as silicates.

Recent discovery of Au-Pb-Sb nanoparticle alloys in strained margins of olivine grains in orogenic lherzolite massif bodies has shown that silicates may contain a significant portion of bulk metal budgets in this form (Ferraris & Lorand, 2014). The initial source of these metals is inferred to have been sulphides. Following initial MSS crystallisation (ca. 1000°C) Pt, Pd, and particularly Au concentrate in residual Cu-rich sulphide liquid, ISS (Peregoedova, 1998; Lorand & Alard, 2001) but once ISS crystallises to form chalcopyrite, Au is incompatible (Wilson *et al.,*1995; Godel *et al.,* 2007; Holwell & McDonald, 2007). In orogenic peridotites, it has been suggested that sulphides underwent subsolidus fluid-based alteration, mobilising Au (Lorand & Alard, 2011; Ferraris & Lorand, 2014). However the peridotites in which nanoparticles were discovered have only undergone mild serpentinisation, suggesting that the abundance of fluids required for Au mobilisation was actually quite low. In the same study, Pt was also noted in conjunction with some Au nanoparticle occurrences within localised strained volumes of olivine margins (Ferraris & Lorand, 2014) further hinting that PGE may also form various alloys on a nanometre scale, and hence be mobilised (physically or chemically). Thus, subsolidus (plastic) deformation of sulphide minerals at high temperatures and pressures ambient in the upper mantle, in conjunction with fluid and/or partial melt infiltration (i.e., metasomatism)

could mobilise precious metal budgets between sulphides and silicate grain boundaries in solution or as reactive nanoclusters (cf. Helmy *et al.,* 2013b).

8.4.2. Implications for bulk rock precious metal geochemistry

The chondrite-normalised whole-rock PGE and Au abundances of spinel lherzolites of Loch Roag have a slightly positive fractionation pattern from Os to Pt and Au. There is a small negative anomaly for Pd, but all other PGE abundances are elevated above primitive upper mantle estimates (e.g., McDonough & Sun, 1995; Palme & O'Neill, 2004). PGE abundances in the western Greenlandic NAC SCLM (Wittig *et al.,* 2010) as well as global examples of Archaean-Proterozoic peridotites predominantly show a variable depletion of Pt and Pd, in both garnet and spinel peridotites (Fig. 8.3d). Hence, based on the current literature, the whole-rock PGE concentrations of the Loch Roag spinel lherzolites are extremely unusual worldwide.

We can investigate the abundances of noble and chalcophile metals, such as the PGE and Cu, according to the effect of partial melting. Pt and Pd concentrations in Loch Roag are coupled with elevated Cu abundances such that Cu/Pd ratios are close to primitive mantle (Fig. 8.4b). Elevated Cu is not coincident with any Ni enrichment (Fig. 8.2d), confirming that Cu (and by inference Pd and the other PGE) is predominantly controlled by sulphide content, while olivine controls the whole-rock Ni signature. IPGE are thought to be mainly hosted by Fe-rich MSS and refractory metal alloys in the mantle (Brenan & Andrews, 2001; Sattari *et al.,* 2002; Bockrath *et al.,* 2004b; Maier *et al.,* 2012). By contrast, PPGE are thought to be predominantly hosted by Cu-rich sulphides (Sattari *et al.,* 2002; Bockrath *et al.,* 2004a). During mantle partial melting, interstitial Cu-rich sulphides are more prone to melting, potentially becoming entrained in the amassing silicate magma, and removing Pd and Pt from the residual mantle to leave a peridotitic restite depleted in these elements (e.g., Maier *et al.,* 2012). In the case of cratonic Pd- and Pt-depleted xenoliths, re-introduction of Pd by transient silicate melts and/or oxidizing fluids has previously been suggested (McInnes *et al.,* 1999; Pearson *et al.,* 2005; Lorand *et al.,* 2008). However the Loch Roag xenoliths demonstrate that PGE mobility and 'refertilisation' may not be restricted to a 'cryptic' process, and that geochemically distinctive Fe-Ni-Cu sulphide liquids can be introduced and crystallise into the SCLM in distinctive petrographic settings and with characteristic internal textural features.

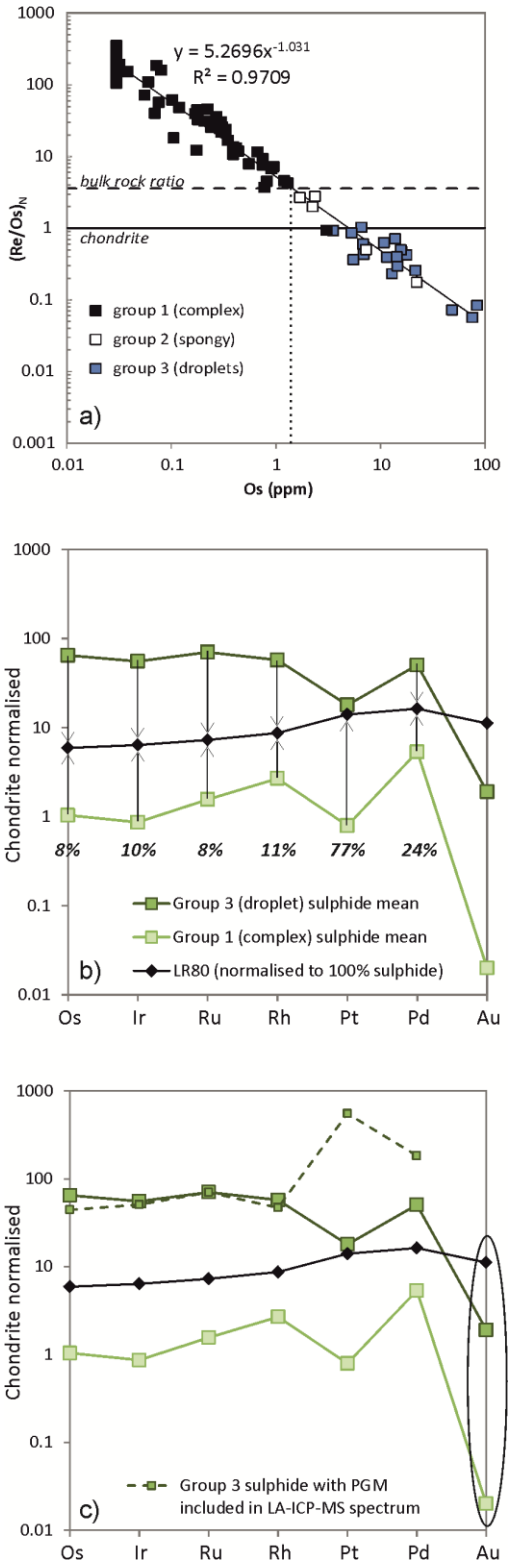

Figure 8.11. Mass balance calculations of bulk rock PGE abundances vs sulphide populations. (a) $(Re/Os)_N$ vs. Os for sulphide all three Loch Roag sulphide groups and bulk rock. (b) Bulk rock PGE multi-element diagram (chondrite normalised) recalculated to 100% sulphide vs. measured Group 1 and 3 sulphide compositions. Arrows show lever rule and percentages labelled refer to the percentage of Group 3 sulphides in the total sulphide population. (c) Chondrite normalised PGE diagram also showing measured LA-ICP-MS composition of a Group 3 sulphide with PGM. Ellipse highlights the relative depletion of Au from both sulphide populations, or the 'invisible' Au fraction. See text for discussion.

Our documentation of multiple sulphide populations within the Loch Roag spinel lherzolite xenolith suite, and especially the 3 populations observed within a single xenolith sample (e.g., LR80), demonstrates the highly complex and geochemically heterogeneous nature of BMS in the SCLM, particularly in a marginal cratonic setting. Given that the bulk PGE concentrations of a rock sample are largely controlled by the sulphide mineral fraction within it, the existence of multiple sulphide populations in a single xenolith or suite of xenoliths, with different precious metal compositions and susceptibilities to melting (based on their textural setting), reveal a level of complexity that has not been apparent previously. Sulphide populations in Loch Roag display a broad variation in PGE concentration on the scale of orders of magnitude between each group. Therefore it is vital that bulk rock precious metal geochemistry and Re-Os isotopic studies (if carried out on sulphide-bearing samples) is tallied back to detailed sulphide petrography before interpretation of bulk geochemical data.

In the absence of measured bulk rock S concentration, distinctive PGE ratios of sulphide minerals can be used to estimate the total abundance of 'sulphide' as a mineral phase in a whole-rock sample. Figure 8.11a shows $(Re/Os)_N$ vs. Os for the three sulphide groups identified in LR80, and a calculated regression through these data (excluding anomalously low $(Re/Os)_N$ data points which have probably undergone Re loss). Previously published results for Re and Os in a powdered bulk sample of LR80 are available in Hughes *et al.* (2014) – Chapter 6. Bulk Re and Os are 0.51 and 1.775 ppb respectively, and we convert this to $(Re/Os)_N$ of 3.56, as shown by the dashed line in Figure 8.11a. Using the equation which describes the sulphide composition trend between the three sulphide groups ($(Re/Os)_N = 5.2696\ Os^{-1.031}$) the Os concentration in a bulk sample normalised to 100 % sulphide is 1.46 ppm. The ratio between measured bulk rock Os abundance (1.775 ppb) and that of 100 % sulphide (1.46 ppm) needed to calculate the total abundance of sulphide in the xenolith (LR80) as 0.12 %. Note that this is calculated as a volume % sulphide mineral fraction, and not the percentage of S.

Recalculating the bulk rock fire assay result for LR80 to 100 % sulphide, assuming 0.12% sulphide abundance in the xenolith, the chondrite normalised PGE diagram of Figure 8.11b is plotted in context with sulphide compositions from Groups 1 and 3 (LA-ICP-MS data). By calculating the difference between the mean abundance of each PGE in Group 1 and Group 3 sulphides, and the difference between each PGE in Group 1 or 3 sulphides and the bulk rock (100 % sulphide normalised), a simple lever rule is used to calculate the relative abundances of each end member sulphide population (low-PGE Group 1 sulphides and high-PGE Group 3 sulphides) making up the bulk rock. For Os, Ir, Ru and Rh, we calculate that Group 3 sulphides

contribute 8-11 % of the total sulphide population (by mass) in LR80, in order to account for the bulk rock composition. This is broadly in line with optical estimations. However for Pt and Pd, Group 3 have apparently greater contributions to bulk rock (77 and 24 % respectively). This can be accounted for once we consider the input of PGM such as cooperite to bulk rock (e.g., Fig. 8.11c). None of our calculations based on sulphide compositions can account for bulk rock Au abundance (as highlighted in Fig. 8.11c), suggesting that the main host of Au is not sulphide minerals (of any group). This 'invisible' Au must instead be hosted by a non-sulphide mineral phase, possibly silicate(s) – an idea recently validated by the discovery of nanoinclusions of Au in strained olivine crystal margins (Ferraris & Lorand, 2014).

8.4.3. The complexity of sulphur in the SCLM – a record of S-bearing events as a 'box model'

General observations of how PGE and chalcophile elements partition between mantle minerals, particularly sulphides, and magma, have been validated by experimental data (e.g., Brenan & Andrews, 2001; Sattari *et al.,* 2002; Bockrath *et al.,* 2004a; Bockrath *et al.,* 2004b), but this oversimplifies the true level of complexity we observe in the SCLM. Multiple populations of base metal sulphides could have been formed by subsolidus plastic deformation, re-melting and/or whole-sale introduction of new sulphide liquids over a vast geologic timescale, as demonstrated by the Loch Roag spinel lherzolite xenolith suite. The lithospheric mantle, particularly its shallowest portion, is a region which magmas and fluids from the deeper mantle (including subducted material) pass through (or become trapped in) during ascent to the crust. However it is certain that the volume of mantle-derived magmas observed at crustal levels represents only a fraction of the total volume of magma within the magmatic plumbing system as a whole, and that the potential for melts becoming trapped and frozen in at deeper levels must be high.

The idea of a heterogeneous SCLM formed during multiple tectonic and magmatic events is well founded (e.g., O'Rielly *et al.,* 2001; Griffin *et al.,* 2003; Griffin *et al.,* 2008), however what this means for the complexities of sulphides, precious metals and metal 'fertility' of the lithospheric mantle is not well constrained (cf. Arndt, 2013). Further, it is likely that long-term magma ascent, melt interaction and metasomatism are predominantly confined along deep lineaments (e.g., Groves & Bierlein, 2007; Begg *et al.,* 2010 and references therein) possibly associated with strain fabrics identified by seismic anisotropy (e.g., Silver *et al.,* 2004; Sodoudi *et al.,* 2013; Youssof *et al.,* 2013). Regions along the margins of cratonic blocks will potentially

be the most prone to deformation and weakening, and hence act as natural pathways for ascending magmas and fluids (Begg *et al.,* 2010; Griffin *et al.,* 2013). Fracture networks developed offshore of southern Africa during the opening of the Atlantic, and rafts of metasomatised cratonic lithosphere (O'Rielly *et al.,* 2009) would appear to support this.

The Loch Roag mantle xenoliths occur at the Scottish margin of the North Atlantic Craton (NAC). This portion became separated from the rest of the NAC in Greenland during the Palaeogene and Eocene rifting and opening of the Atlantic Ocean, initiated by the impingement of the proto-Icelandic mantle plume and ultimately forming the North Atlantic Igneous Province. Prior to this, Caledonian subduction beneath the southwestern margin of the NAC culminated in a sequence of arc-related magmatic and hydrothermal episodes (see Strachan *et al.,* 2002 and references therein). Other magmatic events of note for this region of northern Scotland include Permo-Carboniferous rifting with associated magmatism, including the intrusion of a suite of lamprophyric dykes (see Upton *et al.,* 2004); Neoproterozoic rifting of the Iapetus Ocean at c. 600 Ma (see Trewin, 2002 and references therein); magmatism associated with the West Highland Granite Gneiss c. 870 Ma (Fowler *et al.,* 2013); Palaeoproterozoic orogenesis arc accretion and magmatism of the Laxfordian c. 1.67-1.90 Ga (cf. Goodenough *et al.,* 2013 and references therein, and van Gool *et al.,* 2002) equivalent to the Nagssotoqidian orogenic event in Greenland; and Palaeoproterozoic extension and rifting forming a large igneous province (c. 2.4 Ga; Davies & Heaman, 2014), now represented by the Scourie Dyke Swarm in the Lewisian Gneiss Complex. The Scourie Dykes have an unradiogenic Os-isotopic signature, and coupled with similarly unradiogenic bulk rock Re/Os data from the Loch Roag spinel lherzolite xenolith (LR80) Hughes *et al.* (2014; Chapter 6) suggested that the Scourie Dyke Os-isotopic signature was ultimately derived from melting of the SCLM. We corroborate this finding, however in the light of our new sulphide petrographic data (i.e., three populations of sulphides). If Group 2 and 3 sulphides predate the 2.4 Ga Scourie Dykes, then melting of such sulphides with their low Re/Os ratio and association with spinel-feldspar symplectites, provides a possible mechanism for imparting an unradiogeneic Os-isotopic signature requiring a small melt component. The Scourie Dyke bulk rock lithophile element geochemistry and modelling highlights a significant degree of partial melting of fertile SCLM (Hughes *et al.,* 2014 – Chapter 6) and we suggest that the incorporation of SCLM-derived PGE from readily fusible sulphides appears to be an important process coupled with this.

Overall, the lithospheric keel underlying the Lewisian (NAC) of Scotland has experienced a multitude of magmatic and metasomatic events, all or some of which may have modified the

'S-budget' of the SCLM. We conclude that the sulphide populations identified in the Loch Roag peridotite xenoliths record some of these events. Therefore the SCLM, and particularly its margins, can be likened to a box model with inputs and outputs of S, and correspondingly inputs and outputs of chalcophile precious metals. However this box model is complex with inputs and outputs not necessarily being synchronous with one another, nor with a requirement for there to be a 'balance' of sulphur budget. Sulphides can be added to the mantle keel throughout time, such that multiple populations of sulphide liquids (or minerals) corresponding to various S-bearing events can be observed in the SCLM over small spatial distances, and hence recorded in a single mantle xenolith. This provides an opportunity for geochemical 'mapping' of the SCLM as a way to understand both the 'fertility' of this upper mantle region for (chalcophile) precious metals, and to translate tectonic events below crustal levels.

A key observation regarding the sulphide input into the SCLM is that the Loch Roag spinel lherzolites are 'anhydrous'. Despite evidence of extensive metasomatism, either in a cryptic form for peridotite clinopyroxene (e.g., Hughes *et al.,* in press – Chapter 7), isotopically (e.g., Menzies *et al.,* 1987; Long *et al.,* 1991) or modal metasomatism such as is suggested by the presence of Ca-carbonate inclusions in Group 2 sulphides, the peridotite xenoliths themselves lack hydrous minerals (e.g., mica or amphibole). Xenocrysts of phlogopite and glimmerite xenoliths are both present in the Loch Roag host dyke. However these do not inform us about the hydration of the SCLM itself. It is important to highlight that Loch Roag spinel lherzolites are highly fusible but that this is in no way associated with hydration. Metasomatism is by definition a process associated with low-degree partial melts, and in the case of Loch Roag (and the margin of the NAC craton) metasomatism was both anhydrous and S-bearing.

Maier & Barnes (2004) and Maier & Groves (2011) have proposed that Pt-rich magmas may be derived (at least in part) from a metasomatised SCLM which has undergone enrichment in Pt. Further, they suggest that metasomatic Pt enrichment is a hydrous and fluid-rich process, possibly associated with subduction. Our study of the Loch Roag mantle xenolith sulphide minerals, and particularly cooperite-bearing Group 3 sulphides, clearly demonstrates that components of the SCLM at cratonic margins can be Pt enriched. However, this does not require a hydrous metasomatic process. Metasomatism has doubtless played a role in the geochemistry of these peridotites, however it was probably anhydrous and carbonatitic (forming Group 2 sulphides). This may therefore represent future opportunities to correlate chalcophile element metasomatic events with enrichment of other critical metals in the

lithospheric mantle (e.g., rare earth elements; REE). The process which led to formation of the spinel-feldspar symplectites (and hence Group 3 sulphides) remains unclear, however given the connectivity of these 'melt pockets' and lack of hydrous mineralogy, there is no requirement for it to have been caused by a fluid-rich process.

8.5. Conclusions

1. Detailed petrography reveals three populations of sulphide minerals co-existing within a single mantle spinel lherzolite xenolith (sample LR80). By a combined approach of sulphide morphology and texture, petrographic setting, and sulphide trace element composition we can distinguish between sulphide populations, and recognise some of these in other spinel lherzolite xenoliths of the Loch Roag suite.
2. Given their distinct petrographic setting (i.e., interstitial to silicate grain boundaries vs. within spinel-feldspar symplectite pockets) we can infer a relative chronology of sulphide groups (Groups 1 to 3) with differing and characteristic PGE and Re/Os systematics. The texturally oldest sulphides (Group 1) have the lowest total PGE abundances and highest $Re/Os)_N$ ratios, while the youngest (Group 3) sulphides have micron-scale PtS platinum-group minerals (cooperite) and the lowest $(Re/Os)_N$.
3. We recognise a distinct sulphide population (Group 2) with rounded $CaCO_3$ and polygonal serpentine-filled inclusions. In particular, the co-existence of sulphide and $CaCO_3$ suggests a S-bearing carbonatite event affected this region of the SCLM, and could represent an under-reported association of carbonatitic PGE enrichment, possibly coincident with other metasomatic geochemical features (e.g., REE enrichment).

Acknowledgements

Much of the material (xenolith and dyke) used throughout this study is from B.G.J. Upton's personal collection, now held at the British Geological Survey (BGS), Murchison House, Edinburgh. The BGS, particularly Michael Togher, is thanked for the curation, access and use of these samples. Anthony Oldroyd is thanked for his preparation of polished thin sections and Peter Fisher for his assistance and guidance at Cardiff University's SEM facility. This manuscript greatly benefitted from discussions with Ambre Luguet, Jude Coggan, Graham Pearson, Andrew Fagan, Sebastian Tappe, Nicholas Arndt and Tony Naldrett. H.S.R. Hughes is funded by the Natural Environment Research Council (NERC) studentship NE/J50029X. NERC are thanked for funding open access publication of this paper.

CHAPTER 9

Cobalt and precious metals in sulphides of peridotite xenoliths and inferences concerning their distribution according to geodynamic environment: A case study from the Scottish lithospheric mantle

Submitted as:

Hughes, H.S.R., McDonald, I., Faithfull, J.W., Upton, B.G.J. (under review). Cobalt and precious metals in sulphides of peridotite xenoliths and inferences concerning their distribution according to geodynamic environment: A case study from the Scottish lithospheric mantle. *Lithos.*

Co-author contributions:

I. McDonald, B.G.J. Upton and J.W. Faithfull were involved in discussions during the writing of this paper. B.G.J. Upton and J.W. Faithfull provided xenolith specimens for study. I. McDonald supervised bulk rock and LA-ICP-MS analyses.

Abstract

Studies of precious metal abundances in the lithospheric mantle typically involve bulk geochemical analysis. By contrast, the sulphide mineralogy, texture and composition of mantle xenoliths is relatively under-reported. Further, the abundance of critical metals such as cobalt (Co) is rarely documented. We assess the mineralogy, textures and trace element compositions of sulphides in spinel lherzolites from Scottish lithospheric terranes, which provides an ideal testing ground to examine the variability of sulphides according to terrane age and geodynamic environment. Specifically we test differences in sulphide composition from Archaean-Palaeoproterozoic cratonic sub-continental lithospheric mantle (SCLM) in northern terranes vs. Palaeozoic lithospheric mantle in southern terranes, as divided by the Great Glen Fault (GGF).

Cobalt is consistently elevated in sulphides from Palaeozoic terranes (south of the GGF) with Co concentrations > 2.9 wt.% and Co/Ni ratios > 0.048 (chondrite). In contrast, sulphides from Archaean cratonic terranes (north of the GGF) have low abundances of Co (< 3600 ppm) and low Co/Ni ratios (< 0.030). The causes for Co enrichment remain unclear, but we highlight similarities with ophiolitic Co mineralisation (e.g., Bou Azzer and Outokumpu) and Co-rich sulphides in peridotite-floored deposits at slow-spreading ridges. We also identify a distinction between Pt/Pd ratio across the GGF, such that sulphides in the cratonic SCLM have Pt/Pd ≥ chondrite (consistent with the observation of Pt-bearing PGM in these xenolith suites) while Palaeozoic sulphides have Pt/Pd < chondrite. Xenoliths from north of the GGF have 'pockets' of sulphide-carbonate and/or sulphide-phosphate immiscibility, inferred to record transient carbonatitic melts.

9.1. Introduction

The lithospheric mantle has variably undergone complex magmatic and metasomatic events, dependent upon the age, structure and transient geodynamic environment(s) recorded in any one region. The sub-continental lithospheric mantle (SCLM) as a source of metals has been studied for decades (e.g., Groves *et al.*, 1987; Groves & Bierlein, 2007 and references therein) but recent interest in how the SCLM relates to metals of strategic and economic importance has recommenced this discussion (e.g., Arndt, 2013). For example, platinum-group elements (PGE) and cobalt are designated 'critical metals' in various political reports, summarised by Gunn (2014). Many such metals have a strong affinity to sulphur, and hence the ability of the shallow mantle to store or release these elements is largely dependent on the nature of the sulphur budget.

Studies of the noble metal and chalcophile element composition of the lithospheric mantle (as sampled by mantle xenoliths in dykes and pipes) have focussed on bulk rock geochemistry and isotopic compositions (e.g., Re-Os) of xenoliths (see Lorand *et al.,* 2013 and references therein). Less consideration has been given to the mineralogical and petrographic setting of sulphides, their textural morphology and trace element composition, combined (e.g., Warren & Shirey, 2012 and references therein; Hughes *et al.,* under review, c – Chapter 8) and hence capacity to release critical metals under different melting regimes.

Cobalt has been surprisingly neglected in xenolith studies and other mantle investigations (cf. Pearson *et al.,* 2005). This may largely be because the bulk geochemistry of Co in xenoliths is predominantly controlled and buffered by high modal abundances of Co-bearing silicates, such as olivine, rather than low-abundance sulphide minerals. Hence bulk analysis may not be sensitive enough to identify mineralogical enrichments in precious metals. However, for the metallogenesis of a mantle region, and magmas derived from that region, the petrographic siting of sulphides and their composition (i.e., Co-rich or Co-poor) is a key control, and one that may be reflected in mineralisation at the surface (e.g., Hughes *et al.,* accepted, b – Chapter 10). Classification schemes for mantle-derived magmas have recently been constructed using the abundance and fractionation of Co (e.g., Hastie *et al.,* 2007, 2008). These are based on the strong partitioning of Co into olivine, and Co is thought to be immobile during alteration and weathering of lavas, as demonstrated by laterite profiles over ultramafic terranes (Hastie *et al.,* 2007 and references therein). However, Co exists with a suite of metals in hydrothermal mineralisation settings, for example at mid-ocean ridges (e.g., Von Damm, 2013) and ultramafic-hosted massive sulphides at slow-spreading ridges (Bogdanov *et al.,*

1997; Murphy & Meyer, 1998; Douville *et al.,* 2002). Co is also strongly compatible with respect to sulphides and has been shown to have similar sulphide solid/sulphide liquid partition coefficients as Ni so that there is no discernible fractionation between these elements during crystallisation of sulphide liquids or separation of liquid from residual sulphide under various P-T conditions (e.g., Li *et al.,* 1996; Ohtani *et al.,* 1997; Ballhaus *et al.,* 2001). However, the partition coefficients between sulphide liquid and silicate melt, for both Ni and Co, decrease with increasing pressure and temperature, and this effect is greater for Ni than Co (e.g., Ballhaus *et al.,* 2001, Li & Agee, 2001). Thus, when discussing the sulphide-bearing lithospheric mantle, sulphide minerals play a key role in controlling cobalt geochemistry. Despite this, Co abundances in sulphides are remarkably under-reported in the literature (with the notable exceptions of Aulbach *et al.,* 2004; Davies *et al.,* 2004 and Wang *et al.,* 2010).

In this study we present new whole-rock geochemical data on precious metals and chalcophile elements of mantle xenoliths from terranes north and south of the Great Glen Fault (GGF) in Scotland, together with sulphide mineral compositions (including Co). Sulphide textures and inter-relationships in the xenoliths are also described. Scotland is an ideal place to investigate variations in mantle xenoliths because previous work has demonstrated that the GGF is a significant lithospheric boundary (e.g., Menzies & Halliday, 1988; Canning *et al.,* 1996, 1998). The Scottish terranes record a range of geodynamic environments, from the margin of the Archaean North Atlantic Craton (north of the GGF) to collided Palaeozoic arcs and associated lithosphere (south of the GGF). Furthermore, Scotland as a whole has experienced several intra-plate rifting events. We consider the geochemistry of sulphide 'populations' (particularly for Co) in this geodynamic context.

9.1.1. An overview of Scottish geology

9.1.1.1. Scottish terranes

Scotland is divided into five tectonic terranes by major lithospheric lineaments (Fig. 9.1a). In the far NW of Scotland, and making up the basement of the two terranes north of the GGF (Hebridean and Northern Highland Terranes), the Archaean–Palaeoproterozoic Lewisian Gneiss Complex represents the British portion of the North Atlantic Craton (NAC). The Lewisian sector of the NAC consists of amalgamated Archaean domains with zones of Palaeoproterozoic reworking (broadly correlated to the Nagssugtoqidian orogenic belt of

Greenland) (Fig. 9.1b); (van Gool *et al.,* 2002; Kolb, 2014). In summary, the Lewisian Gneiss Complex can be divided according to the following major tectono-magmatic events: (a) magmatic protolith formation (including ultramafic-mafic bodies now preserved as pods within tonalite-trondhjemite-granodiorite (TTG) gneisses) at 3.0-2.8 Ga; (b) high-grade regional metamorphism followed by initiation of shear zones and associated metamorphism at 2.8-2.5 Ga. (c) Intrusion of mafic-ultramafic dykes (Scourie Dykes) ca. 2.4-2.3 Ga during a period of continental rifting and extension (Davies & Heaman, 2014); and lastly (d) ca. 2.0-1.8 Ga calc-alkaline magmatism and volcanic arc accretion, with formation of Laxfordian metamorphic belts and crustal anatexis (Kinny *et al.*, 2005; Park, 2005; Love *et al.,* 2010; Goodenough *et al.*, 2013; Hughes *et al.*, 2014 (Chapter 6); Crowley *et al.,* 2014).

The Lewisian is part of the basement of the Caledonian foreland bounded to the east by the Moine Thrust Zone (MTZ); a thin-skinned thrust zone which delineates the boundary between the Hebridean Terrane and the Northern Highland Terrane. The MTZ was formed by large-scale horizontal shortening of the crust in the early Silurian which had largely ceased by c. 429 Ma (Goodenough *et al.,* 2011). Archaean gneisses form the crustal basement of the Northern Highland Terrane (e.g., Moorhouse & Moorhouse, 1977; Friend *et al.,* 2008) and similarities between mantle xenolith suites from the Hebridean and Northern Highland Terranes suggest that Archaean lithospheric mantle also continues east beyond the MTZ (Hughes *et al.* in press – Chapter 7). Archaean gneisses are exposed as inliers within the Moine Supergroup: a thick Neoproterozoic sedimentary succession deposited c. 1000-870 Ma, during the Valhalla Orogen (Cawood *et al.,* 2010), that was later affected by the Knoydartian tectono-thermal event (c. 800 Ma – see Strachan *et al.,* 2002).

South of the GGF is the Grampian Terrane. Palaeoproterozoic gneisses (termed 'Rhinnian') are exposed between the GGF itself and a fault splay, the Loch Gruinart Fault (Fig. 9.1) on the Hebridean islands of Colonsay and Islay and the Northern Irish island of Inishtrahull; Marcantonio *et al.* (1988), Daly *et al.* (1991). Rhinnian gneisses form the basement to the late Proterozoic Dalradian super-group that outcrops over most of the Grampian Terrane and are inferred to extend from the Scottish west coast, eastwards for 600 km under the Grampian Terrane (e.g., Westbrook & Borradaile, 1978). Isotopic studies have established that the Rhinnian gneisses were derived from a depleted mantle source and represent comparatively juvenile crust with an age of c. 1.8 Ga. They are not considered to be a reworked or a southern extension of the NAC, but were instead part of an arc which underwent slab roll-back and extension before the break-up of Rodinia (Brown *et al.,* 2003 and references therein). Rhinnian

gneisses have been correlated with the Makkovikian-Ketilidian belt of Labrador and southern Greenland (bordering the NAC to the south, see Fig. 9.1b) – cf. Daly *et al.* (1991), Brown *et al.* (2003). We note that the discovery of deep crustal Rhinnian gneiss xenoliths at Gribun (Upton *et al.,* 1998) on the Isle of Mull (< 20 km north of the GGF) indicates a complexity in deep terrane boundaries (e.g., across the GGF).

Rifting of Rodinia in the late Proterozoic produced another mantle-sourced magmatic event (e.g., the Carn Chuinneag granite, c. 594 Ma; Oliver *et al.,* 2008). More widespread however, are the Late-Caledonian mixed diorite-granitoid, syenite and pyroxenite-syenite intrusions, characterised by high Ba-Sr content, which record extensive Ordovician and Silurian magmatism, particularly in the Northern Highland and Grampian Terranes (e.g., Fowler *et al.,* 2008 and references therein).

The southern margin of the Grampian Terrane is delineated by the Highland Boundary Fault (Fig. 9.1a). Although the southern limit of the Rhinnian basement of the Grampian Terrane cannot be demonstrated, it has been suggested that it is truncated by the Highland Boundary Fault (cf. Pidgeon & Aftalion, 1978). The Grampian event culminated in arc collision during which the Midland Valley Terrane became welded to the southern margin of the Grampian Terrane. The Southern Uplands Terrane is separated from the Midland Valley Terrane by the Southern Uplands Fault and the nature of the basement beneath it is still debated (see Oliver, 2002 and references therein). The Southern Uplands Terrane consists of a sequence of accretionary prisms (Leggett *et al.,* 1979) that may involve both fore-arc and back-arc components (e.g., Stone *et al.,* 1987). Mantle xenoliths from the Southern Uplands Terrane were not studied in the present investigation.

It is widely accepted that in the early Palaeogene, impingement of the Proto-Icelandic mantle plume on the overlying lithosphere led to widespread magmatism affecting all five Scottish terranes. The magmatism, commencing in the Paleocene at 63-62 Ma continued sporadically until 56-55 Ma, generating part of the North Atlantic Igneous Province (Saunders *et al.*, 1997). The tectono-magmatic activity ultimately led to the opening of the Atlantic Ocean and hence the fragmentation of the Archaean–Palaeoproterozoic North Atlantic Craton (Lewisian) and Palaeoproterozoic Makkovikian-Ketilidian-Rhinnian belt (Fig. 9.1b).

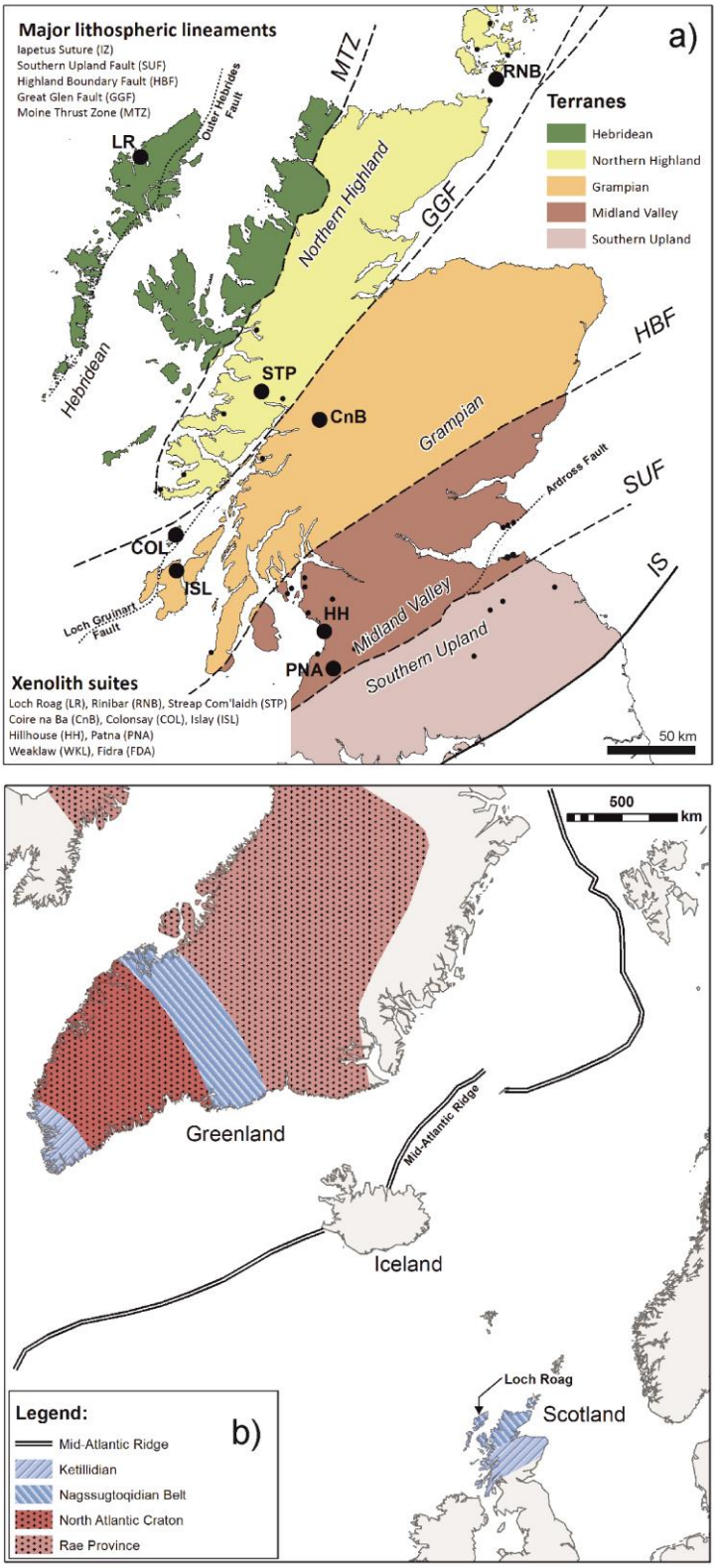

Figure 9.1. (a) Terrane map of Scotland, highlighting mantle xenolith localities (black dots). Suites used in this study are labelled accordingly: Loch Roag (LR), Streap Com'laidh (STP), Rinibar (RNB), Colonsay (COL), Islay (ISL), Coire na Ba (CnB), Hillhouse (HH) and Patna (PNA). These span four Terranes – the Hebridean Terrane, Northern Highland Terrane, Grampian Terrane and Midland Valley Terrane. (b) North Atlantic Craton and neighbouring orogenic belts in Greenland and Scotland, fragmented during the opening of the Atlantic Ocean. Other areas are delineated by light grey shading.

9.1.1.2. Mantle xenoliths

Virtually all mantle and deep crustal xenoliths and xenocrysts in Scotland were carried within Carboniferous and Permian minor intrusions and diatremes. They were entrained in sub-silicic magmas during a period of lithospheric extension north of the Variscan orogenic belt when widespread magmatism occurred. This affected all five Scottish terranes to greater or lesser degrees. One exception is known, namely a small dyke in the Hebridean Terrane intruded in the mid-Eocene (47-46 Ma; Menzies *et al*. 1989; Faithfull *et al.,* 2012). The host magmas range from basanites to silica-deficient compositions that the British Geological Survey usually indicate as monchiquites. A general review of the xenolithic and megacryst-bearing localities was given by Upton *et al*., (1983) and Upton *et al.*, (2011).

The localities containing upper mantle xenoliths span all five Scottish tectonic terranes (Fig. 9.1a). The majority of mantle xenoliths are spinel lherzolites. Whilst most of the associated pyroxenites are considered to be deep crustal cumulates some are probably of sub-crustal derivation. A summary of the geology, geochemistry, petrology and alteration features of the studied mantle xenoliths is provided in Table 9.1.

9.2. Analytical techniques and methodology

The map in Figure 9.1a shows a selection of the xenolith localities included in this study. These include three localities to the north of the GGF; Loch Roag (LR), Streap Com'laidh (STP) and Rinibar (RNB), and four localities south of the GGF; Coire na Ba (CnC), Islay (ISL), Hillhouse (HH) and Patna (PNA). Additionally, we have included two xenolith suites from two different monchiquite dykes on the Isle of Colonsay (COL). Colonsay is regarded as a tectonic sliver within splays of the GGF and it is debatable to which terrane it ought to be ascribed (e.g., McAteer *et al.,* 2010). The three northern localities were selected for the comparative freshness of their peridotite xenoliths, some of which are large enough to be used for both whole-rock and mineral analysis. By comparison, for xenolith suites in western Scotland south of the GGF (included in this study), only samples from Patna and Hillhouse were large enough for bulk geochemistry. Peridotite xenoliths from Coire na Ba, Islay and Colonsay were used for mineralogical studies only. Many of the xenoliths south of the GGF have undergone carbonation, silicification and/or serpentinisation. All of the studied mantle xenoliths are spinel lherzolites.

Table 9.1. Overview table of xenolith suites used in this investigation.

Xenolith Suite	Terrane	Host dyke/sill	Thickness, strike/dip of host	Host dyke age	Xenoliths/Xenocryst suite	Mantle xenolith and xenocryst isotopic data	Peridotite texture(s) (Mercier & Nicolas, 1985)	Pervasive xenolith alternation/replacement (spinel lherzolites)	Melting textures in spinel lherzolites
Loch Roag	Hebridean	Monchiquite dyke	approx. 70cm wide, 075°/ subvertical	45.2 Ma (Ar/Ar dating, Faithfull et al., 2012)	Lower crustal and mantle xenoliths (peridotites, pyroxenites, glimmerites, granulites, anorthosite, gabbros, syenites). Megacrysts (corundum/sapphires, feldspars, apatite, phlogophite)	$^{143}Nd/^{144}Nd$ 0.5118-0.5124, $^{87}Sr/^{86}Sr$ 0.7048-0.7051 (Upton et al., 2011), $^{206}Pb/^{204}Pb$ 17.139-17.348, $^{208}Pb/^{204}Pb$ 36.911-37.570 (Menzies et al., 1987), $^{187}Re/^{188}Os$ 1.411, $^{187}Re/^{188}Os_{intial}$ 0.0703 (Hughes *et al.*, 2014)	Protogranular and porphyroclastic	No pervasive alteration. No alteration at xenolith 'cores' (low LOI/very minor serpentine). Xenolith rims (up to 1cm thick) have abundant Fe-oxides and baryte.	Hercynite-feldspar symplectites, with outer zone of finer crystalline olivine and clinopyroxene.
Rinibar	Northern Highland (NE)	Alkali basalt dyke	approx. 1m wide dyke, striking NE-SW	252 ± 10Ma (K/Ar age, Baxter & Mitchell, 1984)	Spinel lherzolites and pyroxenite megacrysts	$^{143}Nd/^{144}Nd$ 0.5124-0.5128, $^{87}Sr/^{86}Sr$ 0.7033-0.7038, $^{176}Hf/^{177}Hf$ 0.2828-0.2830 (CPX; Bonadiman et al., 2008). Fluid inclusions in olivine $^{3}He/^{4}He$ 2.84 ± 0.29, [^{4}He] 2.78 (Kirstein et al., 2004).	Protogranular and porphyroclastic	No pervasive alteration. Moderate serpeninitisation of olivine. Minor pockets of Ca-, Mg- and Fe-carbonate (interstitial to main silicate mineralogy of spinel lherzolite). Carbonate-filled vugs are small (< 300µm wide) and occur mostly at olivine triple junctions.	A 200-500µm wide zone along the xenolith margin lacks serpentinised fractures (which are otherwise abundant throughout the rest of the xenolith) - suggesting melting and reaction with the host monchiquite dyke. Olivine at the margin has recrystallised to olivine with a higher Si content than 'primary' olivine in the xenolith. 'Pockets' up to 500µm diameter and irregularly shaped occur throughout xenoliths (core and margin). These consist of clinopyroxene, plagioclase, minor ilmenite (all <50µm size crystals), skeletal chromite (<10µm) and granular apatite (generally <10µm).
Streap Com'laidh	Northern Highland (SW)	Monchiquite dyke	approx. 70cm, NE-SW trending/subvertical	c. 290Ma (Walker & Ross, 1954; Upton *et al.*, 2004)	Spinel lherzolites, websterites, pyroxenites, granulite-facies metagabbros and quartzo-feldspathic gneisses	$^{143}Nd/^{144}Nd$ 0.5121-0.5127, $^{87}Sr/^{86}Sr$ 0.7065-0.7083, $^{176}Hf/^{177}Hf$ 0.2825-0.2831 (Bonadiman et al., 2008). Fluid inclusions in olivine $^{3}He/^{4}He$ 6.01-6.33, [^{4}He] 9.26-63.3 (Kirstein *et al.*, 2004).	Protogranular and porphyroclastic	None (low LOI/very minor serpentine). No pervasive alteration. However localised green and brown-coloured veinlets cross-cut some xenoliths (although timing of each set of veinlets is not clear). Green veins contain chlorite, baryte, calcite, clinopyroxene and plagioclase. Brown veins contain clinopyroxene, Ti-Fe-Mn oxide minerals and apatite.	Spinel-hercynite (mm-scale) is partially recrystallisation to higher Cr content (sometimes true chromite) dispersed granular crystals (< 20µm). The spinel-chromite reaction rim is associated with plagioclase, minor grains of Fe-Ti(+/-Mn) oxides and some chlorite. Clinopyroxene can be observed with a high-Ca reaction rim in some xenoliths. In detail, clinopyroxene reaction rims consist of discrete granular crystals of higher-Ca clinopyroxene. 400µm wide zone of xenolith melting at margins with host dyke. In immediate contact with the dyke is a dendritic zone of clinopyroxene intergrown with serpentine. Inward of this is a wider zone of fine granular and intergrown clinopyroxene and orthopyroxene (with chlorite) along with spinel-hercynite which has partially melted and disaggregated to chromite.
Colonsay	Grampian (at boundary with Northern Highland)	Two monchiquite dykes	no data available	Permo-Carboniferous(?) but not dated	Altered spinel lherzolites (in two separate dyke suites; 'CRB' and 'COD')	no data available	Generally protogranular (sometimes pervasively replaced)	Chlorite replacing highly/fully serpentinised olivine along crystal boundaries.	Minor disaggregation at margins of clinopyroxene.
Islay	Grampian	Monchiquite dyke	no data available	Permo-Carboniferous(?) but not dated	Altered spinel lherzolites	no data available	Generally protogranular (sometimes pervasively replaced)	Complex and variable Ca- and Mg-carbonate and quartz replacement textures (i.e., pervasive alteration is present).	Spinel crystals can have extensive reaction rims to chromite. Clinopyroxene crystals sometimes preserve a reaction rim of skeletal or dentritic low-Cr clinopyroxene intergrown with plagioclase (albite). Dendrites (in a zone approximately 100µm wide) abutt a rounded zone (approximately 300µm wide) of graphic melting between fine (< 25µm) orthopyroxene and clinopyroxene.
Coire na Ba	Grampian	Monchiquite dyke	no data available	Permo-Carboniferous(?) but not dated	Altered spinel lherzolites	no data available	Generally protogranular (sometimes pervasively replaced)	Complex serpentine (and chlorite) - quartz replacement textures (i.e., pervasive alteration is present).	Melt pockets of finely crystalline (10-30µm) symplectites of clinopyroxene and olivine, surrounded by coarse un-melted silicates (mostly olivine and orthopyroxene). Melting has been restricted to clinopyroxene-olivine contact zones. Minor partially recrystallised higher-Cr rims to spinel crystals also noted.
Hillhouse	Midland Valley	Olivine dolerite sill	> 20m thick	Permo-Carboniferous (but not dated)	Fresh spinel lherzolites (only)	no data available	Generally protogranular	Very minor serpentine. No pervasive alteration.	n/a (pervasive carbonate and quartz alteration does not show evidence of relic melting textures). Rare relic olivine and clinopyroxene, some spinel.
Patna	Midland Valley	Volcanic breccia (contacts not seen)	> 100m, unknown strike / assumed vertical	Permian(?) but not dated	Altered spinel lherzolites	no data available	Protogranular (pervasively replaced)	Pervasively replaced by Ca-carbonate (zoned in Mn and Fe) and quartz, with relict orthopyroxene now mostly replaced by serpentine. Replacement minerals have preserved the original protogranular texture of the xenolith silicate mineralogy.	

9.2.1. Whole-rock sample preparation and analysis

Samples were provided by the British Geological Survey and the Hunterian Museum, University of Glasgow. For whole-rock analyses this included seven separate xenoliths of approximately 3-6 cm diameter from Loch Roag (see Hughes *et al.,* under review, c, for full details – Chapter 8), two larger angular xenoliths (10-20 cm) from Rinibar, five large xenoliths (ranging 10-15 cm diameter) from Streap Com'laidh, three carbonated xenoliths from Patna (ranging 5-15 cm diameter) and four fresh xenoliths from Hillhouse (2-5 cm). Only xenoliths large enough for powdering were selected for whole-rock analysis but where material was limited, powdered samples weighed at least 25 g (typically 80-150 g for larger xenolith samples). The dykes hosting the xenoliths were also sampled for whole-rock analysis in order to compare their compositions with those of the xenoliths, and to assess whether dyke material remained during xenolith sample preparation.

Major and trace elements were analysed by inductively coupled plasma optical emission spectrometry (ICP-OES) and inductively coupled plasma mass spectrometry (ICP-MS), (see McDonald & Viljoen, 2006). Samples were analysed for PGE and Au by Ni sulphide fire assay followed by tellurium co-precipitation and ICP-MS (Huber *et al.,* 2001; McDonald & Viljoen, 2006). Fire assay samples included multiple blanks and duplicate samples per assay batch, to assess any procedural contamination and nugget effect for smaller samples. Accuracy was constrained by analysis of certified reference materials TDB1, WMG1, WPR1 and WITS1 (for PGE + Au fire assay) and JB1a, NIM-P and NIM-N (for all other major and trace elements) – see Supplementary Material, Tables A and B (on disk). Precision was estimated by repeat analysis of a sub-set of samples (see Supplementary Material, Table C – on disk). Whole-rock analyses are presented in Table 9.1.

9.2.2. Petrography and mineral chemistry analysis

Xenolith textures were studied on polished thin sections and polished blocks. Further examination, mapping and quantitative microanalysis was carried out on a Cambridge Instruments S360 scanning election microscope (SEM) at Cardiff University. Quantitative microanalyses were obtained using an Oxford Instruments INCA Energy EDX analyser attached to the SEM, with operating conditions set at 20kV and specimen calibration current of ~2 nA at a fixed working distance of 25 mm. Analytical drift checks were carried out every 2 hours using

the Co reference standard and a comprehensive suite of standards from MicroAnalysis Consultants Ltd were used to calibrate the EDX analyser.

Polished thin sections, and some corresponding polished blocks for samples requiring sulphide trace element analysis were selected for laser ablation ICP-MS (LA-ICP-MS). LA-ICP-MS was performed on sulphide minerals at Cardiff University using a New Wave Research UP213 UV laser system attached to a Thermo X Series ICP-MS. Analytical procedures and standards followed those of Prichard *et al.* (2013) and Smith *et al.* (2014). Both line and spot analyses were used and independently calibrated, depending on the size of the sulphides. For lines, a minimum line length of ~80 µm and a beam diameter of 15 µm was used, with laser operating conditions of 10 Hz frequency, ~ 5 Jcm^{-2} energy and sample translation at 6µm sec^{-1}. For spot analysis, beam size was 40 µm and the same laser operating conditions were employed. Individual sulphide minerals (or mineral clusters) < 80 µm across were analysed by spot analysis. Acquisition times ranged from 40 to 180s with a gas blank measured for 30-40 s prior to laser ablation. Major element concentrations were measured prior to LA-ICP-MS on the SEM, and ^{57}Fe was used as an internal standard for trace element calibration. Gas blank subtraction and internal standard corrections were carried out on Thermo Plasmalab software. Further procedural details are available in Smith *et al.* (2014). The PGE procedure for LA-ICP-MS was checked by analysis of the standard, Laflamme-Po724 as an unknown against the Cardiff quenched sulphide standards (see Supplementary Material on disk). A representative selection of time resolved analysis spectra (TRA) for sulphide minerals analysed are presented in the Appendix C.

9.3. Results

9.3.1. Xenolith preservation and alteration

The overall texture of xenoliths (e.g., protogranular and porphyroclastic) are summarised in Table 9.1. Xenoliths from suites north of the GGF generally retain their primary silicate mineralogy (olivine, orthopyroxene, clinopyroxene and spinel). In some cases alteration around the margins of xenoliths (restricted to the outermost 5-10 mm) is recorded as overprinting by baryte and Fe-oxides (e.g., Loch Roag – Table 9.1). Xenoliths from Rinibar are moderately serpentinised, as reflected in their elevated LOI (Table 9.2). Despite fracturing, primary silicate chemistry is preserved (see Upton *et al.,* 2011 and references therein). Olivine is partially replaced by serpentine. Small 'pockets' (< 300 µm wide) of Ca-, Mg- and Fe-

carbonates occur interstitially to the primary silicates and can contain sulphide minerals (see Section 3.3).

The xenoliths from south of the GGF are typically altered such that little fresh olivine and/or orthopyroxene remains (see Table 9.1 for details). However, the alteration products are not consistent from one suite to another. For example, while carbonate replacement is commonplace in the Patna and Islay xenoliths, this varies from Ca-carbonate (zoned in Mn and Fe) at Patna, to both Ca- and Mg-carbonates in Islay xenoliths. Quartz replacement is present in some of the Patna, Islay and Colonsay xenoliths, and can be coupled with carbonate and/or serpentine replacement also. The original mineralogy of peridotite xenoliths is locally preserved as patches of some silicates that have been resistant to replacement (for example relic olivine in Colonsay xenoliths). In most cases, pervasive alteration has nonetheless retained patches of the original silicate mineral textures of the peridotites allowing petrography, particularly of interstitial sulphides, to be discerned. We highlight that this pervasive alteration in xenoliths from south of the GGF is distinct from carbonate found in xenoliths from north of the GGF (e.g., Rinibar) in which primary peridotitic mineralogy is retained and the carbonates are strictly as small, rare interstitial melt 'pockets'. Hillhouse xenoliths are the exception, as these are fresh peridotites with unaltered silicate mineralogy (except for very minor serpentinisation of olivine) and lack pervasive alteration of the type(s) described above. The textural relationships of sulphide minerals are outlined in Section 3.3 and Supplementary Table D (on disk).

9.3.2. Whole-rock element abundances

9.3.2.1. Major elements and Ni, Cu and Co

Cr/Al and Al/Si ratios are used as a proxy for the degree of depletion in Figure 9.2a. Mantle xenoliths (harzburgites, lherzolites and wehrlites) from the North Atlantic Craton (NAC) in west Greenland have low Al/Si and extremely variable Cr/Al (Wittig *et al.,* 2010) relative to 'Primitive Upper Mantle' (PUM; McDonough & Sun, 1995). Loch Roag and RInibar xenoliths overlap these compositions – although harzburgites are absent. By comparison, the Streap Com'laidh and Hillhouse xenoliths more closely resemble the PUM. Due to the extensive carbonation of Patna xenoliths, these could not be plotted in Figure 9.2a.

Anhydrous Cu and Ni concentrations are plotted versus MgO (anhydrous) as a proxy for depletion (Figs. 9.2b-c). This highlights a significant enrichment in Cu for all the Scottish

xenoliths (Fig. 9.2b). In particular, the Patna xenoliths have extremely elevated Cu but this is in part an artefact of the anhydrous correction (which is particularly high for these xenoliths due to the abundance of carbonate, also manifest in the very low MgO). 'Raw' (i.e., not LOI corrected) maximum Cu abundance is 253 ppm (see Table 9.2) and hence, Cu abundance in Patna is within range of the other (fresh and not pervasively altered) Scottish xenoliths from north of the GGF. Ni and Co content of Loch Roag, Rinibar, Streap Com'laidh and Hillhouse xenoliths (Fig. 9.2c-d) is within range of the Greenland NAC xenoliths and PUM. The Patna xenoliths (for reasons pertaining to the anhydrous correction) appear to have lower Ni contents. However, for 'raw' Co abundances, the Patna xenoliths are notably enriched and have Co/Ni ratio > 0.1, unlike other xenoliths which have Co/Ni < 0.1 (see Table 9.2) and this enrichment cannot be ascribed to carbonation or to the anhydrous (LOI-based) correction.

9.3.2.2. Platinum-group elements and gold

All the xenoliths are enriched by several orders of magnitude above the composition of their dyke hosts, and fractionation between Ir-group platinum-group elements (IPGE) and Pd-group PGE (PPGE) is notably different, confirming that PGE contamination from the host magmas was insignificant (Fig. 9.3a).

Broadly, the chondrite-normalised (IPGE) incompatible element patterns for the spinel lherzolite xenoliths form a cluster from ~0.002 to 0.01 x chondrite and have flat patterns (Fig. 9.3a). With the exception of one Streap Com'laidh xenolith, the IPGE abundances from north of the GGF are tightly clustered in comparison to PPGE patterns (Fig. 9.3b). The Streap Com'laidh spinel lherzolites display systematic enrichment for Au and a slight negative anomaly for Pt. One of the Streap Com'laidh xenoliths has a PGE pattern with notably lower normalised abundances (displaced by one order of magnitude), although the PGE pattern itself is generally parallel to other Streap Com'laidh xenoliths. Duplicates show that this lower PGE abundance is a consistent feature of the xenolith sample. The Loch Roag xenoliths have elevated Pt in comparison to all other xenolith suites (Fig. 9.3b) whereas Pt is always slightly depleted relative to Rh and IPGE in the other xenolith suites.

A bivariant plot of Pt *vs*. Pd in the xenoliths is presented in Fig. 9.4a, in comparison with Greenlandic NAC xenoliths (Wittig *et al.,* 2010). Whole-rock Pt vs. Pd trends (Fig. 9.4a) for the Scottish xenoliths mainly fall along a linear trend (approximating chondritic ratios). Most of the Greenlandic NAC xenoliths have lower absolute Pt + Pd concentrations than PUM, with Pt/Pd ratios lower than chondrite. Since no published data for the concentration of Au in the

Greenlandic NAC xenoliths are available we compare the Scottish Au contents with those of southern African cratonic xenoliths (Maier *et al.,* 2012; Fig. 9.4b). Au and Cu in the fresh Scottish xenoliths (i.e., from north of the GGF) display a broad positive correlation, in contrast to the southern African xenoliths where the Au concentrations show no correlation with Cu. For the pervasively altered Patna xenoliths, there is no correlation between Cu and Au, although this is probably an artefact of the high anhydrous correction for Cu.

9.3.3. Sulphide petrography and mineralogy

Full details (mineralogy, textures and general petrography) of sulphide minerals in the Scottish peridotite xenoliths are given in Supplementary Table D (on disk). The majority of sulphides are interstitial to the silicates and consist of mixtures of base metal sulphides (pentlandite, pyrrhotite and chalcopyrite). A systematic scheme for categorising sulphide minerals (according to number of sulphide phases, morphology, textures, and replacements) has been adopted in order to ensure clarity and consistency. This scheme is broadly founded upon ore textures in Craig & Vaughan (1994) and describes terms laid out in Figure 9.5. Although the textural classification of sulphide minerals in Fig. 9.5 (and Supplementary Table D, on disk) is not exhaustive, it incorporates all textures encountered in the Scottish xenoliths.

Three populations of mixed base metal sulphides have previously been identified in the Loch Roag lherzolite xenoliths (according to texture, petrography and trace element composition; Hughes *et al.,* under review, c – Chapter 8). A detailed discussion of the petrography of the co-existing sulphide populations in the Loch Roag suite is given in Hughes *et al.* (under review, c – Chapter 8), which outlines the evidence used to establish the relative ages of each population or 'group'. The oldest group (Group 1) are coarse, and irregularly shaped with complex inter-relationships, interstitial to the silicates. Group 2 sulphides tend to be rounded and contain spherical inclusions of Ca-carbonate and polygonal inclusions of serpentine. The Group 2 sulphides are restricted to feldspar-bearing veinlets which extend from spinel-feldspar symplectites. What are inferred to be the youngest sulphides (Group 3) occur as rounded droplets bearing exsolved platinum-group minerals (PGM). These occur only within the spinel-feldspar symplectite pockets.

Table 9.2. *(continued overleaf)*

Sample number	Suite	Lithology	SiO_2	Al_2O_3	Fe_2O_3	MgO	CaO	Na_2O	K_2O	TiO_2	MnO	P_2O_5	LOI	Total	Mg#
Xenoliths:			*(wt.%)*												
LR81*	Loch Roag	Spinel lherzolite	45.34	2.40	10.12	35.78	2.54	0.46	0.54	0.03	0.16	0.15	3.25	100.78	0.89
LR101335*	Loch Roag	Spinel lherzolite	42.85	1.06	11.48	38.16	2.61	0.16	0.03	0.05	0.25	0.22	2.37	99.23	0.88
LR289*	Loch Roag	Spinel lherzolite	43.97	1.89	10.05	37.04	2.53	0.30	0.11	0.06	0.17	0.12	3.29	99.53	0.89
LR80*	Loch Roag	Spinel lherzolite	45.33	1.59	10.20	38.71	2.22	0.44	0.09	0.03	0.13	0.04	0.92	99.70	0.90
E19	Rinibar	Spinel lherzolite	42.34	1.46	7.86	32.90	2.30	0.21	0.07	0.07	0.11	0.07	11.92	99.30	0.91
G8R2xnl	Rinibar	Spinel lherzolite	42.03	2.37	8.59	34.01	3.81	0.28	0.07	0.16	0.15	0.02	7.73	99.22	0.91
2	Streap Com'laidh	Spinel lherzolite	45.77	3.16	9.11	36.82	2.77	0.26	0.03	0.14	0.12	0.01	1.61	99.81	0.91
5	Streap Com'laidh	Spinel lherzolite	47.56	3.37	8.96	34.44	3.46	0.29	0.01	0.15	0.12	0.02	1.20	99.58	0.90
4b	Streap Com'laidh	Spinel lherzolite	46.85	3.42	9.75	35.59	2.75	0.26	0.06	0.12	0.13	0.01	2.31	101.24	0.90
4a	Streap Com'laidh	Spinel lherzolite	43.96	3.11	9.84	37.12	2.71	0.21	0.04	0.12	0.13	0.02	2.61	99.87	0.90
4c	Streap Com'laidh	Spinel lherzolite	47.53	3.19	9.51	34.43	2.89	0.29	0.05	0.13	0.13	0.02	0.96	99.13	0.90
63	Patna	Spinel lherzolite	48.40	3.08	3.13	4.18	22.67	0.01	0.05	0.12	0.27	0.02	19.17	101.10	0.82
64	Patna	Spinel lherzolite	32.93	1.36	2.57	3.67	33.17	0.06	0.08	0.12	1.00	0.05	25.89	100.88	0.84
62	Patna	Spinel lherzolite	36.97	3.06	3.85	7.02	26.14	0.16	0.02	0.07	0.61	0.01	22.80	100.72	0.84
HHX1xnl	Hillhouse	Spinel lherzolite	44.84	3.30	8.13	37.00	2.97	0.34	0.16	0.13	0.13	0.02	2.32	99.33	0.92
HHX4xnl	Hillhouse	Spinel lherzolite	44.54	3.49	9.38	36.13	2.73	0.38	0.25	0.18	0.15	0.03	3.41	100.66	0.90
HHX2xnl	Hillhouse	Spinel lherzolite	42.58	3.77	8.99	36.52	2.02	0.26	0.16	0.15	0.14	0.02	4.38	99.00	0.91
HHX3xnl	Hillhouse	Spinel lherzolite	46.36	1.16	7.62	40.68	0.85	0.25	0.21	0.07	0.13	0.04	2.31	99.68	0.93
Host dykes:															
LRh	Loch Roag	Monchiquite	44.88	14.85	8.48	7.75	10.84	1.91	3.49	2.73	0.21	1.19	4.65	100.95	0.78
HHX4dyke	Hillhouse	Lamprophyre	45.10	14.60	12.17	11.30	10.37	2.57	1.01	1.87	0.20	0.31	1.81	101.31	0.72
HHX1dyke	Hillhouse	Lamprophyre	45.19	14.97	11.10	11.42	10.83	2.68	1.11	1.70	0.20	0.36	1.41	100.98	0.74
R2dyke	Rinibar	Lamprophyre	38.51	9.56	10.33	20.36	8.48	0.79	0.81	1.91	0.22	0.74	8.30	100.01	0.85
P1	Patna	Volcanic breccia plug	52.85	11.01	8.44	8.75	5.74	1.57	1.53	1.19	0.14	0.39	8.49	100.11	0.75

Table 9.2. *(continued overleaf)*

Sample number	Sc	V	Cr	Co	Ni	Cu	Rb	Sr	Y	Zr	Nb	Ba	La	Ce	Pr	Nd	Sm	Eu	Gd	Tb	Dy
Xenoliths:	*(ppm)*																				
LR81*	13.47	60.14	2910	107.4	1756	98.3	5.53	255.6	6.93	4.56	0.37	47.8	100.23	216.44	15.96	40.74	4.36	0.75	3.59	0.33	1.39
LR101335*	9.22	36.56	2599	130.0	2404	69.7	1.19	93.6	9.67	16.41	3.42	25.8	54.65	135.63	12.26	35.78	4.72	0.93	3.78	0.41	2.00
LR289*	11.65	48.21	3001	132.6	2022	97.0	2.73	250.5	9.42	6.53	0.98	37.6	87.14	213.27	20.02	53.41	6.47	1.12	4.80	0.47	2.11
LR80*	12.04	47.35	2456	103.1	2144	182.2	2.27	28.2	4.36	5.70	1.12	13.2	18.91	21.13	2.74	7.89	0.93	0.22	0.82	0.10	0.58
E19	10.00	44.30	2212	98.9	2040	66.8	2.76	148.1	2.24	4.85	3.16	63.9	10.45	17.57	2.00	6.90	1.06	0.27	0.82	0.09	0.41
G8R2xnl	11.24	55.04	2454	90.7	1663	26.9	2.63	209.1	3.47	30.96	5.70	78.1	10.09	15.73	1.68	5.87	1.02	0.32	0.95	0.13	0.65
2	14.74	56.54	2274	87.8	2038	41.4	0.96	26.1	3.22	5.35	1.83	8.3	0.50	1.07	0.16	0.84	0.27	0.11	0.32	0.07	0.48
5	13.48	69.38	3167	98.6	1882	136.6	0.85	45.8	3.67	6.58	1.43	2.7	1.06	2.32	0.31	1.38	0.39	0.13	0.39	0.07	0.55
4b	13.11	59.91	2399	95.3	2227	74.0	2.09	37.5	2.95	3.38	1.90	14.6	1.26	2.24	0.28	1.16	0.29	0.11	0.31	0.06	0.44
4a	13.38	57.88	2656	100.4	2380	57.8	1.36	101.5	3.01	5.12	2.18	9.4	1.31	2.41	0.30	1.29	0.33	0.11	0.35	0.06	0.46
4c	13.89	58.91	2531	96.1	2127	153.2	1.24	54.4	3.00	3.99	1.82	8.3	1.08	2.18	0.29	1.25	0.32	0.11	0.31	0.06	0.47
63	14.11	62.80	4443	149.5	840	253.1	1.45	205.2	7.76	35.26	3.16	28.0	29.81	50.59	5.89	22.37	3.72	0.94	2.92	0.33	1.35
64	15.01	55.51	5238	217.8	1164	175.0	2.28	381.2	6.88	21.82	3.73	82.0	22.14	40.62	4.57	16.37	2.14	0.61	1.97	0.22	1.01
62	19.02	82.72	4164	229.7	1258	93.4	0.47	210.2	6.90	5.66	1.48	11.0	13.71	29.76	4.05	16.20	2.10	0.51	1.87	0.21	0.98
HHX1xnl	13.01	63.41	2640	94.5	1774	25.3	6.64	19.2	2.78	6.26	1.25	26.4	0.64	1.53	0.21	0.90	0.29	0.10	0.33	0.06	0.42
HHX4xnl	11.52	60.98	2272	98.4	1775	95.7	7.32	33.8	3.42	11.35	1.71	35.6	1.45	3.33	0.45	2.00	0.49	0.16	0.52	0.09	0.55
HHX2xnl	10.74	56.51	2538	100.2	1783	42.7	3.76	15.9	2.26	4.83	0.47	13.8	0.34	1.08	0.17	0.86	0.26	0.09	0.28	0.05	0.39
HHX3xnl	6.88	32.59	2870	94.5	2001	15.6	6.37	88.3	2.15	10.96	2.49	61.3	5.91	11.15	1.34	4.82	0.85	0.23	0.64	0.08	0.42
Host dykes:																					
LRh	21.80	212.68	230	36.3	136	51.6	39.88	1797.0	28.03	346.82	100.76	2557.7	132.11	239.79	27.04	91.41	12.87	3.65	10.72	1.24	5.48
HHX4dyke	28.71	235.44	484	55.1	2644	182.0	28.75	438.7	20.91	102.83	28.00	460.1	18.46	38.86	5.07	21.33	4.52	1.51	4.58	0.72	3.72
HHX1dyke	28.11	235.10	469	53.9	258	68.8	31.01	449.7	21.37	120.45	29.74	440.6	19.20	39.82	5.27	21.58	4.65	1.49	4.64	0.70	3.68
R2dyke	21.83	185.39	944	58.9	568	75.0	34.73	392.9	22.23	120.21	72.80	648.8	52.00	92.65	10.90	40.14	7.32	2.18	6.79	0.90	4.27
P1	14.42	131.32	944	35.6	2766	49.2	38.83	283.8	21.37	206.14	39.65	560.5	33.30	63.79	7.82	28.81	5.36	1.51	4.99	0.74	3.67

Table 9.2. Bulk rock geochemistry for xenoliths and host dykes.
Totals are those from oxides with 4 decimal places, displayed to 2 decimal places.

Sample number	Ho	Er	Tm	Yb	Lu	Hf	Ta	Th	U	Os	Ir	Ru	Rh	Pt	Pd	Au	Total PGE+Au	Co/Ni
Xenoliths:										*(ppb)*								
LR81*	0.22	0.64	0.09	0.54	0.08	0.14	0.02	2.71	0.73	2.75	3.08	5.79	1.35	12.52	6.35	2.28	34.10	0.06
LR101335*	0.32	0.89	0.13	0.78	0.11	0.42	0.19	0.89	0.24	3.29	3.48	5.77	1.54	11.69	5.00	2.00	32.77	0.05
LR289*	0.34	0.97	0.14	0.87	0.13	0.17	0.06	2.81	1.02	3.63	3.64	6.41	1.68	11.07	4.70	3.30	34.44	0.07
LR80*	0.11	0.32	0.05	0.32	0.05	0.14	0.07	1.26	0.33	3.45	3.60	6.03	1.47	16.88	11.48	1.96	44.86	0.05
E19	0.08	0.24	0.04	0.19	0.03	0.09	0.17	0.82	0.22	1.92	3.04	6.02	1.03	6.59	4.81	2.11	25.52	0.05
G8R2xnl	0.12	0.34	0.05	0.31	0.06	0.77	0.34	1.37	0.41	3.07	2.99	5.89	0.86	5.23	3.55	0.64	22.22	0.05
2	0.10	0.31	0.05	0.33	0.06	0.09	0.10	0.27	0.06	2.94	2.99	5.73	1.00	7.40	3.98	1.95	26.00	0.04
5	0.11	0.34	0.05	0.34	0.06	0.17	0.08	0.29	0.07	2.76	3.32	6.41	1.16	8.04	6.16	2.57	30.42	0.05
4b	0.09	0.28	0.05	0.30	0.05	0.08	0.11	0.41	0.09	0.43	0.55	1.61	0.31	1.39	1.38	1.48	7.13	0.04
4a	0.09	0.28	0.04	0.28	0.05	0.11	0.11	0.40	0.09	2.89	4.83	6.54	1.96	8.23	6.46	14.47	45.37	0.04
4c	0.09	0.27	0.04	0.31	0.05	0.10	0.11	0.34	0.12	2.97	3.74	6.83	1.32	6.50	5.67	2.88	29.90	0.05
63	0.19	0.49	0.05	0.36	0.06	0.59	0.15	0.55	0.12	3.80	4.10	8.76	1.47	9.55	7.68	2.17	37.52	0.18
64	0.16	0.45	0.06	0.33	0.06	0.41	0.18	0.92	0.25	4.99	5.40	9.42	1.39	7.01	2.41	1.43	32.05	0.19
62	0.16	0.46	0.06	0.37	0.06	0.11	0.08	0.25	0.07	4.63	5.36	10.27	1.80	9.99	7.34	2.81	42.20	0.18
HHX1xnl	0.10	0.31	0.05	0.32	0.05	0.15	0.08	0.17	0.04	0.87	0.85	1.50	0.31	1.49	1.14	0.23	6.38	0.05
HHX4xnl	0.12	0.37	0.06	0.36	0.06	0.25	0.09	0.27	0.12	1.79	3.30	6.22	1.28	7.59	5.91	1.08	27.17	0.06
HHX2xnl	0.08	0.26	0.04	0.28	0.05	0.11	0.03	0.10	0.06	2.96	2.89	6.57	1.17	6.71	5.20	1.48	26.97	0.06
HHX3xnl	0.08	0.21	0.03	0.17	0.02	0.19	0.15	0.59	0.15	5.19	4.77	9.44	1.47	5.29	1.67	1.27	29.10	0.05
Host dykes:																		
LRh	0.95	2.55	0.34	2.06	0.31	8.42	4.97	8.59	2.56	0.02	0.05	0.15	0.05	0.68	0.44	0.05	1.44	0.27
HHX4dyke	0.69	1.91	0.28	1.73	0.26	2.54	1.52	2.57	0.70	0.04	0.04	0.21	0.06	0.75	0.40	0.16	1.66	0.02
HHX1dyke	0.72	2.01	0.28	1.72	0.27	3.01	1.53	2.23	0.74	0.12	0.08	0.17	0.10	2.08	0.64	0.60	3.77	0.21
R2dyke	0.74	1.97	0.26	1.54	0.25	3.08	3.85	6.35	2.03	-	-	-	-	-	-	-	-	0.10
P1	0.69	1.90	0.27	1.72	0.27	5.05	1.97	5.96	1.51	0.27	0.25	0.58	0.17	1.04	0.65	0.51	3.46	0.01

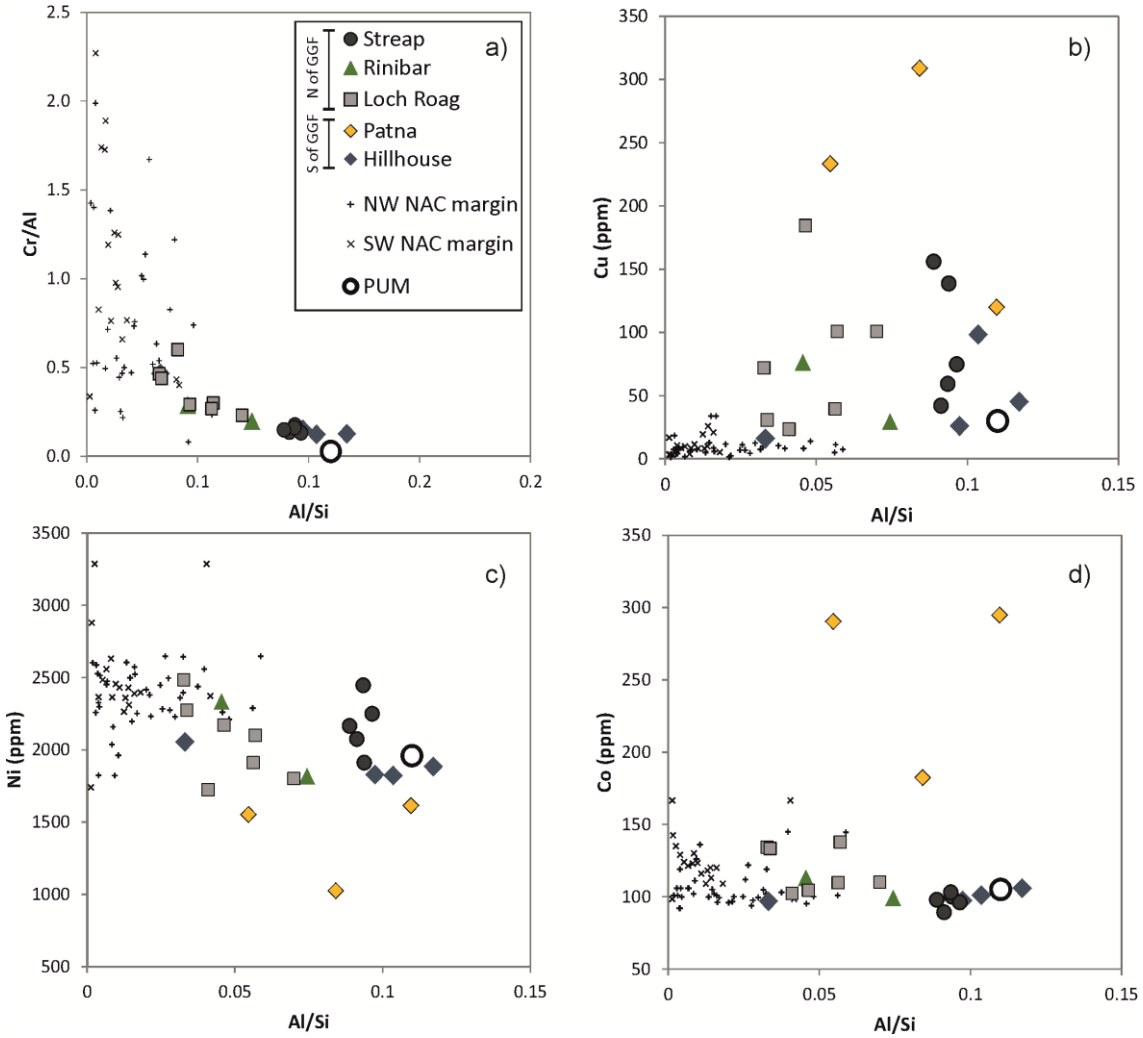

Figure 9.2. Bulk rock geochemistry (a) Major element ratios ; (b) Cu vs. Al/Si; (c) Ni vs. Al/Si; (d) Co vs. Al/Si. Note that Patna xenoliths are highly carbonated and plots displayed are for anhydrous data corrected by LOI (so all bulk rock data is plotted for anhydrous compositions). NW and SW NAC margin xenoliths are from Wittig *et al.* (2010). Primitive Upper Mantle (PUM) is from McDonough & Sun (1995).

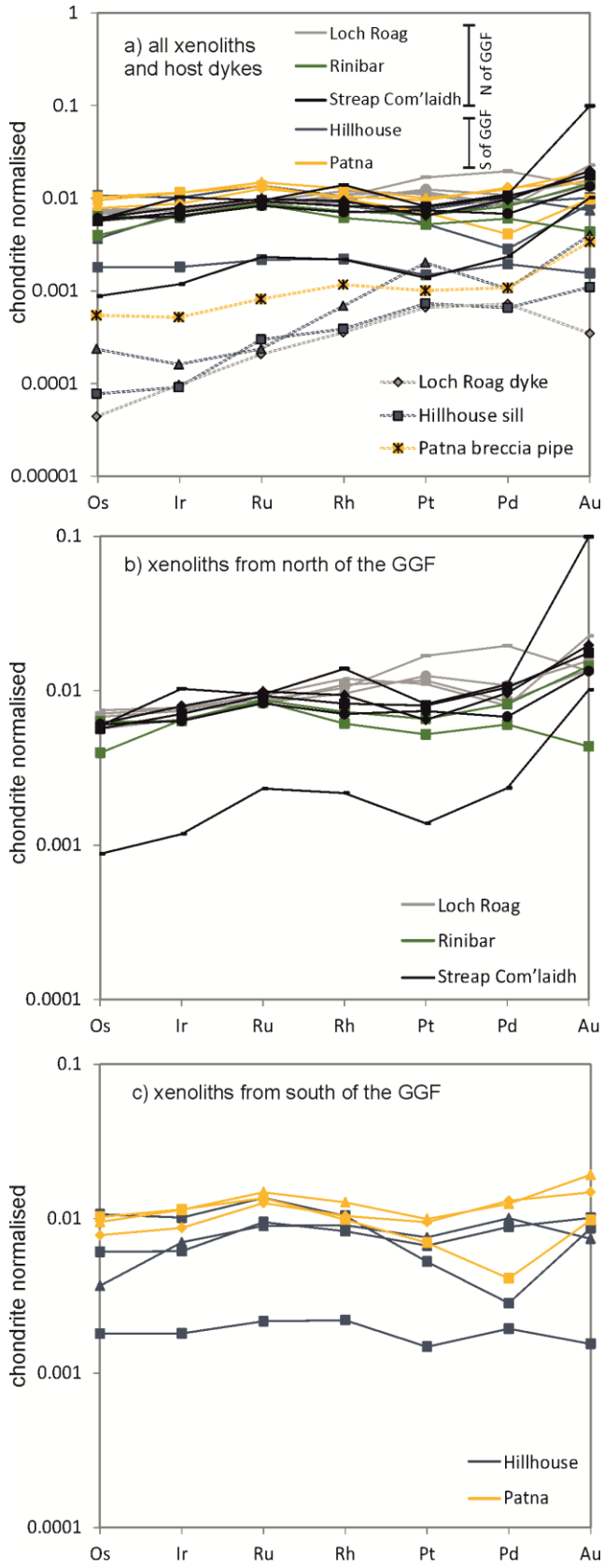

Figure 9.3. Bulk rock platinum-group element multi-element diagrams, chondrite normalised (McDonough & Sun, 1995) and according to xenolith suite; (a) All xenoliths and host dykes, sills and vents which entrained the xenoliths; (b) Xenoliths from north of the Great Glen Fault; (c) Xenoliths from south of the Great Glen Fault.

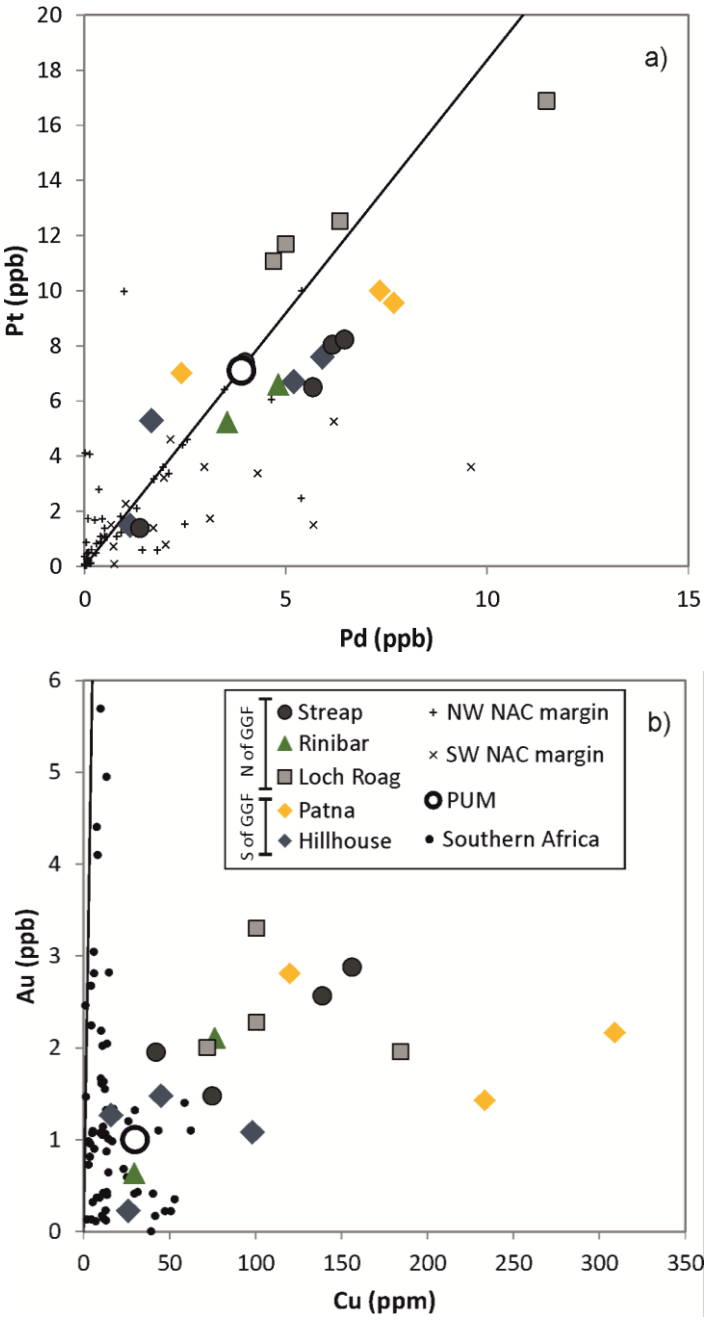

Figure 9.4. Bulk rock bivariant diagrams for Pt vs. Pd (a) and Au vs. Cu (b). NW and SW NAC margin xenoliths are from Wittig *et al.* (2010). Southern African data from Maier *et al.* (2012). Primitive Upper Mantle (PUM) is from McDonough & Sun (1995).

Two populations of mixed base metal sulphides are recognised in the Rinibar xenoliths, the 'reacted' and 'unreacted' groups (Supplementary Table D on disk, and Fig. 9.6). The internal textures of both groups are similar and the complex textures between chalcopyrite, pentlandite and pyrrhotite are best exemplified in 'unreacted' sulphides (e.g., Fig. 9.6e-f). 'Reacted' sulphides occur only in melt 'pockets' which contain fine apatite and skeletal chromite crystals (e.g., Fig. 9.6b) and/or carbonate-filled (carbonatitic) 'pockets' interstitial to silicates (e.g., Fig. 9.6a). The frayed margins of the 'reacted' sulphides and their position in 'pockets' makes it appear that they have been partially melted and/or intergrown with carbonate. In the Streap Com'laidh xenoliths, most sulphides can be ascribed to a single group (Fig. 9.7a-d, Supplementary Table D, on disk). However, small Ni-Fe sulphide droplets (< 2 μm diameter) can be seen nucleating on the edges of clinopyroxenes and spinels (hercynites) that have been partially melted (Fig. 9.7e-f).

As described in Section 3.1, some lherzolite xenoliths included in this study from south of the Great Glen (Patna, Islay, Colonsay) are pervasively (and partially) replaced by carbonates, quartz, serpentine and/or chlorite such that the original peridotite silicate mineral textures are preserved (often with minor relic clinopyroxene and spinel). However base metal sulphides are still readily observed in these xenoliths with varying textures (see Supplementary Table D, on disk). Millerite (NiS) is only observed as micron-scale, rounded, occasionally skeletal grains, in all xenoliths which have pervasive replacement of silicates (i.e., some xenoliths south of the GGF), particularly by quartz (e.g., Coire na Ba; Fig. 9.9a-d). Xenoliths from Colonsay have mixed chalcopyrite, pentlandite and pyrrhotite grains, always interstitial to the (pseudomorphed) silicates – see Figures. 9.8a-d. In one large sulphide grain there is an unusual 'feather-like' intergrowth of chalcopyrite and pentlandite, with striations of pyrrhotite (Fig. 9.8f-h) occurring within quartz replacement at the edge of Ca-carbonate and serpentine replacement zone.

Sulphides are almost entirely absent from the Hillhouse xenoliths, despite their fresh mineralogy. In this respect, the Hillhouse spinel lherzolites are distinctive. However, fine droplets (< 5 μm diameter) of Ni-Fe sulphide occur around the partially melted chromite margins analogous to those of Streap Com'laidh.

Aside from the number of sulphide groups or populations observed in each xenolith suite, sulphide minerals occur in much greater abundance (and indeed are generally coarser) north of the GGF in comparison to those from south of the fault. Further, xenoliths from the Midland Valley have particularly low sulphide abundances (e.g., Patna and Hillhouse).

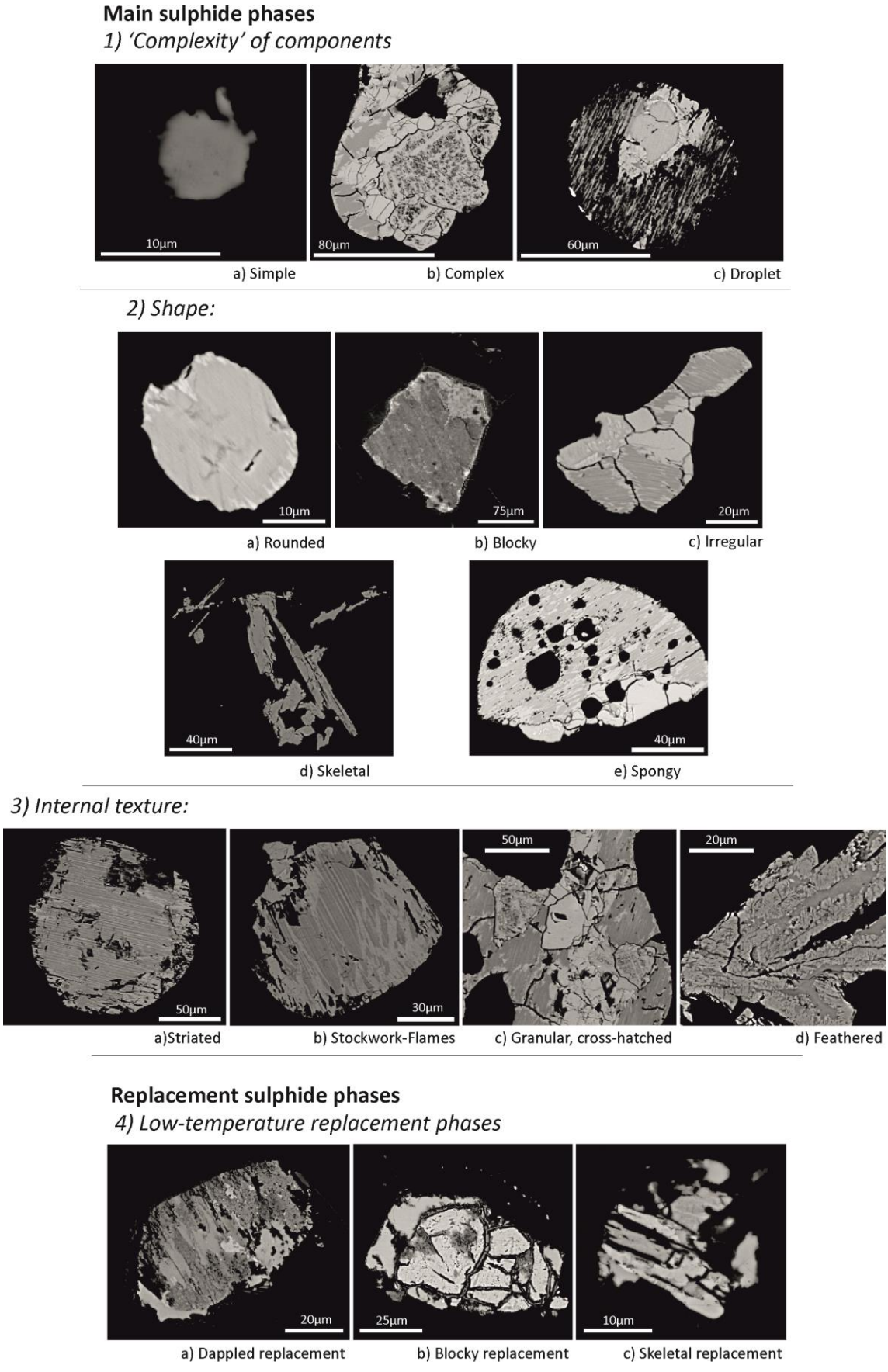

Figure 9.5. Classification categories for sulphide petrography and textures (refers to Supplementary Table D, on disk).

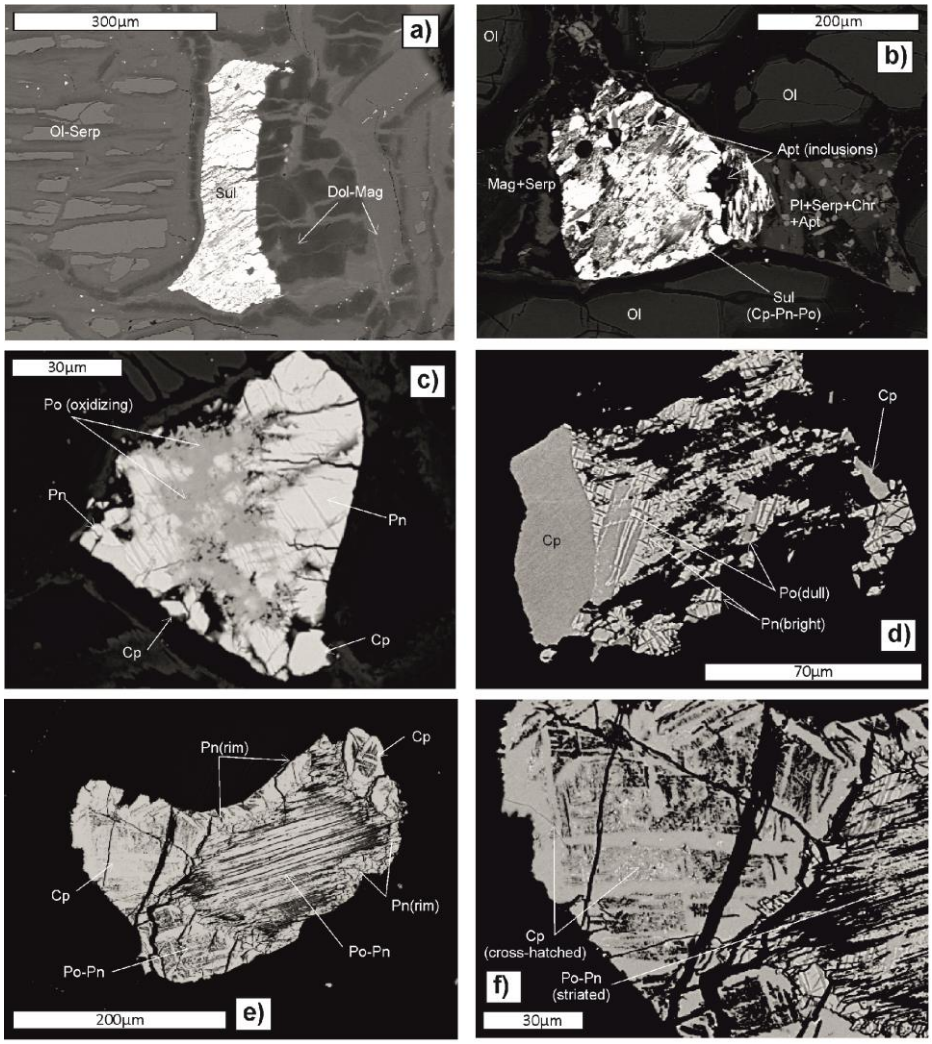

Figure 9.6. Rinibar xenolith SEM backscatter electron images (BSE). (a) Elongate sulphide at margin of carbonate pocket and in contact with serpentinised olivine crystal. Carbonates consist of intergrown dolomite and magnesite. (b) Sulphide at margin of carbonate pocket (left hand side) and melt pocket (right hand side) inbetween granular serpentinised olivine crystals. Carbonate pocket comprises magnesite, with minor serpentine probably entrained from the neighbouring olivines. The melt pocket consists of finely crystalline plagioclase, chromite and apatite, with accessory serpentine. Apatite inclusions occur within the sulphide globule. Sulphide minerals within the globule include chalcopyrite, pentlandite and pyrrhotite. (c) 'Reacted' sulphide at silicate triple junction. Contrast adjusted to show two outer edges of intergrown chalcopyrite and pentlandite with a central 'dappled' zone of pyrrhotite which is oxidising and becoming 'frayed' on the top left hand edge (reacting zone). (d) Another example of a 'reacted' sulphide showing original chalcopyrite and cross-hatched intergrown pentlandite and pyrrhotite, which now has a dappled, skeletal and 'frayed' appearance as a result of partial melting. (e) 'Unreacted' complex sulphide showing multiple and complex sulphide 'domains'. (f) Close-up of left hand side of sulphides in (e) showing cross-hatched and granular appearance of chalcopyrite, next to striated pentlandite-pyrrhotite. Note the fine granular chalcopyrite and pentlandite crystals in the lower right hand corner of this image. This exemplifies the multiple generations of sulphide crystal growth associated with one 'aggregate' of sulphides. Mineral abbreviations are: olivine (Ol), serpentine (Serp), clinopyroxene (CPX), dolomite (Dol), magnesite (Mag), plagioclase (Pl), chromite (Chr), apatite (Ap), iron oxides (Fe-ox), orthoclase (Kfs), biotite (Bt), ilmenite (Ilm), pentlandite (Pn), chalcopyrite (Cp), pyrrhotite (Po).

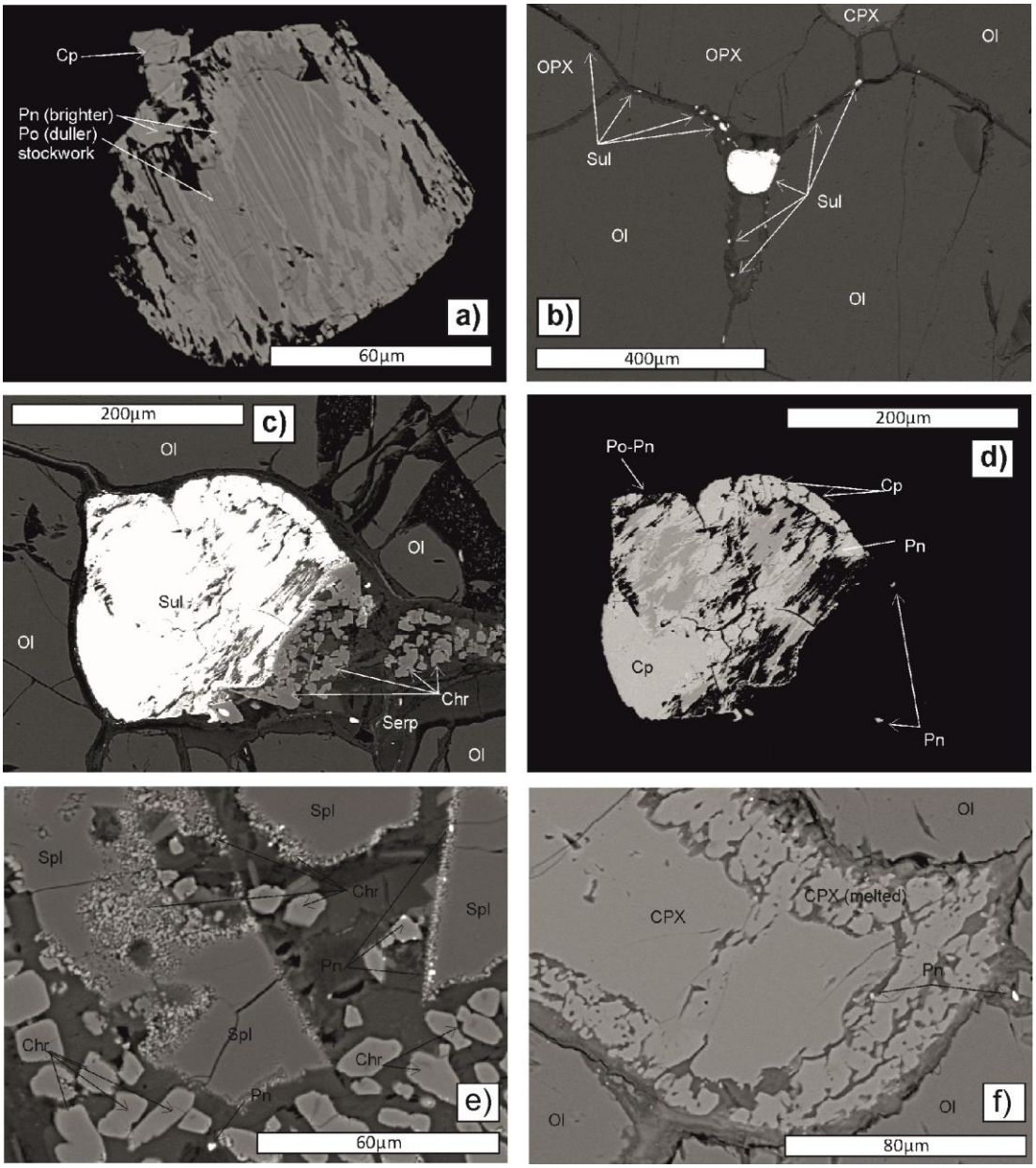

Figure 9.7. Streap Com'laidh xenolith SEM BSE images. (a) Stockwork texture between pentlandite and pyrrhotite with minor chalcopyrite as distinct non-intergrown phases. Overall this is an example of a rounded 'non-reacted' sulphide globule. (b) Large rounded 'unreacted' sulphide globule at olivine-orthopyroxene triple junction. Also note trail of µm-scale sulphides along silicate grain boundaries. (c) Sulphide at olivine grain boundaries (left) which is reacting on the right hand side to a more striated and irregular form. This reacting side is associated with fine-grained granular chromite within a pocket of serpentine. (d) The same sulphide as (c) with the contrast adjusted to display the sulphide internal texture and mineral phases. Note the rim of chalcopyrite vs. the central portion of intergrown pentlandite and pyrrhotite in a stockwork texture. (i) Al-Mg spinel melting at rim and forming granular chromite. Note the two crystal size populations of chromite: > 5 µm granular, sub-euhedral chromite crystals vs. µm-scale rounded chromites. Both chromite populations are associated with µm-scale pentlandite globules at crystal margins. (j) Protogranular clinopyroxene and olivine. Clinopyroxene is melting to form finger-like crystals at its margins. This melt zone is again associated with µm-scale pentlandite globules. Mineral abbreviations are: clinopyroxene (CPX), orthopyroxene (OPX), olivine (Ol), spinel (Spl), chromite (Chr), serpentine (Serp), pentlandite (Pn), chalcopyrite (Cp), pyrrhotite (Po).

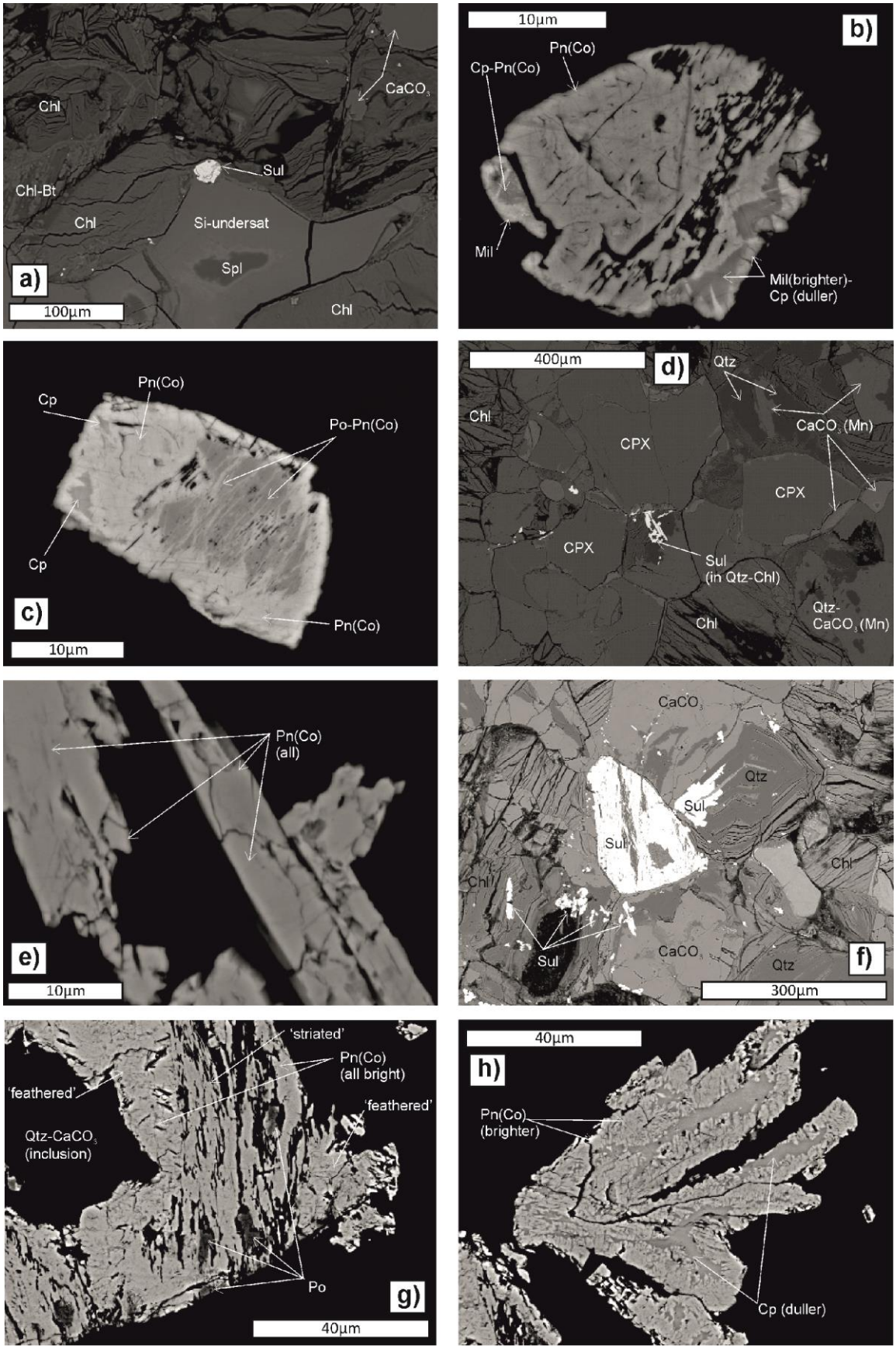

Figure 9.8. *(caption overleaf)*

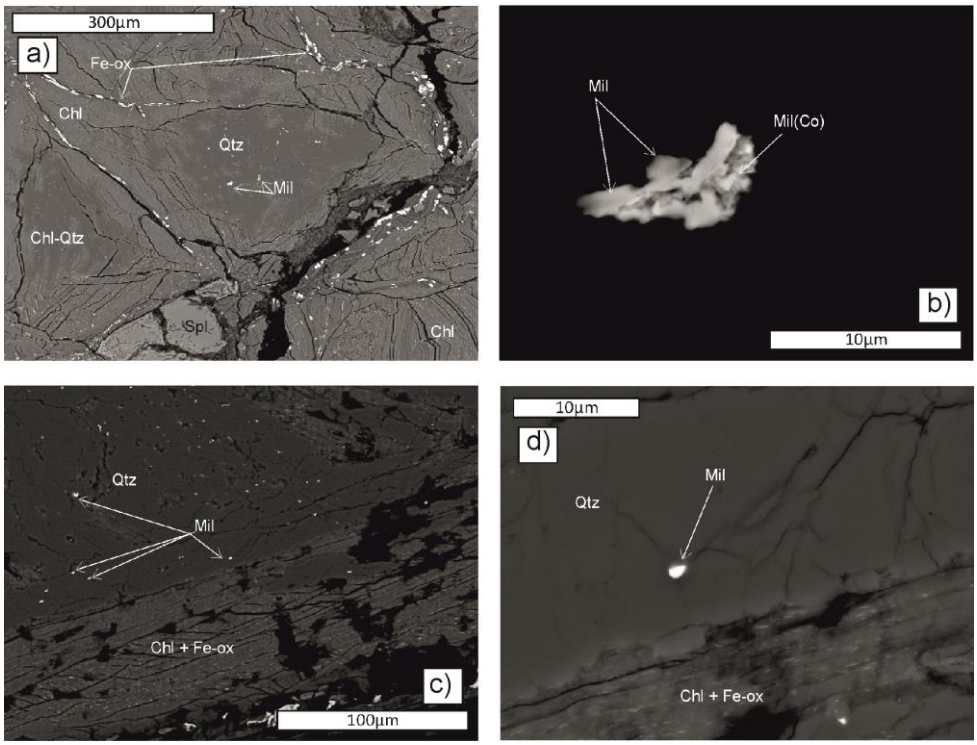

Figure 9.9. Coire na Ba xenolith SEM BSE images. (a) Tiny millerite grains are inclusions in quartz. Quartz is intergrown with serpentine and chlorite (with accessory iron oxide). (b) Close-up image of a millerite grain, showing skeletal texture and areas of Co-bearing millerite (appearing brighter). (c) Widespread µm-scale rounded millerite inclusions in quartz, at margin of serpentine. (d) Close-up of (c) showing simple rounded millerite inclusion in quartz. Mineral abbreviations are: quartz (Qtz), serpentine and/or chlorite (Chl), iron oxide (Fe-ox), clinopyroxene (CPX), orthopyroxene (OPX), plagioclase (Pl), anorthite (Pl(An)), millerite (Mil), Co-bearing millerite (Mil(Co)).

Figure 9.8. Colonsay xenolith SEM BSE images. (a) Al-Mg spinel as relic cores surrounded by wide crystal margins or rims of an unidentified Si-bearing phase of similar Al, Mg, Cr, Fe content to the true spinel core. This has SiO_2 content up to only 13 wt.%, and is therefore not a silicate or feldspathoid. Rounded sulphide is at Si-bearing spinel margin (probably the original spinel margin) and surrounded by serpentine (partially replaced by chlorite) with minor biotite. Minor patches of Ca-carbonate also noted in chlorite. (b) Close-up image of sulphide in (a) showing complex sulphide textures. Co-bearing pentlandite (probably colbaltpentlandite) with millerite and chalcopyrite as intergrown phases in flame-like or stockwork texture. (c) Sulphide complex texture of blocky sulphide multi-phase crystal. Chalcopyrite and colbaltpentlandite as coarser phases around edge of fine stockwork of pyrrhotite and cobaltpentlandite. (d) Skeletal sulphide within quartz-serpentine (chlorite) intergrowth as embayment within granular clinopyroxene. Clinpyroxene is surrounded by further serpentine and chlorite and quartz-Ca(Mn)-carbonate intergrowths. (e) Close-up of skeletal sulphide in (d) showing internal 'granular' texture of cobaltpentlandite. (f) Coarse irregular to skeletal shaped sulphide (multi-phase) in quartz-Ca-carbonate intergrowths (which have replaced original 'primary' silicates of xenolith) and with serpentine/chlorite. (g) Close-up of lower right hand side of main sulphide in (f) showing 'feathered' and 'striated' textures in cobaltpentlandite, with minor elongate inclusions of pyrrhotite. Note quartz-Ca-carbonate inclusion on left hand side of image. (h) Close-up of branched sulphide on right hand side of (f) showing intergrown 'feathered' almost 'dendritic' texture between chalcopyrite (appears duller) and cobaltpentandite (appears brighter). Mineral abbreviations are: serpentine and/or chlorite (Chl), biotite (Bt), quartz (Qtz), Ca-carbonate or calcite ($CaCO_3$), Ca(Mn)-carbonate ($CaCO_3$(Mn)), clinopyroxene (CPX), cobaltpentlandite (Pn(Co)), chalcopyrite (Cp), pyrrhotite (Po), millerite (Mil).

9.3.4. Sulphide compositions

The trace element composition of fifty-seven sulphide grains from spinel lherzolite xenoliths were analysed *in situ* by LA-ICP-MS (all results are in Supplementary Table E, on disk), and compared with seventy-seven sulphide grains previously analysed from Loch Roag (Hughes *et al.,* under review, c – Chapter 8). In bivariant plots in Figures 9.10-9.13, data has been grouped according to xenolith terrane, except for Loch Roag sulphide 'populations' which are so distinct from one another (according to their texture *and* composition), that they span a greater range of compositions than all the other xenolith sulphides included in this study.

9.3.4.1. Major element composition of sulphides – Fe, Ni, Cu and Co

Due to variable grain size, mixed textures of base metal sulphides (BMS), and the nature of 'incision' by the laser, LA-ICP-MS analyses commonly incorporated multiple sulphide phases resulting in mixed spectra (i.e., pentlandite mixed with pyrrhotite and/or chalcopyrite, etc). To account for these mixed spectra, results in Supplementary Table E (on disk) have been classed according to the major BMS end-member (pyrrhotite, Po; pentlandite, Pn; chalcopyrite, Cp) as in Hughes *et al.* (under review, c – Chapter 8).

Total PGE+Re+Au abundance does not appear to strictly correlate with any BMS 'class' (e.g., Po, Pn, Cp, etc; Fig. 9.10a-b). Overall the highest total PGE+Re+Au abundances are in sulphides from the Grampian Terrane, a sub-set from the Patna suite (Midland Valley Terrane), and Group 3 sulphides of Loch Roag. Sulphides from the Northern Highland Terrane have moderate total PGE+Re+Au contents, greater than Group 1 Loch Roag sulphides. Colonsay xenolith sulphides appear to have a bimodal population of sulphides, such that sulphides in a xenolith from one of the two monchiquite dykes has low Co (< 4500 ppm) while sulphides in a xenolith from the other Colonsay monchiquite dyke have extremely high abundances of Co (~ 3-4.5 wt.%) in all base metal sulphides (up to 3.4 wt.%). This extreme elevation in Co abundance in sulphides is also ubiquitous in xenolith suites from south of the Great Glen Fault (GGF), including in Ni-sulphide (millerite). Xenoliths from north of the GGF entirely lack this Co enrichment, and Co is only in trace abundances within sulphides (< 6000 ppm; Fig. 9.10c-d). For xenolith sulphides from north of the GGF, Co appears to gradually increase with increasing Ni and decreasing Cu content. However, for high-Co sulphides from south of the GGF, Co does not strictly correlate with Ni, although there is a broad positive correlation with Cu. There is no correlation between Co and Fe north of the GGF but there is to the south (Fig. 9.10e), where

Fe-poor sulphides have the highest Co abundance. Thus Co concentration appears to be an important discrimination parameter for xenolith suites from either side of the GGF.

9.3.4.2. Platinum-group elements

As shown by Hughes *et al.* (under review, c – Chapter 8), the three sulphide groups initially identified on a textural and petrographic basis in the Loch Roag xenoliths have distinct PGE and Re compositions, such that Group 1 (complex) sulphides have the lowest PGE abundances and highest $(Re/Os)_N$ (> 1), while Group 3 (droplet) sulphides have the highest total PGE concentration and the lowest $(Re/Os)_N$ ratios (< 1). Group 2 sulphides (with carbonate inclusions) have intermediate PGE concentrations and $(Re/Os)_N$ (0.1 to 3). We compare the composition of sulphides from other Scottish xenolith suites to those established for Loch Roag, by plotting the mean Group 1, 2 and 3 sulphide compositions on each chondrite-normalised (McDonough & Sun, 1995) diagram in Figure 9.11. Sulphide compositions in xenoliths from the Northern Highland Terrane (Rinibar and Streap Com'laidh) resemble those of the Group 2 or 3 Loch Roag sulphides, as IPGE are not depleted relative to PPGE and $(Re/Os)_N$, although variable, ranges 0.3 to 6.1 (Fig. 9.11a-c).

Sulphide groups identified on the basis of textural features show subtle variations in composition. For example, 'unreacted' sulphides (Fig. 9.11a) in Rinibar have higher IPGE content (~ 10-50 x chondrite) than 'reacted' sulphides (~ 1-50 x chondrite; Fig. 9.11b) and we note a change in $(Re)_N$ vs. $(Os)_N$ on Figures 9.11a-b, such that $(Re/Os)_N$ ~ 1 for 'unreacted' sulphides, but generally > 1 for 'reacted' sulphides. By contrast (although not exclusively) 'reacted' sulphides associated with carbonate 'pockets' have lower total PGE abundances (approximately 1 x chondrite). 'Reacted' Rinibar sulphides are predominantly composed of pentlandite and pyrrhotite (with a minor chalcopyrite component), while 'unreacted' Rinibar sulphides have notably more chalcopyrite. The trace element compositions of the Streap Com'laidh sulphides most closely resemble those of 'unreacted' Rinibar sulphides, although the former lack IPGE fractionation. Pt vs. Pd is variable, with negative anomalies in Pt indicative of early formation of a Pt-bearing platinum-group mineral (PGM) that detached from the sulphide (cf. McDonald, 2008) or which was not analysed. This is a particular feature of the Streap Com'laidh sulphides (Fig. 9.11c). We note that Streap Com'laidh sulphides have a higher pentlandite component, and this is probably responsible for the negative Pt anomaly in Figure 9.11c. Similarly, a positive Pt anomaly in Figs. 9.11a-b corresponds with sharp peaks in the time spectrum for ^{195}Pt and indicates that the laser sampled a Pt PGM.

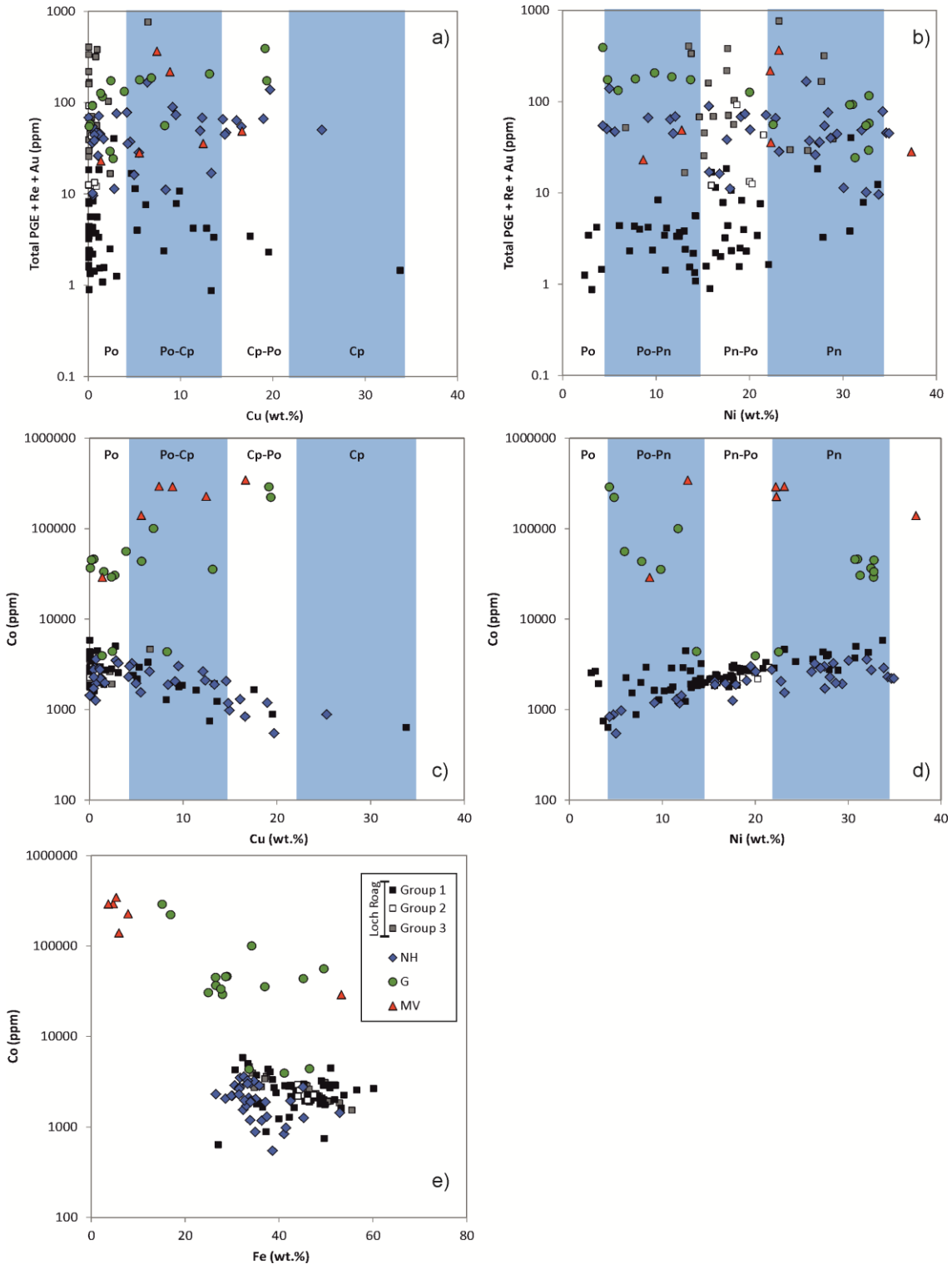

Figure 9.10. Sulphide chalcophile element composition bivariant plots for total PGE + Re + Au vs. Cu (a) and Ni (b). Co vs. Cu (c) and Co vs. Ni (d). Also Co vs. Fe (e). Data is divided according to terrane (Northern Highland = NH, Grampian = G, Midland Valley = MV). For Loch Roag (Hebridean Terrane) data have been divided according to three sulphide populations (as described by Hughes *et al.,* under review, c – Chapter 8); low-PGE (Group 1), spongey (Group 2) and high-PGE (Group 3). LA-ICP-MS data.

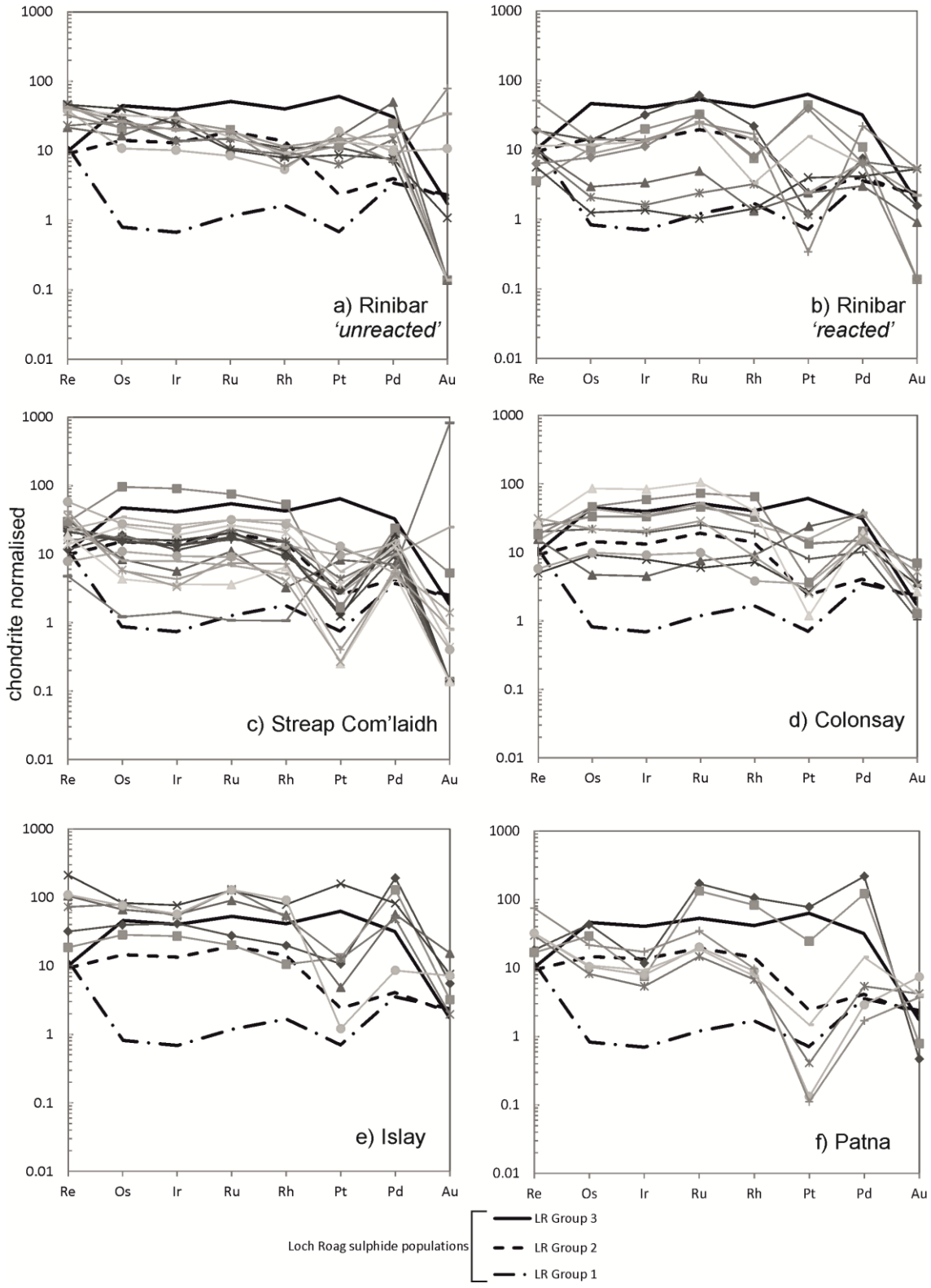

Figure 9.11. Sulphide PGE multi-element diagrams per xenolith suite (chondrite normalised; McDonough & Sun, 1995); (a) Rinibar 'unreacted' sulphides, (b) Rinibar 'reacted' sulphides, (c) Streap Com'laidh, (d) Colonsay, (e) Islay and (f) Patna sulphides. All plots show mean sulphide compositions of groups 1 to 3 sulphides from Loch Roag, for reference. LA-ICP-MS data.

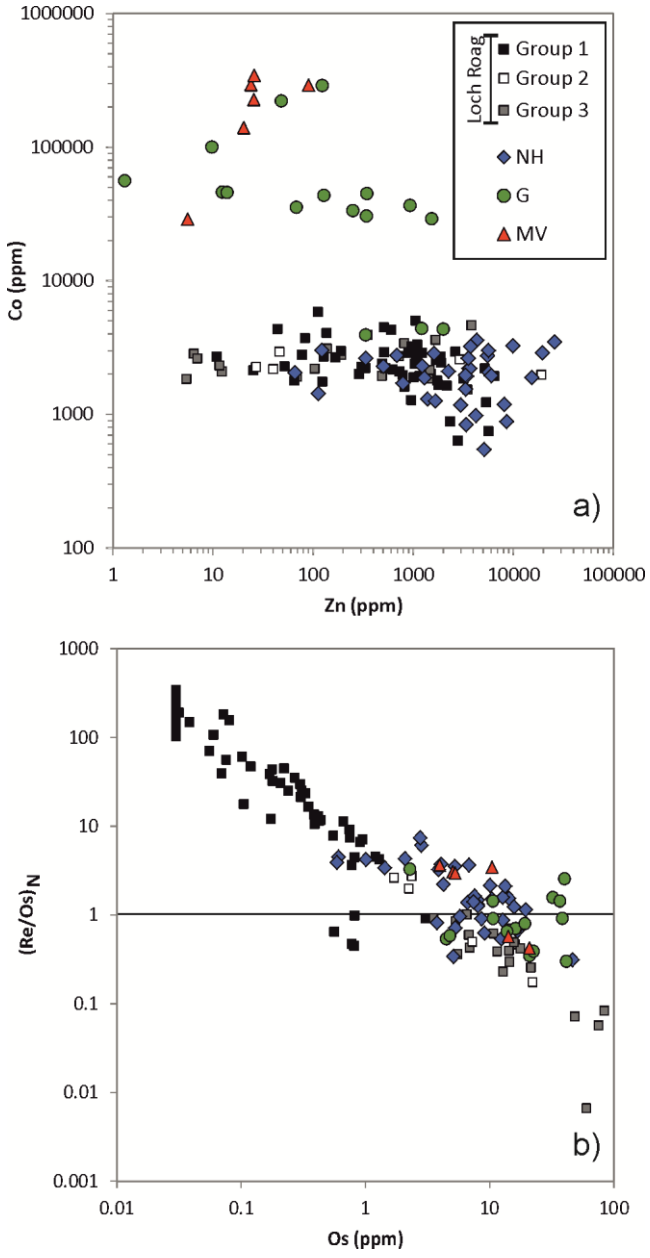

Figure 9.12. Sulphide composition bivariant plots (LA-ICP-MS data); (a) Co vs. Zn and (b) $(Re/Os)_N$ vs. Os. Data is divided according to terrane (Northern Highland = NH, Grampian = G, Midland Valley = MV). For Loch Roag data (Hebridean Terrane), results have been divided according to sulphide population (as described by Hughes *et al.,* under review, c – Chapter 8); low-PGE (Group 1), spongey (Group 2) and high-PGE (Group 3).

In the Grampian terrane, sulphides in the Colonsay xenoliths (Fig. 9.11d) generally have PGE patterns similar to those of Streap Com'laidh and 'unreacted' Rinibar, with approximately 1-100 x chondrite concentrations. Most sulphide analyses show negative Pt anomalies. Sulphides from the Islay xenoliths (Fig. 9.11e) have the highest average PGE abundances, with 10-200 x chondrite (except for Pt). Apart from one analysis, most Islay sulphides have a negative Pt anomalies. Au is less variable in the Grampian Terrane sulphides than those of the Northern Highland Terrane. The latter possess both strong positive and negative anomalies (cf. Fig. 9.11a-c vs. 9.11d-e).

Sulphides from Patna (Midland Valley Terrane) display the most variable PGE patterns (Fig. 9.11f) and have much lower abundances. They are, however, commonly too small for LA-ICP-MS analysis (< 30μm), contrasting with the abundant and coarser sulphides in the other xenolith suites (excluding Hillhouse xenoliths, which generally lack sulphide minerals). The Patna sulphides all have a negative Pt anomaly. However, Ru, Rh, Pt, Pd and Au in the chondrite-normalised patterns are highly variable and appear to define two groups, one with elevated PPGE and a strong negative Au anomaly and the other with IPGE enrichment and no Au depletion relative to Pd. These groups do not correspond to any systematic difference in Ni-, Cu- or Fe-base metal mineral group, and neither is there a systematic difference in Co enrichment.

Sulphides in the mafic host dykes are generally Ni-Fe sulphides or Fe sulphides only although some Cu-Fe sulphides have been noted in the basaltic clasts of the Patna breccia pipe. In all these cases, the sulphides have very low abundances of PGE (typically below detection limit for LA-ICP-MS) and Co (< 350 ppm).

9.3.4.3. Other trace elements in sulphides

There is no correlation between total PGE and Co abundances (cf. Figs. 9.10a and 9.10c) and the high-Co sulphides from xenoliths south of the GGF have a similar range of total PGE abundances as the Loch Roag Group 2 and 3 sulphides. A plot of Co vs. Zn shows that the content of Zn in sulphides from north of the GGF is extremely variable over five orders of magnitude (from 5-20,000 ppm) whilst Co remains low Co (< 6000 ppm: Fig. 9.12a). Sulphides with > 1000 ppm Zn have more variable Co abundances whereas most sulphides from south of the GGF, with very high Co contents, have < 2000 ppm Zn.

$(Re/Os)_N$ has been used as a crucial discrimination factor for the Loch Roag sulphides (Hughes *et al.,* under review, c – Chapter 8). In Fig. 9.12b, sulphides analysed in this study of Scottish

lherzolite xenoliths from late Palaeozoic hosts, are compared with those from Loch Roag according to $(Re/Os)_N$. All xenoliths from the Northern Highland, Grampian and Midland Valley Terranes have $(Re/Os)_N$ values similar to those from the Loch Roag Group 2 and 3 sulphides, although the sulphides in the present study have slightly higher Os abundances.

9.4. Terrane-scale trends in sulphide petrography and precious metals

9.4.1. Sulphide mineral abundance and 'populations'

Various studies of mantle lithologies have shown that the PGE budget is largely controlled by the sulphides, due to their chalcophile behaviour. IPGE are thought to be mainly hosted by Fe-rich monosulphide solid solution and refractory metal alloys where there has been significant partial melting (Brenan & Andrews, 2001; Sattari *et al.,* 2002; Bockrath *et al.,* 2004b; Luguet *et al.,* 2007; Maier *et al.,* 2012). PPGE are thought to be predominantly hosted by Cu-rich sulphides, typically interstitial to the main rock-forming silicates (Sattari *et al.,* 2002; Bockrath *et al.,* 2004a). According to these classic studies, interstitial Cu-rich sulphides are more prone to melting during mantle partial melting events, potentially becoming entrained in the developing silicate magmas. As this takes place, Pd and Pt are lost from the residual mantle, leaving a restite depleted in these elements (e.g., Maier *et al.,* 2012 and references therein). The difference in bulk rock Pt, Pd and Cu abundances between the Greenlandic NAC and the Scottish NAC xenoliths (Loch Roag and Rinibar) may be related to melt extraction from the Greenlandic NAC lithospheric mantle. However, the study of sulphides in the Loch Roag xenoliths (Hughes *et al.,* under review, c – Chapter 8), demonstrates the complexity of sulphide assemblages, melting and entrainment within a single sample. Accordingly, the widely accepted model for PGE behaviour may be valid for the asthenosphere but not necessarily for the lithospheric mantle.

In some instances of PPGE-depleted xenoliths from global cratonic and orogenic suites, re-introduction of Pd by transient silicate melts and/or oxidizing fluids has been suggested (e.g., McInnes*.,* 1999; Pearson *et al.,* 2003; Lorand *et al.,* 2008 a,b). Whilst there is strong evidence for sulphide and chalcophile element re-fertilisation by anhydrous metasomatism in northern Scotland (possibly carbonatatite-related as in the Loch Roag Group 2 sulphides; Hughes *et al.,* under review, c – Chapter 8), we suggest that this metasomatism was pre-Permian in age, and probably occurred in the Precambrian. This metasomatism was not restricted to mobilising only Pd. For example, it has previously been documented that discrete PtS (cooperite) is

present within PGE-rich (low-Re) Group 3 sulphides from Loch Roag (Hughes *et al.,* 2014 (Chapter 6); Hughes *et al.,* under review, c – Chapter 8). We infer comparable discrete Pt-bearing PGM in Rinibar xenoliths from spikes in the TRA spectra obtained by LA-ICP-MS (see Supplementary Material, on disk). Thus both Pt and Pd were mobilised by sulphide melting or S-bearing metasomatism, and re-introduced into the shallow lithosphere. Abundances of precious metal and chalcophile elements at the margin of the NAC in northern Scotland (as recorded in Loch Roag and Rinibar xenoliths) were unaffected by Phanerozoic overprinting, either in the Permo-Carboniferous or Palaeogene tectono-magamatic event (Hughes *et al.,* in press (Chapter 7); Hughes *et al.,* under review, c – Chapter 8). But in the Palaeogene, the process of lithospheric mantle delamination (e.g., e.g., Kerr, 1994; Saunders *et al.,* 1997) may have led to the assimilation and incorporation of Loch Roag-type sulphides (e.g., Pt-rich sulphide populations) – as demonstrated by the changing Pt/Pd ratio of North Atlantic Igneous Province magmas from continental to oceanic rifting (Hughes *et al.,* accepted, b – Chapter 10).

The presence of PGM, multiple coexisting sulphide populations with different textures, petrography and trace element contents, together with the overall abundance of coarse grained (> 50 μm) sulphide minerals (sometimes carbonatite-associated) appears to be a characteristic of the xenoliths from north of the GGF. South of the GGF, sulphides are finer-grained, less complex texturally, and appear to lack discrete PGM. A key factor may be the age of the lithosphere from which xenoliths were derived (cf. Upton *et al.,* 2011). South of the GGF the basement of the Grampian Terrane is thought to be Palaeoproterozoic rather than Archaean as beneath the Hebridean and Northern Highland Terranes.

South of the Grampian Terrane, the nature of the basement to the Midland Valley Terrane remains contentious but could be part of the accretionary prisms from the Lower Palaeozoic Iapetus subduction zone (and thus comparable to the Southern Upland Terrane). Overall the terranes and their associated lithospheric mantle keels are thought to become younger (and less complex) from north to south in Scotland (Upton *et al.,* 2011). Hence, the sulphide mineralogy of the lithospheric mantle across the region reflects a corresponding geodynamic control on sulphur mobility, chalcophile element and precious metal geochemistry (a feature similarly delineated by SCLM-derived lamprophyric magmas; cf. Canning *et al.,* 1996, 1998).

9.4.2. Sulphide-carbonate associations

Hughes *et al.,* (under review, c – Chapter 8) documented sulphides ('Group 2') with rounded inclusions of Ca-carbonate and suggested that this was a rare example of sulphide-carbonate immiscibility, possibly associated with carbonatitic melts. In Rinibar xenoliths we find 'pockets' of carbonates and/or apatite- and skeletal chromite-rich compositions associated with sulphides. Specifically, sulphides are sometimes seen with rounded apatite inclusions (e.g., Fig. 9.6b). The carbonate association of sulphides (albeit, not as inclusions *within* sulphides) could be further evidence of carbonatitic melts having passed through the SCLM north of the GGF. Similar 'pockets' of sulphide-carbonate have been observed in Kerguelen mantle xenoliths (e.g., Lorand *et al.,* 2004; Moine *et al.,* 2004; Delpeche *et al.,* 2012). In addition, a rare account of apatite-rich xenoliths is provided by O'Reilly & Griffin (2000), as well as an account of apatite-rich layers (sometimes with carbonate 'aggregates') in Alpine ophiolitic peridotite (Morishita *et al.,* 2008). Both in these cases, apatite (and carbonate) is thought to have resulted from mantle metasomatism associated with major tectono-magmatic events. Morishita *et al.* (2008) suggest this was associated with a period of rifting, whereas the carbonate-sulphide associations of the Kerguelen xenoliths are thought to be related to mantle plume-derived carbonatites.

In Scotland (and the UK as a whole), only one carbonatite has been documented (Loch Urigill; Young *et al.,* 1994) and this is thought to be related to the alkaline Loch Borralan intrusion (429.2 ± 0.5 Ma; Goodenough *et al.,* 2011). The Urigill carbonatite has been suggested to represent a small-scale partial melt from the lithospheric mantle. Carbonatite metasomatism has also been identified by Sr-, Nd-, and Hf-isotopic studies of Rinibar and Streap Com'laidh xenoliths (Bonadiman *et al.,* 2008) Whether the carbonatitic magma be truly derived from the SCLM itself, or was transient through the SCLM, 'pockets' of carbonatitic affinity appear to have been preserved in xenoliths of the lithospheric mantle, and we suggest that carbonatitic magmatism may therefore occur more widely in Scotland than current surface mapping might suggest. However the age and geodynamic environment associated with Scottish carbonatitic melts has yet to be established.

9.4.3. Changes in Pt/Pd ratio

Sulphides in xenoliths from north of the GGF have some of the highest Pt/Pd ratios recorded across Scotland (i.e., Group 2 and 3 Loch Roag and Northern Highland xenoliths; Supplementary Table E, on disk), frequently with Pt/Pd > chondrite. However, as previously mentioned, these high-Pt sulphides (or sulphides bearing discrete PtS PGM) coexist with low-PGE sulphides in the same xenolith which follow a sub-chondritic Pt/Pd trend, as in Group 1 from Loch Roag. Sulphides with some of the highest total PGE abundances exist in xenoliths from south of the GGF, but crucially these also have a sub-chondritic Pt/Pd ratio (i.e., these are Pd-rich and Pt-poor) and this difference does not strictly correspond to differences in MSS, pentlandite or general base metal sulphide abundances. Thus, strongly Pt-enriched sulphides appear to be restricted to xenoliths derived from terranes underlain by Archaean (Lewisian) SCLM (Hughes *et al.,* under review, c, d – Chapters 10 and 8 respectively). Metasomatism has almost certainly played a role in the geochemistry of these peridotites (silicate and sulphide minerals alike). However, if so, the metasomatism was anhydrous and probably caused by carbonatitic (or Ca-carbonate bearing) fluids.

Craton reconstructions in the North Atlantic show that the NAC was bordered to the north by the Nagssugtoqidian orogenic belt (1900-1680 Ma; van Gool *et al.,* 2002; Kolb 2014) and that this Palaeoproterozoic mobile belt forms the southern border of the Rae Province. The Lewisian Gneiss Complex and its underlying SCLM occur on the very margin of the NAC and are known to have undergone Palaeoproterozoic orogenesis (e.g., accretion of Loch Maree arc terrane c. 1900 Ma; Park, 2002b). This SCLM Pt-enrichment appears to be restricted to lithospheric mantle lineaments such as cratonic block boundaries and their bordering (or overprinting) Palaeoproterozoic orogenic belts (cf. Hughes *et al.,* accepted, b – Chapter 10). Thus Pt enrichment may not be inherited from the bulk of the depleted keel, but is instead a feature restricted to (shallow and re-fertilised) cratonic margins. In particular, whole-rock PGE data alone may mask details pertaining to subtleties in sulphide population(s). For example, while the whole-rock Pt/Pd ratio of cratonic xenoliths may be broadly chondritic (Fig. 9.4a) this gives no information about the 'fusibility' of PGE in subsequent thermal events. If sulphides lie in readily fusible positions (e.g., along grain boundaries or in eutectic melt symplectite pockets, as in the Loch Roag lherzolites), it follows that these may be redistributed in the lithospheric mantle by later transient magmas or ascending metasomatic melts. We emphasise that detailed study of sulphide mineralogy and composition should accompany bulk analyses.

Sulphides in the xenoliths south of the GGF lack the Pt-enrichment observed in the northern xenoliths and Pt/Pd ratio is typically sub-chondritic. This could reflect a sampling bias relating to the relative number of Cu- *vs*. Ni-rich sulphides analysed, as Cu-sulphides are typically depleted in Pd relative to Ni-sulphides (see Holwell & McDonald, 2010). However, we find no correlation between Pt/Pd ratios and Cu content for sulphides analysed from the xenoliths. Similarly we find no correlation of Pt/Pd ratio and Cu for bulk-rock geochemistry. Nonetheless, if Pt-enrichment is specific to the ancient metasomatised SCLM of the craton margins, the *lack* of Pt-enrichment (and therefore relative Pd-enrichment) of the southern Scottish xenoliths suggests that they represent lithospheric mantle formed in an entirely different (non-cratonic) setting. If so, Phanerozoic lavas of equivalent age erupted through basement terranes on either side of the GGF (e.g., the flood basalts of the British Palaeogene Igneous Province) should record different Pt/Pd ratios, so that those north of the GGF have high (approximately chondritic) ratios contrasting with the southern ones that have sub-chondritic values (cf. Hughes *et al.,* accepted, b – Chapter 10).

9.5. Cobalt and the Great Glen Fault – a major lithospheric lineament distinction

A clear division can be made between xenoliths from north and south of the GGF, which can be seen in the concentration of cobalt in their sulphides. Xenoliths from the north have only trace levels of Co in all their base metal sulphides whilst those south are significantly Co-enriched (typically several weight percent). This is shown by Co/Ni, Co/Cu and Co/(Fe+Ni+Cu) ratio plots in Fig. 9.13a-b. Chondritic Co/Ni and Co/(Fe+Ni+Cu) ratios are 0.048 and 0.017 respectively (McDonough & Sun, 1995). Most sulphides from xenoliths north of the GGF have sub-chondritic ratios contrasting with super-chondritic ratios in those from the south, emphasizing their extreme Co-enrichment (Fig. 9.13a). The chondritic Co/Cu ratio is 4.2 (McDonough & Sun, 1995) and we see no spatial correlation for Co/Cu ratios of sulphides on either side of the GGF (Fig. 9.13b). This suggests that Co preferably follows Ni and Fe and is not coupled with Cu nor affected by sulphide liquid fractionation during cooling.

Co-rich sulphides analysed in this study occur along grain boundaries and the majority of southern xenolith silicate minerals have some degree of alteration and replacement (e.g., peridotite silicate textures have been preserved by pervasive replacement of carbonates and quartz). This raises the question of whether alteration has also affected the sulphide minerals and whether this is related to the Co-enrichment, especially given the petrographic setting of

the sulphides (cf. 'fusibility' – see Hughes *et al.,* under review, c – Chapter 8). There is no petrographic evidence for oxidation or break-down of sulphide minerals in the southern xenoliths. Sulphide oxidation would lead to sulphur loss that should be identifiable from the S/Se ratio (e.g., Lorand *et al.,* 2003). Whereas S/Se ratios of the high-Co sulphides may in some cases be nominally lower (minimum 930) than most other Scottish xenolith sulphides (1700 to 5000) Co enrichment is not correlated with S/Se ratio (Fig. 9.13c).

We observed micron-scale millerite grains in quartz pseudomorphs (e.g., Coire na Ba xenoliths; Fig. 9.9) but these low-temperature (hydrothermal?) sulphides are only rarely Co-rich (Fig. 9.9b). Hydrothermal sulphides would also be expected to have high S/Se ratios (as little Se would be available in this low-temperature system). Only two sulphide analyses (from the Grampian Terrane) have S/Se ratio substantially elevated above 5000, and these have approximately 2 wt.% Co (Fig. 9.13c). While it is possible that the breakdown of Co-bearing silicates, such as olivine, may release Co which may then be taken up by sulphides, Co enrichment is not strictly tallied with the degree of xenolith alteration. Crucially, the style of alteration among the southern xenolith suites is highly variable (Table 9.1). For example, some suites have carbonate-only or carbonate-quartz alteration and replacement, while others are serpentinised ± chlorite. Nonetheless, Co-rich sulphides occur in all the southern suites, regardless of alteration style. Further, in many cases olivine has been preserved despite alteration in other portions of a xenolith (e.g., clinopyroxene).

We also discount the possibility of such alteration being a feature of xenolith entrainment with pervasive replacement of silicates by fluids derived from host dykes because the sulphides in the host dykes have extremely low Co (< 350 ppm; Supplementary Table E, on disk). The abundance of sulphide minerals is also unlikely to explain their Co content – whilst we observe that sulphides are generally smaller and are in lower abundances in western Scottish xenoliths from south of the GGF (in comparison to those from the north) we cannot identify a trend between sulphide grain size and Co concentration in the high-Co sulphides. Hence we suggest that the Co-rich sulphides are a primary feature of the xenoliths and lithospheric mantle, and not an artefact of alteration. This Co enrichment of sulphides may not be identified in bulk geochemistry if the sulphide populations are of low abundance, as the whole-rock Co budget may instead be controlled by silicates (olivine). Nonetheless, we tentatively highlight an elevated whole-rock Co/Ni ratio in Patna xenoliths (Table 9.2).

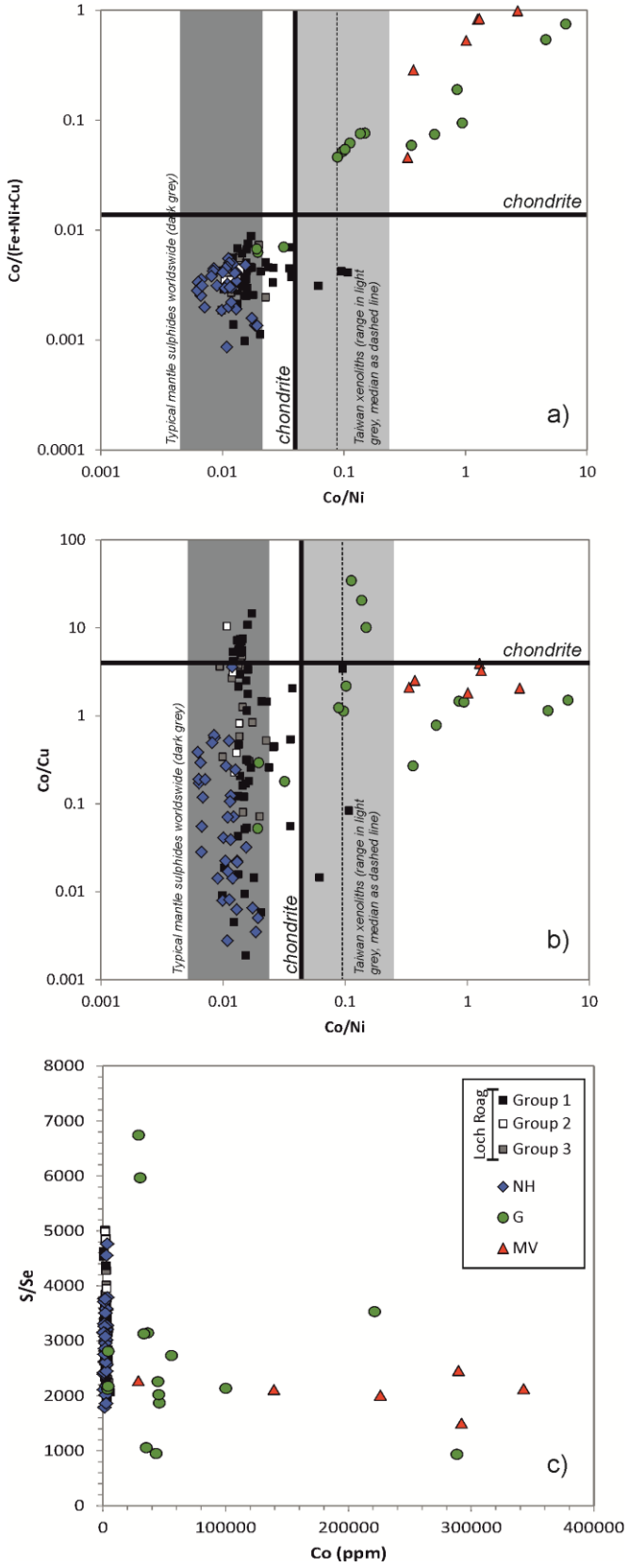

Figure 9.13. Sulphide composition bivariant plots (LA-ICP-MS data) for Co; (a) Co/(Fe+Ni+Cu) ratio vs. Co/Ni ratio, (b) Co/Cu ratio vs. Co/Ni ratio; (c) S/Se ratio vs. Co. Chondritic ratios are labelled (from McDonough & Sun, 1995) as well as worldwide and Taiwanese sulphide Co/metal ratios (according to Wang *et al.,* 2010).

To our knowledge only three examples of Co-rich sulphides in mantle xenoliths and xenocrysts are available in the published literature: these are a) peridotitic sulphide inclusions in micro-diamonds (Lac de Gras, Slave Craton; Davies *et al.,* 2004), b) sulphide grains in xenocrystic olivine and pyroxenes (Lac de Gras, Slave Craton; Aulbach *et al.,* 2004) and c) serpentinised and carbonatised peridotite xenoliths from Taiwan (Wang *et al.,* 2010). For the micro-diamond inclusions, sulphides were recorded with up to 14.7 wt.% Co, while Lac de Gras xenolith sulphides have up to 13.12 wt.% Co. Sulphides from the Taiwan xenoliths (pervasively altered and pseudomorphed spinel lherzolites) have up to 11.5 wt.% Co. Hence the Scottish xenoliths from south of the GGF have the highest recorded Co compositions reported globally thus far (up to 34.3 wt.% Co). Due to the association of sulphides with micro-diamonds and xenolith assemblages from kimberlites, the elevation in Co in the Lac de Gras sulphides could indicate a fundamental control by mantle plume magmatism (e.g., Aulbach *et al.,* 2004 and Davies *et al.,* 2004). The Taiwanese xenolith sulphides have similarly been suggested to be derived from deep mantle plume magmatism, and this interpretation was based primarily on the high $^{3}He/^{4}He$ composition of the xenoliths (Wang *et al.,* 2010). However, two neighbouring suites of xenoliths were present in the study by Wang *et al.* (2010) and only one of these suites contained sulphides with elevated Co. Therefore we question the likelihood of a deep plume signature only being recorded in one of these suites, both of which were entrained and erupted in lavas at similar times (16-8 Ma and 13-10 Ma; see Wang *et al.,* 2010 and references therein). Given the lack of comparable data, we are cautious in our interpretation of the implications for such Co-rich sulphides – perhaps these are generally under-reported due to the similar lack of sulphide-specific studies of mantle xenoliths, as well as being specific to a certain tectonic or geodynamic environment. The relationship of Co-enrichment strictly to a mantle plume setting remains ambiguous, and in the case of the Scottish xenoliths, there is no evidence of a Permo-Carboniferous mantle plume (e.g., Kirstein *et al.,* 2004; Wilson *et al.,* 2004).

Cobalt may be associated with various mineralisation settings and is normally mined as a by-product with other sulphide-hosted metals. Of particular interest are massive and disseminated sulphides in serpentinised (and often carbonated) ultramafic bodies in Morocco (Bou Azzer; e.g., Leblanc & Fischer, 1990; Ahmed *et al.,* 2009), Finland (Outokumpu; e.g., Peltonen *et al.,* 2008), and the Urals (Ivanovka and Ishkinino; see Peltonen *et al.,* 2008 and references therein). As yet there is no clear deposit model to categorise this style of mineralisation and modern analogues for these deposits have not been clearly identified. However we note that high Co concentrations are associated with Mn-nodules and chemical

sediments on the seafloor and oceanic crust (e.g., Calvert & Price, 1970; Burns, 1976; Glasby, 2006). Coupled with Co-rich sulphides in hydrothermal Cu-Zn-Co-Au-(Ni) peridotite-floored deposits of slow-spreading ridges (e.g., the Logatchev and Rainbow fields, Mid-Atlantic Ridge; e.g., Bogdanov *et al.,* 1997, Murphy & Meyer, 1998 and Douville *et al.,* 2002) and the aforementioned connection with ophiolitic features, this provides intriguing information about the geodynamic environment associated with such Co mineralisation – namely obducted oceanic lithosphere (e.g., Ahmed *et al.,* 2009).

In Scotland, Co mineralisation is documented in a number of settings (see Hannis & Bide, 2009). The oldest known Co-bearing mineralisation is associated with Late Caledonian (Silurian) appinite- and diorite-bearing intrusions, such as Talnotry (Southern Uplands; Power *et al.,* 2004) and Sron Garbh (Tyndrum, Grampian Terrane; Graham *et al.,* 2014). In these, Co is associated with Fe-sulphides (bravoite in Sron Garbh) and Ni-Cu-As-sulphides (Talnotry) and PGM have both been reported. Late Carboniferous polymetallic veins, sometimes cross-cutting strata-bound Zn-Pb deposits in the Midland Valley and Grampian Terranes, are also associated with Co mineralisation (at Silver Glen near Alva, Hilderston, Coille-bhraghad and Tyndrum – e.g., Coats *et al.,* 1982; Hall *et al.,* 1982; Stephenson *et al.,* 1983; Pattrick, 1985). In these cases there is often an association of Co with As, Ag and sometimes Au. Indeed we see a similar association of Co-enrichment with elevated As and Ag in sulphides from xenoliths (see Appendix C).

In all of these Scottish mineralised settings, metals such as Ni, Cu and Co are thought to be mantle-derived and appinites (e.g., Sron Garbh) are the product of lithospheric melting (e.g., Platten *et al.,* 1999 and references therein). Crucially, all of these documented occurrences of Co mineralisation occur south of the GGF. This is particularly pertinent because there are analogous Late Caledonian appinitic intrusions bearing Co-poor sulphides and PGM on the northern side of the GGF (e.g., Loch Borralan Complex (Styles *et al.,* 2004). Our distinction of lithospheric mantle terranes between north and south of the GGF (Fig. 9.14) is further corroborated by distinct lamprophyre isotopic compositions on either side of this major lineament (Canning *et al.,* 1996, 1998). Hence it appears that the Co-rich nature of the Scottish mantle xenoliths from southern terranes is complimented by Co-bearing mineralisation south of the GGF. The question arises: what controls this terrane-scale Co-enrichment?

The global association between ophiolite fragments, serpentinised/carbonated ultramafic pod-like bodies (e.g., Outokumpu, Finland) and Co-enrichment may be inherent to a fluid-rich oceanic rifting environment or seafloor sedimentary setting. If the Co-rich mantle beneath

southern Scotland is the subducted relic of formerly rifted oceanic lithosphere, then given the Permo-Carboniferous timing of xenolith entrainment and the oldest Co-bearing mineralisation associated with Silurian appinites, the rifting must have pre-date the Caledonian orogeny. Serpentinised ophiolitic material (south of the GGF) is documented at Ballantrae and Corrycharmaig and both are known to have chromitite-associated PGM (Power & Pirrie, 2000, 2004). The Tyrone Igneous Complex (Northern Ireland) is also an Iapetus ophiolite (accreted onto the outboard segment of Laurentia c. 480 Ma; Cooper *et al.,* 2011 and references therein) and may also contain PGM, although this has not yet been investigated. It is not yet clear as to whether sulphides in these ophiolitic bodies are also enriched in Co (or at least if chemical sediments of the ophiolitic packages are Co-enriched) but the model outlined above predicts that they should be. Iapetus oceanic crust formation was associated with the opening of the Iapetus Ocean and rifting of Rodinia c. 600 Ma in Scotland (see Trewin, 2002 and references therein).

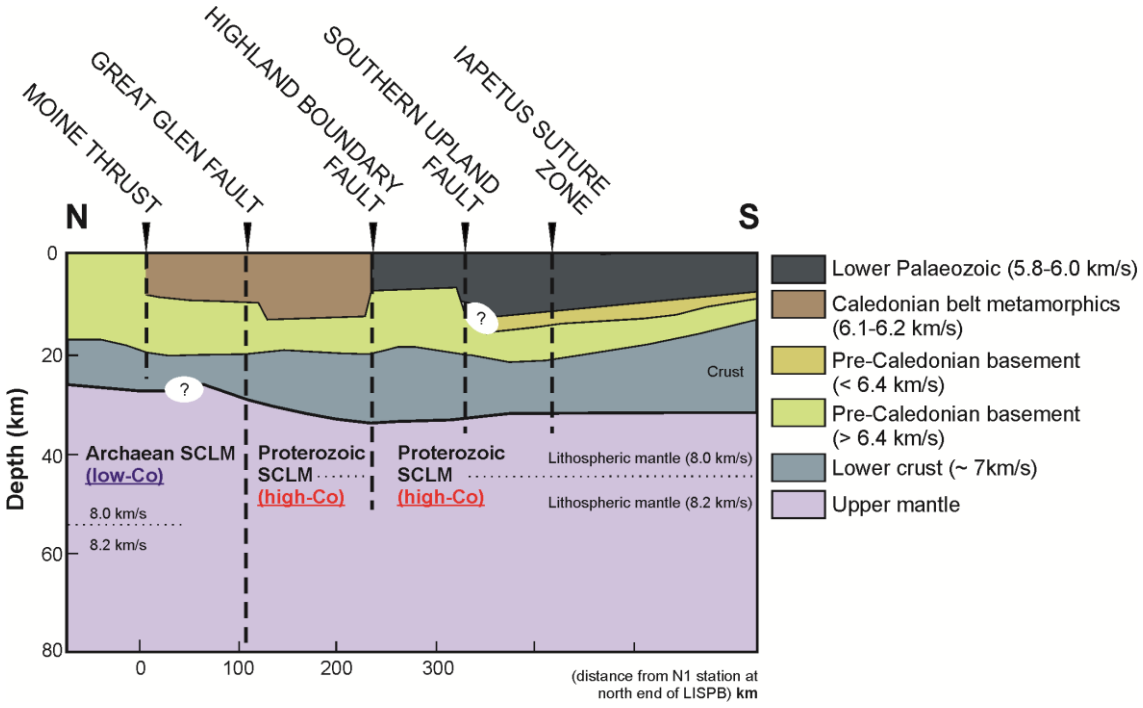

Figure 9.14. Schematic model showing lithospheric mantle below Scotland and the distribution of Archaean (cratonic) SCLM with low-Co sulphides (north of the GGF) vs. Proterozoic (or younger) SCLM with high-Co sulphides (south of the GGF).

Two Permo-Carboniferous dykes host the spinel lherzolites on Colonsay, but no previous work has been published on the xenolith suites they contain. However, based on the abundance of Co in sulphides in xenoliths from each dyke, coupled with Colonsay's position straddling the GGF, we tentatively suggest that xenoliths from these two dykes may be representative of different but neighbouring terranes – the Northern Highland (north) and Grampian (south) Terranes. Overall, given the significant lateral movement along the GGF (estimated to be 1200 km during Caledonian orogenesis between Laurentia and Baltica; Dewey & Strachan, 2003) prior to Permo-Carboniferous entrainment of xenolith suits and the cratonic lithospheric keel beneath northern Scotland; we find that sulphide compositions, petrography and textures (this study and Hughes *et al.,* under review, c – Chapter 8) can distinguish between lithospheric mantle regions (Fig. 9.14). These regions directly correspond with crustal terranes that are distinct between various geodynamic settings. Finally, although the age of sulphide minerals underlying the various terranes of Scotland have yet to be quantitatively determined, we tentatively suggest that sulphide compositions (and sulphide 'populations') may provide a thus far unexplored opportunity for metallogenic 'mapping' of the lithospheric mantle.

9.6. Conclusions

1. Sulphide mineral petrography and composition may be used to identify 'populations' of sulphide minerals from xenolith suites across a region, terrane or even co-existing within a single xenolith (e.g., Loch Roag). This is particularly the case of Archaean-Palaeoproterozoic lithospheric mantle, where numerous (transient) tectono-magmatic and/or metasomatic events may be recorded (e.g., Loch Roag and Rinibar, north of the GGF).
2. We find 'pockets' of sulphides with carbonates and phosphates, and even sulphides with apatite inclusions, in fresh spinel lherzolite xenoliths from the Archaean-Palaeoproterozoic Northern Highland Terrane. Together with sulphide-carbonate immiscibility documented in Loch Roag spinel lherzolites xenoliths (Hebridean Terrane), these highlight a significant PGE-rich sulphide-bearing carbonatitic event(s) in the lithospheric mantle underlying northern Scotland.
3. In contrast, terranes from south of the Great Glen Fault (GGF) record different sulphide compositions and textural characteristics. Pt/Pd ratios in xenolith sulphides north of the GGF are generally ≥ chondritic, whilst sulphides from south of the GGF typically have Pt/Pd < chondrite. Most striking however, is the extreme elevation in Co

concentration in mantle xenolith sulphides south of the GGF (ranging 2.9 to 34.3 wt.%).

4. Co concentration in the mantle (bulk and/or sulphide geochemistry) is generally under-reported. We suggest that Co-rich sulphides in the southern Scottish lithospheric mantle are recording a different geodynamic environment, intrinsic to Palaeozoic terranes south of the GGF, and contrasting with Archaean-Palaeoproterozoic terranes north of the fault. We tentatively propose that this Co enrichment is related to oceanic lithospheric mantle processes (cf. present day Mn-nodules and chemical sedimentary crusts) and that the younger lithospheric mantle below southern Scotland reflects this oceanic affinity. The observed mantle sulphide Co enrichment correlates with Co-mineralisation in ore deposits in overlying crust in central and southern Scotland.
5. A combined approach of sulphide morphology, composition (e.g., Co and PGE), radioisotopic geochronology, general sulphide petrographic setting (i.e., 'fusibility'), and mineralogical associations (e.g., carbonate and phosphate) provides a future opportunity of metallogenic 'mapping' of the lithospheric mantle.

Acknowledgements

Much of the material (xenolith and dyke) used throughout this study is from B.G.J. Upton's personal collection, now held at the British Geological Survey (BGS), Murchison House, Edinburgh. The BGS, particularly Michael Togher, is thanked for the curation, access and use of these samples. New samples from Streap Com'laidh were collected by J.W. Faithfull, and are henceforth curated at the Hunterian Museum, University of Glasgow. Anthony Oldroyd is thanked for his preparation of polished thin sections, and Peter Fisher for his assistance and guidance at Cardiff University's SEM facility. This manuscript greatly benefitted from discussions with Judith Coggon, Ambre Luguet, Graham Pearson, Andrew Fagan, Sebastian Tappe, and Nicholas Arndt. Kathryn Goodenough is particularly thanked for her patient and inspiring discussions. Katie Dobbie provided valuable feedback on the manuscript. H.S.R. Hughes is funded by the Natural Environment Research Council (NERC) studentship NE/J50029X. NERC are thanked for funding open access publication of this paper.

CHAPTER 10

Platinum-group element signatures in the North Atlantic Igneous Province: Implications for mantle controls on metal budgets during continental break-up

Submitted as:

Hughes, H.S.R., McDonald, I., Kerr, A.C. (accepted). Platinum-group element signatures in the North Atlantic Igneous Province: Implications for mantle controls on metal budgets during continental breakup. *Lithos.*

Co-author contributions:

I. McDonald and A.C. Kerr were involved in discussions during the writing of this paper. A.C. Kerr provided bulk rock major and trace element geochemistry from his thesis (although some samples were re-analysed to check comparability of analytical techniques). Isle of Mull and Morvern lava samples are from A.C. Kerr's PhD thesis collection and were therefore crushed and milled by him during his PhD. All Skye, Rum and Ardnamurchan lava samples were collected as part of H.S.R. Hughes's PhD. I. McDonald supervised bulk rock and LA-ICP-MS analyses.

Abstract

The North Atlantic Igneous Province (NAIP) is a large igneous province (LIP) that includes a series of lava suites erupted from the earliest manifestations of the (proto)-Icelandic plume, through continental and ultimately oceanic rifting. The lavas of one of these sub-provinces, the British Palaeogene Igneous Province (BPIP), were some of the first lavas to be erupted in the NAIP and overlie a thick crustal basement and sedimentary succession with abundant S-rich mudrocks. We present the first platinum-group element (PGE) and Au analyses of BPIP flood basalts from the main lava fields of the Isle of Mull and Morvern and the Isle of Skye, in addition to a suite of shallow crustal dolerite volcanic plugs on Mull, and other minor lavas suites. BPIP lavas display both S-saturated and S-undersaturated trends which, coupled with elevated PGE abundances (> MORB), suggest that the BPIP is one of the most prospective areas of the NAIP to host Ni-Cu-PGE-(Au) mineralisation in conduit systems. PGE-Au and chalcophile element abundances in lavas from west and east Greenland, and Iceland, are directly comparable to BPIP lavas, however the relative abundances of Pt and Pd vary systematically between lavas suites of different ages. The oldest lavas (BPIP and west Greenland) have a broadly chondritic Pt/Pd ratio (~ 1.9). Lavas from east Greenland have a lower Pt/Pd ratio (~ 0.8) and the youngest lavas from Iceland have the lowest Pt/Pd ratio of the NAIP (~ 0.4). Hence, Pt/Pd ratio of otherwise equivalent flood basalt lavas varies temporally across the NAIP and appears to be coincident with the changing geodynamic environment of the (proto)-Icelandic plume through time. We assess the possible causes for such systematic Pt/Pd variation, and suggest that this reflects a change in the availability of lithospheric mantle Pt-rich sulphides for entrainment in ascending plume magmas. Hence the precious metal systematics and potential prospectivity of a LIP may be affected by contamination of plume-derived magmas by cratonic subcontinental lithospheric mantle.

10.1. Introduction

Some of the world's most important orthomagmatic Ni-Cu-PGE sulphide deposits reside in continental flood basalt provinces, or large igneous provinces (LIPs) – for example the Norilsk-Talnakh conduit-hosted mineralisation in the Siberian Traps (e.g., Arndt, 2011). Many factors contribute to the formation of such deposits, not least the timing of S-saturation and segregation of immiscible sulphide liquids, triggered by various processes including contamination of magmas by crustal S-rich sediments (e.g., Ripley *et al.,* 2003). S-saturation may also be achieved by magma mixing or fractional crystallisation of ascending magmas (e.g., Irvine, 1975; Naldrett *et al.,* 2011 and references therein). Once formed, immiscible sulphide liquids scavenge chalcophile elements from repeated influxes of silicate magma, and if collected, may form sulphide deposits and mineralisation within intrusions such as mid- to upper-crustal magma conduits (e.g., Naldrett, 2004; 2011).

The North Atlantic Igneous Province (NAIP) is a LIP and certain portions are documented to host Au-Cu-PGE mineralisation, such as the Skaergaard Intrusion, Kap Edvard Holm Complex, and associated Macrodykes in east Greenland (Bird *et al.,* 1991, 1995; Andersen *et al.,* 1998; Arnason & Bird, 2000; Thomassen & Nielsen, 2006; Holwell *et al.,* 2012). Continental flood basalts in west Greenland appear to have undergone assimilation-induced S-saturation, highlighted as potentially overlying significant orthomagmatic PGE mineralisation, and are currently under exploration (e.g., Keays & Lightfoot, 2007 and references therein). In contrast, onshore and offshore continental flood basalts in this region, along with basaltic lavas of the seaward dipping reflectors offshore of the southeast Greenlandic coast, are predominantly S-undersaturated (Philipp *et al.,* 2001; Momme *et al.,* 2002b). However minor S-saturation has taken place in some flows here, following silicate magma differentiation and fractionation (Philipp *et al.,* 2001).

Aside from S-saturation, the initial concentration of PGE, Ni and Cu in mantle-derived magmas is a key factor in the probability of their forming orthomagmatic mineralisation (e.g., Naldrett, 2004). Worldwide, such mineralisation appears to be correlated with the occurrence of mantle plume events impinging on thick cratonic (Archaean) lithospheric mantle (e.g., Groves & Bierlein, 2007; Maier & Groves, 2011 and references therein). The debate over the cause for this association remains unresolved (e.g., Arndt, 2013). This may imply some dependence on there being high-degree melting and/or deeper mantle (or even mantle-core) melting associated with mantle plumes, and hence important geochemical/geophysical constraints on mineralisation potential specific to plumes. Alternatively the association may suggest

enrichment of PGE in cratonic subcontinental lithospheric mantle (SCLM) which could become incorporated in ascending LIP magmas. It may also reflect a biased preservation and/or discovery potential (e.g., Maier & Groves, 2011).

The magmatic centres and plateau lavas of the British Palaeogene Igneous Province (BPIP) formed prior to continental breakup and at a similar time to continental flood basalts in west Greenland (Storey *et al.,* 2007 and references therein). However no significant Ni-Cu-PGE exploration has taken place in the BPIP to date, despite favourable circumstances for crustal S contamination in this region (see Andersen *et al.,* 2002). In this paper we report new platinum-group element (PGE) and Au analyses for a series of BPIP basaltic lavas to establish their S-saturation status, and to assess the fertility and prospectivity of the eastern part of the BPIP.

PGE abundances in various Greenlandic and Icelandic lava suites will be compared with our new BPIP lava dataset in order to assess the implications for mineralisation potential and metal ratios, from early plume impingement beneath the continental lithosphere, throughout continental breakup and ultimately during oceanic rifting (± a non-plume mid-ocean ridge melting component).

10.2. Geology and formation of the North Atlantic Igneous Province (NAIP)

Impingement of the proto-Icelandic mantle plume under the continental lithosphere of Greenland, Canada and Europe (i.e., beneath the North Atlantic Craton; NAC) generated the NAIP. Prior to this, Greenland and Europe were joined and seafloor spreading had previously initiated in the south Labrador Sea between Canada and Greenland (ca. 80 Ma; Roest & Srivastava, 1989) during a period of slow extension devoid of any evidence of extensive volcanism (Chambers, 1991). However, ca. 62 Ma, formation of significant volumes of mafic magma below what is now the UK, Greenland and Baffin Island (Fig. 10.1), signified a dramatic change in thermal mantle conditions, which predated continental rifting (c. 55 Ma) but ultimately led to the opening of the Atlantic Ocean (Saunders *et al*., 1997). The main products of this prolonged period of magmatism were alkali and tholeiitic flood basalts. In total, Palaeocene and Eocene magmas of the NAIP likely ranged from 5 to 10 x 10^6 km^3 in volume (White & McKenzie, 1989; Holbrook *et al.,* 2001 and references therein). The NAIP can be divided into several distinct igneous temporal intervals, as outlined below (Saunders *et al.,* 1997; Chambers & Pringle, 2001; Jolley & Bell, 2002; Storey *et al.,* 2007) – see Figure 10.2.

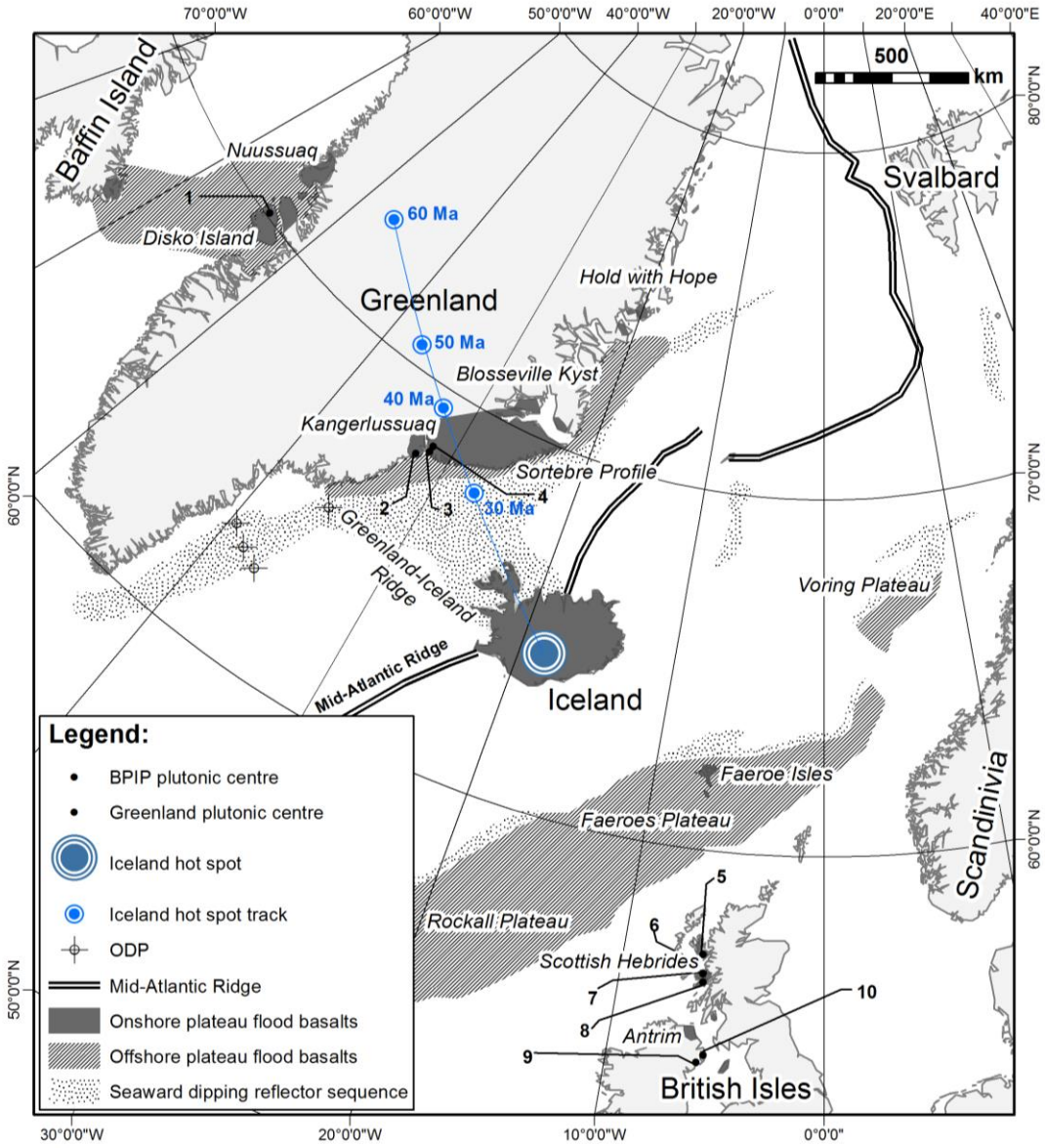

Figure 10.1. Simplified Palaeogene geology of the NAIP, showing locations of the flood plateau basalts associated with early-stage rifting of the Atlantic and a selection of plutonic centres; (1) Hammer Dal Complex, Disko Island, (2) Krusse Fjord Complex, (3) Skaergaard Complex, (4) Miki Fjord and Togeda Macrodykes, (5) Cuillin Central Complex, Isle of Skye, (6) Rum Central Complex, Isle of Rum, (7) Central Complexes of Ardnamurchan, (8) Ben Buie Central Complex, Isle of Mull, (9) Carlingford Complex, (10) Slieve Gulion and Mourne Complexes. ODP are ocean drilling program sites are also labelled. Adapted from Andersen *et al.* (2002).

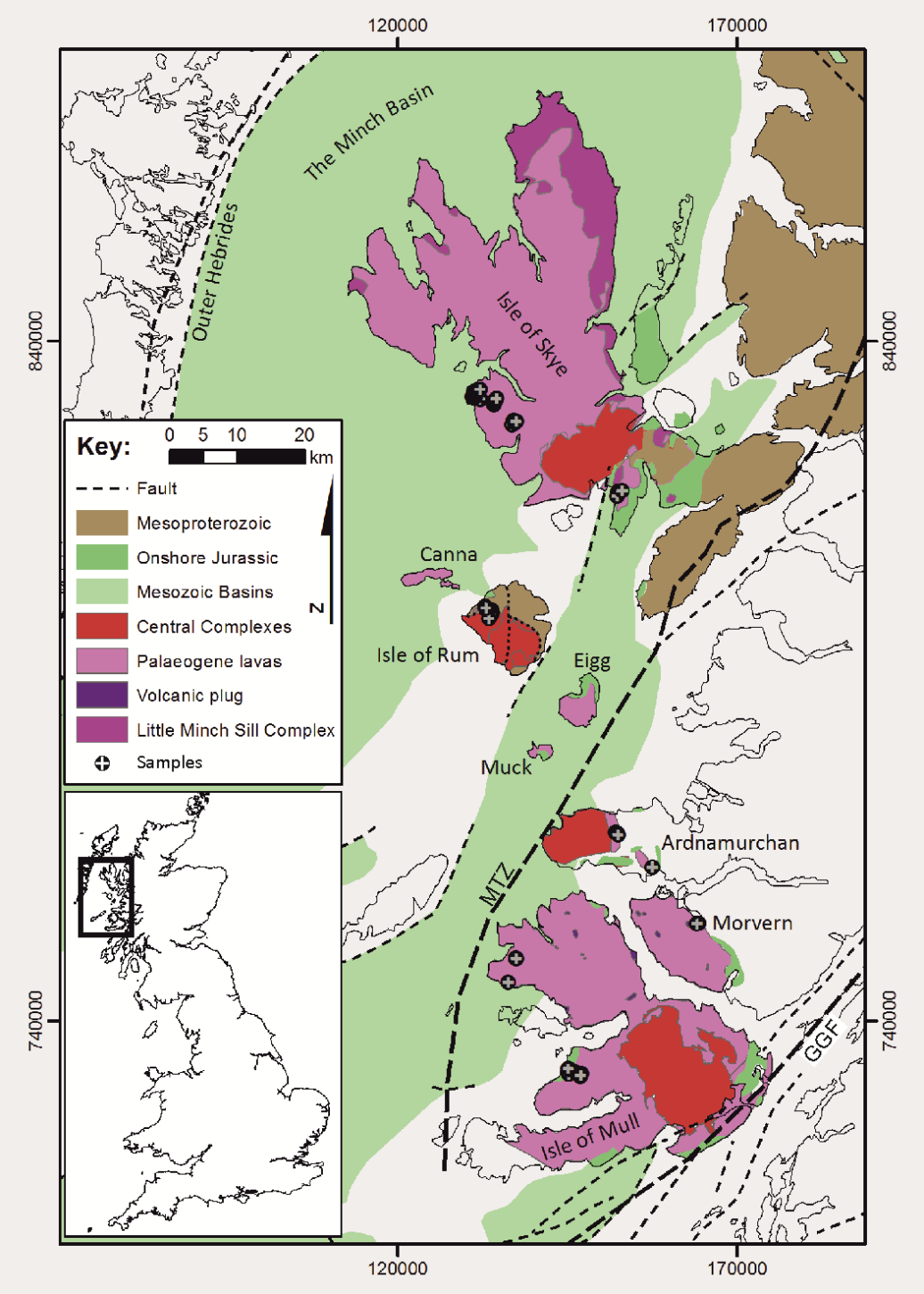

Figure 10.2. Geology of the Hebridean portion of the BPIP and sedimentary rocks of the Torridonian and Hebrides Basin.

Continent-based magmatism and stretching during impingement of the proto-Icelandic mantle plume (pre- and syn-breakup; ca. 62-56 Ma):

1. Phase 1 – The onset of widespread and voluminous volcanism initially in west Greenland and Baffin Island at 61.7 ± 0.5 Ma (Sinton *et al*., 1998) comprising basaltic and picritic lavas up to ~ 7 km thick (Storey *et al.,* 2007), and alkali basaltic lavas in the Faroe-Shetland Basin and Scottish (Hebridean) portion of the BPIP. At the end of this interval there was a switch to localised, and increasingly intermittent, volcanic activity (ca. 57-56 Ma).
2. Phase 2 – Eruption of widespread volcanic sequences due to an increase in melt production rate at 56.1 ± 0.5 Ma which coincided with continental rifting (Storey *et al.,* 2007). Tholeiitic basaltic sequences were erupted in west and east Greenland (e.g., Blosseville Kyst, Kangerlussuaq, and Hold with Hope regions), the Irmiger Basin, Faroe Islands, Vøring Plateau, Faroe-Shetland Basin, Rockall Basin, and the Inner Hebrides and Antrim (BPIP).

Syn- and post-breakup, plate separation at the Mid-Atlantic Ridge (56 Ma to present):

3. Phase 3 – Voluminous volcanism continued, but was restricted to the margins of the proto-North Atlantic rift, forming abnormally thick oceanic crust offshore and along the line of plate separation, ca. 56-50 Ma (Storey *et al.,* 2007; Philipp *et al.,* 2001 and references therein). Basalts from this period are observed in the Irmiger Basin, Faroe Islands, east Greenland margin, and the Vøring Plateau and are seismically imaged as seaward-dipping reflector sequences.
4. Phase 4 – Continuing volcanism of the Iceland plume diminished and narrowed along a restricted portion of the east Greenland margin along the Greenland-Iceland ridge (ca. 50 Ma) to present-day hotspot activity in Iceland (Storey *et al.,* 2007).

The position of the (proto-) Icelandic mantle plume has moved through time relative to the overlying tectonic plates (Fig. 10.1 – e.g., Lawver & Muller, 1994). The various methods used to assess the centre of the plume (e.g., locus of highly magnesian lavas) suggest that the Palaeogene proto-Icelandic plume lay beneath central Greenland in the Palaeogene and Early Eocene, and gradually tracked SE – ESE beneath what is now the Greenland-Iceland ridge (delineated as a zone of thickened oceanic crust) to its present day position beneath Iceland at the Mid-Atlantic Ridge.

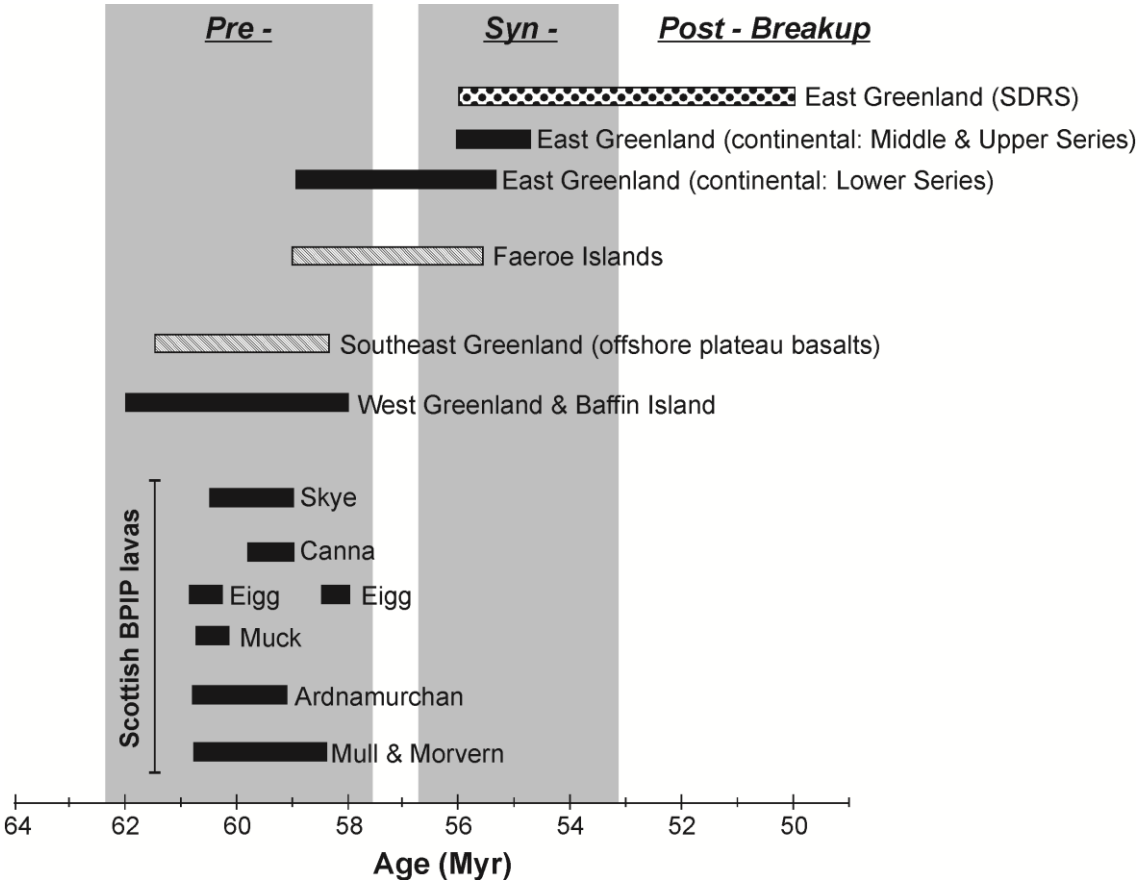

Figure 10.3. Simplified timeline of lava sequences from phases 1 and 2 (pre- and syn-breakup; ca. 62-56 Ma) in the formation of the NAIP. See text for details (Chambers *et al.,* 2005 and references therein).

10.2.1 The Hebridean portion of the BPIP

The BPIP is part of the earliest magmatic series of the NAIP, which includes Palaeogene rocks of the Hebridean Igneous Province (along the west coast of Scotland) and Northern Ireland (Fig. 10.3). In the Scottish Hebrides, the BPIP includes the Isles of Mull, Skye, the Small Isles, and the mainland igneous complex of Ardnamurchan and lava flows of Morvern. The crustal sequence into which the magmas of the Hebridean portion of the BPIP were intruded include the Archaean basement rocks of the Lewisian Gneiss Complex (part of the NAC), Mesoproterozoic Stoer, Sleat and Torridon Group sediments (mostly coarse sandstones, with some shale and silt members), various areas of Neoproterozoic Dalradian and Moine metasediments, Triassic limestones and a thick package (> 1 km estimated total thickness) of Jurassic and minor Cretaceous sediments representing part of the Hebrides Basin (Fig. 10.3). Crustal impingement of mantle-derived mafic magmas resulted in subaerial eruptions along fissure-type feeders (Kent *et al*., 1998) now preserved as a laterally continuous linear array of

dyke swarms. Emeleus and Bell (2005) provide a comprehensive compendium of radiometric and palynological age determinations from various published sources.

Broadly, the eruption of lavas in this province spanned approximately 3 Myr (61-58 Ma) and hence it has been suggested that episodes of lava eruption in the Hebridean portion of the BPIP represent discrete magmatic pulses, rather than continuous plume-driven activity, and could have led to episodic magmatic underplating of the continental shelf of NW Europe (White & Lovell, 1997). Detailed work by Single and Jerram (2004) has revealed volcanic disconformities within eroded lava fields. Such juxtaposition of volcanic sites and lava batches of the same geochemical type, common in the Hebrides, is a feature of continental flood basalt plateaus which were fed by multiple centres or fissure systems, and must be taken into account in regional lava suite correlation (Jerram & Widdowson, 2005).

The Isle of Mull and Morvern lavas and doleritic plugs

The Mull lava succession (Fig. 10.3) is estimated as being 1800m thick and covering approximately 840 km^2 (Emeleus & Bell, 2005), however the maximum thickness presently exposed in a single section is 1000m on Ben More (Kerr, 1995a). These flat-lying lavas display flood basalt trap features, overlying thin Upper Cretaceous rocks, Triassic sandstones, and Moine Supergroup lithologies which displayed significant topographic relief at the time of lava eruption. Jurassic sediments are also observed around various parts of the perimeter of the island, although the extent of these lithologies underlying the flood basalts is unknown.

The Mull Lavas were divided into 3 main groups, originally identified by Bailey *et al.* (1924), correlated in detail and modified according to petrogenetic and geochemical characterisation by Kerr (1993, 1995a) and in subsequent publications. In chronological order, these groups are the Staffa Lava Group, Mull Plateau Group (MPG), the Coire Gorm type and the Central Mull Tholeiites. The MPG is the most complete lava succession on Mull and includes a series of predominantly alkali to transitional alkali Mg-rich basalts and hawaiites with minor mugearites and trachytes. In contrast, the Central Mull Tholeiites outcrop in small marginal areas of the Mull Central Complex. Due to their earlier eruption and the relatively high abundance of high-MgO lavas, all Mull and Morvern lava samples analysed during this study are from the MPG.

A series of elongate volcanic plugs are aligned in the direction of the regional dyke swarm and are found throughout Mull and Morvern. These plugs span a similar range of compositions including the Mull Plateau lavas and so are thought to have been shallow feeder conduits,

particularly in later phases of eruption (Kerr, 1997). A range of tholeiitic dolerite plugs sampled by Kerr (1997) with varying MgO contents were selected for analysis during this study.

Lavas of the Ardnamurchan Peninsula

The Ardnamurchan Peninsula hosts three gabbroic intrusive centres, emplaced concentrically within country rocks of Moine psammites and pelites, Triassic and Jurassic sediments, and partially intruding into thin outliers of the Mull Lava Field (Bell & Williamson, 2002). A selection of these lavas from the lava field east of Beinn an Leathaid were analysed for PGE and Au in the present study.

The Small Isles lavas

Lavas of the Small Isles comprise predominantly olivine and tholeiitic basalts, with minor more evolved compositions (Emeleus & Bell, 2005). Lavas on the Isles of Canna and Sanday are at least 200 m thick, predominantly of alkali olivine basalt, hawaiite, and mugearite. Lavas of the Canna Lava Formation in NW Rum were erupted into steep-sided palaeovalleys, eroded into Torridon Group sediments (Emeleus & Bell, 2005). A series of lava samples from the Canna Lava Formation, outcropping on the Isle of Rum were analysed during this study (Fig. 10.3).

Isle of Skye lavas

The extensive lava field on Skye mainly occurs to the northwest of the Cuillin Central Complex (Fig. 10.3) and comprises alkali olivine basalts, hawaiites, mugearites, benmoreites, and trachytes (Williamson & Bell, 1994). Lavas were extruded onto Mesoproterozoic Torridonian sediments of the Torridon and Sleat Groups, Cretaceous and Jurassic sediments of the Mesozoic Hebrides Basin and parts of the Cuillin Central Complex. The absence of volcanic plugs associated with the lava fields on Skye and the more common observation of inter-lava sediments, may be an artefact of the relatively intermittent nature of Palaeogene volcanic activity in this area (Kerr, 1997).

On the Isle of Skye the Skye Main Lava Series (SMLS), a 1.2-1.7 km thick transitional (tholeiitic-alkali) flood basalt, is overlain by the younger and volumetrically minor Preshal Mor Basalt (PMB) (Thompson, 1982; Williamson & Bell, 1994). Williamson and Bell (1994), amongst others, have divided the SMLS into formations and members based on flow lithological associations in each region of the island (north, north-central, west-central and south-central). These formations range from 10 to 760 m in thickness, however extensive block faulting across the lava field, together with common inter-lava sedimentary units, makes full correlation

across Skye difficult. All samples analysed during this study were sampled from the west-central and south-central sectors of the SMLS.

10.3. Analytical Methods

Extensive major and trace element geochemical data and curated samples, exist for the Isle of Mull and Morvern basaltic lavas and doleritic plugs (Kerr, 1993; Kerr, 1995a; Kerr, 1995b; Kerr, 1998b; Kerr *et al*., 1999). In this investigation, we analyse new samples along with a representative selection of curated BPIP lava and plug samples (Supplementary Material Table A on disk) for the PGE and Au.

Weathered material was removed from each sample before it was crushed to fine gravel. If present, amygdales and filled vesicles were hand-picked and removed from crushed samples before the remainder was milled to a fine powder in an agate planetary ball mill. Loss on Ignition (LOI) was determined gravimetrically by heating at 900^{o}C for two hours. Major and trace elements were measured by inductively coupled plasma optical emission spectrometry (ICP-OES) and inductively coupled plasma mass spectrometry (ICP-MS) respectively at Cardiff University following fusion using methods and instrumentation described by McDonald & Viljoen (2006). PGE and Au analysis was carried out by Ni-sulphide fire assay (sample weight 15 g) followed by Te co-precipitation and ICP-MS (Huber *et al*., 2001; McDonald & Viljoen, 2006). Accuracy for whole-rock elemental geochemistry was constrained by analysis of the certified international reference materials TDB1 and WMG1 for PGE and Au, and JB1a, NIM-P and NIM-N for all other trace and major elements (see Supplementary Material Table B and Ca-b on disk). Precision for fire assay was estimated by repeat analysis of a sub-set of samples (Supplementary Material Table D on disk).

In total, 58 lava samples (including 3 from Ardnamurchan, 1 from Rum, 40 from the Mull Plateau Group and 14 from the Skye Main Lava Series) and 11 dolerite plugs from Mull and Morvern were analysed by fire assay for PGE and Au during this study. All PGE and Au results are presented in Table 10.1. For major and trace element analyses 63 new lava samples were analysed from Skye, Rum and Ardnamurchan, along with a further 24 curated Mull lava samples and 11 curated Mull dolerite plug samples, for cross-checking against previous geochemical analyses by Kerr (1993) and Jones (2005). A full table of major and trace element data are available in Supplementary Material Table E (on disk).

Table 10.1. Bulk rock PGE and Au results for BPIP lavas (in ppb).

Sample number	Location	Category	Rock type	Os (ppb)	Ir (ppb)	Ru (ppb)	Rh (ppb)	Pt (ppb)	Pd (ppb)	Au (ppb)
AN_24	Arnamurchan	lava	Basalt	0.04	0.06	0.16	0.06	0.44	0.16	0.11
AN_52	Arnamurchan	lava	Basalt	0.17	0.24	1.00	0.41	3.98	1.59	0.11
AN_53	Arnamurchan	lava	Basalt	0.11	0.11	0.25	0.14	2.12	0.73	0.21
AM10A(KJ)	Isle of Mull	lava	Basalt	0.10	0.08	0.17	0.08	4.13	2.98	0.81
AM10B(KJ)	Isle of Mull	lava	Basalt	0.16	0.08	0.11	0.09	6.17	2.66	0.71
AM10C(KJ)	Isle of Mull	lava	Basalt	0.07	0.07	0.11	0.14	5.69	2.22	0.62
AM7(KJ)	Isle of Mull	lava	Basalt	0.21	0.15	0.37	0.13	4.87	3.66	2.44
BB19(KJ)	Isle of Mull	lava	Basalt	0.03	0.05	0.12	0.23	2.02	1.77	0.40
BB20(KJ)	Isle of Mull	lava	Basalt	< d.t.	< d.t.	0.06	0.06	1.37	2.01	0.65
BB21(KJ)	Isle of Mull	lava	Basalt	0.31	0.26	0.44	0.15	9.20	2.80	0.78
BHI18(KJ)	Isle of Mull	lava	Basalt	0.15	0.06	0.18	0.08	4.49	2.99	0.58
BHI19(KJ)	Isle of Mull	lava	Basalt	0.79	0.36	0.73	0.25	7.78	4.52	0.52
BHI26(KJ)	Isle of Mull	lava	Basalt	0.07	0.08	0.17	0.14	1.61	1.71	0.23
BHI27(KJ)	Isle of Mull	lava	Basalt	0.21	0.11	0.15	0.08	3.49	1.95	0.84
BHI3(KJ)	Isle of Mull	lava	Basalt	0.04	0.07	0.11	0.07	5.45	2.22	0.98
BHI30(KJ)	Isle of Mull	lava	Basalt	0.81	0.79	1.47	0.43	7.49	7.42	0.78
BM10	Isle of Mull	lava	Basalt	1.00	0.90	1.47	0.38	4.63	1.65	1.01
BM12(KJ)	Isle of Mull	lava	Basalt	0.05	0.10	0.13	0.11	1.66	1.86	0.29
BM14(KJ)	Isle of Mull	lava	Basalt	0.53	0.51	0.64	0.31	7.41	4.03	0.56
BM15(KJ)	Isle of Mull	lava	Basalt	0.81	0.80	1.01	0.35	7.45	6.45	0.90
BM18	Isle of Mull	lava	Basalt	0.03	0.06	0.10	0.08	1.53	0.70	0.64
BM2	Isle of Mull	lava	Basalt	0.05	0.08	0.18	0.12	3.25	1.62	1.72
BM20	Isle of Mull	lava	Basalt	0.04	0.06	0.10	0.07	1.63	1.68	2.20
BM23	Isle of Mull	lava	Basalt	0.15	0.21	0.36	0.14	2.86	1.54	0.99
BM24	Isle of Mull	lava	Basalt	0.28	0.30	0.46	0.19	4.03	1.72	0.90
BM26	Isle of Mull	lava	Basalt	0.26	0.30	0.45	0.20	4.19	2.25	3.45
BM28	Isle of Mull	lava	Basalt	0.13	0.16	0.23	0.11	2.15	1.78	1.29
BM30	Isle of Mull	lava	Basalt	0.02	0.02	0.07	0.06	1.39	1.20	1.72
BM32	Isle of Mull	lava	Basalt	0.02	0.02	0.07	0.06	1.12	0.82	0.61
BM35	Isle of Mull	lava	Basalt	0.03	0.03	0.06	0.10	1.42	1.13	1.53
BM37	Isle of Mull	lava	Basalt	0.03	0.02	0.10	0.10	1.38	0.89	1.34
BM39	Isle of Mull	lava	Basalt	0.09	0.12	0.22	0.20	1.94	0.98	0.25
BM40	Isle of Mull	lava	Basalt	0.12	0.15	0.25	0.10	2.28	0.90	0.55
BM42	Isle of Mull	lava	Basalt	0.15	0.13	0.27	0.11	1.81	0.87	0.82
BM5(KJ)	Isle of Mull	lava	Basalt	0.14	0.10	0.21	0.10	3.50	4.97	0.35
BM6	Isle of Mull	lava	Basalt	0.18	0.16	0.32	0.15	4.06	1.99	2.19
BM6(KJ)	Isle of Mull	lava	Basalt	0.27	0.14	0.40	0.11	4.01	3.12	0.59
BM6A(KJ)	Isle of Mull	lava	Basalt	0.22	0.15	0.29	0.14	14.48	2.87	0.80
BM7(KJ)	Isle of Mull	lava	Basalt	0.38	0.37	0.71	0.28	5.12	5.26	1.12
BM8(KJ)	Isle of Mull	lava	Basalt	0.06	< d.t.	< d.t.	0.06	13.08	1.79	0.64
MR10(KJ)	Isle of Mull	lava	Basalt	0.36	0.40	0.60	0.19	4.42	2.98	13.02
MR11(KJ)	Isle of Mull	lava	Basalt	0.57	0.51	0.75	0.25	6.38	4.26	1.43
MR13(KJ)	Isle of Mull	lava	Basalt	0.24	0.32	0.45	0.18	5.76	3.81	1.20
RM_7	Isle of Rum	lava	Basalt	0.12	0.09	0.19	0.22	2.01	2.57	0.52
SK_14	Isle of Skye	lava	Basalt	0.14	0.36	0.69	0.41	1.40	1.52	1.57
SK_23	Isle of Skye	lava	Basalt	0.03	0.23	0.42	0.48	3.16	1.39	0.79
SK_30	Isle of Skye	lava	Hawaiite	0.04	0.09	0.16	0.09	0.65	0.54	0.09
SK_31	Isle of Skye	lava	Baselt	0.05	0.09	0.46	0.27	9.36	1.36	0.30
SK_32	Isle of Skye	lava	Basalt	0.05	0.05	0.11	0.10	0.65	0.27	0.08
SK_33	Isle of Skye	lava	Hawaiite	0.04	0.07	0.35	0.18	1.24	1.17	0.24
SK_37	Isle of Skye	lava	Mugearite	0.05	0.23	0.51	0.54	8.99	15.15	2.90
SK_38	Isle of Skye	lava	Hawaiite	0.04	0.04	0.11	0.07	0.65	0.42	0.39
SK_41	Isle of Skye	lava	Basalt	0.03	0.19	0.24	0.16	3.18	2.35	0.42
SK_42	Isle of Skye	lava	Mugearite	0.11	0.16	0.22	0.17	0.86	0.64	0.18
SK_44	Isle of Skye	lava	Basalt	0.23	0.48	0.66	0.35	2.91	2.78	0.34
SK_46	Isle of Skye	lava	Hawaiite	0.06	0.06	0.14	0.14	0.63	0.45	0.17
SK_47	Isle of Skye	lava	Picrobasalt	0.24	0.25	0.33	0.17	1.92	1.58	0.43
SK_66	Isle of Skye	lava	Basalt	0.39	0.45	0.75	0.31	4.08	2.86	6.43
P10	Isle of Mull & Morvern	plug	Dolerite	0.03	0.05	0.19	0.11	0.99	2.16	3.61
P11	Isle of Mull & Morvern	plug	Dolerite	0.03	0.10	0.21	0.23	1.40	1.05	0.31
P21	Isle of Mull & Morvern	plug	Dolerite	0.13	0.26	0.26	0.17	2.29	1.93	1.77
P27	Isle of Mull & Morvern	plug	Dolerite	0.08	0.13	0.18	0.09	0.90	0.60	1.12
P28	Isle of Mull & Morvern	plug	Dolerite	0.36	0.28	0.39	0.19	4.87	2.96	3.53
P29	Isle of Mull & Morvern	plug	Dolerite	0.67	0.36	0.50	0.23	4.62	3.48	1.44
P30	Isle of Mull & Morvern	plug	Dolerite	0.10	0.11	0.13	0.11	0.45	0.70	1.24
P34	Isle of Mull & Morvern	plug	Dolerite	0.09	0.21	0.26	0.41	6.30	11.79	4.96
P55	Isle of Mull & Morvern	plug	Dolerite	0.06	0.09	0.21	0.36	4.51	13.46	6.05
P6	Isle of Mull & Morvern	plug	Dolerite	0.05	0.11	0.16	0.13	0.73	0.98	0.26
P9	Isle of Mull & Morvern	plug	Dolerite	0.04	0.05	0.12	0.07	0.41	0.53	0.32
MORB	Atlantic Mid-Ocean Ridge		(Bezos *et al.,* 2005)		0.04	0.07		0.53	0.92	

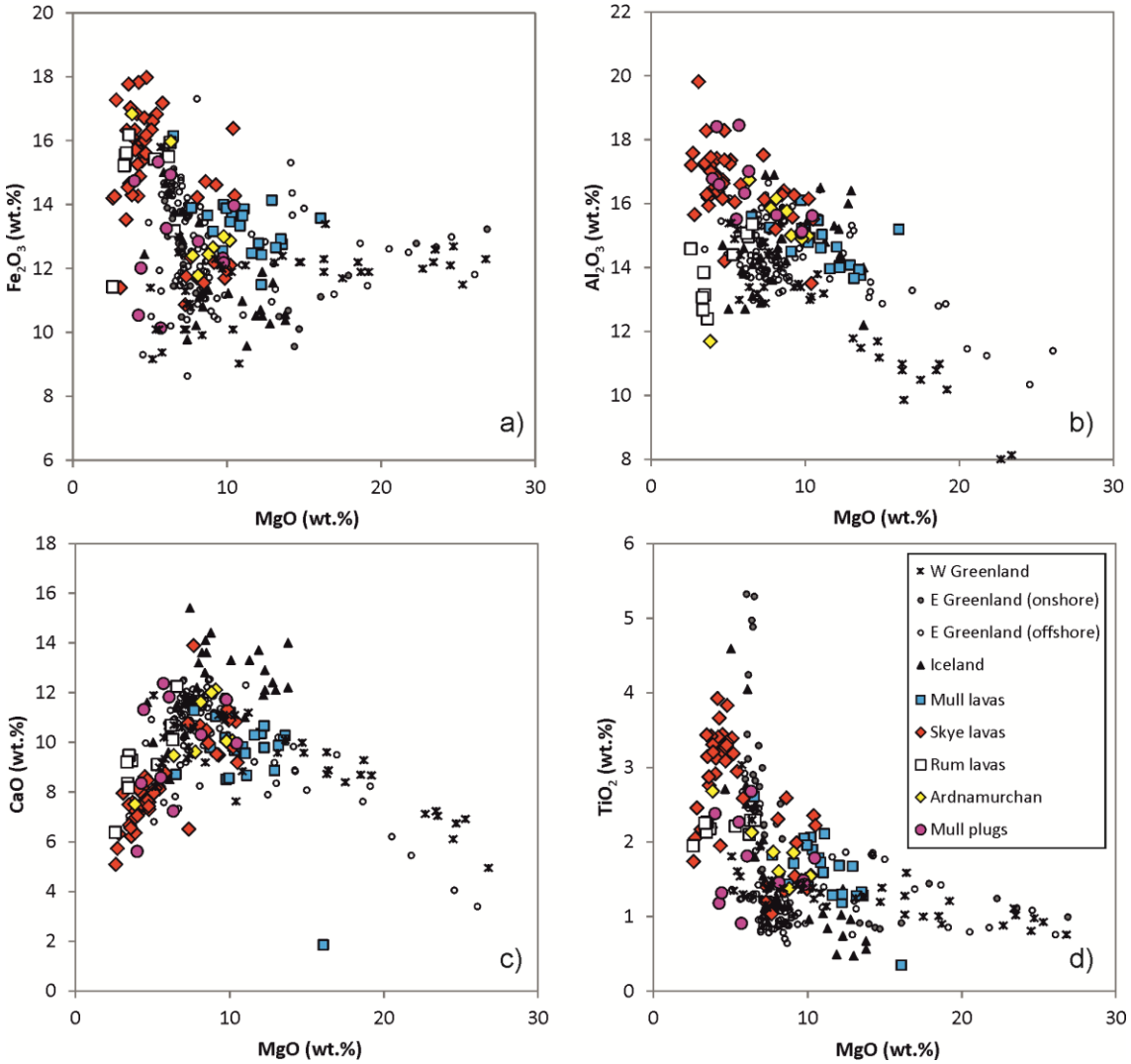

Figure 10.4. Bivariant plots for major elements (anhydrous) vs. MgO (anhydrous) for BPIP lavas (this study; Kerr, 1993), and east Greenlandic, SDRS and Icelandic lavas (Lightfoot *et al.,* 1997; Philipp *et al.,* 2001 and references therein; Momme *et al.,* 2002b; 2003; 2006 and references therein).

10.4. Geochemistry of NAIP and BPIP volcanics

Our results are compared with basaltic lavas collected and analysed for PGE by similar fire assay methods, from onshore Greenlandic plateau suites: west Greenland, Disko Island (Keays & Lightfoot, 2007); east Greenland, the Sortbre Profile in the Kangerlussuaq and Blosseville Kyst areas (Momme *et al.,* 2002b; 2006). Further comparison is made with PGE abundances in the seaward dipping reflector sequence offshore of southeast Greenland (Philipp *et al.,* 2001) and basaltic lavas from Iceland (Momme *et al.,* 2003). Further Au data for Iceland and the Reykjanes Ridge was used for comparison (Webber *et al.,* 2013).

10.4.1. Major elements and petrography

A selection of anhydrous major element variation diagrams (vs. MgO) for suites of lavas and plugs from the BPIP (Mull, Skye, Rum and Ardnamurchan) are shown in Figures 10.4a-d. Data from Greenlandic lavas (onshore plateau basalts and offshore seaward dipping reflector sequences) and Icelandic lavas are also shown for comparison. These major element diagrams broadly define fractionation trends indicating fractionation of olivine and plagioclase, as has previously been detailed for these sequences (Kerr, 1995; Kerr *et al.,* 1995; Fram & Lesher, 1997; Lightfoot *et al.,* 1997; Saunders *et al.,* 1998; Tegner *et al.,* 1998a,b; Philipp *et al.,* 2001; Momme *et al.,* 2003). Overall Figure 10.4 demonstrates that the BPIP, Greenlandic and Icelandic volcanics are directly comparable in terms of lithological classification and major element composition.

10.4.2. Chalcophile elements

All chalcophile elements in Figures 10.5a-d have been plotted relative to Mg# (i.e., MgO/(MgO + FeO)) as a proxy for magma fractionation[1]. High Mg# lavas have high Ni, Cr and Co concentrations, but some of the lowest Cu abundances. Overall Ni, Cr and Co concentrations in BPIP magmas (according to Mg#) overlap those of Greenlandic and Icelandic lavas. Some west Greenlandic lavas with high Mg# (> 50) have anomalously low Ni concentrations (Fig. 10.5a). In contrast, Cu abundances in a significant number of BPIP lavas and plugs do not fully overlap other NAIP compositions (Fig. 10.5b), and some high-Mg# west Greenlandic lavas also have anomalously low Cu concentrations. All onshore east Greenlandic lavas follow an exponential negative trend of increasing Cu content with decreasing Mg#. The majority of offshore east Greenlandic lavas and Icelandic lavas follow a similar trend to onshore east Greenlandic lavas,

[1] Anhydrous FeO content was calculated from anhydrous Fe_2O_3 (total) analytical results according to the following conversion: $[(Fe_2O_3^{Total} – (TiO_2 + 1.5)/1.1)]$ (Irvine & Baragar, 1971).

although these are more scattered. However the BPIP lavas and plugs appear to fall into one of two categories in Figure 10.5b – a cluster that overlaps NAIP lavas for higher Mg# samples vs. a cluster that have lower Cu concentrations (either below this trend at higher Mg# or for samples with Mg# < 50). This division in BPIP samples does not fall rigorously within any one lava suite (e.g., Mull vs. Skye) although most Mull lavas overlap with NAIP.

10.4.3. Platinum-group elements and Au

Chondrite-normalised (McDonough & Sun, 1995) multi-element patterns for PGE and Au are shown in Figures 10.6a-d for the BPIP lavas and plugs along with comparative patterns for Icelandic and Greenlandic lavas (Figures 10.6e-h). It is clear that NAIP lava PGE abundances are typically elevated above MORB (Bezos *et al.,* 2005) – see Table 10.1.

All NAIP samples have fractionated PGE such that Rh, Pt and Pd (Pd-group PGE; PPGE) are enriched relative to Os, Ir and Ru (Ir-group PGE; IPGE), however the relative PGE abundances in each sample suite vary considerably. With the exception of two Skye lava samples, chondrite-normalised Pd is similarly slight enriched over Pt in Figure 10.6b. Lava samples from Mull fall into two categories – some have negative Pd anomalies relative to Pt, while the rest have nearly flat Pt to Pd normalised trends (Fig. 10.6c). Normalised Os and Ir concentrations in some Mull lavas exceed 0.001 x chondrite (0.48 ppb; McDonough & Sun, 1995) whereas lavas from other areas fall consistently below this. In all BPIP lavas, normalised IPGE patterns are relatively flat (with $(Ru/Os)_N$ ranging 0.49 to 6.8), although there is variability in Os vs. Ir. For the BPIP lava samples, normalised Au content is highly variable – most lavas have slight positive Au anomalies (Fig. 10.6e). The normalised PGE patterns for the Mull doleritic plugs broadly overlaps that of the Mull lavas, although the plugs lack any negative Pd anomalies and generally have higher Au. Overall, with the exception of Au, Pd and Pt, all BPIP lava compositions overlap Icelandic and Greenlandic (continental) lavas, although the systematic negative Ru anomaly of the Greenlandic ODP lavas (Fig. 10.6g) has not been found in any of BPIP samples.

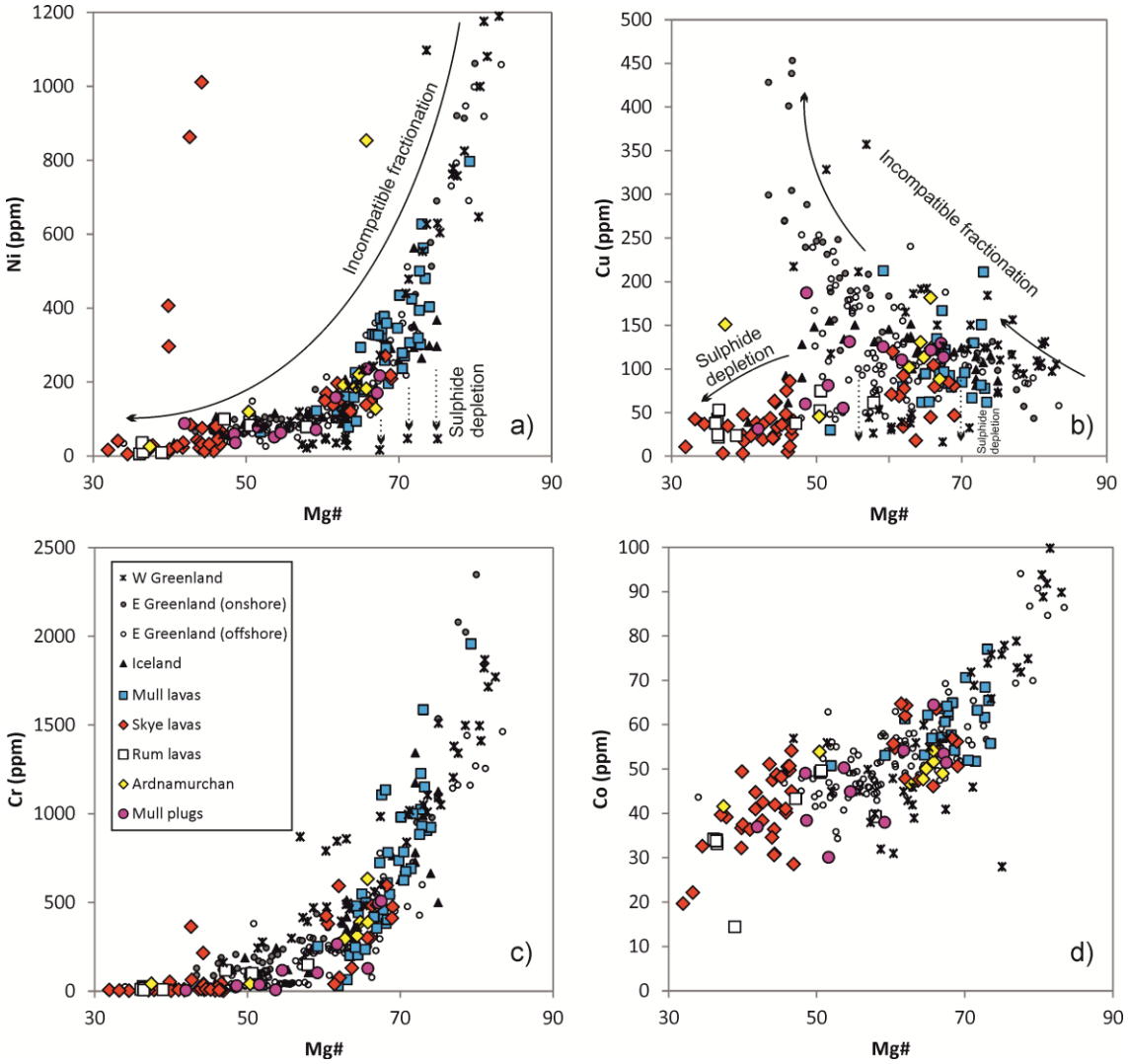

Figure 10.5. Bivariant plots for chalcophile elements vs. Mg#; (a) Ni, (b) Cu, (c) Cr, (d) Co. Symbols and data sources as in Figure 10.4. Silicate fractionation and S-saturation trends indicated schematically in (c). See text for details of Mg# calculation.

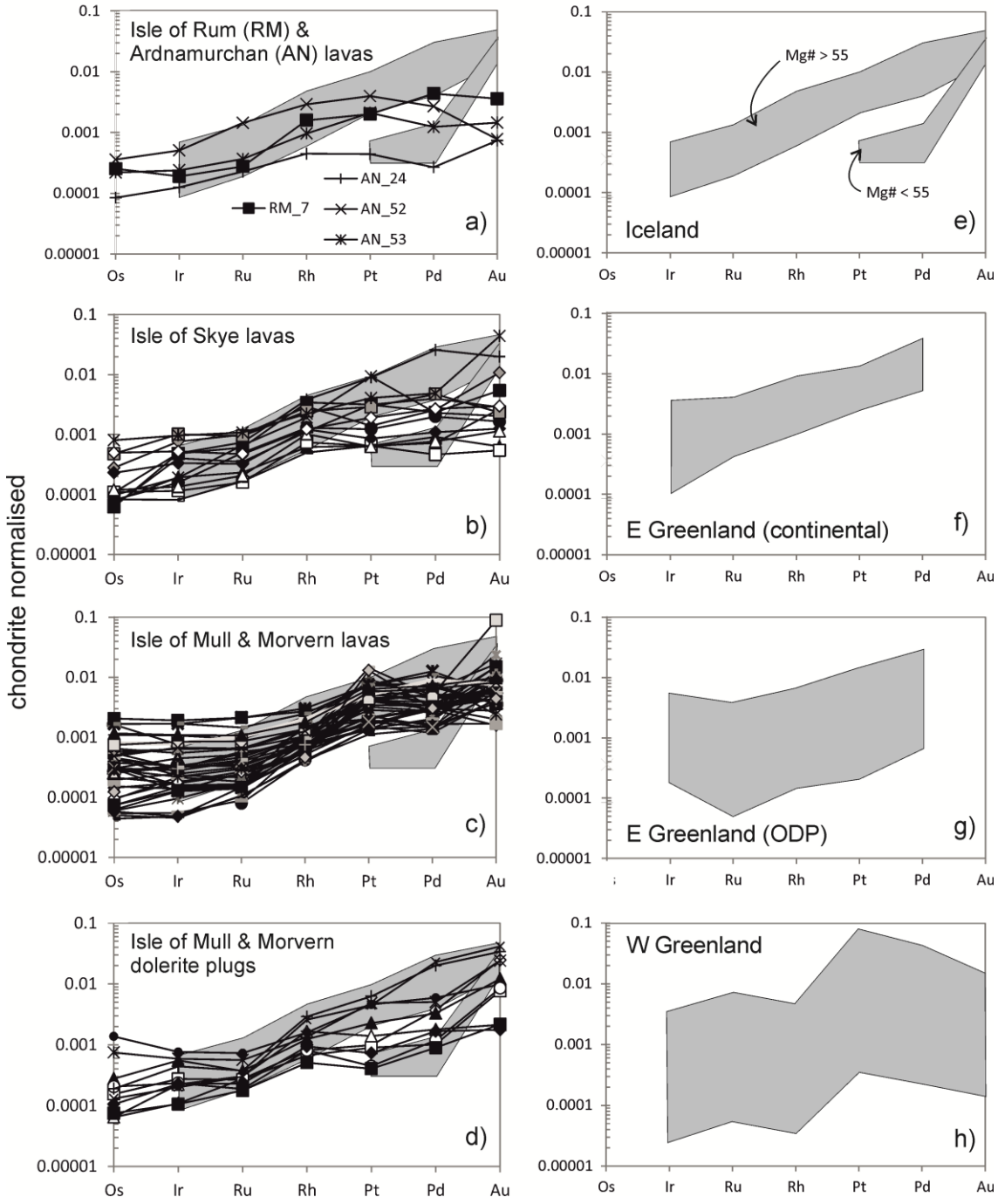

Figure 10.6. Chondrite normalised (McDonough & Sun, 1995) PGE multi-element diagrams for BPIP lavas analysed during this study (a to d) and equivalent plots for Icelandic, east and west Greenlandic lavas (e to h) from Philipp *et al.* (2001), Momme *et al.* (2002b, 2003), Keays & Lightfoot (2007). Two distinct spidergram patterns defined for Icelandic lavas, according to Mg# (e).

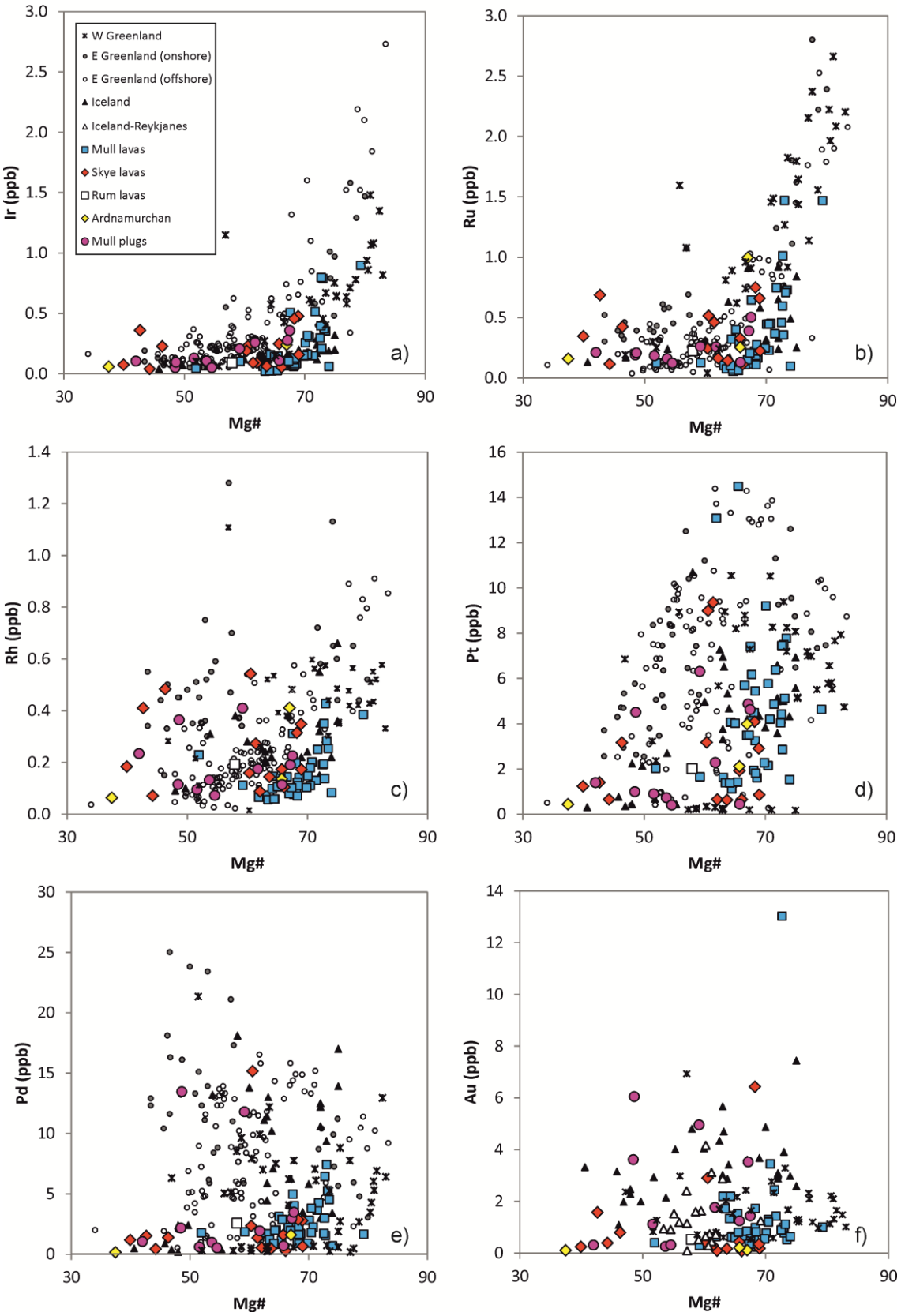

Figure 10.7. Bivariant plots for PGE vs. Mg#; (a) Ir, (b) Ru, (c) Rh, (d) Pt, (e) Pd, (f) Au. Symbols and data sources as in previous figures and as well as Au data from Iceland-Reykjanes Ridge (Webber *et al.,* 2013).

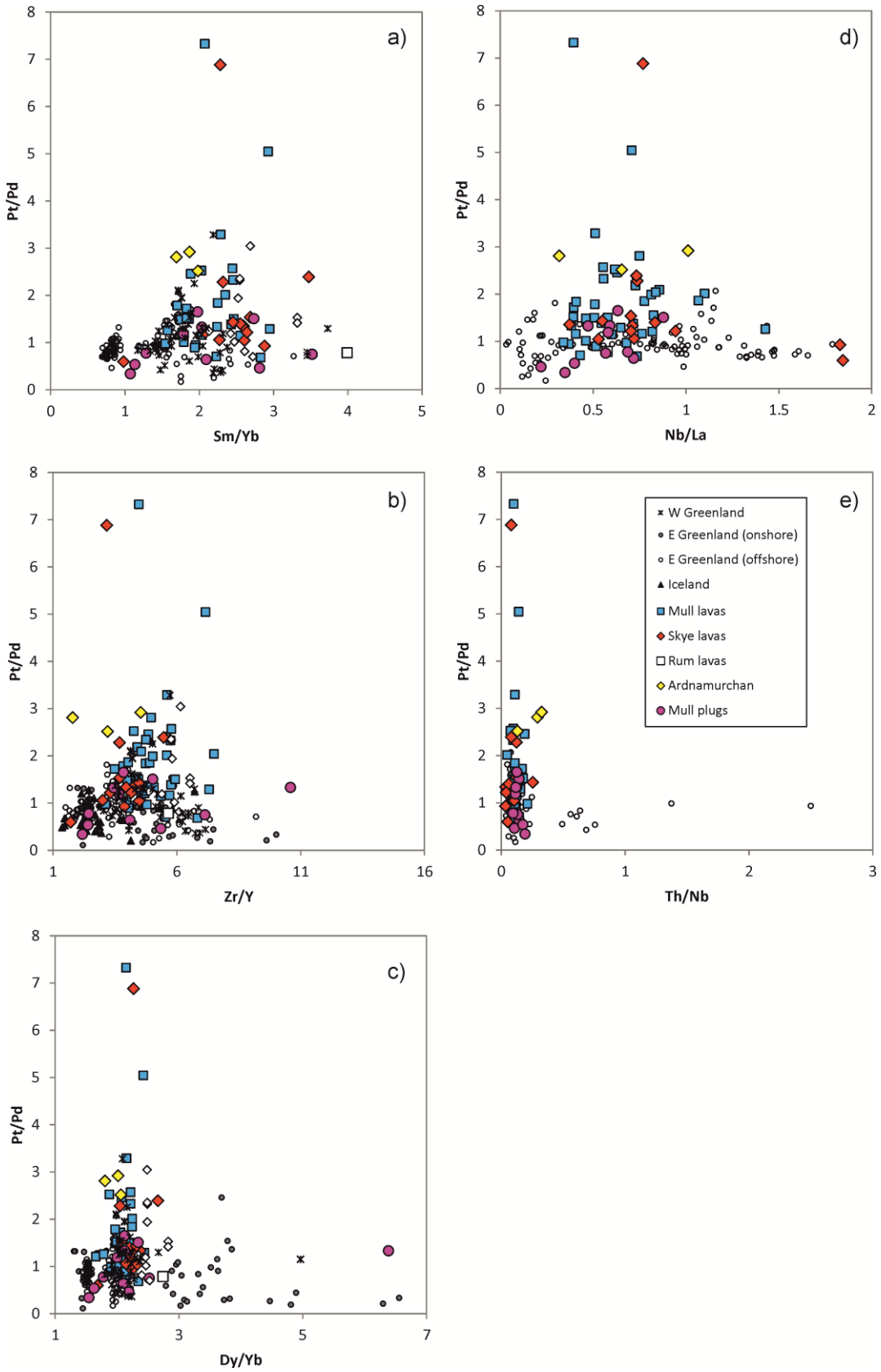

Figure 10.8. Bivariant plots for Pt/Pd ratio vs. (a) Sm/Yb, (b) Zr/Y, (c) Dy/Yb, (d) Nb/La, (e) Th/Nb. Symbols and data sources as in previous figures.

The variation in PGE and Au abundances with Mg# are shown in Figure 10.7a-f. For low Mg# (< 65) BPIP samples, Ir and Ru concentrations are consistently low (< 0.25 ppb for Ir, < 0.5 ppb), but at Mg# > 65, Ir and Ru abundances sharply increase in line with existing data from Greenland. By contrast, Rh, Pt and Pd abundances are more variable and scattered when plotted relative to Mg# (Figs. 10.7c-e). In Figures 10.7c-d, there is a broad positive correlation between increasing Mg# and increasing Rh and Pt concentrations, however this does not appear to be the case for Pd. Overall, BPIP lavas and plugs have lower absolute total PGE concentrations at Mg# > 50, in comparison to Greenlandic and Icelandic equivalents. Au abundances in BPIP and W Greenland samples are highly variable and do not correlate with Mg#, unlike the broad positive correlation for Icelandic lavas. However there is no correlation for Icelandic-Reykjanes Ridge lavas (Fig. 10.7f).

We find no correlation between Pt/Pd ratio with Sm/Yb or Zr/Y (as proxies for mantle source region fertility – see Fig. 10.8a-b) nor with Dy/Yb (as a proxy for the presence of garnet in the mantle source region – Fig. 10.8c). There is also no correlation between Pt/Pd and Nb/La or Nb/Th (Fig. 10.8d-e) as proxies for crustal contamination across NAIP lavas.

Partitioning of PGE into sulphide liquid and silicate minerals can be identified by bivariant correlations between PGE and other chalcophile elements, as shown in Figure 10.9a-d. For example, Ru is incompatible into olivine however Ir is weakly compatible (Capobianco *et al.*, 1991; Brenan *et al.*, 2002; Righter *et al.*, 2004) and there is a positive correlation between in Ir and Ni in Figure 10.9a. Rh and Ru have been experimentally shown to be compatible in Cr-spinel (e.g., Page *et al.,* 2012 and references therein) and there is a positive correlation between Ru and Cr in Figure 10.9b. Cu and Pd are incompatible in silicate minerals but partition strongly into immiscible sulphide liquids (D_{Cu} ~ 1000; D_{Pd} ~ 100,000; Mungall & Brenan, 2014) formed during the S-saturation of silicate magmas. Pd and Cu have a positive correlation for most BPIP samples, although it is a broad correlation (Fig. 10.9c). By contrast, Greenlandic lavas are highly variable and scattered, and Icelandic lavas have a range of Pd concentrations but restricted Cu abundances. A very broad positive correlation is observed between Au and Pd (Fig. 10.9d). However, most BPIP lavas have lower Au abundances than Icelandic lavas.

The Cu/Pd ratio of BPIP lavas ranges 8,000 to 1,000,000 and when plotted against Pd concentration these values overlap with east Greenlandic (offshore), west Greenlandic and Icelandic lavas (Fig. 10.10a). However, east Greenlandic (onshore) lavas form a tigher cluster of Cu/Pd ratios (~ 10,000 to 40,000). Although both elements are compatible into sulphide liquid,

Pd partitions more strongly than Cu (Mungall & Brenan, 2014). Hence a sulphide accumulation trend vs. sulphide depletion magma trend is defined by Cu/Pd ratio. Lavas have been further subdivided according to Mg# in Figures 10.9b-d. The clustered east Greenlandic (onshore) lavas with limited Cu/Pd ratio indicate that for this suite, S-saturation did not play a major role in changing chalcophile element concentration of ascending silicate magmas prior to eruption as lavas. Hence Cu/Pd ratio is 'unmodified' in east Greenlandic (onshore) lavas, irrespective of the degree of silicate magma fractionation. However, evidence of chalcophile element depletion can be identified in most BPIP samples (particularly for lavas with Mg# < 70) and west Greenlandic lavas, as well as some east Greenlandic (offshore seaward dipping reflector sequence) lavas. Additionally some east Greenlandic (offshore) and Icelandic lavas have Cu/Pd ~ 6000 or within range of primitive mantle (McDonough & Sun, 1995) – see Figures 10.9a-d.

Pd/Ir ratio can be used as a proxy for the degree of partial melting in the mantle source region of magmas, indicating whether melting has exhausted Cu-rich (PPGE-bearing) sulphides and begun to incorporate higher temperature IPGE-bearing MSS or metal alloys. With very few exceptions, NAIP and BPIP samples have Pd/Ir ratios > primitive mantle (McDonough & Sun, 1995). However BPIP samples do not overlap with the majority of other NAIP lavas, and sit at systematically lower Ir concentrations at equivalent Pd/Ir ratios (Fig. 10.11).

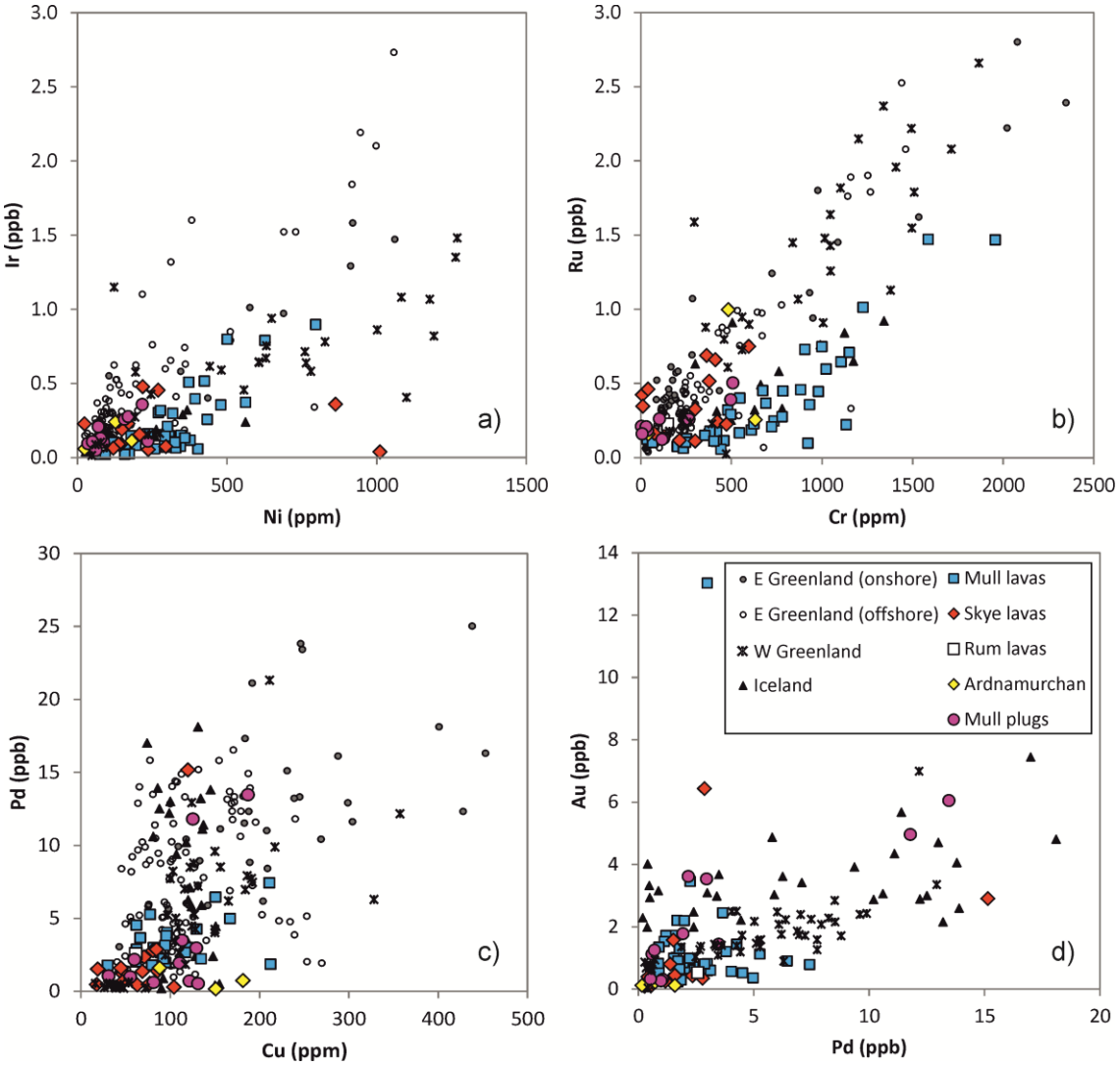

Figure 10.9. Bivariant plots for PGE vs. chalcophile elements, paired according to partitioning behaviour; (a) Ir vs. Ni, (b) Ru vs. Cr, (c) Pd vs. Cu, (d) Au vs. Pd. Symbols and data sources as in previous figures.

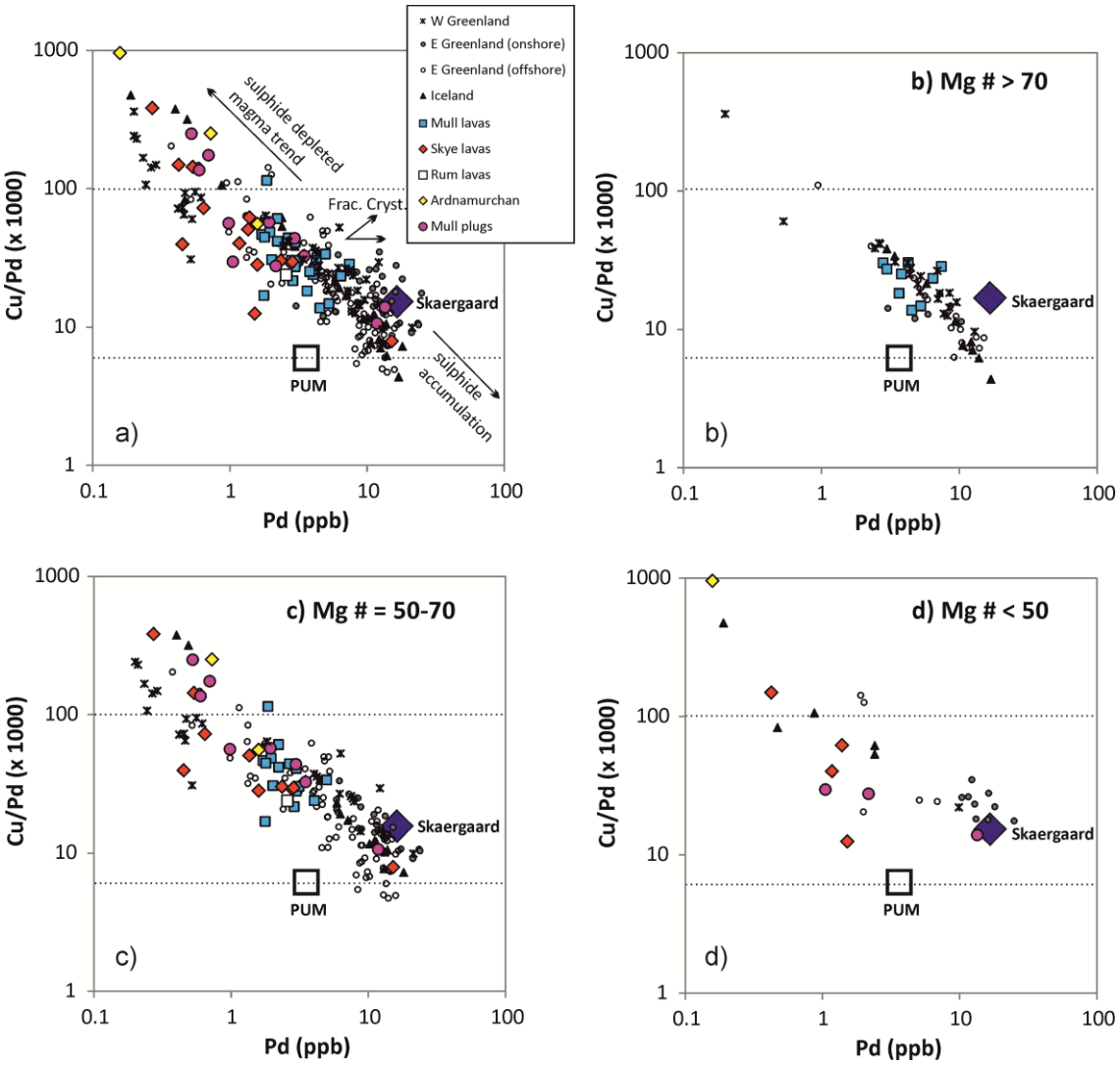

Figure 10.10. PGE ratio plots. Cu/Pd vs. Pd according to Mg#; (a) all lavas, (b) lavas with Mg# > 70, (c) lavas with Mg# 50-70, (d) lavas with Mg# < 50. Primitive mantle from McDonough & Sun (1995). Sulphide depletion vector calculated from silicate/sulphide partition coefficients (Mungall & Brenan, 2014) for R factors (silicate/sulphide ratio) of 100 to 100,000. Skaergaard chilled composition (blue diamond) based on 265 ppm Cu (calculated by Nielsen *et al.,* 2005) and 17 ppb Pd (chilled margin analysis by Vincent & Smales, 1956).

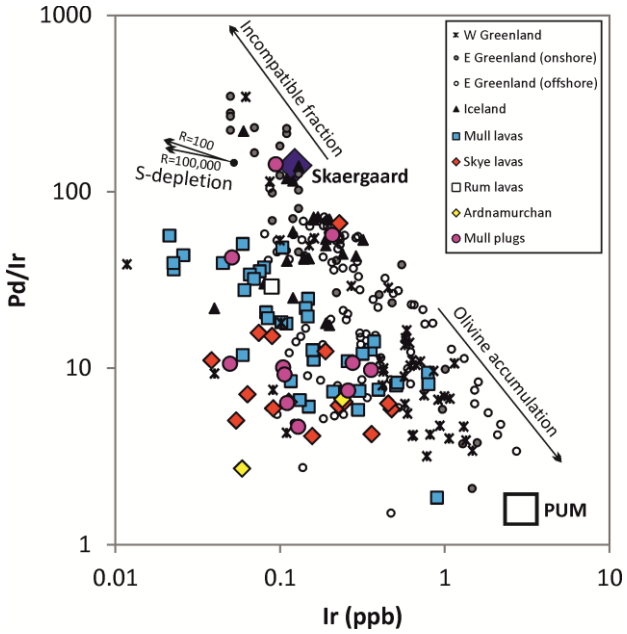

Figure 10.11. Pd/Ir vs. Ir for all NAIP and BPIP lavas. Primitive mantle from McDonough & Sun (1995). Sulphide depletion vector calculated from silicate/sulphide partition coefficients (Mungall & Brenan, 2014) for R factors (silicate/sulphide ratio) of 100 to 100,000. Skaergaard chilled composition (blue diamond) based on 0.1 ppb Ir (estimated) and 17 ppb Pd (chilled margin analysis by Vincent & Smales, 1956).

10.5. Discussion

The partitioning behaviour of chalcophile elements can be used as further evidence of fractional crystallisation throughout magma ascent, in a similar fashion to major elements. For example, the decrease in Ni with decreasing Mg# in Figure 10.5a reflects incremental removal of Ni during olivine fractionation, although there are anomalously elevated Ni contents in four Skye lava samples and one Ardnamurchan lava, which do not fit this fractionation pattern. The anomalously low Ni concentrations in some high-Mg# west Greenlandic lavas suggest that Ni was depleted in these due to prior S-saturation. Hence sulphide depletion must have occurred early in the fractionation of these lavas (Fig. 10.5a). Co weakly partitions into olivine such that the positive correlation between Co and Mg# broadly fits olivine fractionation, although this is more scattered than for Ni. Cr partitions into spinel and hence the decrease in Cr abundance with decreasing Mg# reflects spinel fractionation. Cu is incompatible in silicate minerals so that as a silicate magma fractionates, the concentration of Cu in the remaining silicate magma increases sharply. As labelled in Figure 10.5b, a significant proportion of BPIP lavas display low Cu concentrations (at lower Mg#) that does not fit with typical silicate fractionation, and instead indicates prior sulphide depletion. If a silicate magma achieves S-saturation and

exsolves an immiscible sulphide liquid, Cu partitions strongly into the sulphide ($D^{sul/sil}$ ~ 1000), leaving the remaining silicate magma (which ascends and erupts to form the lavas) depleted in Cu (e.g., Andersen *et al.,* 2002). We identify this feature in most BPIP lavas with Mg# < 60, as well as minor Icelandic and east Greenlandic SDRS lavas. In addition some mafic lavas from Skye (Mg# 60-70) and west Greenland (Mg# 55-75) have anomalously low Cu contents and we suggest these also signify S-saturation prior to eruption.

Various studies have shown that IPGE (such as Ir and Ru) are high-temperature PGE and mainly hosted by Fe-rich monosulphide solid solution (MSS) commonly included in silicate minerals in the mantle, or as refractory metal alloys of Os-Ir-Ru-Pt (Brenan & Andrews, 2001; Ahmed & Arai, 2002; Sattari *et al.*, 2002; Bockrath *et al.*, 2004b). By contrast PPGE (such as Rh and Pd) are predominantly hosted by interstitial Cu-rich mantle sulphides (Sattari *et al.,* 2002; Bockrath *et al.,* 2004a; Lorand *et al.,* 2008). During mantle melting, PPGE are preferentially incorporated into magmas over IPGE (which are retained in unmelted monosulphide solution (MSS) and metal alloy residues), so that the initial Pd/Ir ratio is high and PGE spectra of magmas are positively fractionated (Keays, 1982; Barnes *et al.,* 1988; Barnes, 1990; McDonald *et al.,* 1995; Maier & Barnes, 2004). With increasing degrees of partial melting, the Pd/Ir ratio of partial melts increases until mantle sulphides become exhausted in the source region (Naldrett, 2011). If partial melting exceeds this point of sulphide exhaustion, IPGE-bearing alloys enter the melt while Pd becomes diluted, thereby lowering the Pd/Ir ratio of the magma again. This effect is evident in Figures 10.7a-b, where high Mg# numbers reflect a higher degree of mantle partial melting, enough to begin to significantly melt and incorporate IPGE (at Mg# > 65). Additionally some Greenlandic (offshore) and Icelandic lavas have Cu/Pd ~ 6000 (Fig. 10.10a) within range of primitive mantle (McDonough & Sun, 1995) and coupled with their high concentrations of Cu and Pd, this may suggest that sulphides were largely exhausted from the mantle source region during partial melting.

Palladium partitions very stongly into immiscible sulphide liquid and unlike Pt, tends to remain within the sulpide throughout further fractionation and cooling, rather than forming a discrete Pt-bearing mineral phase or platinum-group mineral (e.g., Holwell & McDonald, 2010 and references therein). The majority of BPIP samples have significantly lower Pd concentrations than wider NAIP lavas of equivalent Mg# (Fig. 10.7e) and this may be a reflection of a previous S-saturation event in BPIP lavas, such that residual silicate magmas which erupted as lavas were depleted in Pd during ascent. This feature can also be identified in some west Greenlandic lavas. Evidence of a systematic S-saturation event prior to BPIP lava eruption is

also evident in Cu/Pd, particularly in lavas with Mg# < 70 (e.g., Fig. 10.10c). Pd/Ir vs. Ir (Fig. 10.11) clearly demonstrates a systematic offset between BPIP lavas and Greenlandic/Icelandic lavas, such that BPIP lavas are strongly controlled by sulphide depletion prior to their eruption, whereas the majority of Greenlandic and Icelandic lavas are controlled by silicate magma processes only (i.e., fractional crystallisation and olivine accumulation).

10.6. The S-saturation status for BPIP and NAIP lavas – regional mineralisation potential

The occurrence of S-saturation in a magma body may be assessed by the concentration of chalcophile elements within it (e.g., Andersen *et al.,* 2002). Crustal contamination of magmas can trigger S-saturation, particularly if the country rocks contain significant amounts of S in the form of sulphides or sulphates (e.g., Li *et al.,* 2002; Ripley *et al.,* 2003; Naldrett, 2004; Keays & Lightfoot, 2009; Naldrett, 2011). Cu is incompatible in silicate minerals but strongly compatible in sulphide liquids. Therefore during S-undersaturated fractional crystallisation of silicate magma, Cu concentration increases sharply in the residual melt. If S-saturation is achieved, the immiscible sulphide liquid formed will strongly deplete the Cu content of the residual silicate magma (i.e., a sulphide depleted trend).

Trends relating to S-undersaturated fractional crystallisation and sulphide depletionhave been identified in BPIP lava suites, including the two main lava series on Mull and Skye (see Fig. 10.5b). Some Mull lavas are S-undersaturated (e.g., Fig. 10.10b), whereas all Skye lavas have experienced S-saturation prior to eruption and follow a sulphide depletion magma trend (e.g., Fig. 10.10c). While Mull lavas generally have higher Mg# and are therefore less fractionated than Skye lavas, the fact that some Skye lavas with Mg# 60-70 also show anomalously low Cu concentrations is noteworthy. Both the Mull and Skye lavas fields erupted through thick lower crustal sequences of Lewisian basement and Moine metasediments, with variable upper crustal sequences of Torridonian and Triassic rocks of the Hebrides Basin. However, current exposures on the Isle of Mull have only thin upper crustal S-rich Lower Jurassic sedimentary units (shales and mudrocks) on the periphery of the island, and it is uncertain how much of this material underlies the lava field. By contrast, a thick package of S-rich Jurassic sediments is prevalent on the Isle of Skye. Thus, we suggest these Jurassic S-rich mudrocks were the main control on ascending BPIP magmas achieving S-saturation during ascent. This is a particularly relevant observation in the context of other NAIP settings.

The vast majority of offshore and onshore east Greenlandic lavas display S-undersaturated (i.e., silicate fractionation only) trends on Cu vs. Mg# plots (see Fig. 10.5b and Andersen *et al.,* 2002). In the case of onshore east Greenlandic lavas, this is also supported by Cu/Pd ratio (Fig. 10.10). Although crustal sediments such as Cretaceous-Palaeocene marine shales, sandstones and marls (Soper *et al.,* 1976; Larsen *et al.,* 2001) are available for contamination on the east Greenlandic continental margin, there are thought to be fewer S-rich lithologies (i.e., a lesser volume of S-rich lithologies and less lateral extent) in comparison to the Scottish BPIP and Mesozoic Hebridean Basin. Icelandic lavas predominantly show a S-undersaturated trend, although some sulphide depletion is recorded in lavas with lower Mg#. Using Mg# as a proxy for fractional crystallisation (e.g., Fig. 10.10), and in the absence of S sources from continental crust on Iceland, this limited S-saturation must be controlled by fractional crystallisation and/or magma mixing. It has been noted by Lightfoot *et al.* (1997) and Andersen *et al.* (2002) that lavas in west Greenland display geochemical features of both sulphide depletion and S-undersaturated silicate fractionation, and like the BPIP, different parts of these lava fields are dominated by predominantly lavas which underwent S-saturation prior to eruption.

The timing of S-saturation is critical in terms of PGE and metal enrichment in magmatic conduits underlying lava fields, and hence the potential for Norilsk-Talnakh style conduit-hosted orthomagmatic Ni-Cu-PGE mineralisation. Lavas near the base of the Vaigat Formation in west Greenland have the most marked crustal contamination signatures (based on lithophile element ratios and radiogenic isotope compositions – see Lightfoot *et al.,* 1997 and Saunders *et al.,* 1997 and references therein). However, because they were among the first lavas to be erupted in the province, Lightfoot *et al.* (1997) suggest that they had limited potential for magmatic mixing and within-conduit 'upgrading' of metal concentrations prior to eruption. This is supported by the observation of high-Mg# lavas with low chalcophile abundances (e.g., Ni depletion – Fig. 10.5a). With sustained magma flow through a conduit, sulphide liquid that ponds within that conduit can become enriched in chalcophile elements, possibly to economic levels, due to its continued interaction with magma continuing to pass through the conduit (e.g., Kerr & Leitch, 2005). According to Lightfoot *et al.* (1997), magmatic conduits or basal intrusions relating to lavas of the Vaigat Formation provide limited potential for significant high tenor orthomagmatic mineralisation. However we suggest that this negates the 'recycling' of magmatic conduits elsewhere in the wider NAIP (i.e., re-activation on conduits with later eruptions) by later silicate magma batches represented by subsequent lavas, sustained flow through the conduit, and the complexity of localised conditions such as variable crustal contamination. For example, the close-association, both spatially and

temporally, of lavas fields in the BPIP shows that comparatively localised districts may have low vs. high S-contamination potential (for Mull and Skye respectively) and hence magmatic conduits underlying and feeding these lava fields may be similarly multifaceted. Therefore regional 'prospectivity', as determined by whether lavas experienced S-saturation or remained undersaturated, must take into account this variability.

In subsurface magmatic conduits, where sulphur has not degassed, S-isotopic studies ($\delta^{34}S$ and $\Delta^{33}S$) can identify the internal or external cause(s) for S-saturation. Hughes *et al.* (accepted, a – Chapter 11) assessed the whole-rock $\delta^{34}S$ signature of a suite of upper crustal narrow basaltic dykes and thick picritic sills intruded into Jurassic mudrocks on the Isle of Skye. Crustal S contamination from these S-rich mudrocks with characteristically light $\delta^{34}S$ can be clearly identified in these dykes, highlighting that crustal S contamination was prevalent in this part of the BPIP. Orthomagmatic sulphides with extremely light $\delta^{34}S$ occur deeper in the magmatic plumbing system in ultramafic volcanic plugs on the Isle of Rum (Power *et al.,* 2003; Hughes *et al.,* accepted, a – Chapter 11). Structural evidence discussed by Hughes *et al.* (under review, a – Chapter 12) suggest that the vertical/subvertical volcanic plugs on Rum erupted through Jurassic sedimentary units, becoming strongly contaminated with isotopically light crustal S, inducing S-saturation and forming an immiscible sulphide liquid which drained down through the partially crystallised conduit when activity ended (Hughes *et al.*, under review, a – Chapter 12).

Overall, the prevalence of fusible S-rich crustal rocks within the BPIP should be considered as a major exploration factor, both for the formation of immiscible sulphide liquids, but also for the collection or concentration of chalcophile elements including PGE in systems where magma input was sustained for long periods. The widespread identification of S contamination and saturation in upper crustal magmatic conduits (by $\delta^{34}S$) and lavas (by chalcophile element geochemistry) very clearly points to the presence of sulphides and enhanced mineralisation potential deeper within the Scottish BPIP magmatic plumbing system (as corroborated by Arndt, pers comm, 2014) and therefore represent thus far unexplored exploration targets.

10.7. Pt/Pd ratio of NAIP magmas throughout continental break-up

Systematic differences in Pt and Pd abundance between lava suites across the NAIP are evident in Figure 10.7. BPIP lavas predominantly have lower Pd concentrations (at equivalent Mg#) in comparison to most Greenlandic and Icelandic lavas (Fig. 10.7e), and Pt vs. Mg# for

BPIP lavas defines an entirely differently shaped trend to Greenlandic and Icelandic compositions, despite there being some overlap in the actual range of Pt (Fig. 10.7d). The sample preparation and analytical methodologies of our study for PGE in lavas are directly comparable to those of Philipp *et al.,* (2001), Momme *et al.,* (2002b), Momme *et al.,* (2003) and Keays & Lightfoot (2007). Therefore differences between Pd and Pt for the NAIP lava suites are unlikely to be due to analytical differences and appear to be true compositional features.

Plots of Pt vs. Pd (Figure 10.12) for lavas from the NAIP are particularly instructive in assessing the compositional differences between the various areas. Lavas from the BPIP and west Greenland have Pt/Pd ratios near chondrite (1.9) and fall along a positive trend (statistically significant, $r^2 > 0.89$; Figs. 10.11a-b). At higher concentrations of either of these elements (i.e., > 9 ppb Pt or Pd) more variability around a chondritic ratio is observed. Continental flood basalts from east Greenland (onshore) have extremely variable and scattered Pt/Pd ratios (Fig. 10.12c) but Pd is consistently enriched over Pt in comparison to BPIP and west Greenlandic lavas. east Greenlandic SDRS (offshore) lavas have a clear positive correlation ($r^2 > 0.88$) between Pt and Pd, but with a different sub-chondritic Pt/Pd ratio (Fig. 10.12d). Icelandic lavas also have a positive correlation between Pt and Pd ($r^2 > 0.90$) but with a much lower Pt/Pd ratio (Fig. 10.12e) than the offshore east Greenland lavas.

All the lava suites discussed in this study compare transitional alkalic-tholeiitic (e.g., BPIP) and tholeiitic (e.g., Iceland) picrites and basalts (with minor andesites). The differences in Pt/Pd ratio do not correspond either with a particular compositional series of lavas, nor with fractionation. Similarly, during magma ascent, S-saturation will not significantly fractionate Pt from Pd, as both elements have similar partition coefficients and will be partitioned equally into an immiscible sulphide liquid. In the NAIP Pt/Pd ratio appears to correspond to the age of the lava suites (i.e., highest Pt/Pd ratio in the earliest lava suites of west Greenland and the BPIP vs. lowest Pt/Pd in recent Icelandic lavas). The question arises whether this temporal change in the Pt/Pd ratio is indicative of a change in the plume-composition or geodynamic setting of the North Atlantic through time: from the initial eruption of picritic and basaltic magmas during early (proto-Iceland) mantle plume impingement, throughout continental rifting, the formation of oceanic lithosphere, and ultimately to the modern plume-oceanic rift setting of Iceland (Fig. 10.12f).

Possible causes for a systematic change in magma PGE geochemistry related to tectonic setting and/or geodynamic environment through time may include: (a) the degree or depth of

partial melting; (b) changes in the mantle source region (i.e., enriched vs. depleted sources); (c) the melting regime and the shape of the melt column (i.e., cylindrical vs. triangular); (d) the mantle potential temperature; (e) the incorporation of deep mantle material in the plume; and/or (f) lithospheric contamination. Each of these possibilities is assessed below.

(a) Degree of partial melting

Relative proportions of fertile mantle PGE concentrations are approximately chondritic (Carlson, 2005), although lower than chondrite in actual concentration by a factor of approximately 100-1000, as indicated by mantle-derived peridotite xenoliths (e.g., Luguet *et al*., 2003; Lorand *et al*., 2008; Maier *et al.,* 2012 and references therein). During mantle melting, the first minerals to melt are sulphides, garnet and clinopyroxene, and so with increasing degrees of partial melting the amount of S in the melt increases until sulphides are exhausted in the mantle source region. However, the timing of sulphide exhaustion is dependent on whether an equilibrium batch melt, fractional melting, continuous melting, or dynamic melting model is used, and the shape and depth of the melting profile (e.g., Rehkamper *et al.,* 1999).

Partial melting of sulphide minerals in the mantle can be identified by fractionation of IPGE from PPGE, and therefore changes in Pd/Ir ratio (as previously outlined in Section 4.3). It is known from both experimental work and natural analogues of mantle materials that partial melting of sulphide phases such as MSS can produce Fe-rich MSS, Cu-Ni-Pd sulphide liquid with Fe-rich MSS and/or Ir-Pt alloys in the residue (e.g., Crocket, 2002; Luguet *et al.,* 2003; Peregoedeva *et al.,* 2004). This will not only fractionate Pd from Ir, but can also potentially fractionate Pd from Pt. However we have already established that the range in Pd/Ir for each of the NAIP lava suites broadly overlaps despite lower absolute Ir concentrations due to PGE removal in sulphide liquids (Fig. 10.11). Coupled with other melting proxies such as MgO content and Mg# (e.g., Figs. 10.4-10.5), a systematic change in Pt/Pd ratio related to the degree of mantle partial melting cannot be identified. Therefore this option is discounted as being a credible control on Pt-Pd ratio across the NAIP.

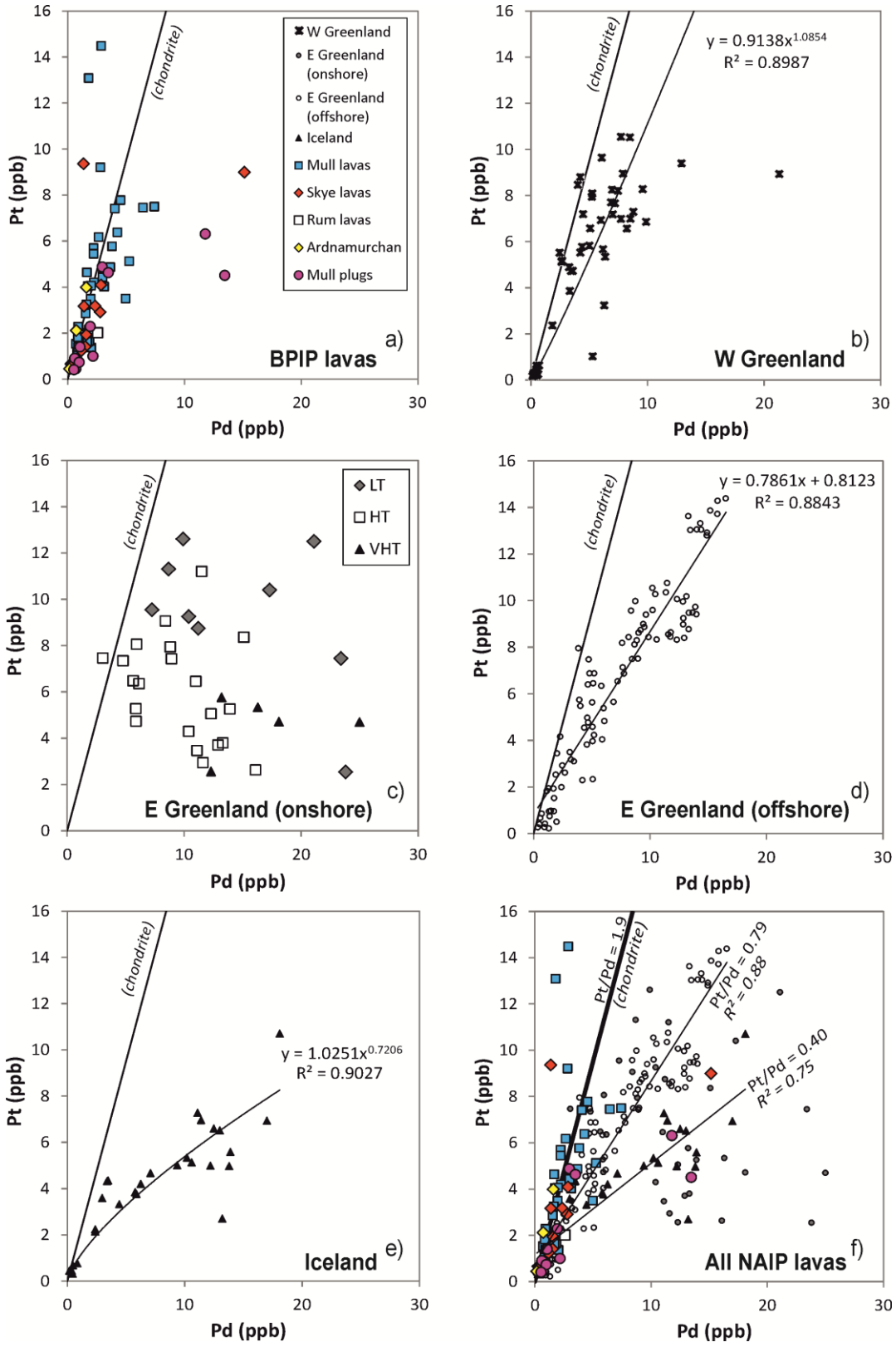

Figure 10.12. Pt vs. Pd bivariant plots for lava suites from across the NAIP; (a) BPIP lavas, (b) west Greenlandic lavas (Disko Island; Keays & Lightfoot, 2007), (c) east Greenlandic lavas (Momme *et al.,*2002b), (d) east Greenlandic SDRS lavas (Philipp *et al.,* 2001), (e) Icelandic lavas (Momme *et al.,* 2003), (f) all NAIP lavas. Chondritic ratio from McDonough & Sun (1995). Calculated trend lines and regressions labelled for plots (b), (d) and (e). Equivalent Pt/Pd ratios and trend line regressions labelled for each lava suite in (f).

(b) Melting source region and depth

Changes in asthenospheric mantle sources undergoing melting have previously been proposed for the NAIP. For example, Kerr (1993; 1995) and Kerr *et al.,* (1999) used REE systematics to identify variations in partial melting of depleted (i.e., due to a prior melting event) vs. enriched asthenospheric mantle at both the spinel- and garnet-stability depths during the magmatism on the Isle of Mull. Similarly other incompatible trace elements in lavas and intrusive rocks have been used to constrain the depth and degree of melting in the BPIP (see Kent & Fitton, 2000 and references therein). Starkey *et al.* (2009) measured REE abundances in whole-rock lava samples and melt inclusions in olivine crystals from picritic lavas for Baffin Island and west Greenland, and identified both enriched and depleted mantle sources. Momme *et al.,* (2006) used TiO_2 and REE contents to infer variations in melting depth and upper mantle sources for onshore east Greenlandic lavas. Isotopic studies by Kempton *et al.* (2000) and Murton *et al.* (2002) point to variations in upper mantle components from up to 6 end members. However, although variations in melt sources of enriched vs. depleted end members and melting depths are clearly identifiable within the lava suites of the NAIP, this does not correlate with the broader temporal change in Pt/Pd observed across the NAIP as a whole (see Fig. 10.8a-c), which must reflect a more fundamental control.

(c) Melting regime

Mantle melting modelling falls into two basic types; either simple batch melting or melt aggregates of near-fractional non-modal melting. In the case of the former, unreasonably high degrees of melting are required to explain the PGE content of Icelandic basalts, which cannot be reconciled with MgO content and other major and trace element systematics (Rehkamper *et al.,* 1999). Therefore more recently, various non-modal melting models have been used to explain the combined lithophile and chalcophile element geochemistry of Icelandic and onshore east Greenlandic lavas (Momme *et al.,* 2006). Non-modal melting models use either a triangular (analogous to spreading ridges; e.g., Momme *et al.,* 2003) or a columnar (i.e., cylindrical; e.g., Keays, 1995; Rehkamper *et al.,* 1999) melting regimes. For the east Greenlandic (onshore) lavas (Fig. 10.11c). Momme *et al.* (2006) suggested that lavas further inland with higher Ti contents were formed by a deeper triangular melting system in a continental rift setting, while lower Ti lavas nearer to the coast formed during continental rupture at greater degrees of shallower melting in a columnar melting regime. Whilst these models reconcile the broad PGE (specifically Pd) and REE features of these east Greenlandic lavas, there is no correlation between Pt/Pd ratios of high- and low-Ti lavas. Both have highly

scattered Pt/Pd (Fig. 10.11c) and so the melting regime and shape of the melt column are unlikely to exert a strong control on Pt/Pd across the NAIP.

(d) Ambient temperature of melting or mantle potential temperature

Various estimates of mantle potential temperature exist for NAIP magmas. However the methods by which temperatures are calculated include; major and trace element thermodynamic modelling (e.g., Herzberg *et al.,* 2007), estimates based on olivine compositions (e.g., Kent, 1995), and modelling based on geophysical constraints (e.g., seismic tomography, lithospheric uplift, buoyancy and/or estimates of active vs. passive upwelling; Brown & Lesher, 2014). All provide strong evidence for elevated mantle temperatures due to the presence of a mantle plume in this region. In particular Brown & Lesher (2014) calculate that the Palaeogene mantle was > 125°C hotter than ambient mantle temperature at the time, but suggest that this temperature elevation is comparatively muted beneath present-day Iceland (85-180°C). Overall, the degree of uncertainty associated with mantle temperature estimates, coupled with the degree of uncertainty inherent in the use of differing methods of estimation, make a comparison of ambient mantle temperatures vs. Pt/Pd ratio difficult for the NAIP lava suites included in the current study. Nonetheless, the possibility that plume-related mantle potential temperatures have diminished during the formation of the NAIP and could systematically affect the Pt/Pd ratio is support by experimental studies that have shown that Pt-alloys have a significantly higher melting temperature than Pd-rich Cu sulphides or MSS (e.g., Peregoedeva *et al.,* 2004).

(e) Incorporation of deep mantle or outer core material in the plume

Involvement of outer core material in mantle plumes could (in part) account for the elevated PGE, Ni and Fe contents observed in some plume-derived magmas, including those of the NAIP (e.g., Andersen *et al.,* 2002). Andersen *et al.* (2002) calculated that PGE concentrations could be enriched 2.5 to 3 times above normal mantle contributions if as little as 0.5 to 1 % of core material were contributed to a plume. Pt-Re-Os isotopic studies of plume-related magmas have widely documented an enriched $^{186}Os/^{187}Os$ signature, particularly noteworthy in lavas from west Greenland and Baffin Island, prompting suggestions that this represents incorporation of deep mantle or outer core-mantle boundary material in the plume magma (e.g., Pearson *et al.,* 1999; Brandon & Walker, 2005). In addition, observations of elevated $^{3}He/^{4}He$ in the Icelandic plume and other plume settings (e.g., Kurz *et al.,* 1983; Rison & Craig, 1983; Hilton *et al.,* 2000 and references therein; Graham *et al.,* 1998; Breddam *et al.,* 2000),

apparently provides further evidence of a deep mantle or core-mantle signature (e.g., Rison & Craig, 1983). However more recent literature has highlighted the likelihood of elevated $^{3}He/^{4}He$ by decoupled entrainment, which implies that the He-isotopic signature cannot directly be used as evidence of core-mantle interaction (e.g., Starkey *et al.,* 2009). Further doubt over the significance of elevated Re/Os, Pt/Os and $^{186}Os/^{187}Os$ signifying a core-mantle signature has come from W-isotopes in Hawaiian basalts, which only have bulk mantle compositions (Schersten *et al.,* 2004; Carlson, 2005 and references therein).

Recent studies suggest that the initial volcanism in the BPIP and NAIP was unlikely to have contained a significant contribution from the outer core or from old recycled crustal material (Dale *et al.,* 2009). Instead Os and He-isotopic studies suggest that early Baffin Island and west Greenlandic picrites were produced from a high percentage of melting in a depleted source region (leading to complete melting of mantle sulphides) at the head of the plume. Later phases of continental rifting and continued magmatism in modern Iceland, contained a greater component of recycled oceanic crust melting (Dale *et al.,* 2009). Kempton et al (2000) identified a higher contribution from a relatively enriched plume component in basalts from the SDRS offshore SE Greenland, than along the Reykjanes Ridge and Iceland today, and they suggest a diminishing plume component in the NAIP through time. Overall, if Dale *et al.* (2009) is accepted, then an outer core contribution to plume magmas cannot be the cause of Pt/Pd variation.

(f) Lithospheric contamination

When assessing lithospheric contamination it is important to distinguish between crustal contamination vs. contamination from the subcontinental lithospheric mantle (SCLM). Deep crustal contamination of magmas by silicic basement is widely documented in lavas from across Greenland and the BPIP, using trace elements and isotopic compositions (see reviews in Saunders *et al.,* 1997 and Kerr *et al.,* 1999). However the concentration of PGE within silicic crustal rocks is typically very low (see Carlson, 2005 and references therein) and they are therefore extremely unlikely to contribute to the PGE budgets of ascending mantle-derived magmas. There is no correlation between Pt/Pd and Nb/La (or other trace element proxies for contamination e.g., Ba/Nb, Nb/Th – see Fig. 10.8d-e) and so crustal contamination cannot be responsible for changing Pt/Pd ratio across NAIP lavas.

Pt/Pd ratios have previously been utilised to infer a metasomatic and 'on-craton' signature for various magmas, with an increased Pt/Pd ratio resulting from input of a metasomatic fluid-

alteration component in the lithospheric mantle (Maier & Barnes, 2004). However, this does not reflect the physical nature of entrainment originally proposed in the instance of kimberlites (McDonald *et al.,* 1995). Metasomatised sulphides are common in mantle peridotites and pyroxenites of the lithospheric mantle, as has been demonstrated in oceanic mantle, abyssal peridotites and alpine peridotites (e.g., Luguet *et al.,* 2003; Alard *et al.,* 2005; Luguet *et al.,* 2008).

Hughes *et al.* (under review, c – Chapter 8) have reported 3 distinctive populations of native base metal sulphides in the SCLM underlying northwest Scotland (Loch Roag, Isle of Lewis). Sulphides from the youngest of these groups are found in frozen melt pockets along grain boundaries (i.e., areas that would be most susceptible to remelting). These sulphides have the highest abundance of PGE and are notably enriched in Pt, with discrete PtS (cooperite) platinum-group minerals, while the peridotite xenoliths themselves have a chondritic bulk rock Pt/Pd ratio. Although the age of the youngest Pt-rich sulphides remains unquantifiable, based on a combination of whole-rock Re-Os isotope analyses and sulphide-specific Re/Os ratios, Hughes *et al.* (under review, c – Chapter 8) propose that this youngest group of sulphides are likely to be pre-Palaeogene, and could record a much older sulphide-bearing magmatic/metasomatic event.

Incorporation of fusible SCLM into plume magmas or ahead of a plume melting front has been suggested previously (e.g., Thompson & Morrison, 1988; Kerr, 1993; Saunders *et al.,* 1997 and references therein; Foulger *et al.,* 2005). This SCLM fusion is particularly feasible given the likelihood of lithospheric thinning or delamination inferred to take place during plume impingement on the base of continents in the North Atlantic (e.g., Kerr, 1994; Saunders *et al.,* 2007). Hence the higher Pt/Pd ratio recorded in the older NAIP lava suites (e.g., BPIP and west Greenland) could reflect assimilation or mixing of ascending asthenospheric magmas with a (complex or multi-phase) Pt-rich lithospheric mantle end member. Given that sulphides are readily fusible and one of the first mineral phases to melt, we suggest that this SCLM interaction could have had a substantial effect on the precious metal budget of plume-derived asthenospheric magmas in the NAIP, essentially dictating the Pt/Pd ratio (> MORB) recorded spatially and temporally across the province.

Incorporation of PGE from the SCLM has previously been suggested for Pt-rich deposits such as the Bushveld Complex and Stillwater Complex (see Maier & Groves, 2011 and references therein). However in these cases, the involvement of SCLM in the PGE budget has been suggested by proxy, either by non-PGE geochemical evidence (e.g., elevated lithophile

element concentrations), or by radiogenic isotopes, and always in the absence of sulphide compositional analyses and petrography of SCLM material (i.e., mantle xenoliths) corresponding to that underlying such deposits. By contrast, in this study and Hughes *et al.* (under review, c – Chapter 8) we can clearly demonstrate that Pt-rich sulphides exist in fusible lithologies (and along silicate grain boundaries) in parts of the Scottish SCLM and would have been available for contamination of asthenospheric plume magmas during the formation of the BPIP. While an ancient metasomatic process may ultimately have been responsible for the pre-enrichment of this cratonic SCLM in sulphide liquids, we suggest that such metasomatic enrichment is itself not necessarily coeval with the LIP magmatism responsible for Pt-deposit formation (c.f., Barnes *et al.,* 2010; Maier & Groves, 2011). Hence the dichotomy of whether SCLM- or plume-based melting is the dominant control on PGE prospectivity and relative Pt/Pd abundances, may obscure a deeper truth. Instead the preconditioning of cratonic SCLM may be an essential precursor to LIP magmatism in defining certain PGE deposit geochemical characteristics. This means that while the majority of magma is derived from asthenospheric mantle (possibly plume) source regions, during ascent precious metal ratios (e.g., Pt/Pd) may be modified by melting and contamination by multiple 'populations' of SCLM sulphides in specific petrographic settings (e.g., pre-existing and preserved melt pockets).

This raises the question – which regions of the SCLM are prone to this preconditioning, and why? For the NAIP lava suites underlain by ancient cratonic gneiss basement and SCLM, the higher Pt/Pd ratio in BPIP and west Greenlandic lavas at first appears to conflict with the more scattered Pt/Pd ratios of east Greenlandic (onshore) lavas. Craton reconstructions in the North Atlantic show that the NAC is bordered to the north by the Nagssugtoqidian orogenic belt (1900-1680 Ma; van Gool *et al.,* 2002; Kolb, 2014) and that this Palaeoproterozoic mobile belt forms the southern border of the Rae Province – see Figure 10.13. The Lewisian gneiss complex of Scotland, and the underlying SCLM (as represented by Loch Roag mantle xenoliths) occur on the very margin of the NAC, and are known to have undergone Palaeoproterozoic orogenesis (e.g., Loch Maree arc terranes c. 1900 Ma; Park, 2002b). Lavas from west Greenland (Disko Island) also sit close to this mobile belt, although they actually overlie the southern margin of the Rae Province. By contrast NAIP lavas in east Greenland span the full width of the Rae Province and in particular lavas of the Sortebre Profile (analysed for PGE by Momme *et al.,* 2002b and included in this study) are notably further from the Nagssugtoqidian orogenic belt than the west Greenlandic lavas.

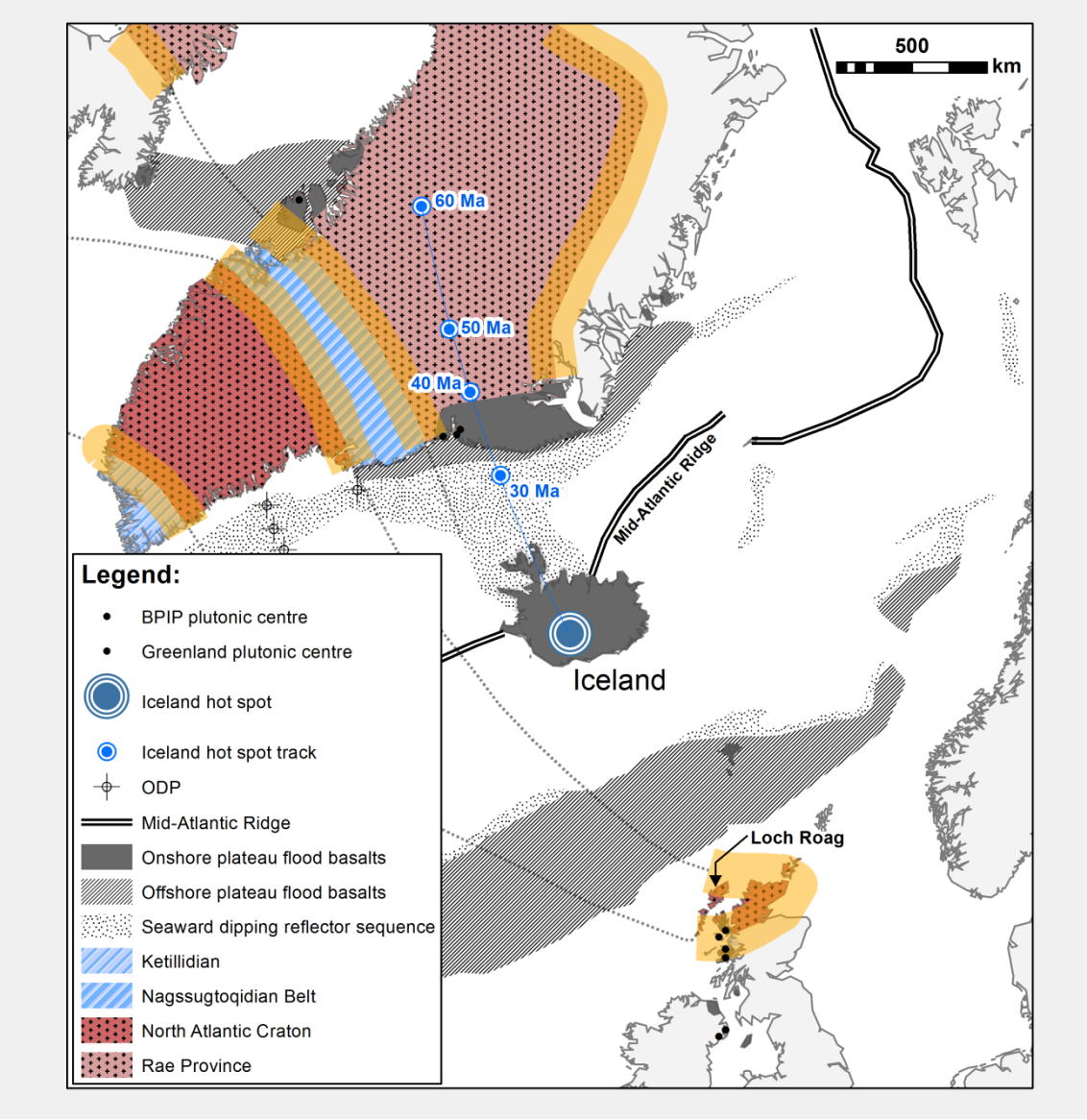

Figure 10.13. Cratonic block reconstruction for the North Atlantic (based on Bleeker, 2003) vs. NAIP lava Pt/Pd ratio. Thick orange lines highlight cratonic margins (nominally to a width of 100-150 km, as a distance of < 100 km was highlighted as being 'near craton margin' by Begg *et al.,* 2010, and the Bushveld Complex sits approximately 130 km from the Kaapvaal cratonic margin).

Hence depending on where the plume head impinges on the lithosphere, parts of the LIP may involve melting of SCLM regions that have experienced older metasomatism, which introduced Pt-rich sulphides. This predisposition of Pt-enrichment is expected to be restricted along lithospheric mantle lineaments such as cratonic block boundaries and/or neighbouring orogenic belts (e.g., Nagssugtoqidian orogenic belt vs. NAC and Rae) and is not inherent in the depleted keel (e.g., Pearson *et al.,* 2004) that makes up the majority of Archaean cratons themselves. While the bulk rock Pt/Pd ratio of depleted cratonic keel mantle xenoliths may be broadly chondritic (e.g., Wittig *et al.,* 2010) this does not inform us about PGE 'fusibility' which will be maximised when PGE-rich sulphides are developed along grain boundaries. In contrast, if the bulk rock PGE budget is strongly controlled by sulphides included within olivine or Cr-spinel, these are unlikely to contaminate passing asthenospheric magmas. Similarly, if sulphides along silicate grain boundaries only carry low PGE concentrations, their effect on asthenospheric magma PGE composition will also be negligible, despite their more feasible entrainment.

Lithospheric lineaments as geophysical conduits for ascending asthenospheric magmas and/or fluids have previously been highlighted as a control on the location of PGE mineralisation (e.g., Begg *et al.,* 2010). We suggest that this is coupled with a fundamental geochemical control too, and that enrichment in precious metals along craton lineaments or margins is not a simple scenario. For example, we see no clear evidence to support a straightforward 'in-out box model' situation whereby SCLM partial melting and S-depletion (thereby enriching PGE in the residual mantle sulphide) is followed by second-stage melting of the same SCLM (as proposed by Hamlyn & Keays, 1986). Instead the multiple mantle xenolith sulphide 'populations' of Loch Roag (Hughes *et al.,* under review, c – Chapter 8) are testament to the true complexity of S-bearing events recorded in the SCLM and therefore the multi-stage enrichment that marginal cratonic lithospheric mantle, or cratonic block/boundary lineaments in the SCLM, may trace. The spatial relationship between ascending plume magmas and whether these magmas interact with pre-enriched (Pt-rich) cratonic boundaries or not, may exert a strong control over the Pt/Pd ratio of LIP magmas.

10.8. Conclusions

Analyses of the platinum-group element geochemistry of a series of lavas from the BPIP, in conjunction with other published studies of Greenlandic and Icelandic NAIP lavas, have

enabled us to tackle two main themes pertaining to mineralisation potential and petrologic constraints on plume-SCLM magmatism and interaction.

1) The apparent enrichment (relative to MORB) in PGE abundances of the NAIP lavas and differing S-saturation controls across the region have been used to assess the mineralisation potential for orthomagmatic Ni-Cu-PGE sulphides in Greenland and Iceland. The widespread opportunity for crustal contamination to take place (particularly in the upper crust with widespread S-rich sediments of the Hebrides Basin) means that the BPIP represents one of the most fertile regions of the NAIP for Ni-Cu-PGE mineralisation.
2) Pt/Pd ratios change systematically across the NAIP, both spatially and temporally, such that the early NAIP lavas in west Greenland and the BPIP have the highest Pt/Pd ratios (approximately chondritic; 1.8). In comparison lavas erupted during the initiation of continental rifting and formation of oceanic crust have progressively lower Pt/Pd, such that modern Icelandic lavas are comparatively Pd-rich. This broad shift in Pt/Pd ratio coincides with changes in the geodynamic setting of the NAIP throughout its evolution – from the first formation of plume-derived magmas beneath thickened SCLM of the North Atlantic Craton and Rae Province, to modern oceanic rifting. Although this geochemical characteristic may be strictly plume controlled and therefore reflect a change in the dominance of the (proto-) Icelandic plume through time, the existence of pre-existing Pt-enriched SCLM underlying the margins of the NAC, and underlying early high Pt/Pd NAIP lavas suggests that there is a fundamental interaction between the plume and lithospheric mantle.
3) We suggest that Pt-enriched SCLM is restricted to the margins of cratons and along cratonic block lineaments such as Palaeoproterozoic inter-block mobile belts. We therefore favour a model whereby fusible sulphides in a fertile and Pt-rich marginal lithospheric keel become mobilised (via partial melting or whole-sale lithospheric delamination) and incorporated into ascending asthenospheric magmas. The spatial relationship between inter-cratonic Proterozoic mobile belts and/or cratonic lineaments vs. the path of ascent of asthenospheric derived (plume) magmas dictates the PGE metal ratios inherent in LIP magmas and hence mineralisation within these provinces.

Acknowledgements

HSRH acknowledges the financial support of the Natural Environment Research Council (NERC) for funding this work (studentship NE/J50029X) and open access publication. Tony Naldrett and Kathryn Goodenough are thanked for their time and discussions.

CHAPTER 11

Contrasting mechanisms for crustal sulphur contamination of mafic magma: evidence from dyke and sill complexes from the British Palaeogene Igneous Province

Submitted as:

Hughes, H.S.R., Boyce, A.J., McDonald, I., Davidheiser-Kroll, B., Holwell, D.A., McDonald, A., Oldroyd, A. (accepted). Contrasting mechanisms for crustal sulphur contamination of mafic magma: evidence from dyke and sill complexes from the British Palaeogene Igneous Province. *Journal of the Geological Society, London.*

Co-author contributions:

A.J. Boyce, I.McDonald, B. Davidheiser-Kroll and D.A. Holwell were involved in discussions during the writing of this paper. A. McDonald and A. Oldroyd advised on bulk rock sulphur extraction methodology. I. McDonald supervised bulk rock analyses at Cardiff, and A. McDonald supervised S-isotopic analyses at SUERC.

Abstract

The addition of crustal sulphur to magma can trigger sulphide saturation: a process fundamental to the development of some Ni-Cu-PGE deposits. In the British Palaeogene Igneous Province, mafic and ultramafic magmas intrude a thick sedimentary sequence offering opportunities to elucidate mechanisms of magma–crust interaction in a setting with heterogeneous S-isotope signatures. We present S-isotopic data from sills and dykes on the Isle of Skye. Sharp contrasts exist between variably light $\delta^{34}S$ in Jurassic sedimentary sulphide (-35 to -10 ‰) and a local pristine magmatic $\delta^{34}S$ signature of -2.3 ± 1.5 ‰. Flat-lying sills have restricted $\delta^{34}S$ (-5 to 0 ‰) while steeply dipping dykes are more variable (-30 to -2 ‰). We suggest that the mechanism by which magma is intruded exerts a fundamental control on the degree of crustal contamination by volatile elements. Turbulent flow within narrow, steep magma conduits, discordant to sediments, and developed by brittle extension/dilation have maximum contamination potential. In contrast, sill-like conduits emplaced concordantly to sediments show little contamination by crustal S. The province is prospective for Ni-Cu-PGE mineralisation analogous to the sill-hosted Noril'sk deposit and Cu/Pd ratios of sills and dykes on Skye indicate that magmas had already reached S-saturation before reaching the present exposure level.

11.1. Introduction

The Palaeogene North Atlantic Igneous Province (NAIP) formed from the intrusion and eruption of mantle-sourced magmas, after the impingement of the proto-Icelandic mantle plume onto overlying lithosphere. Continental rifting initiated in the Palaeogene, with an initial phase of magmatism at 62 Ma in the UK, Greenland and Baffin Island, and ultimately led to the opening of the Atlantic Ocean (continental rifting initiated c. 55 Ma; Saunders *et al.*, 1997). The main products of this prolonged period of magmatism were tholeiitic basalts, in addition to alkali basalts. Where the mantle plume impinged on continental areas, magma fractionation, differentiation, and contamination were commonplace.

The Isle of Skye and surrounding Western Isles of Scotland host a number of prominent intrusive and volcanic features of the British Palaeogene Igneous Province (BPIP; Fig. 11.1a). On Skye, upper crustal mafic and ultramafic intrusions were injected through Archaean Lewisian gneiss basement of the North Atlantic Craton and Mesoproterozoic Torridonian sandstones, siltstones and mudstones. At the current erosion level, the BPIP intrusions (for example the flat-lying Trotternish Sill Complex and an extensive vertical suite of basalt dykes; Fig. 11.1a) have also penetrated through a thick succession of Mesozoic sedimentary rocks of the Hebrides Basin, which are well exposed and can be demonstrated to be physically contaminating BPIP magmas (e.g., via the presence of xenoliths).

The sulphur content of magma may be dramatically increased during crustal contamination and may exceed the saturation concentration, triggering exsolution of an immiscible sulphide liquid into which chalcophile elements such as Cu, Ni and the PGE may partition (e.g., Naldrett 2004, 2011 and references therein). Magmas that intrude through the Jurassic mudrocks have particular potential for Ni-Cu-PGE mineralisation as these sediments would be expected to contain a high level of pyrite with biogenically-derived sulphur (e.g., Fisher & Hudson, 1987). The source of this crustal sulphur can be established by comparing the $\delta^{34}S$ signature of the magmas with that of the country rocks through which it has ascended. In crustal sediments, a substantial range of $\delta^{34}S$ compositions may be preserved in diagenetic sulphides, mostly pyrite. The sulphide isotopic range arises from mass-dependent fractionation during bacterial reduction of seawater sulphate in the contemporaneous diagenetic marine environment, which produces sulphide typically ≤20 ‰ lighter than the starting sulphate (Ohmoto & Goldhaber, 1997). The range of $\delta^{34}S$ can range over 10's of per mille (‰), with Palaeozoic and Mesozoic sulphides extending to more negative values than Precambrian rocks (Canfield & Teske, 1996; Parnell *et al.,* 2010). By contrast, the $\delta^{34}S$ signature of the mantle usually ranges

from -2 to +2 ‰, and magmatic signatures can range from -4 to +4 ‰ depending on the oxidation state of the magma (Ohmoto & Rye, 1979). Due to the dynamic nature of magma intrusion, the crustal S-isotopic signature may be transported away from the immediate site of contamination throughout magma ascent. Therefore crustal S input could be detected remotely from concentrated sulphide mineralisation. Such contamination is typically revealed by analysis of S-isotopes in sulphide minerals or whole-rock samples. Our study uses and develops both techniques to test for crustal contamination in the BPIP. The addition of crustal sulphur to a magmatic system is commonly considered essential in the formation of orthomagmatic Ni-Cu-PGE mineralisation (e.g., Naldrett 2004, 2011; Ripley & Li, 2013) and hence identifying the controls on crustal sulphur contamination, and where this may be occurring will refine strategies for targeting of Ni-Cu-PGE orthomagmatic mineralisation in the BPIP and elsewhere.

We present the first published sulphur isotope compositions for the BPIP, determining a 'framework' for the country rock $\delta^{34}S$ of the Hebrides Basin vs. $\delta^{34}S$ of the BPIP upper crustal intrusions on Skye (including samples from the Lewisian basement, Torridonian sediments, and various Jurassic sediments of the Hebrides Basin). We identify the 'background' plume magmatic sulphur isotopic composition of the BPIP, and investigate if widespread crustal sulphur contamination of magmas took place in northwest Scotland. Coupled with whole-rock Ni, Cu and platinum-group element (PGE) concentrations, this contributes towards the development of a new model for magmatic sulphur contamination, dependent on the orientation and energy by which magma is intruded through a conduit, which impacts upon near-field exploration models for orthomagmatic Ni-Cu-PGE deposits.

11.2. Geology of the Hebridean portion of the British Palaeogene Igneous Province (BPIP)

The British Palaeogene Igneous Province (BPIP) is part of the earliest magmatic series of the NAIP, which includes Palaeogene rocks of the Hebridean Igneous Province (along the west coast of Scotland) and Northern Ireland (Fig. 11.1a). In Scotland, the BPIP includes the Isles of Mull, Skye, Arran, the Small Isles (Rum, Eigg, Muck, Canna and Sanday), together with the mainland igneous complex of Ardnamurchan and lava flows of Morvern. Thus, the BPIP in Scotland extends over a number of tectonic terranes.

Crustal impingement of mantle-sourced mafic magmas resulted in subaerial eruptions along fissure-type feeders (Kent *et al.*, 1998), now seen as a laterally continuous linear array of dyke

swarms, with individual dykes typically < 10m wide (Emeleus & Bell, 2005). These NW-SE trending dykes are perpendicular to the North Atlantic rift margin and indicative of the contemporaneous NE-SW directed extension of northwest Europe at this time (Emeleus & Bell, 2005). Sills associated with lava fields and central complexes normally occur within Mesozoic sediments below lavas, suggesting a relatively shallow emplacement depth (probably < 1 km). Individual sill thicknesses range from up to 10s of metres, amalgamating to form complexes 100s metres in thickness. Sills are often observed to have their own compositional characteristics, unrelated to other overlying lavas. Sills predominantly consist of alkali olivine basalts and tholeiitic basalts, although trachytes and rhyolites are recognised as minor fractionation products (Emeleus & Bell, 2005).

11.2.1. Palaeogene geology of the Isle of Skye

The Isle of Skye records numerous exposures of BPIP magmatic rocks injecting through and into a thick Mesozoic sedimentary sequence, part of the Hebrides Basin (Harker, 1904). Below the Mesozoic rocks, a thick crustal pile of deformed Mesoproterozoic (Torridon and Sleat Group) sediments are present above Archaean (Lewisian) basement (Fig. 11.1b). Hence the Isle of Skye provides an excellent opportunity to study the sources, extent and controls on crustal sulphur contamination in a continental rift environment.

11.2.1.1. The Trotternish Sill Complex, northern Skye

The Trotternish Sill Complex outcrops on the Trotternish Peninsula on the north of the Isle of Skye intruding Jurassic sandstones, limestones and marls (Fig. 11.1a and Supplementary Material B.1; Gibb & Gibson, 1989). The picrites, picrodolerites, and crinanites (analcite olivine dolerites) present throughout the sill complex are genetically related, and thought to result from differentiation of an alkali-olivine basalt magma (Gibson & Jones, 1991) with varying crustal contamination (Simkin, 1967; Gibson, 1990). This horizontal sill complex post-dates the Skye Lava Group and is at least 250 m thick, with individual sills measuring 10's of metres in thickness. Rafts or 'packages' of Jurassic sediments (now baked) occur sporadically within the thickness of the Trotternish Sill Complex in various locations. Sills can display multiple and composite lithologies or melt generations, with banding commonplace (Gibson & Jones, 1991; Emeleus & Bell, 2005). In these cases, the lower zones of a sill are the most mafic. For a detailed 'stratigraphy' of the Trotternish Sill Complex, the reader is referred to Gibson (1990) and Gibson & Jones (1991).

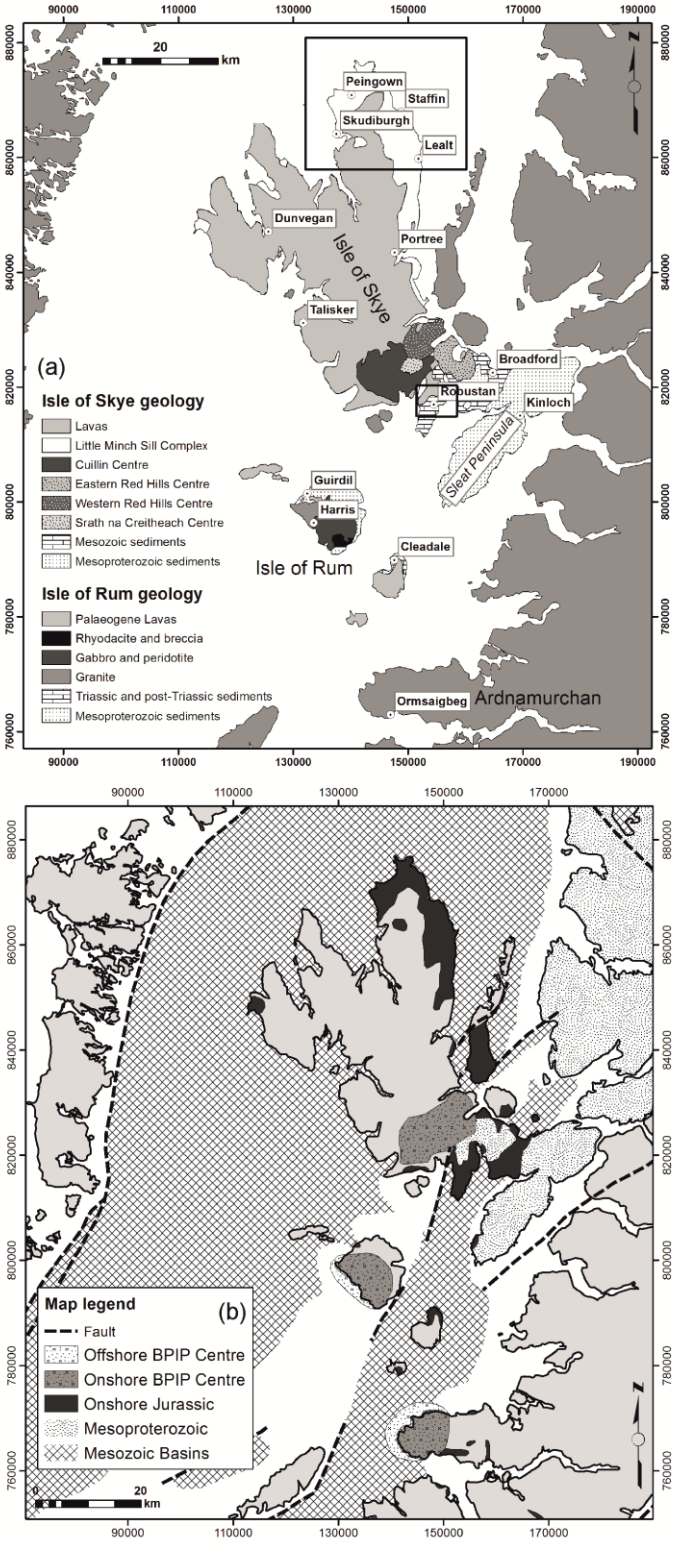

Figure 11.1. (a) Location and simplified geological map of part of the British Palaeogene Igneous Complex (BPIP) – the geology of the Isle of Skye, Rum and the Small Isles. Two black boxes highlight close-up geological maps (see Supplementary Material B). Light grey background does not delineate specific geology, but we highlight that the Lewisian gneisses underlie this entire region (north of the Great Glen Fault). (b) Hebrides Basin area surrounding the Isle of Skye and the Small Isles. Adapted from Fyfe *et al.,* (1993).

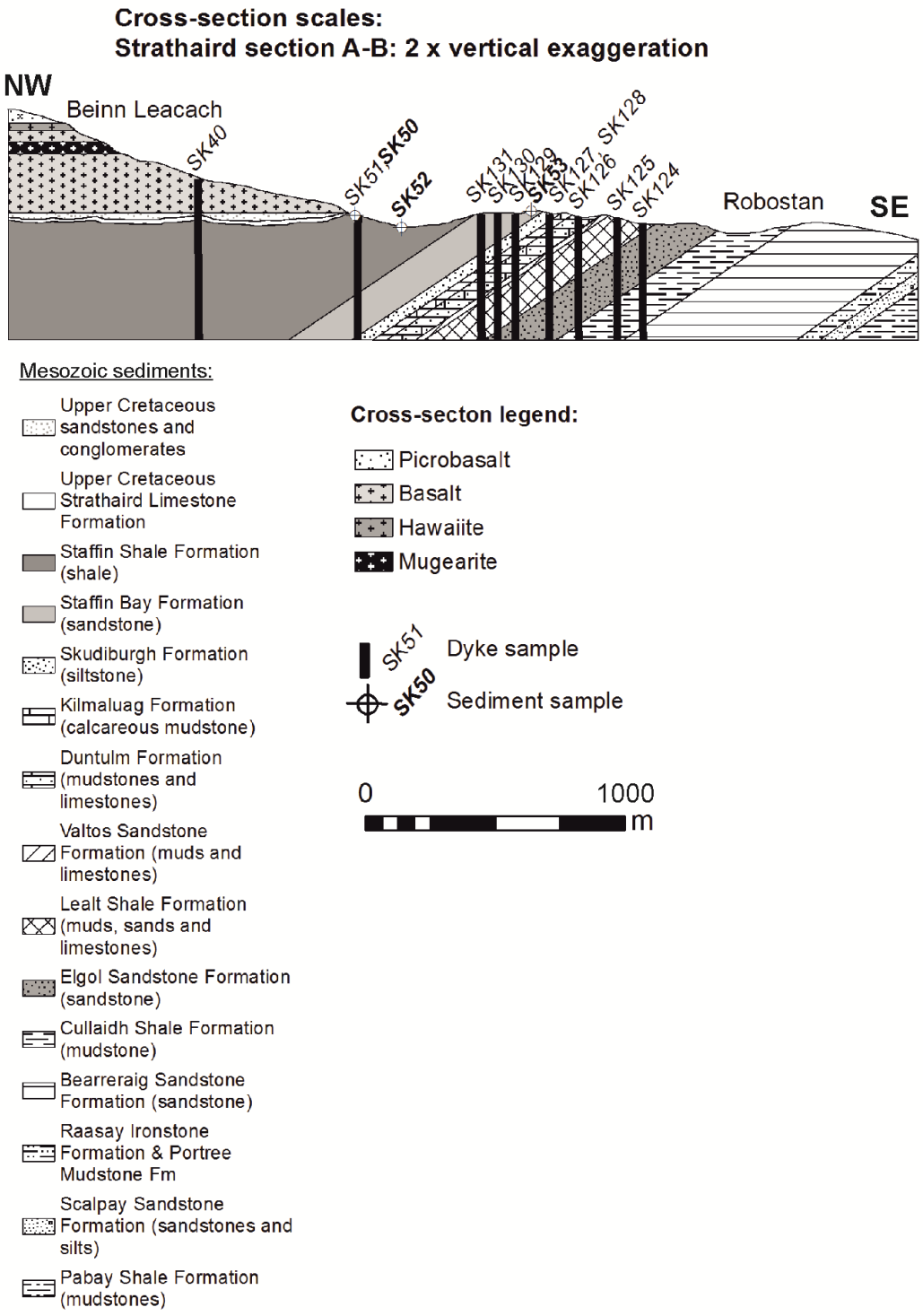

Figure 11.2. Strathaird Peninsula (southern Skye). Line of cross-section displays position of the dyke samples as projected parallel to the strike of the sediment bedding planes, with the exception of sample SK40, which has been projected onto the cross-section along the strike of the dyke itself. Dykes drawn assuming vertical dip. Sediments dip approximately 10° dip NNW below the sediment-lava contact at Scaladal Burn (note cross-section shows 2 x vertical exaggeration). Extent of dyke structure under the current surface level is unknown – cross-section projects dykes for display purposes only. For plan-view geological map see Supplementary Material B.

11.2.1.2. Dykes from the Robustan - Kirkibost area of the Strathaird Peninsula, southern Skye

Dyke swarms on Skye are predominantly directed in a NW-SE azimuth and caused significant local crustal dilation. Most dykes are < 1 m thick, but some wider dykes (e.g., Strathaird Peninsula) display evidence of incremental build-up due to multiple mafic magma injections, resulting in magma mingling and layering within dykes (Platten, 2000). The dykes intrude both lavas and gabbros of the Cuillin Centre, and are mutually cut by cone-sheets (Bell & Williamson, 2002). Compositionally, the Skye Dyke Swarm ranges from silicic pitchstones, to alkali and tholeiitic basalts, and trachytes (Emeleus & Bell, 2005). Ultramafic dykes are predominantly found closest to the Cuillin Central Complex.

At Robustan and Kirkibost on the Strathaird Peninsula, southern Isle of Skye (see Fig. 11.1a), abundant NNW-SSE to NW-SE trending basaltic dykes cross-cut both the lavas and sediments (see cross-section, Fig. 11.2). They represent part of a larger dyke swarm, formed and intruded after the eruption of the Strathaird lavas, and after the intrusion of the Cuillin Central Complexes to the N and NW. The cross-section in Figure 11.2 displays the transect from which dyke and sediment samples were collected (also see Supplementary Material B.2). Rare or minor examples of more evolved dyke compositions are also observed, including basaltic trachyandesites. The dykes are typically vertical and range from 30 cm to 10 m in width. The dykes are finely crystalline (crystal size < 1 mm) and equigranular. Chilled margins are usually absent.

11.3. Stratigraphy of the Hebrides Basin and potential for crustal S contamination

The Mesoproterozoic Torridonian succession of northwest Scotland (Fig. 11.1b and Supplementary Material B.3b) divides into the Sleat, Stoer and Torridon Groups. It is dominated by sandstones and psammites (Stewart, 2002; Kinnaird *et al.*, 2007). Minor siltstone and mudrock units are thinner and less extensive than in the overlying Jurassic units. Recent sulphur isotope studies of Torridonian sulphates and sulphides from the far northwest of Scotland (Stoer to Gruinard Bay) have identified an isotopic shift in $\delta^{34}S$ associated with bacterial sulphate reduction, highlighting that the Mesoproterozoic terrestrial environment was adequately oxygenated to support life (Parnell *et al.*, 2010; Parnell *et al.*, 2012). For example, pyrite-bearing lacustrine siltstones of the Diabaig Formation (basal Torridonian) have $\delta^{34}S$ compositions of -30.1 ± 17.3 ‰. During the present study, 14 Torridonian, Sleat, and Stoer Group sediment samples were collected from the Isle of Skye and Rum for sulphur

isotopic analysis. Of these, only 5 samples yielded enough sulphide precipitate (following whole-rock sulphur extraction – see Section 3.2) to allow for conventional S-isotope analysis.

The anticipated sulphur concentration of the Lewisian crystalline basement and Mesoproterozoic sediments is significantly lower than in the Mesozoic Hebrides Basin, so while the S-isotopic composition of all of these potential contaminants was analysed during this study, the main focus is laid on the Mesozoic. The sedimentary stratigraphy of the Mesozoic Hebrides Basin is presented in Figure 11.1b and Supplementary Material B.3 (based on Morton & Hudson, 1995; Hesselbo & Coe, 2000). While several literature sources document the carbon and oxygen isotopic composition of these rocks, only Yallup *et al.* (2013) report the sulphur isotopic composition of a single unit (in the Middle Jurassic Cullaidh Shale Formation; mean bulk rock $\delta^{34}S$ -0.7 ± 1.8 ‰). Sulphur isotopes for Jurassic sediments from elsewhere in the British Isles have been reported (e.g., Raiswell *et al.*, 1993; Hudson *et al.*, 2001) however until now there has been no Hebridean 'stratigraphy' of sulphur isotopes available in order to establish a S-isotope framework of potential contaminants to BPIP magmas. In the present study, the Palaeogene igneous rocks of interest are observed intruding through, and physically being contaminated by Jurassic sedimentary sequences (via the presence of xenoliths). Thus, it is specifically the Jurassic units which are of most interest for the purposes of this study. This is due to the high proportion and volume of S-rich shales and mudrocks throughout this Jurassic succession, unlike in the older Triassic, or younger Cretaceous sediments that are sulphur poor and sporadically developed across the region (e.g., Hesselbo & Coe, 2000).

The Trotternish Sills intrude through the same thick package of Jurassic sediments as the dykes at Robustan on the Strathaird Peninsula. Thus equivalent Jurassic sedimentary rocks are present as potential contaminants to ascending BPIP magmas and allow for the two different types of intrusive body (sill vs. dyke) to be tested against one another for their degree of crustal S contamination.

11.4. Methodology

11.4.1. Sampling strategy

A full list of sample details and localities can be found in Supplementary Material Table A (on disk) and are shown on maps in Supplementary Material B. In northern Skye, 23 Trotternish Sill

Complex samples were collected, including a range of all rock types (picrites, picrodolerites, and crinanites). Of these, 11 samples were analysed for sulphur isotopes, and PGE and Au.

At Lealt Quarry [NG 5188 6064], a finely crystalline dyke (crystals < 0.5 mm) approximately 2 m wide (strike 338^{o}) with a vertical orientation cuts the Trotternish Sill Complex (comprising an upper crinanite sill, overlying a picrite sill and pegmatitic picrite sill – Fig. 11.3a). The dyke contains 2-20 cm centimetre-scale elongate xenoliths of a baked mudrock (likely of Jurassic origin) and 5-10 cm picrite sill xenoliths at its margins (Fig. 11.3b). The dyke appears to be compound with faint vertical banding (showing indistinct boundaries) at its centre, and elongate xenolith trails within some bands (Fig. 11.3c). This indicates multiple injections of basalt in the dilatational fracture through which the dyke has intruded. Disseminated millimetre-scale (2-10 mm) pyrite crystals are associated with these xenoliths and at the dyke margins, with most disseminated pyrite mineralisation at the contacts with mudrock xenoliths, or forming 'stringers' through the basalt dyke within 30 cm of the xenoliths. There are also trails of white-coloured zeolites (2-10 mm diameter) within 20 cm of the dyke margin (Fig. 11.3d). Four samples from the Lealt Quarry basaltic dyke, which cross-cuts the sill units and four Jurassic sediment samples from packages adjacent to or within the Trotternish Sill Complex, were also collected from northern Skye (e.g. Fig. 11.3e).

In southern Skye, 1 basaltic trachyandesite and 8 basaltic dyke samples were collected from a NW-SE oriented transect approximately 1 km in length through the Jurassic succession at Robustan (Fig. 11.2). All dykes ranged between 30 cm and 8 m in width, with most measuring 1 – 2.5 m wide. One dyke (SK51) displayed rare quartz-filled amygdales up to 0.5 cm in diameter, however all other sampled dykes were amygdale-free. Dyke samples SK124 and SK129 contained visible pyrite within 5 cm of the dyke contact with sediments. Samples were collected from a mixture of dyke margins and central zones. In southern Skye, 5 samples of the Jurassic sediments were collected from this area, including shales, a siltstone, and sandstones.

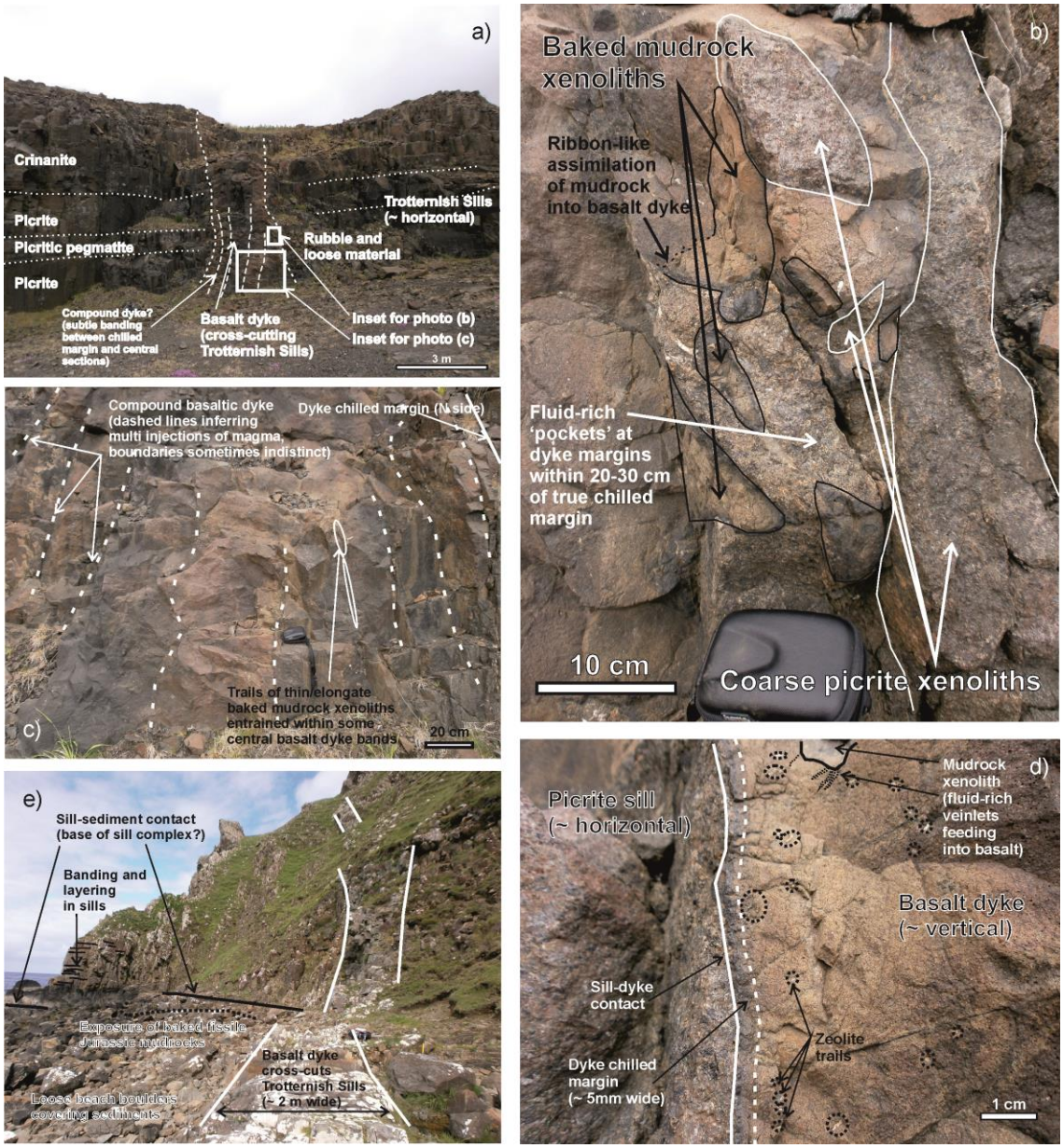

Figure 11.3. Annotated photographs of field relations for the Trotternish Sills and cross-cutting dykes on the Trotternish Peninsula. (a) Lealt Quarry (looking west) – Horizontal Trotternish Sills cross-cut by a later, banded basalt dyke. (b) Close-up of northern margin of basalt dyke in Lealt Quarry showing both picrite (white lines) and mudrock (black lines) xenoliths in a fluid-rich coarser section of the dyke approximately 10cm from the chilled margin. Some mudrock xenoliths have begun to disintegrate and 'fray' at the edges, becoming assimilated or with ribbon-like fluid-rich trails extending into the basalt. (c) Faint banding in the central portions of the dyke. Some 'bands' have elongate mudrock xenolith trails. (d) Close-up of the southern margin of the basalt dyke at Lealt Quarry showing trails of white zeolites close to the chilled margin (annotated by black dashed circles). Baked mudrock xenolith with white coloured fluid-rich stringers extending into basalt shown at top of the image. Basalt dyke contact with picrite sill is annotated by solid white line, and c. 5mm wide basalt chilled margin by dashed white line. (e) Skudiburgh, looking north, with vertical basalt dyke cross-cutting the horizontally banded Trotternish Sills. No offsets of dyke or sills, despite the angle of the photograph. Base of the sill package delineated by black solid line, which overlies a poorly exposed area of baked mudrocks (best observed in the area delineated by dashed black lines).

Table 11.1. Summary of sulphur isotopic composition ($\delta^{34}S$) and measured via conventional (following whole-rock sulphur extraction) and laser combustion methodologies ('Laser'), and whole-rock ('WR') sulphur concentration (S, wt.%). Where 'no precipitate' powdered sample was run through whole-rock sulphur extraction method, but yielded no precipitate, or too small a precipitate to facilitate conventional analysis. *N.B., S concentration too high for calibration - estimation only listed. Samples below detection limit are indicated by < d.t. or < value. Full mineral-specific and duplicate sample details are available in the Supplementary Material.

Sample number				Analytical method	$\delta^{34}S$ (‰)	S (wt%)
Sedimentary:	*Period*	*Group, Formation, Member*	*Sediment type*			
SK50	Upper Jurassic	Staffin Shale Formation	shale	Laser	-32.6	0.113
SK52	Upper Jurassic	Staffin Shale Formation	siltstone	wr	-29.2	-
SK53	Upper Jurassic	Staffin Bay Formation	sandstone	wr	-33.8	<0.02
SK103	Middle Jurassic	Skudiburgh Formation, Great Estuarine Group	fissile, baked mudrock	wr	*no precipitate*	-
SK108	Middle Jurassic	Kilmaluag Formation, Great Estuarine Group	marl	wr	*no precipitate*	-
SK93b	Middle Jurassic	unknown, probably Great Esturarine Group, Lealt Shale Formation	baked mudstone xenolith	Laser	-15.4	-
AN69	Lower Jurassic	Lias Group, Raasay Ironstone Formation	ironstone	wr	-14.7	-
AN71	Lower Jurassic	Lias Group, Raasay Ironstone Formation	pyrite nodule in ironstone	Laser	-18.4	27.746*
AN68	Lower Jurassic	Lias Group, Portree Shale Formation	recrystallised mudstone	wr	-17.6	-
RM78	Mesoproterozoic	Torridon Group, Aultbea Formation	sandstone	wr	*no precipitate*	-
RM3	Mesoproterozoic	Torridon Group, Applecross Formation	sandstone	wr	+1.4	-
RM5	Mesoproterozoic	Torridon Group, Applecross Formation	sandstone	wr	+3.0	-
RM82	Mesoproterozoic	Torridon Group, Diabaig Shale Formation	shale	wr	*no precipitate*	-
SK118	Mesoproterozoic	Sleat Group, Kinloch Formation	mudstone	wr	+4.7	<0.02
SK114	Mesoproterozoic	Sleat Group, Beinn na Seamraig Formation	sandstone	wr	+2.6	-
SK117	Mesoproterozoic	Sleat Group, Loch na Dal Formation	grit	wr	+2.0	-
AN78	Neoproterozoic	Moine coarse micaceous metapelite	n/a	wr	+2.5	-
Basement:	*Period*	*Lithology*				
X66	Archaean	Lewisian amphibolite pod (with minor pyrite) Assynt Terrane		wr	+1.2	-
X11b	Archaean	Lewisian ultrabasic amphibolite (with minor pyrite) Assynt Terrane		wr	-1.4	-
Igneous:	*Location*	*Description*	*Feature type*			
SK83	Dunflodigarry	Picrite sill (sampled from base of cliff on beach)	Picrite sill	wr	-4.9	<0.02
SK89	Staffin	Crinanite sill sampled 20m above contact with limestones	Crinanite sill	wr	-	-
SK90	Lealt Quarry	Pegmatite band in picrite sill	Pegmatitic picrite	wr	-2.2	0.0326
SK92	Lealt Quarry	Picrite sill ~2m below pegmatite band	Picrite sill	wr	-1.7	-
SK93a	Lealt Quarry	East margin of basalt dyke with baked mudrock xenolith bearing pyrite, dyke approx 2m wide	Basalt dyke	wr	-7.5	-
SK96	Lealt Quarry	Basalt dyke (centre), dyke approx 2m wide	Basalt dyke	wr	-6.5	-
SK100	Skudiburgh	Chilled picrite at base of sill complex	Picrite sill	wr	-2.6	<0.02
SK101	Skudiburgh	Finely crystalline picrite (crystals < 0.5 mm), located approx 50cm above base of sill complex	Picrite sill	wr	-3.1	-
SK102	Skudiburgh	Medium crystalline picrite (crystals < 1mm), located approx 2m above base of sill complex	Picrite sill	wr	-10.8	<0.02
SK104	Skudiburgh	Picrite sill sampled approx. 30m above base of sill	Picrite sill	wr	-	-
SK109	Peingown	Base of picrodolerite sill (sampled from chilled margin at contact)	Picrodolerite sill	wr	-2.3	-
SK110	Peingown	Picrodolerite sample located approx 50cm above base of sill	Picrodolerite sill	wr	+0.1	-
SK124	Robustan	Basalt dyke (margin), dyke approx 1m wide	Basalt dyke	wr	-3.7	-
SK125	Robustan	Basalt dyke (margin), dyke approx 1m wide	Basalt dyke	wr	-2.3	-
SK126	Robustan	Basalt dyke (centre), dyke approx 1m wide	Basalt dyke	wr	-2.9	-
SK127	Robustan	Basalt dyke (centre), dyke approx 2.5m wide	Basalt dyke	wr & Laser	-5.1	0.122
SK128	Robustan	Basalt dyke (centre), dyke approx 2.0m wide	Basalt dyke	wr	-3.9	-
SK129	Robustan	Basalt dyke (centre), dyke approx 80cm wide	Basalt dyke	wr & Laser	-15.5	0.4076
SK130	Robustan	Basaltic trachyandesite dyke (margin), dyke approx 1.5m wide	Basaltic trachyandesite dyk	wr & Laser	-19.8	-
SK131	Robustan	Basalt dyke (centre), dyke approx 30cm wide	Basalt dyke	wr	-30.7	1.3389
SK51	Robustan	Basalt dyke (centre), dyke at least 6m wide (contacts not clearly visible)	Basalt dyke	wr	-14.1	-

11.4.2. Whole-rock geochemistry

Major and trace element analyses (including PGE and Au) and S isotopic ($\delta^{34}S$) results are given in Supplementary Table B (on disk) and Table 11.1 respectively. A selection of igneous and sedimentary samples were also analysed for elemental S abundance. Sediment S-isotopic compositions and S concentrations, spanning the upper portion of the Lower to the Upper Jurassic, are presented in Table 11.1, and a sub-selection of 4 sediments were analysed for their major and trace element geochemistry (Supplementary Material Table C – on disk). For the Lower Jurassic, samples were obtained from outcrops on the Ardnamurchan Peninsula, mainland Scotland. In addition, we analysed the S-isotopic composition of 2 sulphide-bearing samples from the Lewisian gneisses of northwest Scotland (X66 and X11b), and 1 sample of Moine metapelite from Ardnamurchan (AN78 – Table 11.1).

Unweathered material was crushed, split, and milled to a fine powder in an agate planetary ball mill. Major and trace elements were analysed by inductively coupled plasma optical emission spectrometry (ICP-OES –JY Horiba Ultima-2) and inductively coupled plasma mass spectrometry (ICP-MS - Thermo X Series 2) respectively at Cardiff University using methods and instrumentation described by McDonald & Viljoen (2006). Platinum-group element (PGE) and Au analysis for samples was carried out by Ni-sulphide fire assay followed by Te co-precipitation and ICP-MS (Huber *et al.*, 2001; McDonald & Viljoen, 2006). Accuracy for whole-rock elemental geochemistry was constrained by analysis of the certified reference materials TDB1 and WMG1 for PGE and Au, and JB1a for all other trace and major elements (see Supplementary Material, parts E - F). Precision was determined by repeat analysis of a sub-set of samples, with most elements repeatable to within 10 % or better.

11.4.3. Sulphur isotope analyses

Samples with visible sulphide minerals >500 μm^2 were cut into blocks (up to 40 x 20 mm in area) and polished. *In situ* laser combustion of polished sulphides was carried out following the technique of (Wagner *et al.*, 2002). Based on experimental results, laser combustion causes a small and predictable fractionation of sulphur isotope compositions for $\delta^{34}S$ of the SO_2 gas produced, compared to the actual $\delta^{34}S$ of the sulphide mineral (Wagner *et al.*, 2002). Therefore the raw $\delta^{34}S$ data were corrected by the following factor: $\delta^{34}Spyrite = \delta^{34}S_{SO2}laser + 0.8$ ‰. Whole-rock S extracted from the rocks (see below), and a series of samples from which

sulphide separates could be picked, were analysed following the technique of Robinson & Kusakabe (1975).

SO_2 gas samples were analysed at the Scottish Universities Environment Research Centre (SUERC) using a ThermoFisher Scientific MAT 253 dual inlet mass spectrometer (for conventional samples) and an on-line VG Isotech SIRA II mass spectrometer (for laser combustion samples). Standards used throughout all analyses were IAEA-S-3 and NBS-123 international standards, alongside an SUERC laboratory chalcopyrite standard, CP-1. The results for these gave -31.5 ‰ (IAEA-S-3, certified to be -31.5 ‰), -4.5 ‰ (CP-1, certified -4.6 ‰) and +17.1 ‰ (NBS-123; certified +17.1 ‰), with $2\sigma < \pm 0.2$ ‰ reproducibility, based on repeated standard analyses. All data are reported in standard per-mille variations from the Vienna Cañon Diablo troilite standard, V-CDT. Full analytical run details can be found in the Supplementary Material.

Our Chromium Reducible Sulphur (CRS) sulphide extraction procedure (for whole-rock powders) is based on and adapted from numerous published and unpublished procedures (Zhabina & Volkov, 1978; Canfield *et al.*, 1986; Tuttle *et al.*, 1986; Hall *et al.*, 1988; Newton *et al.*, 1995; Nielsen & Hanken, 2002; Labidi *et al.*, 2012). A diagram and written description for the procedure can be found in the Supplementary Material.

11.4.4. Whole-rock sulphur concentration analysis

A selection of powdered rock samples were analysed for bulk rock S concentration by LECO CS230 Carbon/Sulphur Determinator at the University of Leicester, UK. Between 0.1 and 1.0 g of sample were used depending on relative bulk S content. Samples were ignited in an O_2 stream and the SO_2 produced was analysed by infra-red absorption. Each sample was run in triplicate to monitor precision. Accuracy was monitored by regular analysis of the reference material BAS ECRM 877-1. The limit of minimum detection for this method is 0.018 wt.% S, which is calculated based on 3 x standard deviation of the mean blank value. A total of 11 samples (both BPIP intrusives and sedimentary rocks) were analysed by this method.

11.5. Results of $\delta^{34}S$ and S determinations

11.5.1. Trotternish Sill Complex

The $\delta^{34}S$ of the Trotternish Sill Complex (including samples from the chilled margins at the base of the sill complex) ranges from +0.1 to -4.9 ‰, however sample SK102 from 2m above the base of the complex at Skudiburgh, gave -10.8 ‰ (Fig. 11.4). Excluding sample SK102, the mean $\delta^{34}S$ of the Trotternish Sills is -2.3 ± 1.5 ‰. Total PGE concentrations for these sills ranges from 12.6 to 30.9 ppb with no clear correlation between whole-rock total PGE content and whole-rock $\delta^{34}S$. Whole-rock Pd concentration ranges from 2.1 to 10.2 ppb and Cu from 57 to 252 ppm (Fig. 11.5). The Cu/Pd ratio varies from 8020 to 46200 with one anomalously high ratio of 81100 (sample SK83, base of picrite sill complex at Dunflodigarry, $\delta^{34}S$ = -4.9 ‰). Pd/Ir ratio ranges from 3.1 to 14.1 with an anomalous value of 56.5 for sample SK90 (a pegmatitic pircite sill from Lealt Quarry, $\delta^{34}S$ = -2.2 ‰). Overall, Pt/Pd ratio for the sills varies from 0.94 to 2.55.

The basaltic dyke at Lealt Quarry, which cross-cuts the Trotternish Sill Complex (Fig. 11.3a and b), has a $\delta^{34}S$ of -7.5 ‰ at the margins (Fig. 11.4a), where the dyke has entrained baked mudrock xenoliths ($\delta^{34}S$ signature of -15.4 ‰; Fig. 11.6). At the centre of the dyke, where xenoliths are absent, the basalt has $\delta^{34}S$ = -6.5 ‰. At the dyke margin, the total whole-rock PGE concentration is 17.9 ppb, as opposed to 1.18 ppb at the dyke centre. Cu/Pd ratio at the margin is 18650 but is significantly higher in the centre of the dyke (77800). Pt/Pd and Pd/Ir show little variance from the dyke margin to its centre, ranging 12.1 to 14.1, and 1.02 to 1.35 respectively.

11.5.2. Robustan basalt dyke swarm

The $\delta^{34}S$ of 8 samples of basaltic dykes from Robustan ranges from -2.3 to -30.7 ‰ (Table 11.1, Fig. 11.4a). Sample SK131 (from the centre of a 30 cm wide basalt dyke) gave the lightest $\delta^{34}S$, at -30.7 ‰, and had a measured whole-rock sulphur concentration of 1.339 wt.%. Sample SK129 (from the centre of an 80 cm wide basalt dyke) gave 0.408 wt.% S and -15.5 ‰, and SK127 (from the centre of a 2.5 m wide dyke) had 0.122 wt.% S and -5.1 ‰. This distribution of S-isotope composition and S concentration, indicates a strong correlation between the S-isotope signature and concentration of S in the dykes (Fig. 11.4b) – dykes with a higher concentration of S having significantly lower $\delta^{34}S$ (correlation r^2 = 0.99). A basaltic

trachyandesite, SK130, with approximately 1 mm diameter rounded pyrite crystallised in some portions of the dyke (mostly at the margins) produced $\delta^{34}S$ of -19.8 ± 1.4 ‰.

Total whole-rock PGE concentrations in the dykes range from 6.4 to 52.4 ppb, and Pd ranges from 1.25 to 16.2 ppb (Fig. 11.5a). Cu concentration ranges from 90.3 to 207 ppm (Fig. 11.5b). Cu/Pd ratios vary between 5590 and 167200. Pd/Ir varies from 11.9 to 48.8 and Pt/Pd ratio ranges from 0.74 to 2.20. The Cu/Pd and Pt/Pd ratios of the dykes are chiefly controlled by Pd concentration (Fig. 11.5c-d). Transposing all samples onto a NW-SE oriented section (Figs. 11.2 and 11.5) we observe that the $\delta^{34}S$ composition of the dykes becomes significantly lighter from SE to NW. This broadly coincides with an increase in the stratigraphic level of the Jurassic sediments that the dykes cross-cut, and into which they intrude. Arranging the results in this manner, we see that between samples SK126 and SK131 a sharp decrease in Pd concentration coincides with a considerable shift in $\delta^{34}S$ (from -2.9 to -30.7 ‰ respectively) and a sharp rise in Cu/Pd (Fig. 11.5c). Pt/Pd broadly follows this increasing Cu/Pd trend from SE to NW (Fig. 11.5d), however SK126 is anomalous due to the significantly higher Pt concentration (25.1 ppb) in this sample.

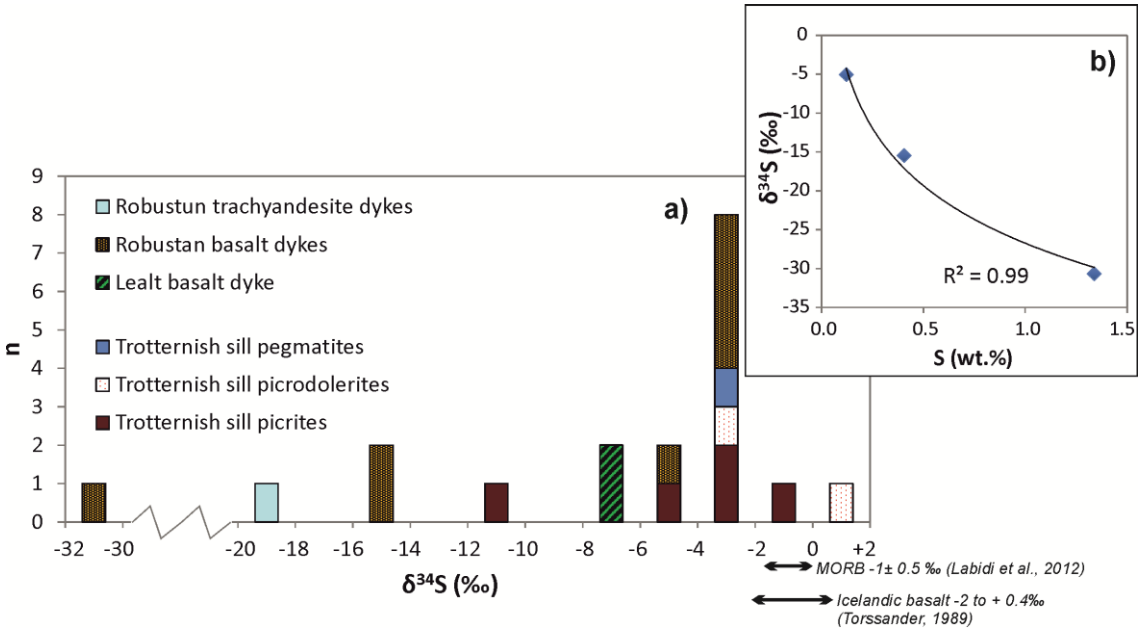

Figure 11.4. Sulphur isotope ($\delta^{34}S$) results for Isle of Skye sills and dykes (a) All sills and dykes. (b) Correlation between whole-rock S concentration and $\delta^{34}S$ (line of best fit is a logarithmic fit as shown, but a linear fit also produces r^2 value > 0.95).

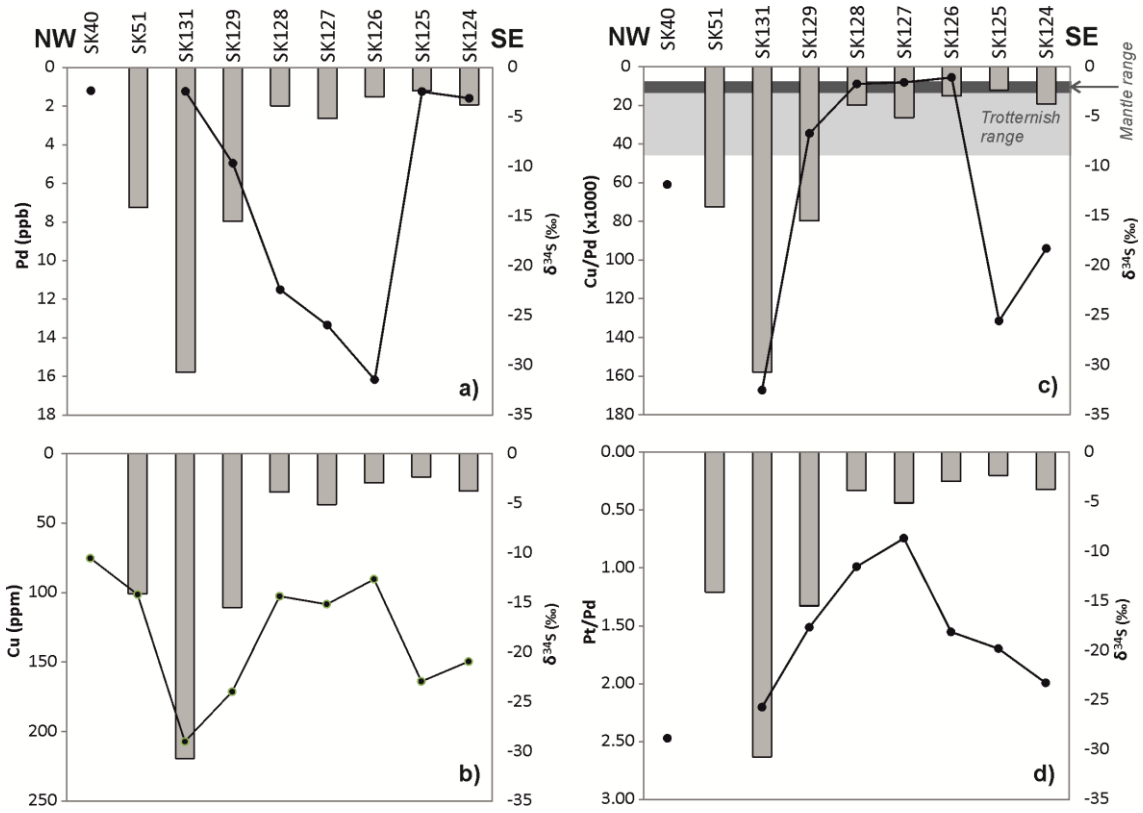

Figure 11.5. Sulphur isotope ($\delta^{34}S$) results and whole-rock PGE and Cu concentrations and ratios for the Robustan basalt dykes, aligned according to a NW-SE transect, as displayed in the cross-section of Figure 11.4. (a) Pd (ppb) and $\delta^{34}S$, (b) Cu (ppm) and $\delta^{34}S$, (c) Cu/Pd x 1000 ratio and $\delta^{34}S$, and (d) Pt/Pd ratio and $\delta^{34}S$. The light grey shaded areas in (c) delineates the range of Cu/Pd ratios measured in samples from the Trotternish Sill Complex and dark grey delineates mantle ranges (according to McDonough & Sun, 1995).

11.5.3. Sedimentary and contaminant country rock units

Of the Jurassic sediments collected from Robustan (Fig. 11.2 and Supplementary Material B.2-3) and analysed by whole-rock sulphur extraction and conventional analysis, the shale member of the Staffin Shale Formation and the Staffin Bay Formation Carn Mor Sandstone Member have the lightest sulphur isotopic signature, with $\delta^{34}S$ = -32.6 and -33.8 ‰ respectively (Table 11.1, Fig. 11.6). The measured sulphur concentration of the shale was 1130 ppm S, but the concentration of sulphur in the sandstone was below detection limit (< 180 ppm). A siltstone member of the Staffin Shale Formation also yielded an average $\delta^{34}S$ = -29.2 ‰. As previously mentioned, the assumed Jurassic mudrock xenolith in the Lealt Quarry basalt dyke, produced $\delta^{34}S$ = -15.4 ‰. Samples of the Staffin Shale Formation (SK103) and Kilmaluag Formation marl (SK108) had very low concentrations of sulphur. Similarly low/absent S contents were recorded in Duntulm Formation limestone. A recrystallized mudstone (Portree Shale Formation) and 2 ironstone samples (Raasay Ironstone Formation with abundant pyrite

nodules) from Ardnamurchan produced $\delta^{34}S$ = -17.6 ‰ and -14.7 ‰ respectively. The pyrite-rich nodules themselves had $\delta^{34}S$ = -18.4 ‰ but had the highest concentration of S with up to 28 wt.% (Table 11.1).

The two pyrite-bearing samples of Lewisian amphibolite gneisses collected from the Assynt Terrane in northwest Scotland gave a $\delta^{34}S$ of -1.4 to +1.2 ‰. The Moine metapelite from the Ardnumurchan Peninsula produced $\delta^{34}S$ = +2.5 ‰. Torridon and Sleat Mesoproterozoic sediments collected from the Isles of Skye and Rum (Fig. 11.6a) have $\delta^{34}S$ ranging +1.4 to +4.7 ‰, although few samples out of the total number collected had sufficient S to produce a useable whole-rock Ag_2S precipitate. Samples from the Aultbea Formation sandstone and a shale from the Diabaig Formation were S poor and did not yield sufficient precipitate for analysis. Together with the Archaean Lewisian gneisses and Moine metasediments, the Mesoproterozoic lithologies delineate a limited range of $\delta^{34}S$, from -1.4 to +4.7 ‰, with a mean of +2.0 ± 1.8 ‰. This is clearly distinct from the mean Jurassic sediment $\delta^{34}S$ of -21.5 ± 8.0 ‰ (e.g., Fig. 11.6) and offers the potential to act as a tracer of upper shallow crustal contamination in the BPIP intrusive suites.

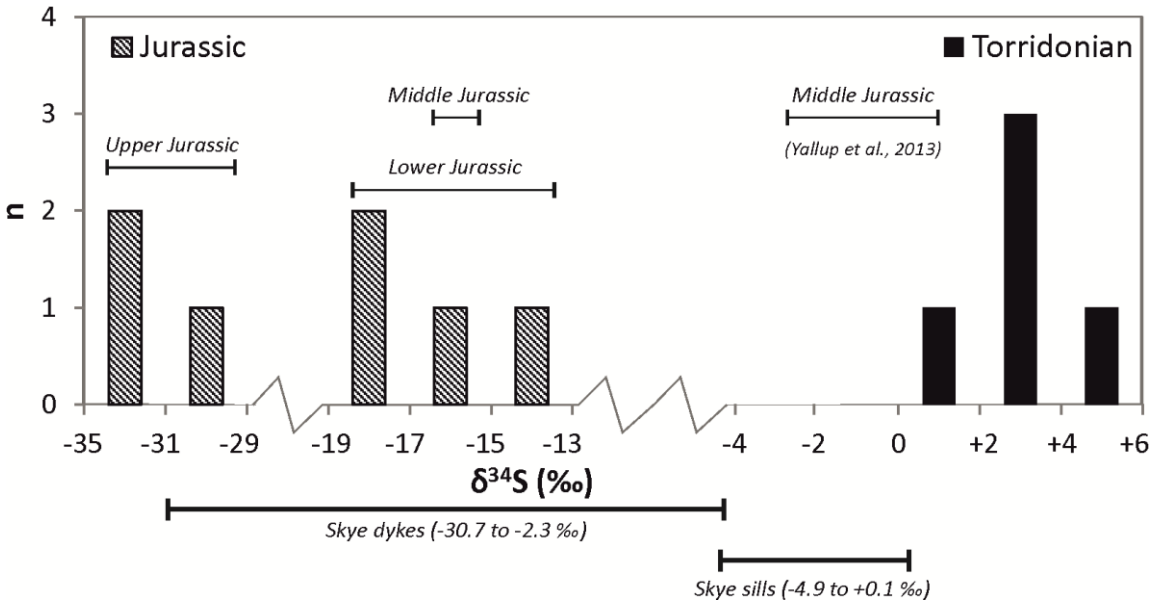

Figure 11.6. Sulphur isotope ($\delta^{34}S$) results for Jurassic and Torridonian (Mesoproterozoic) sediment samples from the Hebrides Basin area, Isle of Skye, Isle of Rum, and Ardnamurchan.

11.6. Discussion

The results of this study provide the first comprehensive S-isotope framework for the BPIP through determining the regional crustal signatures and those of the BPIP magmas on Skye. Our work has identified the following key features:

1. Local Precambrian basement has a limited range of $\delta^{34}S$ values (-1.4 to +4.7 ‰) with a mean of +2.0 ± 1.6 ‰, which overlaps typical magmatic values. This contrasts markedly with the Mesoproterozoic values found on the mainland by Parnell et al (2010).

2. Local Jurassic sediments have a distinct light $\delta^{34}S$ signature ranging -35 to -10 ‰ and a mean of -21.5 ± 8.0 ‰.

3. The flat-lying intrusions of the Trotternish sill complex intruded into Jurassic sediments have restricted $\delta^{34}S$ signatures of -5 to 0 ‰ (with one outlier of -10.8 ‰).

4. The late vertical Robustan dykes *cross-cutting the same Jurassic units* have much lighter $\delta^{34}S$ ranging from -30 to -2 ‰.

Thus the data show that the potential contaminants of the BPIP intrusive rocks on Skye have distinct S-isotope signatures, and our study has identified differences in S-isotope signature between different styles of intrusion. This provides insights into the sources of S, including local mantle and crustal signatures, and to shed light on models for emplacement and contamination in these intrusives. These aspects are explored in detail below.

11.6.1. What is the value of the local mantle S-isotope signature in the BPIP?

Several studies of the sulphur isotopic composition of oceanic basalts have previously been conducted (Kusakabe *et al.*, 1990; Alt *et al.*, 1993; Labidi *et al.*, 2012). Most recently, the reappraisal of MORB $\delta^{34}S$ by Labidi *et al.* (2012) indicated that the mantle has a mean value around -1 ± 0.5 ‰. The sulphur content of such basalts is usually coupled with Fe, Ni and Cu, and is either found within sulphides or dissolved in the silicate melt. At magmatic temperatures, fractionation between the dissolved and segregated sulphide fractions of these basalts would be negligible and the bulk system reduced (Ohmoto & Rye, 1979; Labidi *et al.*, 2012). $\delta^{34}S$ of MORB and primary plume-derived magmas can thus be anticipated to broadly represent the $\delta^{34}S$ of the local mantle, particularly for primitive high-MgO magmatic rocks,

where sulphur exsolution is assumed to be minimal, and contamination *en route* from the mantle likely to be limited (e.g., Iceland).

S-isotope analysis of Icelandic basalts show $\delta^{34}S$ from -2.0 ‰ to +0.4 ‰, with a mean of -0.8‰ (Torssander, 1989). Both tholeiitic and alkaline basalts displayed similar isotopic compositions, although intermediate and acid rocks extend to heavier $\delta^{34}S$, up to +4.2 ‰. For the Icelandic alkaline and tholeiitic samples of Torssander (1989), the homogeneity of the $\delta^{34}S$ distribution provides strong evidence that the sulphur isotopic composition of the parental magmas had not changed significantly from the mantle source to crustal emplacement.

The mean $\delta^{34}S$ of the Trotternish Sills (excluding one anomalously light sample, SK102) is -2.3 ± 1.5 ‰, which is comparable to the signature of basalts from the Iceland plume (Torssander, 1989) and MORB (Labidi *et al.,* 2012), although the range of sulphur isotopic compositions is somewhat larger. Therefore we have confidence that the picritic Trotternish Sill Complex is representative of the mantle S-isotopic signature of the plume in this portion of the NAIP and BPIP.

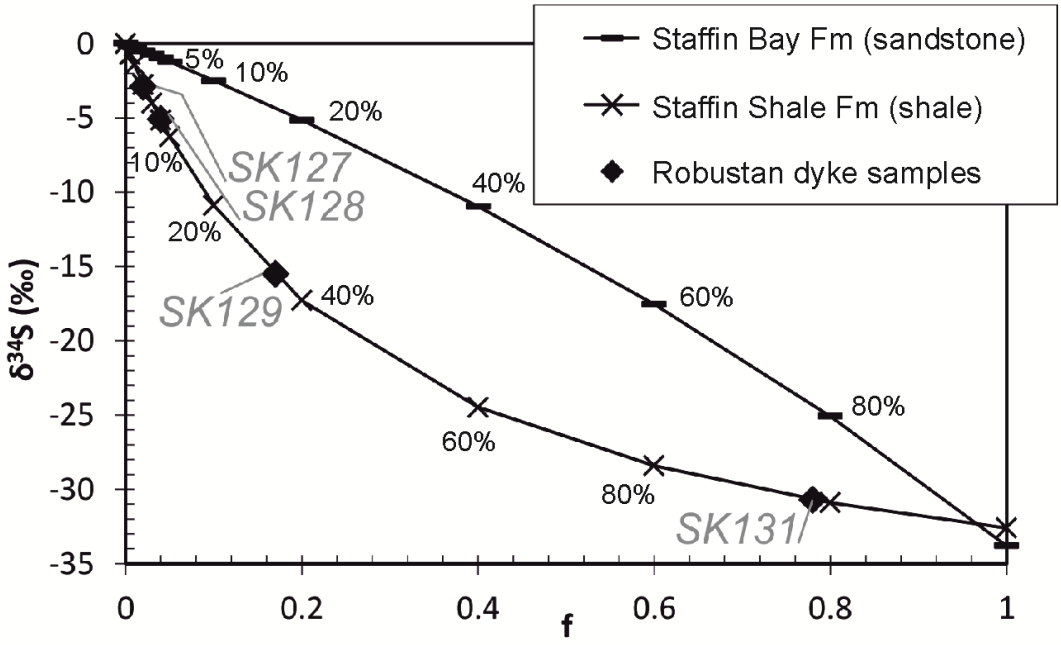

Figure 11.7. (a) Simple binary mixing model between a mantle melt (starting $\delta^{34}S$ = 0.0 ‰, 250 ppm S) end member, and a contaminating end member of either Staffin Bay Formation sandstone, sample SK53 ($\delta^{34}S$ = -33.8 ‰, < 180 ppm S) or Staffin Shale Formation shale unit, sample SK50 ($\delta^{34}S$ = -32.6 ‰, 1130 ppm S). Overlain on the plot are basalt dyke samples SK127, SK128, SK129 and SK131, with estimates of 'f' (mass fraction of S from the contaminating end member) for each sample.

11.6.2. Crustal sulphur contamination in dykes from southern Skye

The sulphur isotopic composition and sulphur concentration for the basalt dykes at Robustan (SK127, SK129 and SK131) indicate that the magmas which formed these intrusions were contaminated by crustally-derived sulphur with an isotopically light $\delta^{34}S$ signature. Assuming contamination is dominated by the Jurassic rocks a simple binary mixing model may be used, as follows:

$$\delta^{34}S_{mix} = [(\delta^{34}S_C \cdot X_C \cdot f) + (\delta^{34}S_M \cdot X_M \cdot (1\text{-}f))] / [(X_C \cdot f) + (X_M \cdot (1\text{-}f))] \qquad \textit{(equation 11.1)}$$

where the contaminated magma = $\delta^{34}S_{mix}$; the isotopic composition of the uncontaminated magma and contaminating sediment = $\delta^{34}S_M$ and $\delta^{34}S_C$ respectively; the concentration of sulphur in the uncontaminated magma and contaminating sediment = X_M and X_C respectively; and the fractional abundance of the contaminant mixing with the magma = f.

Figure 11.7 shows a simple binary mixing model for $\delta^{34}S$ between an uncontaminated mantle melt and Jurassic sediments (SK50 and SK53). Assuming the $\delta^{34}S$ of the contaminant is similar to siltstone SK50, for dyke samples SK126 and SK127, between 2 to 4% input from the sediment S reservoir would account for the measured $\delta^{34}S$ in these dykes; whereas for SK129, 17% contamination is (-15.5 ‰).

For sample SK131, the $\delta^{34}S$ of the contaminated dyke is calculable by accounting for 78 % of the sulphur isotopic signature as coming from a contaminant (e.g., SK50). Sample SK131 was taken from a 30cm wide basalt dyke. While the field evidence, and whole-rock major and trace element geochemistry (Supplementary Material Table B – on disk) indicate that it is likely to be related to the other dyke samples from this area (with the exception of the basalt trachyandesite SK130), it is probable that the S concentration of this dyke is not fully representative of the parental magma composition that was intruded through these conduits. Local sulphur concentration could likely be extremely variable in the dykes, particularly if physical entrainment of crustal material is considered. Further, the sulphur concentration within the Jurassic sediments is extremely variable (e.g., sandstone vs. pyrite nodule rich shale). Therefore, as the dykes were intruded through the Jurassic sediment package, they could have experienced contamination by each S-rich horizon in turn as the dyke intruded upwards.

Although we cannot eliminate the possibility of multi-component progressive contamination having taken place in the parental magmas of the dykes during ascent, we can use a mass balance calculation to interpret the maximum contamination scenario. Assuming an initial

concentration of 250 ppm sulphur in the parental basaltic magma (based on primitive mantle concentrations; McDonough & Sun, 1995) for a volume of 1 m^3 of magma in a 1 m x 1 m x 1 m conduit with a 10 cm wide baked margin in the wall rocks either side (equivalent to 0.2 m^3 wall rock volume and based on visible field evidence) the concentration of sulphur in the wall rock would need to be approximately 7.6 wt.%, assuming a density of 3000 kgm^{-3} and 2600 kgm^{-3} for the basalt and shale respectively. This concentration is considerably higher than that measured in SK50. Assuming that the entire sedimentary S budget is accommodated within pyrite, this is equivalent to a shale containing 14 % pyrite. Given that pyrite-nodules are recorded within the Jurassic sediment pile of the Hebrides Basin, with 27.7 wt.% S (e.g., sample AN71; Table 11.1) this is a feasible composition for the contaminant of SK131. Thus, our model can readily accommodate the observed dyke S concentrations and $\delta^{34}S$ if the high variability of S concentration in Jurassic shales and ironstones is taken into consideration. Dyke SK131 could have intruded through an isotopically light, pyrite-rich portion of the sedimentary pile with unusually higher S concentrations than the surrounding shales, thus dramatically reducing the volume of country rock required to be contaminating the magma conduit and accounting for the S-signature of the dyke.

11.6.3. Contrasting S-isotope signatures of sills and dykes on Skye

This study has presented two examples of high-level informs of intrusion from the BPIP and shows that the dykes have incorporated substantial proportions of Jurassic S in both study areas on the Strathaird and Trotternish Peninsulas (e.g., Lealt Quarry). In stark contrast, the sills of the Trotternish Sill Complex display limited sedimentary S contamination, even at the chilled sill margins. Therefore we have a dichotomy – crustally derived sulphur (with a characteristically light isotopic signature) is widely available in high concentrations within the country rocks of both areas, yet other factors appear to control whether or not this is mobilised or preserved in the local magmatic intrusions.

The possibility of post-magmatic sulphur mobility must be considered – is the sulphur signature observed in the dykes a feature of contamination during the magmatic event, or has this been imparted post-emplacement via *in situ* bacterial reduction in the basalts themselves, within fractures, or by low-temperature fluid remobilisation? At Strathaird, the dykes are volumetrically small, and surrounded by isotopically light sulphur-bearing sediments. It is plausible that post-emplacement fluids could have circulated through these sediments and

through the dykes, imparting the sedimentary $\delta^{34}S$ in this manner. However, textural diagnosis for the timing of sulphide mineral formation might be a better indicator. Where present, pyrite forms subhedral crystals up to 2 mm in diameter, typically within 20 cm of the dyke margin, and less common at dyke centres, although as highlighted above, this has not precluded the light whole-rock $\delta^{34}S$ signature from penetrating the dyke centres. As far as can be determined, there are no veinlets or stringers observed connecting these. In hand specimens, there is no correlation between the presence of oxidised fractures and pyrite, and oxidised/weathered material along with any vugs/amygdales was deliberately removed from the sample before sulphur extraction and analysis. Surface contamination from overlying peat bogs is a feature of the geography of both the dyke and sill areas, and therefore is unlikely to be a realistic modern source of S to one, and not the other. Therefore at Strathaird, there is no reasonable evidence to presume that the sulphide signature is not a 'primary' feature.

Lastly, we can demonstrate physical evidence of high-level crustal contamination by sedimentary rocks taking place in BPIP magmatic intrusions. The vertical basalt dyke at Lealt Quarry, Trotternish Peninsula, is observed in outcrop intruding through the horizontal picritic Trotternish Sills (Fig. 11.3a). 50-80 m below this quarry, the sills overlie the Jurassic Lealt Shale Formation and it is assumed that the vertical basalt dyke extends through the sills and into the sedimentary pile below it. Field evidence of contamination comes from the centimetre-scale mudrock xenoliths entrained and preserved at the dyke margin (Fig. 11.3b-d). Pyrite crystals (up to several millimetres in diameter) nucleate within the basalt at the xenolith margins and the xenoliths themselves contain minor pyrite (mostly at the xenolith margins). The $\delta^{34}S$ of Trotternish Sills at Lealt Quarry are -2.2 and -1.7 ‰ (SK90 and SK92). Critically, this demonstrates that it would not be possible to impart the light sulphur isotopic signature observed in the dyke from sulphur present in the host picritic sills. The mudrock xenoliths, although baked and with no characteristically distinguishing features, are undoubtedly from the Jurassic strata, possibly the Lealt Shale Formation or similar lithology, below the current level of exposure. The $\delta^{34}S$ of pyrite within the dyke at its margin is -7.5 ‰, while the whole-rock sulphur signature of the dyke centre is -6.5 ‰. The whole-rock sulphur signature of a mudrock xenolith is -15.4 ‰, suggesting that the light $\delta^{34}S$ of the dyke has been imparted from Jurassic mudrocks during dyke intrusion and ascent, and involved their physical attrition and brecciation. Accordingly the intact wall rocks to the dyke were baked and chemically interacted with the intruding magma. This is analogous to the dykes on the Strathaird Peninsula, although xenoliths were not observed here, and is in complete contrast to the Trotternish Sills surrounding this dyke exposure.

Mass-independent sulphur diffusion profiles between the Platreef of the Bushveld Complex and footwall country rocks showed that the $\Delta^{33}S$ isotopic ratio is particularly sensitive to wall rock sulphur interaction (Penniston-Dorland *et al.*, 2008). For example, the $\Delta^{33}S$ profile indicates enrichment of S at the Platreef footwall contact via back diffusion controlled by fluids emanating from the cooling and crystallising magma. This process appears to be limited to 5m inside the igneous contact, however the diffusive and advective distances into the country rocks ranges from 6 to 9 m and 16 to 27 m respectively (Penniston-Dorland *et al.*, 2008). In the Lealt Quarry dyke, it is unsurprising therefore, that we observe the margins of the dyke to have a stronger sulphur contamination signature than at the centre, as this is where most magma-sediment interaction and element transfer was taking place during intrusion. Further, we demonstrate that it is highly unlikely that the sulphur isotopic signature of the dyke has been imparted post-emplacement by low-temperature fluids from the immediately surrounding host rocks, as the host rocks are picrite sills with a 'magmatic' $\delta^{34}S$ and are therefore not isotopically light enough to impart the $\delta^{34}S$ found in the basalt dyke.

We have established that the strongly negative $\delta^{34}S$ observed in the Skye dykes is a characteristic feature of the magmatic intrusions, inherited from Jurassic sedimentary pyrite with a bacteriogenic $\delta^{34}S$ signature, during the magmatic stage. The question arises, why is this signature so rare or absent in the Trotternish Sills? Is there an intrinsic difference between the sills and dykes and their capacity for local, high-level crustal contamination? After all, the sills and the dykes intrude through the same package of sediments on the Strathaird Peninsula as they do on the Trotternish Peninsula. And if contamination is taking place, is it wholesale melting/contamination (with inputs of all elements within the sediment being mixed with the magma), or is there preferential mobilisation of only the most volatile elements like sulphur?

11.6.3.1. The role of emplacement mechanism on the crustal contamination signature

During intrusion, many mechanisms can control the upwards movement of magmas through the crust. These include zone melting, penetrative intrusion, and stoping (Oxburgh *et al.*, 1984). The physical method by which a magma body is emplaced could affect the degree of contamination that results. For example, the 'assimilability' of a country rock xenolith entrained in a magma depends on the size of that xenolith, viscous flow (Sachs & Stange, 1993), as well as the mineralogical composition and melting temperature of the xenolith. In addition to these details, the hydration and temperature of the entraining magma will also be a factor. It has been demonstrated that high-Mg basaltic magmas can ascend turbulently if they have a sufficiently high flow rate and conduit width (Campbell, 1985; Huppert & Sparks,

1985) delaying the formation of chilled margins and bringing hot magma in direct contact with country rocks for longer periods of time. Huppert and Sparks (1985) proposed that maximum contamination can occur in dykes which are at the minimum width for fully turbulent flow (approximately 3 m) and evidence of turbulent flow in a basalt conduit has previously been described on the Isle of Mull (Kille *et al.*, 1986).

The Jurassic mudrocks of the Hebrides Basin will predominantly comprise clay minerals and micas, with variable trace element compositions (e.g., Supplementary Material Table C – on disk) rich in Al, Si, Fe, Mg and Ti. Early-stage melting of micaceous xenoliths has been shown to occur as an active melt zone at the xenolith rim, depleted in Al_2O_3 and enriched in CaO, MgO and TiO_2 relative to the bulk composition of the xenolith (Shaw, 2009). Trace element mobility (e.g., large ion lithophile elements) will also be affected by the water content of this partial melt. We have tried to relate changes in Skye dyke whole rock geochemistry with $\delta^{34}S$ but cannot resolve any correlation between dyke trace element composition and S-isotopes. This is possibly because magma compositions were already significantly contaminated by deeper crustal silicic rocks (e.g., Moine and Lewisian basement – see Section 4.4), or due to variations in the original magma compositions (i.e., magma batches) such that trace element variation resulting from later input of Jurassic micaceous material would be masked. In addition, while field relations and hand specimens in our study provide good evidence for mudrock baking, *in situ* anatexsis of these crustal rocks is not observed. This is in contrast to millimetre-scale veinlets of anatectic melt a few centimetres from a sill–shale contact (sill is 3 m wide) at Elgol, Skye (Yallup *et al.,* 2013).

Sulphur and carbon will be mobilised, even without the need for partial melting *senso stricto* (therefore decoupling the trace element geochemistry), and transported as oxidised volatiles released from the baking of the xenolith and/or sedimentary wall rock. Evidence from mudrocks in contact with the Cuillin igneous centre on the Isle of Skye suggests that carbon can remain within these wall-rocks despite severe baking and the high temperatures of the intrusion (Lindgren & Parnell, 2006), however this Cuillin study did not investigate the preservation of sulphur. The thermal effect of the Cuillin Complex was previously been recognised as highly localised, using organic geochemical molecular maturity parameters (Thrasher, 1992). Similarly this has been found to be the case in limestone beds underlying the Trotternish Sills at Staffin Bay (Lefort *et al.*, 2012), although sediments underlying sills at Duntulm show a more developed contact metamorphic sequence, including grossular garnet

and pyroxene (contact metamorphism) and low-temperature alteration in microfactures containing clays (Kemp *et al.*, 2005).

A doleritic sill at Elgol (southern Skye) that intruded through the Middle Jurassic Cullaidh Shale formation demonstrates that both sulphur and carbon may be baked out of sediments in this setting, up to 80 cm from the sill-sediment contact (Yallup *et al.,* 2013). We suggest that a similar amount of sulphur assimilation took place during the intrusion of the Trotternish Sill Complex (scaled to the thicker, and presumably long-lived, sill complex). Yallup *et al.* (2013) also demonstrated that $\delta^{34}S$ became lighter towards the sediment-sill contact, and suggested that this is due to loss of ^{34}S-enriched SO_2 gas during sediment baking. We cannot demonstrate this feature in the Jurassic sediments at the base Trotternish sills due to the extremely low concentration of sulphur remaining in these rocks (almost devoid of S) probably due to substantial baking (and complete loss) of the sedimentary volatile budget. On a global scale, the intrusion of sills (as part of large igneous provinces) into thick organic-rich sedimentary basins has been investigated by Svensen and co-workers. For example, hydrothermal vents originating from the base of sills have been identified in the Karoo Basin of South Africa (Svensen *et al.,* 2006, 2007), Siberian Traps (Svensen *et al.,* 2009) and Vøring Basin offshore Norway (Svensen *et al.,* 2004; Planke *et al.,* 2005). These form when large volumes of volatiles (C, S, H_2O) are baked out of sediments into which magmas have been intruded, and represent significant input of greenhouse gases into the atmosphere at a time coincident with global warming events and/or mass extinctions (e.g., Svensen *et al.,* 2012 and references therein). However most of the aforementioned studies are concerned with the input of C or C-based gases, and have not fully investigated fluxing of S. Nonetheless, in this study we demonstrate the decoupled mobility of S from other trace elements, and highlight the requirement for future investigations into the relative mobilities of C and S (SO_2 is also an important greenhouse gas).

As magma ascends between clay-poor and clay-rich horizons, the amount of water and volatiles released will vary, with volatile-rich shales expected to chemically perpetuate the contamination process. Furthermore the mechanical properties of a shale horizon may actively promote magma penetration. At shallow depths, over-pressured shale units can act as 'ductile horizons', permitting sill formation below the expected level of neutral buoyancy, leading to sill inflation and fracturing of the country rock. This has been documented in the NAIP in the Judd Basin where Palaeogene magmas have intruded through a thick sequence of Jurassic-Palaeocene sediments, forming saucer-shaped sills (Thomson & Schofield, 2008). It is possible

that a similar mechanism of intrusion was in operation during formation of the Trotternish Sill Complex on Skye (Fig. 11.8a). We suggest that this entailed a comparatively 'passive' (i.e., predominantly non-brittle) emplacement mechanism for the magma, such that limited brecciation and entrainment of Jurassic country rock material took place. Where sediment-magma interaction did take place, probably at the chilled base of the sill complex, and in the vicinity of within-sill rafts of Jurassic sediments up to 10 m in thickness (Gibson & Jones, 1991) the sediments became so baked, via contact metamorphism, that volatiles such as S and H_2O appear to have been entirely expelled. Many of the sills formed as a result of multiple injections, therefore magma flowing through the centre of the sill complex (i.e., from later injections) would have been effectively isolated from contamination effects in ~ horizontal the sill conduit itself (see Fig. 11.8a).

The large magma volume represented by the sill complex, and sustained magma throughput (at least in comparison to individual basaltic dykes), could have effectively 'diluted' any crustal sulphur, thereby resulting in a limited change in sulphur concentration and/or $\delta^{34}S$ signature in the magma body. This is potentially analogous to conduit settings in Noril'sk, where sulphides which initially evolved following S-saturation, became flushed out (Brügmann *et al.*, 1993; Lightfoot & Keays, 2005). Further, Cu/Pd, S-isotope and S/Se evidence from the sill-like intrusions of the Platreef (Bushveld Complex) suggests that S contamination from crustal rocks occurred early and deeper in the plumbing system below the Platreef (McDonald & Holwell, 2007; McDonald *et al.,* 2009; Sharman *et al.,* 2013). These sulphides were transported away from this deeper zone during renewed/continued magma batch injections and ultimately emplaced in the Platreef itself (Ihlenfeld & Keays, 2011). At Trotternish, prior contamination by deeper crustal material during fractionation is demonstrable through other isotope systems (e.g., Sr, Nd and Pb; Gibson, 1990), and we suggest that contamination continued throughout the ascent of the sill complex's parental magmas. However, it is plausible that the change in the emplacement mechanism, due to the change in orientation (i.e., from vertical ascent to horizontal emplacement) or rheology of the country rocks (i.e., brittle vs. non-brittle deformation), would have significant implications for the conduit shape (Schofield *et al.*, 2012) and degree of magma contamination, and, crucially, influenced element mobility during chemical reaction (Fig. 11.8a).

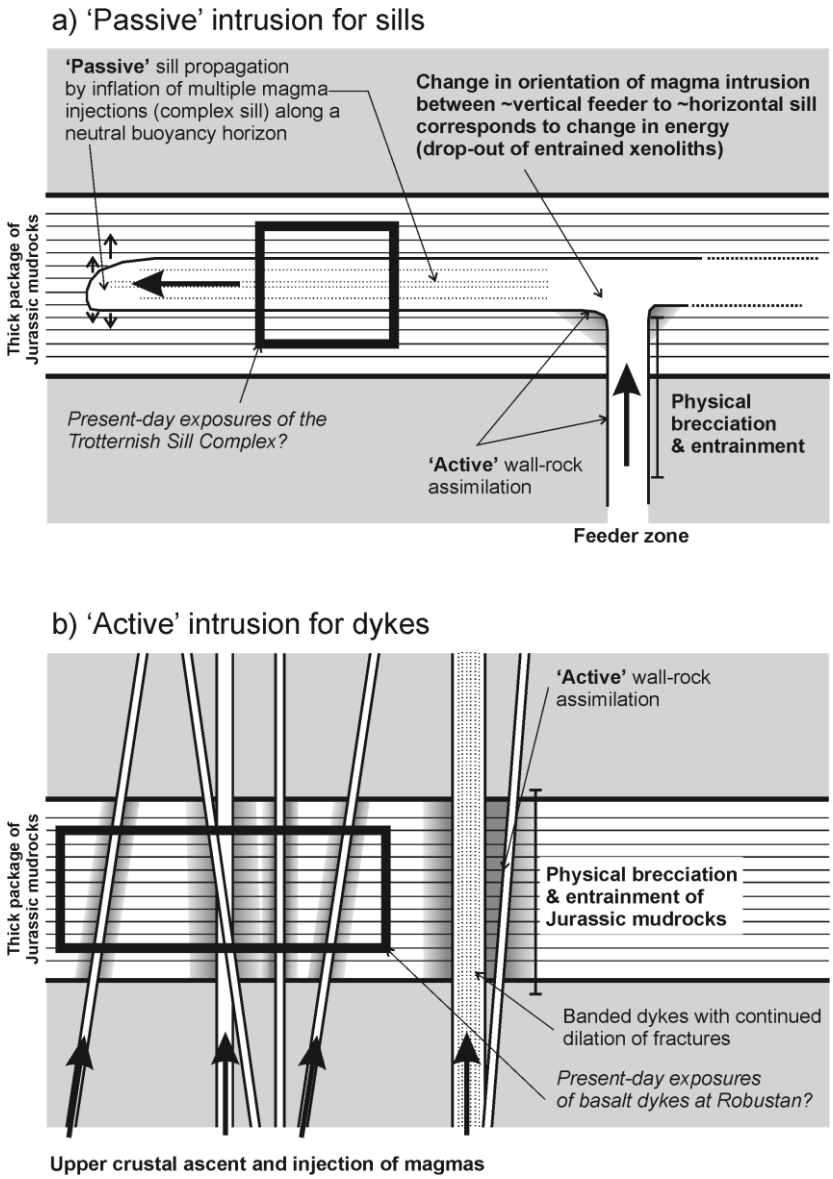

Figure 11.8. (a) Passive intrusion of magmas forming sills – while the ~vertical oriented feeder zones are likely to actively assimilated and become contaminated by wall rocks during magma ascent, once the magma reaches a ductile horizon or zone of neutral buoyancy and spreads out horizontally, magma is injected as a series of batches (i.e., sill complex) in a 'passive' environment or inflation. Little physical attrition of wall rocks will occur and therefore little/no crustal S-isotope signature will be imparted. Crustal S contamination that took place in the feeder zone may have already dropped out following S-saturation and/or been flushed through the sill system so that it is very rarely recorded in the Trotternish Sills. (b) Active intrusion of magmas forming dykes – the ~ vertical and high-energy intrusion of magmas into upper crustal levels forming dykes (e.g., Lealt Quarry or Robustan) causes physical attrition/brecciation of wall rocks. This entrains xenoliths and crustal contamination and S signature is imparted in a higher energy and 'active' or physical mechanism. Initial intrusion of dyke magmas will have taken place along dilation cracks or fractures in country rocks. Continued dilation and magma injection leads for the formation of banded dykes, each with slightly different records of degree of wall rock contamination and various 'stringers' of xenoliths or fluid-rich trails (e.g., zeolites). In both cases (a) and (b), the contamination signature is inferred to be a local effect (magmas have transported the signature on a maximum scale of 100's meters).

By contrast, the vertical dykes on Skye show widespread and exceptional degrees of sedimentary sulphur contamination. As previously mentioned, physical brecciation and entrainment of Jurassic mudrocks is observed, and we suggest that the strong crustal chemical 'interaction' of the dykes (as demonstrated by the correlation between sulphur concentration and $\delta^{34}S$; Fig. 11.4b) is directly related to the magma emplacement mechanism (Fig. 11.8b). These narrow magma conduits, with comparatively limited magma volume, cooled more rapidly than the sills (as shown by their finer crystalline texture), evidently freezing in the local sulphur contamination signature. Dynamic mixing of magmas between the margins and centre of individual dykes has taken place, thereby imparting the marginal contamination $\delta^{34}S$ signature to the dyke centre prior to crystallisation, however this process did not completely equilibrate the crustal sulphur input, so that measurable differences in $\delta^{34}S$ of up to 1 ‰ are observed between margins and centres of a 2 m wide dyke. A maximum degree of contamination probably occurred within the initial intrusive pulse of a dyke into any one given sedimentary horizon, with later pulses of magma along that conduit and through the dyke becoming progressively shielded from further contamination. Thus the mechanism of contamination in vertical dykes is likely complicated by multiple injections of magma, forming complex dykes (Fig. 11.8b). However, most of the examples sampled during this study do not display zoning or banding (with the exception of the dyke at Lealt Quarry), and therefore probably only represent a single magma pulse.

11.6.4. Crustal sulphur sources and contamination potential for Hebridean Scotland and the BPIP

Identifying the crustal contaminants likely to be responsible for inducing S-saturation in ascending magmas is a key factor in pin-pointing when and where immiscible sulphides and orthomagmatic Ni-Cu-PGE mineralisation might have occurred. Therefore we have evaluated the S-isotopic signature of various potential S-bearing contaminants on a more regional scale for the BPIP and Isle of Skye.

Aside from the Jurassic sedimentary rocks discussed so far, other upper-crustal sedimentary formations could also be contributors to the sulphur regime. For example, members of the Sleat and Torridon Groups present along the Sleat Peninsula on Skye, and on the Isle of Rum (Fig. 11.6, Table 11.1), irrespective of lithology and location, have positive $\delta^{34}S$ signatures, ranging +1.4 to +4.7 ‰. The Kinloch Formation mudstone had the highest $\delta^{34}S$ value of +4.7 ‰

(Fig. 11.6). While it is possible that BPIP magmas could be contaminated by Mesoproterozoic sediments, it is very unlikely that this material produced the light $\delta^{34}S$ signature seen in the sills and particularly the dykes of Skye. This is in contrast to the $\delta^{34}S$ results of certain members of the Stoer Group from the far northwest Scottish mainland at Stoer Point, where values less than -30 ‰ are recorded (Parnell *et al.*, 2010). If this material is widely present in the crust below the Isle of Skye, it is possible that the sulphur isotopic signatures of some of the BPIP magma bodies presented here could have been contaminated by this Stoer Group material. However Parnell *et al.* (2010) highlighted the patchy nature of this light S-isotope signature, with bacterial sulphate reduction constrained within small continental water bodies, the relicts of which are laterally discontinuous along strike. More directly, there is no surface exposure of the Stoer Group extending as far south as the Isle of Skye – only the equivalent Sleat Group is observed in this BPIP area, and as discussed above, analysis of this material indicates that its S-isotope signature is significantly heavier. Therefore the combination of the extremely heterogeneous sulphur isotope signature, and unconstrained subterranean extent of the Stoer Group, and other Torridonian sediments, makes this an unlikely candidate to explain the uniformly light $\delta^{34}S$ of the dykes and sills on Skye.

There is ample evidence that deeper crustal contamination via assimilation fractional crystallization (AFC) and assimilation during turbulent ascent (ATA), took place across the BPIP. This includes large deep staging chamber settings, or in narrower meter-scale magma conduits. Both Lewisian (granulite and amphibolite-facies) and Moinian contaminants have been successfully shown to explain the Sr, Nd, and Pb isotopic heterogeneities observed in BPIP magmas (e.g., Gibson, 1990; Kerr, 1995; Preston *et al.*, 1998). In particular, Gibson (1990) demonstrated that the Trotternish Sill Complex underwent up to ~20 % mid- or lower-crustal contamination, prior to magma injection and emplacement. Thompson (1982) and Gibson (1990) use La/Nb ratios to constrain assimilation of Lewisian rocks by Palaeogene magmas, now preserved as dykes, sills and lavas. In Supplementary Material (C.2) we present La/Nb ratio vs. $\delta^{34}S$ and find no correlation for dykes included in this study. There is a very weak and inconclusive correlation between La/Nb ratio vs. $\delta^{34}S$ for sills (r^2 = 0.31). Lewisian gneisses have variable, but low sulphur concentrations and $\delta^{34}S$ ranging -1.4 to +1.2 ‰ (this study) and -1.4 to +5.5 ‰ on the northwest Scottish mainland (Lowry *et al.,* 2005). Torridonian sediments measured in this study always have $\delta^{34}S > 0$ ‰. Moine metapelites also have low or very low concentrations of sulphur, and where measurable have $\delta^{34}S$ = +2.5 ‰ (this study) and +3.4 to +4.6 ‰ in some psammites (Lowry, 1991). Accordingly, Lowry *et al.,* (2005) found that each crustal terrane across Scotland could be characterised by its dominant crustal units, reflected

in the range of $\delta^{34}S$ for that region. In the Northern Highland Terrane (which includes Skyes) complexities in the terrane-scale $\delta^{34}S$ were suggested as reflecting the thick North Atlantic Craton (i.e., Lewisian and Palaeoproterozoic metasediments of Loch Maree) underlying the upper crustal sedimentary cover.

Our study shows that both the Moine and Lewisian deeper crustal materials are unrealistic sources for the consistent and characteristically light sulphur isotopic signature of the Skye dykes. Therefore, we suggest that while deep crustal contamination of BPIP magmas has taken place, the dominant $\delta^{34}S$ contamination signature observed in these magmas is the result of specific and localised upper-crustal contamination of readily-fusible, organic-rich Jurassic shales and mudrocks. This has taken place in smaller vertical magma conduits, or where the mudrocks were in direct contact with BPIP magmas, allowing for pervasive alteration, mobilisation of volatiles and in some cases physical and chemical assimilation of these country rocks, modelled by a simple binary mixing scenario.

11.6.5. Implications for Ni-Cu-PGE orthomagmatic sulphide mineralisation

Whilst not the sole forcing factor in the occurrence of S-saturation, significant literature points to the common association of crustal contamination with the development of orthomagmatic sulphide mineralisation (e.g., Noril'sk-Talnakh Region (Ripley *et al.*, 2003; Ripley & Li, 2013); Duluth (Arcuri *et al.*, 1998); Voisey's Bay (Ripley *et al.*, 1999); Kambalda (Lesher & Burnham, 2001); and others (see Naldrett 2004, 2011 and references therein). A scenario where crustal sulphur is available for magma contamination is therefore often an important factor in Ni-Cu-PGE exploration. A recent study of lavas by Hughes *et al.* (accepted, b – Chapter 10) has suggested that Scottish BPIP is one of the most fertile regions of the NAIP for Ni-Cu-PGE mineralisation, in part due to the widespread opportunities for shallow crustal contamination by S-rich sediments.

Interpreting sulphide metal tenors and whole-rock chalcophile element abundances of magmas in relation to their degree of crustal sulphur contamination (monitored here by $\delta^{34}S$) can be complicated by the formation of multiple generations of sulphide liquids (i.e., deeper in the magmatic plumbing system; e.g., Holwell *et al.,* 2007) and the effects of prolonged interaction of sulphides with fresh silicate magma(s) (Campbell & Naldrett, 1979). The ultramafic sills have a low Cu/Pd ratio in comparison to basaltic dykes at Robustan, however this ratio is still elevated above that of primitive mantle (c. 7000-8000 based on pyrolite;

McDonough & Sun, 1995), suggesting that sulphide saturation had probably already taken place prior to emplacement of the sills. The highly variable Cu/Pd ratio of the Robustan dykes is likely also recording one or more S-saturation events which occurred prior to dyke emplacement. However because the dykes are demonstrably assimilating local crustal sulphur at the current erosion level, we can further inspect the response of the remaining low-abundance chalcophile elements to this secondary S-saturation event.

Broadly, dyke samples with the lightest crustal $\delta^{34}S$ signatures have the lowest Pd concentration (Fig. 11.5a) and highest Cu/Pd ratio (Fig. 11.5c). Pt, Pd and Au concentrations show the strongest response to localised crustal S contamination, and variations in Cu appear to be weaker (i.e., less variable concentrations) in this secondary S-saturation scenario. This causes a correspondingly 'delayed' spike in Cu/Pd ratio. In PGE mineralised settings (e.g., the Bushveld Complex) this feature is well documented for S-saturation in PGE reefs (Maier, 2005 and references therein) as the partition coefficient of Pd into sulphide liquid is several orders of magnitude greater than that for Cu (Mungall *et al.*, 2005; Mungall & Brenan, 2014). However in a setting where first-stage S-saturation has already occurred deeper in the system, the concentration of chalcophile elements (particularly Pd-group PGE) would be much lower in the remaining silicate magma that continued its ascent to the surface. Therefore the Cu/Pd ratio of that residual silicate magma would be much higher and more variable than that of a magma which had only undergone one S-saturation event (as seen in the Trotternish Sills). From this secondary 'starting point' Cu/Pd ratio, a second-stage localised S-saturation event would lead to further fractionation of Pd from Cu (particularly for systems with low R-factors; the ratio of sulphide liquid to silicate magma), raising Cu/Pd ratio to even higher values (up to 167,000 in sample SK131). Assuming sulphide liquids from the initial S-saturation event had not been entrained during continued magma ascent, the extreme variability in Cu/Pd ratio caused by this first S-saturation (deeper) would lead to even greater erraticism in this parameter during the formation of later sulphide liquids (shallower). Thus, in the absence of entrained sulphide liquids, the detailed interpretation of chalcophile element ratios at/after secondary S-saturation events would be impractical.

The cause for this first-stage S-saturation event remains speculative – given the silicic basement underlying this region, this could have been due to the addition of SiO_2 to the magma (as well as fractional crystallisation during magma ascent) such that S concentration at sulphide-saturation (SCSS) was lowered. Alternatively this could have been triggered by addition of S deeper in the crust, but during this study we have shown that $\delta^{34}S$ of Moine,

Torridonian and Lewisian rocks is within magmatic variation (0 ± 4‰) and therefore would not be detected by this method. However, we have also determined that S abundance in these lithologies is typically very low, and we question the likelihood of these rocks in contributing enough S during deep crustal contamination to induce S-saturation.

Ultimately the effects of multiple S-saturation events might be further investigated by analysis of the S/Se ratio of sulphide minerals (e.g., Ihlenfeld & Keays, 2011). In addition, the earlier S-saturation of magmas would likely preclude significant orthomagmatic Ni-Cu-PGE mineralisation in higher portions of a magmatic province. However, by identifying the physical and structural factors controlling the ability of an ascending magma to assimilate crustal sulphur in a conduit, we can ascertain the locations within a magmatic plumbing system (deep or shallow) where S-saturation is likely to have taken place, leading to mineralisation.

Finally, the small (± 1.4 ‰) and non-systematic variation observed between $\delta^{34}S$ of sulphide minerals (in this case, pyrite) compared to whole-rock values is acceptable for use in identifying the occurrence of contamination of magmas by crustally-derived sulphur. The observed maximum procedural-induced isotopic shift is very small in comparison to the isotopic shift caused by crustal contamination and the natural $\delta^{34}S$ of the country rock samples. However this is dependent on the crustal sulphur source having a characteristic $\delta^{34}S$ signature (either light or heavy), and being statistically different from the typical 'mantle' signature. Therefore the whole-rock CRS method of sample preparation for $\delta^{34}S$ analysis (as used in this study) is suitable for identifying areas of potential sulphur saturation in mantle-derived magmas contaminated by crustal sulphur. This contributes to a rapid and flexible exploration tool for orthomagmatic Ni-Cu-PGE sulphide deposits, applicable even to samples with non-visible sulphide mineralisation, as it identifies crustal sulphur contamination of whole-rock magmatic samples, assuming that there is a significant difference between the sedimentary and mantle $\delta^{34}S$ composition. This method offers the opportunity to vector into areas of increased crustal S contamination, even in relatively S-poor rocks.

11.7. Conclusions

1. The $\delta^{34}S$ range for the Palaeogene alkali picritic Trotternish Sill Complex (+0.1 to -4.9 ‰; mean = -2.3 ± 1.5 ‰) reflects the dominance of mantle-derived sulphur, consistent with that found in other Icelandic mantle plume-derived magmas.

2. In contrast, the observed $\delta^{34}S$ range for the Palaeogene basalt dyke swarm at Robustan is -2.3 to -30.7 ‰. Sulphur isotope evidence for contamination is present throughout the full widths of these dykes: margins and centres alike.

3. Despite similar country rocks with light $\delta^{34}S$ (> -33.8 ‰), there appears to be a fundamental geological control on the degree of crustal contamination of magma bodies, depending of the mechanism (orientation and energy) by which that magma intruded. There is a distinct difference in the S contamination pattern between a flat-lying concordant and thicker magma conduit (as represented by the 10-100 m-scale Trotternish Sill Complex), and a vertically intruded discordant and narrow magma conduit (e.g., meter-scale basalt dykes of the Skye dyke swarm at Robustan).

4. Turbulent flow within narrow magma conduits emplaced discordantly to sediments maximises contamination potential, particularly of volatile and highly mobile elements (such as S) in a high surface-to-volume scenario. Whereas passively emplaced, wide conduits emplaced concordantly to the sediments undergo comparatively little crustal sulphur contamination. This mechanical control may act in addition to other known controls on contamination such as the temperature and flux rate of magma in a conduit system.

5. Despite the absence of sulphide minerals, a S-saturation event prior to dyke emplacement may be identified using Cu/Pd ratio. Given the high concentration of S in these dykes, and their strong $\delta^{34}S$ crustal contamination signature, S-saturation causing this extreme variability in Cu/Pd ratio must have been imparted before dyke emplacement and therefore at a deeper crustal level. This suggests that Ni-Cu-PGE mineralisation may exist below current exposure levels (as corroborated by Hughes *et al.,* accepted, b – Chapter 10). However the trigger for this previous S-saturation remains unresolved.

6. Where sulphide minerals are either too rare or too small to separate, use of whole-rock sulphur extraction to analyse $\delta^{34}S$ in samples can reveal S contamination. We suggest that this technique offers a suitable and rapid method that can be used as a vectoring tool for exploration of orthomagmatic Ni-Cu-PGE mineralisation, to identify where crustal sulphur contamination has taken place in magmatic provinces.

Acknowledgements

Sulphur isotope analysis was undertaken at the Scottish Universities Environment Research Centre (SUERC) and funded by a NERC Isotope Geosciences Facilities Steering Committee grant (IP-1356-1112). HSRH would like to acknowledge the financial support of the Natural Environment Research Council (NERC) for funding this work (studentship NE/J50029X) and open access publication. AJB is funded by NERC funding of the Isotope Community Support Facility at SUERC. The manuscript benefitted from discussions with Ben Manton, Geoff Steed and Andrew Kerr. Sally Gibson and Bernard Bingen are thanked for their thorough and constructive reviews.

CHAPTER 12

Sulphide sinking in magma conduits: evidence from mafic-ultramafic plugs on Rum, North Atlantic Igneous Province

Submitted as:

Hughes, H.S.R., McDonald, I., Boyce, A.J., Holwell, D.A., Kerr, A.C. (under review). Sulphide sinking in magma conduits: evidence from mafic-ultramafic plugs on Rum, North Atlantic Igneous Province. *Journal of Petrology.*

Co-author contributions:

I. McDonald, A.J. Boyce, D.A. Holwell and A.C. Kerr were involved in discussions during the writing of this paper. I. McDonald supervised bulk rock and LA-ICP-MS analyses.

Abstract

Magmatic Ni-Cu-PGE sulphide mineralisation is commonly found in magmatic conduit systems and in many cases the trigger for formation of an immiscible sulphide liquid involves assimilation of S-bearing crustal rocks. Conceptually, the fluid dynamics of what happens to sulphide liquid droplets within such conduits is essentially a balance between gravitational sinking and upwards entrainment. Thus, crustal contamination signatures may be present in sulphides preserved both up- and down-flow from the point of interaction with the contaminant. We examine a suite of ultramafic volcanic plugs on the Isle of Rum, Scotland, to decipher controls on sulphide accumulation in near-surface magma conduits intruded into a variable sedimentary stratigraphy. Whole-rock geochemistry of the plugs broadly overlaps with compositions from ultramafic units within the Rum Layered Complex, although subtle differences between each plug highlight their individuality. Interstitial base metal sulphide minerals occur in all ultramafic plugs on Rum. Sulphide minerals have magmatic $\delta^{34}S$ (ranging from -1.3 to + 2.1 ‰) and S/Se ratios (mean = 2299), and demonstrate that conduit magmas were already S-saturated. However, two plugs in northwest Rum have substantially coarser (sometimes net-textured) sulphides with light $\delta^{34}S$ (-14.7 to -2.9 ‰) and elevated S/Se ratios (mean = 4457), not represented by the immediate host rocks. Based on the Hebrides Basin sedimentary stratigraphy, it is likely that volcanic conduits would have intruded through a package of Jurassic mudrocks with characteristically light $\delta^{34}S$ (-33.8 to -14.7 ‰). We propose that a secondary crustal S contamination event took place at a level above that currently exposed, and that these sulphides sank back down to their present position.

Our modelling suggests that upon the cessation of active magma transport, sulphide liquids could have sunk back through the conduit over a distance of several hundreds of metres and over a period of a few days. This sulphide 'withdrawal' process may be observed in other vertical/steeply inclined magma conduits globally, for example in the macrodykes of east Greenland. Sulphide liquid sinking within a non-active conduit or during magma 'suck-back', may help to explain crustal S-isotopic compositions in magma conduits which appear to lack appropriate lithologies to support this contamination, either locally or deeper in the system.

12.1. Introduction

Upper crustal conduits (pipes, dykes and sills) of mafic-ultramafic magmatic systems provide favourable settings for magmatic sulphide genesis, promoted by crustal contamination, and resulting in some of the world's largest orthomagmatic Ni-Cu and platinum-group element (PGE) deposits. Contamination can trigger S-saturation, particularly if the country rocks contain significant amounts of S in the form of sulphides or sulphates and this can be recognised by S-isotope signatures outside the typical mantle range of 0 ± 3 ‰ (e.g., Li *et al.,* 2002; Ripley *et al.,* 2003; Keays & Lightfoot, 2010). In addition, sulphide liquid that ponds within conduits can become enriched in chalcophile elements, possibly to economic levels, due to its interaction with magma continuing to pass through the conduit (e.g., Kerr & Leitch, 2005; Holwell *et al.,* 2014).

Sulphides within conduits commonly occur as massive to semi-massive accumulations, and are present as rounded globules or droplets of varying sizes; e.g., at Norilsk Talnakh, Russia (Czamanske *et al.,* 1992), the Insizwa Complex, South Africa (Lightfoot *et al.,* 1984), Voisey's Bay, Canada (Huminicki *et al.,* 2008), a mafic dyke in Uruguay (Prichard *et al.,* 2004) and in east Greenlandic macrodykes (Holwell *et al.,* 2012). Droplets are generally interpreted to represent sulphide liquid which has been transported upwards, downwards or laterally along the magmatic plumbing system. The fluid dynamics involved in this transport, such as settling rate versus entrainment rate, have been the subject of many recent studies using both empirical and experimental evidence (e.g., de Bremond d'Ars *et al.,* 2001; Mungall & Su, 2005; Godel *et al.,* 2006; Barnes *et al.,* 2008; Chung & Mungall, 2009; Arndt 2011; Godel *et al.,* 2013).

Sulphide- and chromitite-bearing ultramafic units hosting platinum-group minerals (PGM) are documented within the British Paleogene Igneous Province (BPIP) on the islands of Skye, Mull and Rum (Pirrie *et al.,* 2000; Prout *et al.,* 2002; Hubert *et al.,* 1992; Butcher *et al.,* 1999; Power *et al.,* 2000) and highlighted the potential for PGE mineralisation in the Scottish portion of the North Atlantic Igneous Province (NAIP; Andersen *et al.*, 2002). This is especially the case considering the potential for contamination offered by the thick crustal sequences of S-bearing rocks in the region (e.g., the Mesozoic Hebrides Basin). Recent studies on Skye demonstrate the involvement of sediments, with light S-isotope tenors, in triggering S-saturation in ascending BPIP magmas, particularly in vertical narrow sheeted intrusions such as dyke swarms (Hughes *et al.,* accepted, a; Chapter 11). On Rum, ultramafic, vertical or steeply inclined volcanic plugs (pipes) intrude a variety of country rocks, including sediments at the base of the Mesozoic Hebrides Basin. Power *et al.* (2002) identified a crustal $\delta^{34}S$ signature for

intercumulus (net-textured) sulphides in one volcanic plug in northwest Rum, but could not establish whether the sulphide liquids that formed these had been entrained upwards or sunk downwards through the conduit.

In this study, we use whole-rock geochemistry, whole-rock S-isotope composition, and sulphide-specific (*in situ*) S-isotope and trace element compositions for ultramafic volcanic plugs on Rum to constrain where crustal contamination took place. The size range and trace element composition of sulphide minerals, alongside their textural associations, are established for each plug in order to understand the provenance of sulphide liquids in these conduits. We use these data to decipher what the controls were on sulphide accumulation and compare plug sulphide compositions to those from peridotitic cyclic units of the Eastern Layered Series, part of the Rum Layered Suite. These data are combined with numerical modelling of settling and entrainment rates to investigate the roles of magma entrainment, and gravitational settling and sinking of sulphide liquids within conduit systems. We provide new constraints on the development of orthomagmatic Ni-Cu-PGE mineralisation in small BPIP intrusions and discuss these in relation to wider processes of sulphide migration within magmatic systems.

12.2. Regional geological setting

The North Atlantic Igneous Province (NAIP) formed after the impingement of the Icelandic mantle plume under thick continental lithosphere, during a period of continental flood basalt magmatism (e.g., Saunders *et al.*, 1997). Magmatism initiated c. 62 Ma within what is now the UK, Greenland and Baffin Island, and ultimately led to the opening of the Atlantic Ocean (Saunders *et al.*, 1997). The main products of this prolonged period of magmatism were tholeiitic and alkali basalts. The British Palaeogene Igneous Province (BPIP) is part of the earliest magmatic series of the NAIP, which includes Palaeogene rocks in the Hebrides, along the west coast of Scotland and Northern Ireland (Saunders *et al.,* 1997; Fig. 12.1).

In Scotland, the BPIP includes magmatic rocks on the Isles of Mull, Skye, Arran, the Small Isles (Rum, Eigg, Muck, Canna, and Sanday), and on the mainland at Ardnamurchan and Morvern (Emeleus and Bell, 2005). The Scottish BPIP extends across a number of Archaean and Proterozoic basement terranes (e.g., Emeleus and Bell, 2005). Neoproterozoic (Dalradian and Moine) metasediments cover the basement and are overlain by Mesozoic sediments from the Hebrides Basin. Volcanic plugs occur within or close to lava fields and central complexes, and

are primarily exposed on the Isles of Mull and Rum (Emeleus & Bell, 2005). Emeleus and Bell (2005) provide a detailed review of radiometric and palynological age determinations of various intrusions and lavas across the BPIP.

12.2.1. Geology of the Isle of Rum

The Rum Central Complex straddles the Long Loch Fault (Fig. 12.1), which experienced pre-BPIP movements and likely acted as a crustal lineament that facilitated magma ascent (e.g., Upton *et al.,* 2002). The complex developed over at least three different magmatic phases, forming in < 500 kyr (Emeleus & Bell, 2005; Troll *et al.,* 2008).

In *Phase 1,* silicic magmatism occurred in an arcuate fault system (the Main Ring Fault) at 60.33 ± 0.21 Ma (Troll *et al.,* 2008). This was rapidly followed by *Phase 2*, which formed the mafic-ultramafic Rum Layered Suite (60.53 ± 0.04 Ma; Hamilton *et al.*, 1998). Ultramafic magmas were intruded into the complex as multiple intrusions and replenishment of the chamber with picritic magma is thought to have caused disruption of the previously formed cumulate layers (e.g., Bedard, 1988). The mafic-ultramafic Rum Layered Suite can be divided into the Western, Central and Eastern Layered Series, bounded by the Main Ring Fault (Fig. 12.1). Rare late-stage picrite dykes (described by Upton *et al.,* 2002) are thought to represent the parental magmas to the layered suites. However, the small melt fraction (6-7 % melting) inferred to have formed these mildly alkalic dykes, and two olivine phenocryst populations observed within individual picrites dykes, such as M9 (e.g., Upton *et al.,* 2002), may preclude this from truly representing the bulk parental magma composition. During *Phase 3,* deep subaerial erosion and unroofing of the complex followed caldera collapse and intermittent burial by basalt flows from the Skye lava field (Chambers *et al.*, 2005).

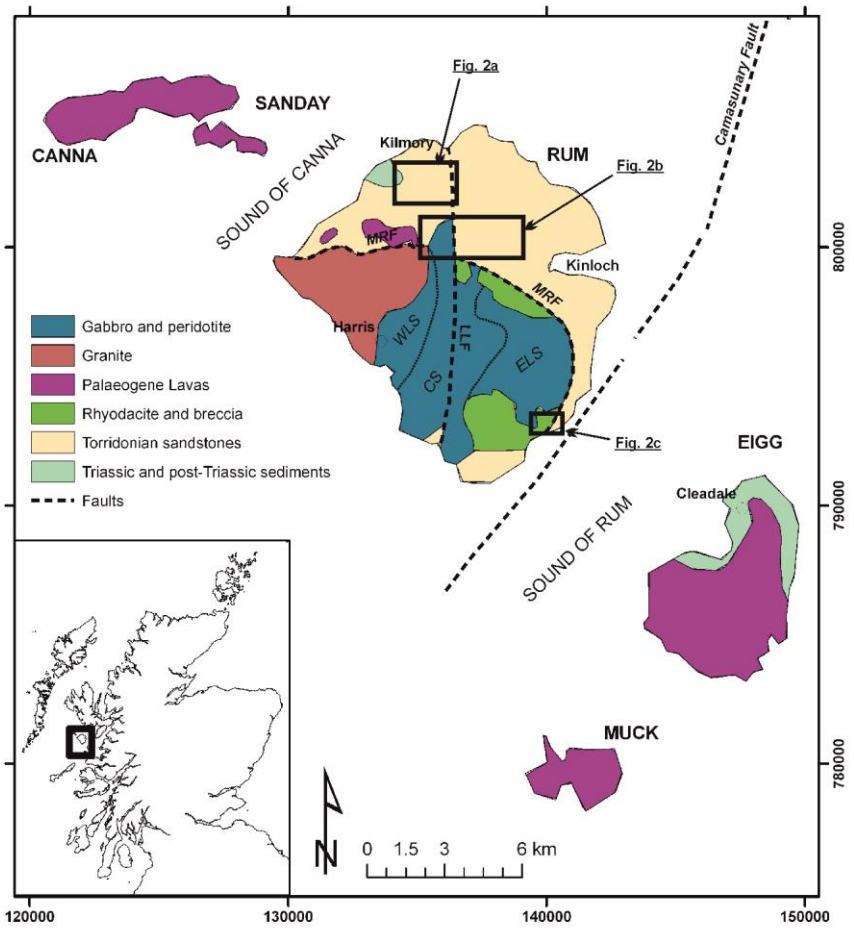

Figure 12.1. Simplified geology of the Isle of Rum and surrounding Small Isles. Inset shows outline map of Scotland. Boxes show map locations in Figure 12.2. Abbreviations are; Long Loch Fault (LLF), Main Ring Fault (MRF), Western Layered Series (WLS), Central Series (CS), and Eastern Layered Series (ELS).

12.2.2. Ultramafic plugs of the Isle of Rum

12.2.2.1. Field relations and structural setting

In excess of 40 volcanic plugs occur on Rum, comprising gabbros and feldspathic peridotite intrusions (*senso stricto* olivine melagabbros) probably formed during *Phase* 2. Plugs predominantly intruded through Torridonian and Triassic sediments, as well as portions of the Rum Layered Suite (McClurg, 1982; Wadsworth, 1994; Holness, 1999). Locality details of the plugs sampled during this study are given in Table A (Supplementary Material – on disk) (also see Figs. 12.2a-c).

The plugs have rounded or elongate/teardrop-shaped outlines (e.g., Fig. 12.2a). Their plan-view shapes probably result from varying angles of conduit intrusion intersecting present-day topography. The plugs sampled during this investigation are distinct from the small

'apophyses' of peridotite within or straddling the Main Ring Fault, which may predate or be contiguous with the Eastern Layered Series (e.g., Fig. 12.2b; Butcher *et al.,* 1985; Wadsworth, 1994). None of the plugs have yet been radiometrically dated, and the timing of their intrusion is reliant upon cross-cutting field relationships alone. Most of the plugs lie within 1-2 km of the Long Loch Fault (Fig. 12.1) and range in size from ~ 100 to 600 m diameter (McClurg, 1982; Volker & Upton, 1990). The plugs may have fed lava flows, but no associated lavas have been proven (Emeleus & Bell, 2005).

The structural setting and silicate mineralogy of volcanic plugs on Rum has been studied in detail by Volker & Upton (1990), Wadsworth (1994), Holness (1999) and Holness *et al.* (2012). Ultramafic plugs are thought to represent the conduits of olivine-rich melts or 'crystal mushes', fed from an underlying magma chamber along faults such as the Long Loch Fault. These crystal mushes were lubricated by interstitial basaltic magma. The contemporaneous series of gabbroic plugs on the island could therefore represent similar conduits, but without an entrained olivine mush. Most plugs are composed of either gabbro or peridotite, and rare plugs (e.g., in S Rum) have rounded troctolite (allivalite), dunite and chromitite xenoliths, probably derived from part of the Rum Layered Suite (Volker & Upton, 1990).

Layering (defined by olivine cumulates) is only recorded in the ultramafic peridotite plugs and typically dips shallowly at the margins (striking parallel to margins) with central portions of plugs taking on a colloform texture. Changes in modal mineralogy can also define layering, now weathered to 'indentation layering'. At the West Sgaorishal plug (Fig. 12.2a, Plug 1) indentation layering is particularly well developed and is observed to be closely spaced at the margins (5-10 cm) dipping inwards towards the plug centre by 30-50°, with layer spacing increasing towards, and ultimately disappearing, at the plug centre. By contrast, in the other plugs layering is generally poorly developed, laterally discontinuous (e.g., Loch Sgaorishal plug; Fig. 12.2a Plug 2) or completely absent, although this may also be an artefact of poor exposure. Layering developed after magma flow had ceased, or perhaps during magma withdrawal back into the feeder system (c.f. 'suck-back' of Hawaiian conduits, as suggested by Upton, 2004).

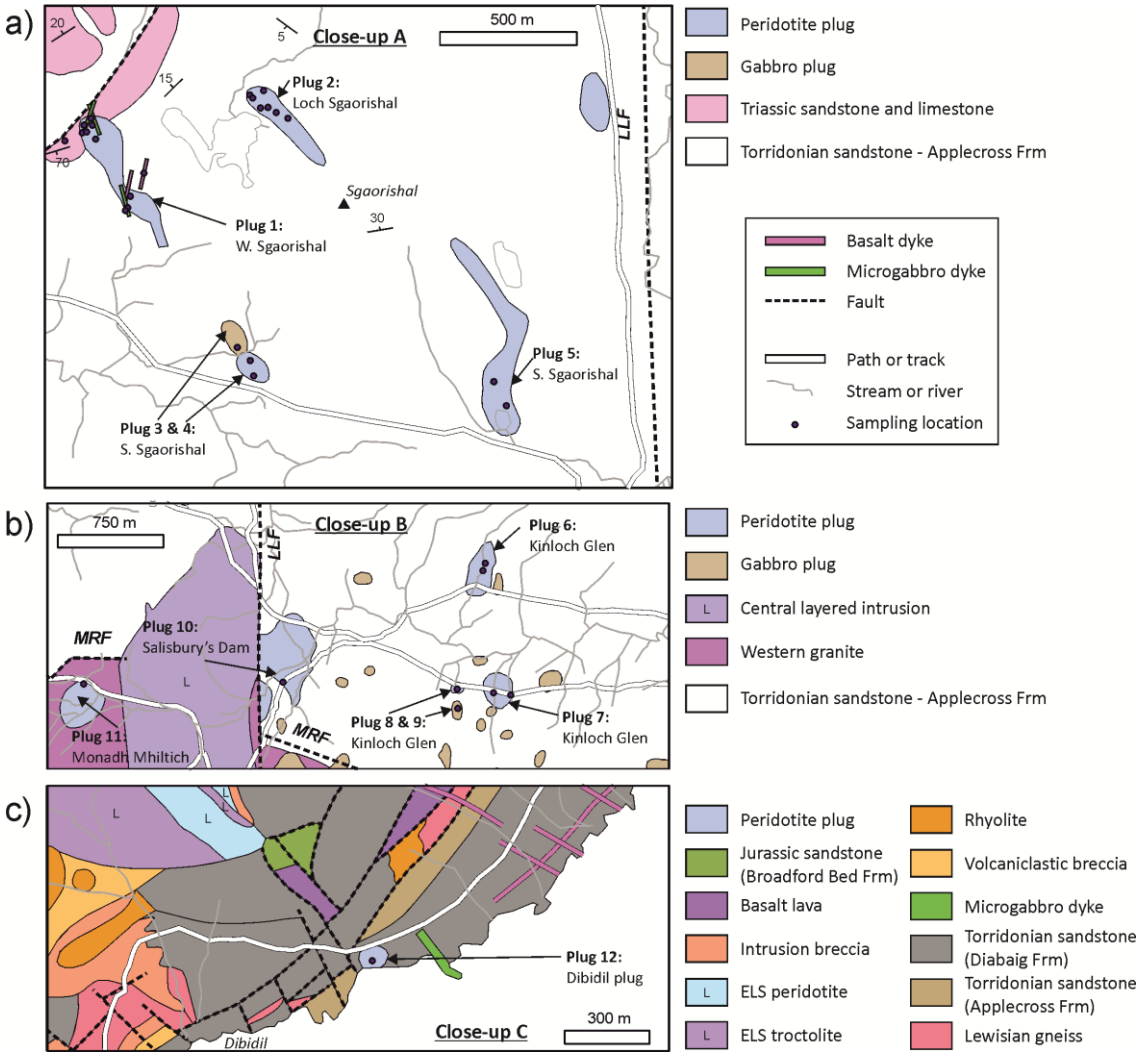

Figure 12.2. Geology of areas surrounding peridotite and gabbro plugs sampled during this study. (a) northwest Rum, (b) central Rum across the Long Loch Fault, (c) SE Rum near Dibidil. Sample locations are shown as dots. Plugs are numbered and correspond to Table A (Supplementary Material – on disk).

The sedimentary host rocks of the volcanic plugs (Triassic; Fig 12.2a, and Torridonian; Fig. 12.2a-c) typically appear bleached, fissile and metasomatised. Studies of *in situ* anatexis of country rocks have provided insights into the longevity of the plugs as active magma conduits (e.g., Holness 1999; Holness *et al.,* 2012). Thermal modelling of the West Sgaorishal plug (Plug 1; Fig. 12.2a), suggests that this was an active magma conduit for only a few months, with magma temperatures of 1400°C and cooling over a period of approximately 30 years (Holness *et al.,* 2012).

12.2.2.2. Mineral compositions and relation to layered intrusions

The peridotite plugs show similarities in mineral composition with layered intrusions of the Rum Central Complex (e.g., Eastern Layered Series). Interstitial to cumulus olivine are plagioclase (10-15 modal %) and clinopyroxene (up to 8 %) with the latter forming poikilitic crystals. Accessory amphibole and biotite are also observed, as well as euhedral and rounded Cr-spinel (Wadsworth, 1994). Olivine compositions in plugs are equivalent to those from feldspathic peridotites in the Eastern Layered Series (Fo_{89-82}) and Western Layered Series (Wadsworth, 1994; Emeleus, 1997 and references therein; Holness *et al.,* 2012) and distinct from olivine compositions in the troctolite portions of the Rum Layered Suite (Fo_{84-70}; Emeleus, 1997 and references therein).

In the West Sgaorishal plug (Plug 1; Fig. 12.2a), olivine accounts for 55-60 vol.% of the rock and delineates layering. However, olivine abundance increases to 88 vol.% at the centre (where layering becomes less clearly defined or colloform) with a marked asymmetry in the olivine content from west to east, such that olivine is more concentrated on the western edge (see Holness *et al.,* 2012).

12.2.3. The Hedridean sedimentary succession and country rocks to the Rum plugs

The crustal sequence on the Isle of Rum includes Archaean basement rocks of the Lewisian Gneiss Complex, Mesoproterozoic Torridonian sediments and Triassic sediments in northwest Rum that are the oldest stratigraphic units of the Hebrides Basin. A thick sequence of Jurassic and Cretaceous sediments probably also covered the island (at least in part) as suggested by extensive outcrops of these rocks preserved on the neighbouring Isle of Skye, and 'wedges' of Jurassic mudrocks preserved in the Main Ring Fault of the Rum Central Complex (Emeleus, 1997; see Hughes *et al.,* accepted, Appendix E for stratigraphic log).

12.2.3.1. S-isotope signatures in western Scotland

Lewisian gneisses generally have variable, but low sulphur concentrations and $\delta^{34}S$ ranging -1.4 to +5.5 ‰ on the northwest Scottish mainland (Lowry *et al.,* 2005). The Neoproterozoic metasediments of the Dalradian and Moine successions (Grampian and Northern Highland Terranes, respectively) are mostly dominated by ^{34}S-enriched metasedimentary sequences (Lowry *et al.,* 2005). Moine metapelites have low or very low concentrations of sulphur, and where measurable have $\delta^{34}S$ = +2.5 ‰ (Hughes *et al.,* accepted, a – Chapter 11) and +3.4 to

+4.6 ‰ in some psammites (Lowry, 1991). Dalradian metasediments (with disseminated diagenetic and metamorphic sulphides, mostly pyrite and pyrrhotite) have a mean $\delta^{34}S$ of +8 ‰ (± 14 ‰; Lowry *et al.,* 2005).

The Mesoproterozoic Torridonian Formations of northwest Scotland include the Stoer, Sleat and Torridon Groups (Stewart, 2002; Kinnaird *et al.*, 2007), however the Stoer Group is thought to be absent on the Isles of Skye and Rum (Figs. 12.1-12.2). Mudrocks are present within the Sleat (and to a lesser extent, Torridon) Group, however they are less extensive and thinner than the mudrocks observed in Jurassic units of the Hebrides Basin. Sulphur isotope studies of Torridonian sulphates and sulphides in Stoer Group mudrocks have identified the light isotopic shift of $\delta^{34}S$ associated with bacterial sulphate reduction in small freshwater pools (Parnell *et al.*, 2010; Parnell *et al.*, 2012). Hughes *et al.* (accepted, a; Chapter 11) found no evidence for bacterial sulphate reduction in Torridonian sediments on Skye or Rum, and established a Mesoproterozoic whole-rock $\delta^{34}S$ range of +1.4 to +4.7 ‰. They also found that these rocks contained low concentrations of sulphur (< 0.018 wt.%, below detection limit).

The stratigraphy of Triassic to Cretaceous rocks of the Hebrides Basin is well correlated (e.g., Morton & Hudson, 1995; Hesselbo & Coe, 2000 and references therein) and has also been investigated for crustal S contamination potential and $\delta^{34}S$ signature (Hughes *et al.,* accepted, a – Chapter 11), with Hebridean Jurassic shales showing a distinctive range in S-isotope composition from $\delta^{34}S$ -33.8 to -14.7 ‰.

12.2.4. Magmatic sulphide mineralisation and S contamination in the NAIP

On the Isle of Rum, disseminated and net-textured coarse sulphides (up to 5 % modal abundance; Power *et al.,* 2003) occur within a few metres of the margin of the West Sgaorishal peridotite plug (Plug 1; Fig. 12.2a). Sulphides become increasingly rare and fine-grained towards the centre of the plug (Power *et al.,* 2003). Sulphide-rich zones have not thus far been identified in the other plugs on Rum, and no sulphide minerals have previously been described in them. PGM are associated with sulphides in the West Sgaorishal plug, including Pt- and Pd-tellurides, bismuth-tellurides, and electrum, however no Ir, Os or Ru-bearing phases are observed (Power *et al.,* 2003). $\delta^{34}S$ of the coarse sulphides vary from -18.3 to -9.2 ‰, suggesting Jurassic sedimentary rock contamination, and resulting in S-saturation and PGE scavenging from silicate magma within the conduit (Power *et al.,* 2003). Given the absence of crustal rocks with low $\delta^{34}S$ currently surrounding the plug, Power *et al.* (2003) suggested that S

contamination either took place in a now-eroded parental magma chamber, or from Jurassic sediments locally surrounding the plug, also now eroded. Both scenarios are plausible, however, the intercumulus texture of sulphides in this plug strongly suggests that sulphide liquid was an integral part of the magma within the conduit, and was likely transported some distance.

More broadly, Jurassic shales of the Hebridean Basin appear an important source of crustal sulphur, inducing S-saturation and strongly contaminating dykes in the BPIP, with implications for exploration for orthomagmatic Ni-Cu-PGE (Hughes *et al.,* accepted, a – Chapter 11). Incorporation of bacterially reduced sulphur from shales show $\delta^{34}S$ signatures in magmatic sulphides of -30.7 to -2.3 ‰, depending on the degree of contamination and the $\delta^{34}S$ signature of the local crustal contaminant, although contamination is not always shown (e.g. horizontal picritic sill complexes; Hughes *et al.,* accepted, a – Chapter 11). Hughes et al. (accepted, a; Chapter 11) show that the mechanism by which a conduit intruded and the ambient flow regime within it (i.e., turbulent or non-turbulent) were important factors in the contamination process.

Magmatic Cu-Ni-PGE-Au sulphide mineralisation within the wider NAIP is recorded in a number of different settings on both sides of the Atlantic. The largest deposit is the Au- and Pd-dominant Platinova Reef in the Skaergaard Intrusion, formed through prolonged fractional crystallisation which triggered S-saturation (e.g. Bird *et al.,* 1991; Andersen *et al.,* 1998; Holwell and Keays, 2014) rather than crustal contamination. Sulphide mineralisation is also found as sulphide globules and disseminations in small hyperbyssal intrusions, such as the Miki Fjord and Togeda Macrodykes (Holwell *et al.,* 2012). Sulphur isotope analyses identified strong crustal S contribution attributed to pyritic Cretaceous black shales, triggering S-saturation (Holwell *et al.,* 2012).

In summary, disseminated mineralisation in magma conduits, such as sills, dykes and plugs, can be used as vectoring tools towards areas of massive sulphide mineralisation (e.g., Lightfoot *et al.,* 1984; Czamanske *et al.,* 1992; Huminicki *et al.,* 2008). Hence understanding the source and location of crustal contamination which triggered S-saturation, in relation to the prevailing fluid dynamic regime in a magmatic conduit, is a valuable method for targeted exploration.

12.3. Methodology

Twenty six whole-rock samples from 12 individual volcanic plugs from across the Isle of Rum were sampled for major and trace elements, S-isotopes, and mineralogical investigations (sample details in Table A (Supplementary Material – on disk), see Figs. 12.2a-c for localities). Additionally, 15 samples of various Torridonian and Triassic sediments were collected from areas adjacent to the plugs, and elsewhere across the island to assess the crustal S-isotopic framework of the island (Table A; Supplementary Material – on disk).

12.3.1. Bulk rock analysis

Weathered material was removed from each sample before crushing to a fine powder by standard procedures. Major and trace elements were analysed by inductively coupled plasma optical emission spectrometry (ICP-OES –JY Horiba Ultima-2 model) and inductively coupled plasma mass spectrometry (ICP-MS – Thermo X Series 2) respectively following McDonald & Viljoen (2006). Platinum-group element (PGE) and Au analysis was carried out by Ni-sulphide fire assay followed by Te co-precipitation and ICP-MS (Huber *et al.*, 2001; McDonald & Viljoen, 2006). Accuracy for whole-rock elemental geochemistry was constrained by analysis of certified reference materials TDB1, WPR1 and WMG1 for PGE and Au, and JB1a, NIM-N and NIM-P for all other trace and major elements (Supplementary Material – Tables F and G, on disk). Precision was determined by repeat analyses of a sub-set of samples (Supplementary Material – Table H, on disk) with all elements repeatable to within 10% or better, and PGE to within < 20%. Results are presented on Table 12.1.

For samples with visible sulphide minerals > 500 μm^2, polished blocks were subjected to sulphide *in situ* laser combustion, sulphide following Wagner *et al.* (2002). Samples without sufficiently large sulphides underwent whole-rock chemical S extraction followed by conventional sulphur analysis: details and evaluation of this method can be found in Hughes *et al.* (accepted, a; Chapter 11). SO_2 gases released by combustion were analysed on a ThermoFisher Scientific MAT 253 dual inlet mass spectrometer (conventional samples) and VG Isotech SIRA II mass spectrometer (for laser samples). Reproducibility for both the laser combustion and conventional analysis is ± 0.4 ‰ (see Hughes *et al.,* accepted, a – Chapter 11) with 2σ of standards < ± 0.2 ‰. Standards used throughout all analyses were IAEA-S-3 (-31.5 ‰) and NBS-123 (sulphate+17.1 ‰) international standards, alongside an SUERC laboratory chalcopyrite standard, CP-1 (-4.6 ‰).

Bulk rock S concentrations were determined using a LECO CS230 Carbon/Sulphur Determinator at the University of Leicester. Sample mass ranged 0.1 to 1.0 g depending on relative bulk S content. Each sample was run in triplicate to monitor precision. Accuracy was monitored by regular analysis of the reference material BAS ECRM 877-1. The limit of minimum detection for this method is 0.018 wt.% S (3 x standard deviation of the mean blank).

12.3.2. Mineralogy and mineral composition methodology

Quantitative microanalysis was carried out on a Cambridge Instruments S360 scanning election microscope, using an Oxford Instruments INCA Energy EDX analyser, with operating conditions set at 20 kV and specimen calibration current of ~2 nA at a fixed working distance of 25 mm. Analytical drift checks were carried out every 2 hours using the Co reference standard and a comprehensive suite of standards from MicroAnalysis Consultants Ltd were used to calibrate the EDX analyser.

Sulphide trace element analysis on selected polished samples were analysed using a New Wave Research UP213 UV laser system attached to a Thermo X Series ICP-MS, followed Prichard *et al.* (2013) and Smith *et al.* (2014). See Supplementary Material (on disk) for standard compositions.

As part of our study, we also analysed the sulphide compositions of a selection of peridotites from each of the major cyclic units in the Eastern Layered Series, in order to put plug compositions into context (e.g., grey shaded backgrounds in Figs. 12.6 and 12.7). The results are presented in Table C of Supplementary Material (on disk), alongside whole-rock $\delta^{34}S$ for corresponding ELS samples (Table D and E, Supplementary Material, on disk).

12.4. Results

12.4.1. Whole-rock geochemistry

Whole-rock major element compositions of peridotite volcanic plugs overlap with those of published compositions for the Eastern Layered Series (see Emeleus, 1997 and O'Driscoll *et al.,* 2009 and references therein). These classify the peridotite plugs as tholeiitic picrobasalts (total alkali silica (TAS) classification Le Maitre *et al.,* 2002) with Mg# ranging between 0.83-0.89

(Table 12.1). Using the TAS classification, the gabbro plugs are basalts, transitional between tholeiitic and alkaline (Mg# 0.56-0.68). Textural evidence from one peridotite plug sample, RM63, suggests this has been significantly altered, and this is reflected a higher SiO_2 content, such that it classifies as basalt under TAS, with anomalously low Mg# (0.52). We present whole-rock trace element compositions of the Rum plugs in Supplementary Material Part B.

12.4.1.1. Platinum-group elements

Chondrite normalised whole-rock PGE concentrations of plug samples are shown in Figure 12.3a-f. Each plug has a systematic signature, and where sampled, we note variations in concentration between the plug centre and margins (e.g., plugs 1, 2, 4, 5 and 7) such that the normalised patterns remain broadly parallel. Generally, all peridotite plugs have a flat normalised pattern, such that Ir-group PGE (IPGE) are neither strongly enriched nor depleted in comparison to Pd-group PGE (PPGE). However, between individual peridotite plugs, the degree of PGE fractionation changes, showing various anomalies. For example, in plug 1, all samples have a slightly positive Os anomaly. The centre of this plug (i.e., sample RM30) has a subtle positive anomaly of Ru, and no Pd anomaly, whereas the plug margins have a spread of positive Pd anomalies over Pt and Au (Fig. 12.3a). Plugs 6, 7 and 8 have the most variable PGE patterns with the centres of plugs 7 and 8 have a notable negative Ir anomaly, and there is a negative Pt anomaly for the centre of plug 8 (Fig. 12.3e). One of the samples from the centre of plug 6 (RM63) has a notably lower PGE abundance than the other plug 6 centre sample and other plugs sampled, but we note that RM63 was serpentinised. The M9 picrite dyke has PPGE enrichment relative to IPGE, with a similar normalised pattern to plugs 1, 2, 10, 11 and 12 (Fig. 12.3f). Platinum-group element abundances for the two gabbro plugs were not measured.

12.4.2. Sulphide mineralogy and trace element compositions

Details of the mineralogy; including size, texture and mineral association of base metal sulphides in the Rum plugs are presented in Table 12.2 together with a record of any PGM present. SEM-based PGM searches were only carried out on samples from Plugs 1, 2 and 10 as previous work had identified a correspondence between sulphide and PGM occurrences (e.g., Power *et al.,* 2003). Thus the main aim of our study was to establish sulphide compositions and abundance. Selected back scattered electron images of sulphide mineral textures are shown in Figure 12.4.

Table 12.1. *(continues overleaf)*

Sample number	Location	Plug number (Fig. 1)	Plug type	Margin/Centre *(wt.%)*	SiO_2	Al_2O_3	Fe_2O_3*	MgO	CaO	Na_2O	K_2O	TiO_2	MnO	P_2O_5	LOI	Total	Mg#
RM81	Dibidil	12	peridotite	centre	42.83	6.56	10.46	32.19	4.75	0.83	0.08	0.29	0.15	0.02	2.29	100.44	0.88
RM58	Kinloch Glen	7	peridotite	margin	41.13	3.43	12.03	38.08	2.86	0.32	0.03	0.39	0.17	0.03	2.36	100.82	0.88
RM59	Kinloch Glen	7	peridotite	centre	43.92	2.58	12.43	35.37	1.61	0.10	0.01	0.22	0.16	0.02	3.19	99.61	0.86
RM60	Kinloch Glen	9	gabbro	margin	46.78	15.45	10.65	8.97	11.24	2.58	0.21	1.01	0.16	0.07	2.99	100.11	0.68
RM61	Kinloch Glen	8	peridotite	centre	41.49	5.93	11.34	32.57	5.26	0.54	0.03	0.28	0.16	0.02	2.03	99.64	0.87
RM63	Kinloch Glen	6	peridotite	centre	48.26	12.94	13.91	5.55	10.93	3.33	0.64	2.45	0.20	0.18	1.86	100.25	0.52
RM64	Kinloch Glen	6	peridotite	centre	42.06	6.10	11.81	33.76	4.01	0.61	0.07	0.22	0.17	0.02	1.38	100.21	0.87
RM17	Monadh Mhiltich	11	peridotite	margin	43.10	3.37	11.40	34.19	2.34	0.19	0.05	0.25	0.15	0.03	4.52	99.97	0.87
RM18	Salisbury's Dam	10	peridotite	margin	42.07	6.10	11.32	29.97	5.04	0.89	0.12	0.59	0.14	0.05	3.16	99.81	0.86
RM35	Loch Sgaorishal	2	peridotite	centre	42.44	4.69	10.74	33.16	3.87	0.69	0.08	0.21	0.15	0.03	2.86	99.36	0.88
RM70	Loch Sgaorishal	2	peridotite	NW margin (at contact)	43.57	7.77	10.14	28.14	6.01	1.19	0.08	0.40	0.16	0.03	2.41	99.90	0.87
RM71	Loch Sgaorishal	2	peridotite	NW margin (5m inwards from contact)	42.54	6.33	10.08	31.97	4.78	0.93	0.08	0.28	0.15	0.02	3.06	100.23	0.88
RM73	Loch Sgaorishal	2	peridotite	centre	42.14	5.04	10.08	34.82	3.85	0.75	0.07	0.25	0.15	0.04	3.56	100.75	0.89
RM74	Loch Sgaorishal	2	peridotite	NE margin	42.90	8.72	9.98	26.03	6.48	1.25	0.15	0.44	0.15	0.05	3.03	99.17	0.86
RM75	Loch Sgaorishal	2	peridotite	NE margin (~ 20m inwards from inferred contact)	42.43	6.24	10.11	32.17	4.88	0.85	0.06	0.28	0.15	0.02	2.90	100.09	0.88
RM85	Southern Sgaorishal	5	peridotite	margin	40.60	5.02	10.93	33.87	3.58	0.40	0.02	0.53	0.16	0.06	4.57	99.74	0.88
RM86	Southern Sgaorishal	5	peridotite	centre	42.12	3.15	11.37	37.26	2.50	0.46	0.02	0.28	0.16	0.03	1.94	99.30	0.88
RM87	Southern Sgaorishal	4	peridotite	margin	41.42	8.94	12.46	26.04	5.80	0.96	0.12	0.45	0.17	0.05	2.87	99.29	0.83
RM88	Southern Sgaorishal	4	peridotite	centre	42.41	6.08	12.03	32.10	4.34	0.85	0.06	0.44	0.17	0.05	2.31	100.85	0.86
RM89	Southern Sgaorishal	3	gabbro	S margin (~ 3m inwards from inferred contact)	43.74	16.15	14.90	7.44	7.54	3.79	0.12	1.97	0.18	0.23	3.22	99.27	0.56
RM29	West Sgaorishal	1	peridotite	N margin (~ 30m inwards from inferred contact)	41.86	4.49	12.00	34.02	3.51	0.56	0.07	0.31	0.15	0.03	1.50	99.15	0.87
RM30	West Sgaorishal	1	peridotite	centre	38.65	3.05	11.01	36.30	2.49	0.23	0.04	0.26	0.14	0.03	6.49	99.38	0.88
RM32	West Sgaorishal	1	peridotite	NW margin (~ 35m inwards from inferred contact)	42.33	5.37	11.54	31.87	4.56	0.67	0.09	0.40	0.15	0.04	1.77	99.35	0.87
RM33	West Sgaorishal	1	peridotite	N margin	39.83	4.32	12.28	32.81	3.73	0.50	0.06	0.32	0.15	0.02	4.67	99.20	0.86
RM91	West Sgaorishal	1	peridotite	S margin	42.17	7.70	11.72	27.66	5.71	0.92	0.12	0.54	0.16	0.05	3.25	100.01	0.85
RM95	West Sgaorishal	1	peridotite	NW margin	42.20	5.98	11.95	31.93	4.43	0.75	0.05	0.44	0.16	0.04	2.14	100.07	0.86
M9	(Upton *et al.,* 2002)	n/a	picrite dyke	n/a	42.77	7.22	11.43	30.07	5.53	1.02	0.11	0.73	0.17	0.04	1.38	100.47	0.87

Table 12.1. *(continues overleaf)*

Sample number	*(ppm)*	Sc	V	Cr	Co	Ni	Cu	Rb	Sr	Y	Zr	Nb	Ba	La	Ce	Pr	Nd	Sm	Eu	Gd	Tb	Dy	Ho	Er	Tm	Yb	Lu
RM81		15	111	2883	-	1771	115	2.8	47	6.0	22	1.55	22	1.46	3.55	0.58	2.62	0.70	0.25	0.94	0.17	0.93	0.20	0.59	0.10	0.64	0.09
RM58		12	100	3216	-	2215	40	0.7	37	2.8	23	0.29	3	0.72	2.35	0.43	2.08	0.63	0.22	0.59	0.11	0.58	0.12	0.30	0.04	0.34	0.05
RM59		9	61	3007	143	2519	30	1.1	10	2.3	13	0.29	9	0.58	1.91	0.33	1.74	0.47	0.16	0.38	0.07	0.49	0.09	0.24	0.04	0.24	0.03
RM60		29	304	361	-	188	108	4.1	157	15.2	59	1.26	60	3.66	9.14	1.50	7.44	2.25	0.74	2.20	0.40	2.49	0.49	1.30	0.21	1.22	0.19
RM61		15	94	2261	-	1686	92	1.1	62	2.6	16	0.13	3	0.59	1.95	0.35	1.78	0.58	0.23	0.72	0.13	0.61	0.11	0.29	0.05	0.28	0.04
RM63		41	483	76	-	54	103	15.7	315	28.7	185	4.88	124	11.65	29.97	4.67	21.47	5.65	1.76	5.68	0.77	4.88	0.93	2.41	0.38	2.29	0.34
RM64		11	68	3414	-	3896	125	2.3	63	2.1	16	0.27	86	1.19	2.75	0.41	1.92	0.48	0.21	0.61	0.11	0.52	0.11	0.28	0.04	0.29	0.04
RM17		9	88	2645	115	2274	27	3.0	39	4.9	21	1.03	33	0.93	2.58	0.40	1.95	0.62	0.21	0.74	0.13	0.76	0.15	0.44	0.07	0.42	0.07
RM18		16	160	2444	104	1816	35	2.4	75	8.3	31	1.23	21	1.52	4.57	0.78	3.97	1.28	0.42	1.36	0.25	1.34	0.25	0.74	0.11	0.66	0.11
RM35		12	87	2969	104	2477	30	1.9	31	5.3	12	0.92	17	0.84	2.20	0.35	1.59	0.54	0.20	0.67	0.13	0.80	0.16	0.49	0.08	0.49	0.09
RM70		17	157	2276	-	1579	104	3.3	44	9.3	30	0.46	22	1.60	4.08	0.66	3.38	1.07	0.36	1.20	0.23	1.43	0.31	0.89	0.15	0.94	0.14
RM71		14	114	2879	-	1873	71	3.2	30	6.3	18	0.27	20	1.19	2.89	0.45	2.26	0.71	0.26	0.85	0.17	0.98	0.21	0.61	0.10	0.64	0.10
RM73		12	97	2922	-	2138	47	2.9	27	4.8	16	0.23	24	0.86	2.28	0.38	1.79	0.57	0.21	0.88	0.15	0.78	0.18	0.49	0.08	0.54	0.08
RM74		18	157	1951	-	1361	101	8.3	97	9.3	28	0.39	44	1.59	4.12	0.67	3.49	1.13	0.38	1.20	0.24	1.50	0.31	0.89	0.16	1.00	0.15
RM75		14	109	2732	-	1936	53	2.5	30	5.9	16	0.22	17	1.03	2.63	0.44	2.11	0.67	0.24	0.89	0.15	0.96	0.21	0.58	0.10	0.63	0.09
RM85		12	124	3494	114	1930	30	1.3	111	5.4	48	1.20	25	1.14	3.58	0.60	3.09	0.96	0.38	1.05	0.17	0.94	0.18	0.54	0.08	0.49	0.08
RM86		11	77	3162	126	2531	38	1.1	34	4.6	27	0.67	11	0.38	1.43	0.29	1.56	0.52	0.22	0.67	0.11	0.74	0.14	0.38	0.05	0.37	0.06
RM87		14	116	1967	111	1233	92	4.6	114	6.1	40	0.99	29	1.64	4.53	0.76	3.47	1.06	0.37	1.09	0.18	1.09	0.20	0.58	0.08	0.54	0.09
RM88		15	119	2925	118	1770	66	2.7	55	7.0	36	0.80	24	0.97	2.78	0.51	2.66	0.87	0.34	1.10	0.16	1.10	0.21	0.66	0.09	0.59	0.08
RM89		26	187	28	61	151	82	3.7	257	35.6	149	2.72	31	3.24	10.27	2.12	12.43	4.46	1.78	5.42	0.96	5.79	1.04	3.15	0.44	2.94	0.42
RM29		13	94	4458	125	2276	56	1.9	44	5.6	25	1.81	21	1.21	3.05	0.50	2.38	0.72	0.25	0.94	0.16	0.89	0.17	0.49	0.08	0.46	0.08
RM30		10	65	4520	106	2600	23	1.2	42	3.8	15	0.91	14	0.69	1.87	0.31	1.59	0.50	0.18	0.60	0.11	0.61	0.11	0.33	0.05	0.33	0.05
RM32		14	117	3708	110	2166	52	2.7	60	7.0	22	2.09	22	1.24	3.43	0.55	2.85	0.95	0.34	1.07	0.20	1.18	0.22	0.63	0.10	0.58	0.10
RM33		13	96	3469	124	3161	215	2.2	46	6.2	22	1.05	16	1.13	2.98	0.48	2.34	0.73	0.26	0.98	0.17	0.97	0.19	0.55	0.08	0.51	0.09
RM91		19	151	2437	114	2000	401	4.9	110	9.8	38	0.74	32	1.32	3.71	0.71	3.77	1.28	0.46	1.49	0.26	1.63	0.30	0.88	0.12	0.75	0.11
RM95		15	120	3163	119	1478	250	2.9	56	7.8	40	0.89	25	1.16	3.02	0.54	2.83	1.00	0.38	1.14	0.20	1.24	0.24	0.72	0.09	0.60	0.08
M9		20	172	2032	101	1561	110	2.9	93	10.8	44	2.30	8	2.21	6.08	1.07	5.20	1.65	0.56	1.50	0.24	1.70	0.32	0.93	0.15	0.91	0.14

Table 12.1. Whole-rock major and trace element results for the Isle of Rum volcanic plugs. Also sulphur isotopic composition ($\delta^{34}S$) measured via conventional (following whole-rock sulphur extraction) and laser combustion methodologies, and whole-rock sulphur concentration (wt.%). Dash marks indicates analysis was not run for that sample. Sample below detection limit are indicated by < d.t. or < value. Detection limit of S is 0.018 wt.%. Totals are those from oxides with 4 decimal places, displayed to 2 decimal places.

Sample number	Hf	Ta	Th	U	*(ppb)* Os	Ir	Ru	Rh	Pt	Pd	Au	Cu/Pd	Pd/Ir	Pt/Pd	$\delta^{34}S$(‰)	S(wt.%)
RM81	0.54	0.10	0.20	0.06	1.43	0.65	2.69	0.31	2.83	3.18	4.74	36.21	4.92	0.89	-0.2	0.03
RM58	0.55	0.02	0.08	0.01	1.16	1.25	3.24	1.01	11.69	8.72	2.05	9.09	4.64	1.94	-0.2	-
RM59	0.30	0.02	0.07	0.01	0.87	0.34	2.12	0.21	2.16	2.14	3.36	13.84	6.31	1.01	-	-
RM60	1.43	0.08	0.40	0.14	-	-	-	-	-	-	-	-	-	-	-	
RM61	0.43	0.01	0.05	0.00	2.49	0.81	3.57	1.14	3.40	10.41	1.55	8.82	12.79	0.33	+1.1	-
RM63	4.33	0.31	1.06	0.31	0.05	0.05	0.08	0.05	1.00	0.31	0.22	332.92	6.69	3.22	-0.6	-
RM64	0.39	0.02	0.16	0.04	2.77	2.46	4.71	1.11	27.27	20.00	13.37	6.26	8.13	1.36	-0.1	-
RM17	0.49	0.06	0.22	0.10	0.75	0.60	1.45	0.35	5.65	3.04	3.75	8.76	5.08	1.86	-	-
RM18	0.79	0.09	0.24	0.05	0.95	1.27	1.83	0.48	3.82	3.32	3.83	10.44	2.61	1.15	+2.1	-
RM35	0.30	0.06	0.22	0.05	1.64	0.79	1.38	0.24	2.42	1.69	1.63	17.93	2.13	1.43	-2.9	-
RM70	0.76	0.03	0.25	0.06	1.16	0.74	1.81	0.35	3.31	3.90	0.58	26.73	5.26	0.85	-5.7	0.05
RM71	0.51	0.02	0.16	0.04	-	-	-	-	-	-	-	-	-	-	-3.7	-
RM73	0.41	0.02	0.18	0.04	-	-	-	-	-	-	-	-	-	-	-4.2	-
RM74	0.76	0.04	0.24	0.07	0.93	0.76	2.07	0.56	5.69	12.51	3.78	8.08	16.50	0.46	-6.5	0.06
RM75	0.45	0.02	0.16	0.04	1.36	0.94	2.30	0.32	3.37	3.22	1.58	16.47	3.44	1.05	-3.9	0.03
RM85	1.07	0.09	0.17	0.04	2.71	2.88	4.06	0.47	2.59	1.66	1.14	22.47	1.36	1.77	-	-
RM86	0.59	0.05	0.07	0.02	8.83	2.16	2.94	0.35	3.04	2.20	1.99	17.46	1.02	1.38	+0.3	0.02
RM87	0.99	0.07	0.18	0.04	2.05	1.71	4.30	0.83	8.22	8.03	1.89	-	-	-	-0.5	-
RM88	0.90	0.06	0.16	0.04	3.18	1.33	4.91	0.67	6.48	4.71	8.56	14.09	3.54	1.38	-1.3	0.04
RM89	3.69	0.17	0.12	0.03	-	-	-	-	-	-	-	-	-	-	-	-
RM29	0.57	0.11	0.25	0.05	2.95	1.18	3.19	0.70	5.24	7.18	2.39	7.74	6.09	0.73	-11.0	-
RM30	0.34	0.05	0.20	0.04	5.13	1.54	5.49	0.74	5.38	3.07	1.47	7.49	1.99	1.75	-10.9	0.02
RM32	0.54	0.13	0.28	0.06	1.51	0.99	2.58	0.66	6.95	11.48	2.58	4.56	11.56	0.61	-14.7	0.08
RM33	0.53	0.07	0.25	0.06	14.15	5.39	12.51	4.67	37.48	116.73	15.20	1.84	21.66	0.32	-11.8	-
RM91	0.95	0.06	0.21	0.05	7.00	3.44	9.69	3.70	25.00	78.38	7.99	5.12	22.80	0.32	-8.0	0.18
RM95	0.89	0.06	0.23	0.05	3.87	0.88	3.68	1.64	13.44	28.34	4.24	8.82	32.23	0.47	-14.3	-
M9	0.96	0.15	0.11	0.03	1.01	0.94	1.58	0.83	8.16	4.43	2.61	24.92	4.72	1.84	-	-

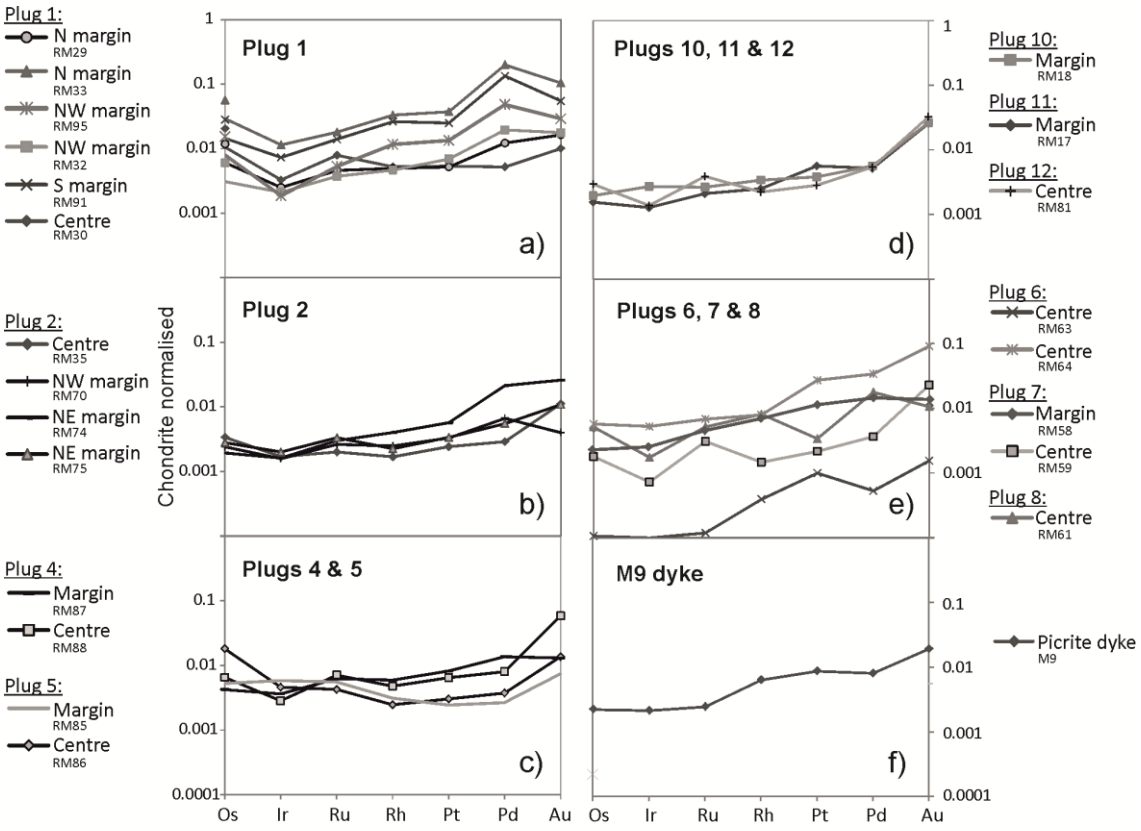

Figure 12.3. Chondrite-normalised whole-rock PGE multi-element diagrams for peridotite plugs. Normalising values from McDonough & Sun (1995).

In summary, with the exception of plugs 1 and 2, all the peridotite plugs have small sulphide blebs (e.g., Fig. 12.4a), typically 20 to 150 µm in length and comprising chalcopyrite, pyrrhotite and pentlandite, with rare bornite and chalcocite (Table 12.2) and are normally rounded or 'granular' in shape, occasionally with a rim of iron oxide in more altered samples (e.g., Fig. 12.4b). Sulphides normally occur at the margins of cumulus olivine (Fig. 12.4a and 12.4c), or within intercumulus plagioclase and clinopyroxene, and sulphides are locally in contact with granular Cr-spinels (e.g., Fig. 12.4d). In rare cases, sulphides occur within the fractured and serpentine-filled margins of cumulus olivine (e.g., Fig. 12.4e). In contrast, plug 1 at West Sgaorishal has coarser sulphide minerals, up to 4 mm in length, occurring as an intercumulus phase with pyroxenes and plagioclase, or 'net textured' where sulphides are most abundant in patches at the plug margin (Fig. 12.4f-h; Table 12.2). Sulphides have been observed to almost enclose cumulus olivine, as well as ilmenite and Cr-spinel (e.g., Fig. 12.4g and 12.4h), and include pyrrhotite, pentlandite (and pyrrhotite-pentlandite flames) as well as chalcopyrite. Minor galena is also observed, however unlike the other plugs, no bornite or chalcocite was encountered in plug 1. Finer sulphide minerals are of the same species as the course sulphides occurring in the centre of plug 1.

Table 12.2. *(continues overleaf)*

Sample number	Sulphide minerals	Sulphide size range	Sulphide textures and associations	Silicate and oxides	PGM categories (if detected)	PGM sizes and associations	Other accessory minerals noted
RM18	Cp + Pn + Po	< 20 µm	Very rare rounded sulphides are interstitial to (but adjacent/in contact with) cumulus olivine crystals	Olivine, clinopyroxene, plagioclase, chromite (also as rare discontinuous veins)	none detected	-	Ni-arsenides, Ni-sulphide (nickeline?), Cu-sulphide (chalcocite?), monazite, apatite, magnetite
RM30	Po + Pn + Cp	<200 µm	Sulphides are generally interstitial to cumulus olivine, but much more rare than in RM32, RM33, RM91. Sulphides usually in contact with olivine at the crystal margins. Abundant coarse (0.5 - 4 mm) sulphides as net-textured phases, interstitial to olivine and chromite cumulates. Irregular-shaped to rounded sulphides within intercumulus plagioclase in vicinity of large net-textured	Olivine, clinopyroxene, plagioclase, chromite, ilmenite	not investigated	-	White vein cross-cuts sample, filled with serpentine and chlorite, minor quartz
RM32	Cp + Po + Pn ± Bo, Cc	Two size groups: < 200 µm, and 0.5 to 4.0 mm	sulphides. Additionall, rounded sulphides (< 200µm) within cumulus olivine marginal areas (not serpentised cracks) or embayed at edges of cumulus olivine crystals, and not in vicinity of net-textured coarse sulphides. Additionally, small sulphides (also < 200 µm) within serpentine-filled alteration cracks throughout slide. Abundant coarse sulphides as net-textured phase, interstitial to olivine cumulates.	Olivine, clinopyroxene, plagioclase, chromite, ilmenite, serpentinite	Pd-telluride (merenskyite), Pd bismuthide-tellurides	0.5 - 4 µm wide PGM, mostly within sulphides (Pn, Po or Cp) and some at silicate-sulphide mineral boundaries	Co-arsenide
RM33	Cp + Po + Pn ± Bo, Cc	0.5 to 2.0 mm	Margins of some of these sulphides have 'variagated' solution textures suggestive of alteration or recrystallisaton. Rarely, elongate sulphides (up to 0.5mm long) can be seen penetrating cumulus olivine crystals along fractures. Chromite crystals both as cumulate phase and sometimes as fine inclusions within granular cumulate olivines. Sulphides within interstitial silicate minerals	Olivine, clinopyroxene, plagioclase, chromite, ilmenite, serpentinite	Pd bismuthide-telluride, Pt-arsenide (sperrylite), Pt-Sb arsenide	0.5 - 7 µm wide PGM, mostly within sulphides (Po, Pn and Cp) and some at silicate-sulphide mineral boundaries (e.g., Po or Pn - silicate)	electrum, Pb-telluride
RM35	Cp + Po + Pn + Ga	50 to 500 µm	(e.g., pyroxene and plagioclase). Smaller rounded sulphides (typically < 100 µm) in contact with margins of cumulus olivine crystals, and associated with serpentine-filled cracks. Rare rounded sulphides (~50 µm) as inclusions in olivine (although crystals are highly fractured).	Olivine, clinopyroxene, plagioclase, chromite, ilmenite, serpentinite	Ir-Pt arsenic sulphide (irarsite-platarsite), Ir-arsenic sulphide (irarsite)	Very rare PGM typically < 1µm wide and found within Pn.	electrum, zircon, chlorite (as replacment mineral overprinting serpentine)
RM58	Cp ± Po ± Pn	< 50 µm	Rounded rare sulphides, as discrete minerals interstitial to cumulate olivine and chromite, and within interstitial pyroxene and plagioclase. Also within serpentinite-filled cracks at margins of cumulus olivines	Olivine, clinopyroxene, plagioclase, chromite	not investigated	-	-

Table 12.2. Sulphide mineralogy, textures and sizes. Modal proportion (%) sulphide minerals in plug are based on Ni content. Details of sulphide metal tenor calculation given in main text. Mineral abbreviations are: chalcopyrite (Cp), pentlandite (Pn), pyrrhotite (Po), bornite (Bo), chalcocite (Cc), galena (Ga).

Sample number	Sulphide minerals	Sulphide size range	Sulphide textures and associations	Silicate and oxides	PGM categories (if detected)	PGM sizes and associations	Other accessory minerals noted
RM61	Cp + Po + Pn ± Bo	< 50 µm	Rounded rare sulphides, as discrete minerals interstitial to cumulate olivine and chromite, and within interstitial pyroxene and plagioclase. Also within serpentinite-filled cracks through cumulate olivines	Olivine, clinopyroxene, plagioclase, chromite	not investigated	-	-
RM64	Cp + Po + Pn ± Bo	< 150 µm	Sulphides are discrete and interstitial to coarse granular cumulate olivine crystals, and sometimes within olivines themselves.	Olivine, clinopyroxene, plagioclase, chromite	not investigated	-	-
RM70	Cp + Pn ± Po	< 90 µm	Sulphides are discrete interstitial to olivine and chromite cumulate crystals, and within intercumulate pyroxenes and plagioclase	Olivine, clinopyroxene, plagioclase, chromite	not investigated	-	-
RM74	Po + Pn ± Cp	< 80 µm	Sulphides are discrete interstitial to olivine and chromite cumulate crystals, and within intercumulate pyroxenes (and variable chlorite-filled zones in OPX ± apatite)	Olivine, clinopyroxene, plagioclase, chromite, ilmenite, serpentinite	not investigated	-	apatite, Fe-oxide
RM75	Cp + Pn ± Po	< 110 µm	Discrete, rounded sulphides, interstitial to granular cumulate olivines, and within intercumulate pyroxenes and plagioclase. Sometimes sulphides at triple junction between cumulate olivine crystals.	Olivine, clinopyroxene, plagioclase, chromite	not investigated	-	-
RM81	Cp ± Po ± Pn	< 50 µm	Sulphides are discrete and both interstitial to granular cumulate olivines, and within olivines (close to olivine crystal margin)	Olivine, clinopyroxene, plagioclase, chromite, serpentine	not investigated	-	Fe-oxide, serpentine, and replacement of serpentine by chlorite
RM85	Pn + Cc + Bo	< 40 µm	Sulphides are discrete, rounded, and interstitial to granular cumulate olivines, and within intercumulate pyroxenes and plagioclase	Olivine, clinopyroxene, plagioclase, chromite, serpentine	not investigated	-	Fe-oxide, serpentine, and replacement of serpentine by chlorite
RM91	Cp + Po + Pn	0.2 to 4.0 mm	Abundant coarse sulphides as net-textured, interstitial to olivine cumulates. Also more rounded sulphide phases (up to 0.2 mm diameter) in contact with cumulus olivine margins or as embayments at olivine margins. Abundant coarse sulphides as net-textured phase, interstitial to olivine cumulates. Rare sulphides filling or partially filling cracks through olivine (± serpentine and Fe-oxides) or as discrete rounded/irregular shaped sulphide crystals (<50 µm) within cracks.	Olivine, clinopyroxene, plagioclase, chromite	not investigated	-	-
RM95	Cp + Po + Pn	Two size groups: < 50 µm, and 0.25 to 2.0 mm		Olivine, clinopyroxene, plagioclase, chromite, serpentine	not investigated	-	-

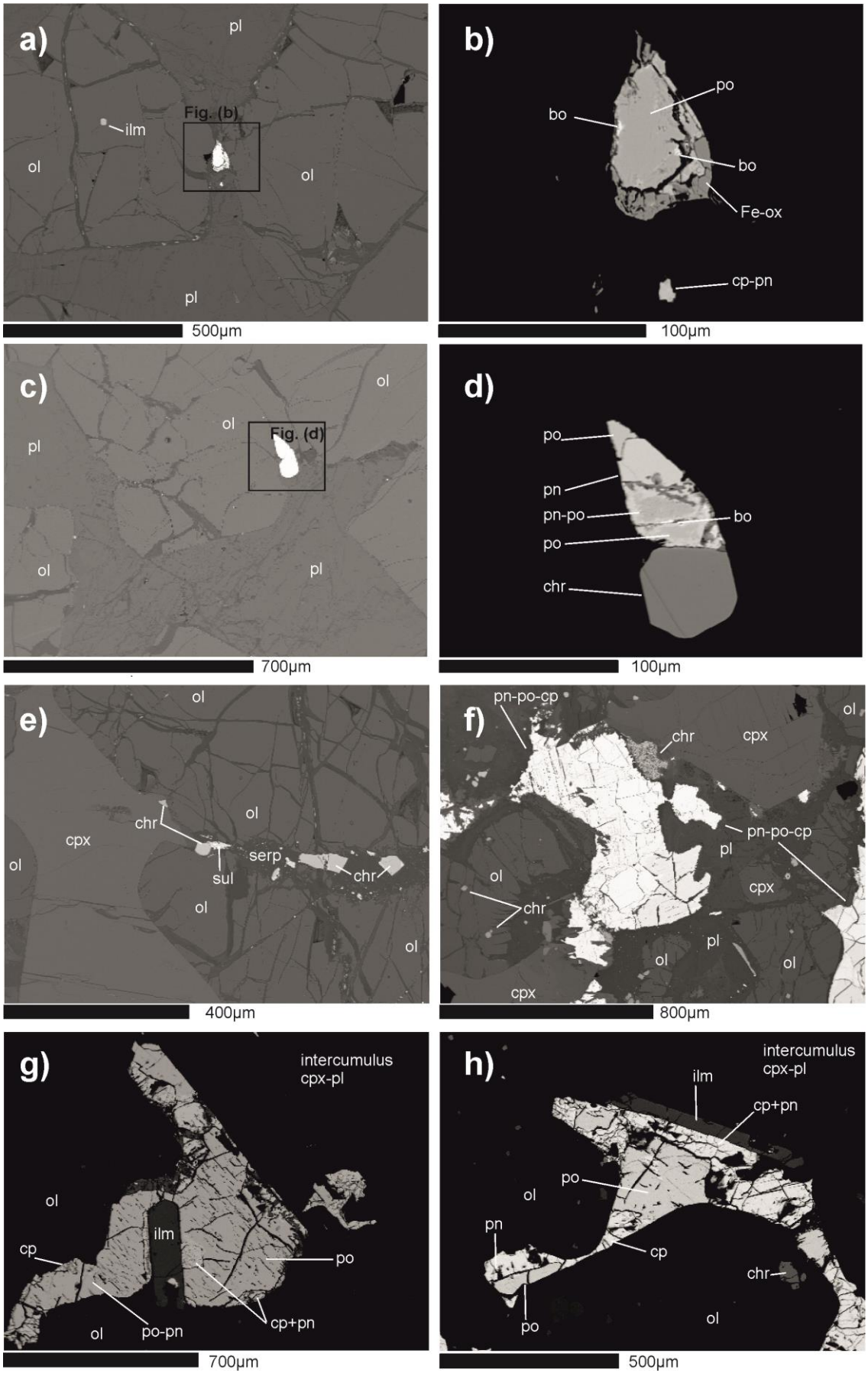

Figure 12.4. *(caption overleaf)*

PGM (plugs 1 and 2 only) are found associated with these sulphides, mostly occurring within sulphide minerals or at silicate-sulphide mineral boundaries. PGM are observed within sulphides or at sulphide-silicate contacts. These range in size from 0.5 – 7 μm wide and include Pd and Pt-tellurides, bismuth-tellurides, Pt-arsenides and Pt-Sb arsenides (Table 12.2). In plug 2 (Loch Sgaorishal) sulphides range 50 – 500 μm and are interstitial to cumulus olivine, with rare rounded sulphides (~ 50 μm) occurring as inclusions within cumulus olivine, albeit in serpentine-filled fractures. Pentlandite in plug 2 contains small (< 1 mm wide) Ir and Pt sulpharsenides of the irarsite-platarsite series. In both plugs 1 and 2, small grains of electrum were observed in pyrrhotite (normally < 5 μm) as well as one crystal of Pb-telluride (Table 12.2).

A representative selection of trace element compositions, including S/Se ratios of sulphide minerals (Table 12.3, and full table in Supplementary Material – Tables C and D, on disk) and PGE abundances in plug sulphides (grouped per region of Rum) are presented in Figures 12.5a-d. Overall, the variation of PGE concentrations in sulphide minerals from plugs in various areas of Rum (northwest, southeast and central) overlap significantly (Fig. 12.5a-d), such that there is no systematic difference in PGE tenor between plugs. There is no correlation between Pd and Rh for any plugs (Fig. 12.5a), nor are Rh concentrations higher in pentlandite or correlated with Ni content (Fig. 12.5b). Higher Pd concentrations are measured in sulphides optically confirmed to be pentlandite (labelled as 'NW Rum pentlandite', Fig. 12.5c) although concentrations in other northwest Rum sulphide are highly variable and overlap with pentlandite Pd abundances. By contrast, Rh and IPGE abundances in pentlandite (Os, Ir, Ru) are not distinct from other base metal sulphides or 'mixed sulphide' analyses (Figs. 12.5b,d).

Figure 12.4. Back-scattered electron images of sulphides in peridotite plugs from scanning electron microscope investigations. (a) Small sulphide nucleating onto and between two cumulus olivine crystals, within intercumulus plagioclase, plug 6. (b) Close-up of sulphide in (a) with contrast adjusted to show sulphide mineralogy. (c) Sulphide grain nucleating on small Cr-spinel at margin of granular cumulus olivine, plug 6. (d) Close-up of sulphide minerals and Cr-spinel in (c). (e) Sulphides and Cr-spinel within serpentinised fracture at margin of cumulus olivine, with intercumulus clinopyroxene, plug 5. (f) Coarse sulphides as poikilitic phase with clinopyroxene and plagioclase, plug 1 margin. (g) Poikilitic sulphides surrounding cumulus olivine and elongate ilmenite, with intercumulus plagioclase, plug 1 margin. (h) Similar to (g), demonstrating poikilitic, sometimes 'net-textured' sulphides surrounding granular cumulus olivine phenocrysts. In both (g) and (h) the contrast has been adjusted to as to display the sulphide internal texture and mineralogy. A summary of sulphide characteristics and PGM is presented in Table 12.2. Mineral abbreviations are olivine (ol), clinopyroxene (cpx), plagioclase (pl), ilmenite (ilm), Cr-spinel (chr), serpentinite (serp), iron oxide (Fe-ox), pentlandite (pn), pyrrhotite (po), chalcopyrite (cp) and bornite (bo).

Table 12.3. *(continues overleaf)*

Sample number	Mineral	*n*	Plug number	Spot/Line	*S (wt.%)	Se (ppm)	S/Se	Co (ppm)	Ni (wt.%)	Cu (wt.%)	Zn (ppm)
RM30	Sulph (mean)	*4*	1	spot	36	137	2911	3451	28.09	1.45	1252
RM32	Cp (mean)	*2*	1	line	35.27	74	4961	290	1.61	23.54	8491
RM32	pn	*1*	1	line	33.38	111	3015	4540	27.59	1.48	466
RM32	Pn-Po (mean)	*2*	1	line	39.61	79	5067	2200	14.21	2.63	889
RM32	Po (mean)	*4*	1	line	41.62	104	4054	311	2.51	0.06	99
RM33	cp	*1*	1	line	40.78	38	10812	7	0.19	13.36	1804
RM33	Pn (mean)	*2*	1	line	32.34	53	6120	3440	28.21	0.12	38
RM33	pn-po	*1*	1	line	37.40	31	12128	472	1.96	0.49	36
RM33	Po (mean)	*3*	1	line	36.39	46	8195	72	0.81	0.16	34
RM91	Cp (mean)	*3*	1	line	32.03	76	4248	617	5.88	15.41	3778
RM91	Pn (mean)	*3*	1	line	35.00	113	3094	2493	30.31	0.50	239
RM91	Po (mean)	*3*	1	line	41.89	111	3827	51	0.61	0.22	1200
RM95	Cp (mean)	*2*	1	line	33.62	44	7694	298	3.29	28.59	6725
RM95	Pn (mean)	*6*	1	line	35.49	76	4878	6121	27.78	1.28	1295
RM95	Po (mean)	*2*	1	line	39.36	65	6055	191	1.69	0.52	115
RM35	Sulph (mean)	*2*	2	spot	36	359	1030	3571	25.61	0.23	1529
RM70	Sulph (mean)	*4*	2	spot	36	237	1721	2260	13.91	6.07	8199
RM75	Sulph (mean)	*3*	2	spot	36	301	1339	3135	20.12	1.57	907
RM87	Sulph (mean)	*3*	4	spot	36	137	2885	1064	3.46	7.18	10617
RM85	Sulph (mean)	*2*	5	spot	36	630	647	6451	36.24	1.11	1203
RM64	Sulph (mean)	*4*	6	spot	36	292	1450	1621	12.03	8.83	7667
RM58	Sulph	*1*	7	spot	36	146	2463	1015	8.65	9.19	9124
RM61	Sulph (mean)	*3*	8	spot	36	240	1539	1876	7.30	13.20	13940
RM61	po	*1*	8	line	36.19	34	10530	400	0.76	3.58	6767
RM18	Sulph	*1*	10	spot	36	328	1099	805	5.60	8.45	3966
RM81	Sulph (mean)	*4*	12	spot	36	159	2304	1699	12.00	3.96	4295

Table 12.3. Representative selection of LA-ICPMS results for plug sulphides. *S content of sulphide is assumed from quantitative analyses of sulphide mineral or assumed 36 wt. % for spot analyses. See Supplementary Table C (on disk) for all plug sulphide analyses, and Table D (on disk) for all ELS sulphide results.

Sample number	Os (ppm)	Ir (ppm)	Ru (ppm)	Rh (ppm)	Pt (ppm)	Pd (ppm)	Au (ppm)	Cd (ppm)	As (ppm)	Bi (ppm)	Te (ppm)
RM30	3.90	0.35	2.90	0.18	0.40	8.92	0.23	6.99	143.58	5.57	43.62
RM32	0.08	0.04	<0.09	<0.22	<0.02	0.34	0.02	51.51	<15	0.69	16.63
RM32	1.06	0.37	0.84	<0.22	<0.02	0.59	0.02	10.64	<15	1.29	15.71
RM32	0.91	0.19	0.24	<0.22	<0.02	3.49	0.22	9.64	<15	2.33	4.32
RM32	1.30	0.48	1.02	0.51	<0.02	1.29	0.10	3.88	<15	1.79	10.15
RM33	<0.02	<0.02	<0.09	<0.22	<0.02	0.43	0.03	45.53	<15	0.36	17.35
RM33	1.16	0.25	0.50	0.40	<0.02	22.50	1.87	<1.1	<15	0.31	7.90
RM33	0.53	0.13	0.13	<0.22	<0.02	2.96	<0.01	<1.1	<15	0.60	1.60
RM33	0.52	0.16	0.35	0.29	<0.02	0.25	<0.01	<1.1	<15	0.34	2.96
RM91	0.18	0.71	0.54	<0.22	0.02	6.25	0.02	25.78	20.03	0.61	9.06
RM91	2.39	1.10	2.00	1.16	0.04	40.11	<0.01	1.35	20.42	1.52	21.87
RM91	1.33	0.61	1.35	0.71	0.02	0.98	<0.01	7.42	<15	1.41	11.18
RM95	0.02	0.02	<0.09	0.24	<0.02	<0.2	0.04	66.06	<15	2.17	12.42
RM95	0.49	0.20	0.23	0.24	0.06	28.11	0.02	6.01	46.11	1.39	12.17
RM95	0.33	0.07	0.10	<0.22	<0.02	1.02	<0.01	<1.1	<15	1.61	11.15
RM35	72.78	21.86	13.84	1.49	4.79	9.03	0.01	1.25	38.58	5.43	27.39
RM70	0.68	0.24	1.07	0.23	1.14	6.48	<0.01	36.32	54.86	0.64	15.55
RM75	1.71	0.80	5.32	0.70	0.23	8.23	0.07	3.29	36.13	11.33	20.03
RM87	4.25	1.58	3.90	0.42	0.12	0.71	0.03	14.97	16.50	0.33	1.17
RM85	1.73	0.10	0.10	0.13	0.23	13.84	0.06	7.35	637.68	3.28	110.73
RM64	1.52	1.12	2.04	0.74	3.03	46.60	0.04	13.02	<9	1.87	<0.9
RM58	0.16	0.10	0.14	<0.11	<0.02	<0.25	<0.01	2.72	<9	3.59	5.28
RM61	0.40	0.17	0.12	0.12	<0.02	0.61	0.27	15.99	<9	0.24	3.92
RM61	0.09	0.02	<0.09	<0.22	0.03	<0.2	<0.01	5.70	<15	<0.05	1.30
RM18	0.50	0.35	0.61	1.78	<0.02	1.24	0.20	8.72	<9	0.59	9.98
RM81	1.20	0.13	1.79	0.18	0.52	2.61	1.64	24.90	27.48	0.48	13.75

Table 12.3. *(continues overleaf)*

Sample number	Mineral	*n*	Plug number	Spot/Line	*S (wt.%)	Se (ppm)	S/Se	Co (ppm)	Ni (wt.%)	Cu (wt.%)	Zn (ppm)
RM30	Sulph (mean)	*4*	1	spot	36	137	2911	3451	28.09	1.45	1252
RM32	Cp (mean)	*2*	1	line	35.27	74	4961	290	1.61	23.54	8491
RM32	pn	*1*	1	line	33.38	111	3015	4540	27.59	1.48	466
RM32	Pn-Po (mean)	*2*	1	line	39.61	79	5067	2200	14.21	2.63	889
RM32	Po (mean)	*4*	1	line	41.62	104	4054	311	2.51	0.06	99
RM33	cp	*1*	1	line	40.78	38	10812	7	0.19	13.36	1804
RM33	Pn (mean)	*2*	1	line	32.34	53	6120	3440	28.21	0.12	38
RM33	pn-po	*1*	1	line	37.40	31	12128	472	1.96	0.49	36
RM33	Po (mean)	*3*	1	line	36.39	46	8195	72	0.81	0.16	34
RM91	Cp (mean)	*3*	1	line	32.03	76	4248	617	5.88	15.41	3778
RM91	Pn (mean)	*3*	1	line	35.00	113	3094	2493	30.31	0.50	239
RM91	Po (mean)	*3*	1	line	41.89	111	3827	51	0.61	0.22	1200
RM95	Cp (mean)	*2*	1	line	33.62	44	7694	298	3.29	28.59	6725
RM95	Pn (mean)	*6*	1	line	35.49	76	4878	6121	27.78	1.28	1295
RM95	Po (mean)	*2*	1	line	39.36	65	6055	191	1.69	0.52	115
RM35	Sulph (mean)	*2*	2	spot	36	359	1030	3571	25.61	0.23	1529
RM70	Sulph (mean)	*4*	2	spot	36	237	1721	2260	13.91	6.07	8199
RM75	Sulph (mean)	*3*	2	spot	36	301	1339	3135	20.12	1.57	907
RM87	Sulph (mean)	*3*	4	spot	36	137	2885	1064	3.46	7.18	10617
RM85	Sulph (mean)	*2*	5	spot	36	630	647	6451	36.24	1.11	1203
RM64	Sulph (mean)	*4*	6	spot	36	292	1450	1621	12.03	8.83	7667
RM58	Sulph	*1*	7	spot	36	146	2463	1015	8.65	9.19	9124
RM61	Sulph (mean)	*3*	8	spot	36	240	1539	1876	7.30	13.20	13940
RM61	po	*1*	8	line	36.19	34	10530	400	0.76	3.58	6767
RM18	Sulph	*1*	10	spot	36	328	1099	805	5.60	8.45	3966
RM81	Sulph (mean)	*4*	12	spot	36	159	2304	1699	12.00	3.96	4295

The chondrite-normalised PGE composition of coarse sulphides at the margins of plug 1 (Fig. 12.6a-c) are subtly different from the composition of fine sulphides at the centre of this plug (Fig. 12.6d). This difference is particularly noticeable for Os, Ir and Ru, with the concentration of all PGE in marginal sulphides being lower than the PGE concentrations in finer sulphides at the centre. Overall, for each individual type of base metal sulphide (chalcopyrite, pentlandite, pyrrhotite), the sulphide PGE patterns of plug 1 (particularly the margins) are fairly consistent and parallel to one another. However, chalcopyrite (Fig. 12.6a) generally has lower PGE abundances than pentlandite and pyrrhotite (Figs. 12.6b and 12.6c, respectively), but the overall normalised PGE spectra are similar or parallel between Ni-Fe mineral species (e.g., Fig, 12.6b-c). Sulphides in plug 2 (Fig. 12.6e) also have two distinctive PGE patterns with sulphides at the margin being comparatively homogeneous, and a similar composition to those from the margin of plug 1. However, two sulphides analysed from the centre of plug 2 have differing PGE compositions – one which overlaps sulphide compositions of the margins, and one entirely different sulphide composition with elevated IPGE.

Overall, sulphide compositions from plugs 4-12 are very heterogeneous. This may in part be explained by there being analyses of 'mixed sulphide' species (due to their small size) but this cannot account for all the observed variation. In a similar fashion to the whole-rock geochemistry, it can be demonstrated that the trace element composition of sulphides from plugs 4-12 are generally different from one another (Fig. 12.7a-g). Broadly, peridotite plug sulphide compositions resemble those from peridotite units in the Eastern Layered Series (Fig. 12.7). Further, there are similarities between individual plugs – for example, sulphides in plugs 4 and 6 (Fig. 12.7a and 12.7c), and plugs 1 and 5 (Fig. 12.6b-c and 12.7b).

12.4.3. S-isotope compositions and S/Se ratios of the Rum plugs

Figure 12.8a shows the average $\delta^{34}S$ value for whole-rock samples per plug and for the Eastern Layered Series (ELS), against S/Se ratios per sulphide. S/Se was calculated from LA-ICPMS analyses of Se and quantitative SEM analyses of S, and therefore quantifies S/Se on a mineral-by-mineral basis per sample. Sulphide minerals large enough to be analysed by laser combustion (i.e., only in plug 1) on a sulphide mineral-by-mineral basis (Table 12.4) have been averaged to a mean $\delta^{34}S$ value listed in Table 12.1, so as to be comparable to other samples analysed by whole-rock S extraction and conventional analyses. The $\delta^{34}S$ results of Hughes *et al.,* (accepted, a; Chapter 11) for various sediments on the Isles of Rum and Skye are shown in Figure 12.8b.

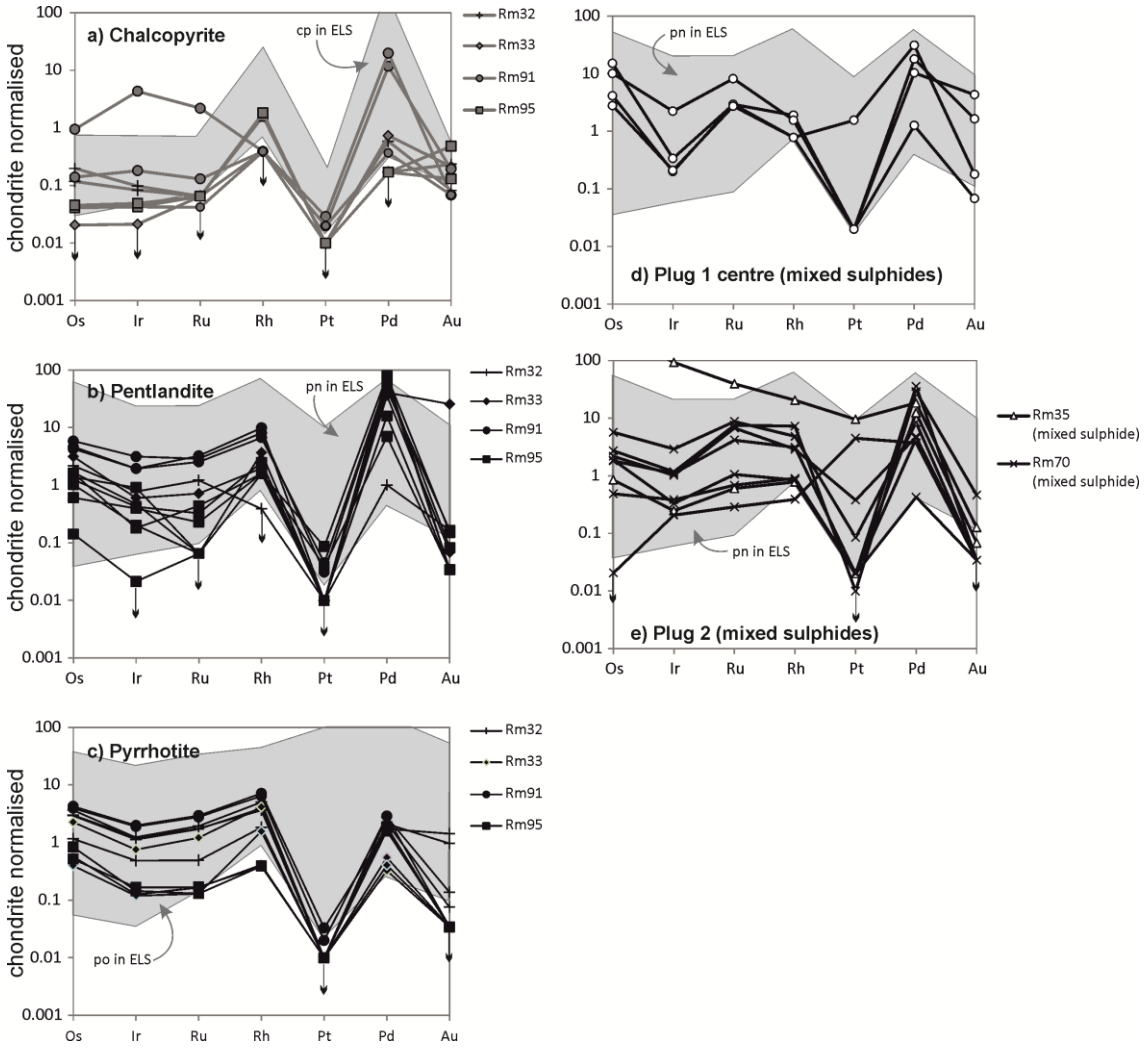

Figure 12.6. Chondrite-normalised PGE spectra for sulphide minerals, measured by LA-ICPMS, for the plugs 1 (centre and margin). Diagrams are divided according to sulphide phase: chalcopyrite (a), pentlandite (b), and pyrrhotite (c). Also for 'mixed sulphides' in Plug 2, and pyrrhotite in the gabbro dyke cross-cutting plug 1 (f). Normalising values from McDonough & Sun (1995). See Table 12.3 for details. Note that where PGE abundances were less than detection limit, results are calculated as half detection limit with small downward arrow. Grey shaded areas delineate range of compositions for chalcopyrite (cp), pentlandite (pn) and pyrrhotite (po) in the Eastern Layered Series (ELS) for comparison in plots (a) to (c). In plots (d) and (e), grey shaded area delineates ELS pn only. ELS data is presented in Supplementary Material Table D (on disk).

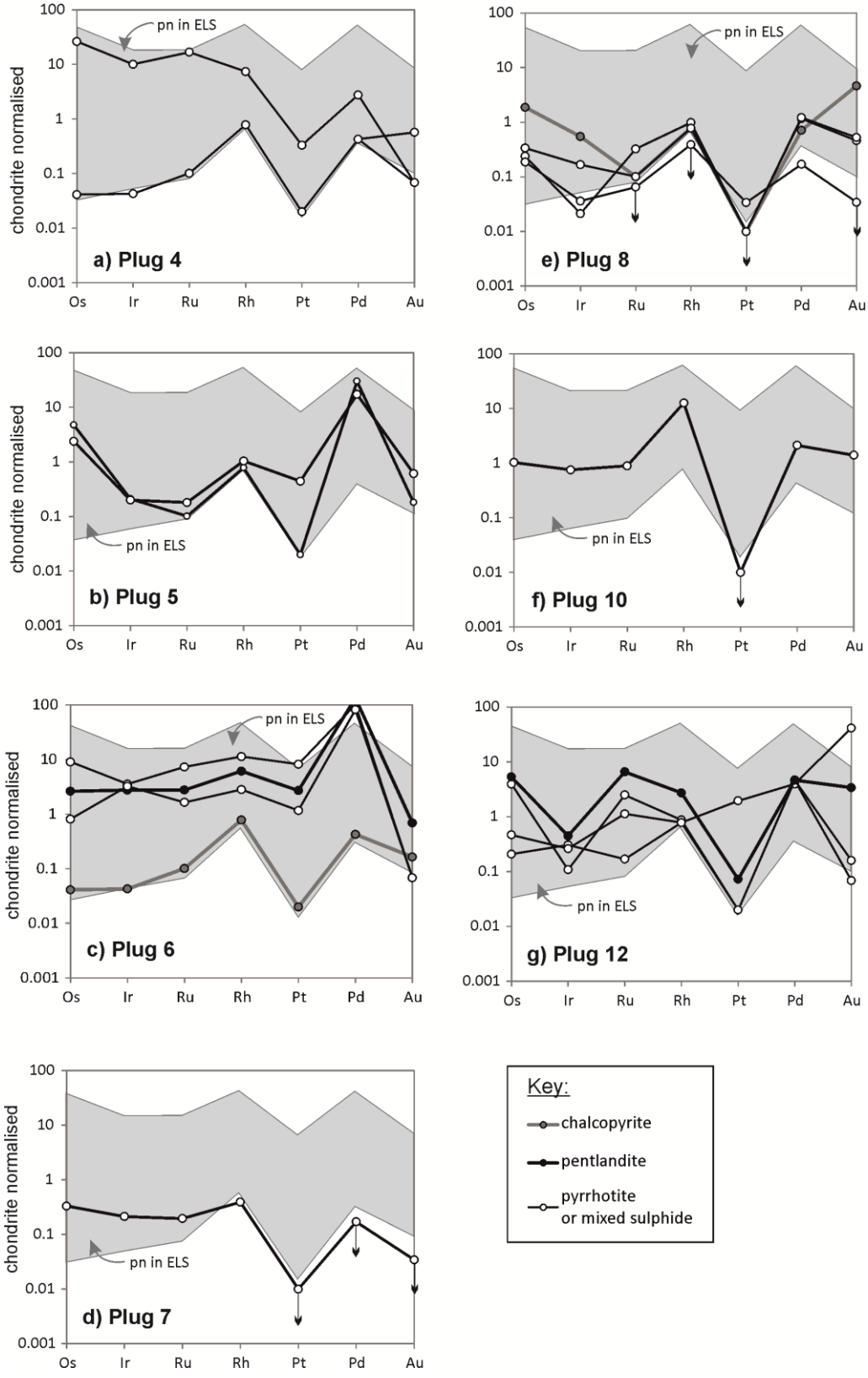

Figure 12.7. Chondrite-normalised PGE spectra for sulphide minerals, measured by LA-ICPMS, for all peridotite plugs, except plugs 1 and 2. Normalising values from McDonough & Sun (1995). See Table 12.3 for details. Note that where PGE abundances were less than detection limit, results are calculated as half detection limit with small downward arrow. Grey shaded areas delineate range of compositions for pentlandite (pn) in the Eastern Layered Series (ELS) for comparison.

The S/Se ratio of ELS samples are mostly within the 'mantle' range of 2850-4350 (Eckstrand & Hulbert, 1987), however the full range of ELS S/Se ratios is 489 to 5416 (Fig. 12.8a) and $\delta^{34}S$ ranges -4.4 to +1.2 ‰. Excluding plug 1 and one anomalous value from plug 8, S/Se ratio of plug sulphides reaches up to 4000. With the exception of plugs 1 and 2, the peridotite plugs have $\delta^{34}S$ ranging -0.6 to +2.1 ‰ in comparison to the ELS peridotites ranging -1.0 to 0.9 ‰. Thus, most of the peridotite plug sulphides have $\delta^{34}S$ and S/Se ratios comparable to, and within range of sulphides from ELS peridotite units. In contrast, sulphides from plug 1 have extremely light $\delta^{34}S$, ranging to -14.7 to -8.0 ‰, and S/Se ratios ranging 3000 to 12,000. The centre of Plug 1 shows least variation and deviation of S/Se from ELS, however $\delta^{34}S$ is -10.9 ‰. Whilst the S/Se ratios of plug 2 are within range of the ELS, the $\delta^{34}S$ composition ranges -6.5 to -2.9 ‰ (Fig. 12.8a and Table 12.1).

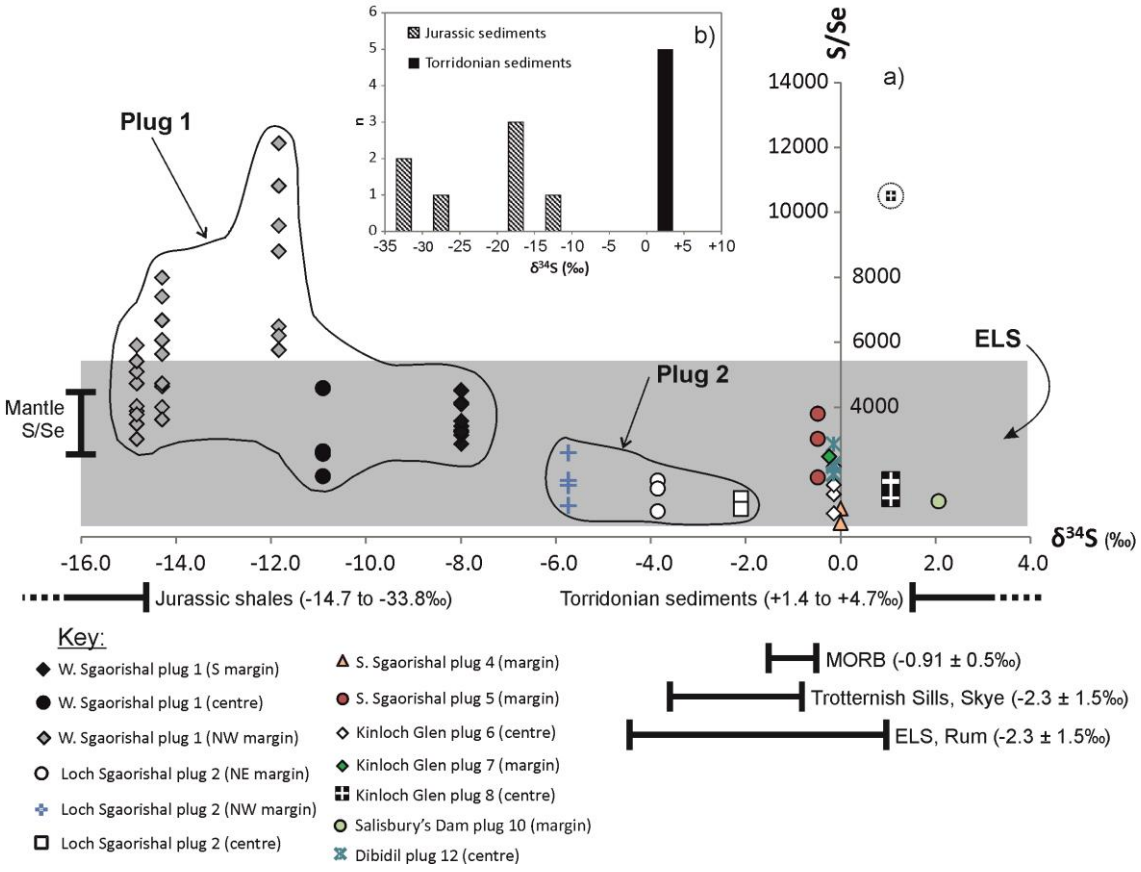

Figure 12.8. (a) S-isotope composition ($\delta^{34}S$) vs. S/Se ratio (see Table 12.3) of peridotite plug sulphides. Grey shaded area delineates variation in S/Se ratio for ELS, and black brackets show range of $\delta^{34}S$ for ELS, for comparison across plug compositions (see Supplementary Material, Tables C and D, on disk). Brackets for mantle S/Se based on Ihlenfeld & Keays (2011). Jurassic shale, Torridonian sediment and Trotternish Sill (Isle of Skye) $\delta^{34}S$ from Hughes *et al.* (accepted, a; Chapter 11). MORB $\delta^{34}S$ from Labidi *et al.* (2012). S/Se and $\delta^{34}S$ for the gabbro dyke at West Sgaorishal is also shown. (b) Histogram of $\delta^{34}S$ for Proterozoic and Mesozoic sediments present in this area of the Hebrides, after Hughes *et al.* (accepted, a; Chapter 11).

Table 12.4. Calculated sulphide metal tenors (*PGE), and $\delta^{34}S$ on a mineral-by-mineral basis for the margins of plug 1.

Sample number	Mineral	$\delta^{34}S$ (‰)	$\delta^{34}S$ (‰) average	Whole-rock S (wt.%)	Calculated modal % Cp	Calculated modal % Pn + Po	*Os (ppm)	*Ir (ppm)	*Ru (ppm)	*Rh (ppm)	*Pt (ppm)	*Pd (ppm)	*Au (ppm)
RM32	cp	-15.6	-14.7	0.08	0.02	0.22	6.89	4.54	11.81	3.01	31.79	52.50	11.79
	pn	-14.6											
	pn	-15.3											
	po	-13.4											
RM33	cp	-12.6	-11.8	*0.18***	0.06	0.47	29.84	11.37	26.38	9.86	79.04	246.18	32.06
	pn	-10.8											
	po	-12.1											
RM91	cp	-8.3	-8.0	0.18	0.12	0.39	17.93	8.80	24.80	9.47	64.00	200.66	20.46
	pn	-7.5											
	po	-8.2											
RM95	cp	-12.7	-14.3	*0.08***	0.07	0.14	27.21	6.19	25.91	11.54	94.63	199.53	29.89
	pn	-14.6											
	po	-15.6											

12.5. Discussion

12.5.1. Magmatic context of the Rum plugs vs. the Rum Central Complex

The peridotite plugs included in this study have whole-rock major, trace and PGE signatures distinctive from one another (e.g., Fig. 12.3 and Supplementary Material Part B). However, broadly the range of major element compositions overlap with those recorded for the various Rum Layered Suites, including peridotite units from the Eastern, Western and Central Layered Series (see Emeleus, 1997 and O'Driscoll *et al.,* 2009 and references therein) and the M9 picritic dyke (Upton *et al.,* 2002).

The Layered Suites on Rum are the result of multiple injections of ultramafic magma, in an open magmatic system of igneous cumulates (e.g., Wager *et al.,* 1960). Current consensus postulates that layering resulted from interaction between cumulates and later magmatic pulses derived from subsequent intruding picrites (e.g., Bedard *et al.,* 1988, Volker & Upton, 1990, 1991; Emeleus, 1997; Holness, 2005; O'Driscoll *et al.,* 2007; Leuthold *et al.,* 2014). The S/Se data for the ELS displays a broad range in ratios from 489 to 5416. Mantle S/Se ratios typically range 2850 to 4350 (Eckstrand & Hulbert, 1987; Ihlenfeld & Keays, 2011 and references therein) and although most of the ELS data is within this range, there are significant deviations. Loss of S via oxidation of sulphide minerals will lower the primary S/Se ratio. This is also consistent with common observations of partially oxidised sulphide minerals in our thin sections from the ELS, and we suggest this to be the cause of ELS S/Se ratios < 2000. By contrast, the causes of an increase in S/Se ratio (i.e., > 3500) are two-fold: this can either be the result of hydrothermal mobilisation of S forming a series of hydrothermal sulphide minerals, or contamination of magmas by crustal S (which is devoid of Se, and thus has a high S/Se ratio). While $\delta^{34}S$ is commonly used as a proxy for crustal S contamination, recent studies suggest that with enough magma throughput in the magmatic (conduit) system, the 'S signal' can be swamped by magmatic $\delta^{34}S$ (0 ± 4 ‰; Ohmoto & Rye, 1979), while S/Se ratio remains a good proxy for crustal contamination (Ihlenfeld & Keays, 2011).

We record a minimum in $\delta^{34}S$ locally in unit 1 (ELS) as -4.4 ‰, but earlier studies have measured $\delta^{34}S$ as low as -14.8 ‰ in ELS unit 1 rocks, associated with sulphide concentrations locally up to 3 modal percent, which have been intruded next to metre-scale rafts of Jurassic mudrocks (Faithfull, 1985; Hulbert *et al.,* 1992). In higher cyclic units in the ELS, $\delta^{34}S$ falls within the typical magmatic range, however sporadic increases in S/Se ratio (> 4350, mantle ratio) observed in the ELS here may indicate localised crustal S contamination. This likely took

place during intrusion of magmas into the layered suite, and may not be recorded in the $\delta^{34}S$ either due to the contaminant having S-isotopic compositions similar to the magma, or because high volumes of magma throughput have obliterated the signal. Ultimately the complexities of sulphide composition, S/Se ratio and S-isotopic composition throughout the ELS and Rum Layered Suite as a whole, requires further investigation, beyond the scope of this paper.

The diversity of S/Se ratios and PGE compositions measured in our ELS sulphides overlap with sulphide compositions from the plugs. Therefore we suggest that plugs (conduits) record various crystal mush injection events broadly coincident with magma (or mush) injections into the Rum Layered Suite. As such, the magma conduits represented by the peridotite plugs were not formed from a single eruption event, and probably represent multiple eruptions.

12.5.1.1. Feeders and magma staging chamber for the plugs and Rum Layered Suite

The presence of dunite, chromitite, and troctolite xenoliths within peridotite plugs situated inside or close to the Main Ring Fault (Volker & Upton, 1990) suggests that ejection of crystal mushes that fed these plugs occurred whilst crystallisation of the layered series was taking place. This demands a physical brecciation of wall rock material, and does not provide evidence that the conduit crystal mushes were derived from the layered suites directly, but instead that it erupted through them. Conversely, the lack of sedimentary xenoliths in the Rum plugs is unsurprising, given that the conduits hosted hot (1400°C) volatile-rich and turbulent magmas, where attrition, partial melting, and ultimately assimilation of brecciated wall rock material is likely; an observation supported by the attrition and rounding of ultramafic xenoliths in some plugs (e.g., Volker & Upton, 1990).

One striking observation regarding the Rum plugs is the lack of troctolite plugs. In contrast, feldspathic peridotites (strictly olivine melagabbros) described throughout our study, exist alongside gabbroic plugs that have no phenocryst assemblage or poilkilitic evidence for their having been intruded as a crystal mush, unlike the peridotite plugs. It is possible that the gabbroic plugs represent the purely basaltic magmas ejected from a staging magma chamber, and there is no evidence to suggest that these gabbroic plugs correlate strictly with the troctolite portions of units in the Rum Layered Suite. Indeed, per cyclic unit in the Rum Central Complex, the peridotite base and troctolite tops are paired, classically in the Eastern Layered Series (O'Driscoll *et al.,* 2014; Emeleus & Troll, 2011 and references therein). Regardless of the

mechanism that formed the overall layering of this suite, it is apparent that each of the troctolite layers is a fractionation feature associated and paired with each peridotite layer. Therefore because the peridotitic crystal mush that ejected through volcanic pipes is of a comparable composition to the peridotite bases of the layered suite cyclic units, this suggests that the crystal mushes of both came from a common source, and not necessarily that the layered suites directly fed the plugs themselves. This is supported by the observation that small entrained sulphide minerals in both the plugs and layered suite peridotites are directly comparable to one another (e.g., S/Se), despite their variable overall trace element composition. In other words, there must have been a separate deeper staging chamber in which a peridotitic crystal mush evolved, before being tapped further up the magmatic plumbing system to both the layered suites and plugs.

12.5.2. The origin of sulphides within the Rum plugs

With the exception of plugs 1 and 2, the sulphide minerals observed are of low abundance and are small, often rounded phases (< 150 μm in diameter). All plugs have distinctive chondrite-normalised PGE patterns, Au systematics and S/Se ratios, some of which closely resemble the compositions of sulphides in peridotite units of the ELS (e.g., Figs. 12.6-12.8). The Fo content of cumulus olivine in the plugs suggest that previously crystallised olivine phenocrysts were entrained within a basaltic or picritic magma, such that the peridotite plugs were essentially crystal mush conduits (e.g., Wadsworth, 1994; Holness *et al.,* 2012) sometimes with entrained chromitite, dunite or troctolite xenoliths (e.g., Volker & Upton, 1990). We propose a similar scenario for the entrainment of sulphide liquids.

The magmatic temperature of peridotite plugs on Rum has previously been estimated as 1400°C, based on picritic magma temperatures (Holness *et al.,* 2012). The solidus temperature of an Fe-bearing sulphide liquid is approximately 1100°C (Bowles *et al.,* 2011 after Kullerud & Yoder, 1959; Arnold, 1971) suggesting that sulphides would be liquid at the estimated temperature of emplacement for the plugs. Given that the 'lubricating' magmas were energetic enough to entrain up to 50% olivine crystals (e.g., Holness *et al.,* 2012) and sizeable xenoliths (e.g., Volker & Upton, 1990), it is highly likely that these were also capable of entraining other phases from within a staging magma chamber – specifically sulphide liquids. Therefore, we suggest that at least some sulphides (with mantle S/Se ratios) were formed

prior to intrusion of the plugs, and were transported as sulphide liquid droplets into the conduits that now form the plugs.

Several examples of sulphide liquid entrainment in magma conduits have been recorded worldwide. For instance, the Noril'sk magma conduit setting for orthomagmatic Ni-Cu-PGE mineralisation, where sulphides were initially exsolved in a deeper staging chamber before being flushed out to higher magmatic plumbing levels (Brügmann *et al.,* 1993; Lightfoot & Keays, 2005). Sulphide entrainment is also suggested for the Platreef (Bushveld Complex) where sulphides were transported away from a deeper zone of sulphide liquid formation (McDonald & Holwell, 2007; McDonald *et al.,* 2009; Ihlenfeld & Keays, 2011; Sharman *et al.,* 2013). In the Platreef, the evidence of this sulphide transportation was based on Cu/Pd, S/Se ratios, S-isotope compositions and trapped sulphide melt inclusions (Holwell *et al.,* 2011). Clearly, the process of entrainment of pre-formed sulphides, other silicate minerals, and xenoliths, is a common feature of many magmatic systems. However, in many of these cases, only one part of the full system is exposed, with processes at depth inferred. The volcanic plugs and the Layered Suite of Rum provide a rare opportunity to compare layered intrusion and volcanic pipe compositions, and mechanisms of sulphide transport at the same present day erosional level.

The $\delta^{34}S$ composition of peridotite plugs (+0.1 ± 1.0‰, excluding plugs 1 and 2) and peridotite cyclic units of the ELS (-0.5 ± 1.4 ‰; Table E – Supplementary Material, on disk) overlap with the typical Icelandic mantle plume range of -2.0‰ to +0.4 ‰ (Torassander, 1989), MORB -0.91 ± 0.5 ‰ (Labidi *et al.,* 2012) and the picritic Trotternish Sills on the Isle of Skye with average $\delta^{34}S$ of -2.3 ± 1.5 ‰ (Hughes *et al.,* accepted, a – Chapter 11). Magmatic $\delta^{34}S$ typically ranges 0.0 ± 4.0 ‰ (Ohmoto & Rye, 1979) with limited S-isotope fractionation resulting from changes in magma oxidation state, at high temperature, and fractional crystallisation during magma ascent. Thus we suggest that for most plugs and the ELS, S-saturation was reached prior to emplacement, in the deeper magmatic plumbing system where olivine crystallisation and fractionation was taking place, and did not involve the addition of crustal sulphur with $\delta^{34}S$ outwith magmatic compositions. Magma fractionation and varying oxidation state led to the slight variations in $\delta^{34}S$ observed in the ELS and plugs (excluding plugs 1 and 2), evolving to slightly heavier compositions (-0.5 to +0.1 ± 1 ‰), away from the Icelandic plume $\delta^{34}S$ signature of -0.8 ‰ to -2.3 ‰ (Torassander, 1989 and Hughes *et al.,* accepted, a – Chapter 11, respectively). During deep-seated olivine crystallisation, the sulphur concentration at sulphide saturation (SCSS) was exceeded, causing the exsolution of an immiscible sulphide liquid. With

ejection of crystal mushes from this staging chamber, sulphide liquid was entrained and emplaced into the peridotite plug magma conduits and Rum Layered Suite alike. However in the case of plugs 1 and 2, significant deviation of $\delta^{34}S$ and elevation of S/Se ratio indicates that localised crustal contamination took place.

12.5.3. Potential crustal S-sources for West and Loch Sgaorishal plugs (plugs 1 and 2)

The $\delta^{34}S$ of plug 1 (West Sgaorishal) ranges -14.7 to -8.0 ‰ with a S/Se ratio of sulphide minerals ranging 3000 to 12,000 while the $\delta^{34}S$ of plug 2 (Loch Sgaorishal) varies from -6.5 to -2.9‰ (Fig. 12.8a). Further, the sulphide S/Se ratios of plug 1 are elevated above the range of most ELS sulphides, and often exceeds 10,000 (a critical value for crustal sedimentary sulphide compositions; Ihlenfeld & Keays, 2011 and references therein). These S-isotope compositions are significantly lighter than typical mantle or the Icelandic plume values, and together with S/Se compositions, demonstrate that crustal S must have been added to these magma conduits (plugs 1 and 2). There is also a change in textural character of the sulphides in plug 1, becoming more abundant and coarser. Hence the questions arise: what was this sulphur source, and why is this light $\delta^{34}S$ only recorded in two plugs from northwest Rum?

The $\delta^{34}S$ of sedimentary S can be highly variable and is preserved in low-temperature diagenetic sulphides, typically pyrite, (Machel, 2001). Bacterial reduction of seawater or lacustrine sulphate during diagenesis, produces sulphide which is commonly ≤ 20 ‰ lighter than the initial sulphate (Ohmoto & Goldhaber, 1997). Within Palaeozoic and Mesozoic sedimentary sulphides, the range of $\delta^{34}S$ can be of the order of tens of per mille (‰), and generally extend to more negative values than those observed in Precambrian rocks (Canfield & Teske, 1996; Parnell *et al.,* 2010).

Most plugs on Rum have intruded through Torridonian (Applecross Formation) sandstones at the current erosion level, but the northwest tip of plug 1 also intrudes the unconformable base of Triassic limestones and calcretes, at the base of the Hebridean Basin sediments (Binns *et al.,* 1974; Fyfe *et al.,* 1993). Hughes *et al.* (accepted, a; Chapter 11) established that the $\delta^{34}S$ of these Triassic sediments, is isotopically heavy (with very low S concentrations) and thus cannot account for the $\delta^{34}S$ of plugs 1 and 2 via assimilation. This leaves three possible explanations; (a) a small patch of lacustrine sediments with light $\delta^{34}S$ (e.g., Parnell *et al.,* 2010) is present below plugs 1 and 2; (b) a segment of Jurassic mudrock with suitably light $\delta^{34}S$ occurs in a downthrown faulted block of a major fault zone (e.g., Main Ring Fault) through

which plugs 1 and 2 have intruded; or (c) the $\delta^{34}S$ signature of plugs 1 and 2 is derived from above the current erosion level and involves the Lower Jurassic Broadford Group that likely covered this area at the time of conduit activity.

Despite Torridonian lacustrine sediments from the mainland Stoer Group with mean reported $\delta^{34}S$ as of -30.1 ± 17.3 ‰ (Parnell *et al.,* 2010) all the Sleat and Torridon Group Mesoproterozoic sediments analysed by Hughes *et al.* (accepted, a; Chapter 11) were > 0.0‰. Further, the Stoer Group is not recorded in the sedimentary pile exposed on either Skye or Rum, suggesting that scenario (a) is extremely unlikely.

Hebridean Jurassic mudrock and ironstone $\delta^{34}S$ ranged -10 to -35 ‰, and associated basaltic dykes recorded $\delta^{34}S$ as light as -30.7 ‰ (Hughes *et al.,* accepted, a – Chapter 11). Blocks of Jurassic mudrocks are recorded as being present within the Main Ring Fault on Rum at Allt nam Bà and near Dibidil (Emeleus & Troll, 2008; Fig. 12.1 and 12.2c). In contrast, no such sedimentary blocks are reported from the Long Loch Fault, not least due to this being a strike-slip fault with no vertical motion which would have downthrown these sedimentary units. It is possible however, that the sub-surface route of the plug magma conduits could have intersected a downthrown block of Jurassic mudrocks, assuming that these conduits were fed from somewhere near the centre of the Rum volcanic edifice. However, only plugs 1 and 2 from the northwest quadrant of the island record this light $\delta^{34}S$ and the absence of such a light $\delta^{34}S$ in plugs 3-5 renders this scenario highly improbable; and necessarily very localised, if true.

By a process of elimination, to account for the light $\delta^{34}S$, we are left with a scenario whereby crustal sulphur contamination demonstrably took place only in plugs 1 and 2. If contamination were taking place above the current erosion level, in Lower Jurassic sediments which very likely overlay this region, there remains a problem as to how these crustally contaminated sulphides are now present below the contaminant. One possibility may be that the sulphides moved down the plug or conduit. In the following section we consider whether this is feasible given the upward injection of magma in a conduit, and whether the observed characteristics of the sulphides in plugs 1 and 2 support this model. What were the physical constraints on sulphides sinking and could this effect have been so localised that the other plugs (3-5) further 'downhill' on the northwest quadrant of Rum, be too low in altitude to record this process?

12.5.4. Dynamic conduit modelling and sulphide sinking

12.5.4.1. Hademard-Rybczinski conduit modelling

The settling of sulphide liquid droplets through a magma conduit can be modelled either by using Stoke's Law, or by the Hadamard-Rybczinsky equation (e.g., Lightfoot *et al.,* 1984) as established by the experiments of de Bremond d'Ars *et al.* (2001). The latter takes into account the non-Newtonian fluid properties in the conduit, as well as both the differences in densities and viscosities of the silicate and sulphide liquids present in the system, and is expressed as:

$$V_s = \frac{1}{3}\frac{\left[\frac{\Delta\rho g r^2}{\mu f}\right][\mu f+\mu d]}{[\mu f+\frac{3}{2}\mu d]} \qquad \textit{(equation 12.1)}$$

where V_s is settling velocity (ms^{-1}), r is sulphide droplet radius (m), Δρ is the difference in density between sulphide liquid and silicate magma (= 1400 kgm^{-3}), μf and μd are the viscosities of silicate magma (0.1 Pa s; Paterson *et al.,* 1998) and sulphide liquid (0.01 Pa s) respectively, and g is the acceleration due to gravity (9.8 ms^{-2}). Sulphide droplets will sink (with velocity V_d) through the conduit pipe once the settling velocity (V_s) exceeds the upward velocity magma intruding into and through the pipe (V_z), such that:

$$V_d = V_z - V_s \qquad \textit{(equation 12.2)}$$

Sulphide droplet settling occurs when $V_d < 0$ ms^{-1}. The analogue experiments of de Bremond d'Ars *et al.* (2001) indicated that sulphide droplets are transported in suspension by flowing magmas, and that due to the large surface tension of the droplets, they do not coalesce during active transport. In part, this could explain the disparity and size of sulphide minerals in peridotite plugs 4 to 12. These plugs generally do not record matrix-banding or indentation layering, suggesting that prolonged quiescent periods were not prevalent during cooling, hence perturbing the ability of the conduit to form crystal layering (e.g., Wadsworth, 1994) and thus arresting sulphide droplet settling and coalescence. Further, the low abundance of sulphides in plugs 4 to 12 would also hamper coalescence. The size and distribution of fine sulphides in these plugs probably reflects the mode of transportation and entrainment which occurred during conduit activity. For scenarios involving higher volumes of sulphide liquid, plots of V_s and V_d according to sulphide droplet radius, are presented in Figures 12.9a-b. Sulphides in the margins of plug 1 range in diameter from 0.5 to 4 mm (Table 12.2) with most intercumulus sulphides 1-3 mm in diameter.

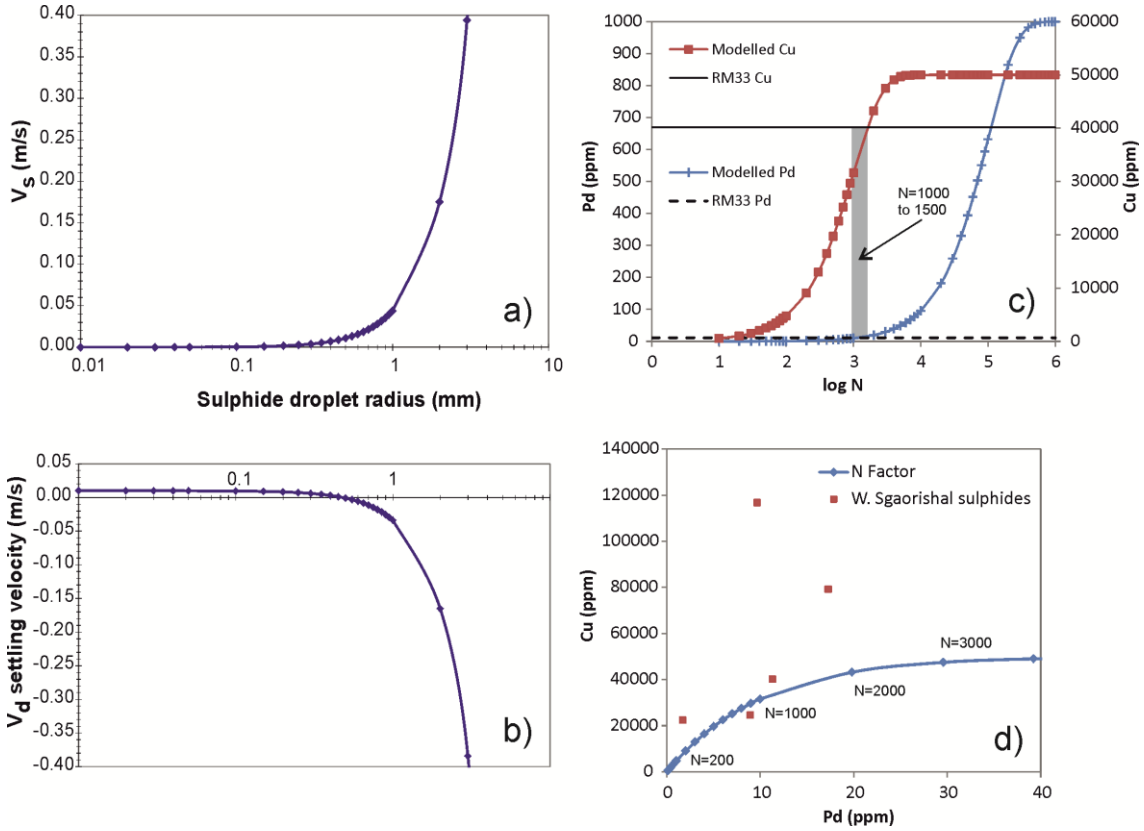

Figure 12.9. Dynamic conduit modelling using Hadamard-Rybczinsky equation for sulphide settling; (a) sulphide settling velocity (V_s) for different sizes of sulphide droplet (radius in mm); (b) sulphide velocity through conduit (V_d) according to sulphide droplet radius. Sulphides will sink if $V_d < 0$ ms^{-1}. N-factor modelling; (c) N factor (expressed as log N) vs. Pd and Cu concentrations in the sulphide liquid. Solid line delineates Cu concentration in sulphides from plug 1 margin (RM33), and dashed line is for Pd. Shaded box shows the range of modelled log N values which fit Cu and Pd; (d) Modelled Cu and Pd concentrations in sulphides according to various values of N (labelled). Also plotted are the measured Cu and Pd abundances for plug 1, centre and margins.

V_z was varied in equation 1, until sulphides of the minimum average radius observed in the margin of plug 1 (r ~ 0.5 mm) had $V_d < 0$ ms^{-1}. This required an upward magma velocity of 0.01 ms^{-1} (Fig. 12.9a-b), such that sulphide droplets would sink through the conduit at a rate of 0.001 ms^{-1} (V_d). By lowering V_z further to 0.001 ms^{-1}, sulphides with r = 0.2 mm would also begin to sink at a similar rate. Thus, the upward flow of magma through the conduit would essentially have to have ceased before sulphide liquids of the sizes observed in the margins of plug 1 would settle. The viscosity of the silicate magma was assumed to be 0.1 Pa s (Paterson *et al.,* 1998), however if the conduit was instead filled with an olivine crystal mush (olivine phenocrysts entrained in basaltic magma) then the overall effective viscosity of the 'silicate magma' would be higher. Holness *et al.* (2012) suggested a crystal load in the range of 10-40 vol.% for the peridotite plugs, based on the volume of phenocrysts entrained in picrite dykes on Rum. Even by increasing viscosity to 1 Pa s (i.e., an assumed 50% crystal mush entrained in a mafic magma, with viscosity = 1 Pa s based on Paterson *et al.,* 1998) at V_z = 0.001 ms^{-1}, sulphides of r ~ 0.5 mm would still be capable of sinking through the conduit. In summary, it is possible that sulphide liquids forming through crustal contamination above the present day level of erosion and exposure of plug 1 (and 2) would have sunk through the conduit once active upwards magma injection had ceased. Sulphide liquid sinking may have taken place either in a passively cooling (stationary) environment and/or become 'sucked' downwards if magma withdrawal were taking place.

By assuming a cooling rate controlled by Newton's Law of Cooling:

$$T = T_a + (T_o - T_a)\, e^{-\kappa t} \qquad \textit{(equation 12.3)}$$

it would take the margin of plug 1 approximately 5 days to cool below 1100°C; where T_a is temperature of the country rock (assumed 600°C, based on Holness *et al.,* 2012; T_o is initial magma temperature of the conduit (assumed 1400°C; Holness *et al.,* 2012); T is the target temperature 1100°C for sulphide liquidus (e.g., Bowles *et al.,* 2011) and κ is thermal diffusivity constant of 10^{-6} m^2s^{-1}. Given a downward velocity V_d of 0.001 ms^{-1} for sulphide droplets through the quiescent conduit, sulphides would be capable of settling through a distance on the order of 400 m, downwards from the initial level of S-saturation. Ultimately, this distance is likely to be subject to estimation errors – for example, as sulphide droplets coalescence during settling, their settling velocity will change. In addition, as the conduit cools towards 1100°C, the effective viscosity of both the sulphide liquid and silicate magma will increase, thus slowing its descent. The 'permeability' of the host silicate mush (i.e., amount of partial melt and degree of ponding of sulphide liquid above areas of low permeability; e.g., Holwell &

McDonald, 2006) may not be uniform throughout a single volcanic plug. However the interfacial tension at silicate-sulphide liquid interfaces may preclude sinking of sulphide droplets below a critical size range (e.g., Mungall & Su, 2005) but this depends on the proportions of silicate melt to solidified silicate minerals in the system, and would suggest that compaction-driven sulphide segregation is possible (Rose & Brenan, 2001).

The estimated thickness of Triassic sediments in the Hebrides Basin in the vicinity of Rum on the 'Skye High' of this Mesozoic sedimentary basin, ranges from tens of metres on Ardnamurchan, to 100 m (Raasay, off the Isle of Skye) and 300 m at Gruinard Bay on the Scottish mainland (Steel *et al.,* 1975). Given that the current erosion level of plug 1 occurs at the base of these Triassic sediments (Figs. 12.2a and 12.10a) and the estimated minimum potential settling distance of sulphide droplets is 400 m, this is within reach of S-rich Jurassic sediment horizon(s), assumed to have been present above the current erosion level (for example the Lower Jurassic mudrocks and ironstones of the Lias Group – see Fig. 12.10a). Assimilation of wall rock sediments, particularly light $\delta^{34}S$ crustal sulphur from Jurassic units, would induce sulphide saturation at a high level in the conduit (above current erosion level; e.g., Fig. 12.10b). Thus, we can reasonably envisage that once active magma-mush injection had ceased in the conduit, silicate and sulphide liquids from above sank through the plug, forming olivine cumulates with interstitial sulphide liquid that recorded light crustal S compositions and high S/Se ratios inherited from 100's metres above (e.g., Fig. 12.10c).

While plug 2 also records $\delta^{34}S$ in sulphides significantly less than the local magmatic compositions around 0 ‰, it has lower abundances of sulphide than plug 1. Projecting the dip of the base of the Triassic sedimentary units near plug 1 (approximately 20° dip NW; Fig. 12.10a) and even accounting for the current topography and elevation of the area between plugs 1 and 2, the lower sulphide abundance in plug 2 may reflect the greater distance between the potential Lower Jurassic contamination zone and the present-day level of exposure (Fig. 12.10a). Further, the lack of crustal $\delta^{34}S$ signature in plugs 3, 4 and 5 is consistent with the model, in that their current level of exposure is > 400 m below the projected contamination horizon so any sulphides that did settle downwards are likely to have been removed by erosion (i.e., Fig. 12.10a). The lack of crustal $\delta^{34}S$ signature in plugs from elsewhere on the island, particularly further east, may also suggest that the Mesozoic sedimentary pile of the Hebrides Basin was not present, as the Isle of Rum sits on the 'Skye high' within the basin such that only the feather-edge of the basin's sediments could have been deposited over part of the island (see Hughes *et al.,* accepted, a – Chapter 11).

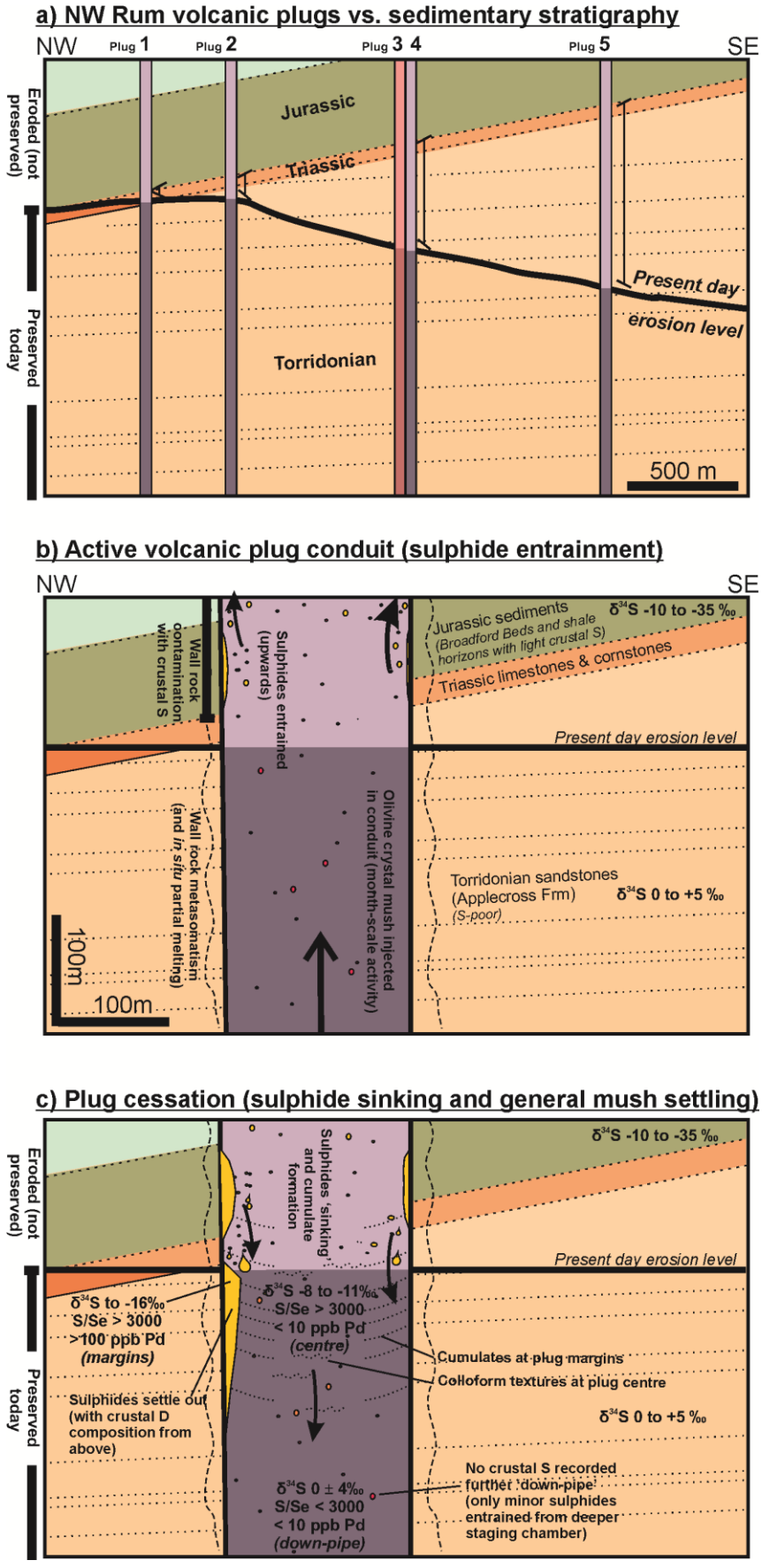

Figure 12.10. (caption overleaf)

Comparison with Paleogene macrodykes in east Greenland and other similar intrusions

A similar set of geological circumstances exist in east Greenland, where Holwell *et al.* (2012) describe a suite of mineralised macrodykes, radiating away from the Skaergaard intrusion, and intruding Archaean basement and overlying pyrite-rich Cretaceous black shales (with $\delta^{34}S$ -23 to -30 ‰) and Paleogene flood basalts. Magmatic Cu-PGE-Au sulphide mineralisation, with crustal $\delta^{34}S$ signatures (-10 to -26 ‰) is present along the margins of the sub-vertical Miki Fjord Macrodyke, which is observed to intrude all three lithological units. Further north, the Togeda Macrodyke, which is exposed at a level where it intrudes the basement gneiss, has similar sulphides that carry light S-isotopes (Holwell *et al.* 2012). Holwell *et al.* (2012) concluded in both cases that Cretaceous shales were the trigger for sulphide saturation and sulphide droplets were entrained within the macrodyke magmas during intrusion. The presence of sulphides in the Togeda Macrodyke*, beneath* the stratigraphic level of the contaminant, was explained by a northward injection of magma which could then incorporate S from sediments exposed deeper to the south (Holwell et al., 2012).

Figure 12.10. Cartoon cross-section model of crustal sulphur contamination scenario for northwest Rum. (a) Schematic cross-section of northwest Rum showing plugs 1 to 5 in the vicinity of Sgaorishal. Due to the orientation of Mesozoic Hebridean Basin Triassic and Jurassic sediments relative to the modern day topography, the current exposures of plugs 3, 4 and 5 are too great a distance below the Jurassic contamination horizon to record crustal $\delta^{34}S$ and voluminous sulphide liquids. However, plugs 1 and 2 still record light crustal $\delta^{34}S$. (b) Active volcanic plug intrudes through Torridonian sediments, and Triassic and Jurassic sediments of the Hebrides Basin (since eroded) above. The plug entrains tiny droplets of high-tenor sulphide liquid from a staging chamber. Wall-rock metasomatism and partial melting (especially recorded in the siliceous Torridonian Applecross Formation sandstones) takes place. In the upper portions of the plug, S-rich shales and siltstones from the Jurassic sediments contaminates magmas with isotopically light crustal S. (c) Active magma intrusion of volcanic plug ceases, and magma-entrained olivine mushes are left to settle through the conduit (forming cumulate layers, particularly at the conduit margins). Sulphide droplets entrained in the plug, including more voluminous sulphide liquids from crustal S contamination horizons (above) at Jurassic sedimentary units, settle through the conduit. Sulphide liquids amalgamate during settling, and form an interstitial/intercumulus phase around cumulate olivine. Sulphide liquid is particularly abundant around conduit margins (due to wall-rock S contamination) and has a higher concentration of PGE, higher S/Se ratio and lighter $\delta^{34}S$.

Alternatively, a similar situation to that described above (for the Rum plugs) is possible for the Togeda Macrodyke. The Cretaceous sedimentary units are inferred to have been present some 500 m or so above the present erosion level. Given the much larger size of the droplets (up to 10 mm) in the macrodykes compared to the Rum plugs (mostly 1-3 mm), the likelihood of large droplets settling down through the dyke conduit by a vertical distance of 500 m is plausible. For example, assuming a sulphide droplet with radius (r) of 0.5 mm, and a silicate liquid (not crystal mush) of viscosity 0.1 Pa s, then due to the silicate-sulphide liquid density difference, the sulphide droplets would be capable of sinking through a magma conduit with upward silicate magma velocities (V_z) of up to 1.1 ms^{-1}. However, in a dyke scenario, lateral movement of magmas along the dyke (due to a pressure gradient from the point of intrusion along an opening fracture) must also be factored in. Hence both lateral and downward migration of sulphide droplets may be envisaged for planar features such as dykes (e.g., Todega Macrodyke), in contrast to pipe-shaped conduits.

The downward movement of sulphide liquids in a cooling magmatic system has also been suggested for ultramafic complexes in Madagascar (McDonald, 2008). In this model, sulphide liquids migrate laterally, as well as downwards, towards the centre of the intrusion during crystallisation. During migration, sulphide liquids fractionated such that Pt- and Pd-bearing PGM exsolved from, and detached from, the sulphide liquid (becoming trapped in olivine mushes) leaving Cu-rich sulphide liquid to continue sinking towards the centre of the intrusion (McDonald, 2008). Notably however, our model of downward sulphide sinking in a cooling (recently cessated) magmatic system differs markedly from sulphide sinking models suggested for other mineralised conduit settings; for example at Noril'sk Talnakh where Arndt (2011) envisaged that sulphide liquids sank through an active silicate magma conduit, with a significant upward velocity of magma injected from beneath.

The significance of sulphide sinking versus upward entrainment

Comparison with examples outside the BPIP shows that a process of sulphide sinking through cooling, recently inactive conduits may well be widespread, and could account for high volume sulphides with crustal S compositions, to be present at levels stratigraphically lower than originally formed. Thus, the study of mineralised magmatic sulphide systems also needs to consider the possibility of contamination from sources above the level of the mineralisation, which may well no longer be exposed. In terms of exploration models, this is significant in that

intrusions exposed below the stratigraphic level of any potential contaminant (or where possible contaminants have been eroded) still have the potential to host magmatic sulphides. Of still further importance, if a settling sulphide liquid had the ability to pond in a depression in the magmatic plumbing system, then massive sulphide accumulations formed from crustal contamination, could potentially be found hundreds of metres below the level of the contaminant that triggered sulphide saturation. As such, the commonly held conceptualisation of sulphides only being entrained with magma injected upwards into intrusions (e.g., Holwell & McDonald, 2007; Naldrett *et al.,* 2009, 2011) should be reconsidered in light of the real possibility of sulphides also moving downwards through magmatic systems, and retaining geochemical signatures imparted by contamination at higher crustal levels.

12.5.4.2. N-factor modelling: Silicate/sulphide liquid ratios

Another parameter which can be calculated for a sulphide-bearing conduit is the proportion of sulphide liquid in the system. This has been modelled for the sill-hosted Noril'sk Ni-Cu-PGE orthomagmatic mineralisation in Siberia (Brügmann *et al.,* 1993; Naldrett *et al.,* 1995; 1996). In an open system, such as a magma conduit, this can be expressed as the *N-factor*, which is the ratio of the volumes of silicate magma to sulphide liquid in a mechanism analogous to zone refining (Brügmann *et al.,* 1993; Naldrett *et al.,* 1995; 1996). In this situation, sulphide droplets are formed at the top of the magma conduit, and slowly settle down through it (e.g., Brügmann *et al.,* 1993). The N-factor equation, based on Cox *et al.* (1979) is as follows:

$$Y_i = X_i \left\{ D - \left[(D-1) e^{-\left(\frac{1}{D} N\right)} \right] \right\} \quad \textit{(equation 12.4)}$$

where Y_i is the concentration of metal, i, in the sulphide, X_i is the initial concentration of metal, i, in the silicate, and D is the partition coefficient for metal, i, between silicate and sulphide.

$$N = \frac{volume\ silicate\ magma}{volume\ sulphide\ liquid} \qquad \textit{(equation 12.5)}$$

As the value of N increases, the concentration of strongly chalcophilic metals such as Pt and Pd rapidly increases. For plug 1, the concentration of trace elements such as Pd, can be modelled using equation 4 (D_{Cu} = 1470; D_{Pd} = 190,000; Mungall & Brenan, 2014), with an initial silicate composition of 50 ppm Cu and 10 ppb Pd (comparable to picritic compositions and Cu and Pd abundances in other low-sulphide plugs such as plug 12). This estimates that the ratio of silicate to sulphide liquid (N) ranged 1000 to 1500 for sample RM33 (Fig. 12.9c). If the average

abundance of Pd measured in sulphides (Table 12.3) is calculated per plug sample for plug 1, and plotted with calculated Cu abundance for a homogenised sulphide liquid (based on assigning all bulk rock Cu to chalcopyrite, and normalising to 100 % sulphide) the Cu and Pd compositions of sulphides in plug 1 can be modelled by equation (4) using N = 200 to 1200 (Fig. 12.9d). This includes the centre of the plug (e.g., RM30), however the outlier of RM95 at the southern plug margin has a substantially higher concentration of Cu (almost 120,000 ppm). This may suggest that the modelled Cu composition of the magma was too low, but it produces the best fit for N-factor modelling across the rest of the plug. Alternatively, the margin of the plug at RM95 has acquired Cu but not Pd from the surrounding wall rock – the Triassic Sandstone Formation in this area has rare malachite reported with carbonate calcretions (Emeleus & Troll, 2008).

12.5.4.3. Sulphide tenor calculations

A mass balance and metal tenor calculation can be carried out to estimate the proportion of PGE present within the sulphides of peridotite plugs. As sulphide assemblages comprise pyrrhotite, pentlandite and chalcopyrite (with only accessory bornite, chalcocite and galena), we have followed the methodology of Huminicki *et al.* (2005) using the whole-rock measured abundances of S, Cu, Ni and Fe. All of the whole-rock Cu budget was assigned to chalcopyrite, and after subtracting the mass of S required, and the mass of Ni bound within olivine (assuming a Ni content of 2400 ppm into olivine and average of 60% olivine in the plug, based on Holness *et al.,* 2012) all of the remaining Ni was assigned to pentlandite. The proportion of pyrrhotite was then estimated from the remaining S. Following the observations and methods of Holwell & McDonald (2007), such that chalcopyrite contains negligible PGE in solid solution, we then recalculate the measured whole-rock PGE content to 100% pyrrhotite + pentlandite, as these are the principle PGE-bearing base metal sulphides. We then compare the measured PGE spectra (chondrite normalised LA-ICPMS data) with the normalised calculated PGE spectra using this mass balance approach (Fig. 12.11). According to Ballhaus & Sylvester (2000), element concentrations in sulphide which are greater than recalculated whole-rock abundances, indicate that element is present in solid solution. In contrast, if element concentrations in sulphide are less than recalculated whole-rock abundances, a proportion of that element must be present in the rock in discrete phases, such as platinum-group minerals (PGM). It should be noted that these tenor calculations were only carried out for plug 1, as the lower sulphide abundances in the other plugs were subject to large uncertainties, particularly

regarding S and Ni content when recalculating chalcophile elements to 100% sulphide. The calculated proportions of each base metal sulphide mineral and calculated PGE tenor for pyrrhotite+pentlandite in Plug 1, used in Figure 12.11, are presented in Table 12.4.

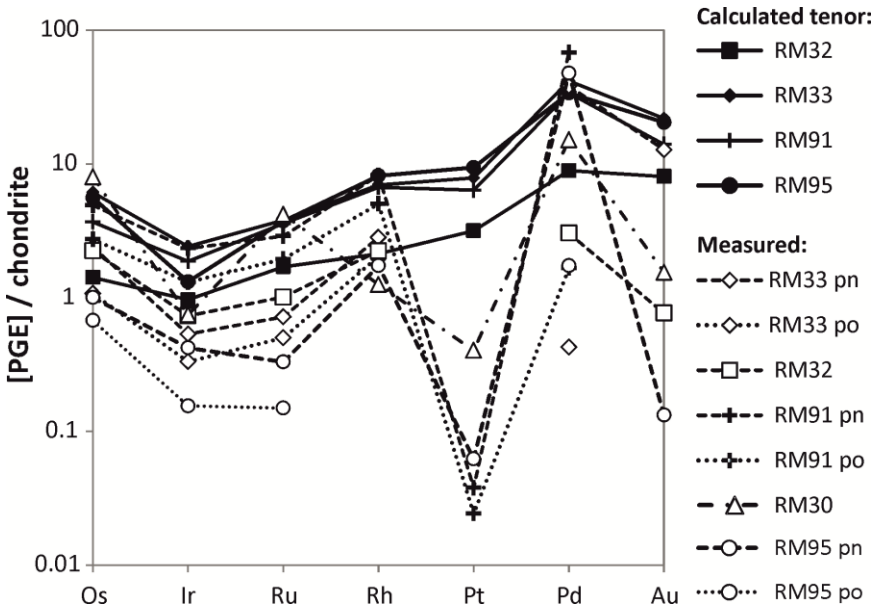

Figure 12.11. Calculated PGE tenor of sulphides vs. measured PGE abundance. PGE values have been normalised to chondrite, based on McDonough & Sun (1995) values.

Based on Figure 12.11, and with the exception of Pt, the measured PGE tenor of sulphides are broadly calculable based on the abundance of sulphides in plug 1, suggesting that the IPGE and Rh are likely to be present in solid solution in pyrrhotite and pentlandite. In contrast, Pt must largely occur as discrete Pt-bearing PGM (a feature well documented by Holwell & McDonald, 2007 and Barnes *et al.,* 2008, for example). This is substantiated by SEM observations of Pt-tellurides, bismuthides, and arsenides (Table 12.2, this study and Power *et al.,* 2003). Measured Pd concentrations in sulphide are highly variable in comparison to calculated metal tenors. The calculated Pd tenor of sulphides is largely based on the accuracy of the estimate of pentlandite abundance, which is affected by the variable olivine content of these plugs, and this may go some way to explaining any discrepancy. Pd-bearing PGM would also offer an explanation for this disparity. Similarly, the variably lower measured abundances of Au in solid solution in the sulphides is supported by the observation of discrete grains of electrum (in agreement with Power *et al.,* 2003). The calculated tenor for IPGE are slightly elevated above measured LA-ICPMS data, and again may suggest a small proportion of Os, Ir and Ru are

occurring as PGM – a feature potentially corroborated in other plugs, such as plug 2, where Ir-Pt and Ir-arsenides have been observed (e.g., RM35; Table 12.2).

The calculated N factor range for plug 1 was 200-1200, which would suggest a range of 0.08 to 0.5 vol.% sulphide minerals preserved in the plug. By summing the calculated modal proportions of chalcopyrite, pentlandite and pyrrhotite in Table 12.4, the proportion of sulphide ranges 0.21 to 0.54 modal % in the margins of this plug, and corroborates the N-factor calculations. This suggests that the same ratio of silicate magma to sulphide liquid which formed in the conduit, remained in the conduit, and ties in with the assumption that this volcanic pipe would have ceased erupting at the time the sulphide liquid settled downwards.

Finally, how do the measured sulphide metal tenors of plug 1 compare to those observed in other peridotite plugs elsewhere on Rum, which do not have a crustal contamination signature? From Figures 12.6-12.9 there does not appear to be a major disparity between the proportion of sulphide minerals in any given plug and the PGE tenor of those sulphides – specifically, the tenor of plugs which only contain small (< 150 µm) sulphides is within range of the sulphide metal tenor of the net-textured and coarser sulphides in plug 1, suggesting no major upgrading of the sulphide liquids took place in plug 1, again validated by calculated N-factor values. Small sulphide liquid droplets entrained from a deeper staging chamber were fed through volcanic conduits in olivine-bearing crystal mush. These would have become amalgamated with secondary more voluminous sulphide liquids (via Ostwald ripening) formed following any high-level crustal S contamination by Jurassic sediments, and would produce a sulphide liquid of intermediate tenor.

12.6. Conclusions

1. The peridotite plugs on the Isle of Rum were intruded as olivine-rich crystal mushes suspended in a basaltic/picritic magma which also entrained sulphide liquid.
2. Based on the elevation and corresponding compositions of the plugs and cyclic units, it is unlikely that the Rum Layered Suite directly fed these volcanic conduits. Instead we suggest that a separate, deeper staging chamber was responsible for the periodic and discrete intrusion of peridotitic crystal mushes with entrained sulphide into both the Rum Layered Suite and the volcanic conduits represented by the plugs.
3. Most plugs have a magmatic whole-rock $\delta^{34}S$ signature of +0.1 ± 1.0 ‰, which overlaps with the whole-rock $\delta^{34}S$ signature of the ELS (-0.5 ± 1.4 ‰) and proto-

Icelandic plume values recorded elsewhere in the NAIP (-2.3 ± 1.5 ‰; Hughes *et al.,* accepted, a – Chapter 11). In addition, whole-rock and sulphide-specific PGE abundances in plugs lacking crustal contamination signatures overlap compositions in the ELS.

4. Two plugs in the northwest of the island have a crustal $\delta^{34}S$ signature (ranging -14.7 to -2.9 ‰) and elevated S/Se ratios (up to 12,130), unlike any of the other plugs on Rum. Projecting the Hebrides Basin sediment stratigraphy above the preserved unconformable base of Triassic rocks (Fig. 12.10a), volcanic conduits would likely have erupted through a thick package of Jurassic mudrocks with characteristically light $\delta^{34}S$ (-33.8 to -14.7 ‰), inducing S-saturation and the formation of voluminous immiscible sulphide liquid, locally and at a near-surface level (Fig. 12.10b).
5. Once active magma transport had ceased, sulphide liquids sunk back through the conduit, and based on modelling of the conduit mush viscosity and cooling rates, this settling would take place over of distance of up to 400 m and over a period of a few days, resulting in the poikilitic and net-textures preserved today. Sulphides previously entrained in the crystal mush from the staging chamber, and this secondary immiscible sulphide liquid, became amalgamated. Given the current topography in northwest of Rum, the other plugs probably record deeper level sulphides in the plug conduit plumbing system, and any crustal S influence (if present) has since been removed by erosion.
6. Based on sulphide PGE tenor and N-factor modelling for the crustally contaminated plugs (1 and 2), we highlight that the volume of sulphide observed in these plugs tallies with that predicted by contamination models. This suggests that while sulphide liquids did sink back through the conduit from a contamination horizon above, sulphides did not pond or become trapped.
7. We suggest that this sulphide sinking process (within a cooling non-active conduit or during magma 'suck-back') may be observed in other vertical/inclined magma conduits globally, for example in the macrodykes of east Greenland. This model may be used to explain S-isotopic and S/Se ratios which are indicative of contamination of magmas by crustal S, and yet no suitable lithology is present either in the direct host package or deeper in the system.

Acknowledgements

Sulphur isotope analysis was funded by NERC Isotope Geosciences Facilities grant, IP-1356-1112. HSRH would like to acknowledge the financial support of the Natural Environment Research Council (NERC) for her PhD studentship (NE/J50029X). We thank Scottish Natural Heritage, the Isle of Rum Community Trust and the residents of the Isle of Rum for granting permission to sample. Alison McDonald, Brett Davidheiser-Kroll, Anthony Oldroyd and Katherine Dobbie are thanked for their assistance in sample preparation, particularly for whole-rock S-extraction and analysis. Peter Fisher carried out PGM searches and is thanked for his assistance with SEM-based studies generally. Discussions with Kathryn Goodenough, Nick Arndt, Ben Hayes, John Faithfull, Brian Upton, John MacLennan and Chris MacLeod helped greatly during the writing of this manuscript.

CHAPTER 13

Synthesis

Chapters 6 to 12 investigate aspects of the PGE and chalcophile element geochemistry, and sulphur budget of the lithosphere of Scotland – both temporally (from the Palaeoproterozoic to the Palaeogene), and spatially, from north to south, and from the upper crust to the lithospheric mantle. Scotland provides an ideal framework to compare different tectono-magmatic events and their potential for PGE metallogenesis. Given Scotland's well-documented long and varied geological history (coupled with that of Greenland), the region represents a unique opportunity to contribute to the ongoing debate over the fundamental influences of asthenospheric mantle and mantle plume(s) vs. lithospheric mantle controls on melting processes and mineralisation. Key questions are: (1) Is there an underlying influence on mineralisation potential or 'prospectivity' according to geodynamic setting? (2) Does the subcontinental lithospheric mantle (SCLM) act as a repository of metals such as the PGE? (3) And to what extent does the SCLM contribute metals during major melting events?

13.1. Cratonisation and 'preconditioning' of the lithospheric mantle

The Lewisian Gneiss Complex (LGC) crops out in NW Scotland and the Outer Hebrides. It comprises mid-late Archaean tonalite-trondhjemite-granodiorite (TTG) gneisses, with minor mafic-ultramafic and metasedimentary components, that have been reworked by several Late Archaean and Palaeoproterozoic tectonic events. The LGC represents a fragment of the North Atlantic Craton (NAC), which can be traced from present day Scotland to Greenland and Canada. Early Palaeoproterozoic extension (c. 2.4 Ga) led to the formation of a large igneous province (LIP), now represented by the Scourie Dyke Swarm (see Chapter 6). These mafic-ultramafic dykes represent the roots of the LIP, presumably feeding shallow intrusions and flood basalts at the palaeo-surface.

The Scourie Dykes are interesting on both geological and metallogenic grounds. They intrude the LGC in between periods of high-grade metamorphism; the earlier Badcallian c. 2.7 Ga and Inverian c. 2.5 Ga events, and the later Laxfordian which commenced c. 1.9 Ga (see Fig. 13.1). Crucially, simple partial melting of the asthenospheric mantle cannot account for the 'continental-like' signature of Scourie Dyke geochemistry (see Section 6.7.4) and instead indicates a significant component of lithospheric mantle melting (up to 40 % of magma was derived from SCLM partial melting – see Table 6.4). Notably, the negative Nb-Ta-Ti anomalies and enrichments in Th, LREE and LILE (particularly marked in the ultramafic dykes) represent an Archaean metasomatic geochemical signature from SCLM of similar composition to that

represented by Loch Roag mantle xenoliths. The 2.4 Ga Scourie Dyke tectono-magmatic event coincides with a carbonatitic metasomatic event recognised in Loch Roag peridotite xenoliths and associated xenocrysts (c. 2.3-2.5 Ga; Long *et al.,* 1991), providing a deeper indication of continental extension (and possibly related to the carbonatitic intrusions in western Greenlandic NAC c. 2.6 Ga; Larsen & Rex, 1992 and references therein).

Whilst the presently exposed Scourie Dykes are unlikely to host any major mineralisation themselves, this has several important implications for the PGE, chalcophile element and sulphide budgets of the Archaean-Palaeoproterozoic SCLM of the NAC in Scotland. Firstly, by 2.4 Ga the SCLM was fertile for PGE and chalcophile elements, and although significant lithospheric mantle melting took place beneath the NAC, this did not severely deplete the shallow SCLM (as represented by Loch Roag peridotite xenoliths) in these elements and/or sulphides. Secondly, sulphide petrography on the Loch Roag xenoliths themselves (see Chapter 8) indicates that by the end of the Scourie LIP rifting event, two coexisting sulphide populations were probably present in the shallow lithospheric mantle (Fig. 13.1). The first; a coarse-grained population of PGE-poor Ni-Fe-Cu sulphides interstitial to the peridotite silicate mineralogy ('Group 1') with $(Re/Os)_N > 1$, and the second a finer-grained population of PGE-rich Ni-Cu-Fe sulphides ('Group 2') with $(Re/Os)_N \sim 1$ and restricted to feldspathic veinlets, themselves interstitial to peridotite modal mineralogy. Crucially, Group 2 sulphides preserve rounded inclusions of Ca-carbonate, suggesting that they were formed from immiscible carbonate-sulphide liquids, introduced into the SCLM by carbonatitic magma. Finally, Re-Os isotopic analyses of a Loch Roag peridotite xenolith (LR80), and picrite and dolerite dykes corroborate the involvement of SCLM partial melting contributing to Scourie Dyke parental magmas (see Table 6.3 and Fig. 13.1). For example, the unradiogenic γOs_i of a Scourie picrite dyke (-7.24 at 2.4 Ga) suggests involvement of a low $(Re/Os)_N$ component in the melting regime that had been isolated from convecting (asthenospheric) mantle prior to partial melting.

Thus, by the early Palaeoproterozoic, the NAC lithospheric mantle keel was enriched in PGE (and REE) in forms that were both heterogeneous and highly 'fusible'. A complex series of compressional events took place later in the Palaeoproterozoic, and the NAC records compressional tectono-magmatic events on both its northern and southern margins. Given the apparent lateral narrowing (or pinching out) of the NAC in Scotland, the LGC records two overlapping geodynamic environments.

Accretion of volcanosedimentary arc terrane(s) took place as juvenile lithosphere became subducted beneath the NAC. In Greenland and southern Labrador this is preserved as the Ketilidian-Makkovikian belt, and is correlated with Rhinnian gneisses in Scotland and Ireland (in the Grampian Terrane – see Section 9.1). Early Laxfordian (c. 1.9 Ga) volcanosedimentary arc terranes (Loch Maree Group) and calc-alkaline magmatism in the Gairloch and Gruinard areas of the southern LGC are probably intrinsically related to the Rhinnian and Ketilidian (see block model, Fig. 13.1) although this relationship has since been complicated by extensive lateral movement along the Great Glen Fault (GGF). Further, the LGC as a whole was overprinted by 1.8-1.65 Ga (Late Laxfordian) crustal thickening, metamorphism, partial melting and pegmatite intrusion. This was likely caused by the continental collision recorded by the Nagssugtoqidian continental orogenic belt, on the northern margin of the NAC in Greenland. Hence given its fortuitous position at the pinched margin of the NAC, the LGC records complicated late Palaeoproterozoic geodynamics at the continental margins during the growth of the Nuna supercontinent.

The 1.9-1.6 Ga reworking of the NAC therefore represents a major tectono-magmatic period, highly likely to be recorded in the geochemistry and/or mineralogy of the sub-Lewisian lithospheric mantle. For example, in Figure 13.1, we propose that a new population of sulphides was formed in Loch Roag-type SCLM ('Group 3') at this time. Group 3 sulphides (see Chapter 8) are PGE-rich droplet-shaped Ni-Fe-Cu sulphides, similar to Group 2 sulphides, but notably lacking any Ca-carbonate inclusions. Group 3 sulphides have $(Re/Os)_N \leq 1$ and micron-scale Pt-S (cooperite) platinum-group minerals (PGM), and they occur strictly within feldspar-spinel symplectites that are physically connected to the feldspathic veinlets that host Group 2 sulphides. Remelting of the (carbonatite-associated) metasomatised 'pockets' and Group 2 sulphides ultimately upgraded and homogenised this sulphide liquid (with the loss of CO_3^{2-}), enriching it in PGE (relative to Re) before cooling to form Group 3 sulphides. This sulphide liquid had become so enriched in PPGE that Pt was exsolved as discrete PGM, while Pd remained in solid solution in pentlandite and pyrrhotite. The PGE-poor Group 1 sulphides were effectively isolated from this remelting, given their shielding away from 'fusible' feldspathic metasomatic 'pockets', and encased in their olivine-pyroxene protogranular petrographic setting (Fig. 13.1).

The co-existence of multiple sulphide populations with distinctly different PGE contents and $(Re/Os)_N$ ratios in a single xenolith, reveals a complexity to the upper mantle sulphur budget thus far not recognised. Specifically, it highlights that the precious metal budget of the SCLM is

dependent on the composition and petrographic setting of each of these populations. Bulk rock Re-Os isotopic analysis of Loch Roag xenolith LR80 gives a calculated γOs_i of 0.07 which is less radiogenic than calculated mantle compositions (γOs_i for asthenospheric mantle ranges 0.11-0.5 at 2.4 Ga – see Section 6.7.4). This suggests the negative γOs_i is controlled by the low $(Re/Os)_N$ sulphides and implies that Loch Roag-type peridotites were already isolated from the convecting mantle by 2.4 Ga. For example, preferential assimilation or melting of Group 2 and/or Group 3-type sulphides may impart an unradiogeneic Os-isotopic signature. Given the considerable differences in PGE abundances and $(Re/Os)_N$ between the three sulphide populations present in Loch Roag-type mantle (see Section 8.4.2), especially the high concentrations of PGE that characterise Group 2 and 3 sulphides, suggests that the formation of Group 2 (which later became Group 3) sulphides at least occurred pre- or syn-2.4 Ga rifting. Hence the 1.9-1.6 Ga orogenesis served only to remobilise some of the already PGE-enriched sulphide budget.

Whilst the other parts of the NAC record a series of complicated tectonic events, from Mesoproterozoic rifting in southern Greenland (e.g., the Gardar Province), to early Neoproterozoic compression associated with the Grenvillian and Valhalla orogenies, no major tectono-magmatic events were recorded in Scotland at this time. Instead, the Scottish part of the NAC records only crustal sedimentary features in the foreland to the Grenville orogenic belt, such as the development of Meso- and Neoproterozoic alluvial sedimentary systems – firstly the Stoer Group of the Torridonian sedimentary succession, and latterly the Sleat and Torridon Groups. The Moine Supergroup of NW Scotland was also deposited in the Neoproterozoic.

Whilst from a global perspective this period represents a long and complicated geological history, from the point of view of Scottish geology, the next major tectono-magmatic event took place during the late Neoproterozoic rifting of Rodinia (Fig. 13.2). During this time, a passive margin developed along the edge of the Scottish NAC, with fault-controlled blocks of continental margin (Rhinnian) basement being covered by deposition of Dalradian sediments. Initially, Ba-rich strataform mineralisation (e.g., of pyritic celsian – Ba-feldspar) was formed, but later Cu-Pb-Zn-Ni mineralisation (with baryte) formed from submarine hot springs in a volcanogenic massive sulphide-type scenario (Fig. 13.2). This latter, metal-rich mineralisation was synchronous to mafic-ultramafic magmatism (e.g., the Tayvallich volcanics). Rifting of Rodinia ultimately culminated in the formation of oceanic crust and the opening of the Iapetus Ocean, after c. 600 Ma. Carbonatitic (and kimberlitic) metasomatic enrichment has been

identified in Streap Com'laidh and Rinibar mantle xenoliths, and based on clinopyroxene Sr-Nd isotopic compositions, this enrichment is thought to have taken place c. 550 Ma (Bonadiman *et al.,* 2008). Metasomatic clinopyroxenes can also be identified (and differentiated from 'primary' clinopyroxenes) using trace element geochemistry, and this can be correlated to Loch Roag mantle xenoliths (see Chapter 7). Further, Ca-carbonate and phosphates (probably carbonatite derived) have been found as 'pockets' associated with base metal sulphides in the Rinibar mantle xenoliths (see Section 9.4.2) providing more evidence for extensive carbonatitic magmatism in Scotland, thus far not correlated to surface expressions of carbonatite intrusions.

This has two important implications for the Scottish SCLM (i.e., north of the GGF). Firstly, it suggests that carbonatitic metasomatism recorded in the Streap Com'laidh and Rinibar xenoliths (c. 550 Ma) extended to the Loch Roag area, indicating that carbonatitic metasomatism at this time was widespread. In fact, Neoproterozoic kimberlites and carbonatites (c. 600 Ma) are widely documented in west Greenland, Norway and Sweden (e.g., Larsen & Rex, 1992). Secondly (and more specifically), despite their unusual trace element bulk geochemistry, geographic location on the leading edge of the (Palaeogene) rifted NAC, and their entrainment in an Eocene dyke (therefore much later than the Permo-Carboniferous entrainment ages of the other Scottish mantle xenolith suites), Loch Roag-type shallow lithospheric mantle shows no evidence for Phanerozoic metasomatism (neither modal or cryptic). This corroborates the Re-Os isotopic and sulphide petrography evidence (e.g., of LR80) and highlights that Loch Roag-type shallow peridotitic SCLM fertility for PGE, chalcophile elements and sulphides was essentially 'preconditioned' by the Neoproterozoic or before.

The opening of the Iapetus Ocean in the late Neoproterozoic and early Palaeozoic, and the formation of Iapetus oceanic crust, also appears to mark significant changes in lithospheric mantle geochemistry and its relationship to geodynamic setting (from continental and/or cratonic, to oceanic). This change is particularly noted in the composition of sulphides in mantle xenoliths north-to-south across Scotland, such that xenoliths from south of the GGF have high-Co sulphides, whereas those from north of the GGF lack Co enrichment (see Chapter 9). This systematic difference in Co enrichment must correspond to a tectono-magmatic event that had significantly more effect on the Scottish lithospheric terranes south of the GGF. As depicted in Figures 13.2 and 13.3, this can be constrained to two possible scenarios: (a) Co enrichment was intrinsic to the formation of Iapetus oceanic crust and related to seafloor spreading (Fig. 13.2), and/or (b) Co enrichment was intrinsic to the deformation of Iapetus

Ocean crust during its subduction in the Grampian event of the Caledonian orogeny (c. 470 Ma – Fig. 13.3).

Sulphide-hosted Co mineralisation occurs in serpentinised (and sometimes carbonated) ophiolites, for example in Morocco and Finland. It has also been noted in seafloor massive sulphide bodies. Further, Co is enriched and concentrated in seafloor Mn-nodules and chemical sediments (see Section 9.5 and Fig. 13.2). But how did these Co-rich components become incorporated in, and be recorded by, the lithospheric mantle of a series of neighbouring Scottish terranes when all of the aforementioned Co-enriching environments were crustal or at the crustal-seawater interface? And why is the GGF such a distinct cut-off for Co enrichment?

Whilst the effects of the Caledonian orogeny as a whole can be observed across all of Scotland, both north and south of the GGF, this only truly reflects the later Scandian event (continent-continent collision of Laurentia-Avalonia and Laurentia-Baltica, c. 430 Ma) – which is evidenced by extensive calc-alkaline granite- and diorite-appinite-granitoid magmatism (Fig. 13.3). In contrast, the earlier Grampian event (c. 470 Ma) is only recorded in terranes now sited south of the GGF (namely, the Grampian, Midland Valley and Southern Upland Terranes). Major strike-slip motion along the GGF was initiated at the start of the Scandian event and at the end of active subduction of Iapetus oceanic crust (although the fault itself probably existed in the Neoproterozoic as a basin-bounding structure), and accommodated continent-continent collision and deformation by sinistral strike-slip motion. Thus the GGF, as a major lithospheric lineament, truncated the marginal areas of the NAC, effectively shortening the spatial transition between true NAC (Lewisian) and Ketilidian (Rhinnian) basement (see Fig. 13.3). In brief, terranes south of the GGF had significant interaction with the oceanic Iapetus slab during active subduction (proximal to the trench). Slab metasomatism and partial melting drove fluids and melts into the overlying lithospheric keel(s) of the (now) Grampian and Midland Valley Terranes, and could have mobilised the Co-bearing components of this oceanic crust. Hence sulphides in the lithospheric mantle regions of the terranes south of the GGF became enriched in Co (Figs. 13.3, 13.4 and Chapter 9), while terranes to the north of the GGF were unaffected.

With the exception of the Loch Roag suite, all Scottish mantle xenoliths studied became entrained in monchiquite (and to a lesser extent, camptonite) dykes and volcanic plugs c. 290 Ma, during Permo-Carboniferous extension and rifting of the Variscan foreland in northern Britain (Fig. 13.4 and see Table 9.1). This provides a 'freeze-frame' for lithospheric mantle

compositions across Scotland, arranged spatially and according to varying preceding geodynamic and tectono-magmatic histories per terrane. This also permits an assessment of the 'preconditioning' stages experienced by different parts of the lithospheric mantle – from Archaean, through Palaeoproterozoic rifting and orogenesis, Neoproterozoic rifting, Caledonian collision(s), and finally Permo-Carboniferous extension.

Chapters 7, 8 and 9 have illustrated the intricate subtleties of metasomatic signatures in the lithospheric mantle, and in particular, highlight the potential for sulphide population and metallogenic 'mapping' of the upper mantle. A holistic study of the lithospheric mantle and mantle-derived magmatism, such as given in Chapters 6 and 8, develops the theme. However, all of this work combined has raised a series of outstanding questions: (1) Can the sulphide populations of mantle xenoliths be dated by Re-Os isotopic analysis on a sulphide-by-sulphide basis, rather than the bulk method more typically used at present? An all-inclusive approach to future lithospheric mantle 'mapping' must surely include sulphide population identification, geochemical characterisation *and* geochronological dating. (2) Is the unusual Co-enrichment of the lithospheric mantle underlying the southern Scottish terranes reflected in features of crustal mineralisation that either involve or tap this mantle source; for example in Scottish and Irish ophiolitic bodies of Iapetus oceanic crust, or in late-Caledonian SCLM-derived magmas (e.g., appinites)? (3) What can PGE geochemistry tell us about the process of cratonisation itself; for example, there are numerous metamorphosed mafic and ultramafic pods within the LGC, but the geodynamic and tectonic environment(s) where the protoliths of these bodies formed remains unresolved? And does this have implications for the upper mantle associated with the craton thereafter?

2.4 Ga Palaeoproterozoic extension and rifting of NAC
SCLM partial melting, Scourie dyke intrusion and formation of a large igneous province

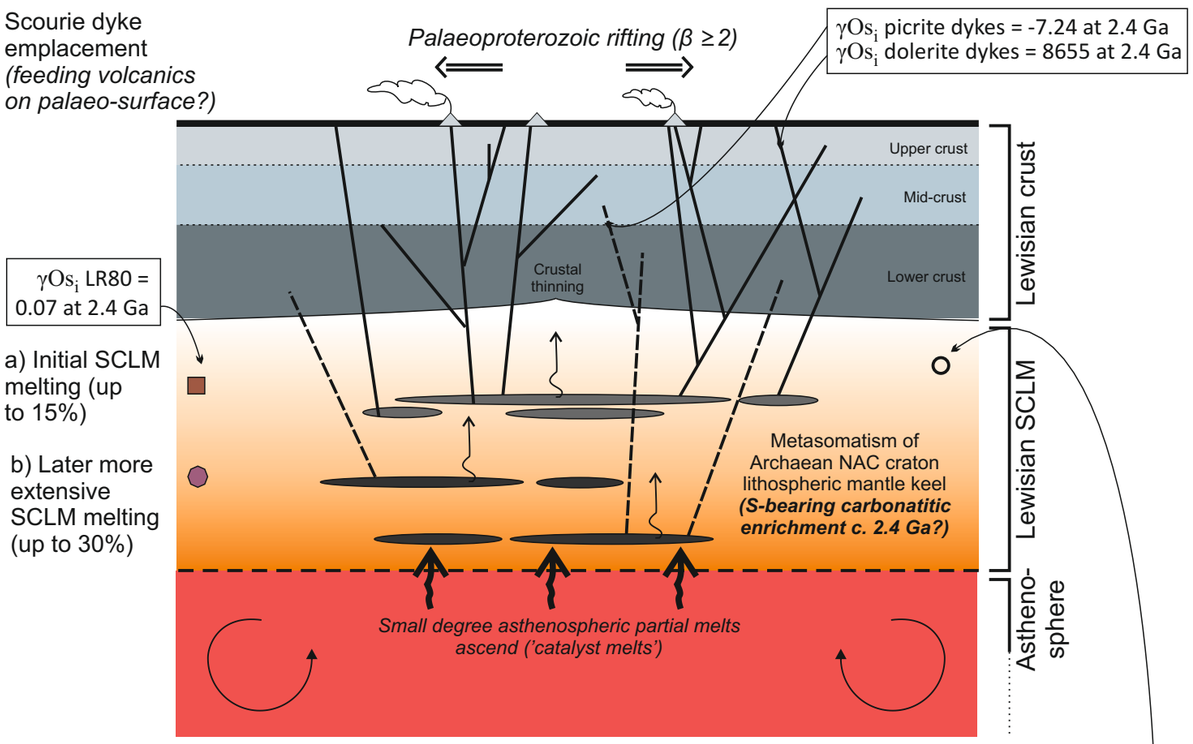

1.8 Ga Palaeoproterozoic growth of Nuna
Movement along Laxfordian shear zones

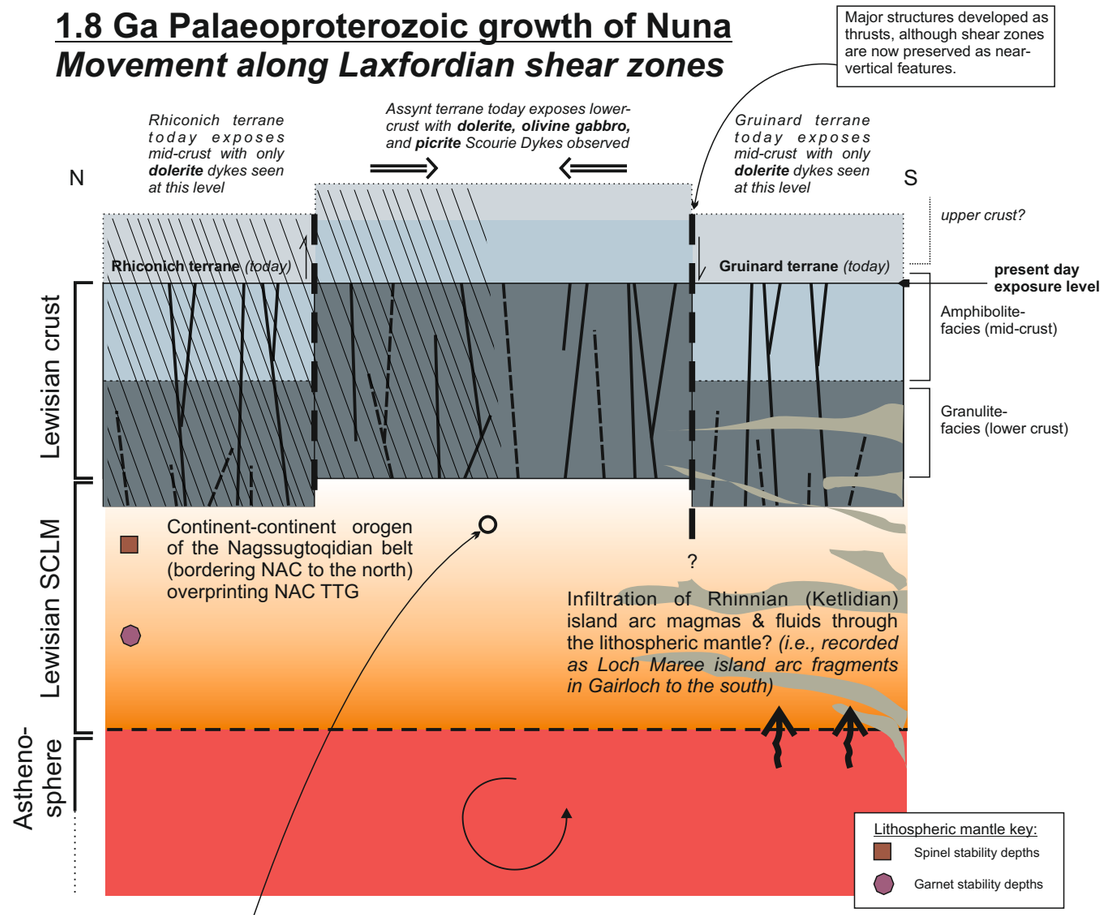

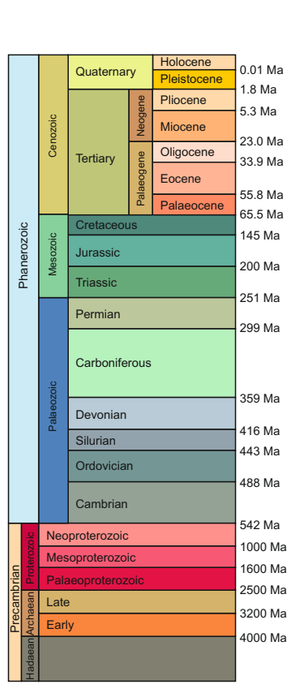

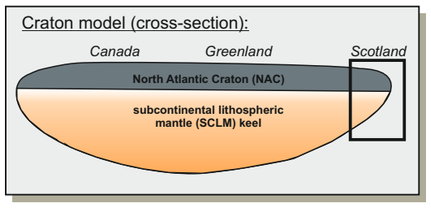

Archaean-Palaeoproterozoic Lewisian schematic timeline:

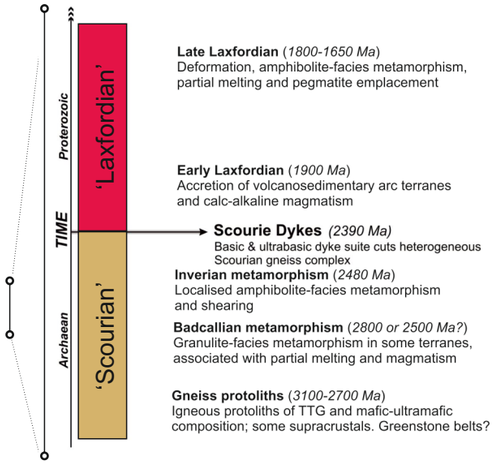

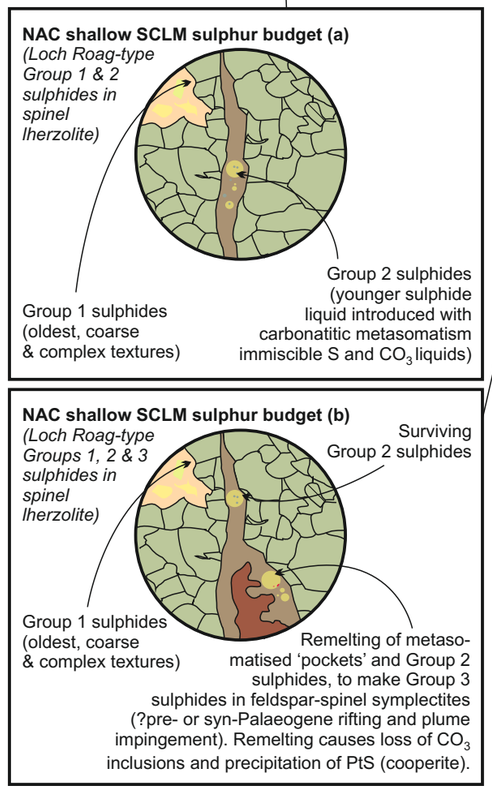

c. 1.9-1.7 Ga block model for growth of Nuna
Ketilidian arcs to the south and Nagssugtoqidian orogenic belt to the north of the NAC 'block'

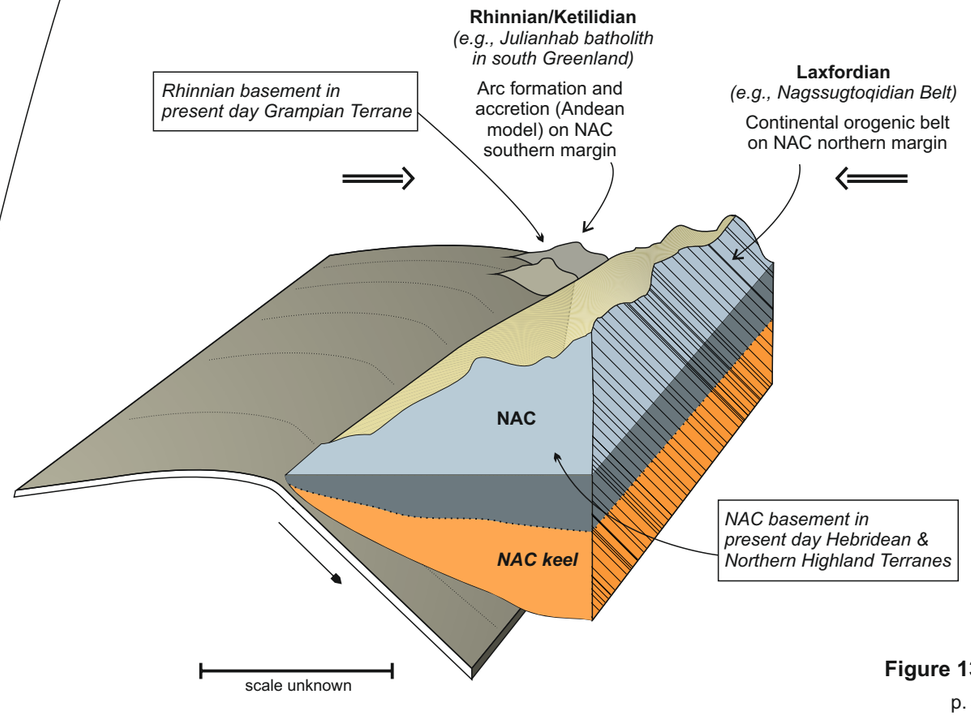

Figure 13.1.

c.600 Ma Neoproterozoic rifting of Rodinia and opening of the Iapetus Ocean *SCLM metasomatism and formation of oceanic lithosphere*

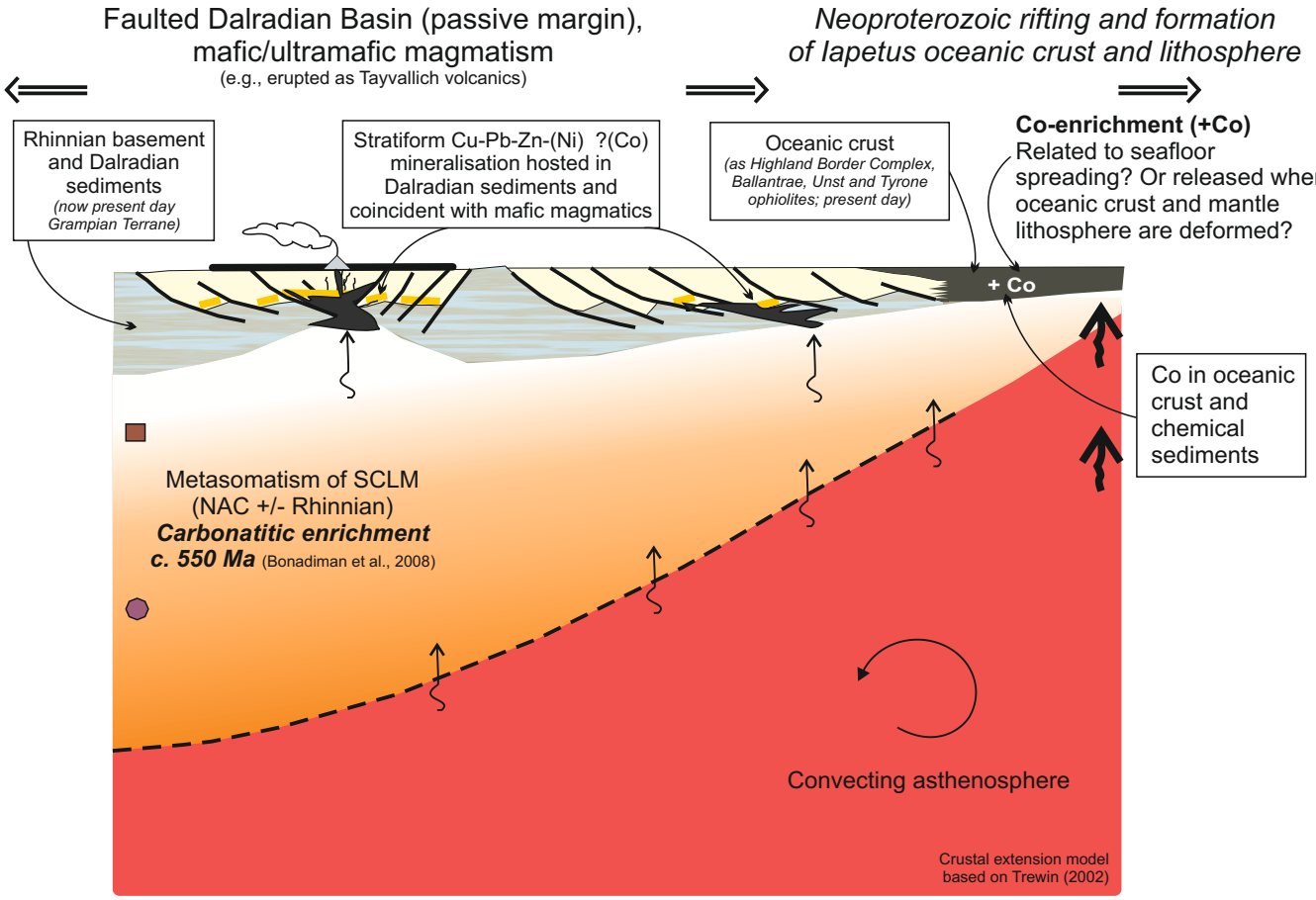

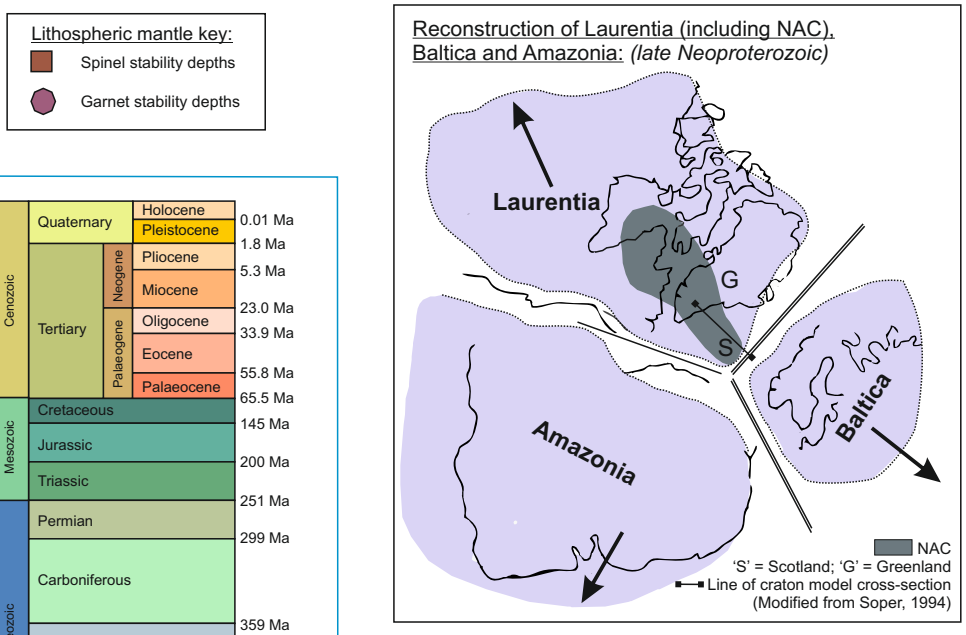

Figure 13.2.

c.470 Ma Grampian event (Caledonian Orogeny) island arc collision and Iapetus subduction

Ophiolite emplacement, and syn- to late-tectonic "Younger Basics" intrusions

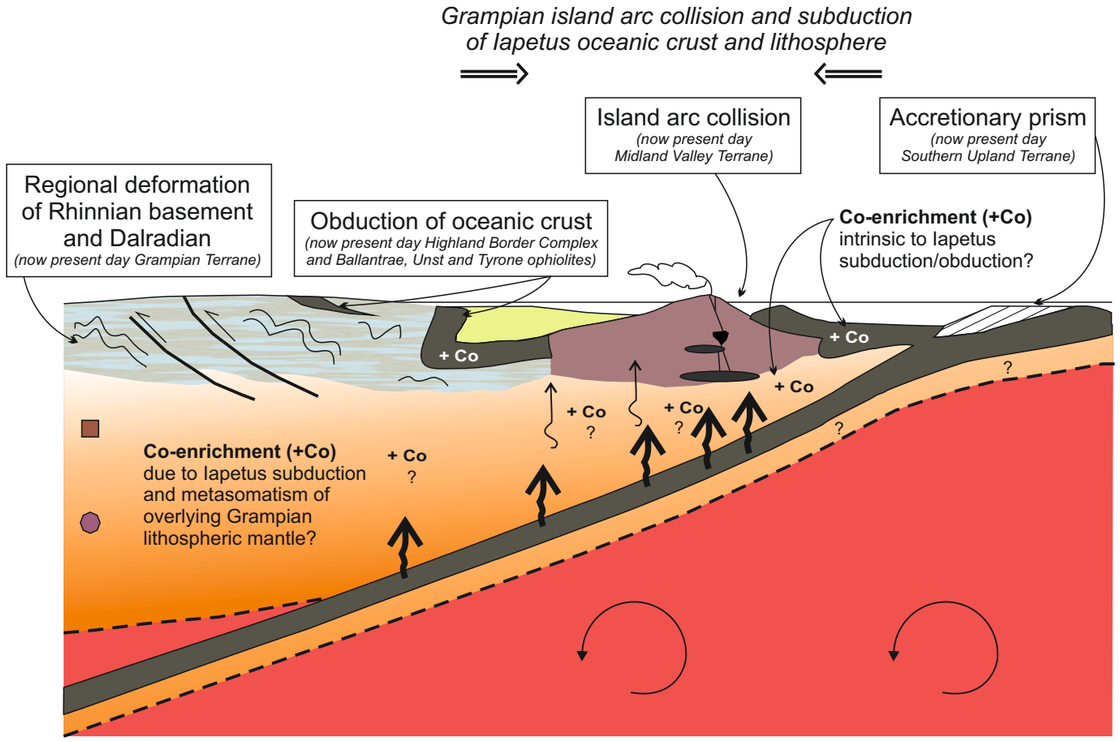

c.430 Ma Scandian event (Caledonian Orogeny) Laurentia-Baltica continent-continent collision

Extensive calc-alkaline and dioritic / 'appinitic' magmatism, Scottish terrane amalgamation and major movement (?initiation) of the Great Glen Fault

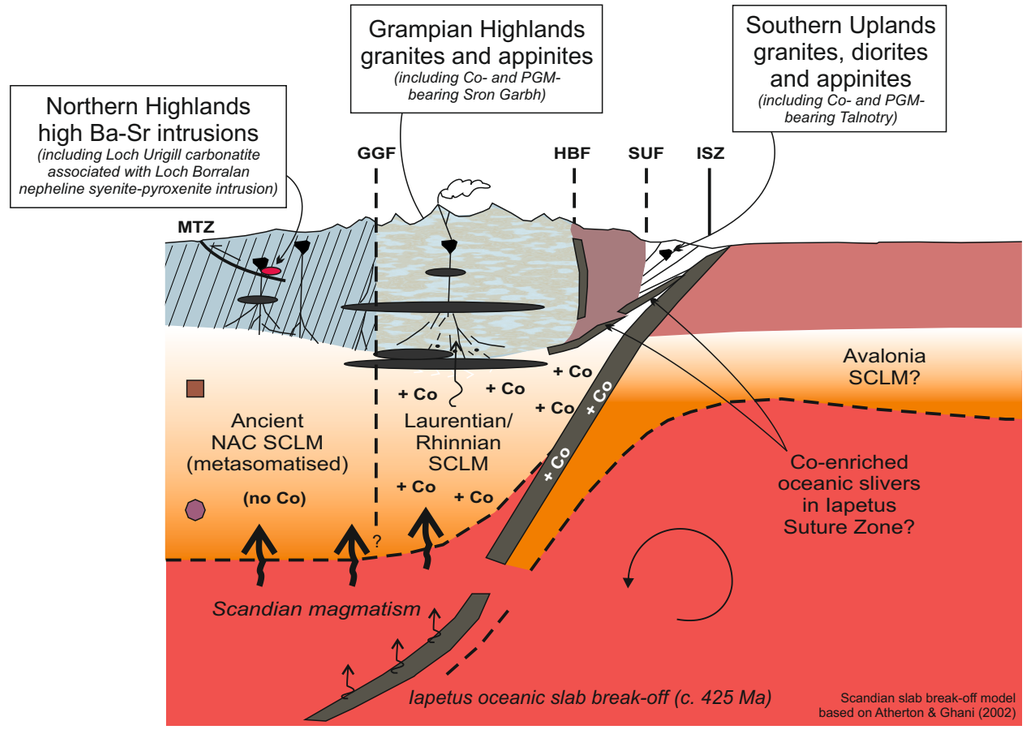

Abbreviations:
'**HT**' = Hebridean Terrane, '**NHT**' = Northern Highland Terrane, '**GT**' = Grampian Terrane, '**MVT**' = Midland Valley Terrane, '**SUT**' = Southern Uplands Terrane, '**MTZ**' = Moine Thrust Zone, '**GGF**' = Great Glen Fault, '**HBF**' = Highland Boundary Fault

Lithospheric mantle key:
- Spinel stability depths
- Garnet stability depths

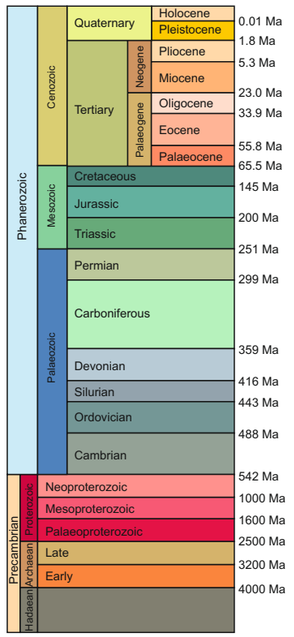

Caledonian schematic timeline:

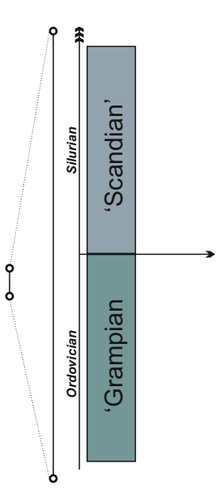

Scandian event: Continent-continent collision between Baltica-Laurentia and Avalonia-Laurentia (435-425 Ma).

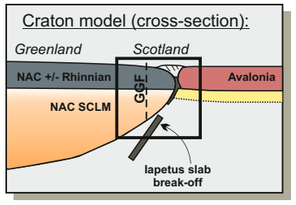

Active Iapetus subduction continued until at least c. 430 Ma. End of active subduction may have initiated the **Great Glen Fault (GGF).**

Grampian event: NW-dipping subduction zone during closure of the Iapetus Ocean (478-460 Ma) in an intra-arc setting (tectonic stacking of Dalradian). Collision of arcs on Laurentia.

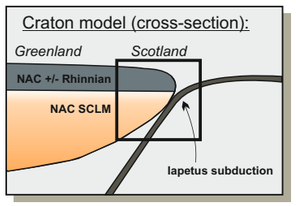

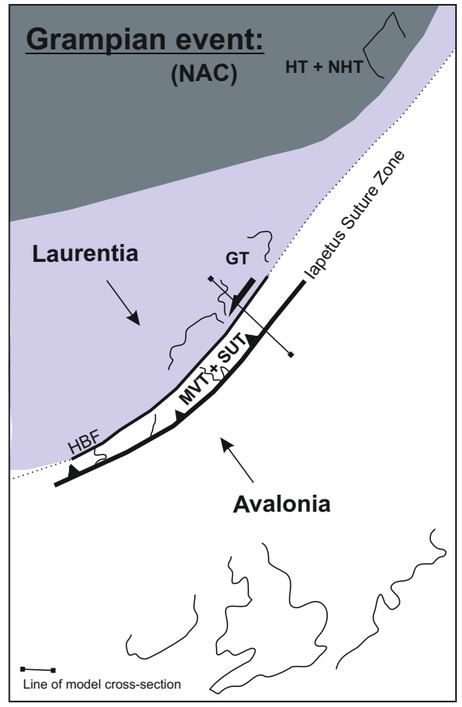

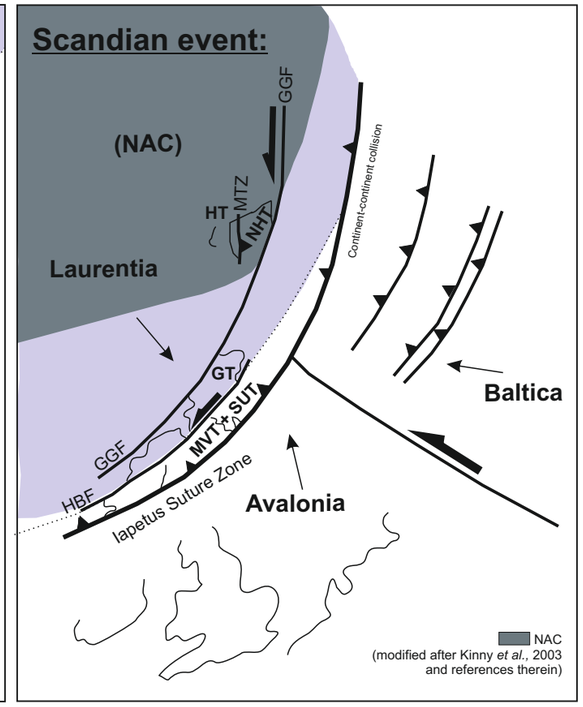

Figure 13.3.

Permo-Carboniferous (Variscan) rifting and extension

SiO_2 - undersaturated alkali basaltic magmatism, lamprophyric dykes and plugs, and mantle xenolith entrainment

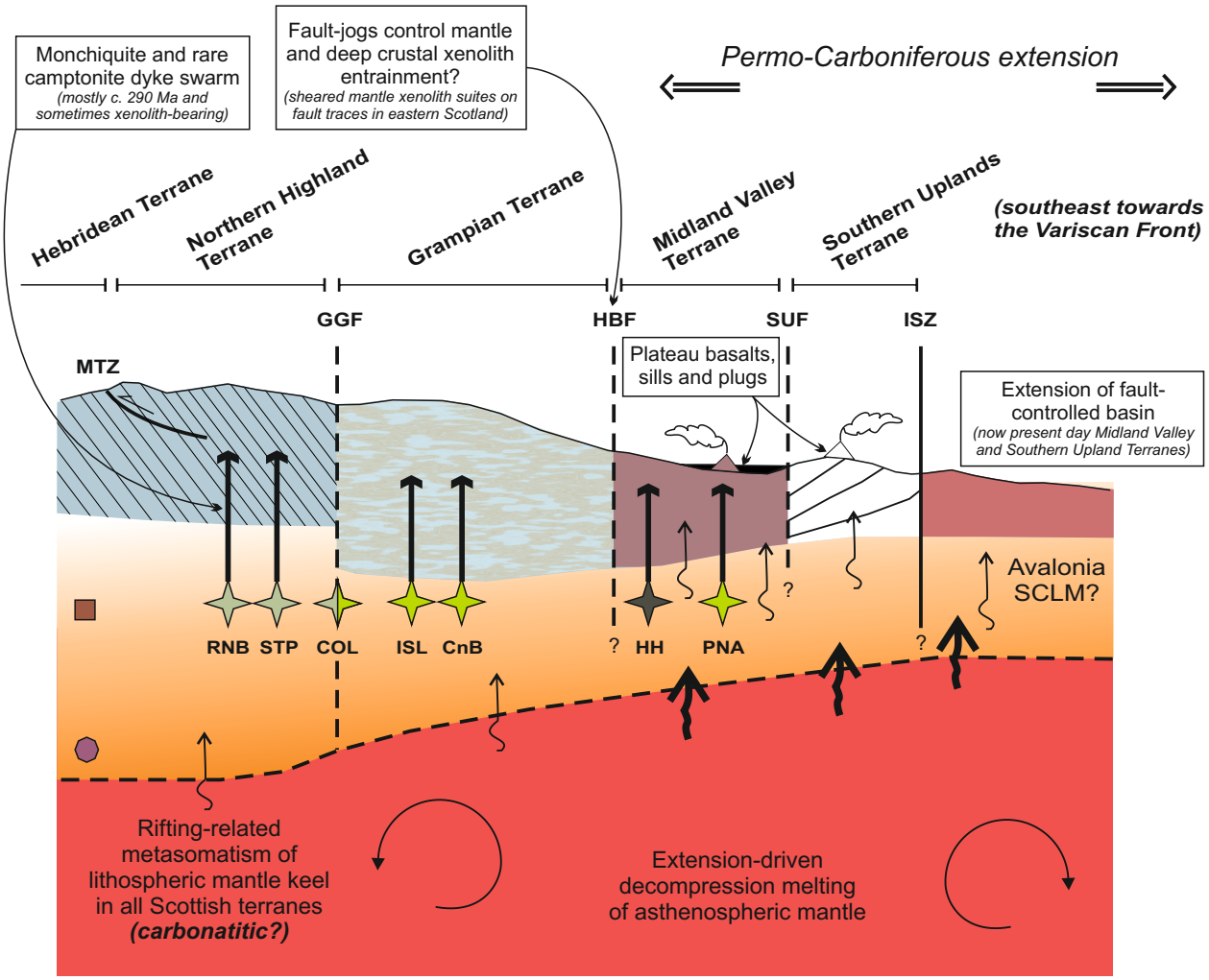

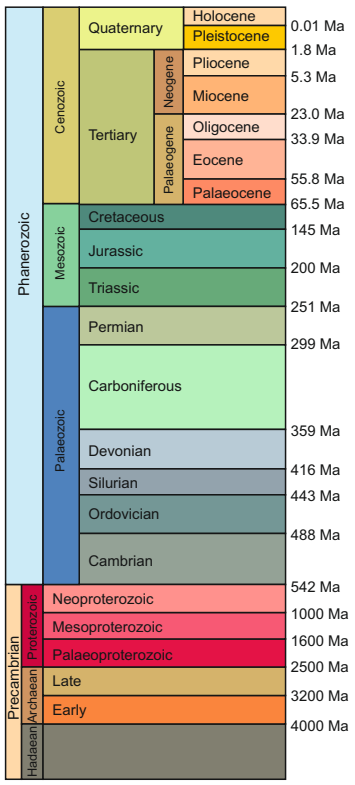

Mantle xenolith suites:
'**RNB**' = Rinibar (Northern Highland Terrane)
'**STP**' = Streap Com'laidh (Northern Highland Terrane)
'**COL**' = Colonsay (?Grampian Terrane - straddles GGF)
'**ISL**' = Islay (Grampian Terrane)
'**CnB**' = Coire na Ba (Grampian Terrane)
'**HH**' = Hillhouse (Midland Valley Terrane)
'**PNA**' = Patna (Midland Valley Terrane)

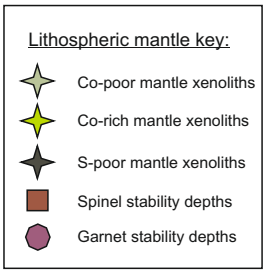

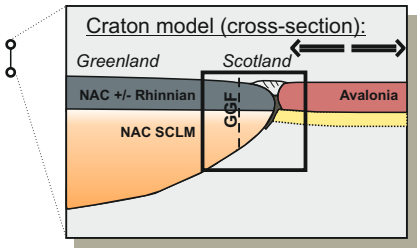

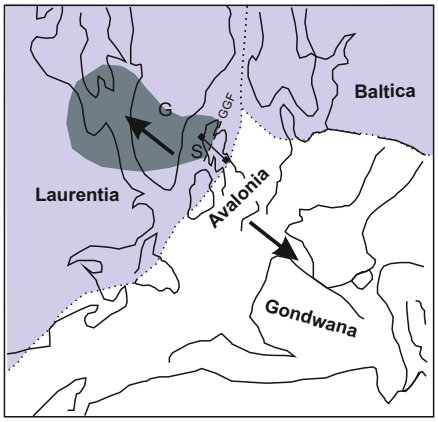

Abbreviations:
'**HT**' = Hebridean Terrane,
'**NHT**' = Northern Highland Terrane,
'**GT**' = Grampian Terrane,
'**MVT**' = Midland Valley Terrane,
'**SUT**' = Southern Uplands Terrane,
'**MTZ**' = Moine Thrust Zone,
'**GGF**' = Great Glen Fault,
'**HBF**' = Highland Boundary Fault

NAC
'S' = Scotland; 'G' = Greenland
Line of craton model cross-section
(Modified from Timmerman 2004)

Figure 13.4. p. 354

13.2. The effects of lithospheric mantle 'preconditioning' on plume-related magmatism in the Palaeogene and regional-scale 'prospectivity' of the Scottish portion of the British Palaeogene Igneous Province

The impingement of the proto-Icelandic mantle plume during the Palaeogene is the most recent major tectono-magmatic event to be recorded in Scottish geology. Its effects can be traced across all five Scottish terranes (e.g., Fig. 13.4) at a crustal level by flood basalts and intrusive complexes (although in the case of the Grampian Terrane, most Palaeogene magmatism is preserved in Northern Ireland, particularly County Antrim). Further, Ni-Cu-PGE mineralisation has been documented in the Greenlandic portions of the North Atlantic Igneous Province (NAIP) but no significant exploration has taken place in the Scottish portion of the British Palaeogene Igneous Province (BPIP) – see Chapter 4. Andersen *et al.* (2002) highlighted the BPIP as being one of the most prospective regions in Europe for orthomagmatic sulphide mineralisation, not least because of the favourable circumstances for crustal sulphur contamination.

In Chapter 10, the geochemistry of BPIP lava suites from Scotland is presented and discussed alongside lavas from across the wider NAIP, which has given an opportunity to test the underlying question of whether the SCLM (and lithospheric mantle generally) contributes metals to magmatic budgets during a major melting event. Pt/Pd ratios of lava suites change systematically across the NAIP, according to the age of eruption. Thus Pt/Pd ratio changes with the geodynamic environment of the NAIP throughout its evolution – from the earliest continental flood basalts erupted as the proto-Icelandic mantle plume impinged upon the base of the SCLM of the NAC and Rae Province (see Fig. 13.5), throughout continental rifting, and ultimately to modern oceanic seafloor spreading at the Mid-Atlantic Ridge and hotspot volcanism in Iceland.

Specifically, Pt/Pd ratio is highest in the oldest lavas of the NAIP (e.g., west Greenland and the BPIP), whereas Pt/Pd ratio is lowest in the youngest lavas (e.g., Iceland). High Pt/Pd ratios are therefore coincident in lava suites which erupted through cratonic lithosphere (at the northern margin of the NAC – see Figs. 10.13 and 13.5). As established in Chapter 8, cratonic Loch Roag-type shallow lithosphere contains a 'fusible' component that is enriched in Pt (including PtS, cooperite). This suggests that there could be a fundamental interaction between the mantle plume (asthenosphere-derived magmas) and pre-enriched, or *'preconditioned'*, cratonic lithospheric mantle. Crucially, as previously indicated in this Synthesis, 'preconditioning' (i.e., Pt-enrichment) of Loch Roag-type shallow mantle appears to

have taken place in the Palaeoproterozoic (i.e., Groups 2 and 3 sulphide populations – Fig. 13.1), and not during initial cratonisation of the NAC itself in the late Archaean. As such, it is the marginal cratonic lithospheric mantle that is Pt-enriched, coincident with Palaeoproterozoic lineaments and orogenic fronts (i.e., c. 1.8 Ga Nagssugtoqidian overprinting of the LGC and NAC). In brief, Pt/Pd ratios in sulphides in mantle xenolith suites from Scottish terranes north of the GGF are > chondrite (~ 1.8), while mantle xenolith sulphides from south of the GGF are < chondrite (see Chapter 9.4.3).

Of further importance is the mechanism by which lithospheric mantle sulphides may be entrained and/or assimilated by ascending (transient) asthenospheric mantle-derived magmas. For example, Group 2 and 3 Loch Roag-type sulphides strictly occur in feldspathic veinlets or symplectite 'pockets', and so they are most vulnerable to partial melting – effectively they sit in a highly 'fusible' petrographic position. Further, the incorporation of fusible SCLM into plume magmas has previously been suggested (e.g., Saunders *et al.,* 1997 and references therein) and SCLM delamination during the Palaeogene may explain the shallow lithospheric mantle thickness observed below present day Scotland (as inferred by seismic tomography). However, the lack of garnet-bearing peridotites in the Permo-Carboniferous mantle xenolith suites may suggest that the mantle lithosphere across all of the Scottish terranes was already thinned by this time. Whether SCLM incorporation of precious metals took place according to selective 'fusibility' of vulnerable sulphide populations, or via wholesale SCLM delamination and assimilation by hot plume magmas, the concentration of comparatively abundant chalcophile elements (e.g., Ni and Cu) in LIP magmas may be largely determined by asthenospheric melting. This work has shown that in Scotland and the NAIP, it can be demonstrated that precious metal abundances (or rather precious metal ratios) may be inherited from 'preconditioned' SCLM (Fig. 13.5).

Finally, from an economic stance, and regarding the exploration potential of the Scottish portion of the BPIP, PGE geochemistry of lava suites (Chapter 10) coupled with S-isotopic studies (Chapters 11 and 12) support the prediction of Andersen *et al.* (2002) – namely that the BPIP represents one of the most fertile regions for orthomagmatic Ni-Cu-PGE sulphide mineralisation in Europe. There is widespread opportunity for S-rich crustal contamination to take place in the Scottish upper crust, and both S-depleted and S-undersaturated lavas and upper crustal intrusions can be identified (e.g., Fig. 10.5). PGE mineralisation has previously been documented in the Scottish BPIP on the Isles of Rum, Mull and Skye (see Chapter 4) but

prior to this study a more general geochemical investigation pertaining to the controls of S-saturation and sulphide accumulation was previously not available for the region as whole.

The most S-rich sediments that the BPIP magmas have interacted with are in the Mesozoic Hebrides Basin, specifically in the Jurassic sedimentary sequences (see Figs. 11.1, Appendix F and Fig. 13.5). The $\delta^{34}S$ framework of the Jurassic sedimentary package vs. the proto-Icelandic plume is outlined in Chapter 11, and has a characteristically light S-isotopic signature ($\delta^{34}S$ ranges -35 to -10 ‰) making it relatively straightforward to identify crustal sulphur contamination in BPIP magmatic rocks. Further, if a whole-rock S-extraction method is used to quantify bulk $\delta^{34}S$, crustal contamination signatures may be identified in locations spatially removed from the actual contamination horizon, and therefore used as a vectoring tool during exploration (see Chapter 11 for methodology). However, the mechanism by which magmas become contaminated by crustal sulphur is not uniform, and there appears to be a fundamental control on the degree of contamination according to the orientation and energy of magma intrusion. For example, the picritic Trotternish Sill Complex (a sub-horizontal series of intrusions) and a suite of narrow vertical basaltic dykes were intruded into a similar sequence of Jurassic sediments on the Isle of Skye (Chapter 11), but only the dykes appear to record a strong crustal $\delta^{34}S$ signature. Thus, it is suggested that turbulent flow within narrow magmatic conduits emplaced discordantly to sedimentary strata developed by brittle processes maximise the potential for assimilation of volatile elements such as sulphur (i.e., by brecciation and increased surface area for wall rock-magma interaction – Section 11.5.3). In contrast, the flat-lying Trotternish Sill Complex was intruded concordantly to Jurassic sedimentary beds, and comparatively little sulphur contamination appears to have taken place in this mechanically 'passive' conduit system.

Once a regional crustal $\delta^{34}S$ framework has been established (e.g., Chapter 11) the particular and localised features of sulphide liquid entrainment and collection may be determined (e.g., Chapter 12). A suite of ultramafic volcanic plugs are exposed on the Isle of Rum, and were broadly coeval with magmatism associated with the Rum Layered Suite (already shown to host PGM – Table 4.1 for details). PGM had previously been discovered in a single volcanic plug on Rum (in the northwest of the island at West Sgaorishal; Power *et al.,* 2003). Sulphides in this plug and a neighbouring plug have light $\delta^{34}S$ compositions (ranging from -14.7 to -2.9 ‰) and high S/Se ratios in sulphide minerals, whereas the other plugs on Rum have magmatic $\delta^{34}S$ and S/Se. This indicates that S-rich crustal contamination was restricted to those plugs in the northwest of the island, and not elsewhere (e.g., Fig. 12.8). Based on the S-isotopic framework

of the BPIP and crustal sequences of the region as a whole, sulphur contamination was doubtless triggered by interaction with Jurassic mudrocks. But at the current exposure level on Rum, Jurassic rocks are absent (except for downthrown fault blocks around the Rum Central Complex), and therefore a simple upward injection of contaminated magma cannot account for the distribution of the $\delta^{34}S$ across the Isle of Rum. Instead, by reconstructing the Hebrides Basin stratigraphy, it is apparent that contamination of magmas by Jurassic sediments must have taken place above the current level of exposure – put simply, sulphide liquids must have sunk through the conduit once active intrusion had ceased (Fig. 12.10).

Given the extent of Mesozoic sedimentary cover across the (now fragmented) NAC in Scotland, Ireland and Greenland, there is a strong potential for upper crustal orthomagmatic Ni-Cu-PGE mineralisation, particularly in a Noril'sk-type conduit setting where sustained throughput of magma was maintained for long periods. However, the spatial relationships between crustal sulphur contamination (triggering S-saturation crucial for chalcophile element mineralisation) and the position of collected sulphides must be reconsidered in the light of the real possibility that sulphides have moved downwards as well as upwards through magmatic systems (e.g., the Greenlandic macrodykes; Section 12.5.4).

13.3. Final statement

Overall, there is a perception amongst the international research community that the 'big questions' about Scottish geology have already been answered by decades of previously published literature, particularly with regards to mineralisation and exploration. However, throughout this thesis it is apparent that the converse may be argued. Whilst the wide-ranging topics of preceding academic and industry-based investigations have provided a detailed tectonic and geodynamic framework for the region, Scottish geology now represents an ideal testing ground for broader and far-reaching ideas. For example, these might relate to lithospheric mantle 'mapping', and/or be reliant upon modern analytical facilities. Working hypotheses developed in this well characterised framework may then be applied to regions across the world where less detailed regional geological information is available. From an economic point of view, Scotland represents a new exploration frontier not yet seriously investigated for orthomagmatic Ni-Cu-PGE mineralisation.

Palaeogene rifting associated with the proto-Icelandic plume culminating in the opening of the North Atlantic

Fragmentation of the NAC, formation of the North Atlantic Igneous Province (NAIP) and British Palaeogene Igneous Province (BPIP), and Loch Roag mantle xenolith entrainment

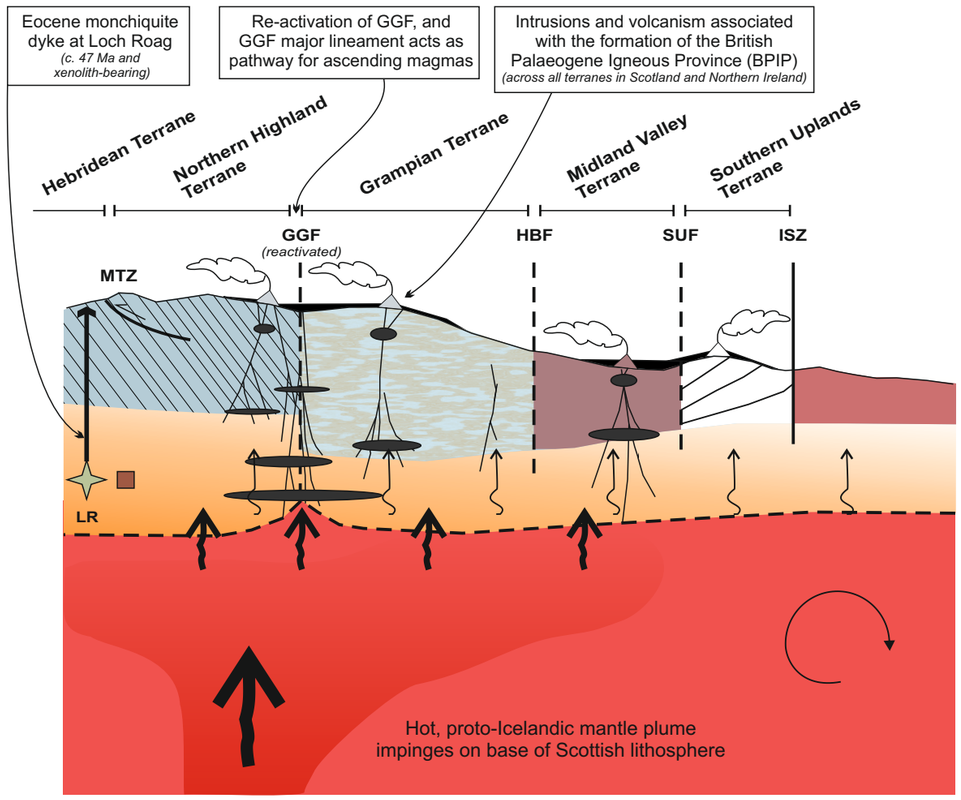

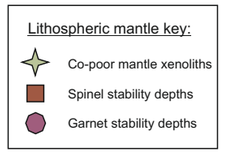

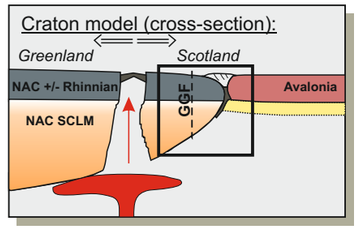

NAC shallow SCLM sulphur budget (c)
(Loch Roag-type Groups 1, 2 & 3 sulphides in spinel lherzolite)

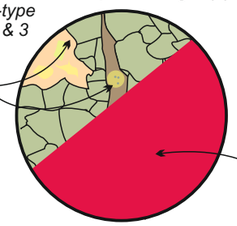

Melting and delamination of the SCLM during proto-Icelandic plume impingement. Sulphides in Loch Roag-type mantle become incorporated into ascending magmas, including Group 3 sulphides with PtS (cooperite). Given their high PGE concentration, Group 3 sulphides particularly contribute PGE to magmas and change the precious metal ratio of plume-derived magmas

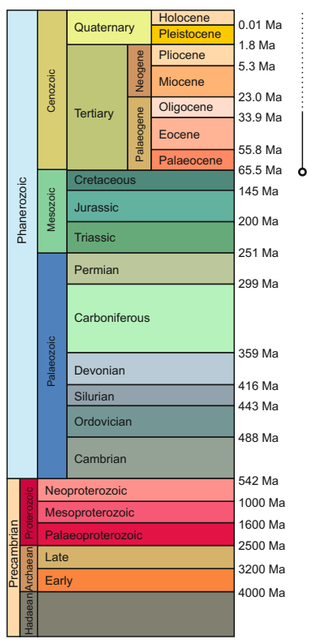

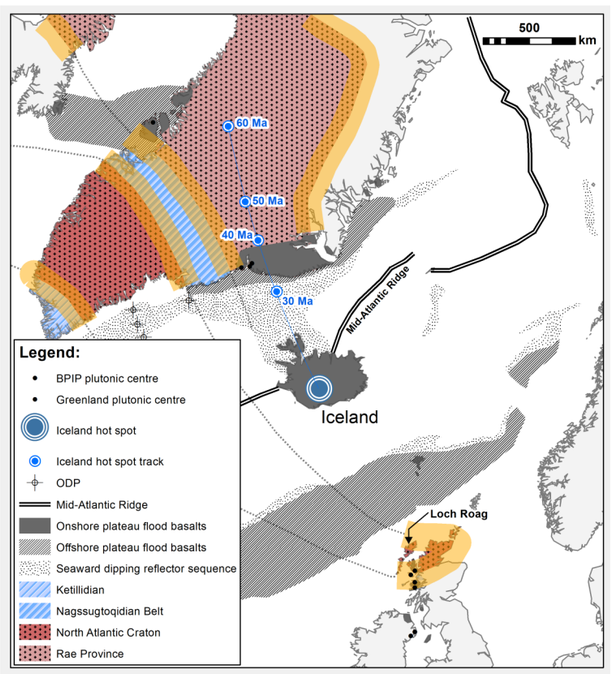

Block model for the fragmentation of the NAC and formation of the NAIP

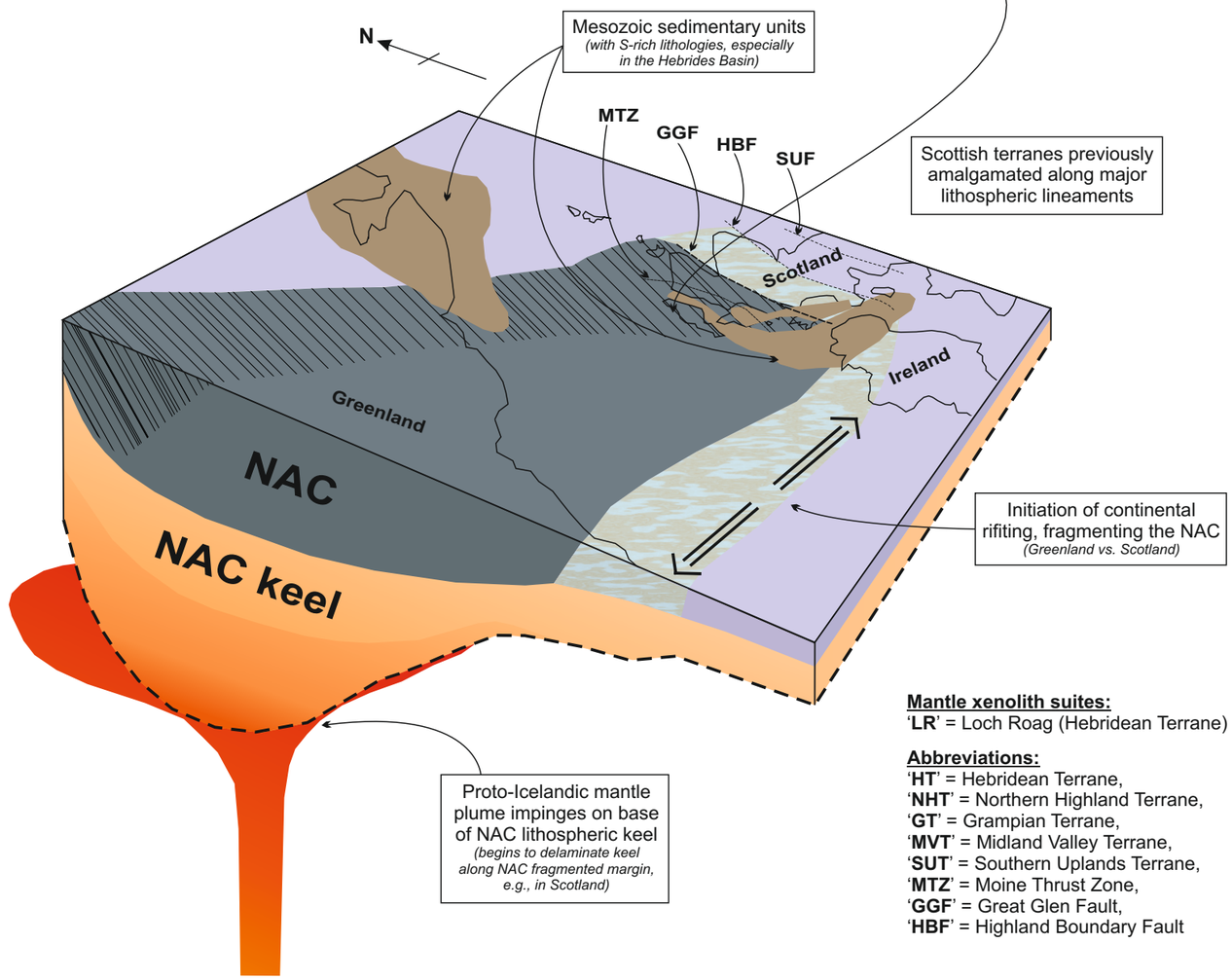

Mantle xenolith suites:
'**LR**' = Loch Roag (Hebridean Terrane)

Abbreviations:
'**HT**' = Hebridean Terrane,
'**NHT**' = Northern Highland Terrane,
'**GT**' = Grampian Terrane,
'**MVT**' = Midland Valley Terrane,
'**SUT**' = Southern Uplands Terrane,
'**MTZ**' = Moine Thrust Zone,
'**GGF**' = Great Glen Fault,
'**HBF**' = Highland Boundary Fault

Figure 13.5.

REFERENCE LIST

AARNES, I., SVENSEN, H., CONNOLLOY, J. A. D. & PODLADCHIKOV, Y. Y. 2010. How contact metamorphism can trigger global climate changes: Modeling gas generation around igneous sills in sedimentary basins. *Geochimica et Cosmochimica Acta,* **74,** 7179-7195.

AARNES, I., SVENSEN, H., POLTEAU, S. & PLANKE, S. 2011. Contact metamorphic devolitization of shales in the Karoo Basin, South Africa, and the effects of multiple sill intrusions. *Chemical Geology,* **281,** 181-194.

AHMED, A. H. & ARAI, S. 2002. Unexpectedly high-PGE chromitite from the deeper mantle section of the northern Oman ophiolite and its tectonic implications. *Contributions to Mineralogy and Petrology,* **143,** 263-278.

AHMED, A. H., ARAI, S. & IKENNE, M. 2009. Mineralogy and paragenesis of the Co-Ni arsenide ores of Bou Azzer, Anti-Atlas, Morocco. *Economic Geology,* **104,** 249-266.

ALAPIETI, T. T., FILEN, B. A., LAHTINEN, J. J., LAVROV, M. M., SMOLKIN, V. F. & VOITSEKHOVSKY, S. N. 1990. Early Proterozoic layered intrusions in the northeastern part of the Fennoscanian Shield. *Mineralogy and Petrology,* **42,** 1-22.

ALARD, O., GRIFFIN, W. L., LORAND, J. -P., JACKSON, S. E. & O'REILLY, S. Y. 2000. Non-chondritic distribution of the highly siderophile elements in mantle sulphides. *Nature,* **407,** 891-894.

ALARD, O., GRIFFIN, W. L., PEARSON, N. J., LORAND, J. -P. & O'REILLY, S. Y. 2002. New insights into the Re-Os systematics of sub-continental lithosperic mantle from in situ analysis of sulphides. *Earth and Planetary Science Letters,* **203,** 651-663.

ALARD, O., LUGUET, A., PEARSON, N. J., GRIFFIN, W. L., LORAND, J. -P., GANNOUN, A., BURTON, K. W. & O'REILLY, S. Y. 2005. In situ Os isotopes in abyssal peridotites bridge the isotopic gap between MORBs and their source mantle. *Nature,* **436,** 1005-1008.

ALARD, O., LORAND, J. -P., REISBERG, L., BODINIER, J. -L., DAUTRIA, J. -M. & O'REILLY, S. Y. 2011. Volatile-rich metasomatism in Montferrier xenoliths (Southern France): Implications for the abundances of chalcophile and highly siderophile elements in the subcontinental mantle. *Journal of Petrology,* **52,** 2009-2045.

ALT, J., SHANKS, W. & JACKSON, M. 1993. Cycling of sulphur in subduction zones: the geochemistry of sulphur in the Mariana Island Arc and back-arc trough. *Earth and Planetary Science Letters,* **119,** 477-494.

ANDERSON, T. & NEUMANN, E. R. 2001. Fluid inclusions in mantle xenoliths. *Lithos,* **55,** 301-320.

ANDERSEN, J. C. Ø. 2006. Postmagmatic sulphur loss in the Skaergaard Intrusion: Implications for the formation of the Platinova Reef. *Lithos,* **92,** 198-221.

ANDERSEN, J. C. Ø., RASMUSSEN, H., NIELSEN, T. F. D. & RONSBO, J. G. 1998. The Triple Group and the Platinova gold and palladium reefs in the Skaergaard Intrusion: stratigaphical and petrographic relations. *Economic Geology,* **93,** 488-509.

ANDERSEN, J. C. Ø., POWER, M. R. & MOMME, P. 2002. Platinum-group elements in the Palaeogene North Atlantic Igneous Province. *In: The Geology, Geochemistry, Mineralogy and Benefication of Platinum-Group Elements.* (eds. CABRI, L. J.), pp. 1-30. CIM Special Volume, **54,** 637-668.

ANDREWS, J. E., HAMILTON, P. J. & FALLICK, A. E. 1987. The geochemistry of early diagenetic dolostones from a low-salinity Jurassic lagoon. *Journal of the Geological Society, London,* **144,** 687-698.

ARCURI, T., RIPLEY, E. M. & HAUCK, S. A. 1998. Sulphur and oxygen isotope studies of the interaction between pelitic xenoliths and basaltic magma at the Babbitt and Serpentine Cu-Ni deposits, Duluth Complex, Minnesota. *Economic Geology,* **93,** 1063-1075.

ARNASON, J. G. & BIRD, D. K. 2000. A gold- and platinum-mineralized layer in gabbros of the Kap Edvard Holm Complex: Field, petrologic, and geochemical relations. *Economic Geology,* **95,** 945-970.

ARNASON, J. G., BIRD, D. K., BERNSTEIN, S. & KELEMEN, P. B. 1997a. Gold and platinum-group element mineralization in the Kruuse Fjord Gabbro Complex, East Greenland. *Economic Geology,* **92,** 490-501.

ARNASON, J. G., BIRD, D. K., BERNSTEIN, S., ROSE, N. M. & MANNIN, C. E. 1997b. Petrology and geochemistry of the Kruuse Fjord Gabbro Complex, East Greenland. *Geological Magazine,* **134,** 67-89.

ARNDT, N. T. 2005. The conduits of magmatic ore deposits. *Mineralogical Association of Canada Short Course,* **35,** 161-182. Ottawa.

ARNDT, N. T. 2011. Insights into the geologic setting and origin of Ni-Cu-PGE sulfide deposits of the Norilsk-Talnakh region, Siberia. *Reviews in Economic Geology,* **17,** 190-215.

ARNDT, N. T. 2013. The lithospheric mantle plays no active role in the formation of orthomagmatic ore deposits. *Economic Geology,* **108,** 1953-1970.

ARNDT, N. T., Czamanske, G. K., Walker, R J., Chauvel, C. & Fedorenko, V. A. 2003. Geochemistry and origin of the intrusive hosts of the Noril'sk-Talnakh Cu-Ni-PGE deposits. *Economic Geology,* **98,** 495-515.

ARNOLD, R. G. 1971. Evidence for liquid immiscibility in the system FeS-S. *Economic Geology,* **66,** 1121-1130.

ATHERTON, M. P. & GHANI, A. A. 2002. Slab breakoff: a model for Caledonian, Late Granite syn-collisional magmatism in the orthotectonic (metamorphic) zone of Scotland and Donegal, Ireland. *Lithos,* **62,** 65-85.

AULBACH, S., GRIFFIN, W. L., PEARSON, N. J., O'REILLY, S. Y., KIVI, K. & DOYLE, B. J. 2004. Mantle formation and evolution, Slave Craton: constraints from HSE abundances and Re–Os isotope systematics of sulfide inclusions in mantle xenocrysts. *Chemical Geology,* **208,** 61-88.

BAILEY, E. B., CLOUGH, C. T., WRIGHT, W. B., RICHEY, J. E. & WILSON, G.V. 1924. *Tertiary and post-Tertiary geology of Mull, Loch Aline and Oban*.

BALLHAUS, C. & SYLVESTER, P. 2000. Noble metal enrichment processes in the Merensky Reef, Bushveld Complex. *Journal of Petrology,* **41,** 545-561.

BALLHAUS, C., RYAN, C. G., MERNACH, T. P. & GREEN, D. H. 1994. The partitioning of Fe, Ni, Cu, Pt and Au between sulfide, metal and fluid phases: A pilot study. *Geochimica et Cosmochimica Acta,* **58,** 811-826.

BALLHAUS, C., TREDOUX, M. & SPATH, A. 2001. Phase relations in the Fe-Ni-Cu-PGE-S system at magmatic temperature and application to massive sulphide ores of the Sudbury Igneous Complex. *Journal of Petrology,* **42,** 1911-1926.

BALLHAUS, C., BOCKRATH, C., WOHLGEMUTH-UEBERWASSER, C., LAURENZ, V. & BERNDT, J. 2006. Fractionation of the noble metals by physical processes. *Contributions to Mineralogy and Petrology,* **152,** 667-684.

BARNES, S. -J. 1990. The use of metal ratios in prospecting for platinum-group element deposits in mafic and ultramafic intrusions. *In: Journal of Geochemical Exploration.* (eds. DUNN, C. E., CURTIN, G. C. & HALL, G. E. M.), pp. 91-99.

BARNES, S. -J., BOYD, R., KORNELIUSSEN, A., NILSSON, L. P., OFTEN, M., PEDERSEN, R. B. & ROBINS, B. 1988. The use of mantle normalization and metal ratios in discriminating between the effects of partial melting, crystal fractionation and sulphide segregation on platinum group elements, gold, nickel and copper: examples from Norway. *In: Geo Platinum.* (eds. PRICHARD, H. M., POTTS, P. J., BOWLES, J. F. W. & CRIBB, S. J.), pp. 113-143. London: Elsevier.

BARNES, S. -J., COUTURE, J. F., SAWYER, E. W. & BOUCHAIB, C. 1993. Nickel-copper occurrences in the Belleterre-Angliers belt of the Pontiac Subprovince and the use of Cu-Pd ratios in interpreting platinum-group element distributions. *Economic Geology,* **88,** 1402-1419.

BARNES, S. -J., MAKOVICKY, E., MAKOVICKY, M., ROSE-HANSEN, J. & KARUP-MOLLER, S. 1997. Partition coefficients for Ni, Cu, Pd, Pt, Rh, and Ir between monosulfide solid solution and sulfide liquid and the formation of compositionally zoned Ni-Su sulfide bodies by fractional crystallization of sulfide liquid. *Canadian Journal of Earth Sciences,* **34,** 366-374.

BARNES, S. J., FIORENTINI, M. L., AUSTIN, P., GESSNER, K., HOUGH, R. M. & SQUELCH, A. P. 2008. Three-dimensional morphology of magmatic sulfides sheds light on ore formation and sulfide melt migration. *Geology,* **36,** 655-658.

BARNES, S. -J., MAIER, W. D. & CURL, E. 2010. Composition of the marginal rocks and sills of the Rustenburg Layered Suite, Bushveld Complex, South Africa: implications for the formation of the platinum-group element deposits. *Economic Geology,* **105,** 1491-1511.

BARTON, P. J. 1992. LISPB revisited: a new look under the Caledonides of northern Britain. *Geophysical Journal International,* **110,** 371-391.

BARTON, J. M., CAWTHORN, R. G. & WHITE, J. 1986. The role of contamination in the evolution of the Platreef of the Bushveld Complex. *Economic Geology,* **81,** 1096-1104.

BAXTER, A. N. & MITCHELL, J. G. 1984. Camptonite-monchiquite dyke swarms of northern Scotland; age relationships and their implications. *Scottish Journal of Geology,* **20,** 297-308.

BECKER, H., HORAN, M. F., WALKER, R. J., GAO, S., LORAND, J. -P. & RUDNICK, R. L. 2006. Highly siderophile element composition of the Earth's primitivemantle: constraints from new data on peridotite massifs and xenoliths. *Geochimica et Cosmochimica Acta,* **70,** 4528-4550.

BECKINSALE, R. D., PANKHURST, R. J., SKELHORN, R. R. & WALSH, J. N. 1978. Geochemistry and petrogenesis of the Early Tertiary lava pile of the Isle of Mull, Scotland. *Contributions to Mineralogy and Petrology,* **66,** 415-427.

BEDARD, J. H., SPARKS, R. S. J., RENNER, R., CHEADLE, M. J. & HALLWORTH, M. A. 1988. Peridotite sills and metasomatic gabbros in the Eastern Layered Series of the Rhum complex. *Journal of the Geological Society, London,* **145,** 207-224.

BEGG, G. C., HRONSKY, J. A. M., ARNDT, N. T., GRIFFIN, W. L., O'REILLY, S. Y. & HAYWARD, N. 2010. Lithospheric, cratonic, and geodynamic setting of Ni-Cu-PGE sulfide deposits. *Economic Geology,* **105,** 1057-1070.

BELL, B. R. & WILLIAMSON, I. T. 2002. Tertiary Igneous Activity. *In: The Geology of Scotland.* (eds. TREWIN, N. H.), pp. 371-408. London: The Geological Society. 4th edition ed.

BERNSTEIN, S. 2011. Noril'sk-type magmatic nickel target in West Greenland. Avannaa Resources.

BERNSTEIN, S., KELEMEN, P. B. & BROOKS, C. K. 1996. Evolution of the Kap Edvard Holm Complex: a mafic intrusion at a rifted continental margin. *Journal of Petrology,* **37**.

BERNSTEIN, S., KELEMEN, P. B. & BROOKS, C. K. 1998. Depleted spinel harzburgite xenoliths in Tertiary dykes from East Greenland: Restites from high degree melting. *Earth and Planetary Science Letters,* **154,** 221-235.

BERNSTEIN, S., HANGHØJ, K., KELEMEN, P. B. & BROOKS, K. 2006. Ultra-depleted shallow cratonic mantle beneath West Greenland: dunitic xenoliths from Ubekendt Ejland. *Contributions to Mineralogy and Petrology,* **152,** 335-347.

BERNSTEIN, S., KELEMEN, P. B. & HANGHØJ, K. 2007. Consistent olivine Mg# in cratonic mantle reflects Archean mantle melting to the exhaustion of orthopyroxene. *Geology,* **35,** 459.

BERNSTEIN, S., SZILAS, K. & KELEMEN, P. B. 2013. Highly depleted cratonic mantle in West Greenland extending into diamond stability field in the Proterozoic. *Lithos,* **168-169,** 160-172.

BÉZOS, A., LORAND, J. P., HUMLER, E. & GROS, M. 2005. Platinum-group element systematics in Mid-Oceanic Ridge basaltic glasses from the Pacific, Atlantic, and Indian Oceans. *Geochimica et Cosmochimica Acta,* **69,** 2613-2627.

BINNS, P. E., MCQUILLIN, R. & KENOLTY, K. 1974. The geology of the Sea of the Hebrides. *Report of the Institute of Geological Sciences.*

BIRD, D. K., BROOKS, C. K., GANNICOTT, R. A. & TURNER, P. A. 1991. A gold-bearing horizon in the Skaergaard intrusion, East Greenland. *Economic Geology,* **86,** 1086-1092.

BIRD, D. K., ARNASON, J. G., BRANDRISS, M. E., NEVLE, R. J. RADFORD, G., BERNSTEIN, S., GANNICOTT, R. A. & KELEMEN, P. B. 1995. A gold-bearing horizon in the Kap Edvard Holm Complex, East Greenland. *Economic Geology,* **90,** 1288-1300.

BIZZARRO, M. & STEVENSON, R. K. 2003. Major element composition of the lithospheric mantle under the North Atlantic craton: Evidence from peridotite xenoliths of the Sarfartoq area, southwestern Greenland. *Contributions to Mineralogy and Petrology,* **146,** 223-240.

BLEEKER, W. 2003. The late Archaean record: a puzzle in ca. 34 pieces. *Lithos,* **71,** 99-134.

BLICHERT-TOFT, J., LESHER, C. E. & ROSING, M. T. 1992. Selectively contaminated magmas of the Tertiary East Greenland macrodike complex. *Contributions to Mineralogy and Petrology,* **110,** 154-172.

BOCKRATH, C., BALLHAUS, C. & HOLZHEID, A. 2004a. Fractionation of the platinum-group elements during mantle melting. *Science,* **305,** 1951-1953.

BOCKRATH, C., BALLHAUS, C. & HOLZHEID, A. 2004b. Stabilities of laurite RuS_2 and monosulphide solid solution at magmatic temperatures. *Chemical Geology,* **208,** 265-271.

BODINIER, J. L., GARRIDO, C. J., CHANEFO, I., BRUGUIER, O. & GERVILLA, F. 2008. Origin of Pyroxenite-Peridotite Veined Mantle by Refertilization Reactions: Evidence from the Ronda Peridotite (Southern Spain). *Journal of Petrology,* **49,** 999-1025.

BOGDANOV, K., TSONEV, D. & KUZMANOV, K. 1997. Mineralogy of gold in the Elshitsa massive sulphide deposit, Sredna Gora zone, Bulgaria. *Mineralium Deposita,* **32,** 219-229.

BONADIMAN, C., COLTORTI, M., DUGGEN, S., PALUDETTI, L., SIENA, F., THIRLWALL, M. F. & UPTON, B. G. J. 2008. Palaeozoic subduction-related and kimberlite or carbonatite metasomatism in the Scottish lithospheric mantle. *In: Metasomatism in Oceanic and Continental Lithospheric Mantle.* (eds. COLTORTI, M. & GREGOIRE, M.), pp. 303-333. London: The Geological Society.

BONS, P. D., BAUR, A., ELBURG, M. A., LINDHUBER, M. J., MARKS, M. A. W., SOESOO, A., VAN MILLIGEN, B. P. & WALTE, N. P. 2015. Layered intrusions and traffic jams. *Geology,* **43,** 71-74.

BOWEN, N. L. & SCHAIRER, L. F. 1935. The system MgO—FeO—SiO_2. *American Journal of Science,* **29,** 151-217.

BOWLES, J. F. W., HOWIE, R. A., VAUGHAN, D. J. & ZUSSMAN, J. 2011. *Rock-forming minerals: Non-silicates; oxides, hydroxides and sulphides*, The Geological Society.

BRANDON, A. D. & WALKER, R. J. 2005. The debate over core–mantle interaction. *Earth and Planetary Science Letters,* **232,** 211-225.

BREDDAM, K., KURZ, M. D. & STOREY, M. 2000. Mapping out the conduit of the iceland mantle plume with helium isotopes. *Earth and Planetary Science Letters,* **176,** 45-55.

BRENAN, J. M. & ANDREWS, D. 2001. High-temperature stability of laurite and Ru-Os-Ir alloy and their role in PGE fractionation in mafic magmas. *The Canadian Mineralogist,* **39,** 341-360.

BRENAN, J. M. & ROSE, L. A. 2002. Experimental constraints on the wetting of chromite by silfide liquid. *The Canadian Mineralogist,* **40,** 1113-1126.

BRENAN, J. M., DALPE, C. & MCDONOUGH, W. F. 2002. PGE's are fractionated by olivine-melt partitioning. *Goldschmidt Conference Abstracts.* Davos, Switzerland.

BRIDGWATER, D., WATSON, J. & WINDLEY, B. F. 1973. The Archaean Craton of the North Atlantic Region. *Philosophical Transactions of the Royal Society A: Mathematical, Physical and Engineering Sciences,* **273,** 493-512.

BRIDGWATER, D., MENGEL, F., FRYER, B., WAGNER, P. & HANSEN, S. C. 1995. Early Proterozoic mafic dykes in the North Atlantic and Baltic cratons: field setting and chemistry of distinctive dyke swarms. *Geological Society, London, Special Publications,* **95,** 193-210.

BROOKS, C. K. 1989. Major gold find in Greenland. *Terra Nova,* **1,** 591-593.

BROUGH, C. P., PRICHARD, H. M., NEARY, C. R., FISHER, P. C. & MCDONALD, I. 2015. Geochemical variations within podiform chromitite deposits in the Shetland Ophiolite: Implications for petrogenesis and PGE concentration. *Economic Geology,* **110,** 187-208.

BROWN, E. L. & LESHER, C. E. 2014. North Atlantic magmatism controlled by temperature, mantle composition and buoyancy. *Nature Geoscience,* **7,** 820-824.

BROWN, P. E., DEMPSTER, T. J., HUTTON, D. H. W. & BECKER, S. M. 2003. Extensional tectonics and mafic plutons in the Ketilidian rapakivi granite suite of South Greenland. *Lithos,* **67,** 1-13.

BRÜGMANN, G. E., NALDRETT, A. J., ASIF, M., LIGHTFOOT, P., GORBACHEV, N. S. & FEDORENKO, V. A. 1993. Siderophile and chalcophile metals as tracers of the evolution of the Siberian Trap in the Noril'sk region, Russia. *Geochimica et Cosmochimica Acta,* **57,** 2001-2018.

BUCHAN, K. L., MERTANEN, S., PARK, R. G., PESONEN, L. J., ELMING, S. -A., ABRAHAMSEN, N. & BYLUND, G. 2000. Comparing the drift of Laurentia and Baltica in the Proterozoic: the importance of key palaeomagnetic poles. *Tectonophysics,* **319,** 167-198.

BUCHANAN, D. L. & NOLAN, J. 1979. Solubility of sulfur and sulfide immiscibility in synthetic tholeiitic melts and their relevance to Bushveld-Complex rocks. *Canadian Mineralogist,* **17,** 483-494.

BUCHANAN, D. L. & ROUSE, J. E. 1984. Role of contamination in the Platreef of the Bushveld Complex. *In: Sulphide deposits in mafic and ultramafic rocks*. (eds. BUCHANAN, D. L. & JONES, M. J.), pp. 141-146. IMM, London.

BUFE, N. A., HOLNESS, M. B. & HUMPHREYS, M. C. S. 2014. Contact metamorphism of Precambrian gneiss by the Skaergaard Intrusion. *Journal of Petrology,* **55,** 1595-1617.

BULANOVA, G. P., GRIFFIN, W. L., RYAN, C. G., SHESTOKOVA, O. Y. & BARNES, S. -J. 1996. Trace elements in sulfide inclusions from Yakutian diamonds. *Contributions to Mineralogy and Petrology,* **124,** 111-125.

BURTON, K. W., SCHIANO, P., BIRCK, J. -L. & ALLEGRE, C. J. 1999. Osmium isotope disequilibrium between mantle minerals in a spinel-lherzolite. *Earth and Planetary Science Letters,* **172,** 311-322.

BUTCHER, A. R., YOUNG, I. M. & FAITHFULL, J. W. 1985. Finger structures in the Rhum Complex. *Geological Magazine,* **122,** 491-502.

BUTCHER, A. R., PIRRIE, D., PRICHARD, H. M. & FISHER, P. 1999. Platinum-group mineralization in the Rum layered intrusion, Scottish Hebrides, UK. *Journal of the Geological Society, London,* **156,** 213-216.

BURNS, R. G. 1976. The uptake of cobalt into ferromanganese nodules, soils, and synthetic manganese (IV) oxides. *Geochimica et Cosmochimica Acta,* **40,** 95-102.

CALVERT, S. E. & PRICE, N. B. 1970. Geochemical variation in ferromanganese nodules and associated sediments from the Pacific Ocean. *Marine Chemistry,* **5,** 43-74.

CAMERON, E. M. 1994. Depletion of gold and LILE in the lower crust: Lewisian Complex, Scotland. *Journal of the Geological Society, London,* **151,** 747-754.

CAMPBELL, I. H. 1985. The difference between oceanic and continental tholeiites: a fluid dynamic explanation. *Contributions to Mineralogy and Petrology,* **91,** 37-43.

CAMPBELL, I. H. & BARNES, S. J. 1984. A model for the geochemistry of the platinum-group elements in magmatic sulfide deposits. *The Canadian Mineralogist,* **22,** 151-160.

CAMPBELL, I. H. & NALDRETT, A. J. 1979. The influence of silicate:sulphide ratios on the geochemistry of magmatic sulphides. *Economic Geology,* **74,** 1503-1506.

CAMPBELL, I. H., NALDRETT, A. J. & BARNES, S. -J. 1983. A model for the origin of platinum-rich horizons in the Bushveld and Stillwater complexes. *Journal of Petrology,* **24,** 133-165.

CANFIELD, D.E. & TESKE, A. 1996. Late Proterozoic rise in atmospheric oxygen concentration inferred from phylogenetic and sulphur-isotope studies. *Nature*, **382**, 127-132.

CANFIELD, D., RAISWELL, R., WESTRICH, J., REAVES, C. & BERNER, R. 1986. The use of chromium reduction in the analysis of rediced inorganic sulphur in sediments and shales. *Chemical Geology,* **54,** 149-155.

CANNING, J. C., HENNEY, P. J., MORRISON, M. A. & GASKARTH, J. W. 1996. Geochemistry of late Caledonian minettes from Northern Britain: implications for the Caledonian sub-continental lithospheric mantle. *Mineralogical Magazine,* **60,** 221-236.

CANNING, J. C., HENNEY, P. J., MORRISON, M. A., VAN CALSTEREN, P. W. C., GASKARTH, J. W. & SWARBRICK, A. 1998. The Great Glen Fault: a major vertical lithospheric boundary. *Journal of the Geological Society,* **155,** 425-428.

CAPOBIANCO, C. J. & DRAKE, M. J. 1990. Partitioning of ruthenium, rhodium, and palladium between spinel and silicate melt and implications for platinum group element fractionation trends. *Geochimica et Cosmochimica Acta,* **54,** 869-874.

CAPOBIANCO, C. J., DRAKE, M. J. & ROGERS, P. S. Z. 1991. Crystal/melt partitioning of Ru, Rh and Pd for silicate and oxide phases. *Lunar and Planetary Science,* **22,** 179-180.

CAPOBIANCO, C. J., HERVIG, R. L. & DRAKE, M. J. 1994. Experiments on crystal/liquid partitioning of Ru, Rh and Pd for magnetite and hematite solid solutions crystallized from silicate melt. *Chemical Geology,* **113,** 23-43.

CARLSON, R. W. 2005. Application of the Pt–Re–Os isotopic systems to mantle geochemistry and geochronology. *Lithos,* **82,** 249-272.

CARTWRIGHT, I. & VALLEY, J. W. 1991. Low-^{18}O Scourie dyke magmas from the Lewisian complex, northwestern Scotland. *Geology,* **19,** 578-581.

CATHELINEAU, M. & NIEVA, D. 1985. A chlorite solid solution geothermometer. The Los Azufres geothermal system (Mexico). *Contributions to Mineralogy and Petrology,* **91,** 235-244.

CAWOOD, P. A., STRACHAN, R., CUTTS, K., KINNY, P. D., HAND, M. & PISAREVSKY, S. 2010. Neoproterozoic orogeny along the margin of Rodinia: Valhalla orogen, North Atlantic. *Geology,* **38,** 99-102.

CAWTHORN, R. G. 2010. The platinum group element deposits of the Bushveld Complex in South Africa. *Platinum Metals Reviews,* **54,** 205-215.

CAWTHORN, R. G., EALES, H. V., WALRAVEN, F., UKEN, R. & WATKEYS, M. K. 2006. The Bushveld Complex. *In: The Geology of South Africa* (eds. JOHNSON, M. R., ANHAEUSSER, C. R. & THOMAS, R. J.) Geological Society of South Africa.

CHAMBERS, L. M. & PRINGLE, M. S. 2001. Age and duration of activity at the Isle of Mull Tertiary igneous centre, Scotland, and confirmation of the existence of subchrons during Anomaly 26r. *Earth and Planetary Science Letters,* **193,** 333-345.

CHAMBERS, L. M., PRINGLE, M. S. & PARRISH, R. R. 2005. Rapid formation of the Small Isles Tertiary centre constrained by precise ^{40}Ar/^{39}Ar and U-Pb ages. *Lithos,* **79,** 367-384.

CHUNG, H. -Y. & MUNGALL, J.E. 2009. Physical constraints on the migration of immiscible fluids through partially molten silicates, with special reference to magmatic sulfide ores. *Earth and Planetary Science Letters,* **286,** 14-22.

CLARKE, D. B. & PEDERSEN, A. K. 1976. Tertiary volcanic province of West Greenland. *In: Geology of Greenland.* (eds. ESCHER, A. & WATT, W. S.), pp. 364-385. Greenland Geological Survey.

COATS, J. S., TANDY, B. C. & MICHIE, U. M. 1982. Geochemical drainage survey of central Argyll, Scotland. *Mineral Reconnaissance Programme Report No. 50.* Natural Environment Research Council.

COATS, J. S., SHAW, M. H., GUNN, A. G., ROLLIN, K. E. & FORTEY, N. J. 1997. Mineral exploration in Lewisian supracrustal and basic rocks of the Scottish Highlands and Islands. *Mineral Reconnaissance Programme Report.* Nottingham: British Geological Survey.

COLEMAN, M. L. & MOORE, M. P. 1978. Direct reduction of sulphates to sulphur dioxide for isotopic analysis. *Analytical Chemistry,* **28,** 199-260.

CONDIE, K. C. 1997. Sources of Proterozoic mafic dyke swarms: constraints from Th/Ta and La/Yb ratios. *Precambrian Research,* **81,** 3-14.

COOPER, M. R., CROWLEY, Q. G., HOLLIS, S. P., NOBLE, S. R., ROBERTS, S., CHEW, D., EARLS, G., HERRINGTON, R. & MERRIMAN, R. J. 2011. Age constraints and geochemistry of the Ordovician Tyrone Igneous Complex, Northern Ireland: implications for the Grampian orogeny. *Journal of the Geological Society,* **168,** 837-850.

COX, S. F. 1987. Flow mechanisms in sulphide minerals. *Ore Geology Reviews,* **2,** 133-171.

CRAIG, J. R. & VAUGHAN, D. J. 1994. Applications of ore microscopy in mineral technology. *Ore microscopy and ore petrology.* 2 ed.

CROCKET, J. H. 1974. Handbook of Geochemistry II. *B.-O. Springer-Verlag.*

CROCKET, J. H. 2000. PGE in fresh basalt, hydrothermal alteration products, and volcanic incrustations of Kilauea volcano, Hawaii. *Geochimica et Cosmochimica Acta,* **64,** 1791-1807.

CROCKET, J. H. 2002. Platinum-group element geochemistry of mafic and ultramafic rocks. *In: The geology, geochemistry, mineralogy and mineral benefication of platinum-group elements.* (eds. CABRI, L. J.), pp. 177-210. Canadian Institution of Mining, Metallurgy and Petroleum.

CROWLEY, Q. G., KEY, R. M. & NOBLE, S. R. 2014. High-precision U–Pb dating of complex zircon from the Lewisian Gneiss Complex of Scotland using an incremental CA-ID-TIMS approach. *Gondwana Research,* **in press**.

CZAMANSKE, G. K., KUNILOV, V. E., ZIENTEK, M. L., CABRI, L. C., LIKHACHEV, A.P., CALK, L.C. & OSCARSON, R. I. 1992. A proton microprobe study of magmatic sulfide ores from the Norilsk-Talnakh District, Siberia. *Canadian Mineralogist,* **30,** 249.

CZAMANSKE, G. K., WOODEN, J. L., ZIENTEK, M. L., FEDORENKO, V. A., ZEN'KO, T. E., KENT, J., KNG, B. S., KNIGHT, R. L. & SIEMS, D. F. 1994. Geochemical and isotopic constraints of the ptetrogenesis of the Noril'sk-Talnahk ore-forming system. *Proceedings of the Sudbury-Noril'sk Symposium,* (eds. LIGHTFOOT, P. C. & NALDRETT, A. J.). pp. 313-342.

CZAMANSKE, G. K., ZEN'KO, T. E., FEDORENKO, V. A., CALK, L. C., BUDAHN, J. R., BULLOCK, J. H., FRIES, T. L., KING, B. S. & SIEMS, D. F. 1995. Petrography and geochemical characterization of ore-bearing intrusins of the Noril'sk type, Siberia; with discussion of their origin. *Resource Geology Special Issue,* **18,** 1-48.

DALE, C. W., PEARSON, D. G., STARKEY, N. A., STUART, F. M., ELLAM, R.M., LARSEN, L. M., FITTON, J. G. & MACPHERSON, C.G. 2009. Osmium isotopes in Baffin Island and West Greenland picrites: Implications for the 187Os/188Os composition of the convecting mantle and the nature of high 3He/4He mantle. *Earth and Planetary Science Letters,* **278,** 267-277.

DALY, J. S., MUIR, R. J. & CLIFF, R. A. 1991. A precise U-Pb zircon age for the Inishtrahull syenitic gneiss, County Donegal, Ireland. *Journal of the Geological Society,* **148,** 639-642.

DARE, S. A. S., BARNES, S. -J., PRICHARD, H. M., FISHER, P. C. 2011. Chalcophile and platinum-group element (PGE) concentrations in the sulfide minerals from the McCreedy East deposit, Sudbury, Canada, and the origin of PGE in pyrite. *Mineralium Deposita,* **46,** 381-407.

DAVIES, G. F. 2009. Effect of plate bending on the Urey ratio and the thermal evolution of the mantle. *Earth and Planetary Science Letters,* **287,** 513-518.

DAVIES, J. H. F. L. & HEAMAN, L. M. 2014. New U-Pb baddeleyite and zircon ages for the Scourie dyke swarm: A long-lived large igneous province with implications for the Paleoproterozoic evolution of NW Scotland. *Precambrian Research,* **249,** 180-198.

DAVIES, J. H. F. L., HEAMAN, L. M., DUFRANE, S. A., MUEHLENBACHS, K. & CREASER, R. A. 2012. Geochemical and isotopic insights into the origin of the 'Scourie' Dykes. *Goldschmidt.* Montreal.

DAVIES, R. M., GRIFFIN, W. L., O'REILLY, S. Y. & DOYLE, B. J. 2004. Mineral inclusions and geochemical characteristics of microdiamonds from the DO27, A154, A21, A418, DO18, DD17 and Ranch Lake kimberlites at Lac de Gras, Slave Craton, Canada☆. *Lithos,* **77,** 39-55.

DE BREMOND D'ARS, J., ARNDT, N. T. & HALLOT, E. 2001. Analog experimental insights into the formation of magmatic sulphide deposits. *Earth and Planetary Science Letters,* **186,** 371-381.

DEER, W. A. 1976. Tertiary igneous rocks between Scoresby Sund and Kap Gustav Holm, East Greenland. *In: Geology of Greenland.* (eds. ESCHER, A. & WATT, W. S.), pp. 405-429. Greenland Geological Survey.

DELPECH, G., LORAND, J. -P., GREGOIRE, M., COTTIN, J. -Y., O'REILLY, S. Y. 2012. In-situ geochemistry of sulfides in highly metasomatized mantle xenoliths from Kerguelen, southern Indian Ocean. *Lithos,* **154,** 296-314.

DEPAOLO, D. J. & WASSERBURG, G. J. 1979. Petrogenetic mixing models and Nd-Sr isotopic patterns. *Geochimica et Cosmochimica Acta,* **43,** 615-627.

DEWEY, J. F. & STRACHAN, R. A. 2003. Changing Silurian-Devonian relative plate motion in the Caledonides: sinistral transpression to sinistral trantension. *Journal of the Geological Society, London,* **160,** 219-229.

DE WIT, M. & THIART, C. 2005. Metallogenic fingerprints of Archaean cratons. *In: Mineral Deposits and Earth Evolution.* (eds. MCDONALD, I., BOYCE, A. J., BUTLER, I. B., HERRINGTON, R. J. & POLYA, D.A.), pp. 59-70. London: Geological Society London Special Publication no. 248.

DICKIN, A. P. 1981. Isotope geochemistry of Tertiary igneous rocks from the Isle of Skye. *Journal of Petrology,* **22,** 155-190.

DICKIN, A. P., JONES, N. W., THIRLWALL, M. F. & THOMPSON, R. N. 1987. A Ce/Nd isotope study of crustal contamination processes affecting Palaeocene magmas in Skye, Northwest Scotland. *Contributions to Mineralogy and Petrology,* **96,** 455-464.

DOWNES, H. 2007. Origin and significance of spinel and garnet pyroxenites in the shallow lithospheric mantle: Ultramafic massifs in orogenic belts in Western Europe and NW Africa. *Lithos,* **99,** 1-24.

DOWNES, H., UPTON, B. G. J., HANDRYDE, E. A. J. & THIRLWALL, M. F. 2001. Geochemistry of mafic and ultramafic xenoliths from Fidra (Southern Uplands, Scotland): implications for lithospheric processes in Permo-Carboniferous times. *Lithos,* **58,** 105-124.

DOWNES, H., UPTON, B. G. J., CONNOLLY, J., BEARD, A. D. & BODINIER, J. -L. 2007. Petrology and geochemistry of a cumulate xenolith suite from Bute: evidence for late Palaeozoic crustal underplating beneath SW Scotland. *Journal of the Geological Society,* **164,** 1-15.

DOWNES, H., DE VRIES, C. & WITTIG, N. 2014. Hf–Zr anomalies in clinopyroxene from mantle xenoliths from France and Poland: implications for Lu–Hf dating of spinel peridotite lithospheric mantle. *International Journal of Earth Sciences*.

DOUVILLE, E., CHARLOU, J. L., OELKERS, E. H., BIENVENU, P., JOVE COLON, C. F., DONVAL, J. P., FOUQUET, Y. & PRIEUR, D. & APPROU, P. 2002. The rainbow vent fluids (36°14'N, MAR): the influence of ultramafic rocks and phase separation on trace metal content in Mid-Atlantic Ridge hydrothermal fluids. *Chemical Geology,* **184,** 37-48.

DUNHAM, A. C. 1965. A new type of banding in ultrabasic rocks from central Rhum, Inverness-shire Scotland. *American Mineralogist,* **50,** 1410-1420.

EALES, H. V., TEIGLER, B., DE KLERK, W. J. & MAIER, W. D. 1994. Nature and origin of orthopyroxenites in the western Bushveld Complex, in the light of compositional data. *South African Journal of Geology,* **97,** 399-407.

ECKSTRAND, O. R., & HULBERT, L. J. 1987. Selenium and the source of sulfur in magmatic nickel and platinum deposits. *Geological Association of Canada/Mineral Association of Canada, Programme and Abstracts* 12:40.

ECKSTRAND, O. R., GRINENKO, L. N., KROUSE, H. R., PAKTUNC, A. D., SCHWANN, P.L. & SCOATES, R. F. 1989 Preliminary data on sulphur isotopes and Se/S ratios, and the source of sulphur in magmatic sulphur and magmatic sulphides from the Fox River Sill, Molson Dykes and Thompson nickel deposits, northern Manitoba. *In: Current Research, Part C.* pp. 235-242. Geological Survey of Canada.

EMELEUS, C. H. 1997. *Geology of Rum and the adjacent islands,* London, British Geological Survey.

EMELEUS, C. H. & BELL, B. R. 2005. *British Regional Geology: The Palaeogene volcanic districts of Scotland,* Nottingham, British Geological Survey.

EMELEUS, C. H. & TROLL, V. R. 2008. *A geological excursion guide to Rum*, Edinburgh Geological Society.

EMELEUS, C. H. & TROLL, V. R. 2011. Recent research developments on the Isle of Rum, NW Scotland. *Geology Today,* **27,** 184-193.

ERNST, R. E. & BUCHAN, K. L. 2003. Recognizing mantle plumes in the geological record. *Annual Review of Earth and Planetary Sciences,* **31,** 469-523.

ERNST, R. E. & PECK, D. C. 2010. Using Large Igneous Provinces for Mineral Exploration (e.g., for Ni-Cu-PGE Deposits). *11th International Platinum Symposium.* Ontario Geological Survey.

ERNST, R. E., BLEEKER, W., SÖDERLUND, U. & KERR, A. C. 2013. Large Igneous Provinces and supercontinents: Toward completing the plate tectonic revolution. *Lithos*, **174**, 1-14.

FAITHFULL, J. W. 1985. The lower Eastern Layered Series of Rhum. *Geological Magazine,* **122,** 459-468.

FAITHFULL, J. W., TIMMERMAN, M. J., UPTON, B. G. J. & RUMSEY, M. S. 2012. Mid-Eocene renewal of magmatism in NW Scotland: the Loch Roag Dyke, Outer Hebrides. *Journal of the Geological Society,* **169,** 115-118.

FARQUHAR, J., SAVARINO, J., AIRIEAU, S. & THIEMENS, M. H. 2001. Observation of wavelength-sensitive mass-independent sulfur isotope effects during SO2 photolysis: Implications for the early atmosphere. *J. Geophys. Res.,* **106,** 32829-32839.

FEDORENKO, V. A. & CZAMANSKE, G. K. 1997. Results of new field and geochemical studies of the volcanic and intrusive rocks of the Maymecha-Kotuy area, Siberian flood-basalt province, Russia. *International Geology Review,* **39,** 479-531.

FERRARIS, C. & LORAND, J. -P. 2014. Novodneprite ($AuPb_3$), anyuiite [$Au(Pb, Sb)_2$] and gold micro- and nano-inclusions within plastically deformed mantle-derived olivine from the Lherz peridotite (Pyrenees, France): a HRTEM–AEM–EELS study. *Physics and Chemistry of Minerals*.

FETTES, D. J. & MENDUM, J. R. 1987. The evolution of the Lewisian complex in the Outer Hebrides. *Geological Society, London, Special Publications,* **27,** 27-44.

FISHER, I. ST. J., & HUDSON, J. D. 1987. Pyrite formation in Jurassic shales of contrasting biofacies. *Geological Society Special Publication,* **26,** 69-78.

FLEET, M. E., CHRYSSOULIS, S. L., STONE, W. E. & WEISENER, C. G. 1993. Partitioning of platinum-group elements and Au in the Fe-Ni-Cu-system: experiments on the fractional crystallization of sulfide melt. *Contributions to Mineralogy and Petrology,* **115,** 36-44.

FLEET, M. E., CROCKET, J. H., LIU, M. & STONE, W. E. 1999. Laboratory partitioning of platinum-group elements PGE/and gold with application to magmatic sulfide-PGE deposits. *Lithos,* **47,** 127-142.

FLETCHER, T. A. & RICE, C. M. 1989. Geology, mineralization (Ni-Cu) and precious-metal geochemistry of Caledonian mafic and ultramafic intrusions near Huntly, northeast Scotland. *Transactions of the Institution of Mining and Metallurgy, Applied Earth Sciences, B,* **98,** 185-200.

FOULGER, G. R., NATLAND, J. H. & ANDERSON, D. L. 2005. A source for Icelandic magmas in remelted Iapetus crust. *Journal of Volcanology and Geothermal Research,* **141,** 23-44.

FOWLER, M. B. 1986. Large-ion lithophile element characteristics of an amphibolite facies to granulite facies transition at Gruinard Bay, North-west Scotland. *Journal of Metamorphic Geology,* **4,** 345-359.

FOWLER, M. B., KOCKS, H., DARBYSHIRE, D. P. F. & DREENWOOD, P. B. 2008. Petrogenesis of high Ba-Sr plutons from the Northern Highlands Terrane of the British Caledonian Province. *Lithos,* **105,** 129-148.

FOWLER, M., MILLAR, I. L., STRACHAN, R. A. & FALLICK, A. E. 2013. Petrogenesis of the Neoproterozoic West Highland Granitic Gneiss, Scottish Caledonides: Cryptic mantle input to S-type granites? *Lithos,* **168-169,** 173-185.

FRAM, M. S. & LESHER, C. E. 1997. Generation and polybaric differentiation of East Greenland Early Tertiary flood basalts. *Journal of Petrology,* **38,** 231-275.

FRICK, L. R. 1998. *Application of Re-Os isotopes to the study of lithospheric processes in Archaean terrains.* PhD, Monash University.

FRICK, L. R., LAMBERT, D. D., REEVES, S. J. & HEAMAN, L. M. 1994. Platinum-group element and osmium isotope evidence for the origin of Scourie Dykes. *VM Goldschmidt Conference.* Edinburgh: Mineralogical Magazine, 290-291.

FRIEND, C. R. L. & KINNY, P. D. 2001. A reappraisal of the Lewisian Gneiss Complex: geochronological evidence for its tectonic assembly from disparate terranes in the Proterozoic. *Contributions to Mineralogy and Petrology,* **142,** 198-218.

FRIEND, C. R. L., STRACHAN, R. A. & KINNY, P. D. 2008. U-Pb zircon dating of basement inliers within the Moine Supergroup, Scottish Caledonides: implications of Archaean protolith ages. *Journal of the Geological Society,* **165,** 807-815.

FYFE, J. A., LONG, D. & EVANS, D. 1993. United Kingdom offshore regional report: the geology of the Malin-Hebrides Sea area. London: HMSO for the British Geological Survey.

GAETANI, G. A. & GROVE, T. L. 1997. Partitioning of moderately siderophile elements among olivine sulphide melt and silicate melt: Constraints on core formation in the Earth and Mars. *Geochim. Cosomochim. Acta,* **61,** 1829-1846.

GALLAGHER, K. & HAWKESWORTH, C. J. 1992. Dehydration melting and the generation of continental flood basalts. *Nature,* **358,** 57-59.

GAMMONS, C. H. & BLOOM, M. S. 1993. Experimental investigation of the hydrothermal geochemistry of platinum and palladium: II. The solubillity of PtS and PdS in aqueous sulfide solutions to 300^{o}C. *Geochimica et Cosmochimica Acta,* **57,** 2451-2467.

GHIORSO, M. S., HIRSCHMANN, M. M., REINERS, P. W. & KRESS, V. C. 2002. The pMELTS: A revision of MELTS aimed at improving calculation of phase relations and major element partitioning involved in partial melting of the mantle at pressures up to 3 Gpa. *Geochemistry, Geophysics, Geosystems,* **33,** 1029.

GIBB, F. G. F. & GIBSON, S. A. 1989. The Little Minch Sill Complex. *Scottish Journal of Geology,* **25,** 367-370.

GIBSON, S. A. 1990. The geochemistry of the Trotternish sills, Isle of Skye: crustal contamination in the British Tertiary Volcanic Province. *Journal of the Geological Society, London,* **147,** 1071-1081.

GIBSON, S. A. & JONES, A. P. 1991. Igneous stratigraphy and internal structure of the Little Minch Sill Complex, Trotternish Peninsula, northern Skye, Scotland. *Geological Magazine,* **128,** 51-66.

GLASBY, G. P. 2006. Manganese: Predominant role of nodules and crusts. *In:* SCHULZ, H. D. & ZABEL, M. (eds.) *Marine Geochemistry.* Springer Berlin Heidelberg.

GODEL, B., BARNES, S. -J. & MAIER, W.D. 2006. 3-D distribution of sulphide minerals in the Merensky Reef (Bushveld Complex, South Africa) and the J-M Reef (Stillwater Complex, USA) and their relationship to microstructures using X-Ray computed tomography. *Journal of Petrology,* **47,** 1853-1872.

GODEL, B., BARNES, S. -J. & MAIER, W. D. 2007. Platinum-group elements in sulfide minerals, Platinum-group minerals and whole-rocks of the Merensky Reef (Bushveld Complex, South Africa): implications for the formation of the reef. *Journal of Petrology,* **48,** 1569-1604.

GODEL, B., BARNES, S.J. & BARNES, S. -J. 2013. Deposition mechanisms of magmatic sulphide liquids: Evidence from high-resolution X-Ray computed tomography and trace element chemistry of komatiite-hosted disseminated sulphides. *Journal of Petrology,* **54,** 1455-1481.

GOLDFARB, R. J., BRADLEY, D. & LEACH, D. L. 2010. Secular Variation in Economic Geology. *Economic Geology,* **105,** 459-465.

GOODENOUGH, K. M., PARK, R. G., KRABBENDAM, M. K., MYERS, J. S., WHEELER, J., LOUGHLIN, S. C., CROWLEY, Q. G., FRIEND, C. R. L., BEACH, A., KINNY, P. D. & GRAHAM, R. H. 2010. The Laxford Shear Zone: an end-Archaean terrane boundary? *In: Continental Tectonics and Mountain Building. The Legacy of Peach and Horne.* (eds. LAW, R. D., BUTLER, R. W. H., HOLDSWORTH, R. E., KRABBENDAM, M. & STRACHAN, R.A.), pp. 103-120. London: The Geological Society of London Special Publication no. 335.

GOODENOUGH, K. M., MILLAR, I., STRACHAN, R. A., KRABBENDAM, M. & EVANS, J. A. 2011. Timing of regional deformation and development of the Moine Thrust Zone in the Scottish Caledonides: constraints from the U-Pb geochronology of alkaline intrusions. *Journal of the Geological Society, London,* **168,** 99-114.

GOODENOUGH, K. M., CROWLEY, Q. G., KRABBENDAM, M. & PARRY, S. F. 2013. New U-Pb age constraints for the Laxford Shear Zone, NW Scotland: Evidence for tectono-magmatic processes associated with the formation of a Paleoproterozoic supercontinent. *Precambrian Research,* **233,** 1-19.

GOODENOUGH, K. M., MACDONALD, J. M., JOHNSON, T. E., HUGHES, H. S. R., SHAW, R. A. & MILLAR, I. 2014. Tectoic history and mineralisation in the North Atlantic Craton: A view from Scotland. North Atlantic Craton Conference, 2014 University of St Andrews.

GOODMAN, R. & SLOWLEY, E. 2005. Independent review of exploration interests of Belmore Resources Ltd.

GORBACHEV, N. S. 2010. Experimental study of interaction between fluid-bearing basaltic melts and peridotite: A mantle-crustal source of trap magmas in the Noril'sk area. *Petrology,* **18,** 416-431.

GRAHAM, D. W., LARSEN, L. M., HANAN, B. B., STOREY, M., PEDERSEN, A. K. & LUPTON, J. E. 1998. Helium isotope compostion of the early Iceland mantle plume inferred from the Tertiary picrites of West Greenland. *Earth and Planetary Science Letters,* **160,** 241-255.

GREEN, D. I. & MCCALLUM, D. 2005. Kainosite-(Y) from the Strontian Mines, Highland Region, Scotland. *UK Journal of Mines and Minerals*, **26**, 23-26.

GREEN, D. H. & WALLACE, M. E. 1988. Mantle metasomatism by ephemeral carbonatite melts. *Nature,* **336,** 459-462.

GRIFFIN, W. L. & O'REILLY, S. Y. 1987. Is the continental Moho the crust-mantle boundary? *Geology,* **15,** 241.

GRIFFIN, W. L., O'REILLY, S. Y., ABE, N., AULBACH, S., DAVIES, R. M., PEARSON, N. J., DOYLE, B. J. & KIVI, K. 2003. The origin and evolution of Archean lithospheric mantle. *Precambrian Research,* **127,** 19-41.

GRIFFIN, W. L., O'REILLY, S. Y., AFONSO, J. C. & BEGG, G. C. 2008. The Composition and Evolution of Lithospheric Mantle: a Re-evaluation and its Tectonic Implications. *Journal of Petrology,* **50,** 1185-1204.

GRIFFIN, W. L., BEGG, G. C. & O'REILLY, S. Y. 2013. Continental-root control on the genesis of magmatic ore deposits. *Nature Geoscience,* **6,** 905-910.

GROVE, T. L., CHATTERJEE, N., PARMAN, S. W. & MEDARD, E. 2006. The influence of H_2O on mantle wedge melting. *Earth and Planetary Science Letters*, **249**(1–2), 74–89.

GROVES, D. I. & BIERLEIN, F. P. 2007. Geodynamic settings of mineral deposit systems. *Journal of the Geological Society, London,* **164,** 19-30.

GROVES, D. I., HO, S. E., ROCK, N. M. S., BARLEY, M. E. & MUGGERIDGE, M. T. 1987. Archean cratons, diamond and platinum: Evidence for coupled long-lived crust-mantle systems. *Geology,* **15,** 801-805.

GROVES, D. I., VIELREICHER, R. M., GOLDFARB, R. J. & CONDIE, K. C. 2005. Controls on the heterogeneous distribution of mineral deposits through time. *In: Mineral Deposits and Earth Evolution.* (eds. MCDONALD, I., BOYCE, A. J., BUTLER, I. B., HERRINGTON, R. J. & POLYA, D. A.), pp. 71-102. London: Geological Society of London Special Publication no. 248.

GSNI. 2011. *Platinum Group Metals* [Online, 14th Feb. 2015]. Geological Survey of Northern Ireland. Available: www.bgs.ac.uk/gsni/minerals/prospectivity/pgms.

GUNN, A. G. 2014. *Critical Metals Handbook*, John Wiley & Sons.

GUNN, A. G. & BENHAM, A. 2009. Platinum. *Commoditiy Profile Report.* British Geological Survey.

GUNN, A. G. & SHAW, M. H. 1992. Platinum-group elements in the Huntly intrusion, Abredeenshire, northeast Scotland. *Mineral Reconnaissance Programme Report 124.* British Geological Survey.

GUNN, A. G. & STYLES, M. T. 2002. Platinum-group element occurrences in Britain: magmatic, hydrothermal and supergene. *Transactions of the Institution of Mining and Metallurgy, Applied Earth Sciences, B,* **111,** 2-14.

GUNN, A. G., LEAKE, R. C., STYLES, M. T. & BATESON, J. H. 1985. Platinum-group element mineralization in the Unst ophiolite, Shetland. *Mineral Reconnaissance Programme Report 73.* British Geological Survey.

GUNN, A. G., STYLES, M. T., STEPHENSON, D., SHAW, M. H. & ROLLIN, K. E. 1990. Platinum-group elements in ultramafic rocks of the Upper Deveron Valley, near Huntly, Aberdeenshire. *Mineral Reconnaissance Programme Report 115.* British Geological Survey.

GUNN, A. G., BENHAM, A. & MINKS, A. 2009. Platinum. Nottingham: British Geological Survey.

GUO, J., GRIFFIN, W. L. & O'REILLY, S. Y. 1999. Geochemistry and origin of sulphide minerals in mantle xenoliths: Qilin, Southeastern China. *Journal of Petrology,* **40,** 1125-1149.

GYSI, A.P., JAGOUTZ, O., SCHMIDT, M. W. & TARGUISTI, K. 2011. Petrogenesis of pyroxenites and melt infiltrations in the ultramafic complex of Beni Bousera, Northern Morocco. *Journal of Petrology,* **52,** 1679-1735.

HALD, N. & TEGNER, C. 2000. Composition and age of tertiary sills and dykes, Jameson Land Basin, East Greenland: Relation to regional flood volcanism. *Lithos,* **54,** 207-233.

HALL, I. H. S., GALLAGHER, M. J., SKILTON, B. R. H. & JOHNSON, C. E. 1982. Investigation of polymetallic mineralisation in Lower Devonian volcanics near Alva, central Scotland. *Mineral Reconnaissance Programme Report No. 53.* Natural Environment Research Council.

HALL, G. E. M., PELCHAT, J. -C. & LOOP, J. 1988. Separation and recovery of various sulphur species in sedimentary rocks for stable sulphur isotopic determination. *Chemical Geology,* **67,** 35-45.

HALLIDAY, A. N., AFTALION, M., PARSONS, I., DICKIN, A. P. & JOHNSON, M. R. W. 1987. Syn-orogenic alkaline magmatism and its relationship to the Moine Thrust Zone and the thermal state of the Lithosphere in NW Scotland. *Journal of the Geological Society, London,* **144,** 611-617.

HAMILTON, E. I. 1963. The isotopic composition of strontium in the Skaergaard Intrusion, East Greenland. *Journal of Petrology,* **4,** 383-391.

HAMILTON, M. A., PEARSON, D. G., THOMPSON, R. N., KELLEY, S. P. & EMELEUS, C. H. 1998. Rapid eruption of Skye lavas inferred from precise U-Pb and Ar-Ar dating of the Rum and Cuillin plutonic complexes. *Nature,* **394,** 260-263.

HAMLYN, P. R., KEAYS, R. R., CAMERON, W. E., CRAWFORD, A. J. & WALDRON, H. M. 1985. Precious metals in magnesian low-Ti lavas: Implications for metallogenesis and sulfur saturation in primary magmas. *Geochimica et Cosmochimica Acta,* **49,** 1797-1811.

HANGHOJ, K., KELEMEN, P. B., BERNSTEIN, S., BLUSZTAJN, J. & FREI, R. 2001. Osmium isotopes in the Wiedemann Fjord mantle xenoliths: A unique record of cratonic mantle formation by melt depletion in the Archaean. *Geochemistry Geophysics Geosystems,* **2,** 1-14.

HANNIS, S. & BIDE, T. 2009. Cobalt. *Commodity Profile.* British Geological Survey.

HARDARSON, B. S., FITTON, J. G., ELLAM, R. M. & PRINGLE, M. S. 1997. Rift relocation - a geochemical and geochronological investigation of a palaeo-rift in northwest Iceland. *Earth and Planetary Science Letters,* **153,** 181-196.

HARKER, A. 1904. The Tertiary Igneous Rocks of Skye. *Memoir of the Geological Survey of Great Britain,* HMSO, Edinburgh.

HARKER, A. 1908. The geology of the Small Isles of Invernesshire. *Memoir of the Geological Survey, Scotland*.

HART, S. R. & DAVIES, K. E. 1978. Nickel partitioning between olivine and silicate melt. *Earth and Planetary Science Letters,* **40,** 203-219.

HASTIE, A. R., KERR, A. C., PEARCE, J. A. & MITCHELL, S. F. 2007. Classification of Altered Volcanic Island Arc Rocks using Immobile Trace Elements: Development of the Th Co Discrimination Diagram. *Journal of Petrology,* **48,** 2341-2357.

HASTIE, A. R., KERR, A. C., MITCHELL, S. F. & MILLAR, I. L. 2008. Geochemistry and petrogenesis of Cretaceous oceanic plateau lavas in eastern Jamaica. *Lithos,* **101,** 323-343.

HAUGHTON, D. R., ROEDER, P. L. & SKINNER, B. J. 1974. Solubility of Sulfur in Mafic Magmas. *Economic Geology,* **69,** 451-467.

HAWKESWORTH, C. J., GALLAGHER, K., HERGT, J. M. & MCDERMOTT, F. 1994. Destructive plate margin magmatism: Geochemistry and melt generation. *Lithos,* **33,** 169-188.

HEAMAN, L. M. & TARNEY, J. 1989. U-Pb baddeleyite ages for the Scourie Dyke Swarm, Scotland: Evidence for two distinct intrusion events. *Nature,* **340,** 705-708.

HEFFERNAN, V. 2010. The Right Mix: Combining geophysics and geochemistry with better quality control overcomes challenges in the field. *Earth Explorer.*

HELMY, H. M., BALLHAUS, C., BERNDT, J., BOCKRATH, C. & WOHLGEMUTH-UEBERWASSER, C. 2007. Formation of Pt, Pd and Ni tellurides: experiments in sulfide-telluride systems. *Contributions to Mineralogy and Petrology,* **153,** 577-591.

HELMY, H. M., BALLHAUS, C., FONSECA, R. O. C., NAGEL, T.J. 2013a. Fractionation of platinum, palladium, nickel, and copper in sulfide-arsenide systems at magmatic temperature. *Contributions to Mineralogy and Petrology,* **166,** 1725-1737.

HELMY, H. M., BALLHAUS, C., FONSECA, R. O., WIRTH, R., NAGEL, T. & TREDOUX, M. 2013b. Noble metal nanoclusters and nanoparticles precede mineral formation in magmatic sulphide melts. *Nat Commun,* **4,** 2405.

HERZBERG, C., ASIMOW, P. D., ARNDT, N., NIU, Y., LESHER, C. M., FITTON, J. G., CHEADLE, M. J. & SAUNDERS, A. D. 2007. Temperatures in ambient mantle and plumes: Constraints from basalts, picrites, and komatiites. *Geochemistry, Geophysics, Geosystems,* **8,** n/a-n/a.

HERZBERG, C., CONDIE, K. & KORENAGA, J. 2010. Thermal history of the Earth and its petrological expression. *Earth and Planetary Science Letters,* **292,** 79-88.

HESSELBO, S. P. & COE, A. L. 2000. Jurassic sequences of the Hebrides Basin, Isle of Skye, Scotland. *In: Field Trip Guidebook.* (eds. GRAHAM, J. R. & RYAN, A.), pp. 41-58. Dublin: International Association of Sedimentologists.

HIEBERT, R. S. & BEKKER, A. 2010. Multiple sulfur isotopes: A new tool for identification of sulfur source in magmatic sulfide deposits. *11th International Platinum Symposium.* Ontario Geological Survey.

HILL, E., WOOD, B. J. & BLUNDY, J. D. 2000. The effect of Ca-Tschermaks component on trace element partitioning between clinopyroxene and silicate melt. *Lithos,* **53,** 203-215.

HILTON, D. J., THIRLWALL, M. F., TAYLOR, R. N., MURTON, B. J. & NICHOLS, A. 2000. Controls on magmatic degassing along the Reykjanes Ridge with implications for the helium paradox. *Earth and Planetary Science Letters,* **183,** 43-50.

HIRSCHMANN, M. M., RENNE, P. & MCBIRNEY, A. R. 1997. $^{40}Ar/^{39}Ar$ dating of the Skaergaard Intrusion. *Earth and Planetary Science Letters,* **146,** 645-658.

HOFMANN, A. W. 1997. Mantle geochemistry: the message from oceanic volcanism. *Nature,* **385,** 219-229.

HOLBROOK, W. S., LARSEN, H. C., KORENAGA, J., DAHL-JENSEN, T., REID, I. D., KELEMAN, P. B., HOPPER, J. R., KENT, G. M., LIZARRALDE, D., BERNSTEIN, S. & DETRICK, R. S. 2001. Mantle thermal structure and active upwelling during continental breakup in the North Atlantic. *Earth and Planetary Science Letters,* **190,** 251-266.

HOLLAND, J. G. & LAMBERT, R. S. J. 1973. Comparative major element geochemistry of the Lewisian of the mainland of Scotland. *In: The Early Precambrian of Scotland and related rocks of Greenland.* (eds. PARK, R. G. & TARNEY, J.), pp. 51-62. Keele: University of Keele.

HOLNESS, M. B. 1999. Contact metamorphism and anatexis of Torridonian arkose by minor intrusions of the Rum Igneous Complex, Inner Hebrides, Scotland. *Geological Magazine,* **136,** 527-542.

HOLNESS, M. B. 2005. Spatial Constraints on Magma Chamber Replenishment Events from Textural Observations of Cumulates: the Rum Layered Intrusion, Scotland. *Journal of Petrology,* **46,** 1585-1601.

HOLNESS, M. B., TEGNER, C., NIELSEN, T. F. D., STRIPP, G. & MORSE, S. A. 2007. A textural record of solidification and cooling in the Skaergaard Intrusion, East Greenland. *Journal of Petrology,* **48,** 2359-2377.

HOLNESS, M. B., STRIPP, G., HUMPHREYS, M. C. S., VEKSLER, I. V., NIELSEN, T. F. D. & TEGNER, C. 2011. Silicate liquid immiscibility within the crystal mush: late-stage magmatic microstructures in the Skaergaard Intrusion, East Greenland. *Journal of Petrology,* **52,** 175-222.

HOLNESS, M. B., SIDES, R., PRIOR, D. J., CHEADLE, M. J. & UPTON, B. G. J. 2012. The peridotite plugs of Rum: Crystal settling and fabric development in magma conduits. *Lithos,* **134-135,** 23-40.

HOLWELL, D. A. & BOYCE, A. J. 2012. The generation of precious metal sulfide deposits in the Skaergaard, and related intrusions, East Greenland. The geology of Ni-PGE deposits, Mineral Deposits Studies Group. Cardiff.

HOLWELL, D. A. & JORDAAN, A. 2006. Three-dimensional mapping of the Platreef at the Zwartfontein South mine: implications for the timing of magmatic events in the northern limb of the Bushveld Complex, South Africa. *Applied Earth Science: Transactions of the Institution of Mining and Metallurgy, Applied Earth Sciences, B,* **115,** 41-48.

HOLWELL, D. A. & KEAYS, R. R. 2014. The formation of low-volume, high-tenor magmatic PGE-Au sulfide mineralization in closed systems: Evidence from precious and base metal geochemistry of the Platinova Reef, Skaergaard Intrusion, East Greenland. *Economic Geology,* **109,** 387-406.

HOLWELL, D. A. & MCDONALD, I. 2006. Petrology, geochemistry and the mechanisms determining the distribution of platinum-group element and base metal sulphide mineralisation in the Platreef at Overysel, northern Bushveld Complex, South Africa. *Mineralium Deposita,* **41,** 575-598.

HOLWELL, D. A. & MCDONALD, I. 2007. Distribution of platinum-group elements in the Platreef at Overysel, northern Bushveld Complex: a combined PGM and LA-ICP-MS study. *Contributions to Mineralogy and Petrology,* **154,** 171-190.

HOLWELL, D. A. & MCDONALD, I. 2010. A review of the behaviour of Platinum Group Elements within natural magmatic sulfide ore systems. *Platinum Metals Review,* **54,** 26-36.

HOLWELL, D.A., BOYCE, A.J. & MCDONALD, I. 2007. Sulphur isotope variations within the Platreef Ni-Cu-PGE deposit: Genetic implications for the origin of sulphide mineralization. *Economic Geology,* **102,** 1091-1110.

HOLWELL, D. A., ABRAHAM-JAMES, T., KEAYS, R. R. & BOYCE, A. J. 2010. Marginal Cu-Au-PGE mineralisation in the newly discovered Togeda Macrodyke, Kangerlussuaq Region, East Greenland. *In:* JUGO, P., ed. 11th International Platinum Symposium. Ontario Geological Survey.

HOLWELL, D. A., MCDONALD, I. & BUTLER, I.B. 2011. Precious metal enrichment in the Platreef, Bushveld Complex, South Africa: evidence from homogenized magmatic sulfide melt inclusions. *Contributions to Mineralogy and Petrology,* **161,** 1011-1026.

HOLWELL, D. A., ABRAHAM-JAMES, T., KEAYS, R. R. & BOYCE, A. J. 2012. The nature and genesis of marginal Cu–PGE–Au sulphide mineralisation in Paleogene Macrodykes of the Kangerlussuaq region, East Greenland. *Mineralium Deposita,* **47,** 3-21.

HOLZHEID, A. & LODDERS, K. 2001. Solubility of copper in silicate melts as a function of oxygen and sulfur fugacities, temperature and silicate composition. *Geochim. Cosomochim. Acta,* **65,** 1933-1951.

HOLZHEID, A., SYLVESTER, P., O'NEILL, H. S. C., RUBIE, D. C. & PALME, H. 2000. Evidence for a late chondritic veneer in the Earth's mantle from high-pressure partitioning of palladium and platinum. *Nature,* **406,** 396-399.

HOWARD, J. H. 1977. Geochemistry of selenium: formation of ferroselite and selenium behaviour in the vicinity of oxidizing sulfide and uranium deposits. *Geochimica et Cosmochimica Acta,* **41,** 1665-1678.

HUBER, H., KOEBERL, C., MCDONALD, I. & REIMOND, W. U. 2001. Geochemistry and petrology of Witwatersrand and Dwyka diamictites from South Africa: search for an extraterrestrial component. *Geochimica et Cosmochimica Acta,* **65,** 2007-2016.

HUCHINSON, D. & MCDONALD, I. 2008. Laser ablation ICP-MS study of platinum-group elements in sulphides from the Platreef at Turfspruit, northern limb of the Bushveld Complex, South Africa. *Mineralium Deposita,* **43,** 695-711.

HUDSON, J. D., COLEMAN, M. L., BARREIRO, B. A. & HOLLINGWORTH, N. T. J. 2001. Septarian concretions from the Oxford Clay (Jurassic, England, UK): involvement of original marine and multiple external pore fluids. *Sedimentology,* **48,** 507-531.

HUGHES, H. S. R., MCDONALD, I., GOODENOUGH, K. M., CIBOROWSKI, T. J. R., KERR, A. C., DAVIES, J. H. F. L. & SELBY, D. 2014. Enriched lithospheric mantle keel below the Scottish margin of the North Atlantic Craton: Evidence from the Palaeoproterozoic Scourie Dyke Swarm and mantle xenoliths. *Precambrian Research,* **250,** 97-126. *(Chapter 6 in thesis).*

HUGHES, H. S. R., MCDONALD, I., FAITHFULL, J. W., UPTON, B. G. J. & DOWNES, H. (in press). Trace element abundances in the shallow lithospheric mantle of the North Atlantic Craton margin: Implications for melting and metasomatism beneath Northern Scotland. *Mineralogical Magazine (North Atlantic Craton Conference Special Issue). (Chapter 7 in thesis).*

HUGHES, H. S. R., BOYCE, A. J., MCDONALD, I., DAVIDHEISER-KROLL, B., HOLWELL, D. A., MCDONALD, A. & OLDROYD, A. (accepted, a). Contrasting mechanisms for crustal sulphur contamination of mafic magma: evidence from dyke and sill complexes from the British Palaeogene Igneous Province. *Journal of the Geological Society, London. (Chapter 11 in thesis).*

HUGHES, H. S. R., MCDONALD, I. & KERR, A. C. (accepted, b). Platinum group element signatures in the North Atlantic Igneous Province: Implications for mantle controls on metal budgets during continental breakup. *Lithos. (Chapter 10 in thesis).*

HUGHES, H. S. R., MCDONALD, I., BOYCE, A. J., HOLWELL, D. A. & KERR, A. C. (under review, a). Sulphide sinking in magma conduits: evidence from mafic-ultramafic plugs on Rum, North Atlantic Igneous Province. *Journal of Petrology. (Chapter 12 in thesis).*

HUGHES, H. S. R., MCDONALD, I., FAITHFULL, J. W. & UPTON, B. G. J. (under review, b). Cobalt and precious metals in sulphides of peridotite xenoliths and inferences concerning their distribution according to geodynamic environment: A case study from the Scottish lithospheric mantle. *Lithos. (Chapter 9 in thesis).*

HUGHES, H. S. R., MCDONALD, I., UPTON, B. G. J. & FAITHFULL, J. W. (under review, c). Sulphides and precious metals in the lithospheric mantle: A multi-event record of sulphur-bearing magmatism and metasomatism through time (Loch Roag, Scotland). *Geochimica et Cosmochimica Acta. (Chapter 8 in thesis).*

HULBERT, L. J., DUKE, J. M., EKSTRAND, O. R., SCOATES, R. F. J., THERIAULT, R. J., LECHEMINANT, M. J., GUNN, A. G. & GRINENKO, L. N. 1992. Metallogenic and geochemical evolution of cyclic Unit 1, lower Eastern Layered Series, Rhum. *In: Mineral deposit modelling in relation to crustal reservoirs of the ore-forming elements.* (eds. FOSTER, R. P.). Institue of Mining and Metallurgy.

HULBERT, L. J. & VON GRUENEWALDT, G. 1982. Nickel, copper, and platinum mineralization in the Lower Zone of the Bushveld Complex, South of Potgietersrus. *Economic Geology,* **77,** 1296-1306.

HUMINICKI, M. A. E., SYLVESTER, P. J., CABRI, L. J., LESHER, C. M. & TUBRETT, M. 2005. Quantitative mass balance of platinum group elements in the Kelly Lake Ni–Cu–PGE deposit, Copper Cliff offset, Sudbury. *Economic Geology,* **100,** 1631-1646.

HUMINICKI, M. A. E., SYLVESTER, P. J., LASTRA, R., CABRI, L. J., EVANS-LAMSWOOD, D. & WILTON, D. H. C. 2008. First report of platinum-group minerals from a hornblende gabbro dyke in the vicinity of the Southeast Extension Zone of the Voisey's Bay Ni-Cu-Co deposit, Labrador. *Mineralogy and Petrology,* **92,** 129-164.

HUNTER, R. H. & SPARKS, R. S. J. 1987. The differentiation of the Skaergaard Intrusion. *Contributions to Mineralogy and Petrology,* **95,** 451-461. Chichester: John Wiley.

HUNTER, R. H. & UPTON, B. G. J. 1987. The British Isles - a Palaeozoic mantle sample. *In: Mantle xenoliths.* (eds. NIXON, P. H.), pp. 107-118. Chichester: John Wiley.

HUPPERT, H. E. & SPARKS, S. J. 1985. Cooling and contamination of mafic and ultramafic magmas during ascent through continental crust. *Earth and Planetary Science Letters,* **74,** 371-386.

HURST, E. 1997a. Renewal report for PL 3843 County Louth, reporting period 1995-1997. BHP.

HURST, E. 1997b. Renewal report for PL 3942 County Louth, reporting period 1995-1997. BHP.

HUTCHINSON, D. 2001. *The origin and distribtuion of platinum-group mineralization in the oceanic upper mantle: a comparison of smaples from the Lizard and Troodos ophiolite complexes, and dredge samples from the Tonga Trench.* PhD, Cardiff University.

HUTCHISON, M. & FREI, D. 2009. Kimberlite and related rocks from Garnet Lake, West Greenland, including their mantle constituents, diamond occurrence, age and provenance. *Lithos,* **112,** 318-333.

HUTCHINSON, D. & MCDONALD, I. 2008. Laser ablation ICP-MS study of platinum-group elements in sulphides from the Platreef at Turfspruit, Northern Limb of the Bushveld Complex, South Africa. *Mineralium Deposita,* **43,** 695-711.

IHLENFELD, C. & KEAYS, R. R. 2011. Crustal contamination and PGE mineralization in the Platreef, Bushveld Complex, South Africa: evidence for multiple contamination events and transport of magmatic sulphides. *Mineralium Deposita,* **46,** 813-832.

IONOV, D. A. & HARMER, R. E. 2002. Trace element distribution in calcite-dolomite carbonatites from Spitskop: Inferences for differentiation of carbonatite magmas and the origin of carbonates in mantle xenoliths. *Earth and Planetary Science Letters,* **198,** 495-510.

IRVINE, T. N. 1975. Crystallization sequences in the Muskox intrusion and other layered intrusions—II. Origin of chromitite layers and similar deposits of other magmatic ores. *Geochimica et Cosmochimica Acta,* **39,** 991-1020.

IRVINE, T. N. 1977. Origin of chromitite layers in the Muskox intrusions and other stratiform intrusions: a new interpretation. *Geology,* **5,** 273-277.

IRVINE, T. N. & BARAGAR, W. R. 1971. A guide to the chemical classification of common igneous rocks. *Canadian Journal of Earth Sciences,* **8,** 523-548.

IRVINE, T. N., ANDERSEN, J. C. Ø. & BROOKS, C. K. 1998. Included blocks (and blocks within blocks) in the Skaergaard Intrusion, East Greenland. *Geological Society of America Bulletin,* **110,** 1398-1447.

ISHIKAWA, Y., SAWAGUCHI, T., IWAYA, S. & HORIUCHI, M. 1976. Delineation of prospecting targets for Kuroko deposits based on modes of volcanism of underlying dacite and alteration halos. *Mining Geology,* **26,** 105-117.

JENNER, F. E., BENNETT, V. C., YAXLEY, G., FRIEND, C. R. L. & NEBEL, O. 2013. Eoarchean within-plate basalts from southwest Greenland. *Geology,* **41,** 327-330.

JENNER, G. A. 1996. Trace element geochemistry of igneous rocks: Geochemical nomenclature and analytical geochemistry. *In: Trace element geochemistry of volcanic rocks: Applications for massive sulphide exploration.* (eds. WYMAN, D. A.), pp. 51-78. Winnipeg: Geological Association of Canada.

JENSEN, S. M., LIND, M., RASMUSSEN, T. M. & SECHER, K. 2003. Diamond exploration data from West Greenland a GIS and digital data compilation on DVD. GEUS.

JENSEN, S. M., SECHER, K. & RASMUSSEN, H. 2004. Diamond content of three kimberlitic occurrences in southern West Greeland. GEUS.

JERRAM, D. A. & WIDDOWSON, M. 2005. The anatomy of Continental Flood Basalt Provinces: geological constraints on the processes and products of flood volcanism. *Lithos,* **79,** 385-405.

JOHNSTONE, G. S. & MYKURA, W. 1989. Lewisian. *In: British Regional Geology: The Northern Highlands of Scotland.* pp. 13-29. Nottingham: British Geological Survey.

JOLLEY, D. W. & BELL, B. R. 2002. The evolution of the North Atlantic Igneous Province and the opening of the NE Atlantic rift. *In: The North Atlantic Igneous Province: Stratigraphy, Tectonic, Volcanic and Magmatic Processes.* (eds. JOLLEY, D. W. & BELL, B. R.), pp. 1-14. London: The Geological Society

JUGO, P. J. 2004. An Experimental Study of the Sulphur Content in Basaltic Melts Saturated with Immiscible Sulphide or Sulphate Liquids at 1300°C and 1.0 GPa. *Journal of Petrology,* **46,** 783-798.

KALSBEEK, F., BRIDGWATER, D. & ZECK, H. 1987. A 1950 ± 60 Ma Rb-Sr isochron age from two Kangamiut dykes and the timing of the Nagssugtoqidian (Hudsonian) orogeny in West Greenland. *Canadian Journal of Earth Sciences,* **15,** 1122-1128.

KEAYS, R. R. 1982. Palladium and iridium in komatiites and associated rocks: application to petrogenetic problems. *In: Komatiites.* (eds. ARNDT, N. T. & NISBET, E. G.), pp. 435-455. London: George Allen and Unwin.

KEAYS, R. R. 1995. The role of komatiitic and picritic magmatism and S-saturation in the formation of ore deposits. *Lithos,* **34,** 1-18.

KEAYS, R. R. & LIGHTFOOT, P. C. 2007. Siderophile and chalcophile metal variations in Tertiary picrites and basalts from West Greenland with implications for the sulphide saturation history of continental flood basalt magmas. *Mineralium Deposita,* **42**.

KEAYS, R. R. & LIGHTFOOT, P. C. 2010. Crustal sulphur is required to form magmatic Ni-Cu sulfide deposits: evidence from chalcphole element signatures of Siberian and Deccan Trap basalts. *Mineralium Deposita,* **45,** 241-257.

KEAYS, R. R., NICKEL, E. H., GROVES, D. I. & MCGOLDRICK, P. J. 1982. Iridium and palladium as discriminants of volcanic-exhaltive, hydrothermal, and magmatic nickel sulfide mineralization. *Economic Geology,* **77,** 1535-1547.

KEMP, S. J., ROCHELLE, C. A. & MERRIMAN, R. J. 2005. Back-reacted saponite in Jurassic mudstones and limestones intruded by a Tertiary sill, Isle of Skye. *Clay Minerals,* **40,** 263-282.

KEMPTON, P. D., FITTON, J. G., SAUNDERS, A. D., NOWELL, G. M., TAYLOR, R. N., HARDARSON, B. S. & PEARSON, G. 2000. The Iceland plume in space and time: a Sr-Nd-Pb-Hf study of the North Atlantic rifted margin. *Earth and Planetary Science Letters,* **177,** 255-271.

KENT, R. W. 1995. Magnesian basalts from the Hebrides, Scotland: chemical composition and relationship to the Iceland plume. *Journal of the Geological Society,* **152,** 979-983.

KENT, R. W. & FITTON, J. G. 2000. Mantle sources and melting dynamics in the British Palaeogene Igneous Province. *Journal of Petrology,* **41,** 1023-1040.

KENT, R. W., THOMSON, B. A., SKELHORN, R. R., KERR, A. C., NORRY, M. J. & WALSH, J. N. 1998. Emplacement if Hebridean Tertiary flood basalts: evidence from an inflated pahoehoe lava flow on Mull, Scotland. *Journal of the Geological Society, London,* **155,** 599-607.

KERR, A. C. 1993. *The geochemistry and petrogenesis of the Mull and Morvern Tertiary lava succession, Argyll, Scotland.* PhD, Durham University.

KERR, A. C. 1994. Lithospheric thinning during the evolution of continental large igneous provinces: a case study from the North Atlantic Tertiary province. *Geology,* **22,** 1027-1030.

KERR, A. C. 1995a. The geochemical stratigraphy, field relations and temporal variation of the Mull-Morvern Tertiary lava succession, NW Scotland. *Transactions of the Royal Society of Edinburgh: Earth Sciences,* **86,** 35-47.

KERR, A. C. 1995b. The geochemistry of the Mull-Morvern lava succession, NW Scotland: an assessment of mantle sources during plume-related volcanism. *Chemical Geology,* **122,** 43-58.

KERR, A. C. 1997. The geochemistry and significance of plugs intruding the Tertiary Mull-Morvern lava succession, western Scotland. *Scottish Journal of Geology,* **33,** 157-167.

KERR, A. C. 1998. Mineral chemistry of the Mull-Morvern Tertiary lava succession, western Scotland. *Mineral Magazine,* **62,** 295-312.

KERR, A. & LEITCH, A. M. 2005. Self-Destructive Sulfide Segregation Systems and the Formation of High-Grade Magmatic Ore Deposits. *Economic Geology,* **100,** 311-332.

KERR, A. C., KENT, R. W., BELL, B. R. & JOLLEY, D. 1998. Discussion on application of palynological data to the chronology of the Palaeogene lava fields of the British Province. *Journal of the Geological Society, London,* **155,** 733-735.

KERR, A. C., KENT, W. R., THOMSON, B. A., SEEDHOUSE, J. K. & DONALDSON, C. H. 1999. Geochemical evolution of the Tertiary Mull volcano, Western Scotland. *Journal of Petrology,* **40,** 873-908.

KERRICH, R., GOLDFARB, R. J. & RICHARDS, J. P. 2005. Metallogenic provinces in an evolving geodynamic framework. *Economic Geology 100th Anniversary Volume***,** 1097-1136.

KILLE, I. C., THOMPSON, R. N., MORRISON, M. A. & THOMPSON, R. F. 1986. Field evidence for turbulence during flow of basalt magma through conduits from southwest Mull. *Geological Magazine,* **123,** 693-697.

KINNAIRD, J. A., KRUGER, F. J., NEX, P. A. M. & CAWTHORN, R. G. 2002. Chromitite formation – a key to understanding processes of platinum enrichment. *Applied Earth Science,* **111,** 23-35.

KINNAIRD, J. A., HUTCHINSON, D, SCHURMANN, L., NEX, P. A. M. & DE LANGE, R. 2005. Petrology and mineralization of the southern Platreef: Norhtern limb of the Bushveld Complex, South Africa. *Mineralium Deposita,* **40,** 576-597.

KINNAIRD, T. C., PRAVE, A. R., KIRKLAND, C. L., HORSTWOOD, M., PARRISH, R. & BATCHELOR, R. A. 2007. The late Mesoproterozoic-early Neoproterozoic tectonostratigraphic evolution of NW Scotland: the Torridonian revisited. *Journal of the Geological Society,* **164,** 541-551.

KINNY, P. D., STRACHAN, R. A., KOCKS, H. & FRIEND, C. R. L. 2003. U-Pb geochronology of late Neoproterozoic augen granites in the Moine supergroup, NW Scotland: dating of rift-related, felsic magmatism during supercontinent break-up? *Journal of the Geological Society, London,* **160,** 925-934.

KINNY, P. D., FRIEND, C. R. L. & LOVE, G. J. 2005. Proposal for a terrane-based nomenclature for the Lewisian Gneiss Complex of NW Scotland. *Journal of the Geological Society,* **162,** 175-186.

KIRSTEIN, L. A., DUNAI, T. J., DAVIES, G. R., UPTON, B. G. J. & NIKOGOSIAN, I. K. 2004. Helium isotope signature of lithospheric mantle xenoliths from the Permo-Carboniferous magmatic province in Scotland -- no evidence for a lower-mantle plume. *Geological Society, London, Special Publications,* **223,** 243-258.

KIRSTEIN, L. A., DAVIES, G. R. & HEEREMANS, M. 2006. The petrogenesis of Carboniferous–Permian dyke and sill intrusions across northern Europe. *Contributions to Mineralogy and Petrology,* **152,** 721-742.

KNELLER, B. C. 1991. A foreland basin on the southern margin of Iapetus. *Journal of the Geological Society, London,* **148,** 207-210.

KOGARKO, L. N., HENDERSON, C. M. B. & PACHECO, H. 1995. Primary Ca-rich carbonatite magma and carbonate-silicate-sulphide liquid immiscibility in the upper mantle. *Contributions to Mineralogy and Petrology,* **121,** 267-274.

KOLB, J. 2014. Structure of the Palaeoproterozoic Nagssugtoqidian Orogen, South-East Greenland: Model for the tectonic evolution. *Precambrian Research,* **255,** 809-822.

KOLB, J., DZIGGEL, A. & SCHLATTER, D. M. 2013. Gold occurrences of the Archean North Atlantic craton, southwestern Greenland: A comprehensive genetic model. *Ore Geology Reviews,* **54,** 29-58.

KORENAGA, J. 2008. Urey ratio and the structure and evolution of the Earth's mantle. *Reviews of Geophysics,* **46,** 1-32.

KRUGER, F. J. 1992. The origin of the Merensky cyclic unit: Sr-isotopic and mineralogical evidence for an alternative orthomagmatic model. *Australian Journal of Earth Sciences,* **39,** 255-261.

KRUGER, F. J. & MARSH, J. S. 1982. Significance of $^{87}Sr/^{86}Sr$ ratios in the Merensky cyclic unit of the Bushveld Complex. *Nature,* **298,** 53-55.

KUCHARSKI, M., I. W. & TOGURI, J. M. 1994. The surface tension and density of Cu_2S, FeS, Ni_3S_2 and their mixtures. *Canadian Metallurgical Quarterly,* **33,** 197-203.

KULLERUD, G. & YODER, H. S. 1959. Pyrite stability relations in the Fe-S system. *Economic Geology,* **54,** 533-572.

KUMAR, P., KIND, R., HANKA, W., WYLEGALLA, K., REIGBER, CH., YUAN, X., WOELBERN, I., SCHWINTZER, P., FLEMING, K., DAHL-JENSEN, T., LARSEN, T. B., SCHWEITZER, J., PRIESTLEY, K., GUDMUNDSSON, O. & WOLF, D. 2005. The lithosphere–asthenosphere boundary in the North-West Atlantic region. *Earth and Planetary Science Letters,* **236,** 249-257.

KURZ, M. D., JENKINS, W. J., HART, S. R. & CLAGUE, D. 1983. Helium isotopic variations in volcanic rocks from Loihi Seamount and the Island of Hawaii. *Earth and Planetary Science Letters,* **66,** 388-406.

KUSAKABE, M., MAYEDA, S. & NAKAMURA, E. 1990. S, O and Sr isotope systematics of active vent materials from the Mariana Back Arc Basin spreading axis at 18 N. *Earth and Planetary Science Letters,* **100,** 275-282.

LABIDI, J., CARTIGNY, P., BIRCK, J. L., ASSAYAG, N. & BOURRAND, J. J. 2012. Determination of multiple sulphur isotopes in glasses: A reappraisal of the MORB $\delta^{34}S$. *Chemical Geology,* **334,** 189-198.

LARSEN, L. M. & BROOKS, C. K. 1994. Origin and evolution of gabbroic pegmatites in the Skaergaard Intrusion, East Greenland. *Journal of Petrology,* **35,** 1651-1679.

LARSEN, L. M. & REX, D. C. 1992. A review of the 2500 Ma span of alkaline-ultramafic, potassic and carbonatitic magamtism in West Greenland. *Lithos,* **28,** 367-402.

LARSEN, L. M., FITTON, J. G. & FRAM, M. S. 1998. Volcanic rocks of the southeast Greenland margin in comparison with other parts of the North Atlantic Tertiary Igneous Province. *Proceedings of the Ocean Drilling Program, Scientific Results,* **152,** 315-330.

LARSEN, L. M., FITTON, J. G. & SAUNDERS, A. D. 1999. Composition of volcanic rocks from the southeast Greenland margin, Leg 163: major and trace element geochemistry. *Proceedings of the Ocean Drilling Program, Scientific Results,* **163,** 63-75.

LARSEN M., BJERAGER, M., NEDKVITNE, T., OLAUSSEN, S. & PREUSS, T. 2001. *Geological Survey of Greenland Bulletin,* **189**, 99–106.

LAWVER, L. A. & MULLER, R. D. 1994. Iceland hotspot track. *Geology,* **22,** 311-314.

LEBLANC, M. & FISCHER, W. 1990. Gold and platinum group elements in cobalt-arsenide ores: Hydrothermal concentration from a serpentinite source-rock (Bou Azzer, Morocco). *Mineralogy and Petrology,* **1990,** 42.

LE BRETON, E., COBBOLD, P. R. & ZANELLA, A. 2013. Cenozoic reactivation of the Great Glen Fault, Scotland: additional evidence and possible causes. *Journal of the Geological Society,* **170,** 403-415.

LEE, C. A. & BUTCHER, A. R. 1990. Cyclicity in the Sr isotope stratigraphy through the Merensky and Bastard Reef Units, Atok Section, Eastern Bushveld Complex. *Economic Geology,* **85,** 877-883.

LEE, C. A. & TREDOUX, M. 1986. Platinum-group element abundances in the upper and lower critical zones of the Bushveld Complex. *Economic Geology,* **81,** 1087-1095.

LEFORT, A., HAUTEVELLE, Y., LATHUILIERE, B. & HUAULT, V. 2012. Molecular organic geochemistry of a proposed stratotype for the Oxfordian/Kimmeridgian boundary (Isle of Skye, Scotland). *Geological Magazine,* **149,** 857-874.

LEGGETT, J. K., MCKERROW, W. S. & EALES, M. H. 1979. The Southern Uplands of Scotland: A Lower Palaeozoic accretionary prism. *Journal of the Geological Society,* **136,** 755-770.

LE MAITRE, R. W., STRECKEISEN, A., ZANETTIN, B., LE BAS, M. J. BONIN, B., BATEMAN, P., BELLIENI, G., DUDEK, A., EFREMOVA, S., KELLER, J., LAMERE, J., SABINE, P. A., SCHMID, H., SORENSEN, S. & WOOLLEY, A. R. 2002. *Igneous Rocks: A Classification and Glossary of Termas, Recommendations of the Internation Union of Geological Sciences*, Cambridge University Press.

LESHER, C. E. & BURNHAM, O. M. 2001. Multicomponent elemental and isotopic mixing in Ni-Cu-(PGE) ores at Kambalda, Western Australia. *The Canadian Mineralogist,* **39,** 421-446.

LEUTHOLD, J., BLUNDY, J. D., HOLNESS, M. B. & SIDES, R. 2014. Successive episodes of reactive liquid flow through a layered intrusion (Unit 9, Rum Eastern Layered Intrusion, Scotland). *Contributions to Mineralogy and Petrology,* **168**.

LI, J. & AGEE, C. B. 1996. Geochemistry of mantle-core differentiation at high pressure. *Nature,* **381,** 686-689.

LI, C. & NALDRETT, A. J. 1993. Sulfide capacity of magma: A quantitative model and its application to the formation of sulfide ores at Sudbury, Ontario. *Economic Geology,* **88,** 1253-1260.

LI, C. & RIPLEY, E. M. 2005. Empirical equations to predict the sulfur content of mafic magmas at sulfide saturation and applications to magmatic sulfide deposits. *Mineralium Deposita,* **40,** 218-230.

LI, C. & RIPLEY, E. M. 2009. Sulphur contents at sulfide-liquid or anhydrite saturation in silicate melts: Empirical equations and example applications. *Economic Geology,* **104,** 405-412.

LI, C., BARNES, S. -J., MAKOVICKY, E., ROSE-HANSEN, J. & MAKOVICKY, M. 1996. Partitioning of nickel, copper, iridium, rhenium, platinum, and palladium between monosulfide solid solution and sulfide liquid: Effects of composition and temperature. *Geochimica et Cosmochimica Acta,* **60,** 1231-1238.

LI, C., RIPLEY, E. M., MAIER, W. D. & GOMWE, T. E. S. 2002. Olivine and sulfur isotopic compositions of the Uitkomst Ni-Cu sulfide ore-bearing complex, South Africa: evidence for sulfur contamination and multiple magma emplacements. *Chemical Geology,* **188,** 149-159.

LI, C., RIPLEY, E. M. & NALDRETT, A. J. 2009. A new genetic model for the giant Ni-Cu-PGE sulfide deposits associated with the Siberian flood basalts. *Economic Geology,* **104,** 291-301.

LIGHTFOOT, P. C. 2007. Advances in Ni-Cu-PGE sulphide deposit models and implications for exploration technologies. *In:* MILKEREIT, B., ed. Proceedings of Exploration 07: Fifth Decennial International Conference on Mineral Exploration. 629-646.

LIGHTFOOT, P. C. & HAWKESWORTH, C. J. 1997. Flood basalts and magmatic Ni, Cu, and PGE sulphide mineralization: Comparative geochemistry of the Noril'sk (Siberian Traps) and West Greenland sequences. *Geophysical Monograph Series,* **100,** 357-380.

LIGHTFOOT, P. C. & KEAYS, R. R. 2005. Siderophile and chalcophile metal variations in flood basalts from the Siberian Trap, Noril'sk Region: Implications for the origin of the Ni-Cu-PGE sulphide ores. *Economic Geology,* **100,** 439-462.

LIGHTFOOT, P. C., NALDRETT, A. J. & HAWKESWORTH, C. J. 1984. The geology and geochemistry of the Waterfall Gorge Section of the Insizwa Complex with particular reference to the origin of the nickel sulphide deposits. *Economic Geology,* **79,** 1857-1879.

LIGHTFOOT, P. C., HAWKESWORTH, C. J. & OLSHEFSKY, K. 1997. Geochemistry of Tertiary tholeiites and picrites from Qeqertarssuaq (Disko Island) and Nuussuaw, West Greenland with implications for the mineral potential of comagmatic intrusions. *Contributions to Mineralogy and Petrology,* **128,** 139-163.

LINDGREN, P. & PARNELL, J. 2006. Rapid heating of carbonaceous matter by igneous intrusions in carbon-rich shale, Isle of Skye, Scotland: an analogue for heating of carbon in impact craters? *International Journal of Astrobiology,* **5,** 343-351.

LLOYD, F. E., EDGAR, A. D., FORSYTH, D. M., BARNETT, R. L. 1991. The paragenesis of upper-mantle xenoliths from the Quaternary volcanics South-East of Gees, West Eifel, Germany. *Mineralogical Magazine,* **55,** 95-112.

LOCMELIS, M., FIORENTINI, M. L., BARNES, S. J. & PEARSON, N. J. 2013. Ruthenium variation in chromite from komatiites and kmoatiitic basalts – A potential mineralogical indicator for nickel sulfide mineralization. *Economic Geology,* **108,** 355-364.

LONG, A. M., MENZIES, M. A., THIRLWALL, M. F., UPTON, B. G. J. & APSEN, P. 1991. Carbonatite-mantle interaction: A possible origin for megacryst/xenolith suites in Scotland. *In:* MEYER, H. O. A. & LEONARDOS, O. H. (eds.) *Fifth International Kimberlite Conference.* Brazil.

LORAND, J. -P. & ALARD, O. 2001. Platinum-group element abundances in the upper mantle: New constraints for in situ and whole-rock analyses of Massif Central xenoliths (France). *Geochimica et Cosmochimica Acta,* **65,** 2789-2806.

LORAND, J. -P. & ALARD, O. 2010. Determination of selenium and tellurium concentrations in Pyrenean peridotites (Ariege, France): New insight into S/Se/Te systematics of the upper in mantle samples. *Chemical Geology,* **278,** 120-130.

LORAND, J. -P., PATTOU, L. & GROS, M. 1999. Fractionation of platinum-group elements and gold in the upper mantle: a detailed study in Pyrenean orogenic lherzolites. *Journal of Petrology,* **40,** 957-981.

LORAND, J. -P., ALARD, O., LUGUET, A. & KEAYS, R. R. 2003. Sulfur and selenium systematics of the subcontinental lithospheric mantle: Inferences from the Massif Central xenolith suite (France). *Geochimica et Cosmochimica Acta,* **67,** 4137-4151.

LORAND, J. -P., DELPECH, G., GREGOIRE, M., MOINE, B., O'REILLY, S. Y. & COTTIN, J. -Y. 2004. Platinum-group elements and the multistage metasomatic history of Kerguelen lithospheric mantle (South Indian Ocean). *Chemical Geology,* **208,** 195-215.

LORAND, J. -P., LUGUET, A. & ALARD, O. 2008a. Platinum-Group Elements: A New Set of Key Tracers for the Earth's Interior. *Elements,* **4,** 247-252.

LORAND, J. -P., LUGUET, A., ALARD, O., BEZOS, A. & MEISEL, T. 2008b. Abundance and distribution of platinum-group elements in orogenic lherzolites; a case study in a Fontete Rouge lherzolite (French Pyrénées). *Chemical Geology,* **248,** 174-194.

LORAND, J. -P., LUGUET, A. & ALARD, O. 2013. Platinum-group element systematics and petrogenetic processing of the continental upper mantle: A review. *Lithos,* **164-167,** 2-21.

LORD, R. A. & PRICHARD, H. M. 1997. Exploration and origin of stratigraphically controlled platinum-group element mineralization in crustal-sequence ultramafics, Shetland ophiolite complex. *Transactions of the Institution of Mining and Metallurgy, Applied Earth Sciences, B,* **106,** 179-193.

LOVE, G. J., KINNY, P. D. & FRIEND, C. R. L. 2003. Timing of magmatism and metamorphism in the Gruinard Bay area of the Lewisian Gneiss Complex: comparisons with the Assynt Terrane and implications for terrane accretion. *Contributions to Mineralogy and Petrology,* **146,** 620-636.

LOVE, G. J., FRIEND, C. R. L. & KINNY, P. D. 2010. Palaeoproterozoic terrane assembly in the Lewisian Gneiss Complex on the Scottish mainland, south of Gruinard Bay: SHRIMP U–Pb zircon evidence. *Precambrian Research,* **183,** 89-111.

LOWRY, D., 1991. *The genesis of Late Claedonian granitoid-related minerlization in Northern Britain.* Unpublished PhD thesis, University of St Andrews.

LOWRY, D., BOYCE, A. J., FALLICK, A. E. & STEPHENS, W. E. 1995. Genesis of porphyry and plutonic mineralisation systems in metaluminous granitoids of the Grampian Terrane, Scotland. *Transactions of the Royal Society of Edinburgh: Earth Sciences,* **85,** 221-237.

LOWRY, D., BOYCE, A. J., FALLICK, A. E., STEPHENS, W. E., GRASSINEAU, N. V. 2005. Terrane and basement discrimination in northern Britain using sulphur isotopes and mineralogy of ore deposits. *In: Mineral Deposits and Earth Evolution.* (eds. MCDONALD, I., BOYCE, A. J., BUTLER, I. B., HERRINGTON, R. J., POLYA, D. A.), pp. 133-151. Geological Society, London. Special Publications, **248**, 133-151.

LUGUET, A., LORAND, J. -P. & SEYLER, M. 2003. Sulfide petrology and highly siderophile element geochemistry of abyssal peridotites: a coupled study of samples from the Kane Fracture Zone (45°W 23°20N, MARK area, Atlantic Ocean). *Geochimica et Cosmochimica Acta,* **67,** 1553-1570.

LUGUET, A., SHIREY, S. B., LORAND, J. -P., HORAN, M. F. & CARLSON, R. W. 2007. Residual platinum-group minerals from highly depleted harzburgites of the Lherz massif (France) and their role in HSE fractionation of the mantle. *Geochimica et Cosmochimica Acta,* **71,** 3082-3097.

MACHEL, H. G. 2001. Bacterial and thermochemical sulfate reduction in diagenetic settings - old and new insights. *Sedimentary Geology,* **140,** 143-175.

MAIER, W. D. 2005. Platinum-group element (PGE) deposits and occurrences: Mineralization styles, genetic concepts, and exploration criteria. *Journal of African Earth Sciences,* **41,** 165-191.

MAIER, W. D. & BARNES, S. -J. 1999. Platinum-gruop elements in silicate rocks of the Lower, Critical and Main Zones at Union Section, Western Bushveld Complex. *Journal of Petrology,* **40,** 1647-1761.

MAIER, W. D. & BARNES, S. -J. 2004. Pt/Pd and Pd/Ir ratios in mantle-derived magmas: A possible role for mantle metasomatism. *South African Journal of Geology,* **107,** 333-340.

MAIER, W. D. & GROVES, D. I. 2011. Temporal and spatial controls on the formation of magmatic PGE and Ni–Cu deposits. *Mineralium Deposita,* **46,** 841-857.

MAIER, W. D., BARNES, S. -J., DE KLERK, W. J., TEIGLER, B. & MITCHELL, A. A. 1996. Cu/Pd and Cu/Pt of silicate rocks in the Bushveld Complex: Implications for platinum-group element exploration. *Economic Geology,* **91,** 1151-1158.

MAIER, W. D., BARNES, S. -J. & DE WAAL, S. A. 1998. Exploration for magmatic Ni-Cu-PGE sulphide deposits: a review of recent advances in the use of geochemical tools, and their application to some South African ores. *South African Journal of Geology,* **101,** 237-253.

MAIER, W. D., BARNES, S. -J., GARTZ, V. & ANDREWS, G. 2003a. Pt-Pd reefs in magnetitites of the Stella layered intrusion, South Africa: A world of new exploration opportunities for platinum group elements. *Geology,* **31,** 885.

MAIER, W. D., ROELOFSE, F. & BARNES, S.-J. 2003b. The concentration of the platinum-group elements in South African komatiites: Implications for mantle sources, melting regime and PGE fractionation during crystallization. *Journal of Petrology,* **44,** 1787-1804.

MAIER, W. D., BARNES, S. -J. CHINYEPI, G., BARTON, J. M., EGLINGTON, B. & SETSHEDI, I. 2008. The composition of magmatic Ni-Cu-(PGE) sulfide deposits in the Tati and Selebi-Phikwe belts of eastern Botswana. *Mineralium Deposita,* **43,** 37-60.

MAIER, W. D., PELTONEN, P., MCDONALD, I., BARNES, S. J., BARNES, S. -J., HATTON, C. & VILJOEN, F. 2012. The concentration of platinum-group elements and gold in southern African and Karelian kimberlite-hosted mantle xenoliths: Implications for the noble metal content of the Earth's mantle. *Chemical Geology,* **302-303,** 119-135.

MAO, J., GOLDFARB, R. J., WANG, Z. & YANG, J. 2005. Late Paleozoic base and precious metal deposits, East Tianshan, Xinjiang, China: characteristics and geodynamic setting. *Episodes,* **28,** 23-36.

MARCANTONIO, F., DICKIN, A. P., MCNUTT, R. H. & HEAMAN, L. M. 1988. A 1800-million-year-old Proterozoic gneiss terrane in Islay with implications for the crustal structure and evolution of Britain. *Nature***,** 62-64.

MARTIN, H., MOYEN, J. -F. & RAPP, R. 2010. The sanukitoid series: magmatism at the Archaean-Proterozoic transition. *Geological Society of America Special Papers,* **472,** 15-33.

MASON, A. J. & BREWER, T. S. 2004. Mafic dyke remnants in the Lewisian Complex of the Outer Hebrides, NW Scotland: a geochemical record of continental break-up and re-assembly. *Precambrian Research,* **133,** 121-141.

MAVROGENES, J. A. & O'NEILL, H. S. C. 1999. The relative effects of pressure, temperature and oxygen fugacity on the solubility of sulfide in mafic magmas. *Geochimica et Cosmochimica Acta,* **63,** 1173-1180.

MAYER, B. & KROUSE, H. 2004. Procedures for sulphur isotope abundance studies. *In: Handbook of Stable Isotope Analytical Techniques.* pp. 538-596. Elsevier.

MCATEER, C. A., STEPHEN DALY, J., FLOWERDEW, M. J., CONNELLY, J. N., HOUSH, T. B. & WHITEHOUSE, M. J. 2010. Detrital zircon, detrital titanite and igneous clast U–Pb geochronology and basement–cover relationships of the Colonsay Group, SW Scotland: Laurentian provenance and correlation with the Neoproterozoic Dalradian Supergroup. *Precambrian Research,* **181,** 21-42.

MCBIRNEY, A. R. 1989. The Skaergaard Layered Series, Part I: Structure and average compositions. *Journal of Petrology,* **30,** 363-397.

McBirney, A. R. & Creaser, R. A. 2003. The Skaergaard Layered Series, Part VII: Sr and Nd isotopes. *Journal of Petrology,* **44,** 757-771.

McClurg, J. 1982. *Geology and structure of the norhtern part of the Rhum ultrabasic complex.* PhD, University of Edinburgh.

McDonald, I. 2008. Platinum-group element and sulphide mineralogy from ultramafic complexes at Andriamena, Madagascar. *Applied Earth Science, Transactions of the Institution of Mineralogy and Metallurgy, Applied Earth Sciences, B,* **117,** 1-10.

McDonald, I. & Holwell, D. A. 2007. Distribution of platinum-group elements in the Platreef at Overysel, northern Bushveld Complex: a combined PGM and LA-ICP-MS study. *Contributions to Mineralogy and Petrology,* **154,** 171-190.

McDonald, I. & Holwell, D. A. 2011. Geology of the northern Bushveld Complex and the setting and genesis of the Platreef Ni-Cu-PGE deposit. *In: Magmatic Ni-Cu and PGE deposits: geology, geochemistry, and genesis. Reviews in Economic Geology,* **17,** 297-327.

McDonald, I. & Viljoen, K. S. 2006. Platinum-group element geochemistry of mantle eclogites: a reconnaissance study of xenoliths from the Orapa kimberlite, Botswana. *Applied Earth Science,* **115,** 81-93.

McDonald, I., De Wit, M., Smith, C. B., Bizzi, L. A. & Viljoen, K. S. 1995. The geochemistry of the platinum-group elements in Brazilian and Southern African kimberlites. *Geochimica et Cosmochimica Acta,* **59,** 2883-2903.

McDonald, I., Holwell, D. A. & Wesley, B. 2009. Assessing the potential involvement of an early magma staging chamber in the generation of the Platreef Ni–Cu–PGE deposit in the northern limb of the Bushveld Complex: a pilot study of the Lower Zone Complex at Zwartfontein . *Transactions Institution of Mining & Metallurgy, Applied Earth Sciences, B,* **118**, 5-20.

McDonald, I., Jones, R. E., Holwell, D. A. & Butler, I. B. 2012. Platinum-group element tenors and S/Se ratios of Platreef sulphide melt inclusions. *5th Platreef Workshop.* Mokopane, South Africa.

McDonough, W. F. & Sun, S. 1995. The Composition of the Earth. *Chemical Geology,* **120,** 223-253.

McKenzie, D. 2011. Compaction and crystallization in magma chambers: towards a model of the Skaergaard Intrusion. *Journal of Petrology,* **52,** 905-930.

McKenzie, D. & Bickle, M. J. 1988. The volume and composition of melt generated by extension of the lithosphere. *Journal of Petrology,* **29,** 625-679.

McInnes, B. I. 1999. Osmium Isotope Constraints on Ore Metal Recycling in Subduction Zones. *Science,* **286,** 512-516.

McKervey, J. A., Gunn, A. G. & Styles, M. T. 2007. Platinum-group elements in Ordovician magmatic Ni-Cu sulphide prospects in northeast Scotland. *Canadian Mineralogist,* **45,** 335-353.

McPherson, G. & Lamb, T. 1921. Platinum-bearing rocks in the Lizard district. *Geological Magazine,* **58,** 512-514.

Menzies, M. & Halliday, A. 1988. Lithospheric mantle domains beneath the Archean and Proterozoic crust of Scotland. *Journal of Petrology,* **Special Lithosphere Issue,** 275-302.

Menzies, M. A., Halliday, A. N., Palacz, Z., Hunter, R. N., Upton, B. G. J., Aspen, P. & Hawkesworth, C. J. 1987. Evidence from mantle xenoliths for an enriched lithospheric keel under the Outer Hebrides. *Nature,* **325,** 44-47.

Menzies, M. A., Halliday, A. N., Hunter, R. N., MacIntyre, R. M. & Upton, B. G. J. 1989. The age, composition and significance of a xenolith-bearing monchiquite dyke, Lewis, Scotland. *In:* O'Reilly, S. Y. (ed.) *Kimberlites and Related Rocks: their Mantle/Crust Setting, Diamonds and Diamond Exploration.* Geological Society of Australia, Special Publication.

MERCIER, J. -C. C. & NICOLAS, A. 1975. Textures and fabrics of upper-mantle peridotites as illustrated by xenoliths from basalts. *Journal of Petrology,* **16,** 454-487.

MITCHELL, R. H. & KEAYS, R. R. 1981. Abundance and distribution of gold, palladium and iridium in some spinel and garnet lherzolites: implications for the nature and origin of precious metal-rich intergranluar components in the upper mantle *Geochimica et Cosmochimica Acta,* **45,** 2425-2442.

MOINE, B., GREGOIRE, M., O'REILLY, S. Y., DELPECH, G., SHEPPARD, S. M. F., LORAND, J. -P., RENAC, C., GIRET, A. & COTTIN, J. -Y. 2004. Carbonatite melt in oceanic upper mantle beneath the Kerguelen Archipelago. *Lithos,* **75,** 239-252.

MOMME, P., TEGNER, C. & BROOKS, C. K. 2002a. On the formation of platinum group element-rich continental flood basalt and Platinova Reefs of the Skaergaard Intrusion. 9th International Platinum Symposium. Billings, Montana.

MOMME, P., TEGNER, C., BROOKS, K. & KEAYS, R. 2002b. The behaviour of platinum-group elements in basalts from the East Greenland rifted margin. *Contributions to Mineralogy and Petrology,* **143,** 133-153.

MOMME, P., ÓSKARSSON, N. & KEAYS, R. R. 2003. Platinum-group elements in the Icelandic rift system: melting processes and mantle sources beneath Iceland. *Chemical Geology,* **196,** 209-234.

MOMME, P., TEGNER, C., BROOKS, C. K. & KEAYS, R. R. 2006. Two melting regimes during Paleogene flood basalt generation in East Greenland: combined REE and PGE modelling. *Contributions to Mineralogy and Petrology,* **151,** 88-100.

MOORBATH, S. & THOMPSON, R. N. 1980. Strontium isotope geochemistry and petrogenesis of the Early Tertiary lava pile of the Isle of Skye, Scotland, and other basic rocks of the British Tertiary Province: an example of magma-crust interaction. *Journal of Petrology,* **21,** 295-321.

MOORHOUSE, S. J. & MOORHOUSE, V. E. 1977. A Lewisian basement sheet within the Moine at Ribigill, north Sutherland. *Scottish Journal of Geology,* **13,** 289-300.

MORISHITA, T., HATTORI, K. H., TERADA, K., MATSUMOTO, T., YAMAMOTO, K., TAKEBE, M., ISHIDA, Y., TAMURA, A. & ARAI, S. 2008. Geochemistry of apatite-rich layers in the Finero phlogopite–peridotite massif (Italian Western Alps) and ion microprobe dating of apatite. *Chemical Geology,* **251,** 99-111.

MORTON, N. & HUDSON, J. D. 1995. Field guide to the Jurassic of the Isles of Raasay and Skye, Inner Hebrides, NW Scotland. *In: Field geology of the British Jurassic.* (eds. TAYLOR, P. D.). The Geological Society, London.

MUIR, R. J., EVANS, J. A. & FITCHES, W. R. 1993. Mafic dykes within the Lewisian Complex on Tiree and Coll, Inner Hebrides. *Scottish Journal of Geology,* **29,** 167-176.

MUNGALL, J. E. 2002. Kinetic Controls on the Partitioning of Trace Elements Between Silicate and Sulfide Liquids. *Journal of Petrology,* **43,** 749-768.

MUNGALL, J. E. & BRENAN, J. M. 2014. Partitioning of platinum-group elements and Au between sulfide liquid and basalt and the origins of mantle-crust fractionation of the chalcophile elements. *Geochimica et Cosmochimica Acta,* **125,** 265-289.

MUNGALL, J. E. & SU, S. 2005. Interfacial tension between magmatic sulfide and silicate liquids: Constraints on kinetics of sulfide liquation and sulfide migration through silicate rocks. *Earth and Planetary Science Letters,* **234,** 135-149.

MUNGALL, J. E., ANDREWS, D., CABRI, L., SYLVESTER, P. & TUBRETT, M. 2005. Partitioning of Cu, Ni, Au, and platinum-group elements between monosulphide solid solution and sulphide melt under controlled oxygen and sulphur fugacities. *Geochimica et Cosmochimica Acta,* **69,** 4349-4360.

MURPHY, P. J. & MEYER, G. 1998. A gold-copper association in ultramafic-hosted hydrothermal sulfides from the Mid-Atlantic Ridge. *Economic Geology,* **93,** 1076-1083.

MURTON, B. J., TAYLOR, R. N. & THIRLWALL, M. F. 2002. Plume-ridge interaction: a geochemical perspective from the Reykjanes Ridge. *Journal of Petrology,* **43,** 1987-2012.

MUSSETT, A. E., DAGLEY, P. & SKELHORN, R. R. 1988. Time and duration of activity in the British Tertiary Igneous Province. *In: Early Tertiary volcanism and the opening of the North Atlantic.* (eds. MORTON, A. C. & PARSONS, L. M.), pp. 337-348. Special Publication of the Geological Society of London no. 39.

NALDRETT, A. J. 1989. *Magmatic Sulfide Deposits,* New York, Oxford University Press.

NALDRETT, A. J. 1997. Key factors in the genesis of Noril'sk, Sudbury, Jinchuan, Voisey's Bay and other world-class Ni-Cu-PGE deposits: Implications for exploration. *Australian Journal of Earth Sciences,* **44,** 283-315.

NALDRETT, A. J. 2004. *Magmatic sulphide deposits: geology, geochemistry and exploration,* Berlin, Springer.

NALDRETT, A. J. 2010. Secular variation of magmatic sulfide deposits and their source magmas. *Economic Geology,* **105,** 669-688.

NALDRETT, A. J. 2011. Fundamentals of Magmatic Sulfide Deposits. *In: Magmatic Ni-Cu and PGE deposits: geology, geochemistry, and genesis.* (eds. LI, C. & RIPLEY, E. M.), pp. 1-51. Society of Economic Geologists, Reviews in Economic Geology volume 17.

NALDRETT, A. J. & FEDORENKO, V. 1995. Ni-Cu-PGE deposits of the Noril'sk reion Siberia: Their formation in conduits for flood basalt volcanism. *Transactions of the Institution of Mining and Metallurgy, Applied Earth Sciences, B,* **104,** 18-36.

NALDRETT, A. J. & VON GRUENEWALDT, G. 1989. Association of platinum-group elements with chromitite in layered intrusions and ophiolite complexes. *Economic Geology,* **84,** 180-187.

NALDRETT, A. J., GASPARINI, E. C. & BARNES, S. -J., VON GRUENEWALDT, G. & SHARPE, M. R. 1986a. The upper Critical Zone of the Bushveld Complex and the origin of Merensky-type ores. *Economic Geology,* **77,** 1105-1117.

NALDRETT, A. J., RAO, B. V. & EVENSEN, N. M. 1986b. Contamination at Sudbury and its roles in ore formation *In: Metallogeny of basic and ultrabasic rocks.* (eds. GALLAGHER, M. J., IXER, R. A., NEARY, C. R. & PRICHARD, H. M.), pp. 75-91. London: Institution of Mining and Metallurgy.

NALDRETT, A. J., LIGHTFOOT, P. C., FEDORENKO, V., DOHERTY, W. & GORBACHEV, N. S. 1992. Geology and geochemistry of intrusions and flood basalts of the Noril'sk Region, USSR, with implications for the origin of the Ni-Cu ores. *Economic Geology,* **87,** 975-1004.

NALDRETT, A. J., FEDORENKO, V. A., ASIF, M., LIN, S., KUNILOV, V. E., STEKHIN, A. I. & LIGHTFOOT, P. C., GORBACHEV, N.S. 1996. Controls on the composition of Ni-Cu sulphide deposits as illustrated by those at Noril'sk, Siberia. *Economic Geology,* **91,** 751-773.

NALDRETT, A. J., ASIF, M., KRSTIC, S. & LI, C. 2000. The Composition of Mineralization at the Voisey's Bay Ni-Cu Sulfide Deposit, with Special Reference to Platinum-Group Elements. *Economic Geology,* **95,** 845-865.

NALDRETT, A. J., WILSON, A., KINNAIRD, J. A. & CHUNNETT, G. 2009. PGE tenor and metal ratios within and below the Merensky Reef, Bushveld Complex: Implications for its genesis. *Journal of Petrology,* **50,** 625-659.

NALDRETT, A. J., KINNAIRD, J. A., WILSON, A., YUDOVSKAYA, M. & CHUNNETT, G. 2011. Genesis of the PGE-enriched Merensky Reef and chromitite seams of the Bushveld Complex. *Reviews in Economic Geology,* **17,** 235-296.

NALDRETT, A. J., WILSON, A., KINNAIRD, J. A., YUDOVSKAYA, M. & CHUNNETT, G. 2012. The origin of chromitites and related PGE mineralization in the Bushveld Complex: new mineralogical and petrological constraints. *Mineralium Deposita,* **47,** 209-232.

NIELSEN, T. F. D. 1978. The Tertiary dike swarms of the Kangerlussuaq Area, East Greenland. *Contributions to Mineralogy and Petrology,* **67,** 63-78.

NIELSEN, T. F. D. & BROOKS, C. K. 1995. Precious metals in magmas of East Greenland: Factors important to the mineralization in the Skaergaard Intrusion. *Economic Geology,* **90,** 1911-1917.

NIELSEN, J. K. & HANKEN, N. -M. 2002. Description of the chromium reduction method for extraction of pyrite sulphur. University of Tromso.

NEILSON, J. C., ANDERSEN, J. C. Ø. & BROOKS, C. K. 2005. The Platinova Reef of the Skaergaard Intrusion. *In: Exploration for Paltinum-Group Element Deposits.* (eds. MUNGALL, J. E.). *Mineralogical Association of Canada, Short Course,* **35,** 431-455.

NEILSON, J. C., KOKELAAR, B. P. & CROWLEY, Q. G. 2009. Timing, relations and cause of plutonic and volcanic activity of the Siluro-Devonian post-collisions magmatic episode in the Grampian Terrance, Scotland. *Journal of the Geological Society, London,* **166,** 545-561.

NEWTON, R. J., BOTTRELL, S. H., DEAN, S. P., HATFIELD, D. & RAISWELL, R. 1995. An evaluation of the use of the chromous chloride reduction method for isotopic analyses of pyrite in rocks and sediment. *Chemical Geology,* **125,** 317-320.

NILSSON, M. K. M., KLAUSEN, M. B., SÖDERLUND, U. & ERNST, R. E. 2013. Precise U–Pb ages and geochemistry of Palaeoproterozoic mafic dykes from southern West Greenland: Linking the North Atlantic and the Dharwar cratons. *Lithos,* **174,** 255-270.

O'DRISCOLL, B., HARGRAVES, R. B., EMELEUS, C. H., TROLL, V. R., DONALDSON, C. H. & REAVY, R. J. 2007. Magmatic lineations inferred from anisotropy of magnetic susceptibility fabrics in Units 8, 9, and 10 of the Rum Eastern Layered Series, NW Scotland. *Lithos,* **98,** 27-44.

O'DRISCOLL, B., DAY, J. M. D., DALY, J. S., WALKER, R. J. & MCDONOUGH, W. F. 2009. Rehmium-osmium isotopes and platinum-group elements in the Rum Layered Suite, Scotland: Implications for Cr-spinel seam formation and the composition of the Iceland mantle anomaly. *Earth and Planetary Science Letters,* **286,** 41-51.

O'DRISCOLL, B., DAY, J. M. D., WALKER, R. J. & DALY, J. S. 2012. Chemical heterogeneity in the upper mantle recorded by peridotites and chromitites fom the Shetland Ophiolite Complex, Scotland. *Earth and Planetary Science Letters,* **333-334,** 226-237.

O'DRISCOLL, B., BUTCHER, A. R. & LATYPOV, R. 2014. New insights into precious metal enrichment on the Isle of Rum, Scotland. *Geology Today,* **30,** 134-141.

O'HARA, M. J. 1961. Petrology of the Scourie dykes, Sutherland. *Mineralogical Magazine,* **32,** 848-865.

OHMOTO, H., & GOLDHABER, M. B., 1997, Sulphur and carbon isotopes. *In: Geochemistry of hydrothermal ore deposits*. (ed. Barnes, H. L.), 3rd edition: New York, Wiley, p. 517–611.

OHMOTO, H. & RYE, R. O. 1979. Isotopes of sulphur and carbon. *In: Geochemistry of Hydrothermal deposits.* (ed. Barnes, H. L.), John Wiley & Sons, 509-567.

OHTANI, E., YURIMOTO, H. & SETO, S. 1997. Element partitioning between metallic liquid, silicate liquid, and lower-mantle minerals: implications for core formation of the Earth. *Physics of the Earth and Planetary Interiors,* **100,** 97-114.

OLIVER, G. J. H., WILDE, S. A., WAN, Y. S. 2008. Geochronology and geodynamics of Scottish granitoids from the late Neoproterozoic break-up of Rodinia to Palaeozoic collision. *Journal of the Geological Society, London,* **165,** 661-674.

O'REILLY, S. Y. & GRIFFIN, W. L. 2000. Apatite in the mantle: implications for metasomatic processes and high heat production in Phanerozoic mantle. *Lithos,* **53,** 217-232.

O'REILLY, S. Y., GRIFFIN, W. L., POUDJOM DJOMANI, Y. H. & MORGAN, P. O. 2001. Are lithospheres forever? Tracking changes in subcontinental lithosperic mantle through time. *GSA Today***,** 4-10.

O'REILLY, S. Y., ZHANG, M., GRIFFIN, W. L., BEGG, G. & HRONSKY, J. 2009. Ultradeep continental roots and their oceanic remnants: A solution to the geochemical "mantle reservoir" problem? *Lithos,* **112,** 1043-1054.

ORTEGA, L., PRICHARD, H. M., LUNAR, R., GARCIA PALOMERO, F., MORENO, T. & FISHER, P. 2000. The Aguablanca discovery. *Mining Magazine.*

OXBURGH, E. R., MCRAE, T. & O'HARA, M. J. 1984. Physical Constraints on Magma Contamination in the Continental Crust: An Example, the Adamello Complex [and Discussion]. *Philosophical Transactions of the Royal Society A: Mathematical, Physical and Engineering Sciences,* **310,** 457-472.

PAGE, P., BARNES, S. -J., BEDARD, J. H. & ZIENTEK, M. L. 2012. In situ determination of Os, Ir, and Ru in chromites formed from komatiite, tholeiite and boninite magmas: Implications for chromite control of Os, Ir and Ru during partial melting and crystal fractionation. *Chemical Geology,* **302-303,** 3-15.

PALACZ, Z. 1985. Sr-Nd-Pb isotopic evidence of crustal contamination in the Rhum intrusion. *Earth and Planetary Science Letters,* **74,** 35-44.

PALME, H. & O'NEILL, H. S. C. 2004. Cosmochemical estimates of mantle composition. *Treatise on Geochemistry,* **2,** 1-38.

PARK, R. G. 1994. Early Proterozoic tectonic overview of the northern British Isles and neighbouring terrains in Laurentia and Baltica. *Precambrian Research,* **68,** 65-79.

PARK, R. G. 1995. Palaeoproterozoic Laurentia-Baltica relationships: a view from the Lewisian. *In: Early Precambrian Processes. Geological Society Special Publication 95.* (eds. COWARD, M. P. & RIES, A. C.). The Geological Society, London.

PARK, R. G. 2002a. The Scourie Dyke Suite. *In: Geological Society Memoirs,* **26***,* pp. 21-28. The Geological Society, London.

PARK, R. G. 2002b. *The Lewisian Geology of Gairloch, NW Scotland*, Geological Society, London.

PARK, R. G. 2005. The Lewisian terraine model: a review. *Scottish Journal of Geology,* **41,** 105-118.

PARK, R. G. & TARNEY, J. 1987. The Lewisian complex: a typical Precambrian high-grade terrain? *In: Evolution of the Lewisian and Comparable Precambrian high grade terrains.* (eds. PARK, R. G. & TARNEY, J.), pp. 13-25. The Geological Society.

PARK, R. G., KINNY, P. D., FRIEND, C. R. L. & LOVE, G. J. 2005. Discussion on a terrane-based nomenclature for the Lewisian Gneiss Complex of NW Scotland. *Journal of the Geological Society, London,* **162,** 893-895.

PARNELL, J., BOYCE, A. J., MARK, D., BOWDEN, S. & SPINKS, S. 2010. Early oxygenation of the terrestrial environment during the Mesoproterozoic. *Nature,* **468,** 290-293.

PARNELL, J., HOLE, M., BOYCE, A. J., SPINKS, S. & BOWDEN, S. 2012. Heavy metal, sex and granites: Crustal differentiation and bioavailability in the mid-Proterozoic. *Geology,* **40,** 751-754.

PATERSON, S. R., FOWLER, T. K., SCHMIDT, K. L., YOSHINOBU, A. S., YUAN, E. S. & MILLER, R. B. 1998. Interpreting magmatic fabric patterns in plutons. *Lithos,* **44,** 53-82.

PATTOU, L., LORAND, J. -P. & GROS, M. 1996. Non-chondritic platinum-group element ratios in the Earth's mantle. *Nature,* **379,** 712-715.

PATTRICK, R. A. D. 1985. Pb-Zn and minor U mineralization at Tyndrum, Scotland. *Mineralogical Magazine,* **49,** 671-681.

PEACH, B. N., HORNE, J., GUNN, W., CLOUGH, C. T., Hinxman, L. W. & Teall, J. J. H. 1907. *The geological structure of the North-West Highlands of Scotland,* London, Her Majesty's Stationery Office.

PEACH, C. L., MATHEZ, E. A. & KEAYS, R. R. 1990. Sulfide melt-silicate melt distribution coefficients for noble metals and other chalcophile elements as deduced from MORB: Implications for partial melting. *Geochimica et Cosmochimica Acta,* **54,** 3379-3389.

PEARCE, J. A. 1996. A user's guide to basalt discrimination diagrams. *In: Trace element geochemistry of volcanic rocks: Applications for massive sulphide exploration.* (eds. WYMAN, D. A.), pp. 79-114. Winnipeg: Geological Association of Canada.

PEARCE, J. A. 2008. Geochemical fingerprinting of oceanic basalts with applications to ophiolite classification and the search for Archean oceanic crust. *Lithos,* **100,** 14-48.

PEARCE, J. A., STERN, R. J., BLOOMER, S. H. & FRYER, P. 2005. Geochemical mapping of the Mariana arc-basin system: Implications for the nature and distribution of subduction components. *Geochemistry, Geophysics, Geosystems,* **6,** n/a-n/a.

PEARSON, D. G. 2005. Mantle Samples Included in Volcanic Rocks: Xenoliths and Diamonds. *In:* CARLSON, R. W. (ed.) *The mantle and core.* Treatise on geochemistry.

PEARSON, D. G., LARSEN, L. M., WALKER, R. J., WOODLAND, S. J., PEDERSEN, A. K., CARLSON, R. W. & SHIRLEY, S. B. 1999. The deep sources of plumes: Phenium-osmium platinum-osmium isotopic and platinum-group element systematics of high helium-3/helium-4 West Greenland picrites. Proceedings of the 9th Annual Goldshmidt Conference. 223.

PEARSON, N. J., ALARD, O., GRIFFIN, W. L., JACKSON, S. E. & O'REILLY, S. Y. 2002. In situ measurement of Re-Os isotopes in mantle sulfides by laser ablation multicollector-inductively coupled plasma mass spectrometry: Analytical methods and preliminary results. *Geochimica et Cosmochimica Acta,* **66,** 1037-1050.

PEARSON, D. G., CANIL, D. & SHIREY, S. B. 2003. Mantle samples included in volcanic rocks: Xenoliths and diamonds. *In: Treatise on Geochemistry.* pp. 171-275.

PEARSON, D. G., IRVINE, G. J., IONOV, D. A., BOYD, F. R. & DREIBUS, G. E. 2004. Re–Os isotope systematics and platinum group element fractionation during mantle melt extraction: a study of massif and xenolith peridotite suites. *Chemical Geology,* **208,** 29-59.

PEARSON, D. G., PARMAN, S. W. & NOWELL, G. M. 2007. A link between large mantle melting events and continent growth seen in osmium isotopes. *Nature,* **449,** 202-205.

PECK, D. C. & KEAYS, R. R. 1990. Insights into the behaviour of precious metals in primitive, S-undersaturated magmas: evidence from the Heazlewood River Complex, Tasmania. *Canadian Mineralogist,* **28,** 553-557.

PEDERSEN, A. K., WATT, M., WATT, W. S. & LARSEN, L. M. 1997. Structure and stratigraphy of the Early Tertiary basalts of the Blosseville Kyst, East Greenland. *Journal of the Geological Society, London,* **154,** 565-570.

PELTONEN, P., KONTINEN, A., HUHMA, H. & KURONEN, U. 2008. Outokumpu revisited: New mineral deposit model for the mantle peridotite-associated Cu–Co–Zn–Ni–Ag–Au sulphide deposits. *Ore Geology Reviews,* **33,** 559-617.

PENNISTON-DORLAND, S. C., WING, B. A., NEX, P. A. M., KINNAIRD, J. A. FARQUHAR, J., BROWN, M. & SHARMAN, E. R. 2008. Multiple sulphur isotopes reveal a magmatic origin for the Platreef platinum group element deposit, Bushveld Complex, South Africa. *Geology,* **36,** 979.

PEREGOEDOVA, A. V. 1998. The experimental study of the Pt–Pd partitioning between monosulfide solid solution and Cu–Ni– sulfide melt at 900–840°C. 8th international platinum symposium abstracts. Geol Soc South Africa and South African Inst Min Metall Symposium Series S18, 325-327.

PEREGOEDOVA, A., BARNES, S. -J. & BAKER, D. R. 2004. The formation of Pt–Ir alloys and Cu–Pd-rich sulfide melts by partial desulfurization of Fe–Ni–Cu sulfides: results of experiments and implications for natural systems. *Chemical Geology,* **208,** 247-264.

PHILIPP, H., ECKHARDT, J. -D. & PUCHELT, H. 2001. Platinum-group elements (PGE) in basalts of the seaward-dipping reflector sequence, SE Greenland Coast. *Journal of Petrology,* **42,** 407-432.

PIDGEON, R. T. & AFTALION, M. 1978. Cogenetic and inherited zircon U-Pb systems in granites: Palaeozoic granites of Scotland and England. *Crustal evolution in northwestern Britain and adjacent regions.* Scottish Academic Press Glasgow.

PIRRIE, D., POWER, M. R., ANDERSEN, J. C. Ø. & BUTCHER, A. R. 2000. Platinum-group mineralization in the Tertiary Igneous Province: new data from Mull and Skye, Scottish Inner Hebrides, UK. *Geological Magazine,* **137,** 651-658.

PLANKE, S., RASSMUSSEN, T., REY, S. S. & MYKLEBUST, R. 2005. Seismic characterisitics and dsitribution of volcanic intrusions and hydrothermal vent complexes in the Vøring and Møre basins. In: DORE, T., VINING, B. (eds.), *Petroleum Geology: North-West Europe and Global Perspectives,* Geological Society Publishing House, London.

PLATINARESOURCES 2009. Miki Fjord Dyke & Kangerkussuaq Alkaline Complex, East Greenland. Platina Resources.

PLATINARESOURCES. *Miki Fjord* [Online, 8th June 2012]. Platina Resources Ltd. Available: http://www.platinaresources.com.au/projects/miki-fjord-and-kangerlussuaq.

PLATINARESOURCES. 2012. *Kap Edvard Holm, East Greenland* [Online, 8th June 2012]. Platina Resources. Available: http://www.platinaresources.com.au/files/projects/pc00316_platina_factsheet_kap_edvard_lr.pdf

PLATTEN, I. M. 1999. Ardsheal Hill and Peninsula. *In:* STEPHENSON, D., BEVINS, R. E., MILLWARD, D., HIGHTON, A. J. PARSONS, I., STONE, P. & WADSWORTH, W. J. (eds.) *Caledonian Igneous Rocks of Great Britain.* JNCC.

PLATTEN, I. M. 2000. Incremental dilation of magma filled fractures: evidence from dykes on the Isle of Skye, Scotland. *Journal of Structural Geology,* **22,** 1153-1164.

POLAT, A. & KERRICH, R. 2006. Reading the geochemcial fingerprints of Archean hot subduction volcanic rocks: Evidence for accretion and crustal recycling in a mobile tectonic regime. *American Geophysical Union: Geophysical Monograph Series,* **164,** 189-213.

POWER, M. R. & PIRRIE, D. 2000. Platinum-group element mineralization within ultramafic rocks at Corrycharmaig, perthshire: implications for the origin of the complex. *Scottish Journal of Geology,* **36,** 143-150.

POWER, M. R. & PIRRIE, D. 2004. Platinum-group minerals within the Ballantrae Complex, SW Scotland. *Scottish Journal of Geology,* **40,** 1-5.

POWER, M., PIRRIE, D., ANDERSEN, J. C. Ø. & BUTCHER, A. R. 2000. Stratigraphical distribution of platinum-group minerals in the Eastern Layered Series, Rum, Scotland. *Mineralium Deposita,* **35,** 762-775.

POWER, M. R., PIRRIE, D. & ANDERSEN, J. C. Ø. 2003. Diversity of platinum-group element mineralization styles in the North Atlantic Igneous Province: new evidence from Rum, UK. *Geological Magazine,* **140,** 499-512.

POWER, M. R., PIRRIE, D., JEDWAB, J. & STANLEY, J. 2004. Platinum-group element mineralization in an As-rich magmatic sulphide system, Talnotry, southwest Scotland. *Mineralogical Magazine,* **68,** 395-411.

PRAEGEL, N. -O. 1981. Origin of ultramafic inclusions and megacrysts in a monchiquite dyke at Streap, Inverness-shire, Scotland. *Lithos,* **14,** 305-322.

PRESTON, R. J., BELL, B. R. & ROGERS, G. 1998. The Loch Scridain sill complex, Isle of Mull, Scotland: fractional crystallization, assimilation, magma-mixing and crustal anatexis in sub-volcanic conduits. *Journal of Petrology,* **39,** 519-550.

PRENDERGAST, M. D. 2000. Layering and precious metals mineralization in the Pincon del Tigre Complex, Eastern Bolivia. *Economic Geology,* **95,** 113-130.

PRICHARD, H. M. & LORD, R. A. 1993. An overview of PGE concentrations in the Shetland ophiolite complex. *In: Magmatic processes and plate tectonics.* pp. 273-294. London: Geological Society

PRICHARD, H. M., POTTS, P. J. & NEARY, C. R. 1981. Platinum-group minerals in the Shetland ophiolite complex. *Transactions of the Institution of Mining and Metallurgy, Applied Earth Sciences, B,* **90,** 186-188.

PRICHARD, H. M., HUTCHINSON, D., FISHER, P. C. 2004. Petrology and crystallization history of multiphase sulfide droplets in a mafic dike from Uruguay: Implications for the origin of Cu-Ni-PGE sulfide deposits. *Economic Geology,* **99,** 365-376.

PRICHARD, H. M., FISHER, P. C., MCDONALD, I., KNIGHT, R. D., SHARP, D. R. & WILLIAMS, J. P. 2013a. The distribution of PGE and the role of arsenic as a collector of PGE in the Spotted Quoll Nickel Ore Deposit in the Forrestania Greenstone Belt, Western Austrlia. *Economic Geology,* **108,** 1903-1921.

PRICHARD, H. M., KNIGHT, R. D., FISHER, P. C., MCDONALD, I., ZHU, M. -F. & WANG, C. Y. 2013b. Distribution of platinum-group elements in magmatic and altered ores in the Jinchuan intrusion, China: an example of selenium remobilization by postmagmatic fluids. *Mineralium Deposita,* **48,** 767-786.

RITCHER, L., HELZ, R. T., WALKER, R. J. & PICCOLI, P. 2009. Fractionation of the platinum-group elements and Re during crystallization of basalt in Kilauea Iki Lava Lake, Hawaii. *Chemical Geology,* **260,** 196-210.

PROUT, S. J., ANDERSEN, J. C. Ø., BARNES, S. -J. & POWER, M. R. 2002. Platinum-group element mineralisation within two mafic/ultramafic intrusions of the British Palaeogene Igneous Province. *In:* BOUDREAU, A. E., ed. Proceedings of the 9th International Platinum Symposium. Billings, Montana.

PUCHTEL, I. & HUMAYUN, M. 2001. Platinum group element fractionation in a komatiitic basalt lava lake. *Geochimica et Cosmochimica Acta,* **65,** 2979-2993.

QUEFFURUS, M. & BARNES, S. -J. The use of S/Se ratios in magmatic Ni-Cu-PGE sulfide deposits. 11th International Platinum Symposium, June 21-24, 2010 2010 Ontario. Ontario Geological Survey.

RAISWELL, R., BOTTRELL, S. H., AL-BIATTY, H. J. & TAN, M. M. 1993. The influence of bottom water oxygenation and reactive iron content on sulphur incorporation into bitumens from Jurassic marine shales. *American Journal of Science,* **293,** 569-596.

REHKAMPER, M., HALLIDAY, A. N., FITTON, J. G., LEE, D. -C., WIENEKE, M. & ARNDT, N. T. 1999. Ir, Ru, Pt and Pd in basalts and komatiites: New constraints for the geochemical behavior of the platinum-group elements in the mantle. *Geochimica et Cosmochimica Acta,* **63,** 3915-3934.

REICHOW, M. K., SAUNDERS, A. D., WHITE, R. V., PRINGLE, M. S., AL'MUKHAMEDOV, A. I., MEDVEDEV, A. & KORDA, N. 2002. ^{40}Ar-^{39}Ar data on basalts from the West Siberian basin: extent of the Siberian flood basalt province doubled. *Science,* **296,** 1846-1849.

RICHTER, F. M. 1988. A major change in the thermal state of the earth at the Archean-Proterozoic Boundary: Consequences for the nature and preservation of continental lithosphere. *Journal of Petrology,* **Special Volume,** 39-52.

RIGHTER, K., CAMPBELL, A. J., HUMAYUN, M. & HERVIG, R. L. 2004. Partitioning of Ru, Rh, Pd, Re, Ir, and Au between Cr-bearing spinel, olivine, pyroxene and silicate melts. *Geochimica et Cosmochimica Acta,* **68,** 867-880.

RIPLEY, E. M. & LI, C. 2013. Sulphide saturation in mafic magmas: Is external sulphur required for magmatic Ni-Cu-(PGE) ore genesis? *Economic Geology,* **108,** 45-58.

RIPLEY, E. M., PARK, Y. -R., LI, C. & NALDRETT, A. J. 1999. Sulphur and oxygen isotopic evidence of country rock contamination in the Voisey's Bay Ni-Cu-Co deposit, Labrador, Canada. *Lithos,* **47,** 53-68.

RIPLEY, E. M., LIGHTFOOT, P. C., LI, C. & ELSWICK, E. R. 2003. Sulphur isotopic studies of continental flood basalts in the Noril'sk region: implications for the association between lavas and ore-bearing intrusions. *Geochimica et Cosmochimica Acta,* **67,** 2805-2817.

RISON, W. & CRAIG, H. 1983. Helium isotopes and mantle volatiles in Loihi Seamount and Hawaiian Island basalts and xenoliths. *Earth and Planetary Science Letters,* **66,** 407-426.

ROBB, L. 2005. *Introduction to ore-forming processes*, Blackwell Science Ltd.

ROBINSON, B. W. & KUSAKABE, M. 1975. Quantitative preparation of sulphur dioxide for $^{34}S/^{32}S$ analyses from sulphides by combustion with cuprous oxide. *Analytical Chemistry,* **47,** 1179-1181.

ROEST, W. R. & SRIVISTAVA, S. P. 1989. Sea-floor spreading in the Labrador Sea: A new reconstruction. *Geology,* **17,** 1000-1003.

ROLLINSON, H. R. 2010. Coupled evolution of Archean continental crust and subcontinental lithospheric mantle. *Geology,* **38,** 1083-1086.

ROLLINSON, H. R. 2012. Geochemical constraints on the composition of Archaean lower continental crust: Partial melting in the Lewisian granulites. *Earth and Planetary Science Letters,* **351-352,** 1-12.

ROLLINSON, H. R. & FOWLER, M. B. 1987. The magmatic evolution of the Scourian complex at Gruinard Bay. *In: Evolution of the Lewisian and comparable Precambrian high grade terrains.* (eds. PARK, R. G. & TARNEY, J.), pp. 57-71. Geological Society of London Special Publication no. 27.

ROSE, L. A. & BRENAN, J. M. 2001. Wetting properties of Fe-Ni-Co-Cu-O-S melts against olivine: Implications for sulfide melt mobility. *Economic Geology,* **96,** 145-157.

RUDNICK, L. & FOUNTAIN, D. M. 1995. Nature and composition of the continental crust: A lower crustal perspective. *Reviews of Geophysics,* **33**, 267-309.

SACHS, P. M. & STANGE, S. 1993. Fast assimilation of xenoliths in magmas. *Journal of Geophysical Research,* **98,** 19741.

SAND, K. K., WAIGHT, T. E., PEARSON, D. G., NIELSEN, T. F. D., MAKOVICKY, E. & HUTCHISON, M. T. 2009. The lithospheric mantle below southern West Greenland: A geothermobarometric approach to diamond potential and mantle stratigraphy. *Lithos,* **112,** 1155-1166.

SANGSTER, C. 2012. Highly anomalous Platinum Group Metals, Gold and Base Metals at Sron Garbh. Scotgold Resources Ltd press release 7th March 2012.

SATTARI, P., BRENAN, J. M., HORN, I. & MCDONOUGH, W. F. 2002. Experimental constraints on the sulfide- and chromite-siliicate melt partitioning behavior of rhenium and the platinum-group elements. *Economic Geology,* **97,** 385-398.

SAUNDERS, A. D., FITTON, J. G., KERR, A. C., NORRY, M. J. & KENT, R. W. 1997. The North Atlantic Igneous Province. *In: Large Igneous Provinces: Continental, Oceanic, and Planetary Flood Volcanism.* (eds. MAHONEY, J. J. & COFFIN, M. F.), pp. 45-93. Washington DC: American Geophysical Union.

SAUNDERS, A. D., LARSEN, H. C. & FITTON, J. G. 1998. Magmatic development of the southeast Greenland Margin and evolution of the Iceland plume: Geochemical constraints from Leg 152. *Proceedings of the Ocean Drilling Program, Scientific Results,* **152,** 479-501.

SAUNDERS, A. D., ENGLAND, R. W., REICHOW, M. K. & WHITE, R. V. 2005. A mantle plume origin for the Siberian Traps: uplift and extension in the West Siberian basin, Russia. *Lithos,* **79,** 407-424.

SCHAEFER, B. F., PARKINSON, I. J. & HAWKESWORTH, C. J. 2000. Deep mantle plume osmium isotope signature from West Greenland Tertiary picrites. *Earth and Planetary Science Letters,* **175,** 105-118.

SCHERSTEN, A., ELLIOTT, T., HAWKESWORTH, C. J. & NORMAN, M. 2004. Tungsten isotope evidence that mantle plumes contain no contribution from the Earth's core. *Nature,* **427,** 234-237.

SCHOFIELD, N. J., BROWN, D. J., MAGEE, C. & STEVENSON, C. T. 2012. Sill morphology and comparison of brittle and non-brittle emplacement mechanisms. *Journal of the Geological Society,* **169,** 127-141.

SEABROOK, C. L., CAWTHR & KRUGER, F. J. 2005. The Merensky Reef, Bushveld Complex: Mixing of minerals not mixing of magmas. *Economic Geology,* **100,** 1191-1205.

SEAL, R. R. 2006. Sulfur isotope geochemistry of sulfide minerals. *In: Sulfide mineralogy and geochemistry.* (eds. ROSSO, J. J.), pp. 633-678. Geochemical Society, Reviews in Mineralogy and Geochemistry volume 61.

SEARLE, M. P., LAW, R. D., DEWEY, J. F. & STREULE, M. J. 2010. Relationships between the Loch Ailsh and Borralan alkaline intrusions and thrusting in the Moine Thrust zone, southern Assynt culmination, NW Scotland. *Geological Society, London, Special Publications,* **335,** 383-404.

SECHER, K. 2009. New mineral showings in southern West Greenland found during GEUS field work. *Minex.* Geological Survey of Denmark and Greenland.

SECHER, K. & STENDAL, H. 2010. Greenland's nickel resource potential. *In:* SECHER, K. (ed.) *Geology and Ore 17: Exploration and Mining in Greenland.* Geological Survey of Denmark and Greenland.

SECHER, K., APPEL, P. & NIELSEN, T. F. D. 2007. The PGE potential in Greenland. *In:* SECHER, K. (ed.) *Geology and Ore 8: Exploration and mining in Greenland.* Geological Survey of Denmark and Greenland.

SECHER, K., HEAMAN, L. M., NIELSEN, T. F. D., JENSEN, S. M., SCHJOTH, F. & CREASER, R. A. 2009. Timing of kimberlite, carbonatite, and ultramafic lamprophyre emplacement in the alkaline province located 64°–67° N in southern West Greenland. *Lithos,* **112,** 400-406.

SECHER, K., APPEL, P. & NIELSEN, T. F. D. 2010. PGE deposits in Greenland. *In:* SECHER, K. (ed.) *Exploration and Mining in Greenland: Fact Sheet No. 24 Greenland Mineral Resources.* Geological Survey of Denmark and Greenland.

SHARMAN, E. R., PENNISTON-DORLAND, S. C., KINNAIRD, J. A., NEX, P. A. M., BROWN, M. & WING, B. A. 2013 Primary origin of marginal Ni-Cu-(PGE) mineralization in layered intrusions: $\Delta^{33}S$ evidence from the Platreef, Bushveld, South Africa. *Economic Geology*, **108**, 365-377.

SHAW, C. S. J. 2009. Caught in the act — The first few hours of xenolith assimilation preserved in lavas of the Rockeskyllerkopf volcano, West Eifel, Germany. *Lithos,* **112,** 511-523.

SHAW, M. H., GUNN, A. G. & MENDUM, J. R. 1993. Investigation into the distribution of the platinum group elements, South Harris, Isle of Lewis, Scotland. *Mineral Reconnaissance Programme Report.* Nottingham: British Geological Survey.

SHERATON, J. W., SKINNER, A. C. & TARNEY, J. 1973. The geochemistry of the Scourian gneisses of the Assynt district. *In: The early Precambrian of Scotland and related rocks of Greenland.* (eds. PARK, R. G. & TARNEY, J.), pp. 13-30. Keele: University of Keele.

SHIMA, H. & NALDRETT, A. J. 1975. Solubility of sulfur in an ultramafic melt and the relevance of the system Fe-S-O. *Economic Geology,* **70,** 960-967.

SILVER, P. G., MAINPRICE, D., BEN ISMAIL, A., TOMMASI, W., BARRUOL, G. 1999. Mantle structural geology from seismic anisotropy. *In: Mantle petrology: Field observations and high pressure experimentation. A tribute to Francis R. (Joe) Boyd.* (eds. FEI, Y., BERTKA, C. & MYSEN, B. O.), pp. 79-103. Geochemical Society, Special Publications.

SILVER, P. G., FOUCH, M. J., GAO, S. S. & SCHMITZ, M. 2004. Seismic anisotropy, mantle fabric, and the magmatic evolution of Precambrian southern Africa. *South African Journal of Geology,* **107,** 45-58.

SIMKIN, T. 1967. Flow differentiation in the picritic sills of north Skye. In WYLLIE, P.J. (Ed.), *Ultramafic and related rocks.* Wiley, New York.

SINGLE, R. T. & JERRAM, D. A. 2004. The 3D facies architecture of flood basalt provinces and their internal heterogeneity: examples from the Palaeogene Skye Lava Field. *Journal of the Geological Society, London,* **161,** 911-926.

SINTON, C. W., HITCHEN, K. & DUNCAN, R. A. 1998. $^{40}Ar/^{39}Ar$ geochronology of silicic and basic volcanic rocks on the margins of the North Atlantic. *Geological Magazine,* **135,** 161-170.

SMITH, D. 2007. The Tellus Geochemical Programme - survey and results. The Tellus Conference, 17-18th October 2007. Belfast.

SMITH, J. W., HOLWELL, D. A. & MCDONALD, I. 2014. Precious and base metal geochemistry and mineralogy of the Grasvally Norite-Pyroxenite-Anothosite (GNPA) member, northern Bushveld Complex, South Africa: implications for a multistage emplacement. *Mineralium Deposita,* **49,** 667-692.

SMYTH, D. 2014. Lonmin Plc exploration in Northern Ireland – the contribution of mineral exploration to new observations in regional geology. *Mineral Deposits Studies Group 38th Annual Meeting,* Univeristy of Southampton.

SODOUDI, F., YUAN, X., KIND, R., LEBEDEV, S., ADAM, J. & TILMANN, F. 2013. Seismic evidence for stratification in composition and anisotropic fabric within the thick lithosphere of Kalahari Craton. *Geochemistry Geophysics Geosystems,* **14,** 5393-5412.

SOPER, N. J. 1994. Neoproterozoic sedimentation on the northeast margin of Laurentia and the opening of Iapetus. *Geological Magazine,* **131,** 291-299.

SOPER N. J., HIGGINS A. C., DOWNIE C., MATTHEWS D. W. & BROWN P. E. 1976. Late Cretaceous-early Tertiary stratigraphy of the Kangerdlugssuaq area, East Greenland, and the age of opening of the northeast Atlantic. *Journal of the Geolological Society of London,* **132,** 85–104

STARKEY, N. A., STUART, F. M., ELLAM, R. M., FITTON, J. G., BASU, S. & LARSEN, L. M. 2009. Helium isotopes in early Iceland plume picrites: Constraints on the composition of high 3He/4He mantle. *Earth and Planetary Science Letters,* **277,** 91-100.

STEEL, R. J., NICHOLSON, R. & KALANDER, L. 1975. Triassic sedimentation and palaeogeography in Central Skye. *Scottish Journal of Geology,* **11,** 1-13.

STEPHENSON, D., FORTEY, N. J. & GALLAGHER, M. J. 1983. Polymetallic mineralisation in Carboniferous rocks at Hilderston, near Bathgate, central Scotland. *Mineral Reconnaissance Programme Report No. 68.* Natural Environment Research Council.

STEWART, A. D. 2002. *The Later Proterozoic Torridonian Rocks of Scotland: their sedimentology, geochemistry and origin*, Geological Society, London.

STEWART, M., STRACHAN, R. A., MARTIN, M. W. & HOLDSWORTH, R. E. 2001. Constraints on early sinistral displacements along the Great Glen Fault Zone, Scotland: structural setting U-Pb geochronology and emplacement of the syn-tectonic Clunes tonalite. *Journal of the Geological Society, London,* **158,** 821-830.

STONE, P., FLOYD, J. D., BARNES, R. P. & LINTERN, B. C. 1987. A sequential back-arc and foreland basin thrust duplex model for the Southern Uplands of Scotland. *Journal of the Geological Society, London,* **144,** 753-764.

STONE, W. E., CROCKET, J. H. & FLEET, M. E. 1990. Partitioning of palladium, iridium, platinum, and gold between sulfide liquid and basalt melt at 1200^{o}C. *Geochimica et Cosmochimica Acta,* **54,** 2341-2344.

STOREY, M., DUNCAN, R. A. & TEGNER, C. 2007. Timing and duration of volcanism in the North Atlantic Igneous Province: Implications for geodynamics and links to the Iceland hotspot. *Chemical Geology,* **241,** 264-281.

STRACHAN, R. A., SMITH, M., HARRIS, A. L. & FETTES, D. J. 2002. The Northern Highland and Grampian terranes. *In:* TREWIN, N. H. (ed.) *The Geology of Scotland.* The Geological Society.

STYLES, M. T., GUNN, A. G., FLETCHER, T. A., SHAW, M. H., PEREZ, M., GREENWOOD, P. G., CHACKSFIELD, B. C. & EVANS, A. D. 1992. Data arising from drilling investigations of the Knock Intrusion at Claymires, North-East Scotland. *Mineral Reconnaissance Programme Report 9.* British Geological Survey.

STYLES, M. T., GUNN, A. G. & ROLLIN, K. E. 2004. A preliminary study of the PGE in the Late Caledonian Loch Borralan and Loch Ailsh alkaline pyroxenite-syenite complexes, north-west Scotland. *Mineralium Deposita,* **39,** 240-255.

SUTTON, J. & WATSON, J. V. 1951. The pre-Torridonian metamorphic history of the Loch Torridon and Scourie areas in the NW Highlands and its bearing on the chronological classification of the Lewisian. *Journal of the Geological Society, London,* **106,** 241-308.

SVENSEN, H., PLANKE, S., MALTHE-SØRENSSEN, A., JAMTVEIT, B., MYKLEBUST, R., EIDEM, T. R. & REY, S. S. 2004. Release of methane from a volcanic basin as a mechanism for intial Eocene global warming. *Nature,* **429,** 542-545.

SVENSEN, H., JAMTVEIT, B., PLANKE, S. & CHEVALLIER, L. 2006. Structure and evolution of hydrothermal vent complexes in the Karoo Basin, South Africa. *Journal of the Geological Society, London,* **163,** 671-682.

SVENSEN, H., PLANKE, S., CHEVALLIER, L. MALTHE-SØRENSSEN, A., CORFU, F. & JAMTVEIT, B. 2007. Hydrothermal venting of greenhouse gases triggering Early Jurassic global warming. *Earth and Planetary Science Letters,* **256,** 554-566.

SVENSEN, H., PLANKE, S., POLOZOV, A. G., SCHIDBAUER, N., CORFU, F., PODLADCHIKOV, Y. Y. & JAMTVEIT, B. 2009. Siberian gas venting and the end-Permian environmental crisis. *Earth and Planetary Science Letters,* **277,** 490-500.

SVENSEN, H., CORFU, F., POLTEAU, S., ØYVIND H. & PLANKE, S. 2012. Rapid magma emplacement in the Karoo Large Igneous Provine. *Earth and Planetary Science Letters,* **325-326,** 1-9.

SWEENEY, R. J. 1994. Carbonatite melt compositions in the Earth's mantle. *Earth and Planetary Science Letters,* **128,** 259-270.

SZILAS, K., VAN HINSBERG, V. J., CREASER, R. A. & KISTERS, A. F. 2014. The geochemical composition of serpentinites in the Mesoarchaean Tartoq Group, SW Greenland: Harzburgitic cumulates or melt-modified mantle? *Lithos,* **198,** 103-116.

TANNER, P. W. G. 1970. The Sgurr Beag Slide-a major tectonic break within the Moinian of the Western Highlands of Scotland. *Quarterly Journal of the Geological Society,* **126,** 435-463.

TAPPE, S., FOLEY, S. F., JENNER, G. A., HEAMAN, L. M., KJARSGAARD, B. A., ROMER, R. L., STRACKE, A., JOYCE, N. & HOEFS, J. 2006. Genesis of ultramafic lamprophyres and carbonatites at Aillik Bay, Labrador: a consequence of incipient lithospheric thinning beneath the North Atlantic Craton. *Journal of Petrology,* **47,** 1261-1315.

TAPPE, S., FOLEY, S. F., STRACKE, A., ROMER, R. L., KJARSGAARD, B. A., HEAMAN, L. M. & JOYCE, M. 2007. Craton reactivation on the Labrador Sea margins: 40Ar/39Ar age and Sr–Nd–Hf–Pb isotope constraints from alkaline and carbonatite intrusives. *Earth and Planetary Science Letters,* **256,** 433-454.

TAPPE, S., SMART, K. A., PEARSON, D. G., STEENFELT, A. & SIMONETTI, A. 2011. Craton formation in Late Archean subduction zones revealed by first Greenland eclogites. *Geology,* **39,** 1103-1106.

TARNEY, J. 1963. Assynt dykes and their metamorphism. *Nature,* **199,** 672-674.

TARNEY, J. 1973. The Scourie dyke suite and the nature of the Inverian event in Assynt. *In: The Early Precambrian of Scotland and related rocks of Greenland.* (eds. PARK, R. G. & TARNEY, J.), pp. 105-118. Keele: Univeristy of Keele.

TARNEY, J. & WEAVER, B. L. 1987. Mineralogy, petrology and geochemistry of the Scourie dykes: petrogenesis and crystallization processes in dykes intruded at depth. *In: Evolution of the Lewisian and comparable Precambrian high grade terrains.* (eds. PARK, R. G. & TARNEY, J.), pp. 217-234. The Geological Society.

TEGNER, C., DUNCAN, R. A., BERNSTEIN, S., BROOKS, C. K. BIRD, D. K. & STOREY, M. 1998a. $^{40}Ar/^{39}Ar$ geochronology of Tertiary mafic intrusions along the East Greenland rifted margin: Relation to flood basalts and the Iceland hotspot track. *Earth and Planetary Science Letters,* **156,** 75-88.

TEGNER, C., LESHER, C. E., LARSEN, L. M. & WATT, W. S. 1998b. Evidence from the rare-earth-element record of mantle melting for cooling of the Tertiary Iceland plume. *Nature,* **395,** 591-594.

TEGNER, C., THY, P., HOLNESS, M. B., JAKOBSEN, J. K. & LESHER, C. E. 2009. Differentiation and compaction in the Skaergaard Intrusion. *Journal of Petrology,* **50,** 813-840.

THIRLWALL, M. F. & JONES, N. W. 1983. Isotope geochemistry and contamination mechanics of Tertiary lavas from Skye, NW Scotland. *In: Continental basalts and mantle xenoliths.* (eds. HAWKESWORTH, C. J. & NORRY, M. J.), pp. 186-208. Nantwich: Shiva.

THOMASSEN, B. & NIELSEN, T. F. D. 2006. The mineral potential of the East Greenland Palaeogene intrusions. *In:* SECHER, K. (ed.). Geological Survey of Denmark and Greenland.

THOMPSON, R. N. 1982. Magmatism of the British Tertiary Volcanic Province. *Scottish Journal of Geology,* **18,** 49-107.

THOMPSON, R. N. & MORRISON, M. A. 1988. Asthenospheric and lower-lithospheric mantle contributions to continental extensional magmatism: an example from the British Tertiary Province. *Chemical Geology,* **68,** 1-15.

THOMSON, K. & SCHOFIELD, N. 2008. Lithological and structural controls on the emplacement and morphology of sills in sedimentary basins. *In:* THOMSON, K. & PETFORD, N. (eds) *Structure and emplacement of high-level magmatic systems.* Geological Society, London, Special Publication, **302,** pp. 31-44.

THRASHER, J. 1992. Thermal effect of the Tertiary Cuillins Intrusive Complex in the Jurassic of the Hebrides: an organic geochemical study. *In: Basins on te Atlantic Seaboard: Petroleum Geology, Sedimentology and Basin Evolution.* (eds. PARNELL, J.), pp. 35-49.

TILL, C. B., GROVE, T. L. & WITHERS., A. C. 2012. The beginnings of hydrous mantle wedge melting, *Contributions to Mineralogy and Petrology*, **163,** 669-688.

TIMMERMAN, M. J. 2004. Timing, geodynmaic setting and character of Permo-Carboniferous magmatism in the foreland of the Variscan Orogen, NW Europe. *Geological Society, London, Special Publications,* **223,** 41-74.

TOMKINS, A. G. 2010. Wetting facilitates late-stage segregation of precious metal-enriched sulfosalt melt in magmatic sulfide systems. *Geology,* **38,** 951-954.

TOMPKINS, L. A., BAILEY, S. W. & HAGGERTY, S. E. 1984. Kimberlitic chlorites from Sierra Leone, West Africa; unusual chemistries and structural polytypes*. American Mineralogist,* **69**, 237-249.

TORSSANDER, P. 1989. Sulphur isotope ratios of Icelandic rocks. *Contributions to Mineralogy and Petrology,* **102,** 18-23.

TREDOUX, M., LINDSAY, N. M. & MCDONALD, I. 1991. Cluster chemistry and its relevance to the behaviour of the PGE in magmatic systems. *In:* BARNES, S. J., ed. Abstract volume of the 6th International Platinum Symposium. Perth. 50-51.

TREDOUX, M., LINDSAY, N. M., DAVIES, G. & MCDONALD, I. 1995. The fractionation of platinum-group elements in magmatic systems, with the suggestion of a novel causal mechanism. *South African Journal of Geology,* **98,** 157-167.

TREWIN, N. H. 2002. *Geology of Scotland*, The Geological Society, London.

TROLL, V. R., NICOLL, G. R., DONALDSON, C. H. & EMELEUS, H. C. 2008. Dating the onset of volcanism at the Rum Igneous Centre, NW Scotland. *Journal of the Geological Society,* **165,** 651-659.

TUTTLE, M. L., GOLDHABER, M. B. & WILLIAMSON, D. L. 1986. An analytical scheme for determining forms of sulphur in oil shales and associated rocks. *Talanta,* **33,** 953-961.

UPTON, B. J. G., ASPEN, P. & CHAPMAN, N. A. 1983. The upper mantle and deep crust beneath the British Isles: evidence from inclusions in volcanic rocks. *Journal of the Geological Society,* **140,** 105-121.

UPTON, B. G. J., ASPEN, P., REX, D. C., MELCHER, F. & KINNY, P. 1998. Lower crustal and possible shallow mantle samples from beneath the Hebrides: evidence from a xenolithic dyke at Gribun, western Mull. *Journal of the Geological Society,* **155,** 813-828.

UPTON, B. G. J., HINTON, R. W., ASPEN, P., FINCH, A. & VALLEY, J. W. 1999. Megacrysts and Associated Xenoliths: Evidence for Migration of Geochemically Enriched Melts in the Upper Mantle beneath Scotland. *Journal of Petrology,* **40,** 935-956.

UPTON, B. G. J., SKOVGAARD, A. C., MCCLURG, J., KIRSTEIN, L., CHEADLES, M., EMELEUS, C. H., WADSWORTH, W. J. & FALLICK, A. E. 2002. Picritic magmas and the Rum ultramafic complex, Scotland. *Geological Magazine,* **139**.

UPTON, B. G. J., STEPHENSON, D., SMEDLEY, P. M., WALLIS, S. M. & FITTON, J. G. 2004. Carboniferous and Permian magmatism in Scotland. *In: Permo-Carboniferous Magmatism and Rifting in Europe.* (eds. NEUMANN, E.-R., DAVIES, G. R., TIMMERMAN, M. J., HEEREMANS, M. & LARSEN, B. T.). Geological Society, London.

UPTON, B. G. J., FINCH, A. A. & SLABY, E. 2009. Megacrysts and salic xenoliths in Scottish alkali basalts: derivatives of deep crustal intrusions and small-melt fractions from the upper mantle. *Mineralogical Magazine*, **73**(6), 895–908.

UPTON, B. G. J., DOWNES, H., KIRSTEIN, L. A., BONADIMAN, C., HILL, P. G. & NTAFLOS, T. 2011. The lithospheric mantle and lower crust-mantle relationships under Scotland: a xenolithic perspective. *Journal of the Geological Society,* **168,** 873-886.

VISMAND. 2006. *Greenland* [Online, 13th June 2012]. Vismand Exploration Inc. Available: http://www.vismand.com/greenland.html.

VON DAMM, K. L. 1995. Controls on the chemistry and temporal variability of seafloor hydrothermal fluids. *Hydrothermal Systems: Physical, chemical, biological, and geological interactions.*

VAN GOOL, J. A. M., CONNELLY, J. N., MARKER, M. & MENGEL, F. C. 2002. The Nagssugtoqidian Orogen of West Greenland: tectonic evolution and regional correlations from a West Greenland perspective. *Canadian Journal of Earth Sciences,* **39**(5)**,** 665-686.

VERNON, R., HOLDSWORTH, R. E., SELBY, D., DEMPSEY, E., FINLAY, A. J. & FALLICK, A. E. 2014. Structural characteristics and Re–Os dating of quartz-pyrite veins in the Lewisian Gneiss Complex, NW Scotland: Evidence of an Early Paleoproterozoic hydrothermal regime during terrane amalgamation. *Precambrian Research,* **246,** 256-267.

VOLKER, J. A. & UPTON, B. G. J. 1990. The structure and petrogenesis of the Trallval and Ruinsival areas of Rhum ultrabasic complex. *Transactions of the Royal Society of Edinburgh: Earth Sciences,* **81,** 69-88.

WADSWORTH, W. J. 1994. The peridotite plugs of northern Rum. *Scottish Journal of Geology,* **30,** 167-174.

WAGER, L. R. & BROWN, G. M. 1968. Layered igneous rocks. p. 588. Oliver & Boyd.

WAGER, L. R., BROWN, G. M. & WADSWORTH, W. J. 1960. Types of igneous cumulates. *Journal of Petrology,* **1,** 73-85.

WAGNER, T., BOYCE, A. & FALLICK, A. E. 2002. Laser combustion analysis of $\delta^{34}S$ of sulfosalt minerals: determination of the fractionation systematics and some crystal-chemical considerations. *Geochimica et Cosmochimica Acta,* **66,** 2855-2863.

WALKER, G. P. L. & ROSS, J. V. 1954. A xenolithic monchiquite dyke near Glenfinnan, Inverness-shire. *Geological Magazine,* **91,** 463-472.

WANG, K. -L., O'REILLY, S. Y., HONDA, M., MATSUMOTO, T., GRIFFIN, W. L., PEARSON, N. J. & ZHANG, M. 2010. Co-rich sulfides in mantle peridotites from Penghu Islands, Taiwan: Footprints of Proterozoic mantle plumes under the Cathaysia Block. *Journal of Asian Earth Sciences,* **37,** 229-245.

WARREN, J. M. & SHIREY, S. B. 2012. Lead and osmium isotopic constraints on the oceanic mantle from single abyssal peridotite sulfides. *Earth and Planetary Science Letters,* **359-360,** 279-293.

WATERS, F. G., COHEN, A. S., O'NIONS, R. K. & O'HARA, M. J. 1990. Development of Archaean lithosphere deduced from chronology and isotope chemistry of Scourie Dykes. *Earth and Planetary Science Letters,* **97,** 241-255.

WEAVER, B. L. & TARNEY, J. 1981a. Chemical changes during dyke metamorphism in high-grade basement terrains. *Nature,* **289,** 47-49.

WEAVER, B. L. & TARNEY, J. 1981b. The Scourie Dyke Suite: Petrogenesis and geochemical nature of the Proterozoic sub-continental mantle. *Contributions to Mineralogy and Petrology,* **78,** 175-188.

WEAVER, B. L. & TARNEY, J. 1983. Chemistry of the sub-continental mantle: inferences from Archaean and Proterozoic dykes and continental flood basalts. *In: Continental Basalts and Mantle Xenoliths.* (eds. HAWKESWORTH, C. J. & NORRY, M. J.), pp. 209-229. Nantwich: Shiva publications.

WEBB, S. J., CAWTHORN, R. G., NGUURI, T., JAMES, D. 2004. Gravity modeling of Bushveld Complex connectivity supported by Southern African seismic experiment results. *South African Journal of Geology,* **107,** 207-218.

WEBB, S. J., ASHWAL, L. D., CAWTHORN, R. G. 2011. Continuity between eastern and western Bushveld Complex, South Africa, confirmed by xenliths from kimberlite. *Contributions to Mineralogy and Petrology,* **162,** 101-107.

WEBBER, A. P., ROBERTS, S., TAYLOR, R. N. & PITCAIRN, I. K. 2013. Golden plumes: Substantial gold enrichment of oceanic crust during ridge-plume interaction. *Geology,* **41,** 87-90.

WESTBROOK, G. K. & BORRADAILE, G. J. 1978. The geological significance of magnetic anomlaies in the region of Islay. *Scottish Journal of Geology,* **14,** 213-224.

WHITE, N. & LOVELL, B. 1997. Measuring the pulse of a plume with the sedimentary record. *Nature,* **387,** 888-891.

WHITE, R. & MCKENZIE, D. 1989. Magmatism at rift zones: The generation of volcanic continental margins and flood basalts. *Journal of Geophysical Research,* **94,** 7685.

WILLBOLD, M. & STRACKE, A. 2006. Trace element composition of mantle end-members: Implications for recycling of oceanic and upper and lower continental crust. *Geochemistry Geophysics Geosystems,* **7**.

WILSON, G. C., KILUS, L. N. & RUCKLIDGE, J. C. 1995. Precious metal contents of sulfide, oxide, and graphite crystals: determinations by accelerator mass spectrometry. *Economic Geology,* **90,** 255-270.

WILSON, M., NEUMANN, E. -R., DAVIES, G. R., TIMMERMAN, M. J., HEEREMANS, M. & LARSEN, B. T. 2004. Permo-Carboniferous magmatism and rifting in Europe: introduction. *Geological Society, London, Special Publications,* **223**.

WITTIG, N., BAKER, J. A. & DOWNES, H. 2006. Dating the mantle roots of young continental crust. *Geology,* **34,** 237.

WITTIG, N., PEARSON, D. G., WEBB, M., OTTLEY, C. J., IRVINE, G. J., KOPYLOVA, M., JENSEN, S. M., NOWELL, G. M. 2008. Origin of cratonic lithospheric mantle roots: A geochemical study of peridotites from the North Atlantic Craton, West Greenland. *Earth and Planetary Science Letters,* **274,** 24-33.

WITTIG, N., WEBB, M., PEARSON, D. G., DALE, C. W., OTTLEY, C. J., HUTCHISON, M., JENSEN, S. M., LUGUET, A. 2010. Formation of the North Atlantic Craton: Timing and mechanisms constrained from Re–Os isotope and PGE data of peridotite xenoliths from S.W. Greenland. *Chemical Geology,* **276,** 166-187.

WOHLGEMUTH-UEBERWASSER, C. C., FONSECA, R. O. C., BALLHAUS, C. & BERNDT, J. 2013. Sulfide oxidation as a process for the formation of copper-rich magmatic sulfides. *Mineralium Deposita,* **48,** 115-127.

WOOD, B. J. & FRASER, D. G. 1976. *Elementary thermodynamics for geologists*, Oxford University Press.

WORKMAN, R. K. & HART, S. R. 2005. Major and trace element composition of the depleted MORB mantle (DMM). *Earth and Planetary Science Letters,* **231,** 53-72.

YALLUP, C., EDWARDS, M. & TURCHYN, A. V. 2013. Sulphur degassing due to contact metamorphism during flood basalt eruptions. *Geochimica et Cosmochimica Acta,* **120,** 263-279.

YAXLEY, G., CRAWFORD, A. J. & GREEN, D. H. 1991. Evidence for cabonatite metasomatism in spinel peridotite xenoliths from wetern Victoria, Australia. *Earth and Planetary Science Letters,* **107,** 305-317.

YAXLEY, G. M., GREEN, D. H. & KAMENETSKY, V. 1998. Carbonatite metasomatism in the southeastern Australian lithosphere. *Journal of Petrology,* **39,** 1917-1930.

YOUNG, M. E. & EARLS, G. J. T. 2007. New geochemical and geophysical data of Northern Ireland. *Proceedings of the 9th Biennial SGA Meeting*.

YOUNG, B. N., PARSONS, I. & THREADGOULD, R. 1994. Carbonatite near the Loch Borralan intrusion, Assynt. *Journal of the Geological Society, London,* **45,** 945-954.

YOUSSOF, M., THYBO, H., ARTEMIEVA, I. M. & LEVANDER, A. 2013. Moho depth and crustal composition in Southern Africa. *Tectonophysics,* **609,** 267-287.

ZHABINA, N. & VOLKOV, I. 1978. A method of determination of various sulphur compounds in sea sediments and rocks. 3rd International Symposium on Environmental Biogeochemistry. Ann Arbor Science Publications, 735-746.

ZHANG, M., O'REILLY, S. Y., WANG, K. -L., HRONSKY, J. & GRIFFIN, W. L. 2008. Flood basalts and metallogeny: The lithospheric mantle connection. *Earth-Science Reviews,* **86,** 145-174.

ZHU, W., ZHANG, Z., SHU, L., LU, H., SU, J. & YANG, W. 2008. SHRIMP U-Pb zircon geochronology of Neoproterozoic Korla mafic dykes in the Northern Tarim Block, NW China : Implications for the long-lasting breakup process of Rondinia. *Journal of the Geological Society, London,* **165,** 887-890.

APPENDIX A

(relating to Chapter 6)

Appendix A.1

Table A.1.1. All dyke results used throughout Chapter 6.

Sample	X6	X7	X8	X9	X10	X12	X13	X15	X17	X18
	D.c	D.m	D.c	D.m	OG.c	D.c	D.c	D.c	D.m	D.c
Grid ref.	NC 1415 4418	NC 1477 4485	NC 1473 4488	NC 1480 4485	NC 1548 4474	NC 1637 4872	NC 1645 4866	NC 1726 4975	NC 1889 4531	NC 1889 4531
	(wt%)									
SiO_2	50.92	46.38	43.43	46.84	47.64	48.55	47.09	51.22	49.97	49.97
TiO_2	2.63	3.22	3.14	3.25	1.41	2.25	2.81	1.66	2.01	1.66
Al_2O_3	12.42	12.61	12.12	12.58	7.26	10.57	10.56	12.89	12.59	13.51
Fe_2O_3*	17.72	20.55	21.21	19.19	14.54	20	21.37	15.71	16.33	15.65
MnO	0.27	0.29	0.28	0.27	0.22	0.35	0.29	0.23	0.24	0.25
MgO	4.49	5.02	5.85	4.85	16.51	6.07	5.32	5.63	5.74	6.21
CaO	8.67	9.5	10.01	9.16	9.08	8.41	7.95	8.52	8.94	9.91
Na_2O	2.26	2.57	2.43	2.61	1.56	2.02	2.2	2.78	2.26	2.4
K_2O	1.15	0.55	0.4	0.57	0.12	0.77	0.73	1.09	0.85	0.82
P_2O_5	0.35	0.26	0.22	0.36	0.12	0.24	0.21	0.16	0.21	0.16
LOI	0.13	0.33	0.31	1.28	0.62	1	1.38	1.23	1.3	0.64
Total	101.01	101.28	99.41	100.97	99.09	100.23	99.92	101.12	100.44	101.18
	(ppm)									
Sc	44	42	50	44	28	50	48	42	41	45
V	456	582	566	450	255	559	539	416	383	375
Cr	246	32	33	30	1689	106	110	108	124	146
Co	48	60	59	53	129	59	51	49	55	55
Ni	104	73	70	77	1213	115	68	79	86	123
Cu	108	92	88	90	139	57	94	110	242	173
Rb	28	11	10	12	1	25	20	28	16	12
Sr	150	174	149	186	135	169	92	160	142	204
Y	61	35	35	47	15	45	41	35	38	31
Zr	265	124	115	123	80	151	170	141	168	110
Nb	13.2	8.4	7.6	14.1	6.3	11.7	10.5	6.3	11	7.5
Ba	332	140	123	178	73	190	148	185	163	149
La	25.02	10.01	9.23	13.59	9.34	11.76	6.5	11.75	14.08	10.03
Ce	61.15	24.42	22.63	33.67	23.66	27.77	17.92	28.18	32.81	23.72
Pr	8.25	3.79	3.58	5.3	3.64	4.44	2.84	4.22	4.91	3.6
Nd	34.06	17.12	16.16	23.77	15.4	19.8	13.62	18.01	21.06	15.49
Sm	8.33	4.63	4.62	6.46	3.74	5.39	4.44	4.57	5.49	4.2
Eu	2.13	1.61	1.52	1.85	1.08	1.68	1.41	1.36	1.57	1.22
Gd	7.99	4.87	4.72	6.03	3.21	5.73	4.71	4.67	5.15	4
Tb	1.36	0.85	0.87	1.06	0.51	1.04	0.9	0.82	0.93	0.75
Dy	8.75	5.53	5.54	6.75	2.79	6.79	6.15	5.3	5.93	4.73
Ho	1.81	1.17	1.14	1.4	0.52	1.42	1.28	1.11	1.24	0.97
Er	5.31	3.3	3.38	4.04	1.41	4.29	3.81	3.22	3.65	2.89
Tm	0.76	0.48	0.49	0.57	0.19	0.61	0.55	0.48	0.52	0.43
Yb	4.98	3.18	3.08	3.8	1.15	4.08	3.82	3.1	3.59	2.92
Lu	0.79	0.5	0.5	0.6	0.17	0.66	0.61	0.49	0.54	0.45
Hf	6.95	3.09	3.1	3.13	2.4	4.02	3.8	3.65	4	2.91
Ta	0.73	0.53	0.41	1.06	0.46	1.05	0.62	0.45	0.82	0.46
Th	3.57	1.3	1.09	1.22	1.25	1.34	1.43	1.92	1.46	1.09
U	0.94	0.28	0.26	0.3	0.31	1.25	0.53	0.53	0.41	0.28

Table A.1.1. *(continues overleaf)*

Sample	X20	X21	X22	X23	X24	X25	X26	X27	X28	X29	X30	X31
	D.c	D.m	P.c	P.c	D.c	P.c	P.c	P.m	D.c	D.m	D.c	D.c
Grid ref.	NC 1679 4427	NC 1679 4427	NC 1449 2255	NC 1447 2256	NC 1462 2282	NC 1451 2283	NC 1448 2283	NC 1487 2395	NC 1698 2581	NC 1717 2602	NC 1717 2602	NC 1717 2602
SiO_2	49.73	50.73	48.27	49.63	51	47.43	50.25	52.5	51.12	49.83	50.48	51.07
TiO_2	1.16	0.81	0.47	0.67	0.31	0.47	0.36	0.68	0.71	1.69	1.3	1.63
Al_2O_3	14.96	14.55	6.46	10.61	5.11	7.23	6.19	7.39	15.13	12.91	13.27	12.86
Fe_2O_3*	11.47	12.62	12.06	11.21	11.91	11.1	11.07	12.23	10.17	16.76	15.9	17.19
MnO	0.21	0.2	0.17	0.16	0.17	0.15	0.17	0.19	0.18	0.25	0.23	0.27
MgO	7.47	6.56	22.15	17.36	23.1	19.81	21.52	16.34	6.37	5.04	5.8	4.89
CaO	9.43	10.21	4.92	6.37	4.65	5.16	5.64	7.32	10.6	7.89	9.96	8.23
Na_2O	2.46	2.32	1.32	2.22	0.27	0.47	1.22	1.37	3.07	2.6	2.55	3
K_2O	0.54	0.74	0.53	0.69	0.01	1.03	0.46	0.76	0.65	0.42	0.36	0.66
P_2O_5	0.1	0.06	0.06	0.11	0.03	0.07	0.05	0.1	0.07	0.17	0.12	0.18
LOI	2.96	1.54	2.82	2.06	3.39	6.88	2.54	1.18	0.99	1.77	0.69	0.77
Total	100.47	100.32	99.23	101.09	99.96	99.8	99.46	100.04	99.06	99.3	100.66	100.73
Sc	41	35	17	19	19	18	19	25	32	36	42	38
V	335	290	142	176	116	146	132	218	250	445	411	410
Cr	112	71	3134	1918	4051	3891	4432	2823	320	258	41	56
Co	57	58	160	114	148	142	157	93	48	64	63	60
Ni	109	153	1841	1261	1712	1474	1587	909	161	84	66	99
Cu	247	146	51	112	18	167	54	42	56	239	231	164
Rb	9	11	16	22	1	31	12	22	6	4	10	15
Sr	182	216	171	258	17	109	155	78	339	173	166	218
Y	28	19	10	14	7	10	9	15	20	36	29	37
Zr	96	63	64	73	34	70	55	81	65	108	87	153
Nb	5.9	3.5	2.5	3.1	0.9	2.9	1.6	3.7	3.5	7.4	4.5	7.8
Ba	123	189	317	366	10	174	315	239	261	108	95	159
La	7.81	5.23	9.78	13.87	2.16	10.78	8.43	14.02	12.92	9.42	7.54	12
Ce	18.73	12.39	20.22	28.58	6.54	21.75	17.27	30.45	29.31	23.13	17.51	27.41
Pr	2.81	1.9	2.64	3.76	1.15	2.84	2.23	3.97	4.08	3.57	2.65	4.04
Nd	12.56	8.27	10.1	14.11	5.11	10.3	8.42	14.65	15.72	15.59	11.72	17.66
Sm	3.66	2.34	2.09	2.8	1.16	2	1.68	2.88	3.29	4.32	3.34	4.83
Eu	1.11	0.79	0.58	0.8	0.29	0.62	0.52	0.75	1.13	1.45	1.06	1.52
Gd	3.5	2.32	1.73	2.41	1.07	1.83	1.54	2.62	3.1	4.59	3.33	4.74
Tb	0.66	0.45	0.27	0.38	0.17	0.27	0.24	0.42	0.51	0.87	0.63	0.87
Dy	4.24	2.9	1.67	2.15	1.06	1.6	1.37	2.44	3.15	5.69	4.12	5.67
Ho	0.88	0.6	0.33	0.42	0.21	0.31	0.27	0.48	0.64	1.15	0.85	1.15
Er	2.64	1.8	0.93	1.2	0.6	0.91	0.81	1.38	1.85	3.45	2.55	3.44
Tm	0.38	0.26	0.13	0.18	0.09	0.13	0.11	0.2	0.27	0.51	0.38	0.48
Yb	2.49	1.84	0.87	1.15	0.57	0.88	0.75	1.23	1.84	3.47	2.54	3.38
Lu	0.37	0.27	0.13	0.17	0.09	0.13	0.11	0.19	0.28	0.52	0.38	0.51
Hf	2.82	1.63	1.57	1.66	0.83	1.85	1.18	1.89	1.53	3.28	2.42	3.79
Ta	0.37	0.2	0.15	0.21	0.07	0.21	0.09	0.19	0.22	0.49	0.27	0.49
Th	1.29	0.82	1.45	1.66	0.8	1.42	1.22	2.58	0.39	1.55	1.06	1.79
U	0.89	0.2	0.26	0.35	0.11	0.28	0.21	0.6	0.12	0.39	0.26	0.35

Table A.1.1. *(continues overleaf)*

Sample	X44	X45	X47	X50	X51	X52	X53	X54	X55	X56	X59
	D.c	D.c	D.c	D.c	D.m	OG.c	D.c	D.c	D.c	D.c	D.c
Grid ref.	NG 9866 9240	NG 9842 9243	NG 9836 9235	NG 9552 9044	NG 9552 9044	NG 9602 9276	NC 2481 4691	NC 2485 4711	NC 2303 4821	NC 2303 4821	NC 2241 5648
SiO_2	50.05	51.79	51.6	51.94	49.66	48.1	50.67	51.53	47.97	49.08	52.62
TiO_2	1.49	1.84	2.27	1.52	1.63	1.34	1.75	1.62	2.43	3.05	1.79
Al_2O_3	9.57	13.42	12.48	12.56	13.27	10.14	13.06	12.45	14.03	13.99	12.84
Fe_2O_3*	14.6	15.33	16.57	14.02	14.19	13.37	14.05	15.59	16.43	16.76	15.64
MnO	0.22	0.23	0.25	0.22	0.21	0.21	0.25	0.26	0.24	0.28	0.21
MgO	10	5.02	4.53	6.3	6.76	12.25	5.09	5.59	5.72	4.69	4.45
CaO	9.57	8.37	7.38	11.45	9.91	9.71	8.1	10.07	8.62	6.74	8.15
Na_2O	2.39	2.79	2.78	1.8	2.6	2.52	3.42	2.54	2.85	3.04	2.74
K_2O	0.72	0.95	1.78	0.4	0.58	0.28	1.71	1.03	1.8	2.18	1.13
P_2O_5	0.18	0.57	0.25	0.13	0.12	0.12	0.16	0.15	0.37	0.46	0.14
LOI	1.46	0.97	1.1	0.89	0.9	1.44	1	0.67	0.57	0.87	0.84
Total	100.26	101.28	100.98	101.23	99.84	99.49	99.27	101.51	101.02	101.15	100.57
Sc	24	37	35	42	50	25	38	44	36	33	31
V	234	345	408	444	364	297	325	349	330	313	408
Cr	837	42	36	58	106	965	24	63	366	52	15
Co	73	47	51	57	37	69	45	54	48	42	42
Ni	323	61	34	85	90	801	55	196	109	46	40
Cu	143	149	169	314	47	90	103	75	77	52	55
Rb	19	15	73	5	10	4	61	23	75	157	34
Sr	271	375	206	141	161	199	316	252	246	257	270
Y	32	34	48	31	28	17	31	34	50	58	26
Zr	256	200	269	96	114	93	161	134	251	310	97
Nb	16.5	7.7	11.8	5.8	5.5	2.7	12.8	8.5	12.8	21	5.6
Ba	322	788	518	79	148	92	302	127	533	517	346
La	24.38	32.02	25.98	9.1	6.67	4.43	13.71	11.02	25.31	28.37	6.77
Ce	54.09	66.45	57.19	20.77	15.47	12.79	31.58	25.12	55.43	63.15	16.49
Pr	7.67	9.45	8.07	3.12	2.42	2.13	4.52	3.72	7.86	8.81	2.63
Nd	30.69	38.6	32.09	13.26	10.62	10.54	18.82	15.95	32.07	36.24	11.58
Sm	7.16	7.94	7.83	3.95	3.13	3.43	4.82	4.41	7.91	8.98	3.39
Eu	1.62	2.18	1.91	1.06	0.94	1.04	1.27	1.15	1.98	2.27	1.17
Gd	6.26	6.63	7.23	3.76	3.04	2.93	4.12	4.15	7.21	8.48	3.42
Tb	0.96	0.97	1.21	0.67	0.62	0.51	0.72	0.74	1.23	1.4	0.63
Dy	5.53	5.36	7.49	4.39	4.15	2.97	4.45	4.96	7.67	8.82	4.07
Ho	1.06	1.01	1.48	0.91	0.89	0.56	0.93	1.02	1.56	1.77	0.86
Er	2.99	3.17	4.5	2.74	2.67	1.49	2.76	3.03	4.62	5.17	2.47
Tm	0.41	0.44	0.63	0.39	0.41	0.2	0.4	0.44	0.67	0.75	0.37
Yb	2.62	2.91	4.24	2.63	2.74	1.27	2.69	2.95	4.48	5.09	2.48
Lu	0.41	0.49	0.69	0.43	0.44	0.18	0.42	0.46	0.7	0.79	0.38
Hf	6.12	4.65	6.75	2.95	2.86	2.71	3.71	3.15	5.61	7.34	3
Ta	0.85	0.54	0.55	0.33	0.35	0.21	0.71	0.48	1	1.69	0.28
Th	3.81	2.36	5.23	1.24	1.1	1.08	2	1.17	3.14	4.51	1.43
U	1.27	0.55	1.55	0.34	0.23	0.18	0.7	0.24	0.77	1.98	0.33

Table A.1.1. *(continued)*

Sample	X60	X63	X65	X67	X68	X69	X71	X72
	D.c	D.c	D.c	D.c	P.c	D.c	D.c	D.c
Grid ref.	NC 2231 5652	NC 1183 3300	NC 0628 3125	NC 0573 3084	NC 0498 2710	NC 0498 2712	NC 0593 2510	NC 0587 2491
SiO_2	46.09	48.35	48.96	49.02	50.46	49.38	48.01	52.05
TiO_2	2.24	2.46	2.07	1.31	0.43	1.77	1.18	1.14
Al_2O_3	12.76	11.95	12.06	13.09	6.21	13.23	13.43	14.05
Fe_2O_3*	17.88	18.04	15.76	12.69	11.55	15.26	14.7	11.37
MnO	0.25	0.27	0.22	0.2	0.19	0.23	0.22	0.18
MgO	5.49	4.94	4.37	8.75	20.38	6.64	7.08	7.82
CaO	9.63	8.18	7.61	11.33	7.07	11.1	11.21	10.34
Na_2O	2.79	2.54	2.42	1.52	0.76	1.69	1.8	2.45
K_2O	1.47	1.22	1.22	0.91	0	0.78	0.42	0.59
P_2O_5	0.12	0.35	0.22	0.1	0.05	0.14	0.08	0.13
LOI	0.67	0.91	6.4	1.61	2.07	0.66	0.93	0.77
Total	99.4	99.22	101.3	100.54	99.18	100.89	99.07	100.88
Sc	39	41	34	42	23	41	41	37
V	495	420	346	310	162	353	326	340
Cr	26	52	37	367	2949	62	129	204
Co	52	45	44	51	87	49	53	45
Ni	134	53	73	156	1209	83	129	119
Cu	47	137	219	27	66	127	119	164
Rb	24	24	34	21	1	9	3	11
Sr	234	186	196	154	12	199	169	282
Y	26	56	44	17	10	22	24	18
Zr	89	266	236	68	53	91	68	89
Nb	5.6	12.5	12.3	6.5	1.4	8.9	3.7	11.2
Ba	203	367	404	137	1	253	115	188
La	8.37	24.13	24.26	8.29	7.34	9.84	3.65	12.53
Ce	18.6	54.5	51.77	19.21	15.36	23.18	9.6	26.27
Pr	2.77	7.76	7	2.87	2.12	3.46	1.61	3.47
Nd	11.83	31.93	28.23	12.22	8.27	14.82	7.81	13.96
Sm	3.39	8.29	6.88	3.24	2	3.91	2.71	3.31
Eu	1.12	2.02	1.64	0.93	0.45	1.17	0.85	0.99
Gd	3.21	7.29	5.92	2.69	1.69	3.32	2.64	3.07
Tb	0.6	1.29	1.03	0.45	0.27	0.56	0.52	0.51
Dy	3.86	8.28	6.38	2.75	1.65	3.47	3.64	3
Ho	0.82	1.68	1.32	0.54	0.33	0.68	0.77	0.59
Er	2.35	5.07	3.95	1.54	0.95	1.97	2.33	1.71
Tm	0.35	0.74	0.56	0.22	0.13	0.28	0.34	0.23
Yb	2.31	4.97	3.83	1.45	0.88	1.81	2.31	1.57
Lu	0.36	0.79	0.6	0.22	0.14	0.28	0.36	0.26
Hf	2.65	6.51	5.75	1.89	1.21	2.62	1.72	2.19
Ta	0.3	0.65	0.8	0.39	0.11	0.53	0.19	0.59
Th	1.13	3.19	5	0.8	1.2	1.14	0.38	1.96
U	0.36	0.8	1.35	0.37	0.29	0.3	0.09	0.52

Table A.1.2. Analytical Recovery (international rock standard JB1-a) for ICP-OES

	Certified value	Measured value	Analytical Recovery (AR %)
SiO_2	52.16	52.90	101.42
TiO_2	1.30	1.31	101.11
Al_2O_3	14.51	14.21	97.93
Fe_2O_3	9.10	9.25	101.60
MnO	0.15	0.15	99.08
MgO	7.75	7.53	97.15
CaO	9.23	8.72	94.46
Na_2O	2.74	2.83	103.46
K_2O	1.42	1.54	108.67
P_2O_5	0.25	0.26	105.72
LOI	0.78	0.78	100.00
Total	99.39	99.49	100.10
Sc	27.9	27.8	99.7
V	206.0	199.3	96.7
Cr	415.0	422.1	101.7
Co	39.5	43.6	110.3
Ni	134.0	147.0	109.7
Cu	55.0	52.3	95.0
Zn	82.0	86.2	105.2
Sr	443.0	456.5	103.1
Y	24.0	24.8	103.5
Zr	146.0	151.0	103.4
Ba	497.0	504.7	101.5

Table A.1.3. Analytical Recovery (international rock standard JB1-a) for ICP-MS

	Certified value	Measured value	Analytical Recovery (AR %)
$^{49}TiO_2$	1.30	1.28	98.2
^{51}V	206.0	198.0	96.1
^{52}Cr	415.0	410.3	98.9
^{55}MnO	0.15	0.15	96.6
$^{57}Fe_2O_3$	9.1	9.0	98.5
^{59}Co	39.5	37.5	94.9
^{60}Ni	134.0	143.2	106.9
^{65}Cu	55.0	65.1	118.3
^{66}Zn	82.0	81.9	99.8
^{71}Ga	18.0	18.6	103.5
^{85}Rb	42.0	40.1	95.6
^{88}Sr	443.0	438.3	98.9
^{89}Y	24.0	24.5	102.2
^{90}Zr	146.0	144.1	98.7
^{93}Nb	27	28.0	103.6
^{95}Mo	1.29	1.29	100.0
^{118}Sn	2.45	2.45	100.0
^{133}Cs	1.2	1.3	110.3
^{137}Ba	497.0	511.2	102.8
^{139}La	38.1	38.8	101.9
^{140}Ce	66.1	66.7	101.0
^{141}Pr	7.3	7.5	103.3
^{146}Nd	25.5	26.5	104.0
^{147}Sm	5.02	5.14	102.5
^{153}Eu	1.47	1.48	100.5
^{157}Gd	4.54	4.53	99.8
^{159}Tb	0.69	0.67	97.1
^{163}Dy	4.19	3.84	91.7
^{165}Ho	0.72	0.73	102.0
^{166}Er	2.18	2.09	95.9
^{169}Tm	0.31	0.31	100.2
^{172}Yb	2.1	2.00	95.1
^{175}Lu	0.32	0.32	99.6
^{178}Hf	3.48	3.45	99.1
^{181}Ta	1.6	1.6	100.4
^{232}Th	8.8	8.9	101.3
^{238}U	1.6	1.6	99.1

Appendix A.2

Mantle and contaminant compositions:

Table A.2.1. Trace element compositions of end members used in this study. Data from [1](Workman & Hart, 2005) [2](Willbold & Stracke, 2006) [3](McDonough & Sun, 1995) [4](Rollinson, 2012).

Element (ppm)	[1]DMM	[2]EM1	[3]PM	[4]Lewisian amphibolite	[4]Lewisian granulite TTG
Th	0.01	0.03	0.08	6.14	0.33
Nb	0.15	0.38	0.66	4.06	2.57
Ta	0.01	0.03	0.04	0.29	0.07
La	0.19	0.60	0.65	27.1	22.6
Ce	0.55	1.75	1.68	48.7	40.5
Nd	0.58	1.47	1.25	19.1	15.8
Zr	5	13	10.5	121	118
Hf	0.16	0.36	0.28	3.04	2.48
Sm	0.24	0.52	0.41	2.83	2.48
Eu	0.10	0.20	0.15	0.70	0.98
Ti	716	1433	1205	1393	2930
Gd	0.36	0.72	0.54	1.84	1.83
Tb	0.07	0.13	0.10	0.22	0.26
Dy	0.51	0.92	0.67	1.12	1.34
Y	3.33	5.77	4.30	5.63	6.94
Ho	0.12	0.20	0.15	0.21	0.27
Er	0.35	0.60	0.44	0.58	0.72
Yb	0.37	0.62	0.44	0.51	0.68

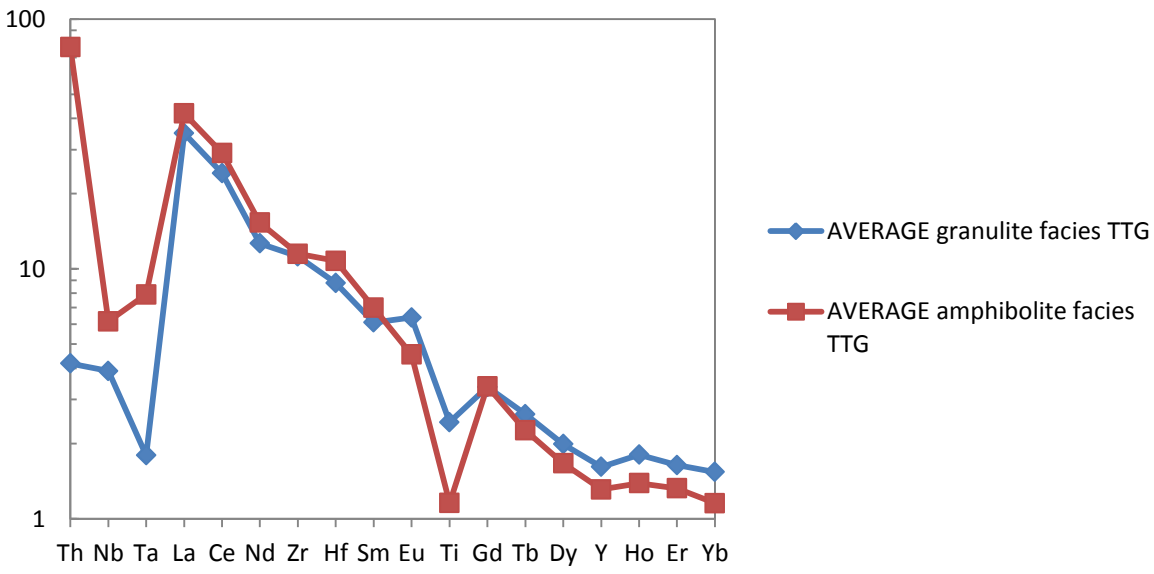

Figure A.2.1. Primitive mantle normalised multi-element plots for potential contaminants – Lewisian amphiblite and granulite, and Archaean SCLM partial melt. Average TTG compositions from Rollinson (2012).

Modal mineralogy:

Table A.2.2. Modal mineralogy spinel lherzolite, garnet lherzolite, transitional spinel-garnet lherzolite and partial melts. Partial melts model mineralogy from Johnson et al. (1990).

	Olivine	Orthopyroxene	Clinopyroxene	Garnet	Spinel
Spinel lherzolite	0.55	0.25	0.18	0.00	0.02
Garnet lherzolite	0.55	0.20	0.15	0.10	0.00

Modelling equations:

Non-batch partial melting:

$$C_L = \frac{C_0}{D + F - FP}$$

(*equation A.1)*

Assimilation with concomitant fractional crystallisation:

$$C_L = C_0\left(f' + \frac{r}{r-1+D} \cdot \frac{C_A}{C_0}(1-f')\right)$$

(equation A.2)

$$f' = F^{\frac{-(r-1+D)}{r-1}}$$

(equation A.3)

Binary mixing (between magma and crustal assimilant):

$$C_{Mix} = \frac{C_{magma} + xC_A}{1-x}$$

(equation A.4)

Fractional (Rayleigh) crystallisation:

$$C_L = C_0 F^{(D-1)}$$

(equation A.5)

C_L = Concentration in liquid

C_0 = Initial concentration

F = Fraction of melting

D = Bulk distribution coefficient

P = Bulk distribution coefficient of the minerals making up the melt

C_{Mix} = Trace element concentration in resultant mixture

C_{magma} = Concentration in uncontaminated magma

C_A = Concentration in assimilant (e.g. contaminant)

r = Ratio of assimilation rate to fractional crystallisation rate

x = Fraction of assimilant added to the magma

Partition coefficients:

Table A.2.3. Partition coefficients used in geochemical modelling. Partition coefficient data from the following sources: Olivine - (Kelemen *et al.*, 1993; Beattie, 1994; Bedini & Bodinier, 1999); Orthopyroxene - (McKenzie & O'Nions, 1991; Kelemen *et al.*, 1993; Salters & Longhi, 1999); Clinopyroxene - (Hauri *et al.*, 1994; Johnson, 1998); Spinel - (Kelemen *et al.*, 1993; Elkins *et al.*, 2008); Plagioclase - (Aigner-Torres *et al.*, 2007); Magnetite - (Haskin *et al.*, 1966; Okamoto, 1979; Lemarchand *et al.*, 1987; Nielsen *et al.*, 1992). Partition coefficients for Pr, Dy, Er, and Tm into magnetite are inferred. Ta coefficients have generally been inferred to be the same as Nb, unless published data is available. Partition coefficients for Pr, Gd, Tb, Ho, Tm, and Lu in silicates and spinel have been inferred where absent in the literature.

	Olivine	Orthopyroxene	Clinopyroxene	Spinel	Plagioclase	Magnetite
Th	0.0000001	0.0004	0.014	0.013	0.3435	0.1
Nb	0.0001	0.002825	0.00605	0.01	0.09725	0.7
Ta	0.0001	0.002825	0.00605	0.01	0.0795	0.23
La	0.000007	0.0000535	0.05025	0.0006	0.0631	0.015
Ce	0.00001	0.0026	0.089	0.0006	0.0457	0.016
Nd	0.00007	0.010267	0.178	0.0006	0.0478	0.026
Sm	0.0007	0.018	0.3775	0.0006	0.06575	0.024
Zr	0.0005	0.01775	0.1975	0.07	0.0094	0.71
Hf	0.0038	0.027225	0.2115	0.003	0.082	0.16
Eu	0.00095	0.0215	0.458	0.0006	0.3254	0.025
Ti	0.015	0.082	0.3955	0.15	0.0473	16.5
Gd	0.002	0.028	0.487	0.0009	0.07175	0.018
Tb	0.003	0.035	0.516	0.0012	0.084	0.019
Dy	0.004	0.041	0.5455	0.0015	0.057167	0.018
Y	0.007365	0.0935	0.412	0.002	0.00989	0.0039
Ho	0.0065	0.05	0.603	0.0023	0.0592	0.017
Er	0.009	0.063917	0.66	0.003	0.07633	0.017
Yb	0.023	0.093917	0.5165	0.0045	0.0903	0.018

Further ratio plots for trace element modelling:

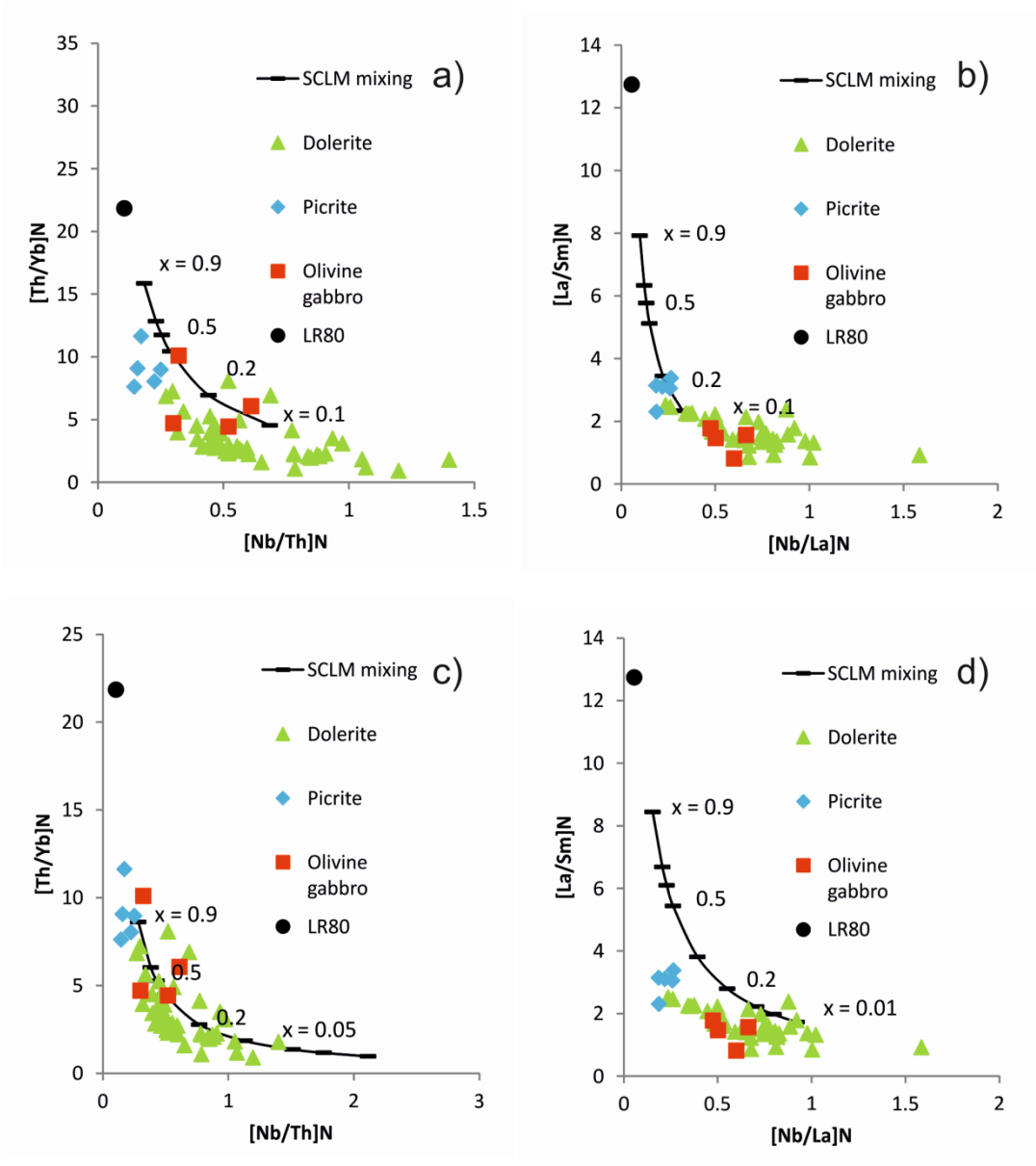

Figure A.3.1. Additional ratio plots (N denotes primitive mantle normalised ratios) for models described in Figure 6.8. (main text). X is the fraction of SCLM partial melt mixed into model. No subsequent fractional crystallisation or AFC has been modelled in these plots, however assimilation of any Lewisian TTG partial melts would adjust La/Sm and Zr/Hf ratio (not plotted – see main text for discussion).

a) and b) display model for picrite dykes – 10% partial melting of DMM garnet lherzolite mixing with 30% SCLM partial melt (LR80) in binary mixing model.

c) and d) display model for dolerite dykes – 2-5% DMM spinel lherzolite partial melt mixing with 15% SCLM partial melt (LR80) in binary mixing model.

Mobility of PGE:

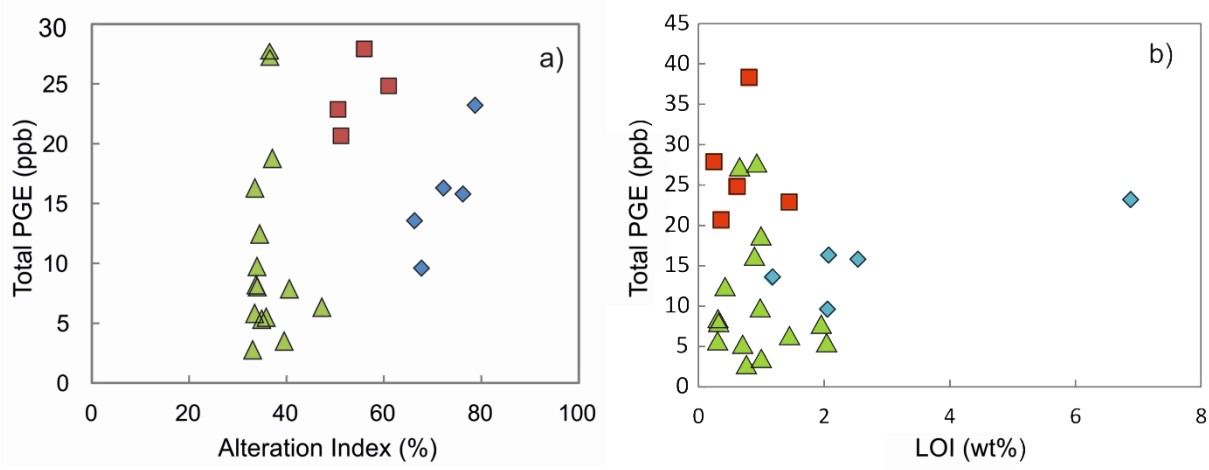

Figure A.3.2. PGE treated as immobile in Scourie Dykes – no correlation between PGE abundance (total) and any alteration index (as in plots (a) and (b).

a) Alteration Index (AI) = $(K_2O+MgO)/(Na_2O+K_2O+CaO+MgO)$% used to assess PGE immobility during metamorphism and alteration.

b) Loss on ignition (LOI).

Appendix A.3

Os isotope systematics and model ages:

$^{187}Os/^{188}Os$ initial (Os_i):

$$\frac{187Os}{188Os_{initial\ sample}} = \left(\frac{187Os}{188Os_{measured}} - \frac{187Re}{188Os_{measured}}\right) \times \left(e^{[\lambda t]} - 1\right)$$

(equation A.6)

γOs (initial):

$$\gamma Os_i = \left(\left(\frac{\frac{187Os}{188Os_{initial\ sample}}}{\frac{187Re}{188Os_{initial\ O-chondrite}}}\right) - 1\right) \times 100$$

(equation A.7)

T_{MA} Os model ages, using λ (^{187}Re decay constant) of 1.666$^{e\text{-}11}$ (Lindner *et al.,* 1989):

$$OsT_{MA} = \frac{1}{\lambda} ln\left(\frac{\frac{187Os}{188Os_{sample}} - \frac{187Os}{188Os_{O-chondrite}}}{\frac{187Re}{188Os_{sample}} - \frac{187Re}{188Os_{O-chondrite}}} + 1\right)$$

(equation A.8)

Re-depletion Os model age (T_{RD}), which assumes all Re is metasomatic, so that model age is calculated so that Re/Os = 0:

$$OsT_{RD} = \frac{1}{\lambda} ln\left(\frac{187Os}{188Os_{sample}} - \frac{187Os}{188Os_{O-chondrite}} + 1\right)$$

(equation A.9)

Re-depletion model eruption age (T_{RD}^{erupt}), which assumes all Re is metasomatic, but is calculated prior to time of magmatic sampling (i.e., Re/Os = 0) and Re/Os (measured) is corrected for radiogenic Os produced post-eruption. This expresses Os-isotopic composition at the time of eruption:

$$OsT_{RD}^{erupt} = \frac{1}{\lambda} ln\left(\frac{187Os}{188Os_{initial\ sample}} - \frac{187Os}{188Os_{initial\ O-chondrite}} + 1\right)$$

(equation A.10)

APPENDIX B

(relating to Chapter 8)

Appendix B

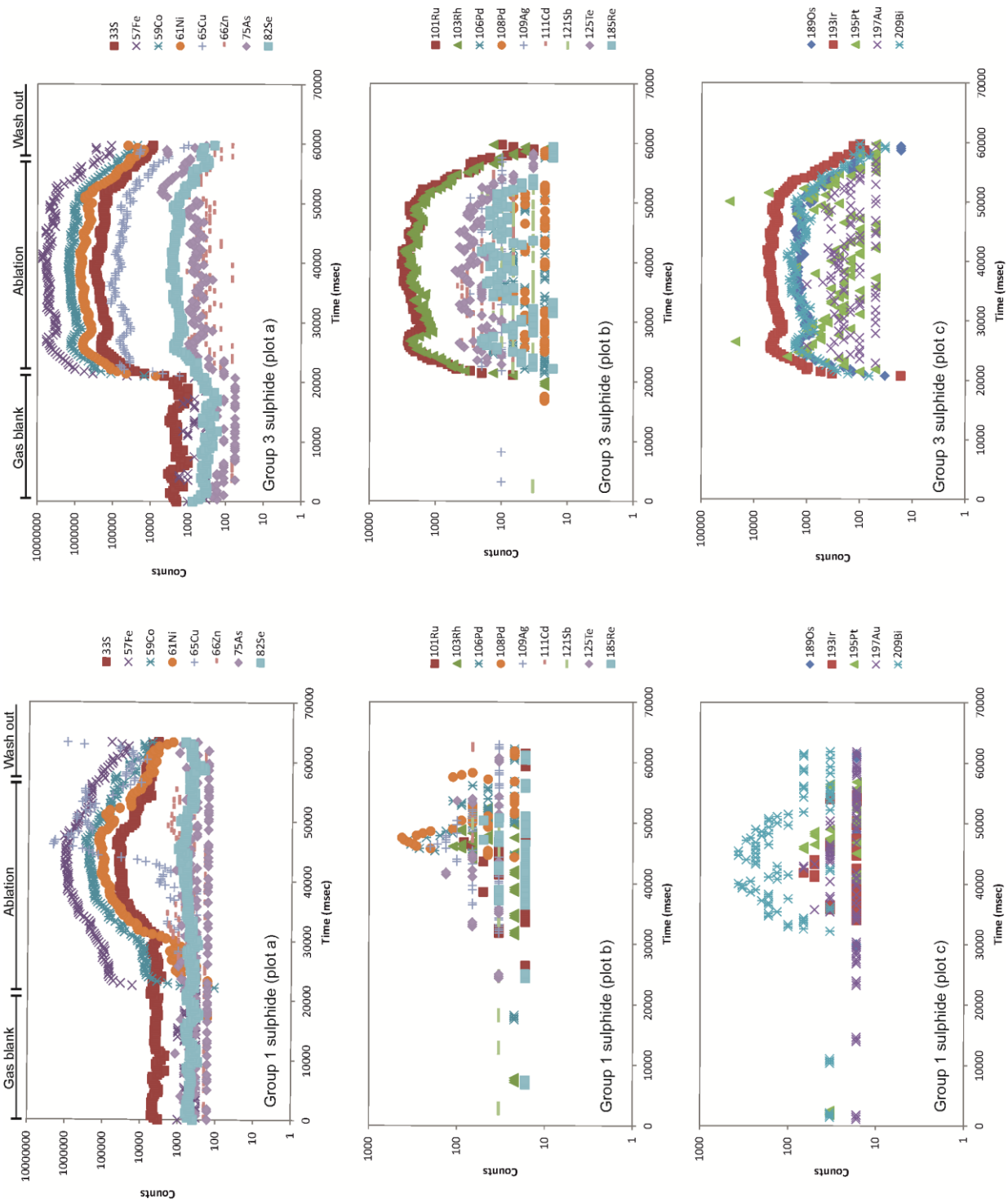

Figure B.1. Representative time resolution analysis (TRA) plots for Group 1 and Group 3 sulphides

APPENDIX C

(relating to Chapter 9)

Appendix C

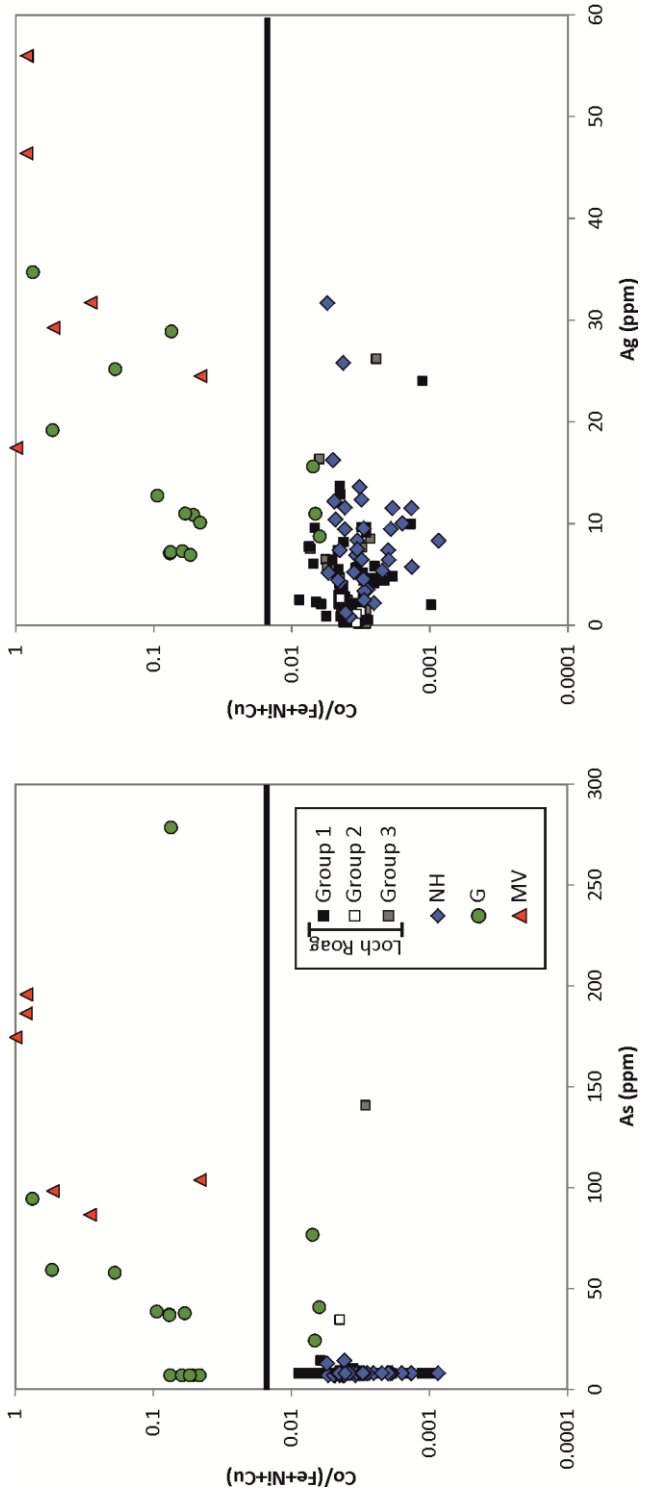

Figure C.1 As and Ag vs Co/(Fe+Ni+Cu) for LA-ICP-MS data from mantle xenolith sulphides

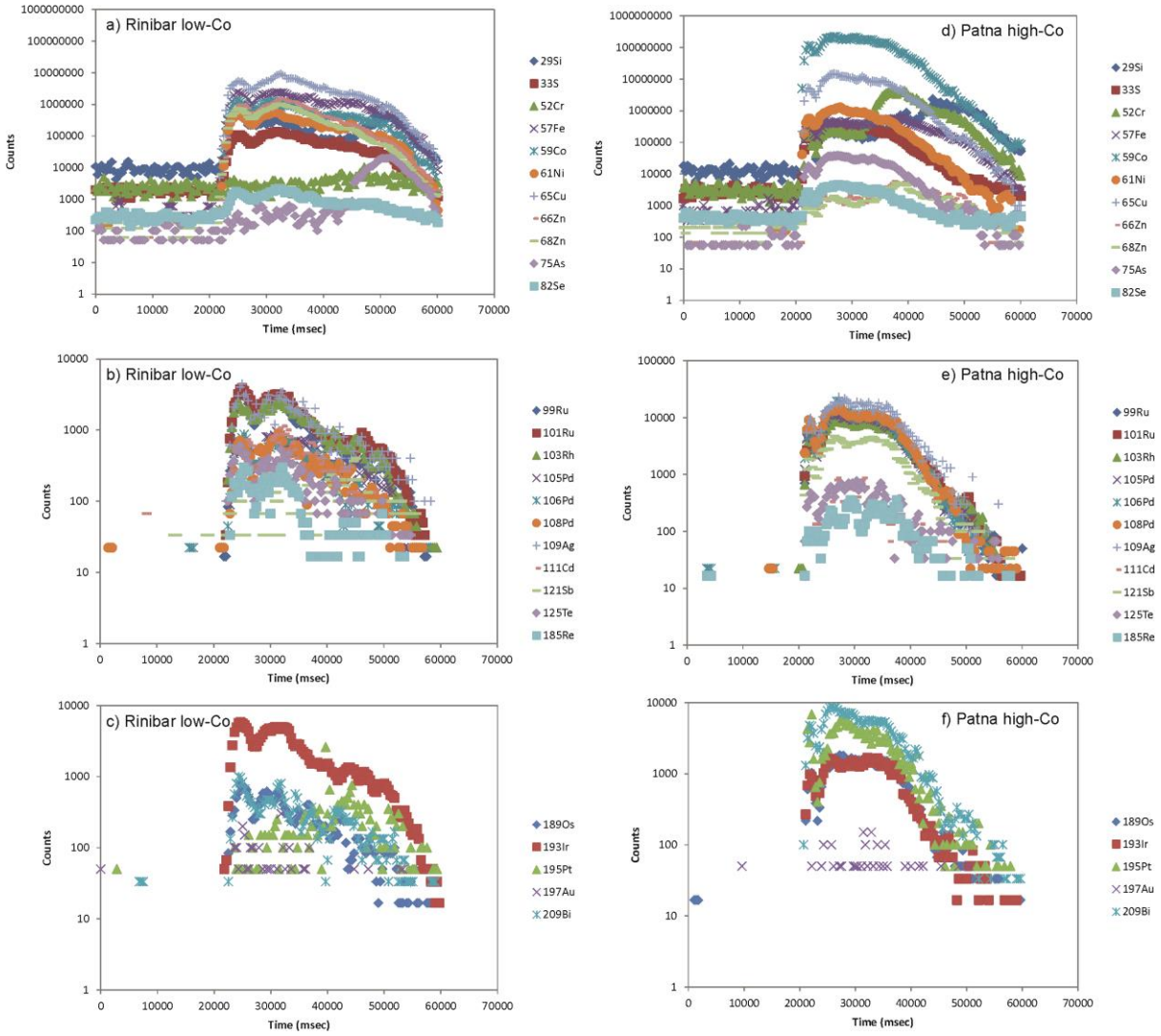

Figure C.2. Examples of time resolution analysis (TRA) spectra for LA-ICP-MS of mantle xenolith sulphide grains

APPENDIX D

(relating to Chapter 10)

Appendix D

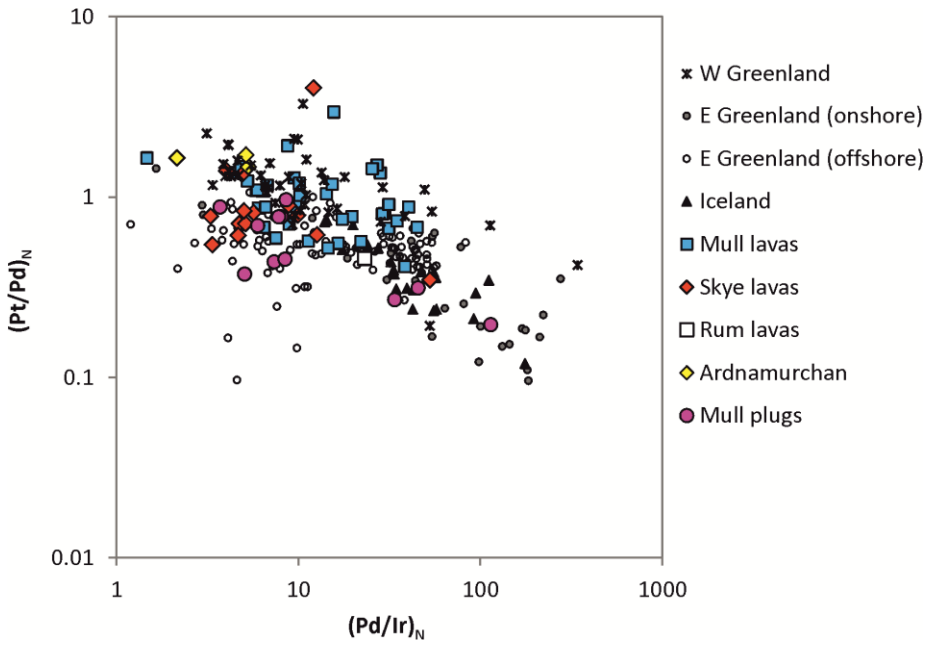

Figure D.1. $(Pt/Pd)_N$ vs, $(Pd/Ir)_N$ for NAIP and BPIP lavas

APPENDIX E

(relating to Chapter 11)

Appendix E.1

E.1.1. Whole-rock chemical sulphur extraction: detailed methodology

Powdered rock samples were loaded into a flat-bottomed glass reaction vessel, with a large magnetic stirrer. A five-leg lid was used to seal the vessel, and clamped in position. The vessel was installed on a magnetic hotplate. A nitrogen gas line was fitted into the vessel lid. In addition, a rubber septum was fitted to one of the other legs, and a condenser clamped and installed vertically from the leg at the top of the vessel. The remaining two legs were blocked off. A Nalgene pipe fitting was connected from the top of the condenser to a gas bell jar, with a glass tube (no gas disperser) feeding down into 100ml of 0.1M $AgNO_3$ solution. The whole apparatus was constructed and operated in a fume cupboard.

At the start of the experiment, the nitrogen gas was turned on and allowed to circulate and equilibrate through the apparatus for a minimum of 20 minutes (at a rate of two or three gas bubbles a second bubbling into the gas bell jar). Once the apparatus was purged and under a N_2 atmosphere, the hotplate and stirrer were set to approximately 150^{o}C, and a 1M solution of chromous chloride ($CrCl_2$) injected through the septum so that the entire powdered sample was submerged (approximately 80-100ml). The condenser was turned on to cool the sulphurous gases (mostly H_2S) produced by the reaction. The reaction was allowed to equilibrate for 3 hours.

During the reaction, chromous chloride solution reduces sulphur in the sample by the following reaction:

$$2Cr^{2+} + S^0 + 2H^+ \rightarrow 2Cr^{3+} + H_2S \qquad \textit{(equation E.1)}$$

This process leads to the complete breakdown of elemental and reduced sulphur species into H_2S, including in the presence of Fe^{3+}. During the reaction, H_2S was continually removed by the stream of N_2 gas and bubbled through the condenser and into the 0.1M $AgNO_3$ solution in the gas bell jar. Reaction with $AgNO_3$ produced a black precipitate of Ag_2S. At the end of the 3 hour period, the hotplate and nitrogen gas line were turned off. The contents of the gas bell jar (Ag_2S precipitate suspended in $AgNO_3$ solution) were filtered under a vacuum through a 0.45µm Millipore® cellulose filter paper. The filtrate was washed twice (still under vacuum) using 100ml of 18.2MΩ deionised water. The paper was collected and freeze dried overnight (or for a minimum of 4 hours). The dry Ag_2S was scraped off the filter papers using a spatula and collected and sealed in a clean sample bottle, ready for conventional sulphur isotope analysis.

E.2.2. Whole-rock chemical sulphur extraction: apparatus diagram

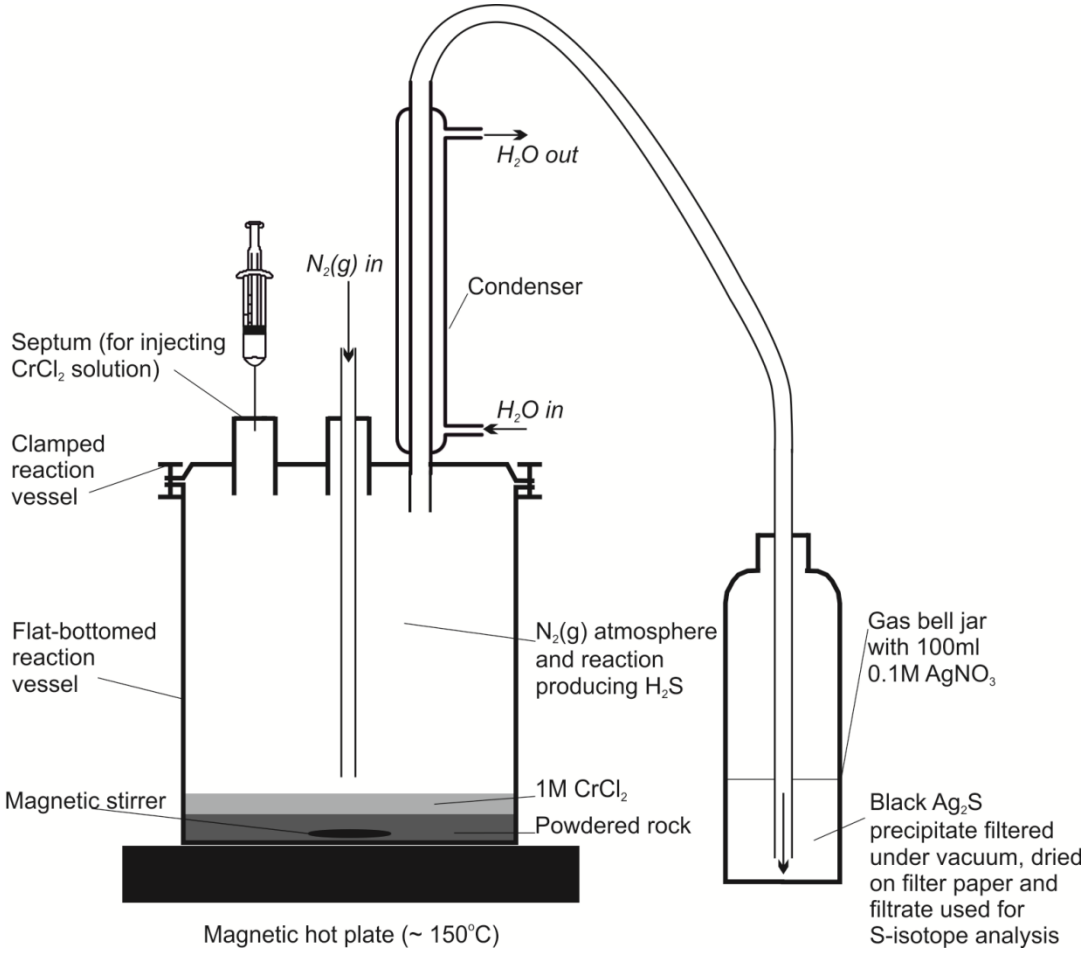

Figure E.1: Apparatus set-up and procedure for whole-rock S-extraction, as described in Supplementary Material section A.

Appendix E.2

E.2.1. Supplementary northern Skye map

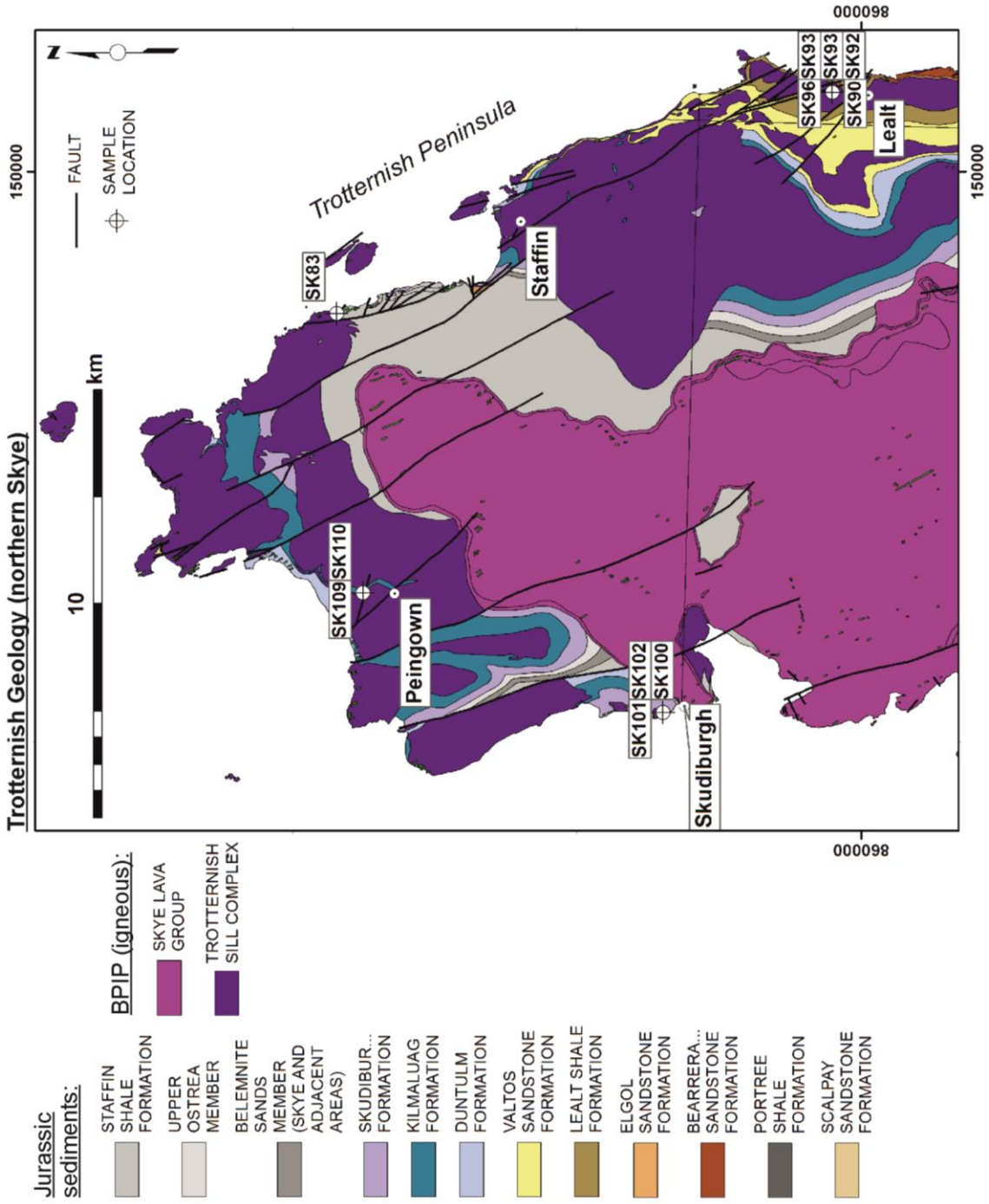

Figure E.2.1. Simplified geology of the Trotternish Sill Complex on the Trotternish Peninsula, showing sample locations

E.2.2. Supplementary southern Skye map

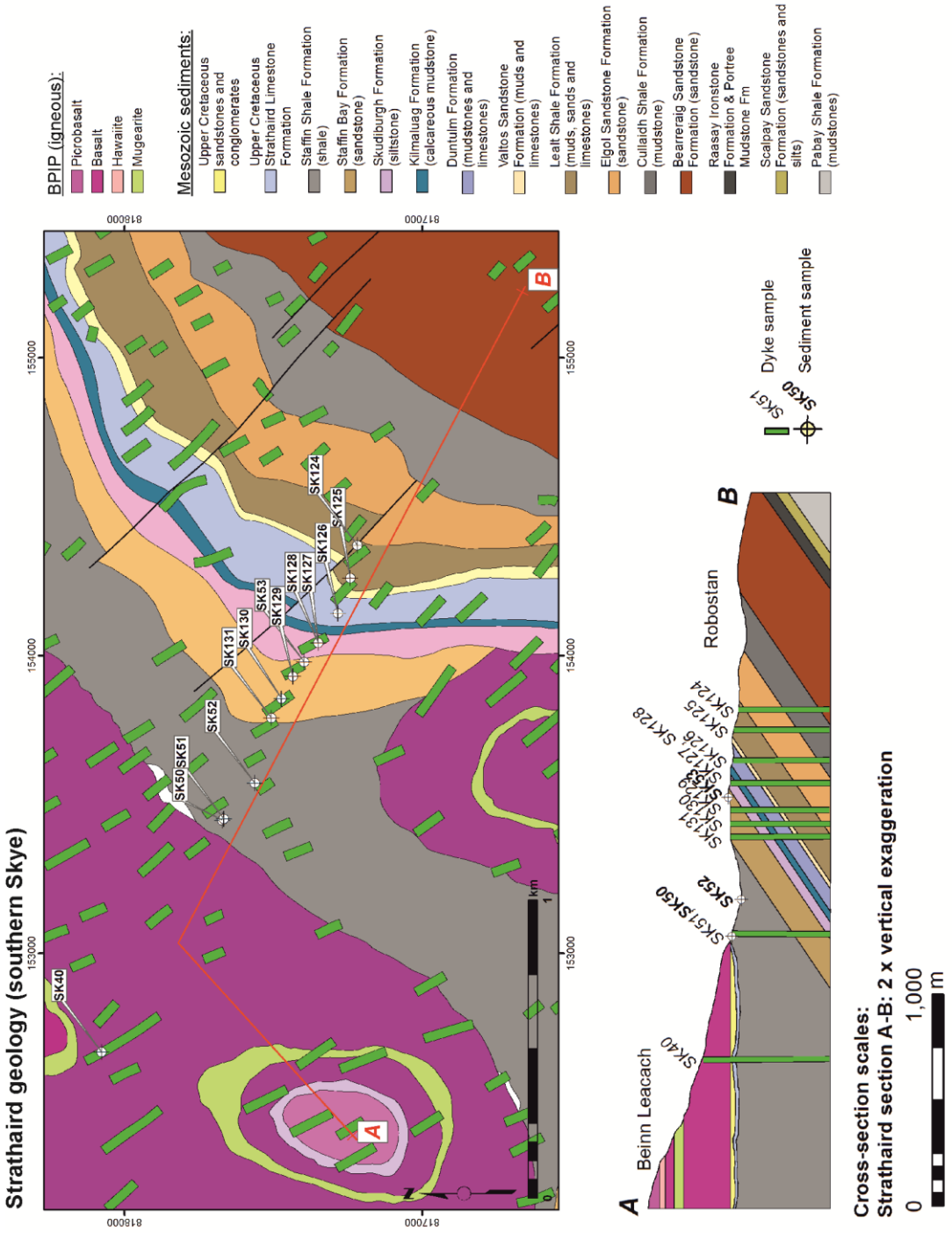

Figure E.2.2. Strathaird Peninsula and Robustan-Kirkibost area. Simplified geological map and sample locations. Line of cross-section displays position of the dyke samples as projected parallel to the strike of the sediment bedding planes, with the exception of sample SK40, which has been projected onto the cross-section along the strike of the dyke itself. Dykes drawn assuming vertical dip. Sediments dip approximately 10^{o} dip NNW below the sediment-lava contact at Scaladal Burn (note cross-section shows 2 x vertical exaggeration). Extent of dyke structure under the current surface level is unknown – cross-section projects dykes for display purposes only.

E.2.3. Supplementary stratigraphic section

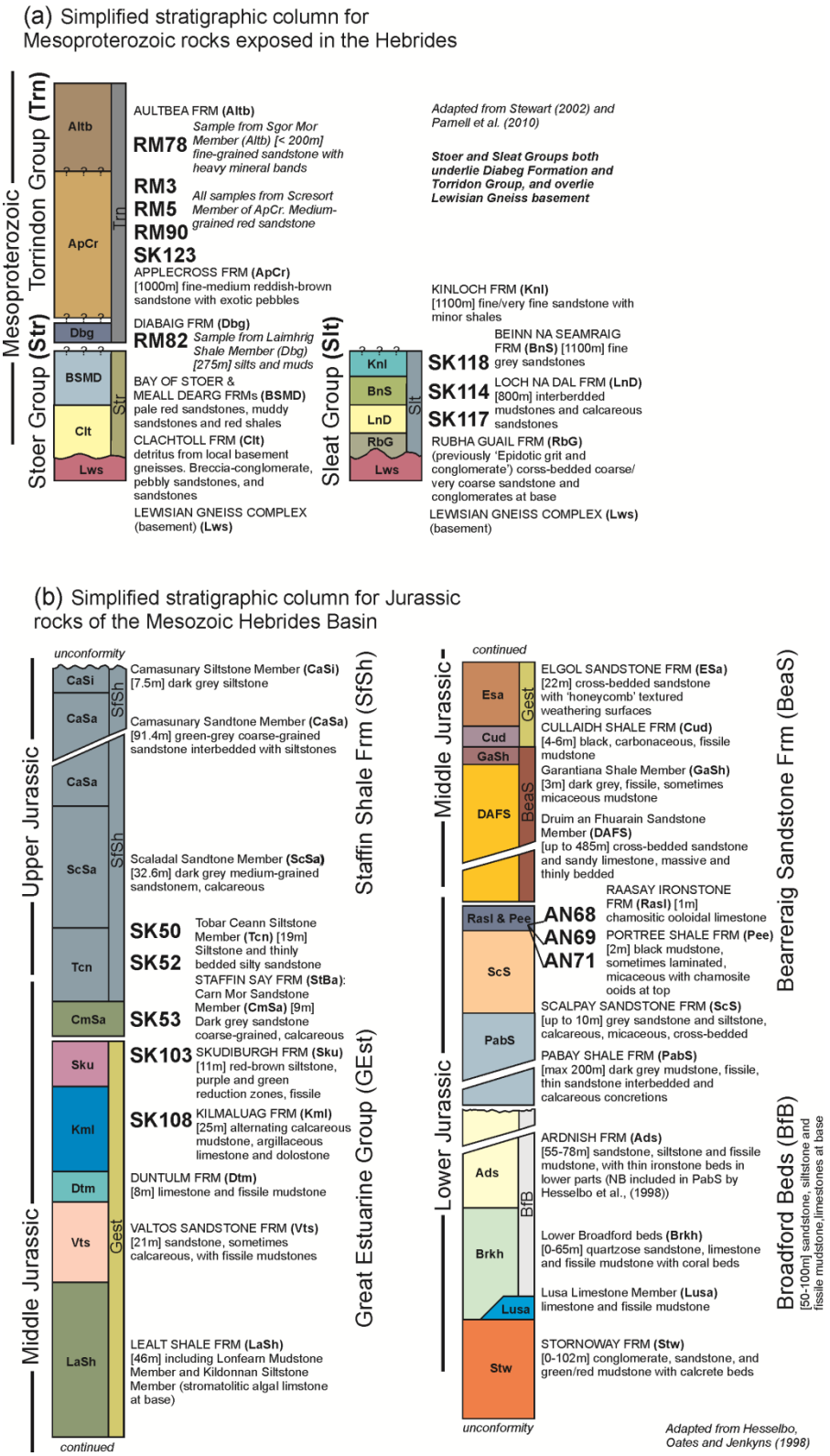

Figure E.2.3. (a) Simplified Mesoproterozoic sedimentary log, based on Stewart (2002) and Parnell *et al.,* (2010). (b).Simplified Hebrides Basin Jurassic sedimentary log, based on and adapted from Hesselbo *et al.,* (1998).

Appendix E.3

E.3.1. Trace element diagrams sills and dykes

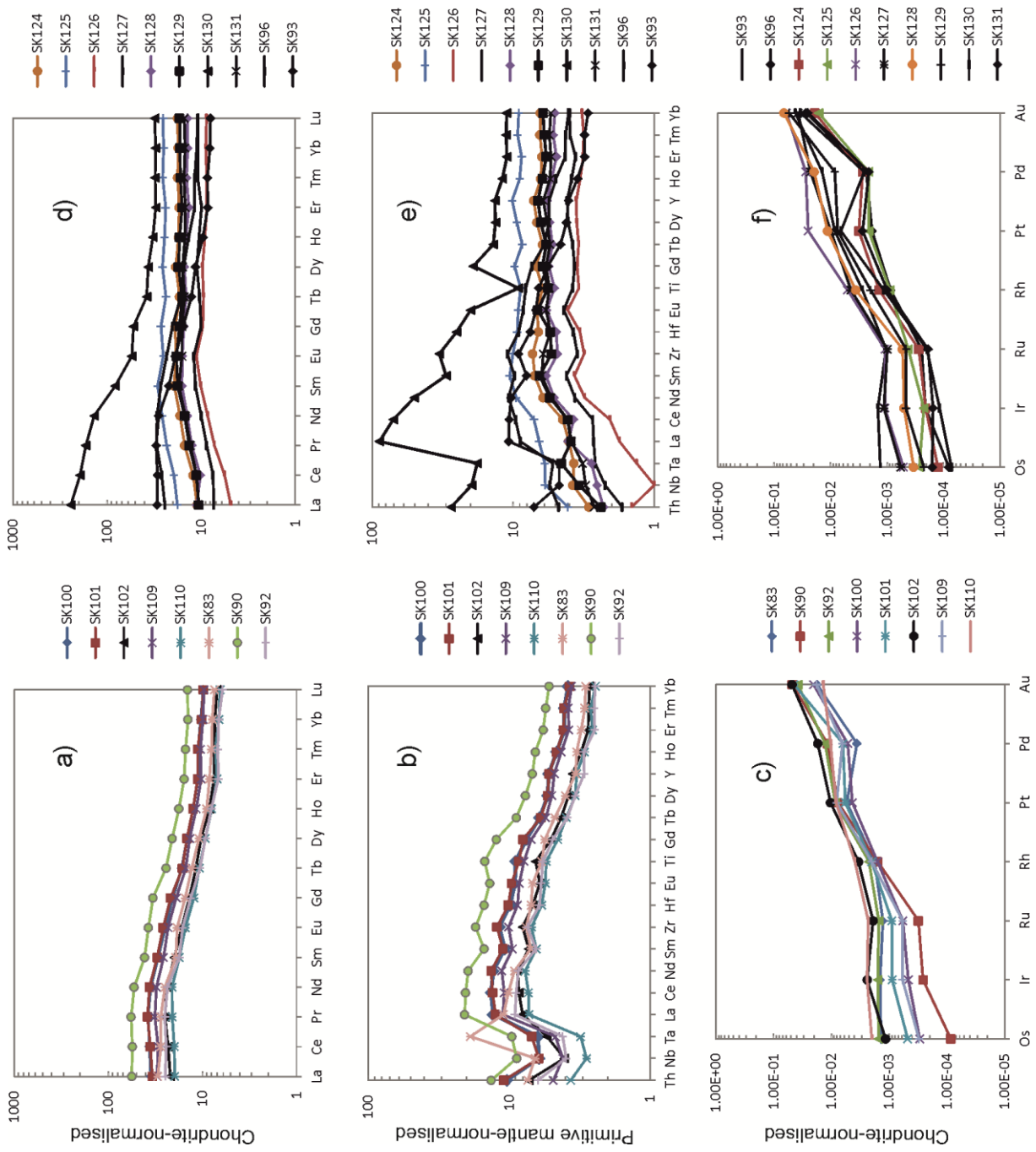

Figure E.3.1. Multi-element normalised diagrams for dykes (a-c) and sills (d-f). Normalisation values from McDonough & Sun (1995). Samples in black highlight those with $\delta^{34}S < -5‰$.

E.3.2. La/Nb ratio of dykes and sills vs. $\delta^{34}S$

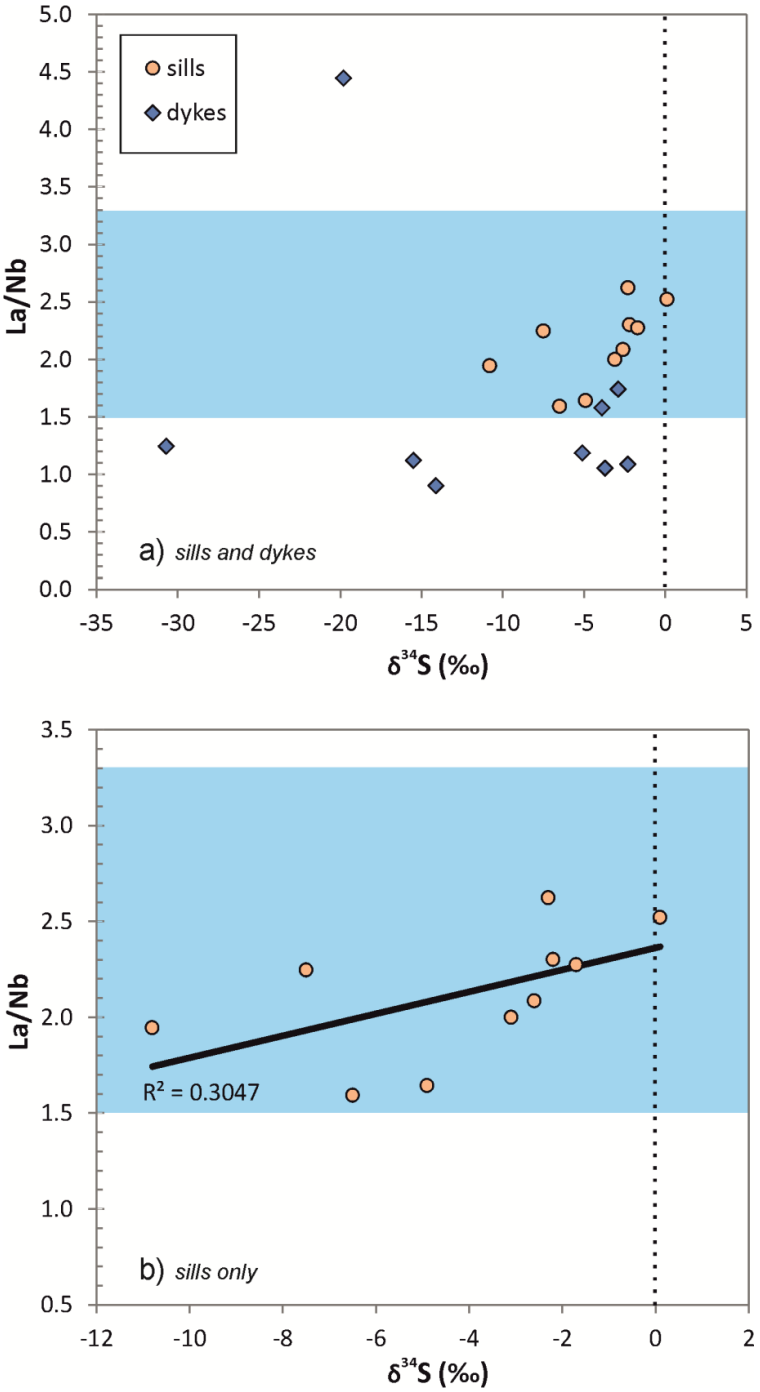

Figure E.3.2. Blue shaded area denotes range of La/Nb ratios in Gibson (1990). Dashed line highlights 0‰ $\delta^{34}S$. (a) All sills and dykes. (b) sills only – with linear trend line displayed with calculated regression.

Appendix E.4

E.4.1. Sulphur isotope results: sulphur extraction and conventional analysis vs. laser combustion

Conventional analyses of Ag_2S precipitates from our whole-rock sulphur extraction method were checked and cross-referenced with laser combustion analyses for sulphide minerals from corresponding samples. A maximum variance of ± 1.4‰ was found between laser and precipitated samples for three sets of corresponding samples (SK127, SK129 and SK130). This variation was not systematic (i.e. neither a positive or negative shift in $\delta^{34}S$), but results from the laser combustion method usually had lighter $\delta^{34}S$ than the Ag_2S precipitates. This variation is likely the result of slightly differing $\delta^{34}S$ of elemental S, sulphide and sulphate species and within various silicate phases of the rock vs. sulphide minerals (normally pyrite), which would be averaged out during whole-rock sulphur extraction. In addition, a repeated sulphur extraction was run for a duplicate sample (SK52 – Jurassic siltstone). $\delta^{34}S$ results for this duplicate extraction varied only ± 0.2‰.

Table E.4.1: $\delta^{34}S$ results for three dykes comparing whole-rock S-extraction methodology followed by conventional analysis (WRS/C) vs. laser combustion of pyrite (Py/L).

Sample	SK127	SK127	SK127	SK127	SK129	SK129	SK129	SK130	SK130	SK130
Method	WRS/C	WRS/C	Py/L	Py/L	WRS/C	Py/L	Py/L	WRS/C	Py/L	Py/L
$\delta^{34}S$ (‰)	-6.6	-6.3	-3.9	-3.6	-15.5	-15.2	-15.7	-21.3	-17.9	-18.4

E.4.2. Sulphur isotope sample duplicates

Table E.4.2: Duplicate $\delta^{34}S$ results for rock samples (conventional analysis) and pyrite-bearing samples (laser combustion). Note that SK52(2) was re-run through the whole S-extraction procedure and conventional analysis to check the consistency of the S-extraction reaction.

Conventional method:

SK127	SK127	SK131	SK131	SK52	SK52	SK52(2)	SK51	SK51
-6.6‰	-6.3‰	-30.7‰	-30.7‰	-29.2‰	-29.6‰	-29.0‰	-13.9‰	-14.2‰

Laser combustion:

SK50	SK50	SK50	SK93b	SK93b	SK127	SK127	SK129	SK129	SK130	SK130
-33.1‰	-33.2‰	-31.6‰	-8.0‰	-6.9‰	-3.9‰	-3.6‰	-15.2‰	-15.7‰	-17.9‰	-18.9‰

APPENDIX F

(relating to Chapter 12)

Appendix F

F.1. Mineralogy and mineral composition methodology (LA-ICP-MS)

Both line and spot analysis were used, depending on the size of the sulphides in each sample. For lines, a minimum line length of ~80µm and a beam diameter of 30µm was used, with laser operating conditions of 10Hz frequency, 0.063 mJ at 4.98 Jcm^{-2}. For spot analysis, the same beam size and laser operating conditions were employed, however the laser beam remained fixed over the static sample, rather than following a designated line along the sample at a rate of 6µm/s (i.e., spatial resolution of ~2µm) as in line analyses. Sulphide minerals (or mineral clusters) < 80µm in length were analysed by spot analysis. Acquisition times ranged 80 to 400s with a gas blank measured for 30-40s prior to laser ablation. Sulphur concentrations were measured prior to LA-ICPMS on the SEM, and ^{33}S (for spots) and ^{57}Fe (for lines) were used as internal standards for trace element calibration. Gas blank subtraction and internal standard corrections were carried out on Thermo Plasmalab software. Further procedural details are available in Smith *et al.* (2014).

Synthetic Ni-Fe-S quenched sulphide standards were used for LA-ICPMS machine calibration, including S, Ni, Fe and Cu as major elements, and Co, Zn, As, Se, Ru, Rh, Pd, Ag, Cd, Sb, Te, Re, Os, Ir, Pt, Au and Bi as trace elements. The compositions and details of analysis methods for these standards is presented in the supplementary material of Prichard *et al.* (2013). Standards 1, 2 and 3 were used for calibration of Cu, Co and Zn, as well as matrix-matched corrections for argide species which interfere with light PGE isotopes ($^{59}Co^{40}Ar$, $^{61}Ni^{40}Ar$, $^{63}Cu^{40}Ar$, $^{65}Cu^{40}Ar$ and $^{66}Zn^{40}Ar$). Standard 1 was also used in corrections for ^{106}Cd on ^{106}Pd and ^{108}Cd on ^{108}Pd, with Cd concentrations in the sulphides up to 66 ppm. Argide and isobaric-corrected data are presented in Table 4 for Ru, Rh and Pd. Independent corrections for various isotopes of the same element (e.g., $^{66}Zn^{40}Ar$ and ^{106}Cd on ^{106}Pd, and ^{108}Cd on ^{108}Pd) showed <20% (commonly <5%) variance, indicating that the correction criteria are suitable. The PGE procedure for LA-ICPMS was checked by analysis of the standard, Laflamme-Po724 as an unknown against the Cardiff quenched sulphide standards (results in Supplementary Material). A representative selection of time resolved analysis spectra (TRA) for sulphide minerals analysed are presented in the Supplementary Material.

F.2. Whole-rock geochemistry of the Rum plugs

CIPW norm calculations (Supplementary Material Table B) using the whole-rock major and trace element compositions from the West Sgaorishal plug (plug 1) corroborate the point counting results of Holness *et al.* (2012) and illustrate an increase in olivine content from the margins to the centre of the plug (RM30) and corresponding decrease in intercumulus minerals such as clinopyroxene and plagioclase. The *CIPW norm* mineralogy estimates support the silicate mineralogical observations listed in Table 2.

F.2.1. Rare earth elements

The chondrite-normalised (McDonough & Sun, 1995) rare earth element (REE) abundances of the peridotite and gabbro plugs are presented in Figure F.2.1.a-f. Most REE multi-element diagrams have smooth patterns, with no or minor Eu anomalies. Most peridotite plugs display arched or smooth REE patterns, with light REE (LREE; La to Nd) depletion in comparison to middle REE (MREE; Sm to Dy). Heavy REE patterns (HREE; Ho to Lu) are generally flat. Broadly, the REE patterns for each plug have parallel or overlapping compositions between samples obtained from the plug margin vs. centre. For example, the centre of plug 1 (RM30) has lower concentrations of REE in comparison to the samples from the margin of this plug, but parallel patterns (Fig. F.2.1.a). However the REE patterns vary significantly between each plug, such that plug 2 has a much flatter pattern than for plug 1 (e.g., Figs. F.2.1.a-b). Plugs 4 and 5 (Fig. F.2.1.c) appear to have similar REE compositions, although sample RM86 from the centre of plug 5 has been offset to lower total abundances, particularly noticeable for LREE. Single samples from plugs 10and 11 follow similar trends with slightly elevated MREE over LREE (Fig. F.2.1.d). The altered sample from the centre of plug 6 (RM63) has considerably elevated REE concentrations in comparison to its margin (RM64), although broadly the REE patterns are parallel to one another (Fig F.2.1.e). The gabbro plugs (plugs 3 and 9; Fig. F.2.1.f) generally have higher REE abundances than peridotites.

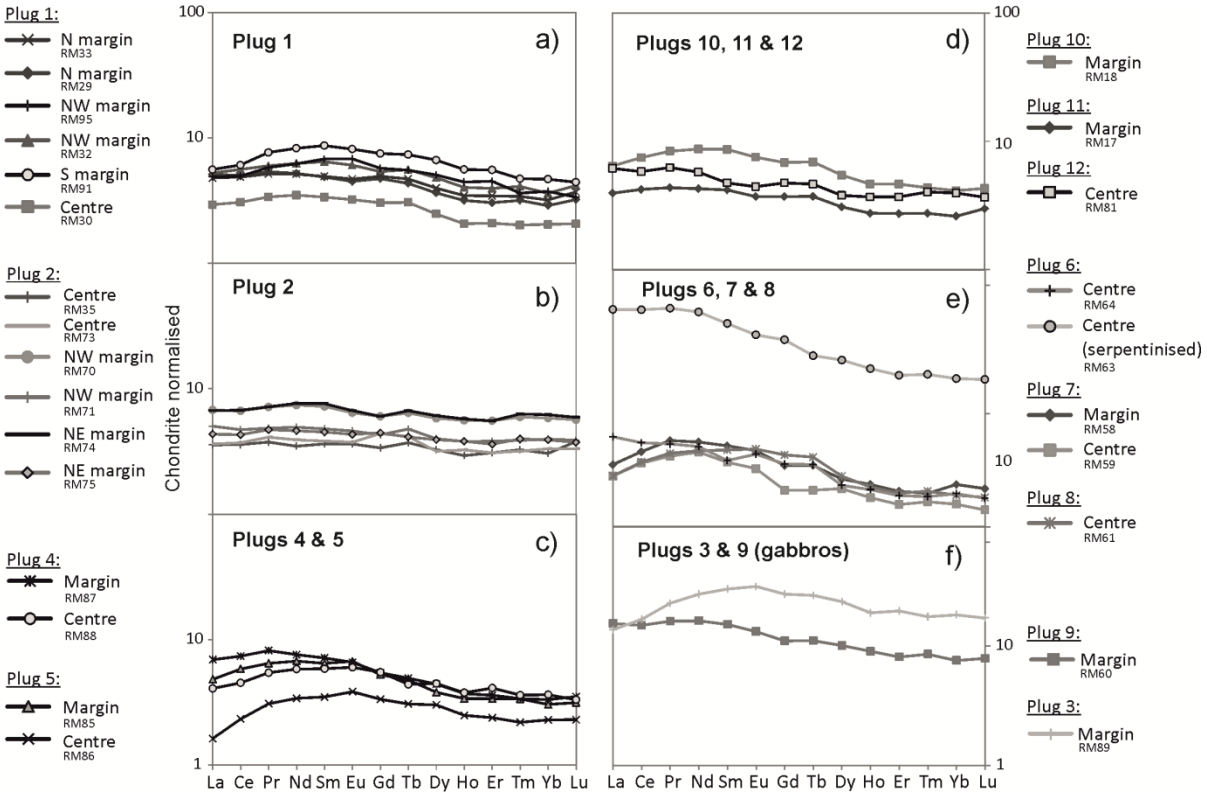

Figure F.2.1. Chondrite-normalised whole-rock REE multi-element diagrams for peridotite plugs (a-e) and two gabbro plug (f). Normalising values from McDonough & Sun (1995).

F.2.2. Multi-element normalised trace element patterns

Multi-element plots have been normalised to primitive mantle compositions (McDonough & Sun, 1995) (Fig. F.2.2.a-f). As for REE, there are consistent trace element characteristics and anomalies per plug, with only slight (parallel) differences between the centre and margins, but more significant differences between plugs. Plugs 2, 6, 7, 8 and gabbro plug 9 have prominent Nb-Ta negative anomalies. In some plugs, subtle non-parallel differences in normalised trace element abundances can be identified – RM29 and RM32 from plug 1 have no Th-Nb-Ta anomalies, while all other samples from that plug have Th elevated above Nb (Fig. F.2.2.a). Similarly sample RM35 from the centre of plug 2 has a lower Th/Nb ratio than other samples from the plug margin, with sizeable negative Nb-Ta anomalies (Fig. F.2.2.b). Gabbro plugs 3 and 9 have divergent normalised trace element abundances, particularly evident for Th, Nb, Ta, Zr, Hf and Ti.

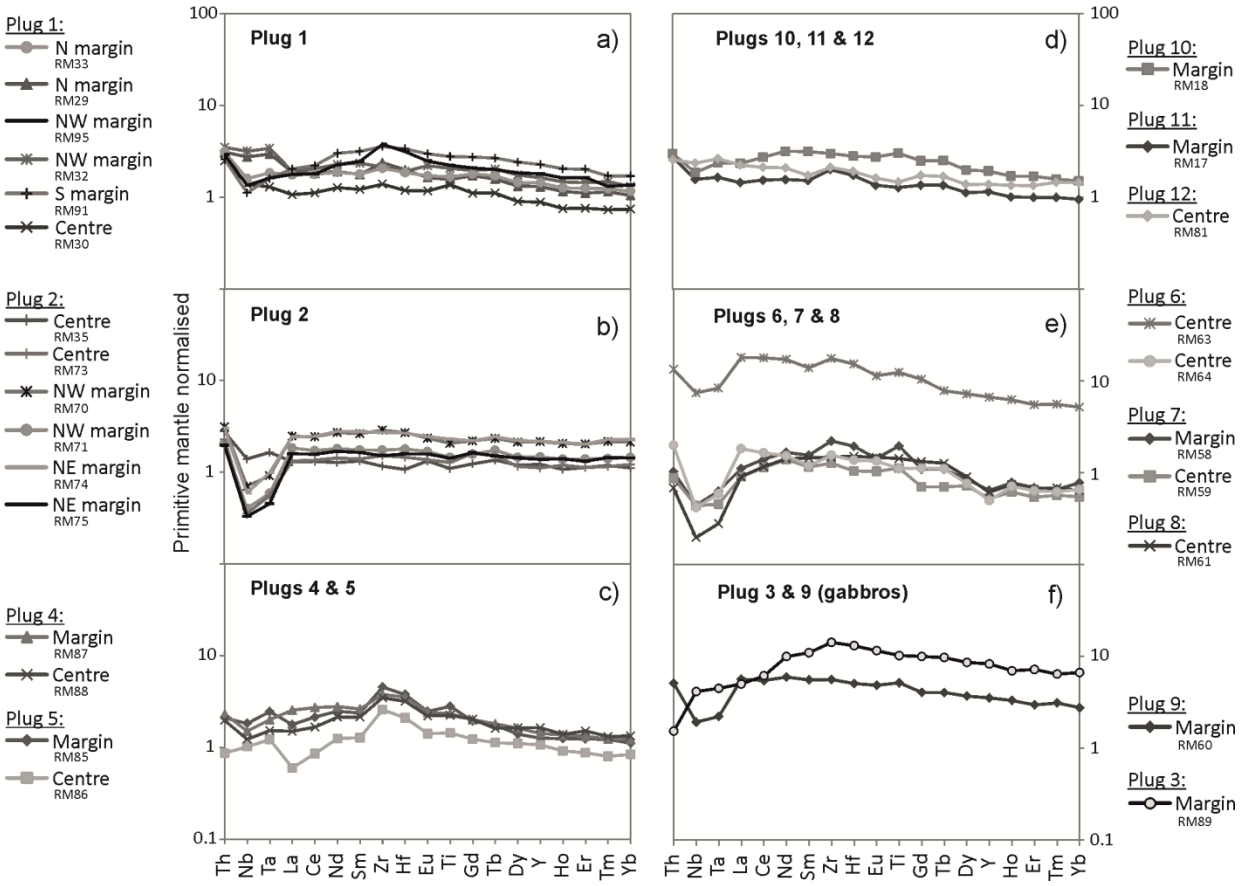

Figure F.2.2. Primitive mantle-normalised whole-rock trace element multi-element diagrams for peridotite and gabbro plugs. Normalising values from McDonough & Sun (1995).

SUPPLEMENTARY TABLES ON CD

CONTENTS

Access Database file

- READ_ME_Geochemical Database Details.pdf
- Hannah_PhD_Thesis.accdb
- Geochemical_Plotting_NORMALISATION_TEMPLATE.xlsx

Chapter 7 Supplementary Tables file

- Supplementary_Material_Table_A.xlsx (BCR-2g glass LA-ICP-MS standard)
- Supplementary_Material_Table_B.xlsx (all LA-ICP-MS results)
- Supplementary_Material_Table_C.xlsx (CIPWnorm calculated mineralogy)

Chapter 8 Supplementary Tables file

- Supplementary_Material_Table_A.xlsx (fire assay rock standards)
- Supplementary_Material_Table_B.xlsx (ICP-OES and ICP-MS rock standards)
- Supplementary_Material_Table_C.xlsx (fire assay duplicates)
- Supplementary_Material_Table_D.xlsx (PGE and semi-metals in the Laflamme-Po724 sulphide standard for LA-ICP-MS)

Chapter 9 Supplementary Tables file

- Supplementary_Material_Table_A.xlsx (fire assay rock standards)
- Supplementary_Material_Table_B.xlsx (ICP-OES and ICP-MS rock standards)
- Supplementary_Material_Table_C.xlsx (fire assay duplicates)
- Supplementary_Material_Table_D.xlsx (sulphide petrography for all xenolith sulphides)
- Supplementary_Material_Table_E.xlsx (all LA-ICP-MS results)
- Supplementary_Material_Table_F.xlsx (PGE and semi-metals in the Laflamme-Po724 sulphide standard for LA-ICP-MS)

Chapter 10 Supplementary Tables file

- Supplementary_Material_Table_A.xlsx (lava and plugs samples analysed by fire assay)
- Supplementary_Material_Table_B.xlsx (fire assay rock standards)
- Supplementary_Material_Table_C.xlsx (ICP-OES and ICP-MS rock standards)
- Supplementary_Material_Table_D.xlsx (fire assay duplicates)
- Supplementary_Material_Table_E.xlsx (all major and trace element results for all lavas)

Chapter 11 Supplementary Tables file

- Supplementary_Material_Table_A.xlsx (sample information for all samples analysed)
- Supplementary_Material_Table_B.xlsx (all whole-rock major and trace element results)
- Supplementary_Material_Table_C.xlsx (whole-rock major and trace element compositions of Jurassic mudrocks)

Chapter 12 Supplementary Tables file

- Supplementary_Material_Table_A.xlsx (Isle of Rum sample information)
- Supplementary_Material_Table_B.xlsx (CIPWnorm mineralogy calculations)
- Supplementary_Material_Table_C.xlsx (all LA-ICP-MS results for sulphides from peridotite plugs)
- Supplementary_Material_Table_D.xlsx (all LA-ICP-MS results for sulphides from the Eastern Layered Series)
- Supplementary_Material_Table_E.xlsx (whole-rock S-isotope compositions of Eastern Layered Series cyclic units)
- Supplementary_Material_Table_F.xlsx (fire assay rock standards)
- Supplementary_Material_Table_G.xlsx (ICP-OES and ICP-MS rock standards)
- Supplementary_Material_Table_H.xlsx (fire assay duplicates)
- Supplementary_Material_Table_I.xlsx (PGE and semi-metals in the Laflamme-Po724 sulphide standard for LA-ICP-MS)

Analytical Methodologies.pdf